

AFRL-IF-RS-TR-2000-44
Final Technical Report
April 2000



TIME-FREQUENCY RECEIVERS FOR NONSTATIONARY INTERFERENCE EXCISION IN SPREAD SPECTRUM COMMUNICATION SYSTEMS

Villanova University

**Moeness G. Amin, Alan R. Lindsey, Adel Belouchrani, Chenshu Wang, Steve Lach,
Xuemei Ouyang, Raja Ramineni, and Ismail Jouny**

APPROVED FOR PUBLIC RELEASE; DISTRIBUTION UNLIMITED.

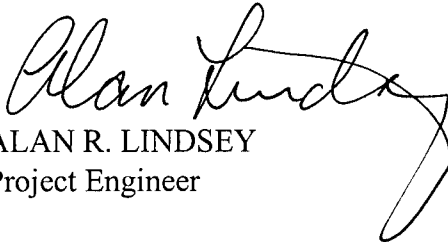
20000606 023

**AIR FORCE RESEARCH LABORATORY
INFORMATION DIRECTORATE
ROME RESEARCH SITE
ROME, NEW YORK**

This report has been reviewed by the Air Force Research Laboratory, Information Directorate, Public Affairs Office (IFOIPA) and is releasable to the National Technical Information Service (NTIS). At NTIS it will be releasable to the general public, including foreign nations.

AFRL-IF-RS-TR-2000-44 has been reviewed and is approved for publication.

APPROVED:



ALAN R. LINDSEY
Project Engineer

FOR THE DIRECTOR:



WARREN H. DEBANY, Technical Advisor
Information Grid Division
Information Directorate

If your address has changed or if you wish to be removed from the Air Force Research Laboratory Rome Research Site mailing list, or if the addressee is no longer employed by your organization, please notify AFRL/IFGC, 525 Brooks Road, Rome, NY 13441-4505. This will assist us in maintaining a current mailing list.

Do not return copies of this report unless contractual obligations or notices on a specific document require that it be returned.

REPORT DOCUMENTATION PAGE			Form Approved OMB No. 0704-0188	
<small>Public reporting burden for this collection of information is estimated to average 1 hour per response, including the time for reviewing instructions, searching existing data sources, gathering and maintaining the data needed, and completing and reviewing the collection of information. Send comments regarding this burden estimate or any other aspect of this collection of information, including suggestions for reducing this burden, to Washington Headquarters Services, Directorate for Information Operations and Reports, 1215 Jefferson Davis Highway, Suite 1204, Arlington, VA 22202-4302, and to the Office of Management and Budget, Paperwork Reduction Project (0704-0188), Washington, DC 20503</small>				
1. AGENCY USE ONLY (Leave blank)		2. REPORT DATE APRIL 2000		3. REPORT TYPE AND DATES COVERED Final Jan 96 - Jul 99
4. TITLE AND SUBTITLE TIME-FREQUENCY RECEIVERS FOR NONSTATIONARY INTERFERENCE EXCISION IN SPREAD SPECTRUM COMMUNICATION SYSTEMS			5. FUNDING NUMBERS C - F30602-96-C-0077 PE - 62702F PR - 4519 TA - 42 WU - 98	
6. AUTHOR(S) Moeness G. Amin, Alan R. Lindsey, Adel Belouchrani, Chenshu Wang, Steve Lach, Xuemei Ouyang, Raja Ramineni, and Ismail Jouny				
7. PERFORMING ORGANIZATION NAME(S) AND ADDRESS(ES) Villanova University 800 Lancaster Ave. Villanova PA 19085			8. PERFORMING ORGANIZATION REPORT NUMBER N/A	
9. SPONSORING/MONITORING AGENCY NAME(S) AND ADDRESS(ES) Air Force Research Laboratory/IFGC 525 Brooks Road Rome NY 13441-4505			10. SPONSORING/MONITORING AGENCY REPORT NUMBER AFRL-IF-RS-TR-2000-44	
11. SUPPLEMENTARY NOTES Air Force Research Laboratory Project Engineer: Alan R. Lindsey/IFGC/(315) 330-1879				
12a. DISTRIBUTION AVAILABILITY STATEMENT APPROVED FOR PUBLIC RELEASE; DISTRIBUTION UNLIMITED.			12b. DISTRIBUTION CODE	
13. ABSTRACT (Maximum 200 words) <p>Time-Frequency distribution are being recognized as powerful tools in signal analysis and processing. Although time-frequency analysis has been of interest for some-time, several advances in recent years have broaden its application areas to include both civilian and military use. The capability of the time-frequency distributions to properly represent multiple component signals in time and frequency permits the development of new and efficient approaches for interference excision in direct sequence spread spectrum communication systems.</p> <p>This report addresses techniques for mitigating nonstationary interference in spread spectrum communication systems; and fast algorithms and efficient realizations of excision techniques based on time-frequency distributions. The scope of this effort is to develop technology to immunize the spread spectrum communication systems to smart jamming and demonstrate the ability to yield improved receiver performance in a highly nonstationary interference environment. This is achieved by utilizing the jammer temporal, spectral, and spatial characteristics to provide accurate and sufficient information leading to its full and effective excision.</p>				
14. SUBJECT TERMS Interference Excision, Spread-Spectrum, Time-Frequency Distribution, Instantaneous Frequency, Nonstationary Interference, Jamming, Jammer, Signal Conditioning, Immune Receivers			15. NUMBER OF PAGES 326	
			16. PRICE CODE	
17. SECURITY CLASSIFICATION OF REPORT UNCLASSIFIED	18. SECURITY CLASSIFICATION OF THIS PAGE UNCLASSIFIED	19. SECURITY CLASSIFICATION OF ABSTRACT UNCLASSIFIED	20. LIMITATION OF ABSTRACT UL	

Table of Contents

Topic	Page
Acknowledgement	1
1. Executive Summary	2
1.1 Notch Filtering Approach for Nonstationary Interference Excision in DSSS Communications	4
1.2 Spatial Time-Frequency Distributions and Array Signal Processing for DSSS Communications	7
1.3 Broadband Interference Excision for Software Radio DSSS Communications Using Time-Frequency Distribution Synthesis	10
1.4 Linear Interference Excision in DSSS Communications Using Short Time Fourier Transforms (STFT's)	11
1.5 Interference Excision in DSSS Communications Using Projection Techniques	12
1.6 High Resolution Time-Frequency Distributions	13
1.7 Broadband Interference Mitigation in Multi-sensor Arrays Using Wavelets and Subbands	13
2. Publications	
2.1 Notch Filtering Approach for Nonstationary Interference Excision in DSSS Communications	15
2.2 Spatial Time-Frequency Distributions and Array Signal Processing for DSSS Communications	16
2.3 Broadband Interference Excision for Software Radio DSSS Communications Using Time-Frequency Distribution Synthesis	17
2.4 Linear Interference Excision in DSSS Communications Using Short Time Fourier Transforms (STFT's)	17
2.5 Interference Excision in DSSS Communications Using Projection Techniques	18
2.6 High Resolution Time-Frequency Distributions	18
2.7 Broadband Interference Mitigation in Multi-Sensor Arrays Using Wavelets and Subbands	19/20

4. Appendix

<i>Notch Filtering Approach for Nonstationary Interference Excision in DSSS Communications</i>	21
Time-frequency distribution spectral polynomials for Instantaneous frequency estimation	22
Optimum interference excision in spread spectrum communications using time-frequency distributions (TFD's)	29
Performance analysis of instantaneous frequency based interference excision techniques in spread spectrum (SS) communications	40
An improved instantaneous frequency based interference excision in DS/SS communication systems	53
Open loop adaptive filtering for interference excision in spread spectrum (SS) systems	64
Zero-tracking time-frequency distributions	69
Performance analysis of interference excisions in spread spectrum communication systems using bilinear transforms	73
<i>Spatial Time-Frequency Distributions and Array Signal Processing for DSSS Communications</i>	77
Jammer mitigation in spread spectrum communications using blind source separation	78
A two sensor array blind beamformer for direct sequence spread spectrum communications	89
Blind source separation based on time-frequency signal representations	99
On the use of spatial time-frequency distributions for signal extraction	109
A two sensor blind beamformer for direct sequence spread spectrum communications	119
Blind source separation using joint signal representations	123

Interference mitigation in spread spectrum communications using blind source separation: approach and analysis	133
Blind source separation using time-frequency distributions: algorithms and asymptotic performance	139
Interference mitigation in SS communications using blind source separation	143
A new approach for blind source separation using time-frequency distributions	148
<i>Broadband Interference Excision for Software Radio DSSS Communications Using Time-Frequency Distribution Synthesis</i>	159
Broadband nonstationary interference excision for software radio spread spectrum communications using time-frequency distribution synthesis	160
A comparison between two bilinear based interference excision in spread spectrum communications	171
Broadband nonstationary interference excision in spread spectrum communications using time-frequency synthesis	175
Multiple component interference excision in spread spectrum communications using Wigner distribution synthesis technique	179
<i>Linear Interference Excision in DSSS Communications Using Short Time Fourier Transforms (STFT's)</i>	183
Short-time Fourier transform receiver for nonstationary interference excision in direct sequence spread spectrum communications	184
Suppression of nonstationary interference in direct sequence spread spectrum communications using short-time Fourier transforms	214
Performance analysis of the DS/SS communications receiver implementing a short time transform interference excision system	242
Time-Frequency concentration measures for nonstationary interference excision in DS/SS communications	246
Recursive Fourier transforms for interference suppression in PN spread spectrum communications	250

<i>Interference Excision in DSSS Communications</i>	255
Suppression of FM interference in DSSS communication systems using projection techniques	256
Interference excision in DSSS communications using projection techniques	260
Analysis of nonstationary interference excision in spread spectrum communications using orthogonal projections	290
Performance analysis of subspace projection technique for interference excision in DSSS communications	294
<i>High Resolution Time-Frequency Distributions</i>	298
High spectral resolution time-frequency distributions	299
<i>Broadband Interference Mitigation in Multi-Sensor Arrays Using Wavelets and Subbands</i>	308
Performance of uniform and nonuniform subband constrained adaptive beamforming under broadband correlated arrivals	309

Acknowledgement

The Principle Investigator, Prof. Moeness Amin, would like to thank Dr. Alan Lindsey, the Contract Technical Manager at the Air Force Research Laboratory (AFRL) for his professional management of this contract. His involvement, patience, flexibility, appreciation, and competence have allowed the project team to carry out the research tasks for four years with continuous enthusiasm and unfading drive.

1. Executive Summary

TIME-FREQUENCY RECEIVERS FOR NONSTATIONARY INTERFERENCE EXCISION IN SPREAD SPECTRUM COMMUNICATIONS SYSTEMS

This is the final report that includes all results of the research work performed under the contract # F30602-96-C-0077 with the Air Force Research Laboratory (Previously, Rome Lab), Rome, NY over the period from January 1st, 1996 to July 31st, 1999. The research project is titled "Time-Frequency Receivers For Nonstationary Interference Excision In Spread Spectrum Communications Systems." This report includes contributions from Professor Moeness Amin (Principle Investigator), Dr. Alan Lindsey (AFRL), Dr. Adel Belouchrani (Postdoctoral Fellow), Dr. Ismail Jouny (Visiting Professor), Mr. Chenshu Wang (Graduate Student), Ms. Xuemei Ouyang (Graduate Student), Mr. Steve Lach (Graduate Student), and Mr. Sekhar Ramineni (Graduate Student). Below, we summarize the major advances made by the above contributors to the general area of interference mitigation in direct sequence spread spectrum communications (DSSS) for a single and multi-antenna receivers, and include in the appendix copies of all journal and conference papers published under the support of this contract. Assuming that the two final papers submitted to the IEEE Transactions on Signal Processing will eventually be accepted for publications, then we are pleased to report that the F30602-96-C-0077 contract has produced one book chapter, eleven journal articles, nineteen conference papers, and nine technical reports. Copies of the book chapter as well as all journal and conference papers are included in the appendix.

The principle contribution of the research work under this contract is in advancing the theory of time-varying spectrum analysis and its applications to the two important areas of communications and sensor array processing. The research team at Villanova University has pioneered the development of a single antenna and multi-sensor receivers based on quadratic time-frequency and joint-variable distributions. We have provided the theoretical framework for solving blind source separation and direction finding problems using bilinear transforms, and established the fundamental role of time-frequency distributions for the rejection of nonstationary interferers in direct sequence spread spectrum communication systems. We have utilized the time-frequency signatures of signal arrivals for improved detection, angle-of-arrival estimation, and blind signal recovery. We were also the first to use the signal power distributions in the time-frequency domain for optimum excision of smart jammers and mitigation of a large class of undesired waveforms through time-varying filtering, least-square synthesis methods, short time Fourier transforms, and subspace projection techniques.

Below, we state our major contributions in each of the following seven areas: 1) Notch filtering approach for nonstationary interference excision in direct sequence spread spectrum (DSSS) communications, 2) Spatial time-frequency distributions and array signal processing for DSSS communications, 3) Broadband interference excision for software radio DSSS communications using time-frequency distribution synthesis, 4) Linear interference excision in DSSS communications using short time Fourier transforms, 5) Interference excision in DSSS communications using projection techniques, 6) High resolution time-frequency distributions, 7) Broadband interference mitigation in multi-sensor arrays using wavelets and subbands.

1.1 Notch Filtering Approach for Nonstationary Interference Excision in DSSS Communications

The first problem tackled is the suppression of nonstationary interference using a notch filtering approach. The main difference between our work in this area and previous contributions is that the position of the filter notch is set by the estimate of the interference instantaneous frequency (IF). Although, there are several techniques devised in the literature for IF estimation for a mono-component and multi-component signal, the prime focus has been set on the new and powerful tool of time-frequency distributions. There were three phases of research on this topic, namely, regress analysis and improvement of the IF-based interference suppression techniques in DSSS communications; devising an optimum receiver for mitigation of the nonstationary jammer using both its amplitude and instantaneous frequency estimates; and development of fast implementation algorithms for IF estimates from TFDs,

In the first phase, analyses of the open-loop adaptive filtering for interference excision spread spectrum communication receiver were provided. We focused on a class of jammers that are characterized by their IFs. Multiple-zero FIR filters whose notches are in synchronization with the jammer IF have been applied to remove the jammer power at every time-sample. These filters are described by three parameters, namely the zero location, the zero multiplicity, and the group delay. Expressions of the receiver SNR incorporating these three parameters have been derived. It is shown that for improved receiver performance, the filter group delay must depend on the filter zero multiplicity, specifically, even-multiplicity excision filters must be of zero-phase. Higher order interference excision filters than those of three and five taps have been proposed for two

primary reasons. First, these filters have broad notches, which will tolerate reasonable bias in the jammer IF estimate. Second, broad notch filters are more effective in excising the jammer energy when it is widely spread around the instantaneous frequency. The two specific cases of three- and five-coefficient filters and their corresponding correlator outputs and signal-to-noise ratios, which had already been devised in the literature, were shown to be special cases of the proposed general interference excision approach.

In the second phase, an optimum open-loop adaptive notch filtering approach for interference excision in PN spread spectrum communications was developed. It has been shown that the FIR filter with variable depth notch that partially removes the jammer achieves significantly higher receiver SNR over both extreme cases of full jammer excision and no excision. The optimum performance is reached by trading off the jammer power and the filter self noise. The filter notch is controlled by a new parameter whose optimum value is a function of the jammer power. For the three-coefficient interference excision filter, the expression for the optimum parameter value can be obtained by solving for a root of a third-order polynomial under both fixed frequency and randomly changing jammer IF. On the other hand, one should seek a numerical solution in the case of the five-coefficient filter, due to the difficulty in getting the solution in a closed form. Several examples have been generated that clearly illustrated the improvement in the receiver signal-to-noise ratio achieved by using the optimum excision filter over both cases of preprocessing disabled and preprocessing enabled, but only based on the jammer IF information. This improvement is exhibited over a wide range of jammer-to-signal ratios (JSR) and is shown using exact values of interference amplitude and IF. As in the case of IF-based interference excision, the noise and the kernel both

affect the estimation of these two parameters when applying TFDs, and yield a lower performance than the case when using exact values.

In the third phase, two zero tracking algorithms were introduced for IF estimation. Both algorithms operate on the local autocorrelation function of the time-frequency distribution and construct a spectral polynomial whose zeros correspond to the IFs of the multicomponent signal. The zero trajectories of this polynomial are either provided by using the sensitivity formula relating, to the first order approximation, the changes in the polynomial coefficients and roots, or by applying Newton's method for zero finding. The sensitivity formula requires all polynomial zeros to be updated simultaneously. That is, the zeros corresponding to the signal autoterms cannot be tracked separately from those that represent cross-terms or extraneous. As such, this method becomes computationally prohibitive for high polynomial orders, i.e., large extent of the local autocorrelation function. From the performance perspective, it has been shown that Newton's method outperforms zero-tracking based on the sensitivity formula, specifically under low signal to noise ratio. In low SNR cases, the spectral polynomial extraneous zeros are significantly perturbed. This perturbation propagates to the signal zero trajectories, leading to tremendous bias in the IF estimates. The employment of the Choi-Williams (CW) distribution kernel may, however, rectify this situation due to its effects on the noise components. The advantage of Newton's method is that we may only track a specific signal root, which simplifies the spectral polynomial zero-tracking operations. However, in rapidly time-varying environment and closely separated frequency components, we stand to lose the signal true zero trajectories to others corresponding to extraneous or cross-term zeros. To mitigate this problem, we have introduced an

extension of Newton's method for TFD applications. This extension was stemmed from the fact that the TFD provides the signal power distribution over time and frequency and may be frequently used to discriminate between true and extraneous signal components. We have shown improved tracking using the extended version over the original version of Newton's method for different nonstationary signals.

1.2 Spatial Time-Frequency Distributions and Array Signal Processing for DSSS Communications

The research involving jammer mitigation in DSSS systems using multi-sensor array receivers have gone through three different phases. The first phase did not deal with the DSSS communication per say, but rather developed a general framework for integrating TFDs in array processing. The second and the third phases both utilized the differences in both the time-frequency and spatial signatures of the DSSS and the interference source signals to achieve improved receiver performance.

In the first phase of the research on multi-sensor array receivers, a new blind separation approach using spatial t-f distributions (STFDs) was introduced. This approach has been devised to primarily separate sources with temporal nonstationary signal characteristics. This new approach is based on the joint diagonalization of a combined set of spatial t-f distribution matrices, which are made up of the auto and cross-TFDs of the data snapshots across the multisensor array, and are expressed in terms of the TFD matrices of the sources. The TFD matrices of the data and sources appear, respectively, in place of the spatial and signal correlation matrices commonly used under stationary environments. The diagonal structure of the TFD matrix of the sources is essential for the proposed approach and is enforced by incorporating only the t-f points

corresponding to the auto-terms. The off-diagonal elements are cross-terms that become negligible by using a reduced interference distribution kernel. We have focused on TFDs of Cohen's class; however, we can use, for the same purpose, any other bilinear t-f distributions and signal representation, such as the affine and hyperbolic classes. The proposed approach has shown a number of attractive features. In contrast to blind source separation approaches using second order and/or high-order statistics, the proposed approach allows the separation of Gaussian sources with identical spectral shapes but with different t-f localization properties. The effect of spreading the noise power while localizing the source energy in the time-frequency domain amounts to increasing the robustness of the proposed approach with respect to the noise. We have run several experiments of simple nonstationary signals as well as real data. These experiments have demonstrated the effectiveness of the proposed technique in separating a wide class of signals. The asymptotic performance analysis of the proposed technique has also been provided.

In the second phase of research on multi-sensor array receivers, we proposed an efficient two sensor blind beamformer for single jammer mitigation in spread spectrum communication systems based on second-order statistic blind identification of the channel coefficients. This second order identification has been made possible because of the difference in the temporal properties between the spread spectrum signal and the jammer. Closed form expressions of the channel coefficients have been derived. Analytical expressions of the optimum beamformer weights have been compared from the perspective of maximum signal to interference plus noise ratio (SINR) at the output of the demodulator. Three structure designs of the mitigation receiver have been suggested. In

solving the underlying problem, the second order channel identification (SOCI) has been compared with the well known JADE in terms of both computational cost and the achieved SINR. It has been shown that, while SOCI has a low computational cost, it provides a comparable performance of JADE when the asymptotic conditions are reached. Because of the inherent ambiguity related to the general blind problem solved by the JADE algorithm, a selection of the desired signal signature and the jammer signature from the estimated signatures should be performed. Therefore, some a priori knowledge of the desired signal is needed in association with the JADE. In contrast, the proposed SOCI does not need this extra processing, since it implicitly selects the desired signature during the identification process.

In the third phase of the research on multi-sensor array receiver, we introduced a new jammer mitigation scheme for DSSS communications. Blind source separation techniques were applied to increase the interference rejection capability of the DSSS communication systems. The main motivation behind the proposed approach was to further immune the DSSS system against strong interference and its multipath. With the inclusion of blind source separation methods, the overall DSSS receiver consists of a single separator, selector, and despreader, followed by a detector. Closed form expressions of the receiver signal-to-noise ratios have been derived. BER curves were provided for multipath and coherent signal environments. These curves have clearly shown the significant reduction in the bit error rates when employing blind source separations.

1.3 Broadband Interference Excision for Software Radio DSSS Communications Using Time-Frequency Distribution Synthesis

Our contribution in this area has been the mitigation of broadband nonstationary interference in DSSS communication systems by jammer signal synthesis. Jammer suppression is achieved by subtracting an estimate of the interference from the received signal. This estimate is obtained by masking out the signal and noise components of the received data in the time-frequency domain, and synthesizing the result. When the interference is known a priori to be a polynomial phase, which is uniquely described by its instantaneous frequency characteristics, an improved estimate can be generated by projecting the synthesized jammer estimate onto a circle of its constant modulus. The direct synthesis of the spread spectrum signal, rather than the interference from the time-frequency domain is shown to be undesirable due to lack of clear t-f signature, the retention of the jammer power in its sidelobes, cross-terms of the signal, noise, jammer spreading over the entire t-f domain, and the loss of meaningful phase reference. A method for extending this technique to the multi-jammer scenario where each term of the interference is of constant modulus is also presented. Computer simulations were performed using two masking techniques. It was shown that the lowest bit-error rates are obtained when the jammer estimate is the result of both a phase-matching and a projection operation on a correctly masked t-f distribution. The implementation of this technique in the simulations showed that different masks should be applied to the TFD of the received signal, depending on the relative power of the interference.

In software radio architectures, the system has the discretion to invoke the proper algorithms, such as the one provided, should a specific jammer type appear. When no

interference signal is present, the receiver should disable preprocessing of the received signal, and rely solely on the spreading gain inherent in DSSS. As the nature of the interference changes and a jammer appears, the receiver can take some corrective action and changes modes, depending on the situation. When a single jammer that is of constant modulus is detected, the method described in this paper becomes applicable. On the other hand, when the jammer is amplitude modulated, more appropriate algorithms may be invoked. Although these interference excision techniques are computationally demanding, the processing power of the spare channel on the multiband, multimode system may be dedicated to them when only channel is in use. By so doing, a signal lost in broadband nonstationary interference may often be recovered.

1.4 Linear Interference Excision in DSSS Communications Using Short Time Fourier Transforms (STFTs)

For linear interference excision, a new adaptive time-frequency technique for interference excision in direct sequence spread spectrum communication has been introduced. The proposed technique implements recursive analysis windows to allow efficient generation of a large class of STFTs with different spectral/temporal resolution properties. Concentration measures were applied to select the analysis window that provides the best jammer time-frequency power concentration. The jammer signal is excised in t-f domain using a binary mask. Central to our contribution is the demonstration that the strength as well as the localization of the jammer power in the t-f domain affects the STFT receiver performance. This demonstration underscores the fact that knowledge of the type of the interference excision system deployed at the receiver can be exploited by the jammer to reduce the system effectiveness to interference

suppression. We have also derived the optimum receiver for interference excision based on STFT analysis. Traditional detectors correlate the receiver PN sequence with the reconstructed PN sequence after interference excision. The proposed optimum scheme, however, takes into account the distortion of the PN sequence caused by the jammer cancellation and is shown to yield enhanced receiver performance. Simulation results have shown significant improvement in the receiver SNR when the optimum receiver is implemented in place of its suboptimum counterpart.

1.5 Interference Excision in DSSS Communications Using Projection Techniques

We have explored the applicability of subspace techniques to nonstationary interference excision in DSSS communications. We continued to focus on FM interference signals that are uniquely characterized by their instantaneous frequencies (IFs). In the proposed subspace technique, the received data over one symbol period is partitioned into blocks. The data in each block is projected on the subspace orthogonal to the respective interference subspace, which is provided using the IF estimate. The projected results are then combined and correlated with the PN sequence at the receiver. Closed form expressions of the receiver SINR have been derived. From these expressions and computer simulations, the performance of the proposed receiver implementing preprocessing subspace techniques has been evaluated as a function of the number of blocks and the noise variance. It has been shown that the receiver performance deteriorates when excision is separately performed on successive data blocks rather than over the entire symbol period. We have compared the proposed projection approach with the recently introduced notch filtering techniques for nonstationary interference excisions

in DSSS. The comparison has shown that subspace techniques outperform the notch filter approach in all jamming cases.

1.6 High Resolution Time-Frequency Distributions

We have introduced a new class of time-frequency distribution kernels. The members of this class satisfy the desirable time-frequency properties for power localization in nonstationary environment, yet they produce local autocorrelation functions (LAF) that are amenable to exponential deterministic modeling during periods of stationarity. The proposed high spectral resolution kernels are required to meet two basic conditions: 1) the frequency marginal 2) an exponential behavior in the ambiguity domain for constant values of the frequency lag. In dealing with sinusoidal data, the first property guarantees that the autoterm sinusoids in the local autocorrelation function are undamped. The second property enforces an exponential damping on all crossterms. As a result, the sinusoidal components in the data translate into damped/undamped sinusoids in the LAF. High-resolution techniques such as reduced rank approximation of the backward linear prediction data matrix can then be applied for frequency estimation. All simulations were presented using noise-free signals. The effect of the noise on the performance of the proposed class of kernels was briefly discussed.

1.7 Broadband Interference Mitigation in Multi-sensor Arrays Using Wavelets and Subbands

We have examined the problem of mitigation of multipath interference in multi-sensor array receivers using wavelets and subbands. Our work has dealt with narrowband

as well as broadband signal arrivals, and uncorrelated as well as coherent signal environments. Performance analysis of subbands for both sensor-space and beamspace processing of the source signals impinging on the array has been provided.

2. Publications

2.1 Notch Filtering Approach for Nonstationary Interference Excision in DSSS Communications

- [1] C. Wang and M. Amin, "Time-frequency distribution spectral polynomials for instantaneous frequency estimation," *Signal Processing*, vol. 76, no.2, pp. 211- July 1999.
- [2] M. Amin, C. Wang, and A. Lindsey, "Optimum interference excision in spread spectrum communications using time-frequency distributions (TFD's)," *IEEE Transactions on Signal Processing*, vol. 47, no. 7, pp. 1966-1976, July 1999.
- [3] C. Wang and M. Amin, "Performance analysis of instantaneous frequency based interference excision techniques in spread spectrum (SS) communications," *IEEE Transactions on Signal Processing*, vol. 46, no. 1, pp. 70-82, January 1998.
- [4] R. Ramineni, M. Amin, and S. Lach, "An improved instantaneous frequency based interference excision in DS/SS communication systems," *Proceedings of the SPIE Conference on Advanced algorithms and Architectures for Signal Processing*, San Diego, CA, July 1998.
- [5] C. Wang, M. Amin, and A. Lindsey, "Open loop adaptive filtering for interference excision in spread spectrum (SS) systems," *Proceedings of the ASILOMAR Conference on Signals, Systems and Computers*, Pacific Grove, CA, November 1997.
- [6] C. Wang and M. Amin, "Zero-tracking time-frequency distributions," *Proceedings of IEEE International Conference on Acoustics, Speech and Signal Processing*, Germany, April 1997.
- [7] C. Wang and M. Amin, "Performance analysis of interference excisions in spread spectrum communication systems using bilinear transforms," *Proceedings of the Fourth International Symposium on Signal Processing and its Applications*, Gold Coast, Australia, August 1996.

2.2 Spatial Time-Frequency Distributions and Array Signal Processing for DSSS Communications

- [1] A. Belouchrani and M. Amin, "Jammer mitigation in spread spectrum communications using blind source separation," Accepted, Signal Processing.
- [2] A. Belouchrani and M. Amin, "A two sensor array blind beamformer for direct sequence spread spectrum communications," IEEE Transactions on Signal Processing, vol. 47, no. 8, pp. 2191-2199, August 1999.
- [3] A. Belouchrani and M. Amin, "Blind source separation based on time-frequency signal representations," IEEE Transactions on Signal Processing, vol. 46, no. 11, pp. 2888-2897, November 1998.
- [4] A. Belouchrani and M. Amin, "On the use of spatial time-frequency distributions for signal extraction," Multidimensional Systems and Signal Processing, Kluwer Academic Publishers, October 1998.
- [5] A. Belouchrani and M. Amin, "A two sensor blind beamformer for direct sequence spread spectrum communications," Proceedings of the IEEE Workshop on Statistical Signal and Array Processing, Portland, Oregon, September 1998.
- [6] A. Belouchrani and M. Amin, "Blind source separation using joint signal representations," Proceedings of the SPIE Conference on Advanced Algorithms and Architectures for Signal Processing, San Diego, CA, August 1997.
- [7] A. Belouchrani and M. Amin, "Interference mitigation in spread spectrum communications using blind source separation: approach and analysis," Proceedings of the International Wireless and Telecommunications Symposium, Shah Alam, Malaysia, May 1997.
- [8] A. Belouchrani and M. Amin, "Blind source separation using time-frequency distributions: algorithms and asymptotic performance," Proceedings of the IEEE International Conference on Acoustics, Speech and Signal Processing, Germany, April 1997.
- [9] A. Belouchrani, M. Amin, and C. Wang, "Interference mitigation in SS communications using blind source separation," Proceedings of ASILOMAR Conference on Signals, Systems and Computers, Pacific Grove, CA, November 1996.

[10] A. Belouchrani and M. Amin, "A new approach for blind source separation using time-frequency distributions," Proceedings of the SPIE Conference on Advanced Algorithms and Architectures for Signal Processing, Denver, CO, August 1996.

2.3 Broadband Interference Excision for Software Radio DSSS Communications Using Time-Frequency Distribution Synthesis

[1] S. Lach, M. Amin, and A. Lindsey, "Broadband nonstationary interference excision for software radio spread spectrum communications using time-frequency distribution synthesis," IEEE Journal on Selected Areas in Communications, vol. 17, no. 4, pp. 704-713, April 1999.

[2] S. Lach, M. Amin, and A. Lindsey, "A comparison between two bilinear based interference excision in spread spectrum communications," Proceedings of the IEEE Workshop on Digital Signal Processing, Bryce Canyon National Park, UT, August 1998.

[3] S. Lach, M. Amin, and A. Lindsey, "Broadband nonstationary interference excision in spread spectrum communications using time-frequency synthesis," Proceedings of the IEEE International Conference on Acoustics, Speech and Signal Processing, Seattle, WA, May 1998.

[4] S. Lach and M. Amin, "Multiple component interference excision in spread spectrum communications using Wigner distribution synthesis technique," Proceedings of the IEEE Sarnoff Symposium on Advanced in Wired and Wireless Communications, College of New Jersey, Trenton, NJ, March 1998.

2.4 Linear Interference Excision in DSSS Communications Using Short Time Fourier Transforms (STFT's)

[1] X. Ouyang and M. Amin, "Short-time Fourier transform receiver for nonstationary interference excision in direct sequence spread spectrum communications," Accepted, IEEE Transactions on Signal Processing, December 1998.

[2] M. Amin and X. Ouyang, "Suppression of nonstationary interference in direct sequence spread spectrum communications using short time-fourier transforms," Book Chapter, To Appear, Wavelet, Transforms and Time-Frequency Signal Analysis, editor: L. Debnath.

[3] X. Ouyang and M. Amin, "Performance analysis of the DS/SS communications receiver implementing a short time Fourier transform interference excision system," IEEE International Symposium on Time-Frequency and Time Scale Analysis, Pittsburgh, October 1998.

[4] X. Ouyang and M. Amin, "Time-Frequency concentration measures for nonstationary interference excision in DS/SS communications," Proceedings of the IEEE Sarnoff Symposium on Advances in Wired and Wireless Communications, College of New Jersey, Trenton, NJ, March 1998.

[5] M. Amin, X. Ouyang, and A. Lindsey, "Recursive Fourier transforms for interference suppression in PN spread spectrum communications," Proceedings of the ASILOMAR Conference on Signals, Systems and Computers, Pacific Grove, CA, November 1997.

2.5 Interference Excision in DSSS Communications Using Projection Techniques

[1] R. Ramineni, M. Amin, and A. Lindsey, "Suppression of FM interference in DSSS communication systems using projection techniques," Proceedings of the ASILOMAR Conference on Signals, Systems and computers, Pacific Grove, CA, November 1999.

[2] R. Ramineni, M. Amin, and A. Lindsey, "Interference excision in DSSS communications using projection techniques," Submitted to the IEEE Transactions on Signal Processing, December 1999.

[3] R. Ramineni and M. Amin, "Analysis of nonstationary interference excision in spread spectrum communications using orthogonal projections," Proceedings of the IEEE Sarnoff Symposium on Advances in Wired and Wireless Communications, College of New Jersey, Trenton, NJ, March 1999.

[4] R. Ramineni, M. Amin, and A. Lindsey, "Performance analysis of subspace projection technique for interference excision in DSSS communications," Proceedings of the IEEE International Conference on Acoustics, Speech and Signal Processing, Turkey, 2000.

2.6 High Resolution Time-Frequency Distributions

[1] M. Amin and W. Williams, "High spectral resolution time-frequency distributions," IEEE Transactions on Signal Processing, vol. 46, no. 10, pp. 2796-2804, October 1998.

2.7 Broadband Interference Mitigation in Multi-Sensor Arrays Using Wavelets and Subbands

[1] I. Jouny and M. Amin, "Performance of uniform and nonuniform subband constrained adaptive beamforming under broadband correlated arrivals," Proceedings of the SPIE International Symposium on Aerospace/Defense Sensing and Control, Orlando, FL, April 1996.

Notch Filtering Approach for Nonstationary Interference Excision in DSSS Communications

Time–frequency distribution spectral polynomials for instantaneous frequency estimation

Chenshu Wang, Moeness G. Amin*

Department of Electrical and Computer Engineering, Villanova University, Villanova, PA 19085, USA

Received 14 April 1998; received in revised form 16 December 1998

Abstract

The local autocorrelation function of the time–frequency distribution (TFD), defined by an appropriate kernel, is used to form a spectral polynomial. Some of the roots of this polynomial correspond to the instantaneous frequencies of the input signal. In this paper, we use extended version of Newton's method for root-finding to obtain the trajectories of the signal IF zeroes. It is shown that the proposed TFD-based zero-tracking technique provides good tracking performance for both mono- and multi-component signals. © 1999 Elsevier Science B.V. All rights reserved.

Zusammenfassung

Die durch einen geeigneten Kern definierte lokale Autokorrelationsfunktion einer Zeit–Frequenz-Darstellung wird verwendet, um ein spektrales Polynom zu bilden. Einige der Wurzeln dieses Polynoms entsprechen den Momentanfrequenzen des Eingangssignals. In diesem Artikel verwenden wir eine erweiterte Version der Newton-Methode zur Nullstellenberechnung, um die Trajektorien der den Momentanfrequenzen des Signals entsprechenden Nullstellen zu erhalten. Es wird gezeigt, daß die vorgeschlagene, auf Zeit–Frequenz-Darstellungen beruhende Methode zur Nullstellen-Nachführung eine gute Leistungsfähigkeit sowohl bei einkomponentigen als auch bei mehrkomponentigen Signalen aufweist. © 1999 Elsevier Science B.V. All rights reserved.

Résumé

La fonction d'autocorrélation locale de la distribution temps–fréquence (TFD), définie par un noyau approprié, est utilisée pour former un polynôme spectral. Certaines des racines de ce polynôme correspondent aux fréquences instantanées (IF) du signal d'entrée. Nous utilisons dans cet article la version étendue de la méthode de Newton pour la recherche des racines afin d'obtenir les trajectoires des zéros IF du signal. Il est montré que la technique de poursuite de zéros basée sur la TFD proposée donne de bonnes performances en poursuite, à la fois pour des signaux mono- et multi-composantes. © 1999 Elsevier Science B.V. All rights reserved.

Keywords: Time–frequency distributions; Instantaneous frequency estimation; Adaptive zero tracking

* Corresponding author. Tel.: (610) 519-7305; fax: (610) 519-4436; e-mail: moeness@ece.vill.edu

1. Introduction

Time-frequency distributions (TFDs) have recently been shown to be a powerful alternative for instantaneous frequency estimation in rapidly time-varying environments [5]. These distributions do not assume a model which is signal specific, as in the case of extended Kalman filters [2], nor are they encumbered by high computational requirements, as in the case of hidden Markov models [12]. Further, TFDs can handle multicomponent signals, and as such outperform existing techniques which are only applicable to a single tone scenario [8]. Finally, TFDs are able to handle signals with rapidly changing IF for which adaptive filter techniques, such as RLS and LMS, fail [3,6].

Because of the localization properties of time-frequency distributions, the location of the spectral peak at time n represents the signal instantaneous frequency. Cohen's class of TFDs are obtained by taking the Fourier transform of the local autocorrelation function (LAF), which captures both the local spectral and temporal characteristics of the signal. The LAF is computed by time-averaging the bilinear data products. The averaging is performed by applying a kernel which acts to satisfy several desirable time-frequency properties [5]. In order to provide a high temporal resolution TFD, the fast Fourier transform (FFT) should be applied at every data sample. At each time instant, it is important to choose a long FFT block length to properly locate spectral peaks, and subsequently provide a good estimate of the signal IFs. This may require extending the data record to include more samples, or by zero padding.

In this paper, the cost of constructing the TFD by applying a high resolution FFT on a data sample by a data sample basis along with a peak picking search routine can be avoided by directly extracting the IF information from the LAF without Fourier transformation. By forming a spectral polynomial for which some roots are located on the unit circle at the TFD peak positions, Newton's method for root finding [4,7,10] can be used as a zero-tracking algorithm to provide the polynomial zero trajectories and subsequently the signal instantaneous frequencies. This technique both simplifies and improves instantaneous frequency estimation, which are the same two motivations

behind zero-tracking adaptive filters techniques introduced by Orfanidis and Vail [9]. Further, the recent application of TFD in interference removal in direct sequence spread spectrum (DS/SS) communication [1] relies on excision filter zeros, which are placed at the jammer IFs.

With Newton's method, tracking of each zero operates independently with computational complexity $O(M)$. Independent tracking of the polynomial roots can also be achieved using other root finding methods such as Bisection, Ridders' and Laguerre's methods [10]. In this paper, however, we focus on Newton's method because of its moderate computational complexity, fast quadratic convergence, and the simplicity of generating the spectral polynomial derivatives.

2. TFD spectral polynomials

Let $R_n(l)$ represent the local autocorrelation function (LAF) at time n and lag l . Cohen's class of time-frequency distributions in the discrete form is given by

$$\rho_n(e^{j\omega}) = \sum_{l=-L/2}^{L/2} R_n(l) e^{-j2\omega l}, \quad (1)$$

where L is the maximum lag of interest, and $R_n(l)$ is given by

$$R_n(l) = \sum_{m=-L/2}^{L/2} \psi(n-m, l) x(m+l) x^*(m-l), \quad (2)$$

where $\psi(n, l) = \psi^*(n, -l)$ is the time-frequency (t-f) two-dimensional kernel of finite extent over the time-time-lag domain. For Wigner distribution, $\psi(n, l) = \delta(n)$, whereas for Choi-Williams distribution, $\psi(n, l) = (1/\sqrt{4\pi l^2/\sigma}) \exp(-n^2/(4l^2/\sigma))$. Both kernels satisfy the instantaneous frequency constraint [5]. $\rho(e^{j\omega})$ is a real-valued function which peaks at several frequencies including the instantaneous frequencies of the multicomponent signal,¹ which are denoted by $\omega_1(n), \omega_2(n), \dots, \omega_M(n)$. Accordingly,

$$\left. \frac{d\rho(e^{j\omega})}{d\omega} \right|_{\omega_i(n), 1 \leq i \leq M} = -j2 \sum_{l=-L/2}^{L/2} l R_n(l) e^{-j2\omega l} \Big|_{\omega_i(n), 1 \leq i \leq M} = 0. \quad (3)$$

¹ The bias in the peak location is dictated by the employed t-f kernel.

Substituting $e^{j2\omega z}$ and multiplying by $z^{L/2}$, Eq. (3) can be rewritten as

$$\sum_{l=-L/2}^{L/2} lR_n(l)z^{-l+(L/2)} = 0, \quad (4)$$

which is the L th-order spectral polynomial

$$f_n(z) = a_n(0) + a_n(1)z + a_n(2)z^2 + \dots + a_n(L)z^L = 0. \\ a_n(l) = (-l + L/2)R_n(-l + L/2). \quad (5)$$

The power series (5) is referred to as the TFD spectral polynomial. The signal instantaneous frequencies correspond to roots of $f_n(z)$ in the exponential form of $\exp(j2\omega_i)$, $1 \leq i \leq M$, and therefore can be directly deduced from the polynomial's zero trajectories. In addition to the signal autoterm zeros, the spectral polynomial (5) has both signal cross-term zeros and extraneous zeros.

It becomes difficult, therefore, to distinguish between the signal autoterm zeros and others. If a signal autoterm zero moves close to an extraneous zero, the zero-tracking algorithm may lock into the "wrong" zero and loses the true trajectory. We place several modifications of the zero-tracking algorithm to circumvent this problem, as discussed in Section 4.

3. Zero-tracking algorithms

A well-known numerical root finding method, Newton's method [7,10], is very suitable for the underlying problem. Given the form of the polynomial (5), the i th root can be found from

$$z_n^{(k)}(i) = z_n^{(k-1)}(i) - \frac{f(z_n^{(k-1)}(i))}{f'(z_n^{(k-1)}(i))}, \quad (6)$$

where k is the iteration number. If the initial guess of the root, $z_n^{(0)}(i)$, is in the neighborhood of the exact root, then the Newton's method is quadratically convergent.

It is assumed that the IF corresponding to the i th root is changing over adjacent time samples such that the root at the n th time sample is in the neighborhood of the new root at time $n+1$. Newton's method can then be applied by using the last root value as the initial guess in Eq. (6). Due to the quadratic convergence, the new root, and sub-

sequently the corresponding IF, will be quickly reached after very few iterations.

Fig. 1 shows the IF estimates and the zero trajectories of Wigner–Ville (WV) distribution spectral polynomial of order $L = 14$, using both the sensitivity formula and Newton's method. The sensitivity formula relates to the first-order approximation, the changes in the polynomial coefficients and roots [9]. The signal is chosen as a chirp with 20 dB SNR. It is clear that Newton's method outperforms the sensitivity method, which yields a substantial bias and deviation from the exact value of IF. In the next section, we propose several modifications of Newton's method to improve its performance in the TFD context.

4. Extended Newton's method for TFD applications

If there is a low signal-to-noise ratio (SNR), fast changing IFs, or multicomponent signals, a situation may arise in which the incorrect zero is tracked. This may occur if we start with an extraneous zero and follow its trajectory, or by starting with the correct zero and lose its trajectory to another one which is extraneous. In order to circumvent, or at least mitigate, this problem, we propose the following four guidance procedures to augment Newton's method. These procedures stem from the fact that the underlying spectral polynomial is derived from the TFD, which, if needed, can be computed at specific time and frequency samples and employed to rectify any potential problems associated with the use of the conventional zero-tracking, as discussed below.

4.1. Zero-tracking correction

This correction is needed to find the exact roots corresponding to the IFs at the initial stage of tracking and whenever tracking of the correct roots is lost due to fast changing IF or spectral resolution problems. In this case, we compute the TFD and apply peak picking routines to find the IFs and thereby identify or redefine the signal zeros. Reduced interference distributions [11] should be used to avoid selecting the signal cross-term zeros.

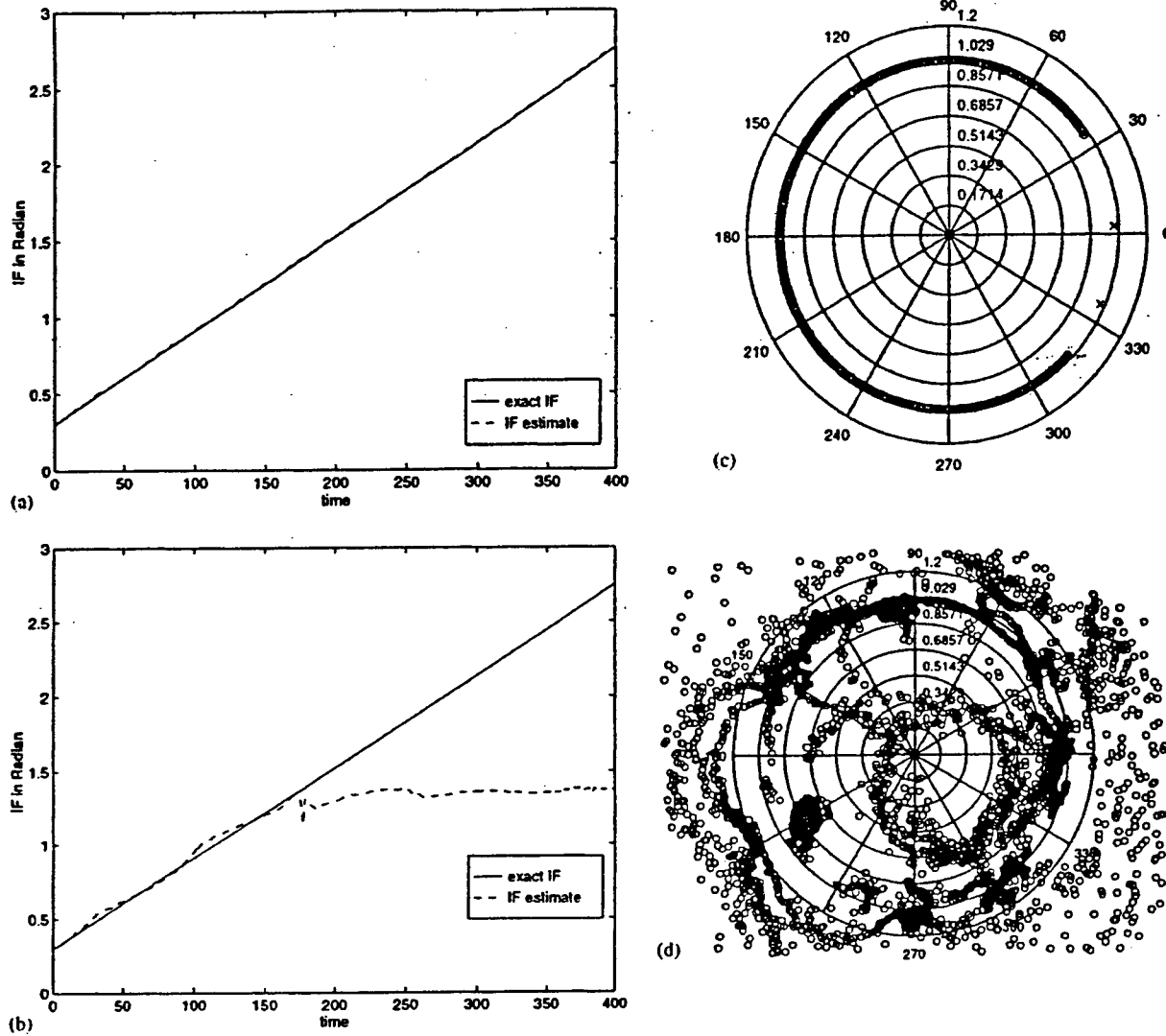


Fig. 1. Zero-tracking of a chirp signal using Wigner-Ville kernel with 14 roots: (a) IF estimate by Newton's method, (b) IF estimate using the sensitivity formula, (c) zero diagram of Newton's method, (d) zero diagram using the sensitivity formula.

4.2. Power monitor

To avoid tracking the wrong trajectory, we frequently monitor the power of the signal at the IF $\omega_i(n)$,

$$P(\omega_i(n)) = \sum_{l=-L_i/2}^{L_i/2} R_l(n) e^{-j2\omega_i(n)l}. \quad (7)$$

When the above power is lower than a threshold, η , it is declared that the algorithm has lost the

correct zero. The zero-tracking correction must then be invoked. This method is most applicable to constant envelope signals where the power is time-invariant. It can be readily shown that the power in the above equation can be evaluated at no additional cost to the overall algorithm. The threshold value may depend on the application. For example, when TFD is used in DS/SS communications, η can be set in direct relation to the bit error rate (BER). In this case, high BER becomes indicative of poor

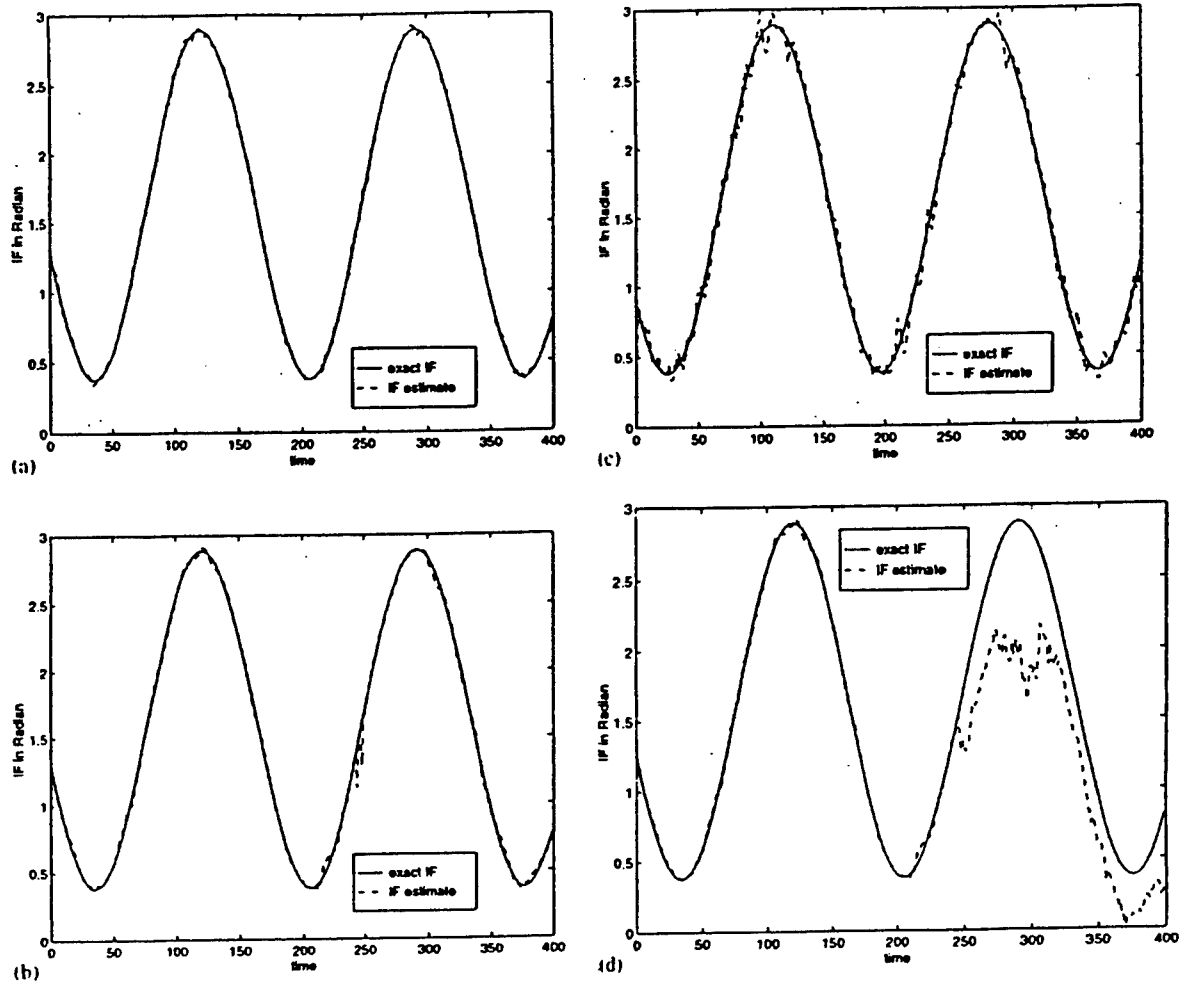


Fig. 2. Sinusoidal IF. SNR = 5 dB, 14 roots: (a) CW distribution, one correction found, (b) WV distribution, three corrections found, (c) spectrogram, four corrections found, (d) WV distribution, no correction is applied during tracking.

tracking and zero-tracking correction should then be invoked.

4.3. Loss of resolution

Due to the finite extent of the LAF, or equivalently, the finite order of the polynomial in Eq. (5), two closely spaced IFs will appear as a single peak in the TFD, and subsequently, will be represented by one zero in the corresponding polynomial. In this case, two zero trajectories will merge into one. In time-varying environment, loss of resolution may, however, last for small periods of time. For example, in the case of two crossing chirps, only the

vicinity of the intersection point represents a resolution problem. Once the two chirps move farther apart, TFD should depict two peaks corresponding to the autoterms, and subsequently, the tracking algorithm should again yield two signal zero trajectories. When two zeros merge to a single root, we record the maximum power at the merged frequency via Eq. (7). When this value significantly drops, the algorithm should go to the correction technique to find the new roots. Again, RID kernels should be used for fast attenuation of cross-terms, which may persist at the intersection frequency upon separation. We maintain that in DS/SS communication applications [1], the BER can be used

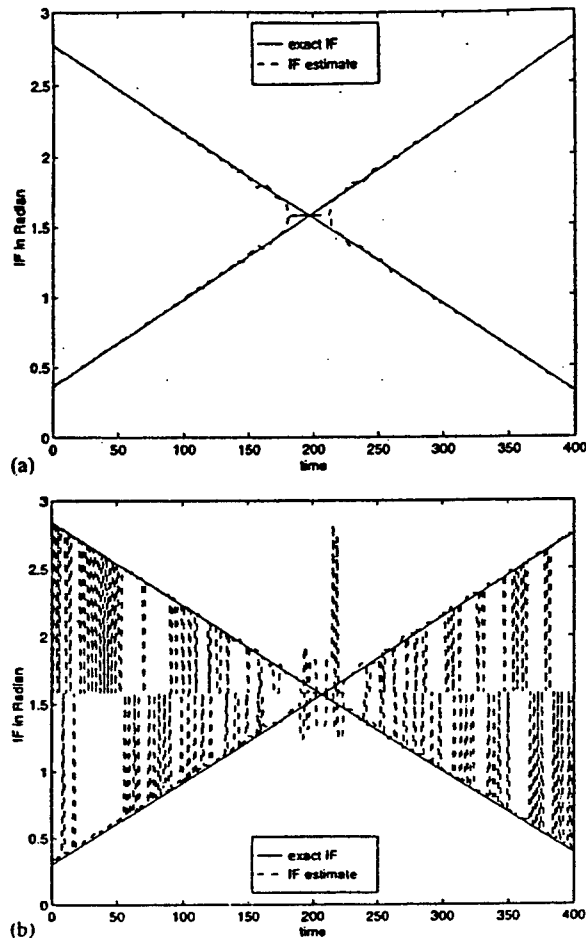


Fig. 3. Two crossing chirps, SNR = 20 dB, 32 lags: (a) WV distribution, two corrections found, (b) 128 points FFT peak picking, WV kernel.

as a measure of loss of resolution and, in general, of how well the tracking algorithm is performing. An increase in the BER should trigger the zero-tracking correction phase of the algorithm to reset the proper conditions.

4.4. Convergence monitor

Newton's method diverges if $|f(z^{(k)})| > |f(z^{(k-1)})|$. In the underlying problem, this means that the root-finding method has lost convergence, and the correction technique must be applied.

5. Simulations

Fig. 2 shows the case of a low SNR single tone fast changing complex sinusoidal FM signal with SNR = 5 dB. In this case, the Choi-Williams distribution kernel [5] based zero-tracking algorithm yields good IF estimates with only one correction, which is needed for initialization, whereas both the WV distribution kernel and spectrogram-based zero tracking algorithms require several zero-corrections to yield reasonable IF estimates (see Fig. 2(b,c)). Fig. 2(d) depicts the case of WV distribution when no corrections are applied. The unextended version of Newton's method has resulted in the loss of the true signal trajectory.

Finally, we considered in Fig. 3 two crossing complex chirps. To achieve better spectral resolution, a high polynomial order is considered. We choose $L = 30$, and as such, WV distributions spectral polynomials have 30 roots. By comparing Fig. 3(a) with Fig. 3(b), the instantaneous frequency estimated using zero-tracking WV distribution is more robust to the effects of cross-terms than that provided by TFD peak-picking. This is mainly because, when no corrections are necessary, zero-tracking does not depend on the relative power of the auto- and cross-terms in the t - f domain.

6. Conclusions

A zero-tracking algorithm based on Newton's method for zero finding has been introduced for instantaneous frequency estimation. This algorithm operates on the local autocorrelation function of the time-frequency distribution and constructs a spectral polynomial whose zeros correspond to the IFs of the multicomponent signal. The primary advantage of Newton's method is that tracking may only be performed for the derived signal root, which simplifies the spectral polynomial zero-tracking operations. However, in rapidly time-varying environment and closely separated frequency components, we stand to lose the signal true zero trajectories to others corresponding to extraneous or cross-term zeros. To mitigate this problem, the paper has presented an extension of Newton's method for TFD applications.

This extension is stemmed from the fact that the TFD provides the signal power distribution over time and frequency and may be frequently used to discriminate between true and extraneous signal components.

Acknowledgements

This work is supported by the US Air Force Research Laboratory, Rome, NY, contract # F30602-96-C-0077.

References

- [1] M. Amin, Interference mitigation in spread spectrum communication system using time-frequency distributions, *IEEE Trans. Signal Process.* 45 (January 1997) 90–102.
- [2] B. Anderson, J. Moore, *Optimal Filtering*, Prentice-Hall, Englewood Cliffs, NJ, 1996.
- [3] B. Boashash, Estimating and interpreting the instantaneous frequency of a signal. Parts 1 and 2, *Proc. IEEE* 80 (12) (April 1992).
- [4] R. Burden, J. Faires, *Numerical Analysis*, PWS Publishing Company, Boston, MA, 1993.
- [5] L. Cohen, *Time-Frequency Analysis*, Prentice-Hall, Englewood Cliffs, NJ, 1995.
- [6] L. Griffiths, Rapid measurement of digital instantaneous frequency, *IEEE Trans. Acoust. Speech Signal Processing*, 1975, pp. 202–221.
- [7] L. Johnson, R. Riess, *Numerical Analysis*, Addison-Wesley, Philipines, 1977.
- [8] S. Kay, Statistically/computationally efficient frequency estimation, in: *Proc. Internat. Conf. Acoust. Speech Signal Process.*, New York, NY, USA, pp. 2292–2295.
- [9] S.J. Orfanidis, L.M. Vail, Zero-tracking adaptive filters, *IEEE Trans. Acoust. Speech Signal Processing* 34 (6), (December 1986) 1566–1571.
- [10] W. Press, S. Teukolsky, W. Vetterling, B. Flannery, *Numerical Recipes*, Cambridge University Press, New York, 1992.
- [11] W. Williams, J. Jeong, Reduced interference time-frequency distributions, in: B. Boashash (Ed.), *Time-frequency Signal Analysis: Methods and Applications*, Longman and Cheshire, 1992.
- [12] L. White, Adaptive tracking of frequency modulated signals using hidden Markov models, in: *Workshop on Hidden Markov Models For Tracking*, Wirrina Cove Resort, February 1992.

Optimum Interference Excision in Spread Spectrum Communications Using Open-Loop Adaptive Filters

Moeness G. Amin, Senior Member, IEEE, Chenshu Wang, and Alan R. Lindsey

Abstract—A generalized approach for interference suppression in PN spread-spectrum communications using open-loop adaptive excision filtering is introduced. The excision filter coefficients under this technique depend on the jammer power and its instantaneous frequency (IF) information, and both values can be gained in the time-frequency domain. The dependency of the excision filter characteristics on the interference power, which was absent in past contributions in this area, is of significant importance as it allows optimum tradeoff between interference removal and the amount of self-noise generated from the induced correlation across the PN chip sequence, due to filtering. This tradeoff is bounded by the two extreme cases of no self-noise, which implies preprocessing disabled, and full interference excision, which the case previously considered. In this paper, we derive the FIR excision filters that maximize the receiver signal-to-noise ratio for narrowband interference and discuss the generalization to nonstationary jamming environment.

Index Terms—Interference excision, spread spectrum communications, time-frequency distributions.

I. INTRODUCTION

ONE OF the most important applications of direct-sequence spread-spectrum (DSSS) communications is that of interference mitigation. A DSSS system is defined as one in which the transmitted signal is spread over a bandwidth much wider than the minimum bandwidth necessary to transmit the information [1] by means of a code independent of the data. The processing gain of a DS/SS system, generally defined as the ratio between the transmission and the data bandwidths, provides the system with a high degree of interference suppression. Since the availability of the code at the receiver enables despreading and recovery of data while spreading and suppressing of interference, any level of interference rejection can be achieved by using sufficient processing gain. This, however, may entail increasing the bandwidth of the transmitted signal beyond the limits of the available frequency spectrum. Therefore, signal processing techniques have been used in conjunction with the DS spread spectrum receiver to augment the processing gain, permitting greater interference protection without an increase in bandwidth [2].

Several past contributions deal with the suppression of narrowband interference [3]–[5]. For nonstationary interference,

adaptive linear prediction methods have been traditionally employed to track and remove the time-varying frequency characteristics of the interference [6], [7]. Recently, two different approaches for nonstationary interference excision in DS/SS communications based on time-frequency (t - f) analysis have been considered for the same task [8]–[11]. One approach is linear and based on multiresolution analysis, whereas the second approach requires a bilinear transformation of the data. In linear transform interference excisions, the data is processed using Gabor transform [10], [12], the short time Fourier transform [13], [14], the wavelet transform [8], or M -band/subband filter banks [9]. Excision of the correlated interference components of the received data is then performed by clipping, or gating, the high coefficient values followed by inverse transformation to recover the desired signal. Correlation with the receiver PN sequence can be either performed in the time or in the transform domain.

The recent advances in instantaneous frequency (IF) estimation have motivated a new open-loop adaptive filtering approach for nonstationary interference excision in SS communications [11]. In this approach, the received data is processed by a short-length time-varying finite impulse response (FIR) filter with a notch (notches) at the jammer IF or IF's. The implementation of IF-based interference excision systems utilizing the localization properties of the time-frequency distributions (TFD's) has been thoroughly discussed in [9], [11], and [15]. Expressions for the general spread spectrum receiver SNR incorporating an IF estimate of the time-varying interference is derived in [16] using three- and five-coefficient open loop adaptive notch filters and extended to multizero FIR filters. In the same reference, the effect of the IF estimation error on performance is also delineated.

The main concept behind the open-loop adaptive filtering approach to interference excision is to place a filter zero synchronous with the jammer. This zero, which is positioned on a unit circle with a phase equal to the jammer IF, causes an infinite deep notch, and thereby, effectively removes the jammer, causing the filter output to be essentially jammer free. However, a filter of such zero characteristics creates a significant amount of self-noise due to the large correlation introduced across the different chips of the PN sequence. In a jammer free-environment, the filter self-noise has the undesired effect of reducing the receiver SNR far below the spreading gain, which is achieved via the spreading/despreading process of the system. In this case, the best solution is to avoid creating any self-noise by shutting off the excision filter. The presence of the jammer gives rise to two conflicting requirements: reduction of the jammer power and

Manuscript received February 19, 1998; revised September 27, 1998. This work was supported by the U.S. Air Force, Rome Laboratory, under Contract F30602-96-C-0077. The associate editor coordinating the review of this paper and approving it for publication was Dr. Xiang-Gen Xia.

M. G. Amin and C. Wang are with the Department of Electrical and Computer Engineering, Villanova University, Villanova, PA 19085 USA (e-mail: moeness@ece.vill.edu; cw@ece.vill.edu).

A. Lindsey is with the Rome Laboratory, Rome, NY 13441 USA (e-mail: lindsey@rl.af.mil).

Publisher Item Identifier S 1053-587X(99)04683-8.

reduction of the self-noise. The fundamental problem with the interference excision system, which is based solely on the IF information [11], is that it does not have either the flexibility or the mechanism to deal with these requirements. It is noted that even under relatively high jammer power, the system performance is still worse than the case when preprocessing is disabled. This situation is intolerable and can be avoided if the filter coefficients are properly chosen.

In this paper, the adaptive open-loop interference excision technique is further developed by making it amenable to a wide range of jammer-to-signal ratio (JSR). The development is based on the fact that several IF estimators also provide estimates of the signal amplitudes. For example, TFD's are distributions of the signal power over time and frequency, and as such, they become unfully utilized if only the IF information is considered in the excision process. Using the interference amplitude, which could be estimated in the t - f plane, the original open-loop adaptive interference excision system introduced in [11] is modified such that the location of the filter notch is set by the jammer IF, whereas its depth is controlled by a new variable, dependent on jammer power. This variable is selected to maximize the receiver SNR, and as such, achieves the optimum tradeoff between the two requirements imposed on the excision system.

It is noteworthy that although the need to have both the instantaneous power and frequency to derive optimum excisions of the interference advocates the use of TFD [17] and clearly distinguishes it from other estimators [18], which either provide the IF or are confined to a single component signal, the analysis provided in this paper can be used in conjunction with any scheme that provides these two values. Following the same practice used in the two sequence papers [11], [16], which have, respectively, introduced IF based interference excision in DS/SS communication using perfect and then perturbed values of IF's, we assume throughout this paper exact knowledge of the jammer amplitude and IF. It is recognized that both of the above parameters, if estimated, will carry an error, depending on the jammer signal characteristics as well as the employed estimator. The effect of inaccuracies in both the amplitude and IF estimates on the receiver performance is an important companion of this work, and it is not within the scope of this paper.

The theoretical development for obtaining the optimum excision performance using the three- and five-coefficient filters for jammers with fixed IF is given in Section II. The expressions for optimum solutions of the filter coefficients are generalized and further applied to the nonstationary case in Section III. Section IV highlights the performance improvement of the new approach through a set of examples and computer simulations. For both fixed and time-varying environment, we assume that the interference is either of constant modulus or of a slowly varying amplitude over one bit period.

II. NARROWBAND INTERFERENCE ANALYSIS

The DSSS signal is given by

$$b_k(t) = \sum_{n=1}^L p_k(n)q(t - n\tau_c)$$

where $p_k(n)$ represents the output sequence from the PN code generator for the k th information bit $b_k(t)$, and L is the PN sequence length. The chip pulse $q(t)$ is of duration τ_c and unit energy. The transmitted signal may be expressed as

$$s(t) = \sum_k I_k b_k(t - kT_b)$$

where I_k represents the binary information sequence, and $T_b = L\tau_c$ is the bit interval (reciprocal of the bit rate). The PN sequence $p_k(n) \forall n, k$ is known to both the transmitter and the receiver and is assumed to be a segment of identically distributed random variables such that $p(n) = 1, -1$ with equal probability. Assuming a transmission of a signal bit "1," we drop the subscript k in the above two equations. With one sample/chip, the desired signal at sample n is equal to the PN sequence, i.e., $s(n) = p(n)$. The channel adds both noise and interference to the DSSS signal. At the receiver, the data at time n takes the form

$$r(n) = s(n) + j(n) + w(n)$$

where $j(n)$ is the jammer waveform whose power is given by σ_j^2 , and $w(n)$ is the additive white noise, which is of zero mean and variance σ^2 . The received signal $r(n)$ is processed by an excision filter, and the result is correlated with $p(n)$ to produce the decision variable for detection.

The receiver SNR is defined as the square value of the mean divided by the variance of the correlator output. The general expression of the receiver SNR using linear time-invariant interference excision filter of coefficients $h_k, k = 1, 2, \dots, N$, is given in [6] and [16] as

$$\text{SNR}_0 = \frac{L^2 h_0^2}{L(1 + \sigma^2) \sum_{k=0}^N h_k^2 - Lh_0^2 + \sigma_{j_0}^2} \quad (1)$$

where $\sigma_{j_0}^2$ is the power of the jammer at the correlator output.

A. Three Coefficient Excision Filter

The simplest form of excision filter that can remove a sinusoid jammer is the three-coefficient causal excision filter

$$\begin{aligned} H(z) &= z^{-1}(z - ae^{-j\omega_0})(1 - az^{-1}e^{j\omega_0}) \\ &= 1 - 2az^{-1} \cos \omega_0 + a^2 z^{-2} \end{aligned} \quad (2)$$

where the parameter a represents the amplitude of the filter zero, which is positioned at the jammer frequency ω_0 . This parameter controls the depth of the filter notch, and its effect on the filter frequency response is depicted in Fig. 1(a). The filter impulse response comes directly from the definition of the Z transform

$$h(n) = \delta(n) - 2a\delta(n-1) \cos \omega_0 + a^2 \delta(n-2). \quad (3)$$

If we denote the filter coefficients by $h_0 = 1, h_1 = 2a \cos \omega_0, h_2 = a^2$, then the corresponding receiver SNR is a special case of (1) and is given by

$$\text{SNR}_0 = \frac{L^2}{L[(1 + \sigma^2)(1 + a^4 + 4a^2 \cos^2 \omega_0) - 1] + \sigma_{j_0}^2} \quad (4)$$

The self-noise introduced by the filter $H(z)$ is given by the first term in the denominator of (4), i.e., those terms dependent

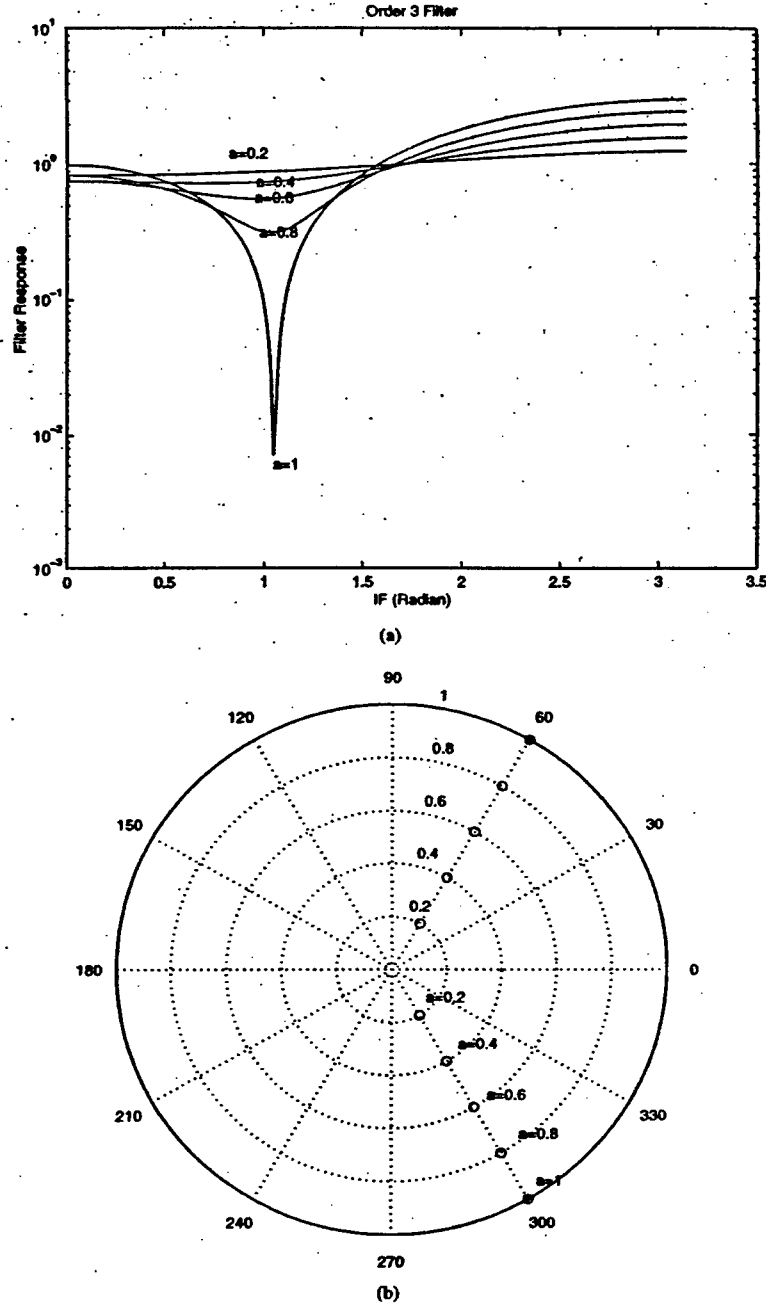


Fig. 1. (a) Frequency responses of the three-coefficient adaptive notch filters with $IF = \pi/3$. (b) Zero diagram of the adaptive notch filter and the exact jammer frequency.

solely on the amplitude of the filter zero

$$\sigma_s^2 = L(a^4 + 4a^2 \cos^2 \omega_0). \quad (5)$$

The white noise sequence also becomes colored at the excision filter output, and its contribution to the receiver SNR_0 in (4) is given by the term

$$\sigma_w^2 = L\sigma^2(1 + a^4 + 4a^2 \cos^2 \omega_0). \quad (6)$$

The quantity $\sigma_T^2 = \sigma_s^2 + \sigma_w^2$ represents the receiver noise in a jammer-free environment; therefore, we may refer to it as the

jammer-free noise or the total self-noise (TSN). Improved SNR_0 can be achieved by reducing either or both components of the TSN. It is clear from (5) and (6) that for a given a , the minimum and maximum values of the total noise occur at $\omega_0 = \pi/2$ and $\omega_0 = 0$, respectively, independent of a . On the other hand, the minimum value of the TSN occurs at $a = 0$ and increases monotonically as a function of a , independent of ω_0 . Fig. 1(b) shows the notch filter zero diagram for different values of a . For high jammer power, $\sigma_j^2 \gg \sigma_T^2$, and

interference removal becomes more important than reducing the TSN to achieve any measurable improvement in the SNR_0 . In this case, a high value of a should be chosen such that a deeper filter notch is introduced. We note that the jammer is entirely removed in the extreme case of $a = 1$, which is the only case discussed in the original design [11]. On the other hand, as the jammer power decreases, the choice of a should tend toward favoring the reduction of the total self-noise over the jammer power and to ultimately shut off the filter for $(\sigma_s^2 + \sigma_w^2) \gg \sigma_j^2$, disabling preprocessing of the received signal prior to despreading. To obtain the jammer power at the correlator output $\sigma_{j_0}^2$, it is prudent to first derive an expression of the jammer waveform $j_0(n)$ that escapes the excision filter when $a \neq 1$. Consider a narrowband sinusoidal jammer of the form $j(n) = A \sin(n\omega_0 + \varphi)$, where A is the jammer amplitude, and φ is its phase. The jammer at the filter output is given by the convolution

$$\begin{aligned} j_0(n) &= A \sin(n\omega_0 + \varphi) * [\delta(n) - 2a\delta(n-1) \cos \omega_0 \\ &\quad + a^2\delta(n-2)] \\ &= A \sin(n\omega_0 + \varphi) - 2aA \sin[(n-1)\omega_0 + \varphi] \cos \omega_0 \\ &\quad + a^2A \sin[(n-2)\omega_0 + \varphi] \\ &= A(1-a) \sin(n\omega_0 + \varphi) + (a^2-a)A \\ &\quad \cdot \sin[(n-2)\omega_0 + \varphi] + aA \sin(n\omega_0 + \varphi) \\ &\quad - 2aA \sin[(n-1)\omega_0 + \varphi] \cos \omega_0 \\ &\quad + aA \sin[(n-2)\omega_0 + \varphi] \\ &= A(1-a) \sin(n\omega_0 + \varphi) + (a^2-a)A \\ &\quad \cdot \sin[(n-2)\omega_0 + \varphi]. \end{aligned} \quad (7)$$

The correlator output due to the jammer is

$$U_j = \sum_{n=1}^L j_0(n)p(n). \quad (8)$$

Accordingly

$$\begin{aligned} \sigma_{j_0}^2 &= E[U_j^2] - E^2[U_j] \\ &= \sum_{n=1}^L j_0^2(n) \\ &= \sum_{n=1}^L A^2(1-a)^2 \{ \sin^2(n\omega_0 + \varphi) \\ &\quad + a^2 \sin^2(n\omega_0 - 2\omega_0 + \varphi) - 2a \sin(n\omega_0 + \varphi) \\ &\quad \cdot \sin(n\omega_0 - 2\omega_0 + \varphi) \} \\ &= A^2(1-a)^2 \frac{L + La^2 - 2La \cos 2\omega_0}{2} \\ &\quad + A^2(1-a)^2 \sum_{n=1}^L \left[a \cos(2n\omega_0 - 2\omega_0 + 2\varphi) \right. \\ &\quad \left. - \frac{\cos 2(n\omega_0 + \varphi)}{2} - \frac{a^2 \cos 2(n\omega_0 - 2\omega_0 + \varphi)}{2} \right]. \end{aligned} \quad (9)$$

For a reasonably high value of L , the summation term in the above equation can be ignored. For example, for a chip sequence of length $L = 128$, and jammer frequency $\omega_0 = \pi/3$ and phase $\varphi = \pi/7$, the summation term for $a = 0.7$ is $0.013A^2$, which is much smaller than the first term $10.589A^2$. An exhaustive study over all ω_0 and φ and a has shown this example to be typical and the claim justified. Therefore

$$\sigma_{j_0}^2 \approx LA^2(1-a)^2 \left[\frac{1}{2} + \frac{a^2}{2} - a \cos 2\omega_0 \right]. \quad (10)$$

Approximation (10) is used from this point forward. Substituting (10) in (4), the receiver SNR becomes as in (11), shown at the bottom of the page. Equation (10) can be rewritten as

$$\sigma_{j_0}^2 = \frac{A^2}{2} [(1-a)^4 + 2a(1-a)^2(1 - \cos 2\omega_0)]. \quad (12)$$

It is evident from the above equation that the jammer output power has a minimum zero value at $a = 1$ and monotonically increases for both increased and reduced values of a . The value of $\sigma_{j_0}^2$ increases faster for $a > 1$ than for $a < 1$, as illustrated in Fig. 2. This is because both factors $(1-a)^4$ and $(1-a)^2$ in (12) are invariant for $a = 1 \pm \Delta$. However, due to the appearance of a as a multiplicative factor in the second term, $\sigma_{j_0}^2$ will be greater for $+\Delta$ than for $-\Delta$. Since the self-noise increases for increased value of a , as stated earlier, we can conclude from the above argument that the minimum value of the dominator in the SNR_0 in (11) should occur for a in the range $[0, 1]$. Below, we prove this argument using the overall combined behaviors of the jammer power and self-noise. The denominator in (11) can be rewritten as a polynomial in a as

$$\begin{aligned} f(a) &= a^4 \left(1 + \sigma^2 + \frac{A^2}{2} \right) + a^3 (-A^2 - A^2 \cos 2\omega_0) \\ &\quad + a^2 (4 \cos^2 \omega_0 + 4\sigma^2 \cos^2 \omega_0 + A^2 + 2A^2 \cos 2\omega_0) \\ &\quad + a (-A^2 - A^2 \cos 2\omega_0) + \left(\sigma^2 + \frac{A^2}{2} \right). \end{aligned} \quad (13)$$

To find the maximum SNR_0 , we simply differentiate $f(a)$ with respect to a

$$\begin{aligned} f'(a) &= a^3 (4 + 4\sigma^2 + 2A^2) + a^2 (-3A^2 - 3A^2 \cos 2\omega_0) \\ &\quad + a [8(1 + \sigma^2) \cos^2 \omega_0 + 2A^2 + 4A^2 \cos 2\omega_0] \\ &\quad - (A^2 + A^2 \cos 2\omega_0) \end{aligned} \quad (14)$$

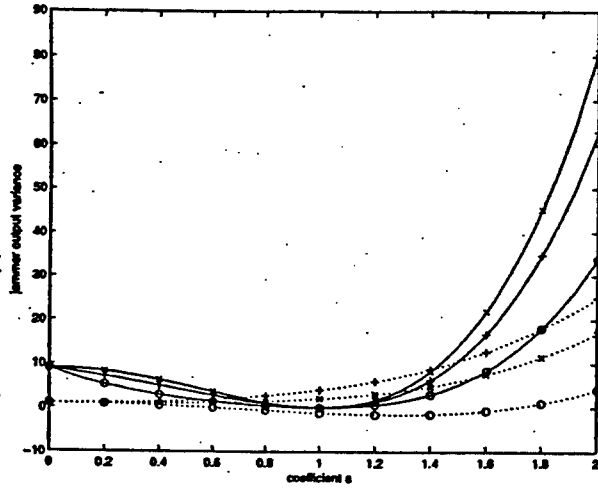
$$f'(a) = ba^3 + ca^2 + da + e \quad (15)$$

and then obtain a , which sets $f'(a) = 0$.

Since $f'(0) < 0 \forall \omega_0$, except at $\omega_0 = \pi/2$, and $f'(1) = 4 + 4\sigma^2 + 8(1 + \sigma^2) \cos^2 \omega_0 > 0$ for all values of ω_0 , then $f'(a)$ must have a real root in the range $[0, 1]$, which represents the

¹Negative values of a change the filter notch position and move it away from a and therefore should be avoided.

$$\text{SNR}_0 = \frac{L}{(1 + \sigma^2)(1 + a^4 + 4a^2 \cos^2 \omega_0) - 1 + A^2(1-a)^2 \left[\frac{1}{2} + \frac{a^2}{2} - a \cos 2\omega_0 \right]} \quad (11)$$

Fig. 2. Jammer output variance changing with a .

optimal a . For the specific value of $\omega_0 = \pi/2$, $f'(0) = 0$, and $f''(0) = -2A^2 < 0$. This means that $f'(0_-) < 0$. With $f'(1) > 0$, $f'(a)$ must then intersect the horizontal axis in the range $[0, 1]$. The same conclusion can be drawn for $\omega_0 = \pi/2$ as for $\omega_0 \neq \pi/2$.

The above argument implies that if (15) has one real root, then this root must be in the range $[0, 1]$ and yields the minimum value of $f(a)$, i.e., the maximum value of SNR_0 . We maintain that in the case that there are three real roots in (15), then one root must be negative since $e < 0$. This leaves two positive roots, and only one of them minimizes $f(a)$ and lies in the range $[0, 1]$. In the Appendix, we present closed-form expressions of the three roots of given by (15).

B. Five-Coefficient Filter

The z transform of the five-coefficient filter with the adaptive coefficient a can be expressed as

$$H(z) = (z - ae^{-j\omega_0})(1 - az^{-1}e^{j\omega_0})(az - e^{-j\omega_0}) \cdot (a - z^{-1}e^{j\omega_0}) \quad (16)$$

$$= a^2(z^2 + z^{-2}) - 2a \cos \omega_0(1 + a^2)(z + z^{-1}) + 1 + a^4 + 4a^2 \cos^2 \omega_0. \quad (17)$$

To normalize the center coefficient to one, $H(z)$ is rescaled as

$$H_1(z) = \frac{a^2}{1 + a^4 + 4a^2 \cos^2 \omega_0} (z^2 + z^{-2}) - \frac{2a \cos \omega_0(1 + a^2)}{1 + a^4 + 4a^2 \cos^2 \omega_0} (z + z^{-1}) + 1. \quad (18)$$

The five filter coefficients are then given by

$$\begin{cases} h_0 = 1 \\ h_1 = h_{-1} = \frac{-2a(1 + a^2) \cos \omega_0}{1 + a^4 + 4a^2 \cos^2 \omega_0} \\ h_2 = h_{-2} = \frac{a^2}{1 + a^4 + 4a^2 \cos^2 \omega_0} \end{cases} \quad (19)$$

The receiver SNR expression of the five-coefficient filter for a fixed frequency interference is derived in [6] and [16] as

$$\text{SNR}_0 = \frac{L^2 h_0^2}{L \left[(2 + \sigma^2) \sum_{k=-2}^2 h_k^2 - 2h_0^2 \right] + \sigma^2} \quad (20)$$

The jammer waveform escaping the five-coefficient filter as a function of A , ω_0 , and a is

$$\begin{aligned} j_0(n) &= A \sin(n\omega_0 + \varphi) * \{h_0 \delta(n) + h_1 [\delta(n-1) + \delta(n+1)] \\ &\quad + h_2 [\delta(n-2) + \delta(n+2)]\} \\ &= A \sin(n\omega_0 + \varphi) (h_0 + 2h_1 \cos \omega_0 + 2h_2 \cos 2\omega_0). \end{aligned} \quad (21)$$

Therefore, the jammer variance is given by the approximation

$$\begin{aligned} \sigma_{j_0}^2 &= \sum_{n=1}^L j_0^2(n) \\ &\approx \frac{LA^2}{2} (h_0 + 2h_1 \cos \omega_0 + 2h_2 \cos 2\omega_0)^2 \end{aligned} \quad (22)$$

where a similar argument to that for (10) holds true here as well. Substituting (22) in the SNR expression (20) gives

$$\text{SNR}_0 = \frac{Lh_0^2}{D(a)} \quad (23)$$

where

$$\begin{aligned} D(a) &= (2 + \sigma^2)(2h_2^2 + 2h_1^2 + h_0^2) - 2h_0^2 \\ &\quad + \frac{A^2}{2} (h_0 + 2h_1 \cos \omega_0 + 2h_2 \cos 2\omega_0)^2. \end{aligned}$$

Since $h_0 = 1$, maximizing SNR_0 requires the minimization of the denominator $D(a)$. The optimum a is then a root of the polynomial $D'(a) = 0$.

$$(2 + \sigma^2)(4h_2 h_2' + 4h_1 h_1') + A^2(2h_2' \cos 2\omega_0 + 2h_1' \cos \omega_0) \cdot (1 + 2h_1 \cos \omega_0 + 2h_2 \cos 2\omega_0) = 0 \quad (24)$$

where h_1' and h_2' are the derivatives of h_1 and h_2 , respectively. It is clear from (19) that the impulse response remains invariant when a is replaced by its reciprocal value $1/a$. Accordingly, $\text{SNR}_0(a) = \text{SNR}_0(1/a)$, which implies that we only need to find the optimum a in the range $[0, 1]$. Define the new variable x such that

$$x = a + \frac{1}{a}. \quad (25)$$

The coefficients h_1 and h_2 in (19) can then be expressed in terms of the new variable x as

$$\begin{cases} h_1 = h_{-1} = \frac{(-2 \cos \omega_0)x}{x^2 + 2 \cos 2\omega_0} \\ h_2 = h_{-2} = \frac{1}{x^2 + 2 \cos 2\omega_0} \end{cases} \quad (26)$$

and (24) becomes

$$D'(x) = c_4 x^4 + c_3 x^3 + c_2 x^2 + c_1 x + c_0 \quad (27)$$

where

$$\begin{aligned} c_4 &= A^2 \cos^2 \omega_0 \\ c_3 &= -(8 \cos^2 \omega_0 + 4\sigma^2 \cos^2 \omega_0 + A^2 \cos 2\omega_0 \\ &\quad + 4A^2 \cos^4 \omega_0) \\ c_2 &= 6A^2 \cos^2 \omega_0 \cos 2\omega_0 \\ c_1 &= 16 \cos^2 \omega_0 \cos 2\omega_0 - 4 + 8\sigma^2 \cos^2 \omega_0 \cos 2\omega_0 \\ &\quad - 2\sigma^2 + 8A^2 \cos^4 \omega_0 \cos 2\omega_0 - 4A^2 \cos^2 2\omega_0 \\ c_0 &= -8A^2 \cos^2 \omega_0 \cos^2 2\omega_0. \end{aligned} \quad (28)$$

The above equation should be first solved to find the real root x in $[2, \infty]$. Numerical methods could be used for this task. This solution is then used via (25) to provide the optimal value of the coefficient a . In the following development, we clearly show that there is a unique optimum value of a in the range $[0, 1]$ that yields the maximum SNR₀. We begin by making two important observations.

- 1) Using trigonometric equalities, it can be easily shown from (27) that $D'(-2) \geq 0$ and $D'(2) \leq 0$, independent of ω_0 , A , and σ^2 . For $A \neq 0$ and $\omega_0 \neq \pi/2$, the leading term of polynomial (27) is positive, i.e., $D'(\pm\infty) > 0$. Therefore, since $D'(2) \leq 0$ and $D(\infty) \geq 0$, then a real root x in $[2, \infty]$ is guaranteed when a jammer is present. For $A \neq 0$ and $\omega_0 = (\pi/2)$,

$$D'(x) = xA^2 \left(x^2 - \frac{4 + 2\sigma^2 + 4A^2}{A^2} \right) \quad (29a)$$

which shows that x still has a positive root that is greater than or equal to 2.

- 2) In a jammer-free environment, $A = 0$, and

$$D'(x) = c_3 x^3 + c_1 x = c_3 x(x^2 + c_1/c_3) \quad (29b)$$

where $|(c_1/c_3)| < 4$. That is, there is no real root in the range $[2, \infty]$. In this case, it is clear from (23) that the lowest possible value of $D(a)$ is reached at $a = 0$. This result is expected as it implies that the maximum receiver SNR is achieved by disabling preprocessing and shutting off the excision filter when the jammer is absent. We note that in both parts of (29), the root $x = 0$ is discarded, as it yields an imaginary value of a .

Let x_1 , x_2 , x_3 , and x_4 represent the roots of (27). From the values of c_0 and c_4 , the product of these roots is negative and given by

$$x_1 x_2 x_3 x_4 \leq -8. \quad (29c)$$

Due to the respective values of $D'(x)$ at $x = -\infty, -2, 2, \infty$, one of the above roots (x_1) is always in the range $[2, \infty]$, whereas another root (x_2) must be in the range $[-\infty, -2]$. Further, the two remaining roots (x_3 and x_4), if real and positive, must both be either in the range $[2, \infty]$ or in the range $[0, 2]$. If both roots are in the range $[2, \infty]$, then x_1, x_3 , and $x_4 \geq 2$, which implies $-1 \leq x_4 \leq 0$ to satisfy (29c). However, these values contradict the fact that according to

(27), the multiplication of the roots pairwise must be equal to or less than 6, i.e.,

$$x_1(x_2 + x_4) + x_3(x_1 + x_4) + x_2(x_3 + x_4) \leq 6. \quad (29d)$$

The only case that the above equality holds is when A and σ^2 are such that $x_1 = x_2 = x_3 = 2$ and $x_4 = -1$ at $\omega_0 = 0$. This is impossible since in this case, the sum of the above roots is 5, which is inconsistent with the value $-c_3/c_0$ at $\omega_0 = 0$, given by (28).

III. NONSTATIONARY INTERFERENCE EXCISION

To develop the optimum receiver based on both the power and IF of the nonstationary interference, we assume that the jammer is stationary over the filter extent. It is then quite straightforward, as shown below, to prove that the optimum receiver performance is achieved by optimizing the parameter a at each data sample.

Contrary to the analysis in Section II, the three-coefficient excision filter impulse response in this case is time dependent and is given by

$$h(n, m) = \delta(m) + h_1(n)\delta(m-1) + h_2(n)\delta(m-2) \quad (30)$$

where

$$\begin{cases} h_1(n) = -2a_n \cos \omega_n \\ h_2(n) = a_n^2. \end{cases} \quad (31)$$

If the interference IF is assumed constant over the filter extent, then $A_n = A_{n+1} = A_{n+2}$, and $\omega_n = \omega_{n-1} = \omega_{n+1}$. Using the three components of the received signal discussed in Section II, the filter output at time n is given by

$$\begin{aligned} y(n) &= p(n) + h_1(n)p(n-1) + h_2(n)p(n-2) \\ &\quad + j_o(n) + w_o(n) \end{aligned} \quad (32)$$

where

$$\begin{aligned} j_o(n) &= j(n) + h_1(n)j(n-1) + h_2(n)j(n-2) \\ w_o(n) &= w(n) + h_1(n)w(n-1) + h_2(n)w(n-2). \end{aligned}$$

The decision variable U at the correlator output is

$$U = \sum_{n=1}^L y(n)p(n). \quad (33)$$

It is easy to show that

$$E[U] = L \quad (34)$$

and

$$\begin{aligned} E[U^2] &= L^2 + \sum_{n=1}^L (h_1^2(n) + h_2^2(n) + \sigma^2 + \sigma^2 h_1^2(n) \\ &\quad + \sigma^2 h_2^2(n) + j_o^2(n)). \end{aligned} \quad (35)$$

Thus, the correlator SNR is

$$\text{SNR}_3 = \frac{E^2[U]}{E[U^2] - E^2[U]} = L^2/D_3 \quad (36)$$

where

$$D_3 = \sum_{n=1}^L h_1^2(n) + h_2^2(n) + \sigma^2 + \sigma^2 h_1^2(n) + \sigma^2 h_2^2(n) + j_o^2(n). \quad (37)$$

Similar to (9)

$$\begin{aligned} \sum_{n=1}^L j_o^2(n) &= \sum_{n=1}^L A_n^2(1-a_n)^2 \\ &\quad \cdot \frac{1+a_n^2-a_n \cos 2\omega_n}{2} + \sum_{n=1}^L A_n^2(1-a_n)^2 \\ &\quad \cdot \left[a_n \cos(2n\omega_n - 2\omega_n + 2\varphi) \right. \\ &\quad \left. - \frac{\cos 2(n\omega_n + \varphi)}{2} \right. \\ &\quad \left. - \frac{a_n^2 \cos 2(n\omega_n + 2\omega_n + \varphi)}{2} \right]. \end{aligned} \quad (38)$$

The subscript n is now attached to a to indicate its dependence on time. The second summation term in (38) can be ignored in most cases, as in (9). Then, (37) can then be rewritten as

$$\begin{aligned} D_3 &= \sum_{n=1}^L (1+\sigma^2)(1+a_n^4+4a_n^2 \cos^2 \omega_n) - 1 \\ &\quad + A_n^2(1-a_n)^2 \left[\frac{1}{2} + \frac{a_n^2}{2} - a_n \cos 2\omega_n \right]. \end{aligned} \quad (39)$$

Since D_3 is a sum of positive terms, its minimum value is obtained by minimizing each term in the summation (39) separately. It is easily recognized that each term in (39) has the same form as the denominator in (11). As such, providing that the approximation of (38) by (39) is valid, the optimum coefficient a_n can be obtained by using (14) at each time sample in a nonstationary jamming scenario. A similar argument can be supplied for the case of the five-coefficient excision.

IV. PERFORMANCE IMPROVEMENT

First, a fixed frequency jammer excised by a three-coefficient filter is considered. The optimal value of a is computed from (A6) and substituted back into the receiver SNR expression to provide the maximum SNR for a given jammer power and frequency. Figs. 3 and 4 compare the correlator SNR's using the original excision filter (full excision), no excision filter, and the optimum excision filter. It is evident that for low jammer-to-signal ratio, shutting off the excision filter leads to a higher receiver SNR than processing the data with the original excision filter, which is insensitive to the jammer power and only depends on the IF information. This situation is reversed for a high JSR where the original

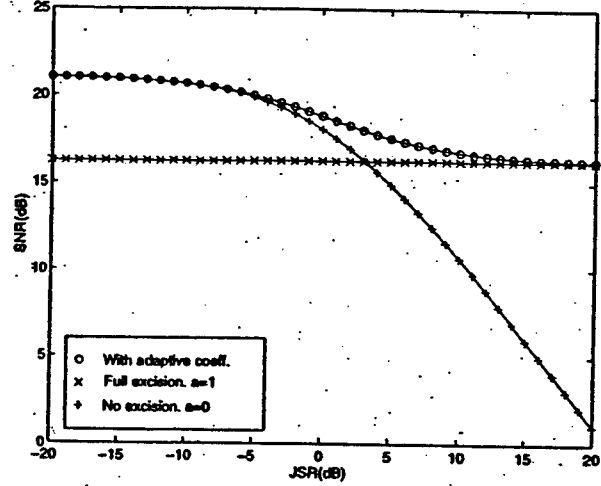


Fig. 3. IF = $\pi/2.1$, 0 dB white noise, PN length = 128. Correlator SNR with three coefficient filters and filter off.

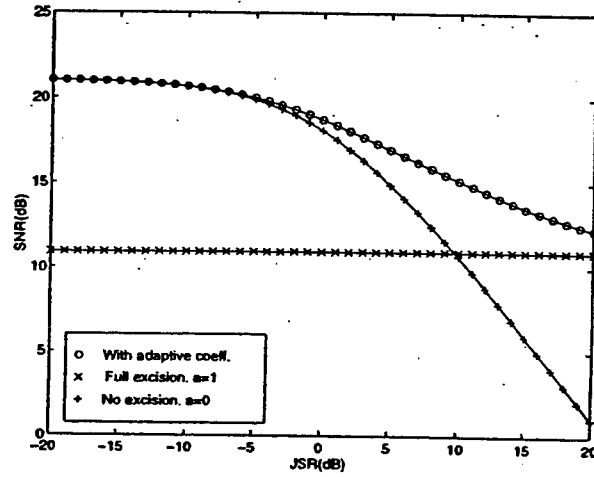


Fig. 4. IF = $\pi/1.1$, 0 dB white noise, PN length = 128. Correlator SNR with three coefficient filters and filter off.

filter, which fully excises the jammer, outperforms the case when preprocessing is disabled. As is evident from Figs. 3 and 4, the performance of the proposed optimum interference excision filter asymptotically reaches the desired performance of both the "IF-based excision" and "no excision" for high and low jammer power, respectively. In between these two extreme cases, the proposed excision filter, which is based on both the amplitude and frequency of the jammer, gives clear improvement over the other two techniques.

In Figs. 5–7, we compare the receiver performance versus the interference IF. The optimum excision filtering curve depicting the change in receiver SNR versus frequency is not only above the other curves, correspondingly to the two alternative aforementioned techniques, but it also becomes much flatter than the receiver SNR curve of the original filter. This means that one attractive by-product of the proposed approach is making the receiver SNR less dependent on the

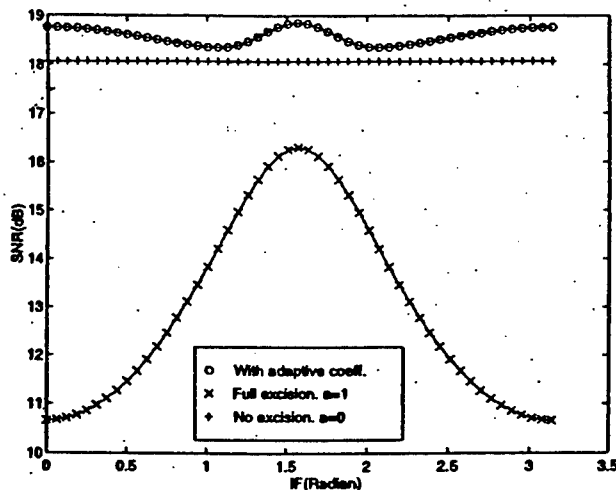


Fig. 5. JSR = 0 dB, 0 dB white noise, PN length = 128. Correlator SNR with three coefficient filters and filter off versus jammer IF.

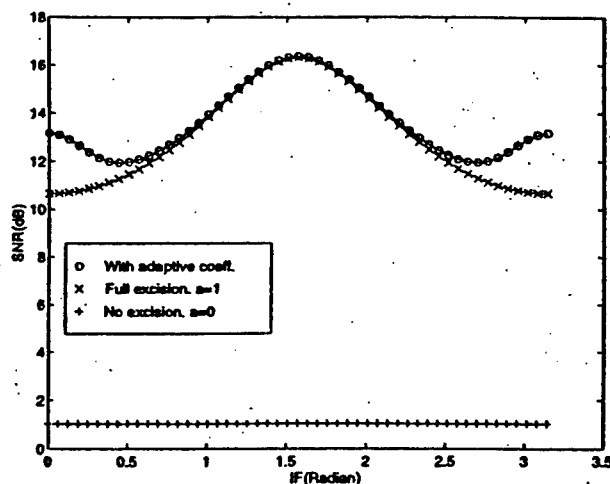


Fig. 7. JSR = 20 dB, 0 dB white noise, PN length = 128. Correlator SNR with three coefficient filters and filter off versus jammer IF.

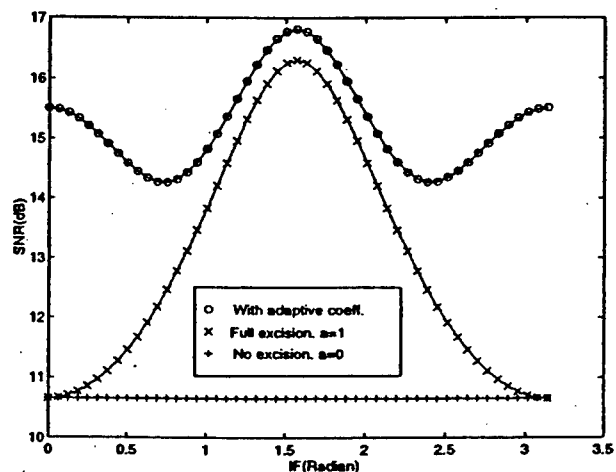


Fig. 6. JSR = 10 dB, 0 dB white noise, PN length = 128. Correlator SNR with three coefficient filters and filter off versus jammer IF.

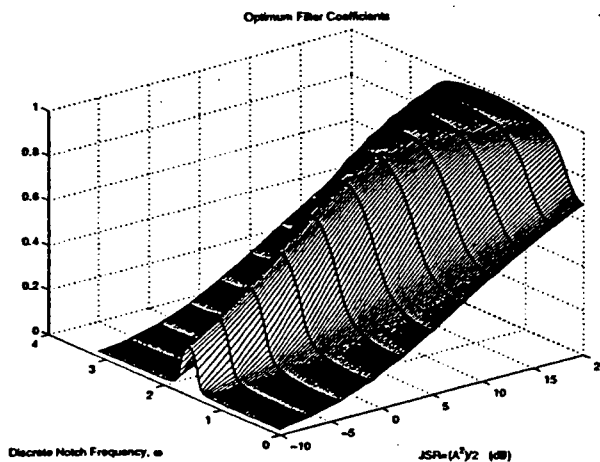


Fig. 8. Optimum filter coefficient a changing versus IF and jammer energy for three coefficient filter. 0 dB white noise, PN length = 128.

jammer IF. The three-dimensional (3-D) plot in Fig. 8 shows the combined effect of the jammer power and frequency on the derived optimum coefficient a . It is clear that a changes from 0 to 1 and becomes less dependent on for higher values of A .

Figs. 9–14 carry the same comparison as Figs. 3–8, but for the five-coefficient adaptive notch filter case. Similar performance can be easily observed. In general, the five-coefficient excision filter gives better overall SNR performance than the three-coefficient filter, as discussed in [11].

Figs. 15 and 16 show the computer simulation results of the bit error curve using three- and five-coefficient filters, respectively. For the three-coefficient filters, a chirp jammer whose frequency changes from 0 to π in every bit duration and a white noise sequence with 0 dB relative to the signal are both added to the PN sequence of length $L = 64$. One million bits are tested at every 2-dB JSR increment from -10 to 10 dB.

Consistent with the result of the receiver SNR analysis, for low jammer-to-signal ratio, applying no filtering leads to lower bit error rate than processing the data with the original excision filter, whereas for a high jammer power, the original filter has lower errors than the case when preprocessing is disabled. The optimum excision filter outperforms both cases above. It gives a BER of 10^{-5} at 10 dB JSR and smaller rates at lower JSR.

For the five coefficient filters, a frequency random hopping jammer is used for the same signal and noise environment as in the previous case. The random hops are uniformly distributed in $[0, \pi]$ with one hop per bit. Because of the good performance of the five-coefficient filter, the PN sequence length is reduced to 32 to yield some reasonable bit errors in one million iterations. The bit error curve of the adaptive coefficient does not significantly outperform the original filter case at high JSR, as illustrated in Fig. 16. This is primarily due

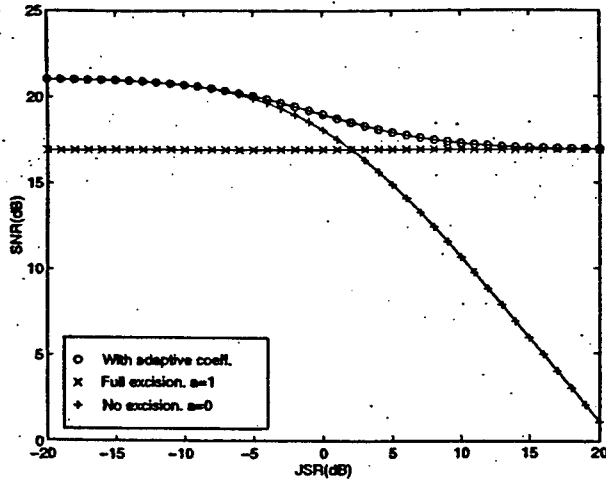


Fig. 9. $IF = \pi/2.1$, 0 dB white noise, PN length = 128. Correlator SNR with five coefficient filters and filter off.

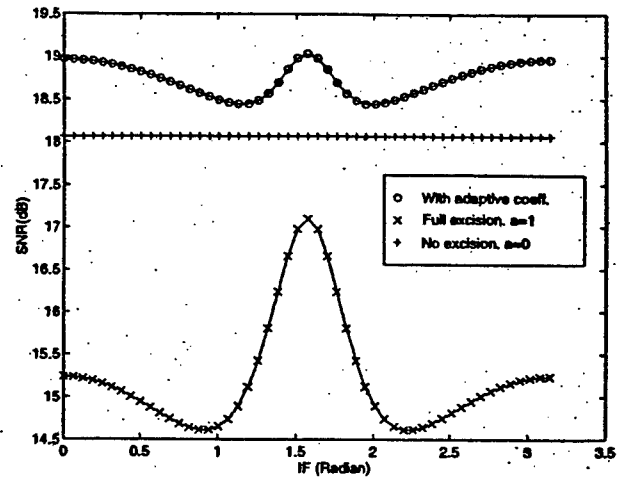


Fig. 11. $JSR = 0$ dB, 0 dB white noise, PN length = 128. Correlator SNR with five coefficient filters and filter off versus jammer IF.

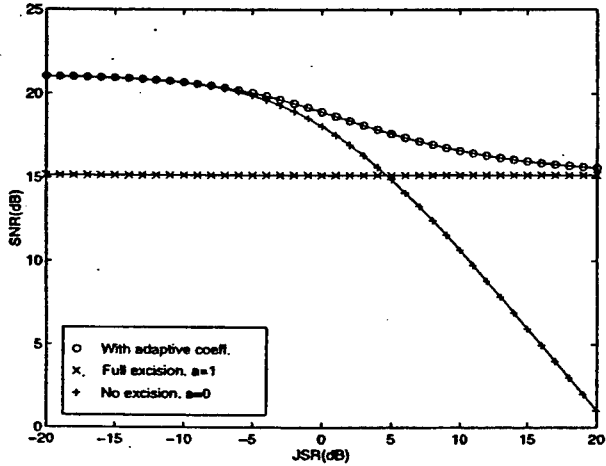


Fig. 10. $IF = \pi/1.1$, 0 dB white noise, PN length = 128. Correlator SNR with five coefficient filters and filter off.

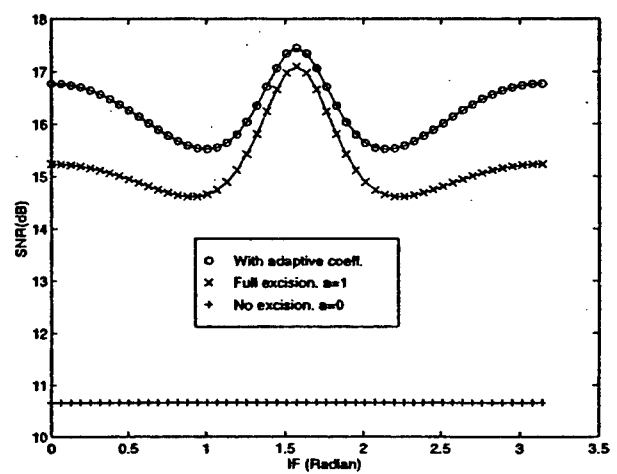


Fig. 12. $JSR = 10$ dB, 0 dB white noise, PN length = 128. Correlator SNR with five coefficient filters and filter off versus jammer IF.

to the slight difference in the receiver SNR using the original and modified excision filters at high JSR for the five-coefficient filter, as shown in Fig. 12.

V. CONCLUSIONS

An optimum open-loop adaptive notch filtering approach for interference excision in PN spread spectrum communications has been developed. The FIR filter with variable depth notch that partially removes the jammer achieves significantly higher receiver SNR over both extreme cases of full jammer excision and no excision. The optimum performance is reached by trading off the jammer power and the filter self-noise. The filter notch is controlled by a new variable whose optimum value is a function of the jammer power, the jammer IF, and the white noise power. For the three-coefficient interference excision filter, the expression for the optimum a can be obtained by

solving for a root of a third-order polynomial under both fixed frequency and randomly changing IF jammer. On the other hand, we should seek numerical solution in the case of the five-coefficient filter, due to the difficulty in getting the solution in a closed form.

Several examples have been presented that show the improvement in the receiver signal-to-noise ratio achieved by using the optimum excision filter over both cases of preprocessing disabled and preprocessing enabled, but only based on the IF information. This improvement is exhibited over a wide range of JSR and is shown using exact values of the interference amplitude and IF. As in the case of IF-based interference excision [11], [16], the noise and the kernel will both affect the estimation of these two parameters when applying TFD's to the underlying problem and will yield a lower performance than when using exact values. The

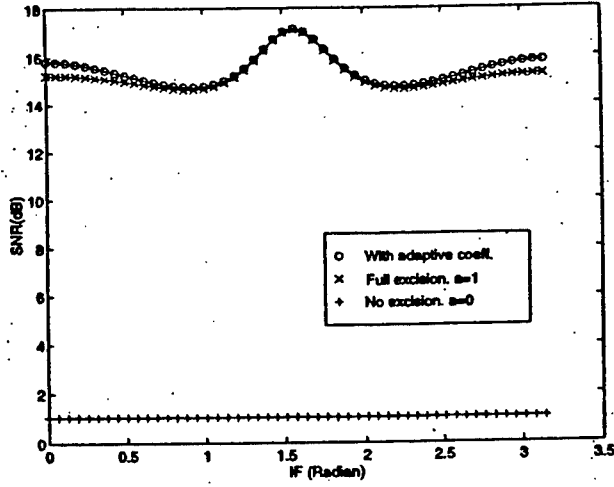


Fig. 13. JSR = 20 dB, 0 dB white noise, PN length = 128. Correlator SNR with five coefficient filters and filter off versus jammer IF.

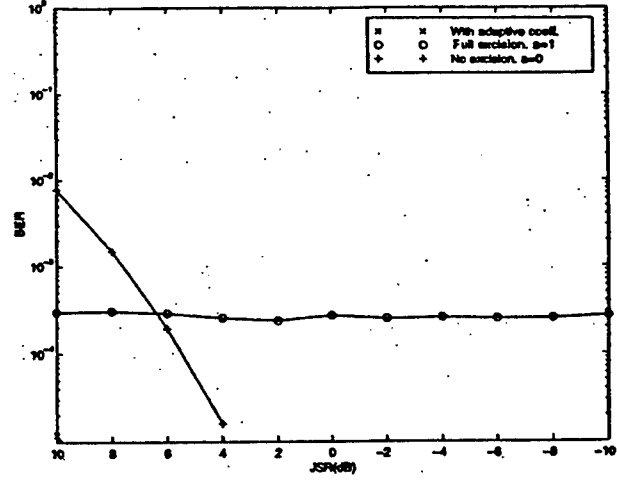


Fig. 15. Bit error rate of the three-coefficient filter with adaptive filter coefficient, fixed coefficient, and filter off. 0 dB white noise, PN length = 64.

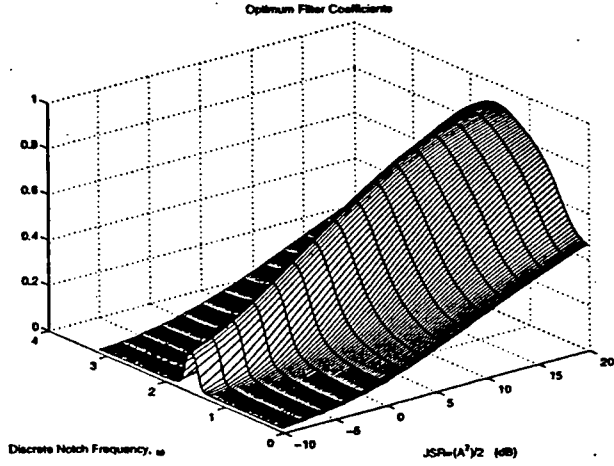


Fig. 14. Optimum filter coefficient a changing versus IF and jammer energy for three coefficient filter. 0 dB white noise, PN length = 128.

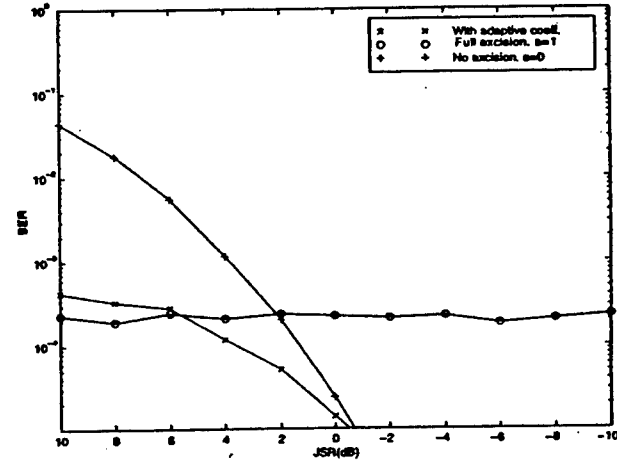


Fig. 16. Bit error rate of the five-coefficient filter with adaptive filter coefficient, fixed coefficient, and filter off. 0 dB white noise, PN length = 32.

Wigner-Hough transform recently proposed for interference excision in the PN spread-spectrum communication problem [19] can be applied for an improved IF estimate in low jammer power scenarios.

APPENDIX

To solve for a , we use the polynomial $f'(a) = 0$ in (15)

$$ba^3 + ca^2 + da + e = 0 \quad (A1)$$

where

$$\begin{cases} b = 4 + 4\sigma^2 + 2A^2 \\ c = -3A^2 - 3A^2 \cos 2\omega_0 \\ d = 8(1 + \sigma^2) \cos^2 \omega_0 + 2A^2 + 4A^2 \cos 2\omega_0 \\ e = \frac{c}{3} = -(A^2 + A^2 \cos 2\omega_0). \end{cases} \quad (A2)$$

Let x define a new variable such that

$$a = x - \frac{c}{3b}. \quad (A3)$$

Substituting (A3) in (A1) yields

$$x^3 + px + q = 0 \quad (A4)$$

where

$$\begin{cases} p = \frac{3bd - c^2}{3b^2} \\ q = \frac{e}{b} - \frac{cd}{3b^2} + \frac{2c^3}{27b^3}. \end{cases} \quad (A5)$$

The closed-form expression of the roots of the simplified polynomial (A4) are given in [20]

$$\left\{ \begin{aligned} x_1 &= \sqrt[3]{-\frac{q}{2} + \sqrt{\left(\frac{q}{2}\right)^2 + \left(\frac{p}{3}\right)^3}} \\ &\quad + \sqrt[3]{-\frac{q}{2} - \sqrt{\left(\frac{q}{2}\right)^2 + \left(\frac{p}{3}\right)^3}} \\ x_2 &= \gamma \left(\sqrt[3]{-\frac{q}{2} + \sqrt{\left(\frac{q}{2}\right)^2 + \left(\frac{p}{3}\right)^3}} \right) \\ &\quad + \gamma^2 \sqrt[3]{-\frac{q}{2} - \sqrt{\left(\frac{q}{2}\right)^2 + \left(\frac{p}{3}\right)^3}} \\ x_3 &= \gamma^2 \sqrt[3]{-\frac{q}{2} + \sqrt{\left(\frac{q}{2}\right)^2 + \left(\frac{p}{3}\right)^3}} \\ &\quad + \gamma \sqrt[3]{-\frac{q}{2} - \sqrt{\left(\frac{q}{2}\right)^2 + \left(\frac{p}{3}\right)^3}} \end{aligned} \right. \quad (\text{A6})$$

where $\gamma = (-1 + i\sqrt{3})/2$, and $\gamma^2 = \gamma^* = (-1 - i\sqrt{3})/2$.

REFERENCES

- [1] M. K. Simon et al., *Spread Spectrum Communications*. New York: Comput. Sci., 1985.
- [2] L. Milstein and R. Iltis, "Signal processing for interference rejection in spread spectrum communications," *IEEE Signal Processing Mag.*, vol. 3, pp. 18-31, Apr. 1986.
- [3] L. B. Milstein, "Interference rejection techniques in spread spectrum communications," *Proc. IEEE*, pp. 657-671, June 1988.
- [4] J. Proakis and M. Salehi, *Communication System Engineering*. Englewood Cliffs, NJ: Prentice-Hall, 1994, Sec. 11.
- [5] L. A. Rusch and H. V. Poor, "Narrowband interference suppression in CDMA spread spectrum communication," *IEEE Trans. Commun.*, vol. 42, pp. 1969-1979, Feb.-Apr. 1994.
- [6] J. Ketchum and J. Proakis, "Adaptive algorithms for estimating and suppressing narrowband interference in PN spread spectrum systems," *IEEE Trans. Commun.*, vol. COMM-30, pp. 913-924, May 1982.
- [7] H. V. Poor and X. Wang, "Adaptive suppression of narrowband digital interference from spread spectrum signals," in *Proc. IEEE Conf. Acoust., Speech, Signal Process.*, Atlanta, GA, May 1996.
- [8] M. Medley, G. Saubier, and P. Das, "Applications of the wavelet transform in spread spectrum communications systems," in *SPIE, Wavelet Appl.*, Orlando, FL, Apr. 1994, vol. 2242.
- [9] M. Tazebay and A. Akansu, "Adaptive subband transforms in time-frequency excisers for DSSS communication systems," *IEEE Trans. Signal Processing*, vol. 43, pp. 2776-2782, Nov. 1995.
- [10] S. Roberts and M. Amin, "Linear vs. bilinear time-frequency methods for interference mitigation in direct sequence spread spectrum communication systems," in *Proc. Asilomar Conf. Signals, Syst., Comput.*, Pacific Grove, CA, Nov. 1995, pp. 925-929.
- [11] M. Amin, "Interference mitigation in spread spectrum communication system using time-frequency distribution," *IEEE Trans. Signal Processing*, vol. 45, pp. 90-102, Jan. 1997.
- [12] D. Wei, D. Harding, and A. Bovik, "Interference suppression in DS spread spectrum communication using the discrete Gabor transform," submitted for publication.
- [13] B. Krongold, K. Ramchandran, D. Jones, and M. Kramer, "Spread spectrum interference suppression using adaptive time-frequency tiling," in *Proc. IEEE ICASSP*, Munich, Germany, Apr. 1997.
- [14] M. Amin, X. Ouyang, and A. Lindsey, "Recursive FT for interference suppression in PN spread spectrum communications," in *Proc. Asilomar Conf. Signals, Syst., Comput.*, Pacific Grove, CA, Nov. 1997.
- [15] M. G. Amin, A. Lindsey, and C. Wang, "On the application of time-frequency distributions in the excision of pulse jamming in spread spectrum communication systems," in *Proc. IEEE Workshop SSAP*, June 1996.
- [16] C. Wang and M. G. Amin, "Performance analysis of instantaneous frequency-based interference excision techniques in spread spectrum communications," *IEEE Trans. Signal Processing*, vol. 46, pp. 70-82, Jan. 1998.
- [17] L. Cohen, *Time-Frequency Analysis*. Englewood Cliffs, NJ: Prentice-Hall, 1995.
- [18] B. Boashash, "Estimating and interpreting the instantaneous frequency of a signal," *Proc. IEEE*, vol. 80, Dec. 1990.
- [19] L. Rade and B. Westergren, *Beta Mathematics Handbook*. Lund, Sweden: Studentlitteratur, Akergrandan, 1989.
- [20] S. Barbarossa and A. Scaglione, "Adaptive suppression of wideband interference in spread spectrum communications using the Wigner-Hough transform," in *Proc. IEEE Conf. Acoust., Speech, Signal Process.*, Munich, Germany, Apr. 1977.



Moeness G. Amin (SM'91) received the B.Sc. degree from Cairo University, Cairo, Egypt, in 1976, the M.Sc. degree from King Fahd University of Petroleum and Mines, Dhahran, Saudi Arabia, in 1980, and the Ph.D. degree in 1984 from the University of Colorado, Boulder, all in electrical engineering.

He has been on the Faculty of the Department of Electrical and Computer Engineering, Villanova University, Villanova, PA, since 1985, where is now a Professor. His current research interests are in the

areas of time-frequency analysis, spread spectrum communications, smart antennas, and blind signal processing.

Dr. Amin was an Associate Editor of the IEEE TRANSACTIONS ON SIGNAL PROCESSING and a member of the Technical Committee of the IEEE Signal Processing Society on Statistical Signal and Array Processing from 1995 to 1997. He is currently a member of the IEEE Signal Processing Society Technical Committee on Signal Processing for Communications. He was the General Chair of the 1994 IEEE International Symposium on Time-Frequency and Time-Scale Analysis. He is the General Chair of the 2000 IEEE Workshop on Statistical Signal and Array Processing. He received the 1997 IEEE Philadelphia Section Award for "Outstanding intellectual and organizational contributions to the IEEE Philadelphia section in the area of signal processing." He is also the recipient of the 1997 Villanova University Outstanding Faculty Research Award.



Chenshu Wang was born in Tianjin, China, in 1969. He received the B.E. degree in electrical engineering from Tsinghua University, Beijing, China, in 1993 and the M.S. degree in electrical engineering in 1997 from Villanova University, Villanova, PA.

From 1993 to 1995, he was working for Full Link Enterprise Inc., Beijing. He is currently employed by GlobeSpan Technologies Inc. His research interests include spread spectrum communications, time-frequency distributions, and xDSL technologies.

Alan R. Lindsey was born in Ohio in 1966. He received the B.S.E.E., M.S.E.E., and Ph.D. degrees in 1989, 1991, and 1995, respectively, from Ohio University, Athens.

Since 1995, he has served the United States Air Force as a Civilian Research Scientist for the Information Grid Directorate of the Air Force Research Laboratory, Rome, NY. He is currently responsible for basic research into the problems of interference mitigation in spread-spectrum communication signals and computationally feasible trellis coding in high-dimensional signal spaces. His main interests include digital communication theory, coding and information theory, digital signal processing, adaptive signal processing, digital control systems, wavelet and multiresolution theory, and applications of time-frequency signal representations.

Performance Analysis of Instantaneous Frequency-Based Interference Excision Techniques in Spread Spectrum Communications

Chenshu Wang and Moeness G. Amin, *Senior Member, IEEE*

Abstract—Jammers characterized by their instantaneous frequencies can be effectively mitigated in direct sequence spread spectrum communications by using open-loop adaptive excision filters. The primary requirement for these filters is that they must possess a notch in tune with the jammer instantaneous frequency (IF) to annihilate the interference power at every time sample. The interference time-varying frequency can be obtained using existing IF estimators, including quadratic time-frequency distribution methods. Without focusing on any specific estimator, we develop expressions for the receiver performance using a general class of multiple-zero FIR excision filters and show the dependence of the bit error rate (BER) on the filter order and its group delay. The effect of inaccuracies in the jammer instantaneous frequency information on the receiver performance is considered and evaluated as a function of the filter notch bandwidth. The latter is defined by the filter zero multiplicity, which is shown to be an important factor in the analysis of the correlator signal-to-noise ratio (SNR).

I. INTRODUCTION

A GREAT DEAL of research has been carried out for estimating the instantaneous frequency (IF) of signals encountered in physics, communications, radar, sonar, and acoustics. A variety of different approaches have been examined, ranging from closed-loop adaptive filtering [1], extended Kalman filters [2], and hidden Markov models [3] to time-varying spectral analysis such as the quadratic time-frequency distributions (TFD's) of Cohen's class [4], the affine class [5], and the hyperbolic class [5]. Some of the IF estimation methods are only applicable to monocomponent signals [6]–[8], whereas others cannot be used for a rapidly time-varying environment [1]. In addition, IF estimators may be encumbered by high computational requirements [3] and may also require a model that is signal specific [2]. In general, computationally efficient IF estimators should be sought out for real-time data processing applications involving on-line signal enhancement and jammer suppression [9]–[12].

The instantaneous frequency information of a nonstationary interference has recently been used in direct sequence spread spectrum (DSSS) communication to mitigate a large class of

polynomial phase jammers using time-frequency distributions [13], [14]. These jammers are characterized by their instantaneous frequency and can be easily removed by applying a time-varying excision filter to the data at the receiver. The basic requirement of this filter is that it must have a notch in tune with the interference IF in order to annihilate the undesired interference power at every time sample and as such improve the interference immunity of the DSSS receiver. This requirement is satisfied by *integrating* or *copying* the IF estimate of the jammer into the coefficients of the excision filter to form a proper notch. This excision method can be categorized as an open-loop adaptive filtering, where the filter coefficients are adjusted using the interference IF estimated in the time-frequency plane [13], [14]. We maintain that the instantaneous frequency-based interference excision approach is not confined to time-frequency signal representations but can be adopted using other IF estimators, including those cited above. The IF-based approach represents a promising alternative to the two primary schemes commonly used for interference rejection, namely, the linear prediction filtering [15] and the transform domain excision [16]–[19]. The high nonstationary property of the interference along with the difficulty to confine it in one or few transform bins make these schemes less attractive for some classes of jammer signals, especially those of polynomial phase characteristics.

The general formulation of the open-loop adaptive filtering interference excision problem, which was introduced in [13] and detailed in [20], assumes exact knowledge of the jammer instantaneous frequency, which is not always the case. Inaccuracies in the IF information may vary from one estimator to another but generally increase with increased noise power level or decreased jammer to signal (JSR) ratio. A bias in the IF may also be the result of poor frequency resolution generated by processing short data records or using an insufficient number of Fourier transform bins [10]. This bias leads to a displacement of the filter notch away from its proper position at the exact interference IF and will, subsequently, allow some of the jammer power to escape through the filter to the correlator, causing significant change in the probability of errors. In this paper, without focusing on any specific IF estimator, we examine the effects of the IF estimation error on the spread spectrum receiver performance. This error is assumed to be a zero-mean white noise process that is independent of the pseudonoise (PN) sequence and the interference frequency. We derive expressions of the correlator output signal-to-noise

Manuscript received November 6, 1996; revised June 5, 1997. This work was supported by the U.S. Air Force, Rome Laboratory, under Contract F30602-96-C-0077. The associate editor coordinating the review of this paper and approving it for publication was Dr. Jose C. Principe.

C. Wang is with GlobeSpan Technologies, Inc., Red Bank, NJ 07701 USA. M. G. Amin is with Department of Electrical and Computer Engineering, Villanova University, Villanova, PA 19085 USA (e-mail: cw@ece.vill.edu; moeness@ece.vill.edu).

Publisher Item Identifier S 1053-587X(98)00532-7.

ratio (SNR_o) as a function of the IF error variance. The SNR_o is a performance measure that is commonly chosen as an appropriate figure of merit of a DSSS receiver incorporating an interference exciser [15].

We broaden the scope of the IF-based interference excision methods by considering a wider class of excision filters than those presented in [14] and [20], where only three- and five-coefficient filters are employed. The task is to quantify the receiver performance as a function of the excision filter characteristics. Specifically, we consider the effect of both the phase and order of the multiple-zero excision filter on the correlator SNR.

In Section II, we derive the general expression for the correlator SNR under a time-varying preprocessing excision filter. Section III presents the framework of open-loop adaptive interference excisions using multiple-zero FIR excision filters. Analysis of the receiver SNR under even and odd values of the filter zero multiplicity is provided. In Section IV, we focus on the special cases of fixed and randomly changing instantaneous frequencies. Section V deals with the effect of the instantaneous frequency estimation errors on the receiver performance. Computer simulations are presented in Section VI.

II. CORRELATOR SNR FOR TIME-VARYING EXCISION FILTERING

Since the proposed instantaneous frequency-based interference-mitigation technique requires the application of a filter with variable coefficients, it is important to derive the correlator SNR using linear time-varying excision filters.

The DSSS signal is given by

$$b_k(t) = \sum_{n=1}^L p_k(n)q(t - n\tau_c) \quad (1)$$

where $p_k(n)$ represents the output sequence from the PN code generator for the k th information bit $b_k(t)$, and L is the PN sequence length. The chip pulse $q(t)$ is of duration τ_c and unit energy. The transmitted signal may be expressed as

$$s(t) = \sum_k I_k b_k(t - kT_b) \quad (2)$$

where I_k represents the binary information sequence, and $T_b = L\tau_c$ is the bit interval (reciprocal of the bit rate). The PN sequence $p_k(n) \forall n, k$ is known to both the transmitter and the receiver. The channel adds both noise and interference to the DSSS signal. At the receiver, the data sample at time t takes the form

$$r(t) = s(t) + j(t) + w(t) \quad (3)$$

where $j(t)$ is the jammer waveform, and $w(t)$ is the additive white noise, which is of zero mean and variance σ^2 . We assume that the PN sequence is identically distributed random variables such that $p(n) = 1$ or -1 with equal probability.

Consider a time-varying filter of length $K + 1$ with coefficient $h_{0,n}, h_{1,n}, \dots, h_{K,n}$ and induced delay l . The filter

impulse response can be written as

$$h(n, m) = \sum_{f=0}^K h_{f,n} \delta(m - f - l) \quad (4)$$

where $\delta(n)$ is the Kronecker delta function. Assuming a transmission of a single bit "1," we drop the subscript k in (1) and (2) and take $s(n)$ as $p(n)$. Processing $r(n)$ with the excision filter $h(n, m)$ and correlating the result with the PN sequence $p(n)$ yields

$$U_1 = \sum_{n=1}^L \sum_{m=-\infty}^{\infty} h(n, m)p(n-m)p(n) \quad (5)$$

which represents the correlator output due to the signal. Substituting (4) in (5), we obtain

$$U_1 = \sum_{n=1}^L \sum_{f=0}^K h_{f,n} p(n-f-l)p(n). \quad (6)$$

The correlator outputs due to the additive noise U_2 and the jammer U_3 , respectively, take the form

$$U_2 = \sum_{n=1}^L \sum_{f=0}^K h_{f,n} w(n-f-l)p(n) \quad (7)$$

$$U_3 = \sum_{n=1}^L \sum_{f=0}^K h_{f,n} j(n-f-l)p(n). \quad (8)$$

The overall correlator output y represents the decision variable $y = U_1 + U_2 + U_3$. The receiver makes the decision as to whether "1" or "-1" was transmitted depending on the value y . Due to the zero-mean property of $p(n)$ and the independence between $p(n)$, $j(n)$, and $w(n)$, $E[U_2] = E[U_3] = E[U_1 U_2] = E[U_2 U_3] = 0$, where $E[\cdot]$ is the expectation operator. On the other hand, the correlator mean value due to the signal is nonzero and is given by

$$m_y = E[U_1] = \sum_{n=1}^L \sum_{f=0}^K E[h_{f,n}] E[p(n-f-l)p(n)]. \quad (9)$$

In the above equation, we make use of the assumption that the jammer and, subsequently, the filter coefficients, is uncorrelated of the PN values. Due to the whiteness property of the PN sequence, the term $E[p(n-f-l)p(n)]$ is zero unless $f = -l$. As such, the induced delay l only in the range $0 \leq l \leq K$ should be considered. In this case, the mean value of correlator output becomes

$$m_y = \sum_{n=1}^L E[h_{-l,n}]. \quad (10)$$

The correlator SNR is defined as the square value of the output mean divided by the output variance [20]. Therefore, if y is the output, the correlator SNR is given by

$$\begin{aligned} \text{SNR}_o &= \frac{m_y^2}{\sigma_y^2} \\ &= \frac{E^2[U_1]}{E[U_1^2] - E^2[U_1] + E[U_2^2] + E[U_3^2] + 2E[U_1 U_3]}. \end{aligned} \quad (11)$$

The contribution of U_1 to the denominator of the SNR_o expression is referred to as the self-noise term, which reflects the effect of the excision filter on the PN uncorrelation property. The corresponding mean square value can be obtained from (6) as

$$E[U_1^2] = E \left[\sum_{n=1}^L \sum_{k=1}^L \sum_{f=0}^K \sum_{g=0}^K h_{f,n} h_{g,k} \cdot p(n-f-l)p(n)p(k-g-l)p(k) \right]. \quad (12)$$

The terms in (12) take zero value except under one of the following exclusive sets of conditions:

Condition 1:

$$\begin{cases} n-f-l=n \\ k-g-l=k \\ n \neq k \end{cases} \Rightarrow \begin{cases} f=g=-l \\ n \neq k \end{cases}. \quad (13)$$

Condition 2:

$$\begin{cases} n-f-l=k-g-l \\ n=k \end{cases} \Rightarrow \begin{cases} f=g \\ n=k \end{cases}. \quad (14)$$

Condition 3:

$$\begin{cases} n-f-l=k \\ k-g-l=n \\ n \neq k \end{cases} \Rightarrow \begin{cases} n-k=f+l=-g-l \\ n \neq k \end{cases}. \quad (15)$$

Under the first set of conditions, the mean square value in (12) is equal to

$$V_1 = \sum_{n=1}^L \sum_{k=1}^L E[h_{-l,n} h_{-l,k}] - \sum_{n=1}^L E[h_{-l,n}^2]. \quad (16)$$

For the second set of conditions, (12) can be simplified to

$$V_2 = \sum_{n=1}^L \sum_{f=0}^K E[h_{f,n}^2]. \quad (17)$$

Under the third set of conditions, we have $n-k=f+l=-g-l \neq 0$. The nonzero terms under condition 3 allow $E[U_1^2]$ to be rewritten as

$$V_3 = \begin{cases} \sum_{n=1}^L \sum_{f=\max[0, -k-2l]}^{\min[k, -2l]} E[h_{f,n} h_{-f-2l, n-f-l}] & f \neq -l \\ 0 & f = -l \end{cases} \quad (18)$$

where the upper and lower bounds on f are due to the limits $0 \leq f \leq K$ and $0 \leq -f-2l \leq K$. It can be readily shown that for the noise component in the received data, the only nonzero terms in the mean square value at the correlator output U_2 is generated under (2). Therefore

$$E[U_2^2] = \sigma^2 V_2 \quad (19)$$

where V_2 is given by (17). The mean square value of the correlator output due to the jammer is denoted as V_4 and

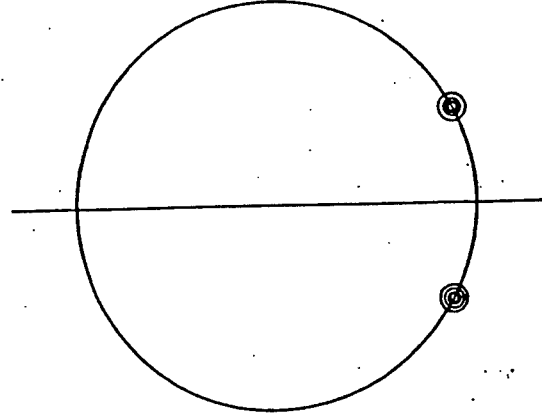


Fig. 1. Zero-diagram of proposed filters.

given by

$$\begin{aligned} V_4 = E[U_3^2] &= E \left[\sum_{n=1}^L \sum_{k=1}^L \sum_{f=0}^K \sum_{g=0}^K h_{f,n} h_{g,k} j(n-f-l) \cdot p(n)j(k-g-l)p(k) \right] \\ &= \sum_{n=1}^L \sum_{f=0}^K \sum_{g=0}^K E[h_{f,n} h_{g,n} j(n-f-l)j(n-g-l)]. \end{aligned} \quad (20)$$

The cross-correlation term in the correlator SNR expression

$$E[U_1 U_3] = E \left[\sum_{n=1}^L \sum_{k=1}^L \sum_{f=0}^K \sum_{g=0}^K h_{f,n} h_{g,k} p(n-f-l) \cdot p(n)j(k-g-l)p(k) \right] = 0 \quad (21)$$

which is due to the fact that $E[p(n)p(k)p(l)] = 0, \forall n, k, l$. From (10)–(21)

$$\text{SNR}_o = \frac{m_y^2}{V_1 + V_2(1 + \sigma^2) + V_3 - m_y^2 + V_4} \quad (22)$$

where m_y , V_1 , V_2 , V_3 , and V_4 are given by (11), (16)–(18), and (20), respectively. If the filter is time invariant, with no induced delay, and assuming that the jammer is of zero mean, then (22) becomes identical to the correlator SNR expression, using a linear predictor exciser, which is given by [15, Eq. (31)].

The improvement in the receiver performance using a filter exciser can be quantified by comparing the correlator SNR with and without applying the preprocessing excision techniques. It can be readily shown that the ratio of these two SNR's is given by

$$\eta = \frac{m_y^2 \left\{ L\sigma^2 + \sum_{n=1}^L E[j^2(n)] \right\}}{[V_1 + V_2(1 + \sigma^2) + V_3 - m_y^2 + V_4]L^2}. \quad (23)$$

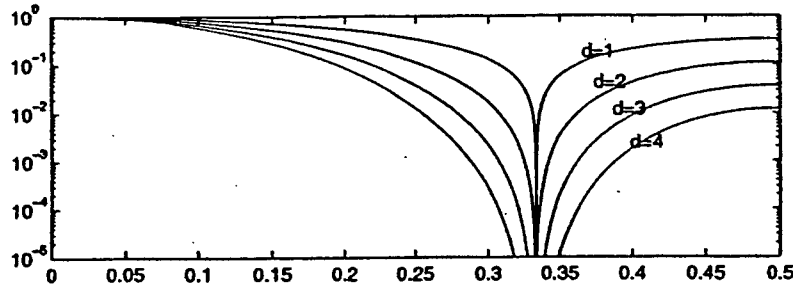


Fig. 2. Multizero filter response of different order IF = 0.33 (normalized frequency).

In general, two constraints often exist on the construction of nonstationary interference open-loop or closed-loop adaptive excision filters. A filter with short impulse response must be used. Long extent filters are likely to span segments of changing frequency content and, as such, allow some of the jammer components to escape to the filter output. This can lead to large bit error rates (BER's) for high jammer-to-signal ratios (JSR's). The filter frequency response should, on the other hand, be close to an ideal notch filter to be able to null the interference with minimum possible distortion of the signal. This property, however, requires filters with infinite or relatively long impulse responses. These conflicting constraints represent, in essence, a tradeoff between temporal and spectral resolutions, which is commonly encountered in time-frequency signal analysis and estimation.

It is shown in [13] and [20] that short multiple-zero excision filters, which are formed based on the IF estimates in the time-frequency plane, effectively improve the overall receiver performance for a large class of nonstationary interference known as polynomial phase signals.

In the following sections, we consider multiple-zero filters with both short and long extents. Excision filters of long impulse responses are used to produce a wide notch, rather than a narrow one. This is achieved by increasing the multiplicity of the filter zero corresponding to the IF (see Fig. 1). With a higher multiplicity, the filter becomes longer in length as well as broader in notch bandwidth (see Fig. 2). Therefore, high notch multiplicity excision filters are most effective in situations where the jammer has an instantaneous bandwidth, i.e., its energy is spread around the instantaneous frequency [21]. In this case, broader instantaneous bandwidth necessitates the use of a wider notch. In addition, wide-notch filters become important in offsetting the effect of inaccuracies in the IF estimates, as discussed in the introduction.

III. GENERAL MULTIZERO EXCISION FILTERS

If $j(t)$ is a polynomial phase jammer that is fully characterized by its instantaneous frequency ω_n , then interference excision can be effectively performed by processing the data $r(t)$ at the receiver by a linear filter with a notch synchronous with ω_n . In dealing with real signals, we focus on nonstationary jammers in the form

$$j(n) = A \sin(\omega_n n + \varphi) \quad (24)$$

where

A sinusoidal amplitude;

ω_n instantaneous frequency;

φ phase.

The z -domain transform function of the corresponding multiple-zero notch filter of order $2d$ is given by

$$H(n, z) = (z - e^{-j\omega_n})^d (1 - z^{-1} e^{j\omega_n})^d z^{-l} \\ = (z^{-1} - 2 \cos \omega_n + z)^d z^{-l} \quad (25)$$

where l now represents the filter group delay. It is well known that the n th-order polynomial can be expanded as

$$(a + b + c + \dots + f)^n \\ = \sum_{p+q+\dots+s=n} \sum_{p!q!\dots s!} \frac{n!}{p!q!\dots s!} a^p b^q \dots f^s \\ 0 \leq p \leq d, 0 \leq q \leq d, \dots, 0 \leq s \leq d; \\ p + q + \dots + s = n. \quad (26)$$

From (25) and (26)

$$H(n, z) = \sum_{q+r+v=d} \frac{d!}{q!r!v!} (-2 \cos \omega_n)^q z^{v-r-l} \\ 0 \leq r \leq d, 0 \leq v \leq d, 0 \leq q \leq d. \quad (27)$$

The corresponding impulse response of $H(n, z)$ is

$$h(n, m) = \sum_{q+r+v=d} \sum_{q!r!v!} (-2 \cos \omega_n)^q \delta(n - r + v - l). \quad (28)$$

If we let $r - v = f$, then the above impulse response can be written in terms of the time-varying filter coefficients as

$$h(n, m) = \sum_{f=-d}^d h_{f,n} \delta(n - f - l) \quad (29)$$

where

$$h_{f,n} = h_{-f,n} = \sum_{r=f}^{[(d+f)/2]} \frac{d! (-2 \cos \omega_n)^{d-2r+f}}{(d-2r+f)! r! (r-f)!} \\ 0 \leq r \leq d, 0 \leq f \leq d \quad (30)$$

and the bounds on r are due to the conditions $0 \leq v = r - f \leq d$ and $0 \leq q = d - 2r + f \leq d$. The operator $[\cdot]$ represents the floor integer.

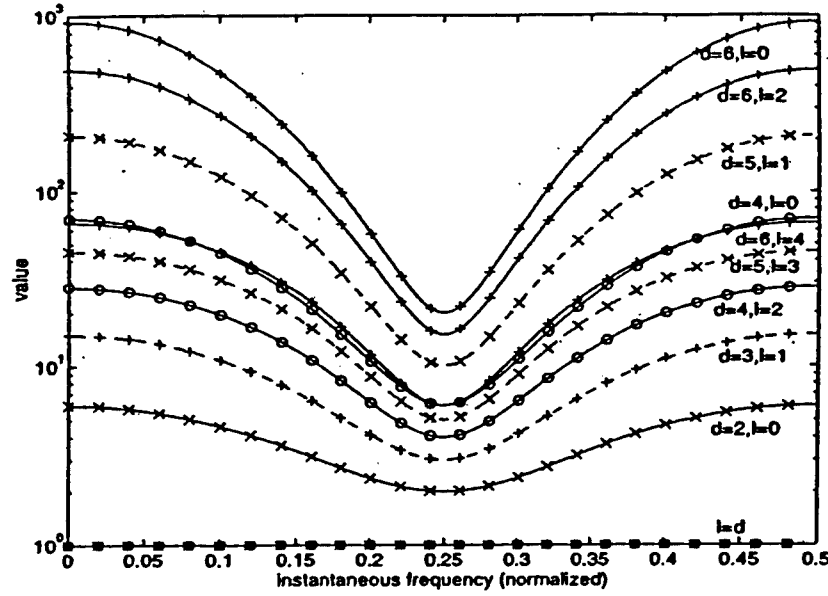


Fig. 3. Filter coefficient $h_{l,n}$ changing with l versus IF ω_n “+,” $d = 6$; “x-,” $d = 5$; “o-,” $d = 4$; “+,” $d = 3$; “x-,” $d = 2$.

We assume that the jammer is stationary over the filter extent. This means $\omega_n = \omega_{n \pm k}$, $1 \leq k \leq d$, and subsequently, $h_{f,n} = h_{f,n \pm m}$ with $0 \leq m \leq d$. For this assumption to hold, rapidly time-varying jammers should be processed by short excision filters. With the filter notch placed at the IF, the jammer is totally removed, and the correlator output is only due to the DSSS signal and additive noise. Because of the symmetry of the filter coefficients, we focus on the range $0 \leq l \leq d$. By changing the sign of l and the range of f in the appropriate terms in the general expression (22), the correlator SNR becomes

$$\text{SNR}_o = \frac{m_y^2}{V_1 + V_2(1 + \sigma^2) + V_3 - m_y^2} \quad (31)$$

where

$$m_y = \sum_{n=1}^L E[h_{l,n}] \quad (32)$$

$$V_1 = \sum_{n=1}^L \sum_{k=1}^L E[h_{l,n} h_{l,k}] - \sum_{n=1}^L E[h_{l,n}^2] \quad (33)$$

$$V_2 = \sum_{n=1}^L \sum_{f=-d}^d E[h_{f,n}^2] \quad (34)$$

$$V_3 = \sum_{n=1}^L \sum_{\substack{f=-d+2l \\ f \neq l}}^d E[h_{f,n} h_{-f+2l,n}] \quad (35)$$

where $h_{f,n}$ is given by (30), and where the bound conditions of f in (35) are due to $-d \leq f \leq d$ and $-d \leq -f + 2l \leq d$.

In order to generate small probability of errors, m_y should be of high magnitude. Since we assume that “1” is transmitted, the output mean value should be positive and, from (32), is maximized if all terms in the summation take positive values, independent of ω_n . From (30), this requirement is satisfied if the group delay l is even for even values of d and odd for

odd values of d . With this condition satisfied, m_y becomes the sum of positive terms. Since the high-order multiplicity filter coefficients result from the convolution of the impulse responses of the lower order multiplicity filters, the values of the filter coefficients decrease as we move away from the center. Therefore, m_y , which is related to only one filter coefficient according to (32), increases in absolute value for decreased values of l . Fig. 3 shows the plots of $h_{l,n}$ over ω_n for different l and d . For the same multiplicity d , the filter coefficient $h_{l,n}$ significantly increases for smaller l .

For a deterministic, rather than a stochastic, type of jammer, we drop the expected value in (32)–(35). In this case

$$V_1 = m_y^2 - \sum_{n=1}^L h_{l,n}^2 \quad (36)$$

In (31), $V_1 - m_y^2$ is insignificant compared with V_2 . We note that V_2 in (34) is constant and independent of l ($0 \leq l \leq d$). Although V_3 is a monotone decreasing function of l , its value is always smaller than V_2 . Fig. 4 compares the values of the inner summations of V_2 and V_3 over ω_n . For the variable V_3 , the maximum value is considered, i.e., $l = 0$ for even d and $l = 1$ for odd d . The summation values in V_2 are almost twice those of V_3 . Therefore, the denominator in (31) is less sensitive to the changes in l than the numerator m_y^2 . Accordingly, the correlator SNR reaches its maximum value when m_y^2 is maximum, which occurs at $l = 0$ for even d and $l = 1$ for odd d . Under these conditions, the correlator SNR can be detailed as shown in (37), shown at the bottom of the next page, where is still given by (30).

IV. SPECIAL CASES OF JAMMING

Two cases of the instantaneous frequency are now considered: a) IF is fixed, independent of time, and b) the normalized IF in radians is a random variable uniformly distributed over $[0, \pi]$. These two cases of fixed and randomly changing

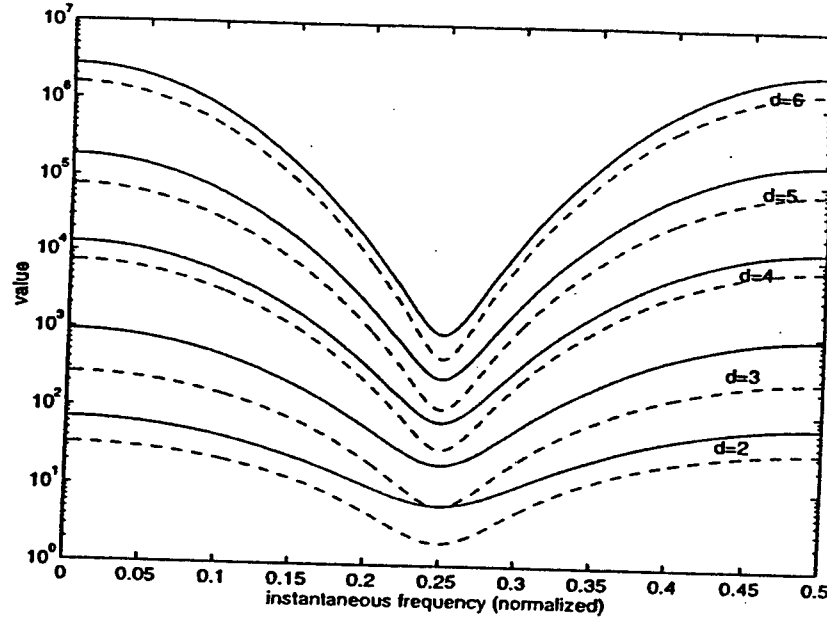


Fig. 4. Inner summation value of V_2 and V_3 versus IF ω_n . Solid line: $\sum_{f=-d}^d h_{f,n}^2$. Dashed line: $\sum_{\substack{f=-d+2 \\ f \neq 1}}^d h_{f,n} h_{-f+2,n}$.

frequencies represent the two extreme cases of time-varying where is the filter coefficients given by environment.

A. Fixed IF

For a fixed frequency jammer, $\omega_n = \omega_0$. The correlator SNR in (37) becomes

$SNR_o \approx$

$$\begin{cases} \frac{h_0^2 L}{(2 + \sigma^2) \sum_{f=-d}^d h_f^2 - 2h_0^2} & d \text{ is even} \\ \frac{h_1^2 L}{(1 + \sigma^2) \sum_{f=-d}^d h_f^2 - h_1^2 + \sum_{\substack{f=-d+2 \\ f \neq 1}}^d h_f h_{-f-2}} & d \text{ is odd} \end{cases} \quad (38)$$

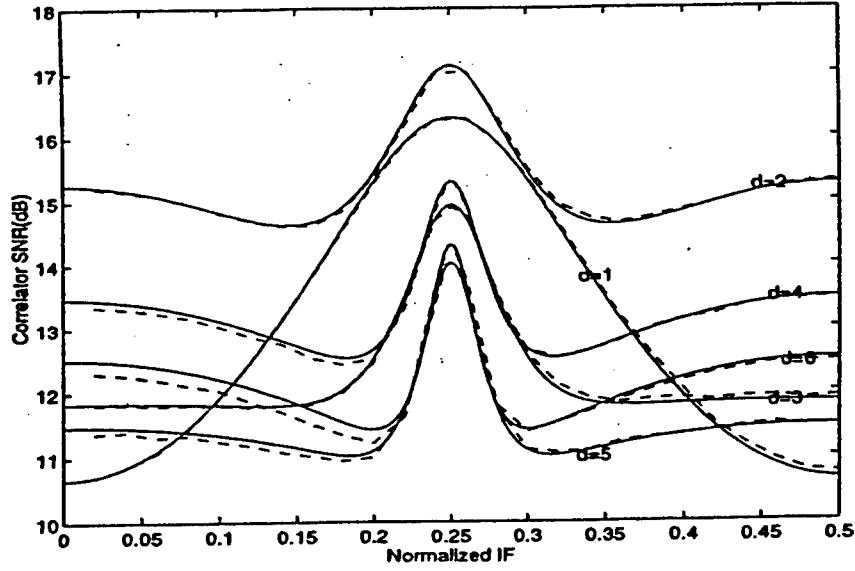
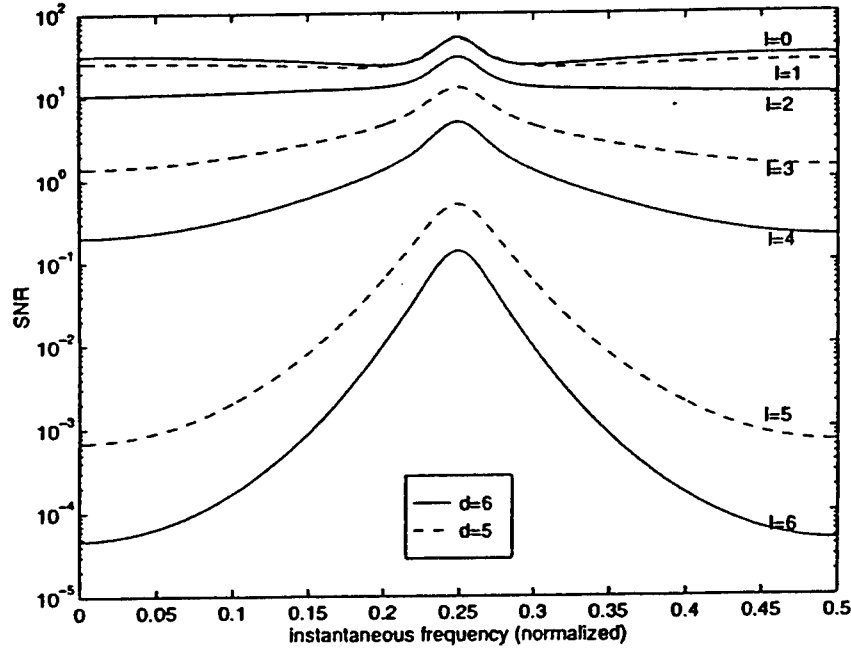
$$h_f = h_{-f} = \sum_{r=f}^{\lfloor (d+f)/2 \rfloor} \frac{d!(-2 \cos \omega_0)^{d-2r+f}}{(d-2r+f)!r!(r-f)!} \quad 0 \leq r \leq d, 0 \leq f \leq d. \quad (39)$$

Fig. 5 depicts the correlator SNR versus the interference fixed frequency ω_0 for a 0-dB signal. The solid line curves correspond to theoretical result using (38), whereas the dashed line curves represent the experimental values using the general expression (11) of the SNR_o . The mean and variance of all terms in (11) were computed over 100 000 runs. There is a clear agreement between the theoretical and the simulated results, which validates the above derivation. In Fig. 5, the delay l was set equal to zero and one for even and odd values of d , respectively, to maximize the SNR, as argued in Section III.

The correlator SNR is not constant and reaches a maximum

$$SNR_o \approx \begin{cases} \frac{\left(\sum_{n=1}^L E[h_{0,n}] \right)^2}{\sum_{n=1}^L \sum_{k=1}^L E[h_{0,n} h_{0,k}] - \left(\sum_{n=1}^L E[h_{0,n}] \right)^2 + (2 + \sigma^2) \sum_{n=1}^L \sum_{f=-d}^d E[h_{f,n}^2] - 2 \sum_{n=1}^L E[h_{0,n}^2]} & \text{even } d \\ \frac{\left(\sum_{n=1}^L E[h_{1,n}] \right)^2}{\sum_{n=1}^L \sum_{k=1}^L E[h_{1,n} h_{1,k}] - \left(\sum_{n=1}^L E[h_{1,n}] \right)^2 + (1 + \sigma^2) \sum_{n=1}^L \sum_{f=-d}^d E[h_{f,n}^2]} & \text{odd } d \end{cases} \quad (37)$$

$$\left\{ - \sum_{n=1}^L E[h_{1,n}^2] + \sum_{n=1}^L \sum_{\substack{f=-d+2 \\ f \neq 1}}^d E[h_{f,n} h_{-f-2,n}] \right\}$$

Fig. 5. Correlator SNR for different zero multiplicity ($L = 128$, $\sigma^2 = 1$).Fig. 6. Correlator SNR for different group delay l .

at $\omega_0 = \pi/2$. This fact is emphasized in Fig. 6, which shows the dependence of SNR_o on l for two different values of d with $L = 128$, $\sigma^2 = 1$.

It is important to note that the correlator SNR expressions for the three- and five-coefficient excision filters in [14], [20], with the coefficients $[1 - 2 \cos \omega_0 \ 1]$ and $[1 - 4 \cos \omega_0 \ 2 + 4 \cos^2 \omega_0 - 4 \cos \omega_0 \ 1]$, respectively, are special cases of (38). By setting $d = 1$ and $d = 2$, the correspondingly correlator SNR is given by (40) and (41), shown at the bottom of the next page.

B. Randomly Changing IF

If ω_n is a random variable uniformly distributed over $[0, \pi]$, then

$$E[(\cos \omega_n)^{2m}] = \frac{1}{\pi} \int_0^\pi (\cos \omega_n)^{2m} d\omega_n = \frac{(2m-1)!!}{(2m)!!} \\ = \frac{(2m-1)(2m-3)(2m-5) \cdots 3 \cdot 1}{(2m)(2m-2)(2m-4) \cdots 4 \cdot 2} \quad (42)$$

$$0 = E[(\cos \omega_n)^{2m+1}]. \quad (43)$$

By substituting (42) and (43) into (37), we have (44)–(46),

TABLE 1
CORRELATOR SNR OF DIFFERENT ZERO
MULTIPLICITY AT DIFFERENT l ($L = 128, \sigma^2 = 1$)

SNR(dB)	$l=0$	$l=1$	$l=2$	$l=3$	$l=4$	$l=5$	$l=6$
$d=2$	15.4790		2.5595				
$d=3$		11.4121		-7.9534			
$d=4$	12.1661		5.2940		-18.8397		
$d=5$		9.7368		-2.0004		-29.9662	
$d=6$	10.0036		5.6118		-10.1248		-41.2516

shown at the bottom of the page. The correlator SNR in terms of u_1 , u_2 , and u_3 takes the form

$$\text{SNR}_o = \frac{u_1 L}{u_2 - 1 + \sigma^2 u_2 + u_3} \quad (47)$$

Again, the special cases of $d = 1$ and $d = 2$ correspond to the three- and five-coefficient excision filters. For these values, the correlator SNR is given by

$$\text{SNR}_o = \frac{L}{3 + 4\sigma^2} \quad d = 1 \quad (48)$$

$$\text{SNR}_o = \frac{16L}{22 + 36\sigma^2} \quad d = 2. \quad (49)$$

The expression in (49) is the same as the one derived in [20].

Table 1 depicts the SNR_o in (47) versus the delay l in the case of random jamming. It is clear that the correlator SNR_o drops significantly for higher values of l .

V. PERTURBATION ANALYSIS

A. Even Multiplicity

When there is an inaccuracy in the IF, the jammer energy at the correlator output is not zero. Let $\Delta\omega(n)$ denote the perturbation error, which is the difference between the exact value and the estimate of the instantaneous frequency, calculated at time n . It is reasonable to assume that $\Delta\omega(n)$ is an uncorrelated stationary zero-mean random process with a variance equal to σ_Δ^2 . This error is independent of both the jammer and the PN sequence. We still consider the class of jammers given by (4). The filter notch is now shifted in position to the frequency $\omega_n + \Delta\omega(n)$. The corresponding filter transfer function is

$$H(\omega) = \{e^{j\omega} - 2 \cos[\omega_n + \Delta\omega(n)] + e^{-j\omega}\}^d. \quad (50)$$

Using the same assumption of stationarity as in Section III, it can be easily shown that the jammer at the correlator output takes the form

$$j_o(n) = 2^d A \sin(\omega_n n + \varphi) \{\cos \omega_n - \cos[\omega_n + \Delta\omega(n)]\}^d. \quad (51)$$

The error in the IF is assumed to be sufficiently small to permit a first-order Taylor series expansion to the cosinusoidal term in (51). This expansion is given by

$$f(x) = f(x_0) + f'(x)|_{x=x_0}(x - x_0) + o(x - x_0). \quad (52)$$

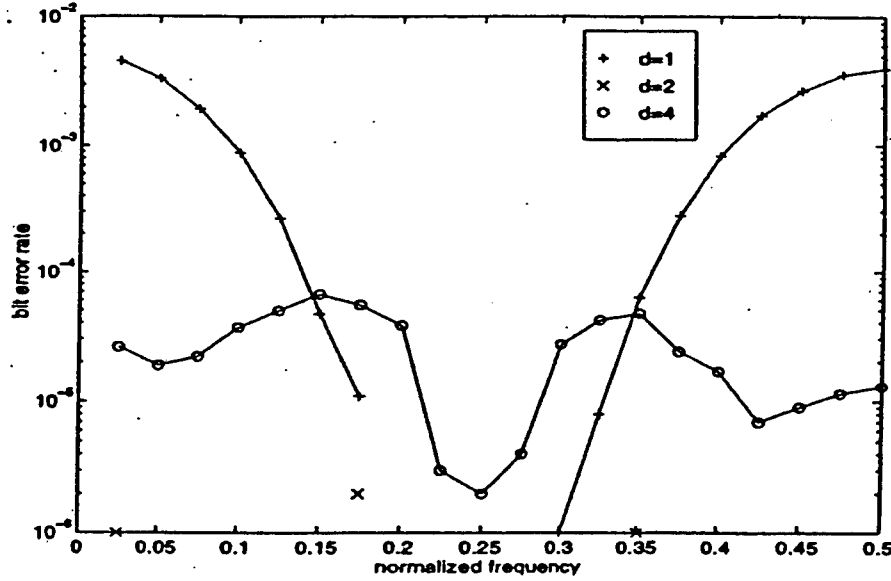
$$\text{SNR}_o = \frac{L}{1 + 4 \cos^2 \omega_0 + 2\sigma^2(1 + 2 \cos^2 \omega_0)} \quad d = 1 \quad (40)$$

$$\text{SNR}_o = \frac{2L(1 + 2 \cos^2 \omega_0)^2}{2 + 32 \cos^2 \omega_0 + \sigma^2 + 16\sigma^2 \cos^2 \omega_0 + 2\sigma^2(1 + 2 \cos^2 \omega_0)^2} \quad d = 2. \quad (41)$$

$$u_1 \approx \begin{cases} E^2[h_{0,n}] = \left\{ \sum_{r=0}^{d/2} \frac{d!(-2)^{d-2r}}{(r!)^2[(d-2r)!]^2} \right\}^2 & (d \text{ is even}) \\ E^2[h_{1,n}] = \left\{ \sum_{r=0}^{[d/2]} \frac{d!(-2)^{d-2r-1}}{(r!)^2[(d-2r-1)!]^2} \right\}^2 & (d \text{ is odd}) \end{cases} \quad (44)$$

$$u_2 = \sum_{f=-d}^d E[h_{f,n}^2] = \sum_{f=-d}^d \sum_{r_1=|f|}^{[(d+|f|)/2]} \sum_{r_2=|f|}^{[(d+|f|)/2]} \frac{d!d!(-2)^{2d-2r_1-2r_2+2|f|} (2d-2r_1-2r_2+2|f|)!}{(2d-2r_1-2r_2+2|f|)!} \quad (45)$$

$$u_3 = \begin{cases} 2 \sum_{f=1}^{d/2} E[h_{2f,n}^2] = 2 \sum_{f=1}^{d/2} \left\{ \sum_{r=0}^{d/2-f} \frac{d!(-2)^{d-2r}}{r!(r+2f)![(d-2r-2f)!]^2} \right\}^2 & d \text{ is even} \\ 2 \sum_{f=1}^{(d-1)/2} E[h_{2f+1,n} h_{1-2f,n}] = \sum_{r_1=2f+1}^{[(d+1)/2+f]} \sum_{r_2=2f-1}^{[(d-1)/2+f]} \frac{(d!)^2(-2)^{2d-2r_1-2r_2+2}}{\{(r_1!)(r_1-2f-1)!(d-2r_1+2f+1)!(r_2!)(r_2+2f+1)!(d-2r_2-2m_2-1)!\}^2} & d \text{ is odd} \end{cases} \quad (46)$$

Fig. 7. BER of different order filters at different IF ($L = 64, \sigma^2 = 1, \text{JSR} = 30 \text{ dB}$).

Accordingly

$$\cos[\omega_n + \Delta\omega(n)] = \cos \omega_n - \Delta\omega(n) \sin \omega_n + o[\Delta\omega(n)] \quad (53)$$

and (51) can be approximated by

$$j_o(n) \approx 2^d A \sin(\omega_n n + \varphi) [\Delta\omega(n) \sin \omega_n]^d. \quad (54)$$

Since the correlator output due to the jammer is

$$U_j = \sum_{n=1}^L j_o(n) p(n) \quad (55)$$

then, the mean and the mean square values of U_j are, respectively, given by

$$E[U_j] = 0 \quad (56)$$

$$\begin{aligned} E[U_j^2] &= E \left[\sum_{n=1}^L \sum_{k=1}^L j_o(n) j_o(k) p(n) p(k) \right] \\ &= \sum_{n=1}^L E[j_o^2(n)] \end{aligned} \quad (57)$$

where we used both the zero-mean property of the PN sequence and the uncorrelation between the PN values and the jammer. Using approximation (53) and the independence of $\Delta\omega(n)$ and ω_n , we obtain

$$\begin{aligned} \sigma_j^2 &= E[U_j^2] = 2^{2d} A^2 E[\Delta^{2d} \omega(n)] \\ &\quad \cdot \sum_{n=1}^L E[\sin^{2d} \omega_n \sin^2(\omega_n n + \varphi)] \\ &= (2\sigma_\Delta)^{2d} A^2 (2d-1)!! \\ &\quad \cdot \sum_{n=1}^L E[\sin^{2d} \omega_n \sin^2(\omega_n n + \varphi)]. \end{aligned} \quad (58)$$

B. Odd Multiplicity

Follow the same procedure of Part A, the jammer variance for odd values of d is

$$\begin{aligned} \sigma_j^2 &= E[U_j^2] = (2\sigma_\Delta)^{2d} A^2 (2d-1)!! \sum_{n=1}^L \\ &\quad \cdot E[\sin^{2d} \omega_n \sin^2(\omega_n(n-1) + \varphi)]. \end{aligned} \quad (59)$$

Equations (58) and (59) give the general results of the jammer variance at the correlator output. When the error in the IF estimate is taken into account, the jammer variance given by (58) and (59) should be added at the denominator of the correlator SNR expression in (37).

For small values of $2\sigma_\Delta$, the term proceeding both summations in (58) and (59) decays with increased d . This is due to the fact that a wider notch eliminates more of the biased jammer energy.

Let us now consider the special cases of fixed and random changing IF's. With the fixed frequency ω_0 , (58) and (59) can be rewritten as

$$\begin{aligned} \sigma_j^2 &= (2\sigma_\Delta)^{2d} A^2 (2d-1)!! \sin^{2d} \omega_0 \\ &\quad \cdot \sum_{n=1}^L \left[\frac{1}{2} - \frac{\cos(2\omega_0 n + 2\varphi)}{2} \right]. \end{aligned} \quad (60)$$

For large values of L , the second term within the brackets in the above equation can be ignored compared with the first term, resulting in

$$\sigma_j^2 = E[U_j^2] \approx 2^{2d-1} \sigma_\Delta^{2d} L A^2 \sin^{2d} \omega_0 (2d-1)!! \quad (61)$$

which reaches a maximum value at $\omega_0 = \pi/2$. Substituting (61) in the correlator SNR (38), the overall correlator SNR with the presence of the jammer energy becomes (62), shown at the bottom of the next page.

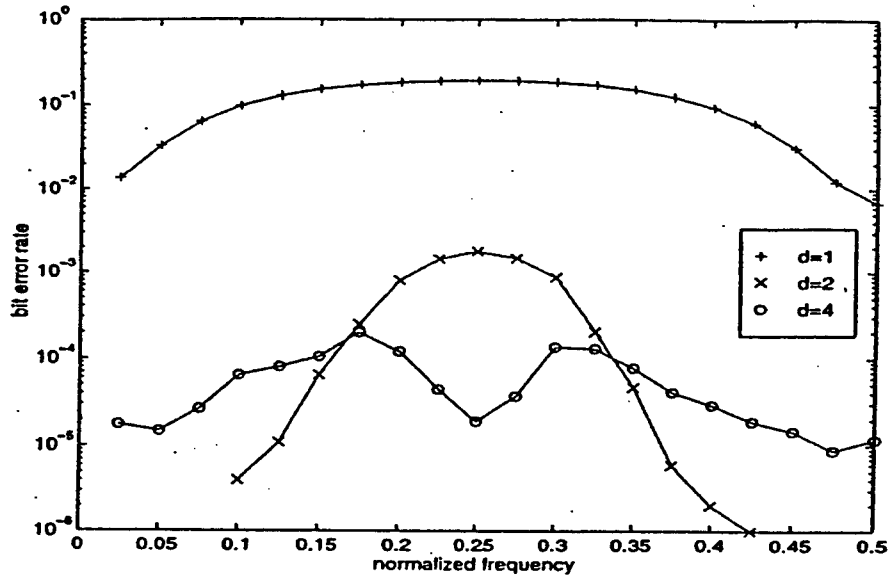


Fig. 8. BER of different order filters versus IF with IF estimate bias ($L = 64$, $\sigma^2 = 1$, JSR = 30 dB, $\sigma_\Delta^2 = 0.02$).

As the special cases of $d = 1$ and $d = 2$, the correlator SNR for the three- and five-coefficient filters is given by (63) and (64), shown at the bottom of the page, where (63) is the same as in [22].

For randomly changing IF, the expected values in (58) and (59) can be easily evaluated. In this case, the SNR becomes

$$\text{SNR}_o = \frac{Lu_1}{u_2 - 1 + \sigma^2 u_2 + u_3 + 2^{2d-1} \sigma_\Delta^2 A^2 \frac{[(2d-1)!!]^2}{2d!!}} \quad (65)$$

where u_1 , u_2 , and u_3 are still given by (44)–(46)

The special cases of $d = 1$ and $d = 2$, yield the three- and five-coefficient filters with

$$\text{SNR}_o = \frac{L}{3 + 4\sigma^2 + A^2 \sigma_\Delta^2} \quad d = 1 \quad (66)$$

$$\text{SNR}_o = \frac{16L}{22 + 36\sigma^2 + 9LA^2 \sigma_\Delta^4} \quad d = 2 \quad (67)$$

where (67) is the same as in [18].

VI. SIMULATIONS

In the first set of simulations, we use the exact instantaneous frequency, assuming no estimation error. The jammer is of 30 dB JSR and is given by (24) with fixed instantaneous frequency. The latter is varied in the range $[\pi/20, \pi]$ with $\pi/20$ increments. Three-, five-, and nine-coefficient multiple-

$$\text{SNR}_o = \begin{cases} \frac{h_0^2 L}{(2 + \sigma^2) \sum_{f=-d}^d h_f^2 - 2h_0^2 + 2^{2d-1} \sigma_\Delta^2 LA^2 \sin^2 \omega_0 (2d-1)!!} & d \text{ is even} \\ \frac{h_1^2 L}{(1 + \sigma^2) \sum_{f=-d}^d h_f^2 - h_1^2 + \sum_{\substack{f=-d+2 \\ f \neq 1}}^d h_f h_{-f-2} + 2^{2d-1} \sigma_\Delta^2 LA^2 \sin^2 \omega_0 (2d-1)!!} & d \text{ is odd} \end{cases} \quad (62)$$

$$\text{SNR}_o = \frac{L}{1 + 4 \cos^2 \omega_0 + 2\sigma^2(1 + 2 \cos^2 \omega_0) + 2A^2 \sigma_\Delta^2 \sin^2 \omega_0} \quad d = 1 \quad (63)$$

$$\text{SNR}_o = \frac{2L(1 + 2 \cos^2 \omega_0)^2}{2 + 32 \cos^2 \omega_0 + \sigma^2 + 16\sigma^2 \cos^2 \omega_0 + 2\sigma^2(1 + 2 \cos^2 \omega_0)^2 + 12A^2 \sigma_\Delta^4 \sin^4 \omega_0} \quad d = 2 \quad (64)$$

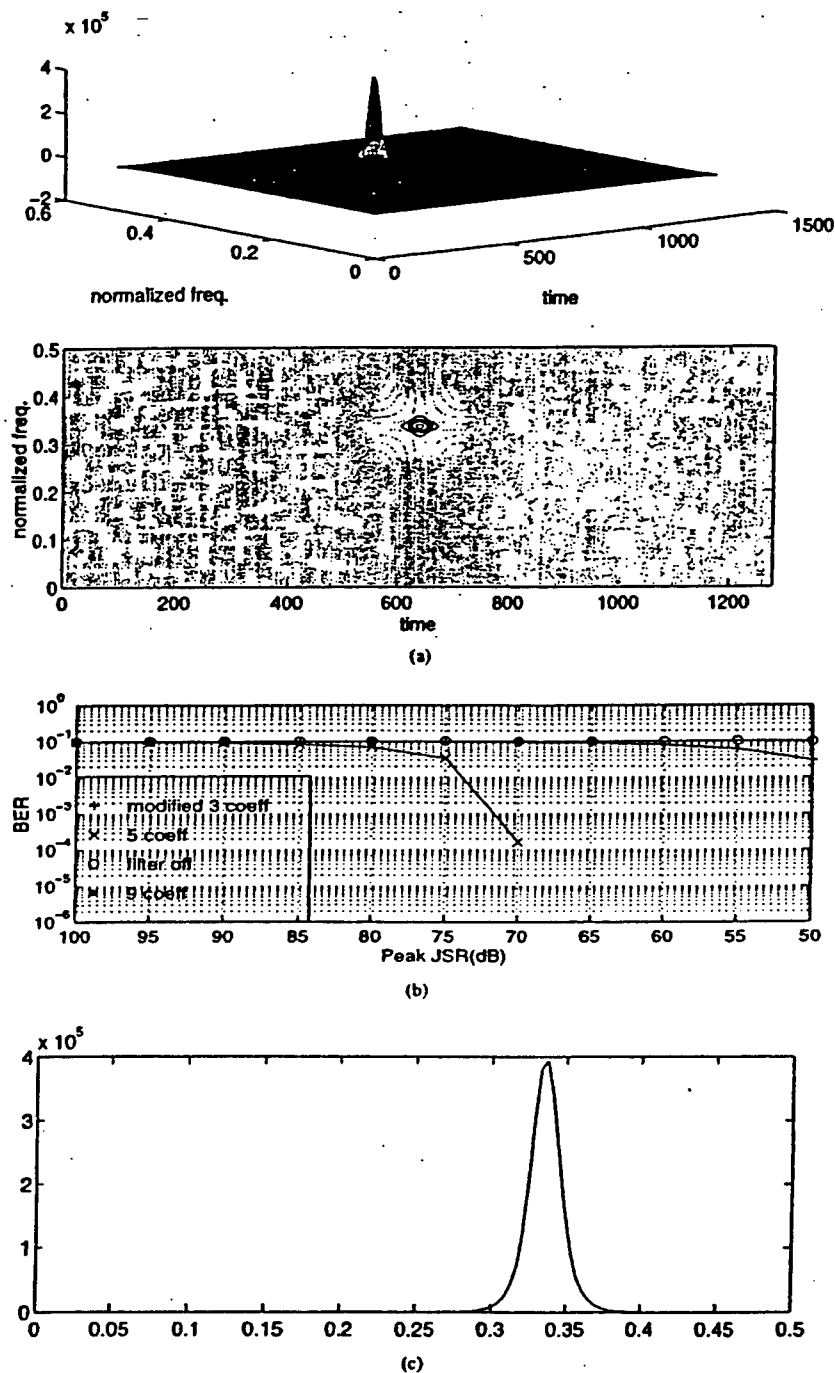


Fig. 9. (a) TFD of the Gaussian amplitude modulated jammer $j(n) = A_j \exp[j(2\pi/3)n - (n - 640)^2/500]$. This jammer is periodical every 10 bits duration, 100% jamming. (b) Bit error rate of different filtering and filter off. The higher the filter order, the better the performance. Curve of nine coefficient filter is already below 10^{-6} , which is not shown on the figure. (c) Jammer instantaneous spectrum at $n = 640$.

zero filters are applied. The additive Gaussian white noise has unit variance and is of 0 dB with respect to the signal. The PN length is $L = 64$. The bit error rate is shown in Fig. 7. The BER curves are consistent with the theoretical correlator SNR_o expressions derived in Section III and shown in Fig. 5. Low SNR_o corresponds to high bit error rate. The

smallest error occurs at $\omega_o = \pi/2$, which is the frequency of the highest SNR_o . The five-coefficient filter has the highest SNR_o , which only shows three points in the BER curve. In all simulation examples, the BER's are provided after running 10^6 bit iterations. Therefore, it is expected that the BER estimates smaller than 10^{-5} appear with relatively high variance.

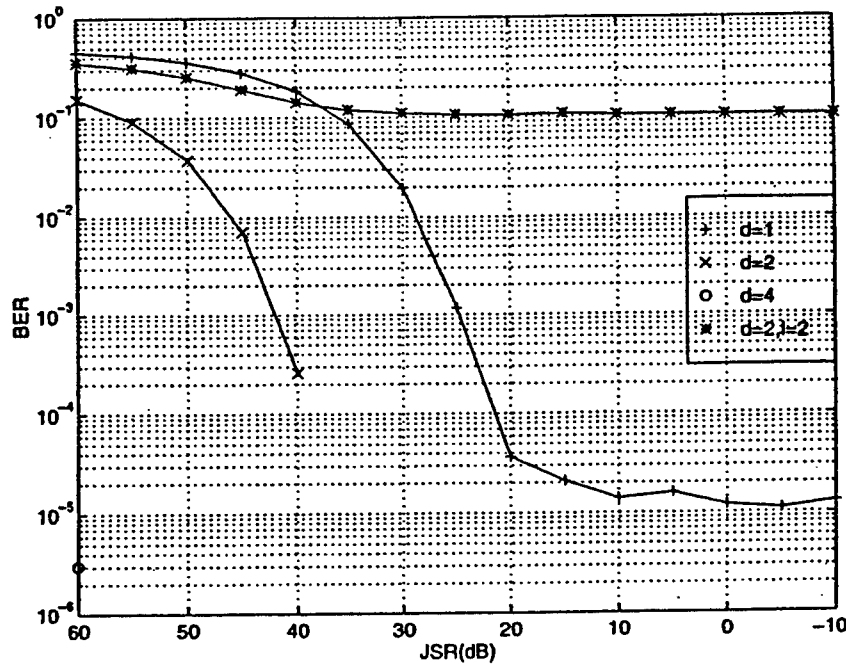


Fig. 10. BER of a chirp jamming with estimation bias using different filters $L = 128$, $\sigma^2 = 1$, $\sigma_{\Delta}^2 = 0.01$, chirp $(0 - \pi)$ in every ten bits.

In the second simulation, we induce a random error in the IF with variance $\sigma_{\Delta}^2 = 0.02$. All other conditions are the same as in the first simulation. The BER is shown in Fig. 8. The BER curves of three- and five-coefficient filter now reach a maximum at $\pi/2$ instead of a minimum, as in the previous example. This is due to the fact that the jammer power at the correlator output is maximum at $\omega_o = \pi/2$. Therefore, as this component becomes dominant in the SNR_o expressions (58) and (61), the poorest receiver performance is bound to occur at $\pi/2$. This is the case in both three- and five-coefficient filters. However, since the jammer variance decreases greatly for increased filter multiplicity d , the effect of IF estimation error on the BER in the nine-coefficient filter case is substantially less than when using smaller-extent excision filters. Fig. 8 demonstrates that the BER for the nine-coefficient filter still shows a minimum at $\pi/2$, even with IF estimation errors.

In the third simulation example, we use the jammer

$$j(n) = A_j \exp \left[j \frac{2\pi}{3} n - \frac{(n - 640)^2}{500} \right]$$

which is Gaussian modulated with fixed frequency at $2\pi/3$ and a wide bandwidth at $n = 640$. Fig. 9(a) shows the jammer time-frequency distribution. In the simulation, we vary the peak jammer power to signal ratio from 40–100 dB at $n = 640$. Using the exact IF, three multiple-zero excision filters are applied with $d = 1, 2, 4$, corresponding to 3, 5, 9 coefficients, respectively. The BER's are shown in Fig. 9(b). In this case, the higher the filter order, the better the performance. For the nine-coefficient excision filter, the error rate is below 10^{-6} , which does not appear in the figure. The reason for this performance is that to effectively remove the underlying jammer whose power spectrum is shown in Fig. 9(c), the

excision filter frequency response should exhibit a wide notch at $2\pi/3$. It is clear from the filter frequency response in Fig. 2 that $d = 4$ should lead to the best performance.

In the fourth set of simulations, we test the filters using a chirp jammer with a random IF estimation error variance $\sigma_{\Delta}^2 = 0.01$. Four filters are applied: $d = 4, l = 0$; $d = 2, l = 0$; $d = 1, l = 1$; and $d = 2, l = 2$. The PN length is $L = 128$. The white noise is 0 dB. The IF changes from 0 to π in every ten bits of duration. The jammer power is varied from -10 to 60 dB with 5-dB increments. We ran 1 000 000 bit iterations for each JSR value. The bit error curve is shown in Fig. 10. The excision filter with $d = 2$ outperforms that with $d = 1$. However, as argued before, the five coefficient filter with $l = 2$ yields poor BER. With the underlying IF estimation error and high jammer power, the nine-coefficient filter provides better results than the excision filter of $d = 2$.

VII. CONCLUSIONS

Analysis of the open-loop adaptive filtering interference excision spread spectrum communication receiver has been provided. We have focused on a class of jammers that are characterized by their instantaneous frequencies. Multiple-zero FIR filters whose notch is in synchronization with the jammer IF have been applied to remove the jammer power at every time sample. These filters are described by three parameters, namely, the zero location, the zero multiplicity, and the group delay. Expressions of the receiver SNR incorporating these three parameters have been derived. It is shown that for improved receiver performance, the filter group delay must depend on the filter zero multiplicity. Specifically, even multiplicity excision filters must be of zero phase.

High-order multiplicity filters have been proposed for two primary reasons. First, these filters have broad notches, which will tolerate reasonable bias in the jammer IF estimate. Second, broad notch filters are more effective in excising the jammer energy when it is widely spread around the instantaneous frequency.

The two specific cases of three- and five-coefficient filters and their corresponding correlator outputs and signal-noise ratios, which have already been devised in the literature, were shown to be special cases of the general approach presented in this paper.

REFERENCES

- [1] S. Haykin, *Adaptive Filter Theory*. Englewood Cliffs, NJ: Prentice-Hall, 1986.
- [2] B. Anderson and J. Moore, *Optimal Filtering*. Englewood Cliffs, NJ: Prentice-Hall, 1979.
- [3] L. White, "Adaptive tracking of frequency modulated signals using hidden Markov models," in *Proc. Workshop Hidden Markov Models Tracking*, Yankalilla, Australia, Feb. 1992.
- [4] B. Boashash, "Estimating and interpreting the instantaneous frequency of a signal," Parts 1 and 2, *Proc. IEEE*, vol. 80, Dec. 1990.
- [5] F. Hlawatsch and G. F. Boudreaux-Bartels, "Linear and quadratic time-frequency signal representations," *IEEE Signal Processing Mag.*, pp. 21-61, 1992.
- [6] D. Rife and R. Boorstyn, "Single tone parameter estimation from discrete time observations," *IEEE Trans. Inform. Theory*, vol. IT-20, pp. 591-598, Sept. 1974.
- [7] S. Kay, "A fast and accurate single frequency estimator," *IEEE Trans. Acoust., Speech, Signal Processing*, vol. ASSP-27, Dec. 1979.
- [8] V. Clarkson, "Efficient single frequency estimator," in *Proc. Int. Symp. Signal Process. Applicat.*, Gold Coast, Australia, Aug. 1992.
- [9] L. Jackson et al., "Frequency estimation by linear prediction," in *Proc. IEEE Int. Conf. Acoust., Speech, Signal Process.*, Tulsa, OK, 1978.
- [10] B. Quinn, "Estimating frequency by interpolation using Fourier coefficients," *IEEE Trans. Signal Processing* vol. 42, pp. 1264-1268, May 1994.
- [11] G. Venkatesan and M. Amin, "Time-frequency distribution kernel design over a discrete powers-of-two space," *IEEE Signal Processing Lett.*, vol. 3, pp. 1-3, Nov. 1996.
- [12] M. Amin, "Recursive kernels for time-frequency signal representations," *IEEE Signal Processing Lett.*, vol. 3, pp. 16-18, Jan. 1996.
- [13] S. Tyler and M. Amin, "Mitigating interference in direct sequence spread spectrum communication systems," *Rome Lab. Tech. J.*, vol. 1, June 1995.
- [14] M. Amin, "Interference mitigation in spread spectrum communication systems using time-frequency distributions," U.S. Air Force, Rome Lab., Tech. Rep., Sept. 1994.
- [15] J. Ketchum and J. Proakis, "Adaptive algorithms for estimating and suppressing narrow band interference in PN spread spectrum systems," *IEEE Trans. Commun.*, vol. COMM-30, pp. 913-924, May 1982.
- [16] S. Davidovici and E. Kanterakis, "Narrow-band interference rejection using real-time Fourier transform," *IEEE Trans. Commun.*, vol. 37, pp. 713-722, July 1989.
- [17] R. DiPietro, "An FFT based technique for suppressing narrow-band interference in PN spread spectrum communications systems," in *Proc. IEEE ICASSP*, 1989, pp. 1360-1363.
- [18] M. Medley, G. Saulnier, and P. Das, "The application of wavelet-domain adaptive filtering to spread spectrum communications," in *Proc. SPIE Wavelet Applicat. II*, Apr. 1995, vol. 2491, pp. 233-247.
- [19] M. Tazebay and A. Akansu, "Adaptive subband transforms in time-frequency excisers for DSSS communication systems," *IEEE Trans. Signal Processing*, vol. 43, pp. 1776-1782, Nov. 1995.
- [20] M. Amin, "Interference mitigation in spread spectrum communication system using time-frequency distribution," *IEEE Trans. Signal Processing*, vol. 45, pp. 90-102, Jan. 1997.
- [21] L. Cohen and C. Lee, "Instantaneous bandwidth," in *Time-Frequency Signal Analysis*, B. Boashash, Ed. Melbourne, Australia: Longman Cheshire.
- [22] C. Wang and M. Amin, "Performance analysis of interference excisions in spread spectrum communications based on instantaneous frequency estimation," in *Fourth Int. Symp. Signal Process. Applicat.*, Australia, Aug. 1996.



Chenshu Wang was born in Tianjin, China, in 1969. He received the B.E. degree in electrical engineering from Tsinghua University, Beijing, China, in 1993 and the M.S. degree in electrical engineering in 1997 from Villanova University, Villanova, PA.

From 1993 to 1995, he was working for Full Link Enterprise Inc., Beijing. He is currently employed by GlobeSpan Technologies, Inc., Red Bank, NJ. His research interests include spread spectrum communications, time-frequency distributions, and xDSL technologies.



Moeness G. Amin (SM'91) received the B.Sc. degree in 1976 from Cairo University, Cairo, Egypt, the M.Sc. degree in 1980 from the University of Petroleum and Minerals, Dharhan, Saudi Arabia, and the Ph.D. degree in 1984 from the University of Colorado, Boulder, all in electrical engineering.

In 1984, he joined the University of Colorado, Denver, as a Visiting Assistant Professor. He has been on the Faculty of the Department of Electrical and Computer Engineering, Villanova University, Villanova, PA, since 1985, where he is now a

Professor. His current research interests are in the areas of time-frequency analysis, spread spectrum communications, smart antennas, and blind signal processing.

Dr. Amin is currently an Associate Editor of the IEEE TRANSACTIONS ON SIGNAL PROCESSING and a member of the Technical Committee of the IEEE Signal Processing Society on Statistical Signal and Array Processing. He was the General Chair of the 1994 IEEE International Symposium on Time-Frequency and Time-Scale Analysis. He is the recipient of the 1997 IEEE Philadelphia Section Award for "Outstanding Intellectual and Organizational Contributions to the IEEE Philadelphia Section in the Area of Signal Processing." He is also the recipient of the 1997 Villanova University Outstanding Faculty Research Award. He is a member of Sigma Xi and Eta Kappa Nu.

An Improved Instantaneous Frequency Based Interference Excision In DS/SS Communications

Raja S. Ramineni, Moeness G. Amin and Stephen R. Lach

Villanova University, Villanova, PA 19085
Dept. of Electrical and Computer Engineering

ABSTRACT

In this paper, the well known notch filtering technique for interference excision in direct sequence spread spectrum (DS/SS) communications is expanded, so as to remove the constraint that the instantaneous frequency (IF) of the jammer must be constant over the filter duration. The time-varying difference equation representation of a polynomial phase signal is used to define a new filter impulse response that can effectively remove any polynomial phase interfering signal. It is shown that this approach, when applied to jammers with constant modulus property, is more efficient than the existing excision methods implementing notch excision filtering. This paper focuses specifically on chirp signals, and provides both the receiver SNR and bit error rate (BER) curves, thus showing the improved performance over similar approaches based on instantaneous frequency information.

1. INTRODUCTION

One of the primary motivations for direct sequence spread spectrum (DS/SS) communications is that of interference mitigation. By definition, a DS/SS system is one in which the transmitted signal is spread over a bandwidth much wider than is required to transmit the information, by means of code independent of the data. The availability of this code at the receiver enables the despreading and recovery of the data, while spreading and suppressing the interference. Thus, any level of interference rejection can be achieved with sufficient processing gain. However, this may require increasing spectrum of the transmitted signal beyond the available limits. Therefore, signal processing techniques are often used in conjunction with a DSSS receiver to combat significant amounts of interference^{1,2,3,4}.

The recent advances in instantaneous frequency (IF) estimation have motivated a new open-loop adaptive filtering approach for nonstationary interference excision in spread spectrum communications. In this approach, the received data is processed by a short length time-varying finite impulse response (FIR) filter with a notch synchronous with the jammer IF. The implementation of IF-based interference excision systems utilizing the localization properties of the time-frequency distributions (TFD's) have been thoroughly analysed^{5,6,7}. Expressions for the spread spectrum receiver SNR incorporating an IF estimate of the time-varying interference using three and five-coefficient notch filters have been derived and extended to the multi-component case⁸. The effect of the IF estimation error on performance has also been considered⁸.

The fundamental concept behind the open-loop adaptive filtering approach to interference excision is to place a filter zero synchronous with the jammer. This zero, which is positioned on a unit circle with a phase equal to the jammer instantaneous frequency, effectively removes the interference, causing the filter output to be essentially jammer free. However, for this excision method to work effectively, the IF of the jammer must remain constant or change slowly over the filter extent. In effect, the excision filter coefficients at time instant n are chosen such that the filter can remove a fixed frequency sinusoid whose frequency is equal to the interference IF at the same instant n . This methodology is illustrated in Fig. 1a. When this condition is strongly violated, much of the jammer power will escape the excision process, leading to increased bit error rates and deteriorating receiver performance. This undesired property of the notch filter approach to interference excision in rapidly time-varying environment will be clearly demonstrated in the simulation section.

In this paper, we overcome the above drawback by presenting a modified version of the notch filter approach to jammer excision in DS/SS communications⁷. Since the jammer IF is already estimated at each sample over the filter extent, it makes sense to use this information in the design of the excision filter. The time-varying difference equation representation of a polynomial phase signal can be used to define a new filter impulse response that can entirely remove any interfering signal of constant modulus characteristics. Further, if an approximation to the IF curve of the interference is to be performed, it is more prudent to approximate the IF by a piece-wise curve, i.e., chirp functions, rather than stair case constant frequency segments⁸. Figure 1b. illustrates this point, as it demonstrates that the piece wise approximation provides a better fit to the IF curve than the stair-case approximation and, as such, will, significantly reduce the jammer power at the filter output.

The paper is organized as follows. In section 2, the time-varying difference equation for the monocomponent complex chirp signal is presented. These equations are then employed to cover the special case of real valued interference signal. In section 3, the expression for the receiver SNR implementing the proposed excision approach is derived. Computer simulations are presented in section 4 to illustrate the advantages of the new method over similar excision techniques which are also based on IF information.

2. TIME-VARYING DIFFERENCE EQUATION REPRESENTATION OF A POLYNOMIAL PHASE SIGNAL

Let $x[n]$ be a polynomial phase signal, representing the nonstationary interference with time-varying frequency

$$x[n] = e^{j\theta[n]} \quad (1)$$

where $\theta[n] = a_0 + a_1 n + a_2 n^2 + \dots$, is the phase function. The phase at any time instant can be written as sum of the phases at the time instant $(n-1)$ and a time increment $\Delta\theta[n]$.

$$\theta[n] = \theta[n-1] + \Delta\theta[n] \quad (2)$$

The instantaneous frequency is therefore given by

$$f[n] = \frac{\Delta\theta[n]}{2\pi} = \frac{(\theta[n] - \theta[n-1])}{2\pi} \quad (3)$$

The discrete-time signal $x[n]$ in (1) can be rewritten as

$$x[n] = e^{j\Delta\theta[n]} e^{j\theta[n-1]} = a[n] x[n-1] \quad (4)$$

where

$$a[n] = e^{j\Delta\theta[n]} \quad (5)$$

Accordingly, if both the first sample and the jammer instantaneous frequency are known, the interfering signal can be easily constructed and removed. If we consider the general case of a signal composed of M complex sinusoids

$$x[n] = \sum_{m=1}^M x_m[n] \quad (6)$$

It can be readily shown that the overall difference equation describing the signal $x[n]$ is⁹

$$x[n] = \sum_{k=1}^M a_k[n]x[n-k] = \sum_{m=1}^M c_m[n]x_m[n-1] \quad (7)$$

where the coefficient c_m are given by the relations⁹

$$d_{mk}[n] = \frac{d_{m(k-1)}[n]}{c_m[n-k+1]}, \quad c_m[n] = \sum_{k=1}^M d_{mk}[n]a_k[n] \quad (8)$$

A real valued sinusoid with time-varying frequency is a special case of the above complex sinusoids. For a real chirp signal, $x[n]$ can be written as the sum of two complex exponentials with phases $\Delta\theta_1[n] = -\Delta\theta_2[n]$. In this case, it is easy to show that the coefficients of the difference equation are given by

$$a_1[n] = \frac{\sin(\Delta\theta[n] + \Delta\theta[n-1])}{\sin(\Delta\theta[n-1])} = h_1[n], \quad a_2[n] = (-1) \frac{\sin(\Delta\theta[n])}{\sin(\Delta\theta[n-1])} = h_2[n] \quad (9a)$$

For the case of a sinusoid of fixed frequency the coefficients of the difference equation reduce to

$$a_1[n] = 2\cos(\Delta\theta[n]), \quad a_2[n] = -1 \quad (9b)$$

3. INTERFERENCE EXCISION

The coefficients of the difference equation, as derived in the previous section, are used as the filter taps for interference excision. The impulse response of the excision filter thus becomes

$$h_k[n] = \delta(n) - h_1[n]\delta[n-1] - h_2[n-2]\delta[n-2] \quad (10)$$

The coefficients in the above equation are updated every time instant, using the jammer instantaneous frequency (IF) information¹. It is important to note that the filter performance is very sensitive to the initial conditions. This is because any error made in the initial stages accumulates quickly and gives rise to a very large error after a short time period. However, if the initial conditions are reasonably accurate, interference excision becomes effective and leads to satisfactory receiver performance.

The received signal is of the form $r(t) = s(t) + w(t) + i(t)$, where $w(t)$ is the uncorrelated white noise signal, $s(t)$ is the desired signal and $i(t)$ is the interfering signal. The input to the excision filter is the sampled received signal $r(n)$, and the filter output is $y(n)$, which is given by the equation

$$y(n) = \sum_{k=0}^2 h_k(n)r(n-k) \quad (11)$$

¹This information can be provided using time-frequency distributions or any other IF estimator

Due to linearity, the filter output can be written as the summation of the outputs due to each of the individual components. This can be expressed as

$$U = \sum_{n=1}^L p(n)p_o(n) + \sum_{n=1}^L w_o(n)p(n) + \sum_{n=1}^L i_o(n)p(n) \quad (12)$$

where the subscript "o" denotes the output of the filter, L is the number of chips/bit, $p(n)$, $w(n)$ and $i(n)$ represent the sampled versions of the direct sequence, noise and interference components of the input data over a bit period, and U is the decision variable. Let

$$U = U_1 + U_2 + U_3 \quad (13)$$

where the term U_1 is given by

$$U_1 = \sum_{n=1}^L \sum_{k=0}^2 h_k(n)p(n-k)p(n) \quad (14)$$

and its expected value is

$$E\{U_1\} = \sum_{n=1}^L \{p(n)p(n) + h_1(n)p(n)p(n-1) + h_2(n)p(n)p(n-2)\} = L \quad (15)$$

Assuming the interference signal to be a real valued chirp signal, the mean square value and the variance of U_1 are, respectively given by

$$E\{U_1^2\} = \sum_{n=1}^L \left[\left(\frac{\sin(\Delta\theta[n] + \Delta\theta[n-1])}{\sin(\Delta\theta[n-1])} \right)^2 + \left(\frac{\sin(\Delta\theta[n])}{\sin(\Delta\theta[n-1])} \right)^2 \right] + L^2 \quad (16)$$

$$Var\{U_1^2\} = \sum_{n=1}^L \left[\left(\frac{\sin(\Delta\theta[n] + \Delta\theta[n-1])}{\sin(\Delta\theta[n-1])} \right)^2 + \left(\frac{\sin(\Delta\theta[n])}{\sin(\Delta\theta[n-1])} \right)^2 \right]$$

The expected value of the variable U_2 due to the additive noise is

$$E\{U_2\} = \sum_{n=1}^L \sum_{k=0}^2 h_k(n)w(n-k)p(n) = 0 \quad (17)$$

which is the result of the uncorrelation property between the noise and the PN sequence. The mean square value of U_2 is

$$E\{U_2^2\} = \sigma^2 \left[L + \sum_{n=1}^L \left[\left(\frac{\sin(\Delta\theta[n] + \Delta\theta[n-1])}{\sin(\Delta\theta[n-1])} \right)^2 + \left(\frac{\sin(\Delta\theta[n])}{\sin(\Delta\theta[n-1])} \right)^2 \right] \right] \quad (18)$$

With full excision

$$E\{U_2^2\} = 0 \quad \text{and} \quad E\{U_3\} = 0 \quad (19)$$

The receiver signal to noise ration (SNR) is

$$SNR = \frac{E^2\{U\}}{E\{U^2\} - E^2\{U\}}$$

From equations (10-19) the SNR of the receiver with chirp like approximation for real valued chirp interference signal is

$$SNR = \frac{L^2}{(1 + \sigma^2) \left[\sum_{n=1}^L \left[\left(\frac{\sin(\Delta\theta[n] + \Delta\theta[n-1])}{\sin(\Delta\theta[n-1])} \right)^2 + \left(\frac{\sin(\Delta\theta[n])}{\sin(\Delta\theta[n-1])} \right)^2 \right] \right] + L\sigma^2} \quad (20)$$

It is noteworthy that for the case of a sinusoidal interference signal with fixed frequency $\omega = \omega_n$, it can be seen that the above expression for the receiver SNR simplifies to

$$SNR = \frac{L}{\left[1 + 4\cos^2\omega_n + 2\sigma^2(1 + 2\cos^2\omega_n) \right]} \quad (21)$$

which is the same as the expression (40) derived in reference ⁸.

4. COMPUTER SIMULATIONS

In this section we present computer simulations to illustrate the performance of the proposed method, and compare it to the stair-like filter. Both the real and complex interference scenarios are considered for the polynomial phase approximation filter. Figure 2 depicts the staircase approximation filter output in both the time and frequency domains for a real-valued chirp signal with $\omega_0 = 0.3 + \alpha(2n-1)$. It is evident from Fig. 2 that the filter output is more pronounced for $\alpha = \frac{1}{256}$ (Fig. 2e to Fig. 2h) than the case of small rate chirp signal alone, i.e. $\alpha = \frac{1}{2560}$ (Fig. 2a to Fig. 2d). However this is not the case for the chirp-like approximation filter. Figure 3a shows the frequency spectrum of the Interfering signal and Fig. 3b. shows the corresponding frequency domain output of the piece-wise approximation filter. Figure. 3c and Fig. 3d present the signal in time domain. These figures illustrate that the polynomial phase filter output is practically zero when the input signal is composed of the interference.

Finally, bit error simulations were performed with 128 chips/bit over a variety of Jammer-to-Signal ratios(JSR). The curves in Fig. 4 were produced. Figure 4a presents the results for the stair-like approximation filter. Figure 4b. presents the results for the piece-wise approximation filter. 1,000,000 trials were used for these plots. These curves show that the BER for the case of piece-wise approximation are lower than those that can be obtained with the stair-case approximation.

5. CONCLUSIONS

This paper has presented an improvement to the notch filtering method of interference excision in DSSS communications. This newly proposed technique eliminates the constant IF constraint assumed by the stair-like approximation, and allows the IF information to be utilized to the fullest extent. Improved performance has been demonstrated both mathematically and through computer simulations. For the case of sinusoidal interference signals, it can be shown that the polynomial phase approximation filter is the same as the three coefficient filter³. A closed form expression for the receiver SNR were derived for the case of sinusoidal interference signals

6. REFERENCES

1. M. K. Simon *et al.*, *Spread Spectrum Communications*. New York: Computer Science, 1985.
2. J. Ketchum and J. Proakis, "Adaptive algorithms for estimating and suppressing narrow band interference in PN spread spectrum systems," *IEEE Transactions on communications.*, Vol. COM-30, pp. 913-924, May 1982.
3. L. Milstein and R. Iltis, "Signal processing for interference rejection in spread spectrum communications," *IEEE Acoustic, Speech, Signal Processing Magazine*, Vol. 3., pp. 18-31, April, 1986.
4. J. Doherty, "Linearly constrained direct-sequence-spread-spectrum interference rejection," *IEEE Trans. Commun.*, Vol. 423, nos. 2/3/4, Feb./Mar./Apr., 1994.
5. M.G. Amin, "Interference excision in spread spectrum communication systems using time-frequency distributions," *Tech. Report, AFOSR, Rome Lab*, Sept. 1994.
6. M. Tazebay and A. Akansu, "Adaptive subband transforms in time-frequency excisers for DSSS communication systems," *IEEE Trans. on Signal Processing*, Vol.11, pp. 2776-2782, Nov. 1995.
7. M. Amin, "Interference mitigation in spread spectrum communication system using time-frequency distribution," *IEEE Trans. on Signal Proc.* Vol. 45., pp. 90-102, Jan. 1997.
8. C. Wang and M.G. Amin, "Performance analysis of instantaneous frequency-based interference excision techniques in spread spectrum communications," *IEEE Transactions on Signal Processing*, Vol.46, no.1. January, 1998.
9. A.S. Kayhan, "Representation and analysis of complex chirp signals," submitted to the *IEEE Transactions on Signal Processing*, August, 1996.

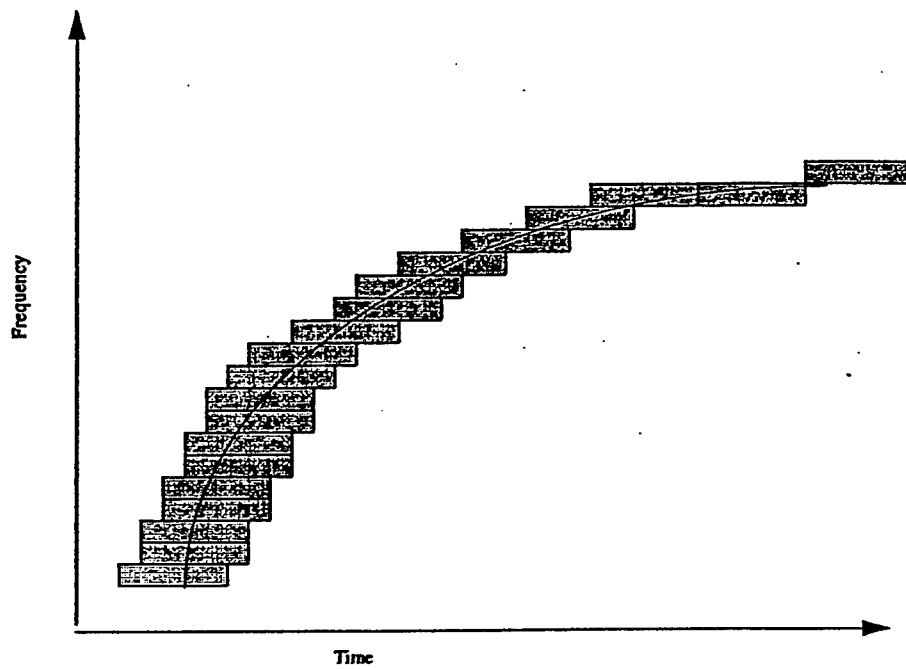


Figure 1a. The stair like approximation of the instantaneous frequency of the signal under consideration

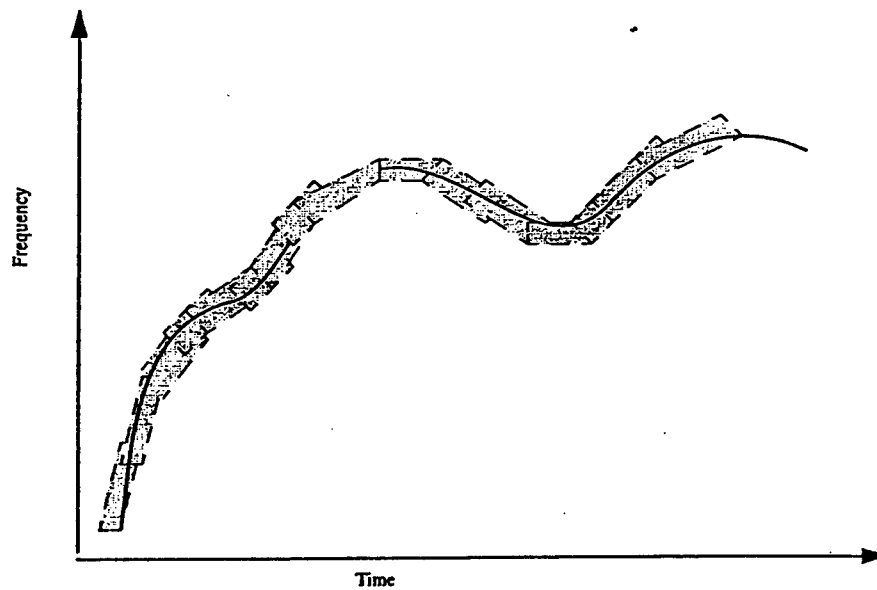


Figure 1b. The Chirp like approximation of the instantaneous frequency of the signal under consideration

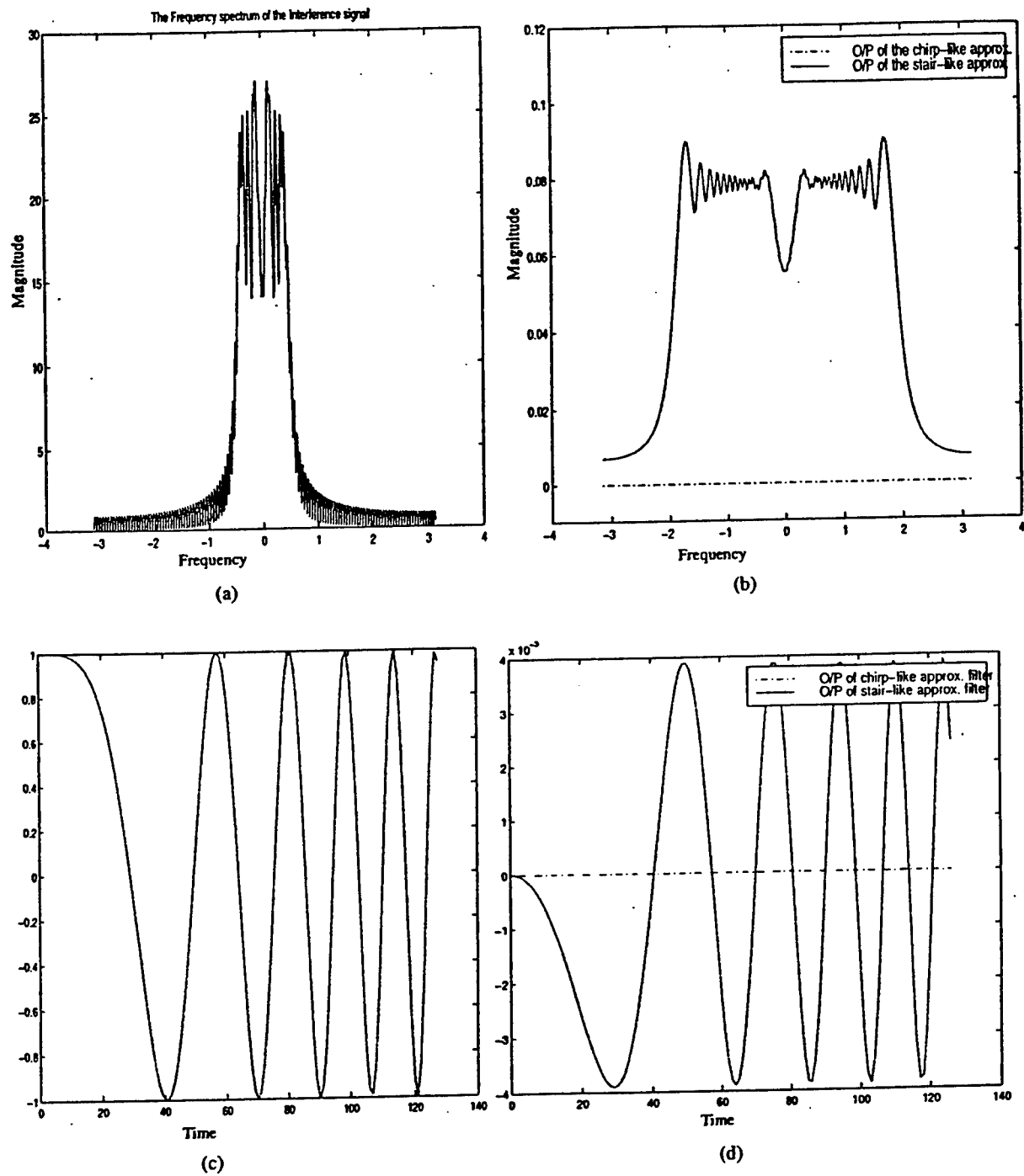
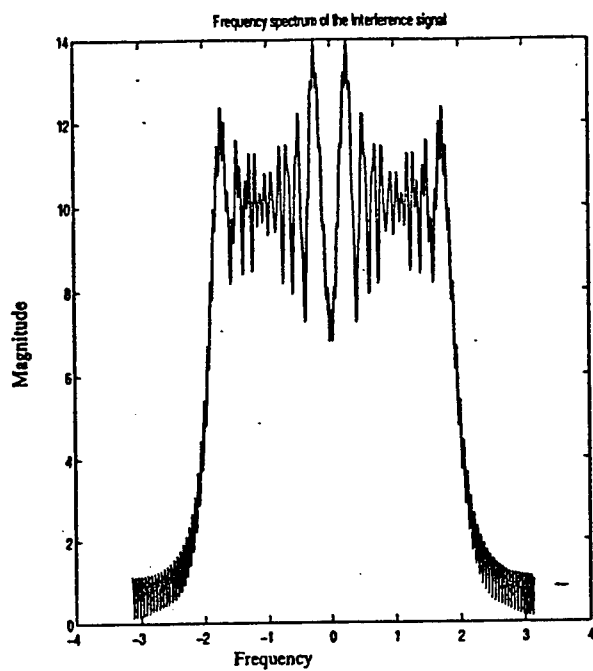
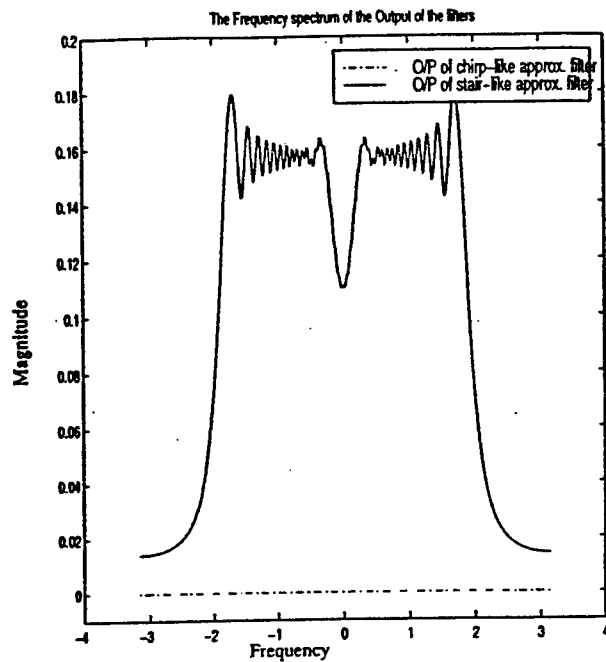


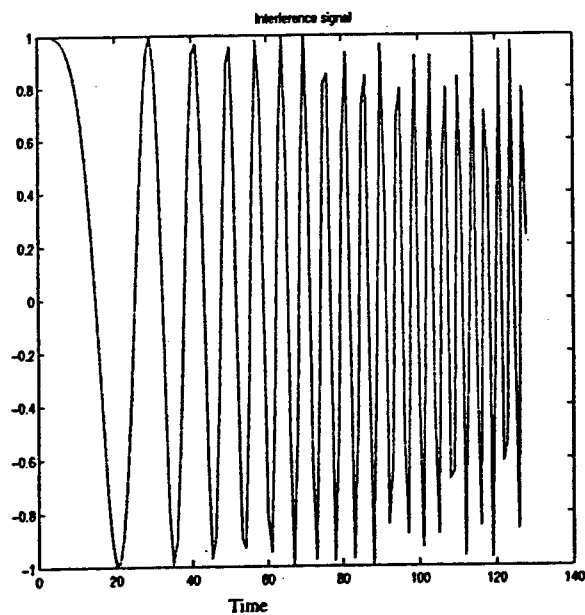
Figure 2a, 2b. The frequency spectra of the interference and the output of the filters (stair like and chirp like approximations).
 (c) The interference signal in time domain. (d) The output of the filters in time domain. (The chirp-rate is $\alpha = \frac{1}{2560}$.)



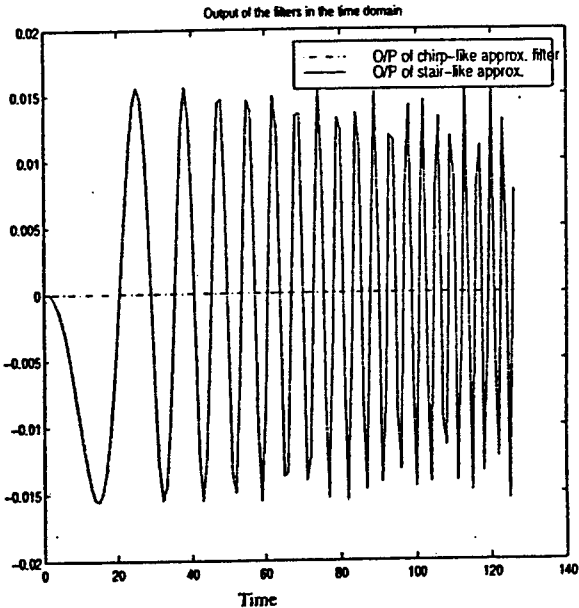
(e)



(f)



(g)



(h)

Figure 2e, 2f. The frequency spectra of the interference and the output of the filters (stair like and chirp like approximations).
(g) The interference signal in time domain. (h) The output of the filters in time domain (chirp rate $\alpha = \frac{1}{256}$).

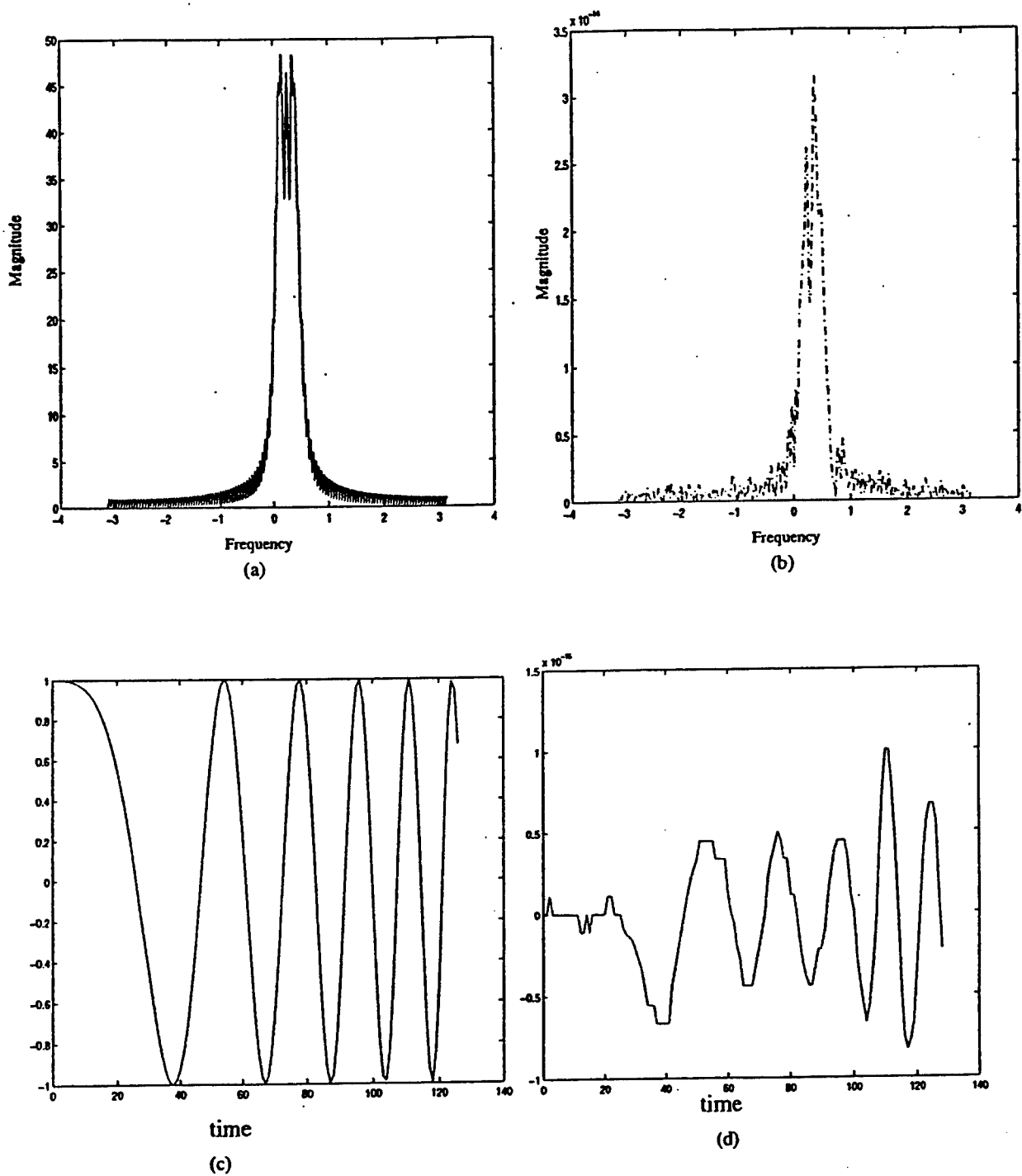


Figure 3a, 3b. The Frequency Spectrum of the complex interference signal and the output of the Chirp-like and Stair-like approximation filters. (3c) Real part of the interference signal (3d) Real part of the output of the filter.

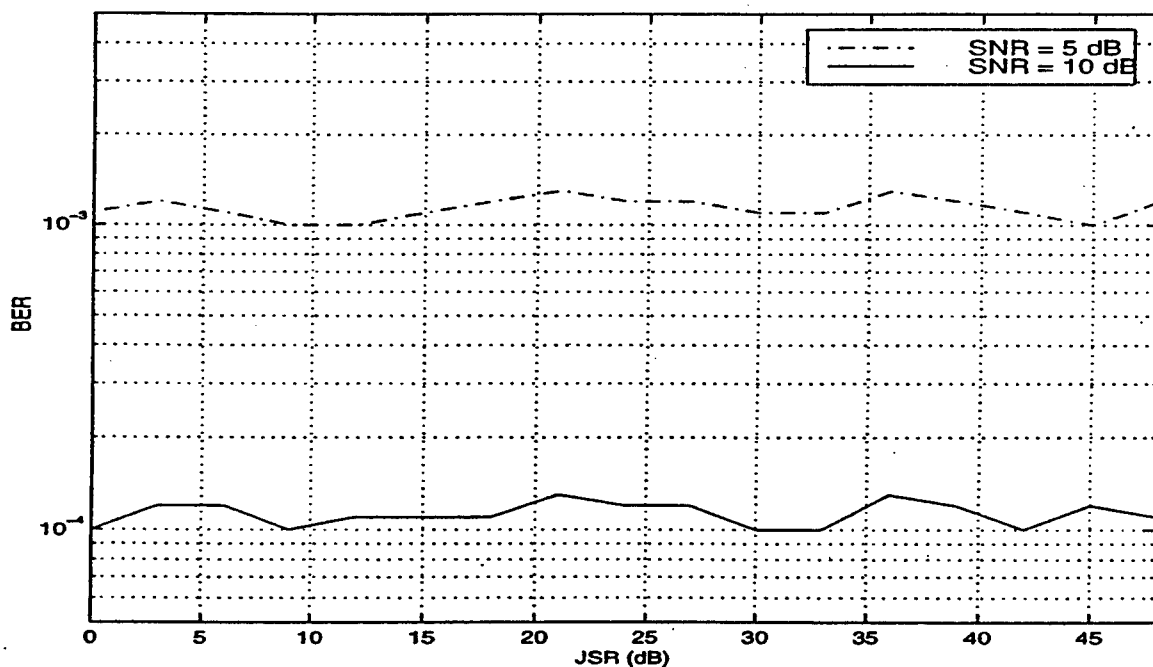
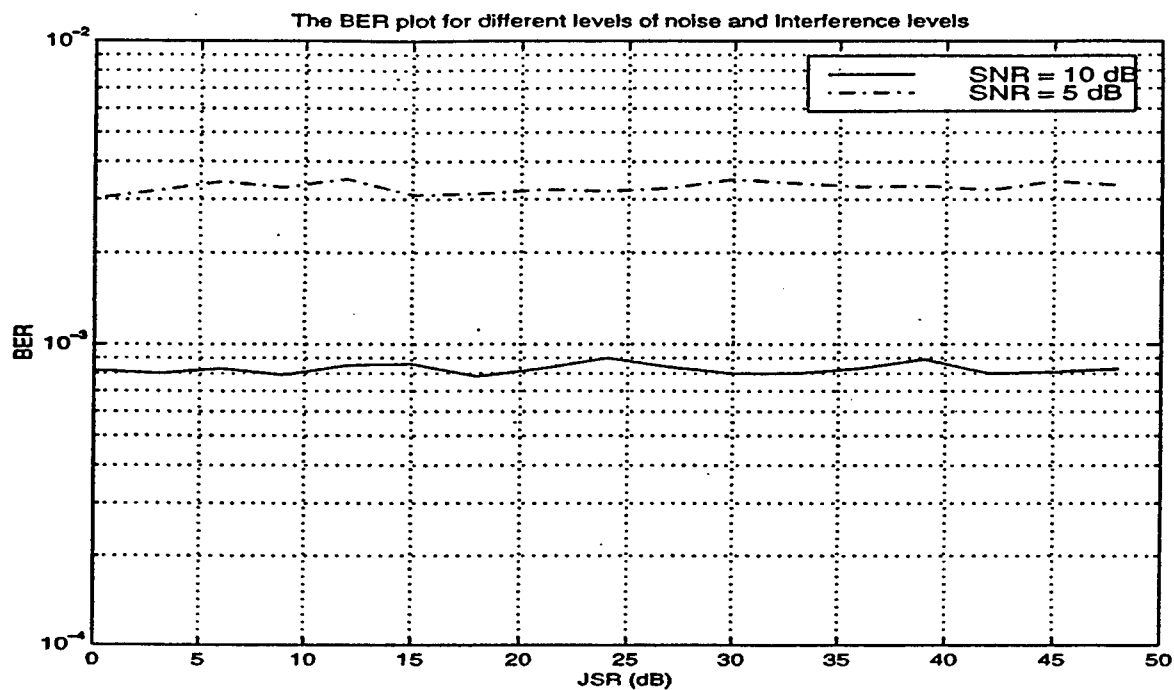


Figure 4. The plot of the BER for different values of the JSR as a function of the Signal to Noise Ratio SNR(dB). The number of trials in the simulation is 1,000,000. Fig. 4a. BER curves for the stair-like approximation. Fig.4b. BER curves for the piece-wise approximation

Open Loop Adaptive Filtering for Interference Excision in Spread Spectrum Systems

Chenshu Wang[†] Moeness G. Amin[†] and Alan Lindsey^{**}

[†]Dept. of Electrical and Computer
Engineering
Villanova University
Villanova, PA 19085
Email: moeness,cw@ece.vill.edu

^{**} Rome Laboratory
RL/C3BB
525 Brooks Road
Rome, NY 13441-4505
Email: lindseya@rl.af.mil

Abstract

A new technique for interference excision in PN spread spectrum communications using time-frequency distributions is introduced. The excision filter coefficients under this technique depend on the jammer power and its instantaneous frequency information, both values are gained in the time-frequency domain. The dependency of the excision filter characteristics on the interference power, which was absent in previous contributions in this area, is of significant importance, as it allows optimum trade-off between interference removal and the amount of the filter self-noise generated from the induced correlation across the PN chip sequence. This trade-off is bounded by the two extreme cases of no self-noise, which implies preprocessing disabled, and full interference excision, which the case previously considered. In this paper, we derive the FIR excision filters that maximize the receiver signal-to-noise ratio for a simple jammer case.

I. Introduction

Several past contributions deal with the suppression of narrowband interference [1,2,3,4]. For broadband interference, adaptive linear prediction filters have been commonly employed to track and remove the time-varying frequency characteristics of the interference [5]. Two different approaches for nonstationary interference excision in DS/SS communications based on time-frequency analysis have been recently considered [6,7,8,9]. One approach is linear and based on multiresolution analysis, whereas the second approach requires a bilinear transformation of the data. In linear transform interference exci-

sions, the data is processed using Fourier, Gabor, or wavelet transforms or M-band/subband filter banks. Excision of the correlated interference components of the received data is performed by clipping, or gating, the high coefficient values followed by inverse transformation to recover the desired signal.

In the recently developed open-loop adaptive filtering approach for interference excision [9, 11,12], a filter zero is put synchronous with the jammer instantaneous frequency (IF), which is estimated using Cohen's class [10] of time-frequency distributions (TFDs). This zero, which is placed on a unit circle with a phase equal to the jammer IF, causes an infinite deep notch, and thereby, effectively removes the jammer, causing the filter output to be essentially jammer free. However, this type of filter characteristics also create significant amount of self-noise, due to the correlation introduced across the different chips of the PN sequence. In a jammer free-environment, the filter self-noise reduces the receiver performance from the case when no preprocessing is applied as it limits the maximum attainable value of the correlator SNR. Depending on the filter characteristics, this value may very well be far below the spreading gain. Although in general, excision filters should be shut off if no jammer is present, the problem with the aforementioned interference excision system which is based solely on the IF information [9] is that even under significant jammer power, the performance is still worse than when preprocessing is disabled. This should not be the case if the filter coefficients are properly chosen.

In this paper, the TFD-based interference excision technique is further developed for application to a wide range of jammer to signal ratios (JSR). Since the TFD is the distribution of the signal power over time and frequency, then, in addition to the IF estimate, TFDs depict the instantaneous power of the different compo-

The work is supported by Rome Lab, contract No. F30602-96-C-0077

nents of the received signal. The amplitude information of the interference gained in the t-f plane is used to control the notch of the excision filter, achieving a higher receiver SNR than the case of a fixed depth notch. Preprocessing the data before despreading produces a trade-off between the self-noise introduced by the filter and the effective removal of the jammer power. In order to account for this trade-off, the original open-loop adaptive interference excision system introduced in [9] is herein modified such that the filter notch location depends on the jammer IF, whereas the depth of the filter notch is controlled by a new variable, which is a function of jammer power. This variable is selected to achieve an optimum receiver performance for a given jammer environment.

It is noteworthy that the need to have both the instantaneous power and frequency to derive the proposed optimum excision of the interference advocates the use of TFD [10] and clearly distinguishes it from other estimators, which only give the IF. The analysis provided in this paper, however, can be used in conjunction with any detection scheme that provides the above two values [13]. Perfect knowledge of the jammer amplitude and IF is assumed. It is recognized that in using TFD, both of the above parameters will carry an error, depending on the jammer signal characteristics as well as the employed t-f kernel.

II. Narrowband Interference Analysis

A simple jammer with a fixed frequency is now considered. The general expression of the receiver SNR using linear time-invariant interference excision filter of coefficients h_i , $i=1,2,\dots,N$, is derived in [12] and given by

$$SNR_o = \frac{L^2 h_0^2}{L(1 + \sigma^2) \sum_{k=0}^N h_k^2 - L h_0^2 + \sigma_j^2} \quad (1)$$

where L is the PN length, σ^2 is the white noise variance, and σ_j^2 is the jammer power. In the following analysis, we focus on the three-coefficient causal notch excision filter

$$H(z) = z^{-1}(z - ae^{-j\omega_0})(1 - az^{-1}e^{j\omega_0}) \\ = 1 - 2az^{-1}\cos\omega_0 + a^2z^{-2} \quad (2)$$

where the parameter a represents the amplitude of the filter zero that controls the depth of the filter notch at the jammer frequency ω_0 . The effect of this parameter on the filter frequency response is shown in Fig. 1(a). The filter impulse response comes directly from the definition of the Z-transform

$$h(n) = \delta(n) - 2a\delta(n-1)\cos\omega_0 + a^2\delta(n-2) \quad (3)$$

If we denote the filter coefficients by

$h_0 = 1$, $h_1 = 2a\cos\omega_0$, $h_2 = a^2$, then the corresponding receiver SNR is a special case of (1) and is given by

$$SNR_o = \frac{L^2}{L[(1 + \sigma^2)(1 + a^4 + 4a^2\cos^2\omega_0) - 1] + \sigma_j^2} \quad (4)$$

The self-noise introduced by the filter $H(z)$ is given by the first term in the denominator of equation (4), i.e., those terms dependent solely on the filter zero amplitude parameter a ,

$$\sigma_s^2 = L(a^4 + 4a^2\cos\omega_0). \quad (5)$$

The white noise sequence also becomes colored at the excision filter output and its contribution to the receiver SNR_o in (4) is given by

$$\sigma_w^2 = L\sigma^2(1 + a^4 + 4a^2\cos\omega_0). \quad (6)$$

The quantity $\sigma_T^2 = \sigma_s^2 + \sigma_w^2$ is the receiver noise in a jammer-free environment, so, we may refer to it as the jammer-free noise or the total self-noise (TSN). It is clear from equations (5) and (6) that the minimum value of the TSN occurs at $a=0$, and increases monotonically as a function of a . Figure 1(b) shows the zero-diagram of the notch filter for different values of a . For high jammer power, $\sigma_j^2 \gg \sigma_T^2$, the interference removal becomes more important than reducing the TSN. In this case, a high value of a should be chosen such that a deeper notch is introduced. The jammer is entirely removed in the extreme case of $a=1$, which is discussed in the original design [9]. On the other hand, as the jammer power decreases, the choice of a should tend towards favoring the reduction of the total self-noise over the jammer power, and to ultimately shut off the filter, for $\sigma_s^2 + \sigma_w^2 \gg \sigma_j^2$, disabling preprocessing of the received signal prior to despreading.

To obtain σ_j^2 , it is prudent to first derive an expression of the jammer waveform that escapes the excision filter when $a \neq 1$. Consider a narrowband sinusoidal jammer of the form $j(n) = A\sin(n\omega_0 + \varphi)$, where A is the jammer amplitude and φ is its phase. The jammer at the filter output is given by

$$j_0(n) = A(1-a)\sin(n\omega_0 + \varphi) + (a^2-a)A\sin[(n-2)\omega_0 + \varphi]$$

The correlator output due to the jammer is

$$U_j = \sum_{n=1}^L j_0(n)p(n) \quad (7)$$

where the $p(n)$ is the PN chip sequence. Accordingly,

$$\sigma_j^2 = E[U_j^2] - E^2[U_j] = \sum_{n=1}^L j_0^2(n). \quad (8)$$

It can be readily shown that for $L \gg 1$,

$$\sigma_j^2 = LA^2(1-a)^2 \left[\frac{1}{2} + \frac{a^2}{2} - a \cos 2\omega_0 \right] \quad (9)$$

Substituting (9) in (4), the receiver SNR becomes

$$SNR_o = L / \left\{ (1 + \sigma^2)(1 + a^4 + 4a^2 \cos^2 \omega_0) - 1 + A^2(1-a)^2 \left[\frac{1}{2} + \frac{a^2}{2} - a \cos 2\omega_0 \right] \right\} \quad (10)$$

The jammer power given by (9) has a minimum value at $a=1$, and monotonically increases for both increased and reduced values of a . Equation (9) can be rewritten as

$$\sigma_j^2 = \frac{A^2}{2} [(1-a)^4 + 2a(1-a)^2(1 - \cos 2\omega_0)] \quad (11)$$

Careful study of the above equation reveals that the value of σ_j^2 increases faster for $a > 1$ than for $a < 1$. This is because both factors $(1-a)^4$ and $(1-a)^2$ are invariant for $a = 1 \pm \Delta$. Due to the appearance of a as a multiplicative factor in the second term, σ_j^2 will be greater for $+\Delta$ than for $-\Delta$. Negative values of a change the filter notch position and move it away from ω_0 , and therefore should be avoided. Since the self-noise increases for increased value of a , as stated earlier, one can conclude that the minimum value of the dominator in the SNR_o expression (10), σ_j^2 , should occur for a in the range $[0, 1]$.

IF $f(a)$ represents the denominator in (10), then in order to find the maximum SNR_o , we simply differentiate $f(a)$ with respect to a ,

$$f'(a) = a^3(4 + 4\sigma^2 + 2A^2) + a^2(-3A^2 - 3A^2 \cos 2\omega_0) + a[8(1 + \sigma^2) \cos^2 \omega_0 + 2A^2 + 4A^2 \cos 2\omega_0] - (A^2 + A^2 \cos 2\omega_0) \quad (12)$$

and sets $f'(a)=0$. Since $f'(0) < 0 \quad \forall \omega_0$, except at $\omega_0 = \pi/2$ where $f'(0) = 0$, and $f'(1) > 0$ for all values of ω_0 , then $f'(a)$ must have a real root in the range $[0, 1]$, which represents the optimal a . For the specific value of $\omega_0 = \pi/2$, $f'(0) = 0$ and $f''(0) = -2A^2 < 0$. This means $f'(0_-) < 0$. With $f'(1) > 0$, $f(a)$ must then intersect the $f'(a) = 0$ axis in the range $[0, 1]$, and the same conclusion can be drawn for $\omega_0' = \pi/2$ as for $\omega_0 \neq \pi/2$.

To solve for a , we rewrite the polynomial $f'(a)=0$ as

$$ba^3 + ca^2 + da + e = 0 \quad (13)$$

where

$$\begin{cases} b = 4 + 4\sigma^2 + 2A^2 \\ c = -3A^2 - 3A^2 \cos 2\omega_0 \\ d = 8(1 + \sigma^2) \cos^2 \omega_0 + 2A^2 + 4A^2 \cos 2\omega_0 \\ e = -(A^2 + A^2 \cos 2\omega_0) \end{cases} \quad (14)$$

and substitute $b = a - \frac{d}{3c}$,

$$a^3 + pa + q = 0 \quad (15)$$

where

$$p = \frac{3bd - c^2}{3b^2}, \quad q = \frac{c}{b} - \frac{cd}{3b^2} - \frac{2c^3}{27b^3} \quad (16)$$

The roots of polynomial (15) are given in [14],

$$\begin{cases} a_1 = \sqrt[3]{-\frac{q}{2} + \sqrt{\left(\frac{q}{2}\right)^2 + \left(\frac{p}{3}\right)^3}} + \sqrt[3]{-\frac{q}{2} - \sqrt{\left(\frac{q}{2}\right)^2 + \left(\frac{p}{3}\right)^3}} \\ a_2 = \gamma \left(\sqrt[3]{-\frac{q}{2} + \sqrt{\left(\frac{q}{2}\right)^2 + \left(\frac{p}{3}\right)^3}} \right) + \gamma^2 \sqrt[3]{-\frac{q}{2} - \sqrt{\left(\frac{q}{2}\right)^2 + \left(\frac{p}{3}\right)^3}} \\ a_3 = \gamma^2 \sqrt[3]{-\frac{q}{2} + \sqrt{\left(\frac{q}{2}\right)^2 + \left(\frac{p}{3}\right)^3}} + \gamma \sqrt[3]{-\frac{q}{2} - \sqrt{\left(\frac{q}{2}\right)^2 + \left(\frac{p}{3}\right)^3}} \end{cases} \quad (17)$$

where $\gamma = \frac{-1 + i\sqrt{3}}{2}$.

If $q < 0$, then a_2 and a_3 are complex due to the presence of γ and its complex value γ^2 . Accordingly, a_1 should be real. On the other hand, if $q=0$ as in the case of $\omega_0 = \pi/2$, then a_1 becomes zero and p is given by

$$p = \frac{d}{b} = \frac{-2A^2}{4 + 4\sigma^2 + 2A^2} < 0, \quad (18)$$

In this case, it can be easily shown that a_2 and a_3 are both real, and have opposite signs with magnitude smaller than one. Accordingly, there is only one positive real root which should be in the range $[0, 1]$, as argued before.

III. Performance Improvement

A fixed frequency jammer excised by a three-coefficient filter is considered. The optimal value of a is computed from equation (12) and substituted back into the SNR expression to provide the maximum SNR for a given jammer power and frequency. Figure 2 compares the correlator SNRs using the original excision filter, no excision filter, and the optimal excision filter. It is evident that for low jammer-to-signal ratio, shutting off the excision filter, leads to a higher receiver SNR than processing the data with the original excision filter, which only depends on the IF information. This situation is reversed for a high jammer power where the original filter outperforms the case when preprocessing is disabled. But, the performance of the proposed optimum interference excision filter asymptotically reaches the desired performance of both the IF-based excision and no excision for high and low jammer power, respectively. In between these two extreme cases, the proposed excision filter, which is based on both the amplitude and frequency of the jammer, gives

clear improvement over the other two techniques. That is, the optimal notch filter gives an excellent trade-off between filtering and no filtering and as expected, α increases with increased jammer power.

In Figures 3-4, we compare the receiver performance versus the interference IF. The optimal excision filtering curve depicting the change in SNR vs frequency is not only above the other curves, correspondingly to the two alternative aforementioned techniques, but also it becomes much flatter than the receiver SNR curve of the original filter. This means that a by-product of the proposed approach is to make the receiver SNR less dependent on the jammer IF.

Figure 5 shows the computer simulation results of bit error curve. A chirp jammer whose frequency changes from 0 to π in every bit duration and a white noise sequence with 0 dB relative to the signal are both added to the PN sequence of length $L=64$. One million bits are tested at every 2 dB JSR increment from -10dB to 10dB. Consistent with the result in SNR analysis, for low jammer to signal ratio, applying no filter leads to lower bit error rate than processing the data with the original excision filter, whereas for a high jammer power, the original filter has lower errors than the case when preprocessing is disabled. Because the optimum notch, adaptive coefficient filter outperforms both cases above. It gives a bit error rate of 10^{-5} at 10 dB JSR and smaller rates at lower JSR.

Conclusions

An optimum open-loop adaptive notch filtering approach for interference excision in PN spread spectrum communications has been developed and discussed in this paper. The FIR filter with variable depth notch that partially removes the jammer achieves optimum receiver SNR over both extreme cases of full jammer excision and no excision. The optimum performance is reached by trading-off the jammer power and filter self-noise. The filter notch is controlled by a new variable whose optimum value is a function of the jammer power, the jammer instantaneous frequency, and the white noise power. Several examples have been presented which show the improvement in the receiver signal-to-noise ratio achieved by using the optimum excision filter over both cases of preprocessing disabled and preprocessing enabled, but only based on the IF information. This improvement is exhibited over a wide range of JSR, and is shown using exact value of the interference amplitude and instantaneous frequency.

References

- [1] L. B. Milstein, "Interference rejection techniques in spread spectrum communications," *Proc. of IEEE*, pp.657-671, June 1988.
- [2] J. Proakis and M. Salehi, *Communication system engineering*, (Section 11), Prentice Hall, Englewood Cliffs, New Jersey, 1994.
- [3] L. A. Rusch and H. V. Poor, "Narrowband interference suppression in CDMA spread spectrum communication," *IEEE Trans. on Communications*, vol.42, no. 2/3/4, pp. 1969-1979, February, March, April 1994.
- [4] H. V. Poor and X. Wang, "Adaptive suppression of narrowband digital interference from spread spectrum signals," *Proc. of the IEEE conf. on Acoustics, Speech and Signal Processing*, Australia, CA, May 1996.
- [5] J. Ketchum and J. Proakis, "Adaptive algorithms for estimating and suppressing narrowband interference in PN spread spectrum systems," *IEEE Trans. on Comm.*, pp. 913-924, May 1982.
- [6] M. Medley, G. Saulnier, and Das, "Applications of the wavelet transform in spread spectrum communications systems," *SPIE, Wavelet Applic.*, Orlando, FL, April 1994.
- [7] M. Tazebay and A. Akansu, "Adaptive subband transforms in time-frequency excisers for DSSS communication systems," *IEEE Trans. on SP*, pp. 2776-2782, Nov. 1995.
- [8] S. Roberts and M. Amin, "Linear vs. bilinear time-frequency methods for interference mitigation in direct sequence spread spectrum communication systems," *Proc. Asilomar Conf. on Signals, Systems and Computers*, Pacific grove, Ca, Nov. 1995.
- [9] M. Amin, "Interference mitigation in spread spectrum communication system using time-frequency distribution," *IEEE Transactions on Signal Processing*, Vol. 45, pp. 90-102, January 1997.
- [10] L. Cohen, *Time-Frequency Analysis*, Prentice Hall, Englewood Cliffs, New Jersey, 1995.
- [11] M. G. Amin, A. Lindsey, and C. Wang, "On the application of time-frequency distributions in the excision of pulse jamming in spread spectrum communication systems," *IEEE Workshop on SSAP*, Greece, June 1996.
- [12] C. Wang and M. G. Amin, "Performance analysis of instantaneous frequency-based interference excision techniques in spread spectrum communications," *IEEE Transactions on Signal Processing*, January, 1998.
- [13] S. Peleg and B. Porat, "Estimation and classification of signals with polynomial phase," *IEEE Trans. on Information Theory*, vol. 37, pp. 442-430, 1991.
- [14] L. Rade and B. Westergren, *Beta Mathematics Ha book*, Studentlitteratur, Akergrandan 1, S-221 00 Lund, 1989.

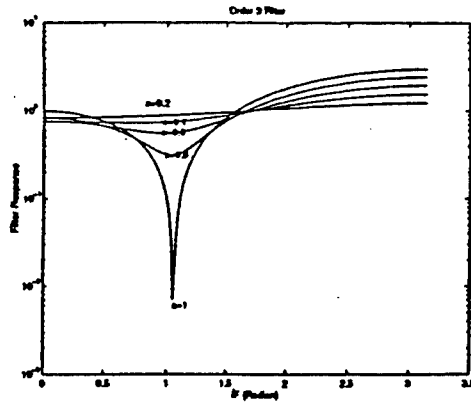


Fig. 1(a) Frequency responses of the three-coefficient adaptive notch filters with $IF=\pi/3$.

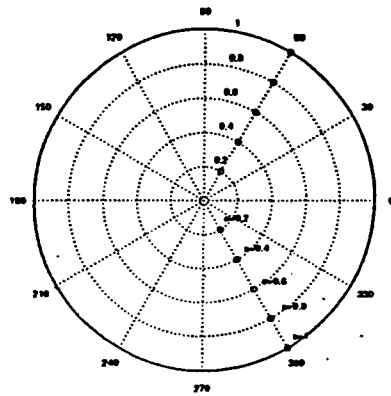


Fig.1 (b) Zero diagram of the adaptive notch filter and the exact jammer frequency. 'o', zero position, '+' exact jammer frequency.

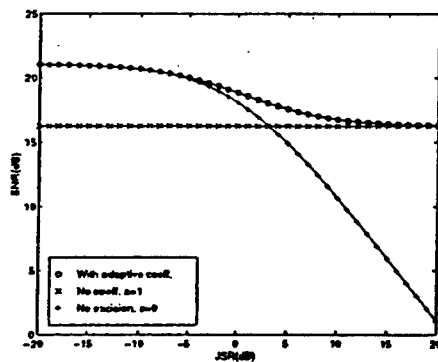


Fig.2 $IF=\pi/2.1$, 0dB white noise, PN length=128. Correlator SNR with 3 coefficient filters and filter off.

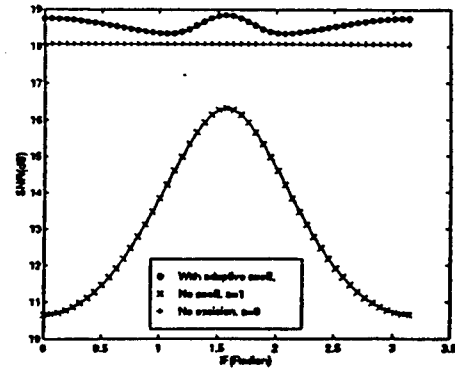


Fig.3 JSR=0dB, 0dB white noise, PN length=128. Correlator SNR with 3 coefficient filters and filter off versus jammer IF.

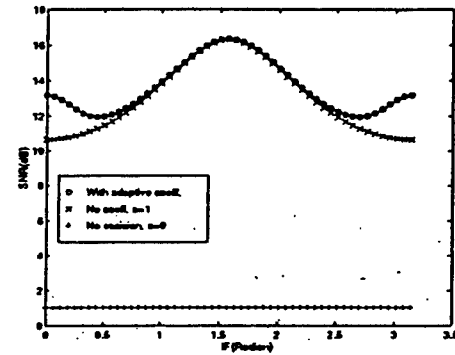


Fig.4 JSR=20dB, 0dB white noise, PN length=128. Correlator SNR with 3 coefficient filters and filter off versus jammer IF.

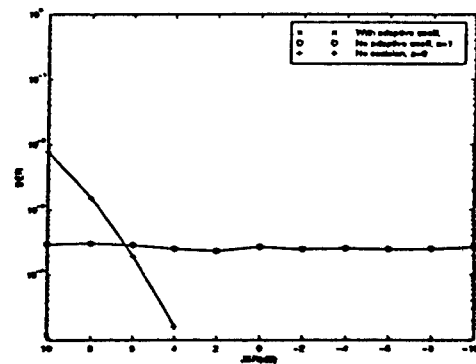


Fig.5 Bit error rate of the three-coefficient filter with adaptive filter coefficient, fixed coefficient and filter off. 0dB white noise, PN length=64.

ZERO-TRACKING TIME-FREQUENCY DISTRIBUTIONS

Chenshu Wang and Moeness G. Amin

Department of Electrical and Computer Engineering
Villanova University
Villanova, PA 19085

ABSTRACT

The zero-tracking time-frequency distribution (TFD) is introduced. The local autocorrelation function of the TFD, defined by an appropriate kernel, is used to form a polynomial whose roots correspond to the instantaneous frequencies of the multicomponent signal. Two techniques for zero-tracking based on TFD are presented. The first technique requires updating all of the polynomial signal and extraneous zeros, and is based on the formula relating to the first order approximation, the changes in the polynomial roots and coefficients. The second technique employs the zero-finding Newton's method to only obtain the zero-trajectories of interest.

1. INTRODUCTION

Recently, quadratic time-frequency distributions (TFD), including of Cohen's class [1], the affine class, and the hyperbolic class [2], have been introduced for nonstationary signal analyses. TFDs have been shown to be a powerful tool for instantaneous frequency (IF) estimation in rapidly time-varying environment [3]. These distributions do not assume a model which is signal specific, as in the case of extended Kalman filters [4], nor they are encumbered by high computational requirements, as in the case of Hidden Markov Models [5]. Further, TFDs can handle multicomponent signals, and as such, outperform existing techniques which are only applicable to a single tone scenario [6]. TFDs are obtained by taking the Fourier transform of the local autocorrelation function (LAF). The later is computed by time-averaging the bilinear data products. The averaging is performed by applying a kernel which acts on satisfying several desirable time-frequency properties including the marginal, support, instantaneous frequency, and reduced cross-terms.

In this paper, we introduce zero-tracking time-frequency distribution methods for instantaneous frequency

estimation. The motivation is two fold and is analogous to that of zero-tracking adaptive filters, namely computational savings and enhanced performance. The proposed methods avoid the Fourier transform and utilize the fact that the local characteristics of the signal are captured in its LAF.

Because of the localization properties of the time-frequency distributions, the location of the spectral peak at time n represents the signal instantaneous frequency. Multiple peaks are a property of a multicomponent signal. In TFD computation, the FFT is used at each time instant. It is important to choose a long FFT block length to properly locate spectral peaks and estimate the IFs. This may require extending the data record to include more data samples, or by zero padding. The cost of applying a high resolution FFT on a data sample by a data sample basis along with a search routine can be avoided by directly extracting the information from the local autocorrelation function without Fourier transformation.

By constructing a polynomial whose roots are located at the TFD peak positions, one can apply zero tracking algorithms to provide the zero trajectories, i.e., the signals instantaneous frequencies. Two methods for zero updating are introduced. The first follows the same approach adopted in zero-tracking adaptive filters [7], but with application to the local autocorrelation function, instead of the filter coefficients. In this case, the zero trajectories are provided using the formula relating the changes in the LAF coefficients to the polynomial zeros. The second method is introduced to mitigate the problems inherent in the first method, namely the need to update all zeros including those which are extraneous, i.e., do not correspond to the signal IFs. In the second method, new polynomial zero positions are obtained by applying an iterative technique similar to that of *Newton's method* [8] for root finding. It is shown that this method works well in low signal-to-noise ratio and under both evolutionary and abrupt changes in frequency.

2. POLYNOMIAL DERIVATION

The basic idea of zero-tracking applied to the underlying problem is to find a polynomial in which all the signal instantaneous frequencies (IFs) are among its roots. We then proceed to identify the signal roots and follow their trajectories.

Let $R_f(n)$ denote the local autocorrelation function at time n and lag l . The TFD is given by

$$Y_n(e^{j\omega}) = \sum_{l=-L/2}^{L/2} R_f(n) e^{-j2\omega l} \quad (1)$$

where $L/2$ is the maximum lag of interest. $Y(e^{j\omega})$ is real and it peaks at the instantaneous frequencies of the multi-component signal, represented by $\omega_1(n), \omega_2(n), \dots, \omega_M(n)$. Accordingly,

$$\left. \frac{dY(e^{j\omega})}{d\omega} \right|_{\omega_i(n), 1 \leq i \leq M} = -j2 \sum_{l=-L/2}^{L/2} l R_f(n) e^{-j2\omega l} = 0 \quad (2)$$

Substituting $e^{j2\omega} = z$, (2) can be rewritten as

$$\sum_{l=-L/2}^{L/2} l R_f(n) z^{-l} = 0 \quad (3)$$

By multiplying the above equation by $z^{L/2}$, we obtain

$$\sum_{l=-L/2}^{L/2} l R_f(n) z^{-l+L/2} = 0 \quad (4)$$

which is the L -th order polynomial:

$$f_n(x) = a_0(n) + a_1(n)z + a_2(n)z^2 + \dots + a_L(n)z^L = 0 \quad (5)$$

$$a_l = (-l + L/2) R_{-l+L/2}(n), \quad l=0, 1, \dots, L \quad (6)$$

The instantaneous frequencies are among the above polynomial roots in the form of $e^{j2\omega_i}, 1 \leq i \leq M$, and therefore can be obtained from the polynomials' zero trajectories.

It is important to note that since the polynomial $f_n(x)$ is based on the LAF, time-frequency kernels which yield reduced cross-terms should be used for proper IF estimation.

3. ZERO-TRACKING ALGORITHMS

Two techniques for zero-tracking based on the LAF of the TFD are considered below.

A. Orfanidis-Vail's Method

This method is based on using the formula, relating to the first-order approximation, the changes in the polynomial coefficients and its roots. Equation (5) can be written in the factorized form as

$$a_0(n) + a_1(n)z^{-1} + a_2(n)z^{-2} + \dots + a_L(n)z^{-L} = a_0(n)(1 - z_1(n)z^{-1})(1 - z_2(n)z^{-1}) \dots (1 - z_L(n)z^{-1}) \quad (7)$$

where $z_i(n)$ is i th root. The roots are updated by

$$z_i(n+1) = z_i(n) + \Delta z_i(n), \quad 1 \leq i \leq L \quad (8)$$

where

$$\Delta z_i(n) = \sum_{m=0}^L \frac{\partial}{\partial a_m(n)} z_i(n) \Delta a_m(n) \quad (9)$$

The partial derivatives in the above equation are given by

$$\frac{\partial}{\partial a_m(n)} z_i(n) = \frac{z_i(n)^{L-m}}{a_0(n) \prod_{j \neq i} (z_i(n) - z_j(n))} \quad (10)$$

This algorithm can therefore be summarized as: 1) At time n , the LAF is available, and so are the coefficients $a_m(n)$. 2) Compute the zero updates using (9), and update the zeros using (8).

The problem with the above zero-tracking method is that all the polynomial roots need to be updated, as evident from equation (10). This entails heavy computations and becomes inefficient, especially for small values of M as well as high spectral resolution requirements. As shown below, zero-tracking based on Newton's method can allow only selected zeros corresponding to the IFs to be updated.

B. Zero-Tracking Based On Newton's Method

A well-known numerical root finding method, *Newton's Method*, is very suitable for the underlying problem. Given the form of the polynomial (5), the i th root can be found by

$$z_i^{(k)} = z_i^{(k-1)} - \frac{f(z_i^{(k-1)})}{f'(z_i^{(k-1)})} \quad (11)$$

where k is the iteration number. If the initial guess of the root, $z_i^{(0)}$, is in the neighborhood of the exact root, then the Newton's method is quadratically convergent [8].

It is assumed that the IF corresponding to the i th root is changing over adjacent time samples such that the root at the n th time sample is in the neighborhood of the new root at time $n+1$. Newton's Method can then be applied by using the last root value as the initial guess in (11). Due to the quadratical convergence, the new root value, and subsequently the corresponding IF, will be quickly reached after very few iterations.

A situation may arise, however, in which the incorrect zero is tracked. This may occur if we start with an extraneous zero and follow its trajectory, or by starting with the correct zero and losing its trajectory to another

one, which is extraneous. In order to circumvent or mitigate this problem, we propose the following four guidance procedures.

- The Zero-Tracking Correction Technique

It is needed to find the exact roots corresponding to the IFs at the early stage of tracking and whenever tracking of the correct roots is lost due to fast changing IF or other problems. In this case, we use TFD and peak picking to identify the signal zeros.

- Power Monitor

To find out whether the tracking follows the wrong trajectory, we simply monitor the power of the signal at the IF $\omega_i(n)$.

$$P(\omega_i(n)) = \sum_{l=-L/2}^{L/2} R_f(n) e^{-j2\omega_i(n)l} \quad (12)$$

Whenever the power of a tracked IF is lower than a threshold, it is declared that the algorithm has lost the correct zero. The zero-tracking correction technique must then be applied.

- Loss of Resolution

Due to the finite extent of the LAF, or equivalently, the finite order of the polynomial in (5), two closely spaced IFs will be presented by one peak in the TFD, and subsequently, one zero in the corresponding polynomial. In this case, the two zero trajectories will merge into one. In time-varying environment, loss of resolution may, however, lasts for small periods of time. For example, in the case of two crossing chirps, only the vicinity of the intersection point may represent a resolution problem. Once the two chirps move farther apart, TFD should show two peaks corresponding to the autoterms, and subsequently the tracking algorithm should again yield two trajectories. When two zeros merge to one, we keep record of the merged peak value. Whenever the peak maximum value drops in half, the algorithm should go to the correction technique to find the exact roots.

- Convergence Monitor

A simple way to test the divergence of the *Newton's Method* is given in [8]. The inequality, $|f(x^k)| > |f(x^{k-1})|$, means that the root finding method has lost convergence. If this occurs, we need to apply the correction technique.

C. The Basic Algorithm

The complete version of the proposed zero-tracking algorithm is summarized as follows

- 1) At time n , perform the zero-tracking correction technique. Find the IFs and the corresponding roots $z_{n,i}$.
- 2) Calculate the new polynomial coefficients a_0, a_1, \dots, a_L at time $n+1$ using equation (4).

- 3) Calculate $f(z_{n,i})$ using (5), and $f'(z_{n,i})$ by

$$f(z_{n,i}) = a_1 + 2a_2 z_{n,i} + 3a_3 z_{n,i}^2 + \dots + La_L z_{n,i}^{L-1} \quad (13)$$

$$4) z_{n+1,i} = z_{n,i} - \frac{f(z_{n,i})}{f'(z_{n,i})}$$

- 5) Calculate $f(z_{n+1,i})$, and put $z_{n,i} = z_{n+1,i}$

- 6) If $|f(z_{n+1,i})| > |f(z_{n,i})|$ or $P(z_{n,i}) < \text{threshold}$, apply the correction technique in step 1).

- 9) If $z_{n,i}$ is equal to any other IF root, keep record of the maximum value of the merged peak until it drops in half, then apply the correction technique in step 1).

- 10) If $|f(z_{n+1,i})| < \text{accuracy threshold}$, go to the next time sample, and apply step 2), otherwise go to the step 3).

The calculation of zero-tracking in term of number of multiplication is approximately $4L$, where L is the number of roots. The time efficiency is linear.

4. SIMULATIONS

First, consider the case of single tone frequency hopping signal with SNR=20dB. We use Choi-Williams kernel applied to the LAF with $\sigma=1$ and $L=14$. The result is shown in Fig.1. The zero-tracking correction technique was used once for each hop.

Second, we use a single tone signal with a fast sinusoidal changing IF and high noise level, SNR=5dB. Again, Choi-Williams kernel with $\sigma=1$ and 14 roots is applied. The IF tracking is shown in Fig.2. In this example, the correction technique was used only once at the beginning of tracking.

Next, two component IFs are tested. The signal consists of two crossing chirps with SNR=20dB. To provide good spectral resolution, we use a polynomial of 30 roots and Choi-Williams kernel with $\sigma=10$. The two chirps are nicely tracked in Fig.3. The correction technique was only applied twice, at the initial phase and at the split point past the chirp crossing region.

CONCLUSION

Two zero-tracking algorithms have been introduced for instantaneous frequency estimation. Both algorithms operate on the local autocorrelation function of the time-frequency distribution and construct a polynomial whose zeros correspond to the IFs of the multicomponent signal. The zero trajectories of this polynomial are either provided by using the formula relating, to the first order approximation, the changes in the polynomial coefficients and roots, or by applying *Newton's method* for zero-finding.

Unlike TFDs, providing the IFs via the zero-trajectories of a polynomial whose coefficients are generated

from the LAF does not require the application of either FFT or peak finding techniques every time sample.

Computer simulations illustrating the performance of the zero-tracking algorithm using Newton's method under evolutionary and abrupt frequency changes are presented. All simulations demonstrate the fast tracking and convergence properties of the proposed algorithm when applied to LAFs of reduced interference distributions.

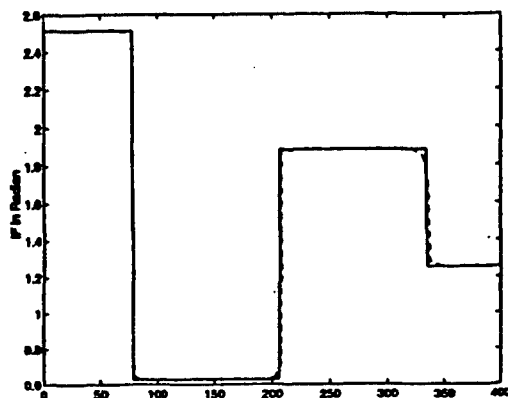


Fig.1 Frequency Hopping.
'.' is the exact IF, '- -' is the IF estimate.

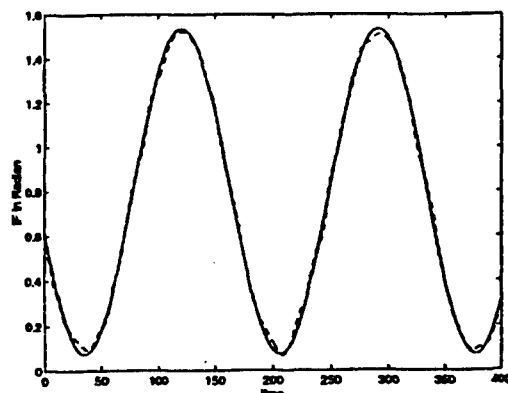


Fig.2 Sinusoidal IF.
'.' is the exact IF, '- -' is the IF estimate

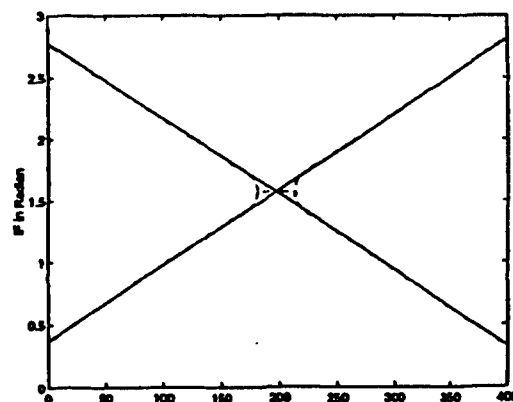


Fig.3 Two Crossing Chirps.
'.' is the exact IF, '- -' is the IF estimate.

References

- [1] L. Cohen, *Time-Frequency Analysis*, Prentice Hall, Englewood Cliffs, New Jersey, 1995.
- [2] F. Hlawatsch and G. F. Boudreaux-Bartels, "Linear and quadratic time-frequency signal representations," *IEEE Signal Processing Magazine*, pp.21-61, 1992.
- [3] B. Boashash, "Estimating and interpreting the instantaneous frequency of a signal," Parts 1 and 2, *Proceedings of the IEEE*, vol. 80, no. 12, December 1990.
- [4] B. Anderson and J. Moore, *Optimal Filtering*, Prentice Hall, Englewood, NJ, 1979.
- [5] L. White, "Adaptive tracking of frequency modulated signals using hidden markov models," *Workshop on Hidden Markov Models For Tracking*, Worrina Cove Resort, Feb. 1992.
- [6] S. Kay, "A fast and accurate single frequency estimator," *IEEE Transactions on Acoustics, Speech, and Signal Processing*, vol. 37, no. 12, December 1979.
- [7] S. J. Orfanidis and L. M. Vail, "Zero-tracking adaptive filters," *IEEE Transactions on Acoustics, Speech, and Signal Processing*, vol. 34, no. 6, December 1986.
- [8] L. W. Johnson and R. D. Riess, *Numerical Analysis*, Addison-Wesley Publishing Company, Inc. Philippines, 1977.

PERFORMANCE ANALYSIS OF INTERFERENCE EXCISIONS IN SPREAD SPECTRUM COMMUNICATIONS BASED ON INSTANTANEOUS FREQUENCY ESTIMATION

Chenshu Wang and Moeness G. Amin

Department of Electrical and Computer Engineering
Villanova University, Villanova, PA 19085
Email: amin@vill.edu

ABSTRACT

Interference excision in spread spectrum communication systems using time-frequency distributions (TFD) has been recently introduced to mitigate nonstationary interferers. The jammer instantaneous frequency (IF) is estimated and used to construct a time-varying notch filter which eliminates the jammer instantaneous energy. In this paper, we present the effects of the bias in the IF estimates on the receiver performance. Both cases of fixed and random frequency jamming signals are considered. It is shown that the bit error rate (BER) increases with the bias and is dependent on the jammer IF.

1. INTRODUCTION

The notion of applying time-frequency distributions to mitigate nonstationary interference in spread spectrum communications was introduced in [1] and has been successfully used to improve the receiver performance in time-varying jamming environment [2][3][4][5].

The TFD excision approach is based on estimating the instantaneous frequency of frequency modulated jammers using fixed kernels, such as Wigner-Ville and Choi-Williams [6], or data-dependent kernels using weighted least squares methods [7]. This information is then used to control the position of the notch of a short-length FIR filter, which excises the jammer energy over its instantaneous concentration.

Fig.1 shows the block diagram depicting the outlines of this approach. The excision notch filter is preferably of three or five coefficients, as longer filters become inappropriate for rapidly time-varying interferers. A bias in the estimation of the instantaneous frequency will however allow some of the jammer energy to escape to the filter output, causing an increase in the probability of bit errors. This bias may be the result of poor frequency resolution associated with using

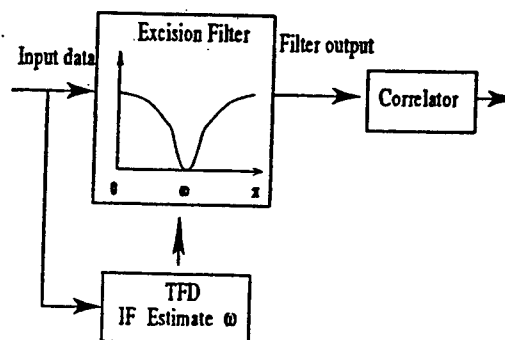


Fig.1 block diagram of the interference excision

insufficient number of DFT samples in implementing the TFD or due to the low jammer-to-signal and noise ratio.

In this paper, we present analysis which shows the effects of the imperfections of the TFDs on the receiver performance. The instantaneous bias is taken as a zero-mean white noise random process. Expressions of the filter output and the receiver SNR due to the jammer are derived for both three coefficient and five coefficient excision filters.

2. PERTURBATION ANALYSIS FOR A FIXED FREQUENCY JAMMER SIGNAL

2.1. Three-Coefficient Excision Filter

We consider the case of a sinusoidal jammer $J(n)$ with fixed frequency ω_0 , amplitude A and phase ϕ

$$J(n) = A \sin(\omega_0 n + \phi) \quad (1)$$

Let $\Delta\omega(n)$ denote the bias in the instantaneous frequency estimate at time n whose variance is σ_Δ^2 . This bias is independent of both the jammer and the PN sequence. The impulse response of the excision notch

filter at the n -th sample is therefore given by

$$h(n) = \delta(n+1) - 2\cos[\omega_0 + \Delta\omega(n)]\delta(n) + \delta(n-1) \quad (2)$$

The output of the filter due to the jammer is

$$J_o(n) = J(n) * h(n) = 2A\sin(\omega_0 n + \phi) \{\cos\omega_0 - \cos[\omega_0 n + \Delta\omega(n)]\}. \quad (3)$$

Below, we present two types of approximations to equation (3), both apply Taylor series expansion to the cosinusoidal term in (2). In each case, we derive expressions for the mean and the variance of the correlator output. First, consider the first order Taylor expansion

$$f(x) = f(x_0) + f'(x)|_{x=x_0}(x - x_0) + o(x - x_0). \quad (4)$$

Accordingly,

$$\cos[\omega_0 + \Delta\omega(n)] = \cos\omega_0 - \Delta\omega(n)\sin\omega_0 + o(\Delta\omega(n)), \quad (5)$$

and (3) becomes

$$J_o(n) \approx 2A\sin(\omega_0 n + \phi)\Delta\omega(n)\sin\omega_0 \quad (6)$$

For the second order Taylor expansion,

$$f(x) = f(x_0) + f'(x)|_{x=x_0}(x - x_0) + \frac{f''(x)}{2}(x - x_0)^2 + o[(x - x_0)^2] \quad (7)$$

In this case,

$$\cos[\omega_0 + \Delta\omega(n)] = \cos\omega_0 - \Delta\omega(n)\sin\omega_0 + \frac{\cos\omega_0}{2}|_{x=x_0}(x - x_0)^2 + o[(x - x_0)^2] \quad (8)$$

Using the expansion (8), equation (3) can be approximated by

$$J_o(n) \approx 2A\sin(\omega_0 n + \phi)[\Delta\omega(n)\sin\omega_0 + \Delta^2\omega(n)\frac{\cos\omega_0}{2}] \quad (9)$$

The correlator output due to the jammer is

$$U_j = \sum_{n=1}^L J_o(n)p(n) \quad (10)$$

Since $E[p(n)] = 0$, then $E[U_j] = 0$. The mean square value is given by

$$E[U_j^2] = E\left[\sum_{n=1}^L \sum_{k=1}^L J_o(n)J_o(k)p(n)p(k)\right] \quad (11)$$

Since $\Delta\omega(n)$ and $p(n)$ are independent, then

$$E[U_j^2] = E\left[\sum_{n=1}^L J_o^2(n)\right] \quad (12)$$

Using the first order approximation (5),

$$E[U_j^2] \approx \sum_{n=1}^L E[4A^2\sin^2\omega_0\sin^2(\omega_0 n + \phi)\Delta^2\omega(n)] \\ = 4A^2\sin^2\omega_0\sigma_\Delta^2\left[\frac{1}{2}L - \sum_{n=1}^L \frac{\cos(2\omega_0 n + 2\phi)}{2}\right] \quad (13)$$

For large value of L , the second term in the brackets in (13) can be ignored. Accordingly,

$$E[U_j^2] \approx 2LA^2\sin^2\omega_0\sigma_\Delta^2 \quad (14)$$

From (14) and the zero mean property, the variance of correlator output due to the jammer can be expressed as

$$\sigma_c^2 = E[U_j^2] - E[U_j]^2 \approx 2LA^2\sin^2\omega_0\sigma_\Delta^2 \quad (15)$$

which reaches a maximum value at $\omega_0 = \pi/2$. Similarly, it can be shown that using the second order approximation (9), the variance of the correlator output is

$$\sigma_c^2 \approx 2LA^2[\sin^2\omega_0 + 3\sigma_\Delta^2\frac{\cos^2\omega_0}{4}]\sigma_\Delta^2 \quad (16)$$

which, for low σ_Δ^2 , also reaches its maximum in the vicinity of $\omega_0 = \pi/2$.

2.2. Five-Coefficient Excision Filter

We assume the same jammer characteristics and bias conditions as in the three-coefficient filter case. In the underlying case, the filter impulse response has five nonzero coefficients obtained by convolving the filter response (2) with itself and is given by

$$h(n) = \delta(n+2) - 4\cos[\omega_0 + \Delta\omega(n)]\{\delta(n+1) + \delta(n-1)\} + \{2 + 4\cos^2[\omega_0 + \Delta\omega(n)]\}\delta(n) + \delta(n-2) \quad (17)$$

where the IF estimate bias is defined as before. It can be readily shown that the five coefficient excision filter output is

$$J_o(n) = J(n) * h(n) = 4A\sin(\omega_0 n + \phi) \{\cos\omega_0 - \cos[\omega_0 n + \Delta\omega(n)]\}^2. \quad (18)$$

Using the 1st order approximation (5), we obtain

$$J_o(n) \approx 4A\sin(\omega_0 n + \phi)[\Delta\omega(n)\sin\omega_0]^2 \quad (19)$$

While the second order approximation (8) yields

$$J_o(n) \approx 4A\sin(\omega_0 n + \phi)[\Delta\omega(n)\sin\omega_0 + \Delta^2\omega(n)\frac{\cos\omega_0}{2}]^2 \quad (20)$$

Similar to Section 2.1, $E[U_j] = 0$. The mean square value is

$$E[U_j^2] = E\left[\sum_{n=1}^L \sum_{k=1}^L J_o(n) J_o(k) p(n) p(k)\right] \quad (21)$$

$$E[U_j^2] = E\left[\sum_{n=1}^L J_o^2(n)\right] \quad (22)$$

Using approximation (19)

$$\begin{aligned} E[U_j^2] &\approx \sum_{n=1}^L E[16A^2 \sin^4 \omega_0 \sin^2(\omega_0 n + \phi) \Delta^4 \omega(n)] \\ &= 48A^2 \sin^4 \omega_0 \sigma_\Delta^4 \left[\frac{1}{2}L - \sum_{n=1}^L \frac{\cos(2\omega_0 n + 2\phi)}{2} \right] \end{aligned} \quad (23)$$

for $L \gg 1$,

$$E[U_j^2] \approx 24LA^2 \sin^4 \omega_0 \sigma_\Delta^4 \quad (24)$$

So, the variance of correlator output is

$$\sigma_c^2 \approx 24LA^2 \sin^4 \omega_0 \sigma_\Delta^4 \quad (25)$$

which reaches a maximum value at $\omega_0 = \pi/2$. It can be shown that using the 2nd order approximation (20), the variance of correlator output is

$$\begin{aligned} \sigma_c^2 &\approx 24LA^2 \left[\sin^4 \omega_0 + 15\sigma_\Delta^2 \frac{\cos^2 \omega_0 \sin^2 \omega_0}{2} + \right. \\ &\quad \left. 35\sigma_\Delta^4 \frac{\cos^4 \omega_0}{4} \right] \sigma_\Delta^4 \end{aligned} \quad (26)$$

As in the case of three coefficient filter, the behavior of the correlator output variance in (25) and (26) depends on the jammer frequency and becomes small at both low and high IF. Fig.2 shows the bit error rates versus the instantaneous jamming frequency with two different values of the frequency bias variance at the JSR of 50dB. In both cases, the highest probability of error occurs at and around $\pi/2$.

2.3. Overall SNR

Using the results in [1][3] and the 1st and 2nd order approximations (4) and (7), the receiver SNR for $L \gg 1$ can be respectively written as

$$SNR_{1st} = \frac{2L \cos^2 \omega_0}{2 + \sigma^2(1 + 2\cos^2 \omega_0) + A^2 \sigma_\Delta^2 \sin^2 \omega_0} \quad (27)$$

and

$$SNR_{2nd} = \frac{2L \cos^2 \omega_0}{\sigma_{n0}^2 + \sigma_{c0}^2} \quad (28)$$

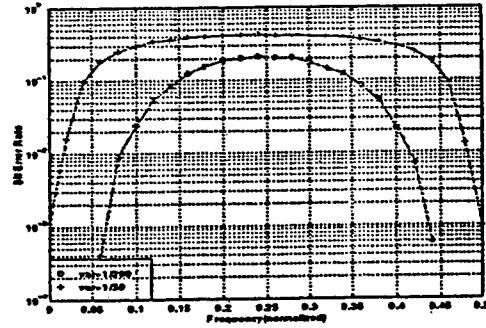


Fig.2 BER versus IF ($0-\pi$) with different σ_Δ^2

where

$$\sigma_{n0}^2 = 2 + \sigma^2(1 + 2\cos^2 \omega_0) \quad (29)$$

$$\sigma_{c0}^2 = A^2 \sigma_\Delta^2 (\sin^2 \omega_0 + 3\sigma_\Delta^2 \frac{\cos^2 \omega_0}{4}) \quad (30)$$

The corresponding expressions of (27) and (28) for the five coefficient excision filter are given by

$$SNR_{1st} = \frac{2L(1 + 2\cos^2 \omega_0)^2}{\sigma_{n1}^2 + \sigma_{c1}^2} \quad (31)$$

where

$$\sigma_{n1}^2 = 2 + 32\cos^2 \omega_0 + \sigma^2 + 16\sigma^2 \cos^2 \omega_0 + 2\sigma^2(1 + \cos^2 \omega_0)^2 \quad (32)$$

$$\sigma_{c1}^2 = 12A^4 \sigma_\Delta^4 \sin^4 \omega_0 \quad (33)$$

and

$$SNR_{2nd} = \frac{2L(1 + 2\cos^2 \omega_0)^2}{\sigma_{n2}^2 + \sigma_{c2}^2} \quad (34)$$

where

$$\sigma_{n2}^2 = 2 + 32\cos^2 \omega_0 + \sigma^2 + 16\sigma^2 \cos^2 \omega_0 + 2\sigma^2(1 + \cos^2 \omega_0)^2 \quad (35)$$

$$\begin{aligned} \sigma_{c2}^2 &= 12A^4 \sigma_\Delta^4 \left[\sin^4 \omega_0 + 15\sigma_\Delta^2 \frac{\cos^2 \omega_0 \sin^2 \omega_0}{2} + \right. \\ &\quad \left. 35\sigma_\Delta^4 \frac{\cos^4 \omega_0}{4} \right] \sigma_\Delta^4 \end{aligned} \quad (36)$$

3. PERTURBATION ANALYSIS FOR A RANDOM FREQUENCY JAMMER SIGNAL

In this case, we consider a sinusoidal jammer with random frequency uniformly distributed over $[0, \pi]$. But we assume that the jammer frequency is constant within the filter extent. So the correlator outputs of both the three-coefficient and five-coefficient filter are still the same as in Section 2.

The receiver SNR for the random frequency jammer can be derived using the same assumptions and

procedure followed in Section 2. Detailed analysis can be found in [8]. It can be readily shown that for three coefficient filter, $SNR_{1st} = SNR_{2nd} = 0$, and for five coefficient filter,

$$SNR_{1st} \approx \frac{L}{22/16 + 36/16\sigma^2 + 9/16A^2\sigma_\Delta^4} \quad (37)$$

$$SNR_{2nd} \approx \frac{L}{\sigma_{n3}^2 + \sigma_{c3}^2} \quad (38)$$

where

$$\sigma_{n3}^2 = 22/16 + 36/16\sigma^2 \quad (39)$$

$$\sigma_{c3}^2 = 9/16A^2\sigma_\Delta^4(45/2\sigma_\Delta^2 + 315/16\sigma_\Delta^4) \quad (40)$$

4. SIMULATIONS

Fig.3 compares the bit error rates in the case of sinusoidal jamming with different fixed normalized frequencies using 128 chips/bit for the five-coefficient excision filter. The IF bias variance is $\pi/50$. It is clear that the BER curve at $IF = 0.25(2\pi)$ gives the poorest performance, consistent with the analytical results given in Section 2.

Fig.4 compares the bit error rates in the same case as in Fig.3, but under a fixed IF bias of $\pi/100$.

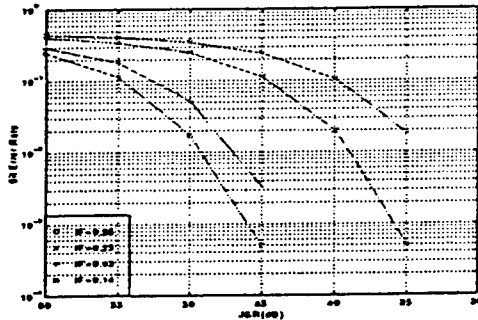


Fig.3 BER for random IF bias

5. CONCLUSIONS

In this paper, we have presented analysis of the effect of bias in the IF estimation on a TFD based spread spectrum receiver. As the IF defines a notch filter, which acts as a preprocessing interference excision system, a bias in the IF will prevent a total removal of the instantaneous jammer energy and as such, increases the probability of bit error.

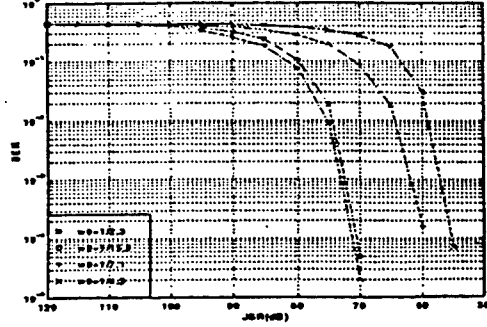


Fig.4 BER for fixed IF bias

6. REFERENCES

- [1] M. G. Amin, "Interference excision in spread spectrum communication systems using time-frequency distributions," *Technical Report, Rome Lab*, Sept. 1994.
- [2] S. Tyler and M.G. Amin, "Mitigating interference in direct sequence spread spectrum communication systems," *Rome Lab Technical Journal*, June 1995.
- [3] M. G. Amin, G. Venkatesan, and S. Tyler, "A new approach for spread using time-frequency distributions," in *Proceedings of the SPIE Conference on Advanced Algorithms and Architectures for Signal Processing*, San Diego, CA, July 1995.
- [4] S. Roberts and M. G. Amin, "Linear vs. bilinear time-frequency methods for interference mitigation in direct sequence spread spectrum communication systems," in *Proceedings of the Asilomar Conference*, Pacific Grove, CA, Nov. 1995.
- [5] M. G. Amin, A. Lindsey, and C. Wang, "On the application of time-frequency distributions in the excision of pulse jamming in spread spectrum communication systems," *IEEE Workshop on SSAP*, Greece, June 1996.
- [6] L. Cohen, *Time-Frequency Analysis*. Prentice Hall, Englewood Cliffs, New Jersey, 1995.
- [7] M. G. Amin, G. Venkatesan and J. Carroll, "A constrained weighted least squares approach for time-frequency kernel design," *IEEE Transactions on Signal Processing*, May 1996.
- [8] M. G. Amin and C. Wang, "Statistical analysis of tfd-based interference excision systems in ss communications," *Technical Report, Rome Lab*, July 1996.

Spatial Time-Frequency Distributions and Array Signal Processing for DSSS Communications

Jammer Mitigation in Spread Spectrum Communications Using Blind Source Separation.

Adel Belouchrani and Moeness G. Amin

* Electrical and Computer Engineering Departement,
Ecole Nationale Polytechnique, El Harrach 16200, Algiers, Algeria.

** Department of Electrical and Computer Engineering,
Villanova University, Villanova PA 19085 USA

Fax: (610) 519-4436, E-mail: moeness@ece.vill.edu

Abstract

This paper introduces a new approach for interference rejection in direct sequence spread spectrum communication systems based on blind source separation techniques. These techniques strive to separate the interference from the desired signal and as such produce the spread spectrum signal with reduced jammer contamination. The proposed approach is robust under multipath and array imperfections. The paper presents the performance analysis and evaluation of the spread spectrum receiver incorporating the blind source separator. Closed form expressions of the receiver SNR using the proposed preprocessing scheme are derived. A numerical example, including the bit error rates, is provided to illustrate the effectiveness of the blind source separation-based interference mitigation approach.

Key words : Interference mitigation, Spread spectrum communications, Blind source separation, Performance analysis.

I. Introduction

One of the most important applications of direct sequence (DS) spread spectrum (DS/SS) communications is that of interference mitigation. A DS/SS system is defined as one in which the transmitted signal is spread over a bandwidth much wider than the minimum bandwidth necessary to transmit the information [1], by means of a code independent of the data. The availability of this code at the receiver enables despreading and recovery of data, while spreading and suppression of interference. The processing gain of an DS/SS system, generally defined as the ratio between the transmission and data bandwidths, provides the system with a high degree of interference suppression. In fact, any

Dr. Moeness Amin's work is supported by Rome Lab, NY, contract # F30602-96-C-0077.

form

$$s(t) = \sum_{k=-\infty}^{\infty} b_k m_k(t - kT), \quad (2)$$

where $m_k(t) = \sum_{l=1}^L c_l^k p(t - (l-1)T_c)$ with T^{-1} the data (bit) rate, and T_c^{-1} the chip rate. The integer $L = T/T_c$ is the number of chips per bit (SS processing gain). $\{b_k\}$ and $\{c_l^k\}_{l=1,\dots,L}$ represent the k -th bit data sequence and the corresponding chip sequence, and $p(t)$ is the chip pulse. The chip sequence (the PN spreading code) is a pseudo-random signal which is known by both the transmitter and the receiver. The matrix A , which in general corresponds to the steering matrix, is assumed to be full column rank, but otherwise is unknown in structure. This relaxation is important to handle interference multipath.

III. A New Interference Mitigation Design

The block diagram shown in Fig.1 illustrates the proposed spread spectrum communication system. The standard spread spectrum demodulation is augmented by a preprocessor, which consists of a separator followed by a selector. The separator acts on separating the interference from the signal by utilizing the spatial diversity provided by the multi-sensor array. This separation can be performed only up to a permutation. Hence, a selection device is needed to label the separated waveforms as signal and jammer. The demodulation process recovers the original data by despreading the selected (desired) signal, while spreading the background noise and any interference component which might have not been separated from the signal. In the following, we describe each processing step.

Separation The separation of the signal from the interference is achieved by using blind source separation techniques. These techniques strive to recover the source vector $y(t)$ from the array output $x(t)$ *without the knowledge of matrix A*. The benefit of such a 'blind' processing is that the separation is essentially unaffected by errors in the propagation model or in array calibration. Source separation techniques are based on the assumption of statistical independence of the source signals.

Various algorithms have been proposed for the blind source separation [5, 6]. In this paper, we only focus on the so called SOBI (Second Order Blind Identification) algorithm [7]. This algorithm is based on the simultaneous diagonalization of a combined set of spatio-temporal correlation matrices of the received signals (for more details see reference [7]).

It is well established that there is two inherent ambiguities in the blind source separation problem, irrespective of the employed technique. First, there is no direct or indirect way of knowing

the original labeling of the sources, hence any permutation of the estimated sources is also a satisfactory solution. The second ambiguity is that it is impossible to uniquely identify the source signals. This is because the exchange of a fixed scalar factor between a source signal and the corresponding column of the mixture matrix \mathbf{A} does not affect the observations. Hence, the blind source separation is a technique for recovering the source signals up to a fixed permutation and complex scalar multiplication.

Selection Because of the inherent ambiguity stated above, a selector at the output of the separator is necessary to identify the desired signal for postprocessing. For this purpose, several strategies can be considered. The selection can be based on the signature of the desired signal which may be known by the receiver. As such, the problem of the selection becomes a pure problem of signal classification [8]. Note that the classical adaptive array interference nulling algorithm also requires some a priori information on the desired signal before processing.

Spread Spectrum Demodulation This last step consists of despreading the selected signal for recovering the original data bit sequence $\{b_k\}$. This is accomplished by the correlation of the received signal with a synchronized replica of the spreading signal $\{c_l^k\}_{l=1,\dots,L}$ used to spread the information. While the correlator despreads the desired signal, it spreads any interference components which might have escaped to the desired signal in the separation process.

IV. Analysis

Throughout the following analysis, the additive noise is assumed to be a zero mean white Gaussian complex circular process with variance σ_w^2 . The desired signal $s(t)$ and the jammer $j(t)$ are treated as if they have unit power. The actual dynamic range of both waveforms are accounted for by the magnitude of the corresponding columns of the steering matrix \mathbf{A} . Hence, matrix \mathbf{A} has the following structure:

$$\mathbf{A} = \begin{bmatrix} \sigma_s & \sigma_j \\ \sigma_s e^{j\theta_s} & \sigma_j e^{j\theta_j} \end{bmatrix} \quad (3)$$

where σ_s^2 and σ_j^2 represent the powers of the signal $s(t)$ and the jammer $j(t)$, respectively, and θ_s and θ_j are their corresponding directions-of-arrival.

Further, in the analysis herein, we assume the transmission of the information bit "1", i.e., $s(n) = c(n)$, and a narrowband jammer of the form: $j(n) = e^{j\omega n + \phi}$, where ω is the jammer frequency and the phase ϕ is a uniform random variable. The receiver SNR is defined as the ratio of the square

of the mean to the variance of the correlator output U [4],

$$SNR = \frac{|E[U]|^2}{Var[U]} \quad (4)$$

where $U = \sum_{n=1}^L r(n)c(n)^*$. In the above equation, $r(n)$ is the sampled version of the correlator input, $c(n)$ is a zero-mean complex circular i.i.d. chip sequence such that $|c(n)|^2=1$ and L is the length of the chip sequence per information bit. Note that the decision of receiving 1 or -1 is based on the sign of the real part of U [9].

Pre-processor Disabled When no DS/SS signal-interference separation is performed, the input to the correlator (the received signal) is the average of the sensor outputs,

$$r(n) = \frac{1}{2}[x_1(n) + x_2(n)] \quad (5)$$

In this case, the correlator output is given by

$$U = \frac{1}{2} \sum_{n=1}^L [x_1(n) + x_2(n)]c(n)^* \quad (6)$$

The uncorrelation between the zero mean PN sequence and both the jammer and noise sequences, along with the properties of the white noise process, is used below to obtain the mean and variance expressions of the correlator output U ,

$$E[U] = \frac{1}{2}\sigma_s(1 + e^{j\theta_s})L \quad (7)$$

$$Var[U] = \frac{L}{2}[\sigma_j^2(1 + \cos(\theta_j)) + \sigma_w^2] \quad (8)$$

According, the correlator SNR is

$$SNR_{off} = \frac{(1 + \cos(\theta_s))\sigma_s^2 L}{(1 + \cos(\theta_j))\sigma_j^2 + \sigma_w^2} = \frac{(1 + \cos(\theta_s))L}{(1 + \cos(\theta_j))JSR + \frac{1}{SNR}} \quad (9)$$

where JSR and SNR are the jammer-to-signal and signal-to-noise ratios, respectively. Since (5) amounts to a beamformer with unit coefficients, then, for a given jammer position, the correlator SNR reaches a maximum value for a broadside desired signal arrival. Adversely, SNR_{off} reaches a minimum value for a given DOA of the desired signal when the jammer DOA is perpendicular to the array. The correlator SNR using only one array sensor and without applying any auxiliary interference excision scheme is

$$SNR_{one} = \frac{L\sigma_s^2}{\sigma_j^2 + \sigma_w^2} = \frac{L}{JSR + \frac{1}{SNR}} \quad (10)$$

Therefore, the SNR improvement factor achieved via the use of 2-sensor array is the array gain,

$$\nu_1 = \frac{SNR_{off}}{SNR_{one}} = \frac{(1 + \cos(\theta_s))(JSR + \frac{1}{SNR})}{(1 + \cos(\theta_j))JSR + \frac{1}{SNR}} \quad (11)$$

whose maximum value is $\nu_1 \approx 2$, i.e., 3 dB improvement.

Pre-processor Enabled When the SS signal/interference separation is performed, the correlator input is the selected signal

$$\begin{aligned}
r(n) = \hat{s}(n) &= [\hat{\mathbf{A}}^{-1}\mathbf{x}(n)]_1 \\
&= [\hat{\mathbf{A}}^{-1}\mathbf{A}]_{11}s(n) + [\hat{\mathbf{A}}^{-1}\mathbf{A}]_{12}j(n) + \{[\hat{\mathbf{A}}^{-1}\mathbf{A}]_{11}[\mathbf{A}^{-1}]_{11} + [\hat{\mathbf{A}}^{-1}\mathbf{A}]_{12}[\mathbf{A}^{-1}]_{21}\} \\
&\quad w_1(n) + \{[\hat{\mathbf{A}}^{-1}\mathbf{A}]_{11}[\mathbf{A}^{-1}]_{12} + [\hat{\mathbf{A}}^{-1}\mathbf{A}]_{12}[\mathbf{A}^{-1}]_{22}\}w_2(n)
\end{aligned} \tag{12}$$

The mixing matrix $\hat{\mathbf{A}}$ is estimated by the SOBI algorithm using K correlation matrices. In the following analysis, we make use of the performance study of SOBI algorithm as derived in [7]. Hence, at the first order approximation, we have:

$$[\hat{\mathbf{A}}^{-1}\mathbf{A}]_{11} \approx 1 \tag{13}$$

$$[\hat{\mathbf{A}}^{-1}\mathbf{A}]_{12} \approx \frac{-1}{2} \sum_{|k| \leq K, k \neq 0} \frac{\rho_k^*}{|\rho|^2} [\mathbf{A}^{-1}\delta\mathbf{R}(k)\mathbf{A}^{-1H}]_{12} \tag{14}$$

where $\rho = [\rho_1, \dots, \rho_K]$, $\rho_k = E[j(n)j(n-k)^*]$, for $k = 1, \dots, K$, and $\delta\mathbf{R}(k) = \hat{\mathbf{R}}(k) - \mathbf{R}(k)$ with $\hat{\mathbf{R}}(k) = \frac{1}{L} \sum_{n=1}^L \mathbf{x}(n)\mathbf{x}(n-k)^*$ and $\mathbf{R}(k) = E[\mathbf{x}(n)\mathbf{x}(n-k)^*] = \mathbf{A}\mathbf{A}^H$, for $k \neq 0$.

Incorporating the three different components of the array outputs in equation (14), it can be readily shown that

$$[\hat{\mathbf{A}}^{-1}\mathbf{A}]_{12} = \frac{-1}{2L} \sum_{|k| \leq K, k \neq 0} \frac{\rho_k^*}{|\rho|^2} \sum_{n=1}^L [s(n) + N_1(n)][j(n-k) + N_2(n-k)]^* \tag{15}$$

where $N_1(n) = \frac{1}{\sigma_s(e^{j\theta_j} - e^{j\theta_s})} [e^{j\theta_j} w_1(n) - w_2(n)]$ and $N_2(n) = \frac{1}{\sigma_j(e^{j\theta_s} - e^{j\theta_j})} [e^{j\theta_s} w_1(n) - w_2(n)]$.

From (12), (13) and (15), the received signal is

$$r(n) = [s(n) + N_1(n)] - \frac{1}{2L} \sum_{|k| \leq K, k \neq 0} \frac{\rho_k^*}{|\rho|^2} \sum_{m=1}^L [s(m) + N_1(m)][j(m-k) + N_2(m-k)]^* [j(n) + N_2(n)] \tag{16}$$

It is appropriate to partition U into two components, one is interference-free and the other is interference-dependent, which becomes zero when the jammer is absent. That is,

$$U = \sum_{n=1}^L r(n)c(n)^* = U_1 + U_2, \tag{17}$$

$$U_1 = \sum_{n=1}^L [c(n) + N_1(n)]c(n)^* \tag{18}$$

$$U_2 = \frac{-1}{2L} \sum_{|k| \leq K, k \neq 0} \frac{\rho_k^*}{|\rho|^2} \sum_{n=1}^L \sum_{m=1}^L [c(m) + N_1(m)][j(m-k) + N_2(m-k)]^* [j(n) + N_2(n)]c(n)^* \tag{19}$$

It can then be shown that the mean and variance of the correlator output U are given by ,

$$E[U] = L - 1 \quad (20)$$

$$Var[U] = \gamma_0 + \gamma_1 \sigma_w^2 + \gamma_2 \sigma_w^4 + \gamma_3 \sigma_w^6, \quad (21)$$

$$\gamma_0 = 1 - \frac{1}{L} \quad (22)$$

$$\gamma_1 = \frac{1}{\sigma_j^2(1 - \cos(\theta_s - \theta_j))} \left[1 + \frac{\sigma_j^2}{\sigma_s^2} \left(L - 1 + \frac{1}{2K} \right) + \frac{1}{L} \left\{ \frac{\sigma_j^2(3 + \cos(\theta_s - \theta_j))}{2\sigma_s^2} + 2 - \frac{1}{2K} \right\} - \frac{K+1}{L^2} \right]$$

$$\gamma_2 = \frac{1}{\sigma_j^4(1 - \cos(\theta_s - \theta_j))^2} \left[\frac{1}{2K} + \frac{\sigma_j^2}{\sigma_s^2} \left(1 + \frac{1}{2K} \right) + \frac{1}{L} \left\{ \frac{1}{2K} + \frac{\sigma_j^2}{\sigma_s^2} \left(1 + \frac{1}{2K} + \frac{(3 + \cos(\theta_s - \theta_j))}{4K} \right) \right\} - \frac{1}{L^2} \left\{ \frac{K+1}{4K} + \frac{\sigma_j^2}{\sigma_s^2} (K+1) \left(1 + \frac{1}{4K} \right) \right\} \right]$$

$$\gamma_3 = \frac{1}{\sigma_j^6(1 - \cos(\theta_s - \theta_j))^3} \left[\frac{1}{2K} \frac{\sigma_j^2}{\sigma_s^2} \left\{ 1 - \frac{2}{L} + \frac{K+1}{2L^2} \right\} \right]$$

From (20) and (21), the correlator output signal-to-noise ratio is

$$SNR_{on} = \frac{(L-1)^2}{\gamma_0 + \gamma_1 \sigma_w^2 + \gamma_2 \sigma_w^4 + \gamma_3 \sigma_w^6} \quad (23)$$

It is noteworthy that the above analysis hold as well for coherent arrivals. In this case, the vector $[\sigma_j \sigma_j e^{j\theta_j}]^T$ in (3) represents the generalized steering vector (spatial signature) associated to the jammer and all of its multipath.

A. Remarks

In the case of a noise free channel, equations (9) and (23) become,

$$SNR_{on} = \frac{(L-1)^2}{\gamma_0}, \quad SNR_{off} = \frac{(1 + \cos(\theta_s))\sigma_s^2 L}{(1 + \cos(\theta_j))\sigma_j^2} \quad (24)$$

According to (24), SNR_{on} is independent of the array geometry, the jammer power, and the number of correlation matrices used in the SOBI algorithm. This invariance property is not satisfied when the pre-processor is disabled, as shown by SNR_{off} . Note from (23) that for small jammer power, the detection becomes sensitive to noise through γ_1 , γ_2 and γ_3 . However, as the jammer power σ_j^2 increases, the SNR_{on} increases, leading to conclude that *the higher the jammer power the better the detection*. For $L \gg 1$ and high SNR, the receiver SNR improvement factor using a two-sensor array and SOBI over one-array element is

$$\nu_2 = \frac{SNR_{on}}{SNR_{one}} \approx L(JSR) \quad (25)$$

whereas the receiver SNR improvement factor with/without SOBI in a two-element array is

$$\nu_3 = \frac{SNR_{on}}{SNR_{off}} \approx L \frac{(1 + \cos(\theta_j))}{(1 + \cos(\theta_s))} (JSR) \quad (26)$$

It is clear that $\nu_2 = \nu_3$ for $\theta_s = \theta_j$, as expected. In figure 2, we plot expressions (23) and (9) versus the number of chips/bit, for $\theta_s = 0^\circ$, $\theta_j = 9^\circ$ and $K=4$.

V. Numerical Example

Consider a uniform linear array of 2 sensors separated by half a wavelength. The desired signal is a BPSK arriving at $\theta_0 = 0^\circ$. The jammer is composed of a chirp signal whose frequencies are $\omega_1 = 0.1\pi$ and $\omega_2 = 0.6\pi$. The direct path of the jammer arrives at $\theta_1 = 2^\circ$ whereas its multipath arrive at $\theta_2 = 10^\circ$ and $\theta_3 = -10^\circ$, respectively. The noise used is zero-mean white Gaussian process. The first four lags spatio-temporal correlation matrices are considered in the SOBI algorithm. Figure 3 presents the Bit Error Rate (BER) in dB versus JSR for 0 dB SNR and 8 chips/bit, 16 chips/bit, 32 chips/bit and 64 chips/bit. For 32 chips/bit and 64 chips/bit, the proposed method offers no error over 10^6 runs for JSR up to 90 dB. The BER is remarkably reduced under the proposed method.

VI. Conclusions

In this paper, we have introduced a new jammer mitigation scheme for spread spectrum communications. Blind source separation techniques are applied to increase the rejection capability of the direct sequence SS communication systems. The main motivation behind the proposed approach is to further immune the DS/SS system against strong interference and its multipath. The later is most appropriately handled by blind source separation methods, which do not lead to reduced array aperture, as in the case of spatial averaging methods. With the inclusion of blind source separation methods, the overall DS/SS receiver consists of a signal separator, selector, despreader followed by a detector. Closed form expressions of the receiver signal-to-noise ratios have been derived. BER curves were provided for multipath and coherent signal environment. These curves clearly show the significant reduction in bit error rates when employing blind source separations.

References

- [1] M. K. Simon, et al, *Spread Spectrum Communication*. Computer Science Press, 1985.

- [2] L. Milstein, "Interference rejection techniques in spread spectrum communications," *Proceedings of the IEEE*, vol. 66, pp. 657-671, June 1988.
- [3] B. D. Van Veen and K. M. Buckley, "Beamforming: A versatile approach to spatial filtering," *IEEE SP Magazine*, pp. 4-24, Apr. 1988.
- [4] J. Ketchum and J. Proakis, "Adaptive algorithms for estimating and suppressing narrow band interference in PN spread spectrum systems," *IEEE Trans. on Comm.*, vol. 30, pp. 913-924, May 1982.
- [5] P. Comon, "Independent component analysis," in *Proc. Int. Workshop on Higher-Order Stat., Chamrousse, France*, pp. 111-120, 1991.
- [6] M. Gaeta and J.-L. Lacoume, "Source separation without a priori knowledge: the maximum likelihood solution," in *Proc. EUSIPCO*, pp. 621-624, 1990.
- [7] A. Belouchrani and K. Abed Meraim and J.-F. Cardoso and E. Moulines, "A blind source separation technique using second order statistics," *IEEE Trans. on SP*, vol. 45, pp. 434-444, Feb. 1997.
- [8] L. Dominguez, J. Borrallo, J. Garcia, "A general approach to the automatic classification of radiocommunication signals," *Signal Processing*, vol. 22, pp. 239-250, Mar. 1991.
- [9] A. W. Lam and F. M. Ozluturk, "Performance bounds for DS/SSMA communications with complex signature sequences," *IEEE Trans. on Comm.*, vol. 40, pp. 1607-1614, Oct. 1992.

- [2] L. Milstein, "Interference rejection techniques in spread spectrum communications," *Proceedings of the IEEE*, vol. 66, pp. 657-671, June 1988.
- [3] B. D. Van Veen and K. M. Buckley, "Beamforming: A versatile approach to spatial filtering," *IEEE SP Magazine*, pp. 4-24, Apr. 1988.
- [4] J. Ketchum and J. Proakis, "Adaptive algorithms for estimating and suppressing narrow band interference in PN spread spectrum systems," *IEEE Trans. on Comm.*, vol. 30, pp. 913-924, May 1982.
- [5] P. Comon, "Independent component analysis," in *Proc. Int. Workshop on Higher-Order Stat., Chamrousse, France*, pp. 111-120, 1991.
- [6] M. Gaeta and J.-L. Lacoume, "Source separation without a priori knowledge: the maximum likelihood solution," in *Proc. EUSIPCO*, pp. 621-624, 1990.
- [7] A. Belouchrani and K. Abed Meraim and J.-F. Cardoso and E. Moulines, "A blind source separation technique using second order statistics," *IEEE Trans. on SP*, vol. 45, pp. 434-444, Feb. 1997.
- [8] L. Dominguez, J. Borrillo, J. Garcia, "A general approach to the automatic classification of radiocommunication signals," *Signal Processing*, vol. 22, pp. 239-250, Mar. 1991.
- [9] A. W. Lam and F. M. Ozluturk, "Performance bounds for DS/SSMA communications with complex signature sequences," *IEEE Trans. on Comm.*, vol. 40, pp. 1607-1614, Oct. 1992.

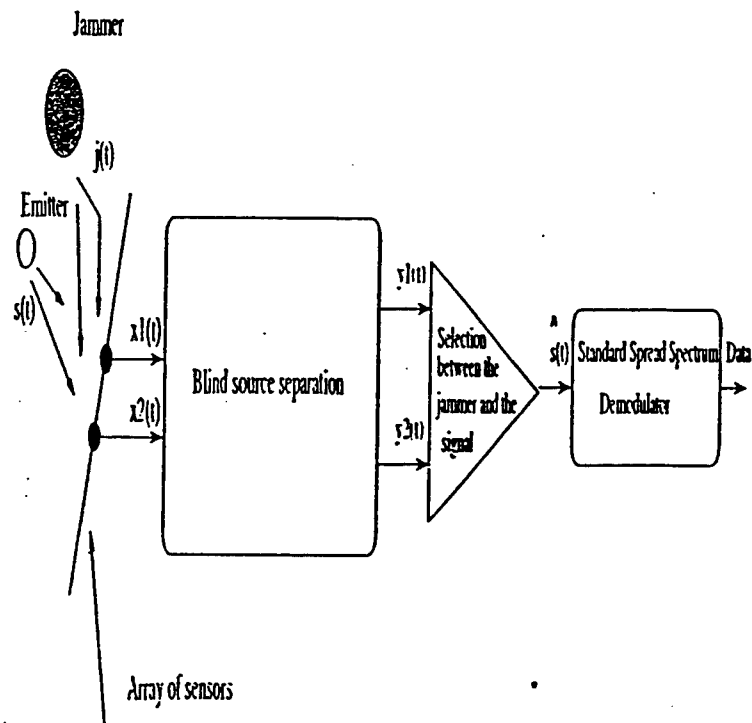


Figure 1: Spread spectrum system using blind source separation.

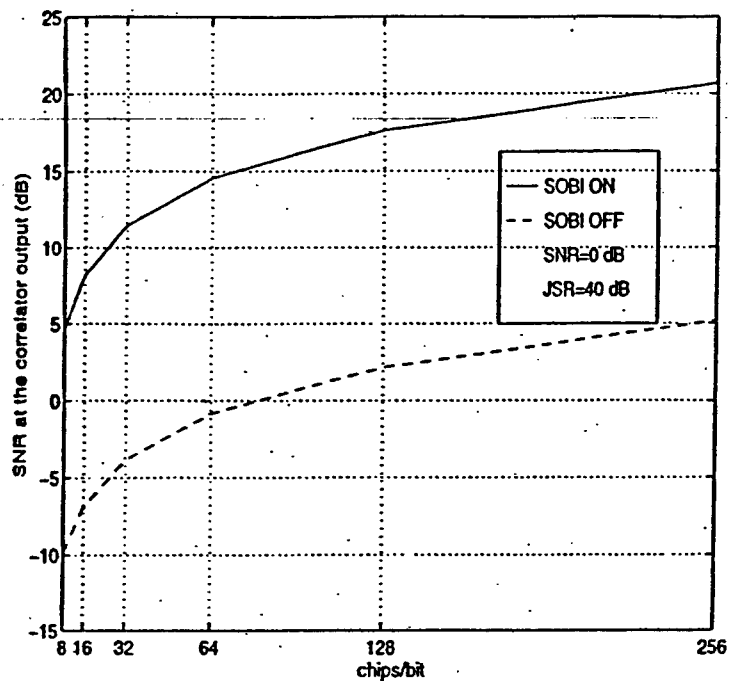


Figure 2: SNR at the correlator output in dB vs chips/bit.

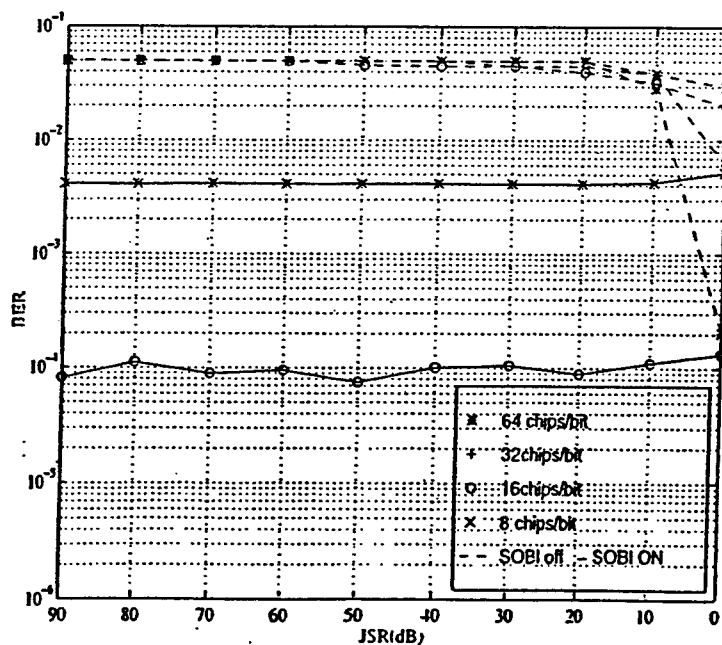


Figure 3: BER in (dB) vs JSR

A Two-Sensor Array Blind Beamformer for Direct Sequence Spread Spectrum Communications

Adel Belouchrani, *Member, IEEE*, and Moeness G. Amin, *Senior Member, IEEE*

Abstract—In this paper, we present an efficient blind beamformer dedicated to the problem of interference mitigation in direct sequence spread spectrum (DSSS) communication systems using a two sensor array. A closed-form solution for the blind identification of the communication channel is derived by exploiting the temporal properties of the desired signal and the interference. The optimal beamformer is derived from the maximization of the signal-to-interference and noise ratio (SINR) at the output of the receiver in terms of the blindly estimated channel coefficients. Three structures of the DSSS receiver are presented. One structure consists of the blind beamformer followed by the spread spectrum demodulator. The other two structures consist of the spread spectrum demodulator followed by the blind beamformer. The performance of these structures is discussed in terms of the achieved SINR and the computational cost. Simulation results are provided to illustrate the effectiveness of the proposed blind beamformers in interference excision.

Index Terms—Author, please supply index terms. E-mail keywords@ieee.org for info.

I. INTRODUCTION

THE RECENT developments of spread spectrum communications [1], [2] and digital beamforming [3], [4] provides a formidable set of technologies for jammer resistance systems. These technologies are compatible and often used in the same system [5], [6]. The integration of these two technologies can be achieved by cascading their corresponding processing techniques, that is, the multidimensional problem can be first translated into a single dimension problem via beamforming, where the sensor array outputs are weighted and added to attenuate a strong jammer signal received by the multisensor antenna array. Spread spectrum techniques [7] may then be employed to neutralize large numbers of weak jammers that may not be totally eliminated by the spatial filtering implemented by the beamformer. A different order of cascade is to first apply the spread spectrum techniques at the output of each sensor followed by spatial filtering. This paper investigates the performance of these two approaches in terms of both the computational cost and the achieved receiver SINR. For this purpose, new beamformers dedicated to the problem of a single jammer mitigation in DSSS communications systems

using a two-sensor array according to the two aforementioned approaches are proposed.

Several beamforming approaches have been proposed in the literature. Unfortunately, these methods may have significant drawbacks in practice. Methods requiring direction-finding and array calibration often fail in coherent environments and for unknown array manifolds. Herein, we consider blind beamforming techniques that are robust under multipath and array imperfections [8].

The main contribution of this paper is the derivation of a closed-form solution for the blind identification of the communication channel by exploiting the whiteness property of the desired signal and the coherence property of the interference. The two sensor optimum beamformer weights are derived from the maximization of the SINR at the output of the receiver. The DSSS receiver is implemented in two different structures. One structure consists of the blind beamformer followed by the spread spectrum demodulator. In the other structure, the cascading order is reversed where the spread spectrum demodulators are applied at both sensors, and the results are then processed by a blind beamformer. The performance of the each structure is discussed in terms of the achieved SINR and the computational cost.

The paper is organized as follows. In Section II, the system model is described, and the relevant assumptions are stated. A closed-form expression of the estimated communication channel is derived in Section III.

II. PROBLEM FORMULATION

A. Data Model

The DSSS communication system under consideration employs binary phase-shift-keying (BPSK) for both chip and data modulation. An array of two sensors receiving the signals from two sources [an i.i.d. desired signal and a temporally correlated jammer (\mathcal{H}_1)]¹ is considered. The array output vector $\mathbf{x}(t)$ is two-dimensional (2-D) and is expressed by the low-rank model [8]

$$\mathbf{x}(t) = \mathbf{H}\mathbf{y}(t) + \mathbf{n}(t), \quad \mathbf{y}(t) = [s(t) \ j(t)]^T \quad (1)$$

where $\mathbf{y}(t)$ is the signal vector whose entries are $s(t)$ and $j(t)$, which represent the desired signal and the jammer signal, respectively. The superscript T denotes the transpose

¹In some military applications, this assumption is often verified when the spread spectrum signal is white in the baseband and the jammers are narrowband.

Manuscript received August 7, 1997; revised February 8, 1999. This work was supported in part by Rome Laboratory Contract F 30602-96-C-0077 and by the Office of Naval Research under Grant N00014-98-1-0176. The associate editor coordinating the review of this paper and approving it for publication was Dr. Eric Moulines.

The authors are with the Department of Electrical and Computer Engineering, Villanova University, Villanova, PA 19085 USA (e-mail: moeness@ece.vill.edu).

Publisher Item Identifier S 1053-587X(99)05418-5.

the signal direct path and all its multipaths. The desired signal, the jammer signal, and the noise components are assumed uncorrelated $\mathcal{H}(3)$. In the baseband, the desired signal $s(t)$ has the form

$$s(t) = \sum_{k=-\infty}^{\infty} b_k m_k(t - kT) \quad (2)$$

$$m_k(t) = \sum_{l=1}^L c_l^k p(t - (l-1)T_c) \quad (3)$$

In (2) and (3), T^{-1} is the data (bit) rate, and T_c^{-1} is the chip rate. The integer $L = T/T_c$ is the number of chips per bit (SS processing gain). $\{b_k\}$ and $\{c_l^k\}_{l=1, \dots, L}$ represent the k th bit data sequence, and the corresponding chip sequence and $p(t)$ is the chip pulse. The chip sequence is a pseudorandom signal that is known to both the transmitter and the receiver. Perfect synchronization between the transmitter and the receiver chip sequences is assumed.

The multiplicative nature of the low-rank model (1) is valid for small delay spread, i.e., when the relative time delays for different propagation paths are small compared with the inverse of the bandwidth of each signal arrival. This assumption is often satisfied under local scattering conditions. Moreover, model (1) assumes the signal complex envelop received by each sensor is identical except for phase and possibly amplitude differences that depend on path angle-of-arrival. This is typically the case when the inverse signal bandwidth is large compared with the travel time across the array.

B. Blind Identification

In the blind context, a full identification of the channel matrix \mathbf{H} is impossible because the exchange of a fixed scalar factor between a given signal and its corresponding channel vector does not affect the observations

$$\mathbf{x}(t) = \mathbf{H}\mathbf{y}(t) + \mathbf{n}(t) = \sum_{k=1}^2 \frac{h_k}{\alpha_k} \alpha_k y_k(t) + \mathbf{n}(t) \quad (4)$$

where α_i is an arbitrary complex factor. It is assumed without any loss of generality that

$\mathcal{H}(4)$ the waveforms $s(t)$ and $j(t)$ are treated as if they have unit variance so that their dynamic range is accounted for by the magnitude of the corresponding channel vector;

$\mathcal{H}(5)$ the first entries of the channel vectors \mathbf{h}_k , $k = 1, 2$ are real and positive, i.e.,

$$h_{k1} = h_{k1}^*, \quad h_{k1} > 0 \quad k = 1, 2 \quad (5)$$

where the superscript $*$ denotes the complex conjugate operator. These conventions are shown to be convenient in the sequel. If $h_{k1} = 0$, $k = 1, 2$, then the first sensor neither receives the jammer or the desired signal. In this case, the spatial dimension provided by the two-sensor array will not improve jammer excision.

C. Receiver Design

The block diagrams shown in Figs. 1–3 illustrate the three structures of the proposed spread spectrum communication

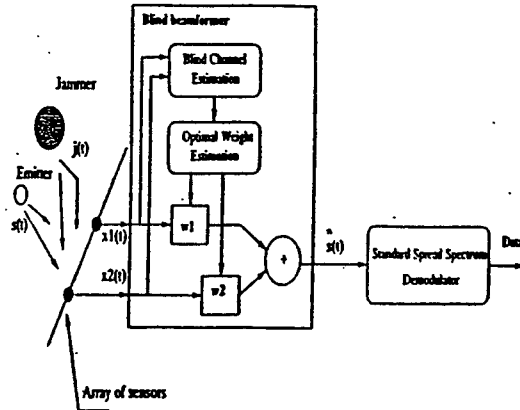


Fig. 1. Jammer mitigation system: Structure I.

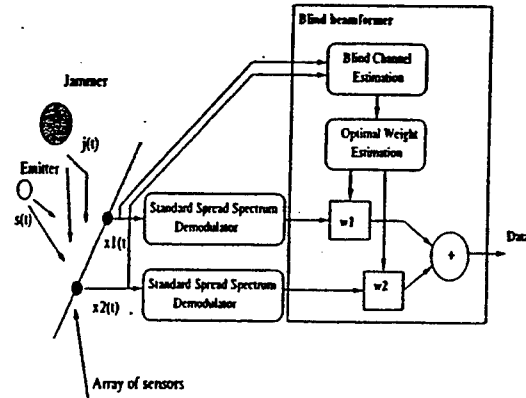


Fig. 2. Jammer mitigation system: Structure II.

receiver. In Fig. 1, structure I describes a receiver that consists of the standard spread spectrum demodulation preceded by a blind beamformer. The task of the beamformer is to fully or partially remove the jammer with minimum distortion to the desired signal. This is achieved by utilizing the spatial diversity provided by the two-sensor array as well as the difference in the temporal characteristics of the two signal arrivals. The demodulation process recovers the original data by despreading the separated desired signal while spreading the background noise and, in part, suppressing any jammer component that might have escaped to the beamforming output. As depicted in Fig. 2 and 3, structures II and III of the receiver consist of the spread spectrum demodulations applied at each sensor followed by a blind beamformer. The difference between these structures is in the estimation of the channel coefficients. In structure II, the channel coefficients are estimated from the observed data directly before despreading, whereas in structure III, these coefficients are estimated from the despread data.

III. SECOND-ORDER CHANNEL IDENTIFICATION (SOCI)

Consider the sampled version of the data model ($t = T_s$, where T_s is the sampling period)

$$\tilde{\mathbf{x}}(n) = \mathbf{H}\tilde{\mathbf{y}}(n) + \tilde{\mathbf{n}}(n), \quad \tilde{\mathbf{y}}(n) = [\tilde{s}(n) \ \tilde{j}(n)]^T. \quad (6)$$

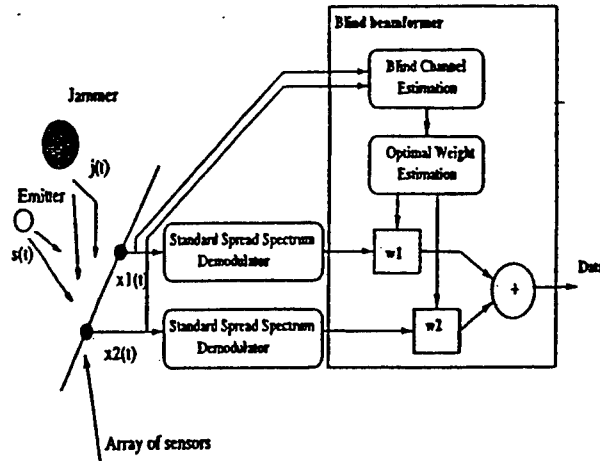


Fig. 2. Jammer mitigation system: Structure II.

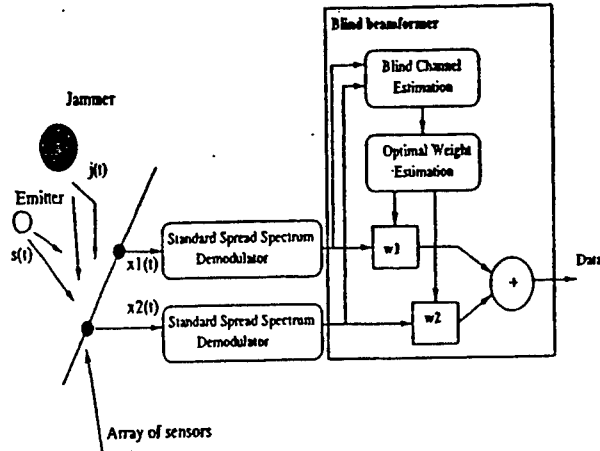


Fig. 3. Jammer mitigation system: Structure III.

$$\tilde{n}(n) = \sum_{l=1}^L n(n-l)c(l)^*$$

$$\tilde{s}(n) = \sum_{l=1}^L s(n-l)c(l)^*$$

and

$$\tilde{j}(n) = \sum_{l=1}^L j(n-l)c(l)^*.$$

In the above expressions, $x(n)$, $n(n)$, $s(n)$, and $j(n)$ are the sampled versions of $x(t)$, $n(t)$, $s(t)$, and $j(t)$, respectively. $c(l)$ is a zero-mean i.i.d. chip sequence, and L is the length of the chip sequence per information bit. The correlation matrices of $\tilde{x}(n)$ are given by

$$R_{\tilde{x}, \tilde{x}} = h_{11}^2 \tilde{L}^2 I + h_{21}^2 \tilde{L} R_{jj} + \tilde{L} \sigma^2 I \quad (7)$$

$$R_{\tilde{x}, \tilde{s}} = |h_{12}|^2 \tilde{L}^2 I + |h_{22}|^2 \tilde{L} R_{jj} + \tilde{L} \sigma^2 I \quad (8)$$

$$R_{\tilde{x}, \tilde{j}} = h_{11} h_{12}^* \tilde{L}^2 I + h_{21} h_{22}^* \tilde{L} R_{jj} \quad (9)$$

where I is the $N \times N$ identity matrix, $\tilde{x}_i(n)$, $i = 1, 2$ are the element of $\tilde{x}(n)$, and R_{xy} is defined by

$$R_{xy} = E([x(1), \dots, x(N)]^T [y(1), \dots, y(N)]^*). \quad (10)$$

In the above equation, $E(\cdot)$ is the expectation operator, and N is some length of the data. Expressions (7)–(9) are derived under the assumptions $\mathcal{H}1)$ – $\mathcal{H}5)$, where

$$\tilde{L} = \begin{cases} 1 & \text{if structures I and II} \\ L & \text{if structure III.} \end{cases} \quad (11)$$

Let us define the operators $\text{off}(\cdot)$ and $\text{tr}(\cdot)$ by

$$\text{off}(M) = \frac{1}{N(N-1)} \sum_{i \neq j} M_{ij} \quad (12)$$

$$\text{tr}(M) = \frac{1}{N} \sum_i M_{ii} \quad (13)$$

where M is any square matrix of dimension $N \times N$, and M_{ij} are the entries of M . By applying these operators to (7)–(9), we get

$$F_1 = \text{off}(R_{\tilde{x}, \tilde{x}}) = h_{21}^2 \tilde{L} \text{off}(R_{jj}) \quad (14)$$

$$F_{12} = \text{off}(R_{\tilde{x}, \tilde{s}}) = h_{21} h_{22}^* \tilde{L} \text{off}(R_{jj}) \quad (15)$$

$$T_1 = \text{tr}(R_{\tilde{x}, \tilde{x}}) = h_{11}^2 \tilde{L}^2 + h_{21}^2 \tilde{L} + \tilde{L} \sigma^2 \quad (16)$$

$$T_2 = \text{tr}(R_{\tilde{s}, \tilde{s}}) = |h_{12}|^2 \tilde{L}^2 + |h_{22}|^2 \tilde{L} + \tilde{L} \sigma^2 \quad (17)$$

$$T_{12} = \text{tr}(R_{\tilde{x}, \tilde{s}}) = h_{11} h_{12}^* \tilde{L}^2 + h_{21} h_{22}^* \tilde{L} \quad (18)$$

where $|\cdot|^2$ indicates the square modulus. Note that $\text{off}(R_{jj})$ is unknown and can be eliminated by combining (1) and (14). From (14)–(18), we obtain the expressions of the channel coefficients as

$$h_{21} = \sqrt{\frac{1}{\tilde{L}} \frac{T_1 T_2 - |T_{12}|^2 - \tilde{L} \sigma^2 (T_1 + T_2) + \tilde{L}^2 \sigma^4}{T_2 + T_1 |\beta|^2 - 2 \text{Re}(\beta^* T_{12}) - \tilde{L} \sigma^2 (1 + |\beta|^2)}} \quad (19)$$

$$h_{22} = h_{21} \beta^* \quad (20)$$

$$h_{11} = \frac{1}{\tilde{L}} \sqrt{T_1 - h_{21}^2 \tilde{L} - \tilde{L} \sigma^2} \quad (21)$$

$$h_{12} = \frac{1}{\tilde{L}} \frac{T_{12} - h_{21}^2 \tilde{L} \beta}{\sqrt{T_1 - h_{21}^2 \tilde{L} - \tilde{L} \sigma^2}} \quad (22)$$

where $\beta = F_{12}/F_1$, and $\text{Re}\{\cdot\}$ denotes the real part operator.

An estimate of the noise variance σ^2 is needed for a robust estimation of the channel coefficients. It can be obtained by eigendecomposition of the data covariance matrix [9] if a third sensor is available. Otherwise, σ^2 can be estimated using only two sensors before transmission begins, i.e., in the absence of the spread spectrum signal (see the Appendix). Note that in practice, the temporal correlation matrices of the data are replaced by their time averages.

It should be noted that if there is no jammer present, then $h_{21} = h_{22} = 0$, and (19) and (20) do not carry any new information to estimate h_{11} and h_{12} . Further, in the case that the jammer is an uncorrelated signal, where $\text{off}(R_{jj}) = 0$, then $F_1 = F_{12} = 0$, and, as such, there is no unique solution of the channel. In addition to reducing the jammer power, the despreading in structure II also weakens the temporal coherence of the jammer signal while estimating the channel coefficients. For high number of chips by bit (L), the despreading operation makes the jammer temporally white, and similar to the above case, the values of F_1 and F_{12} in (14) and (15) are reduced to zero. Hence, (16)–(18) become insufficient to solve the identification problem. Whether the jammer is originally or made white, we have to use higher order blind identification techniques for blind notations [10]–[12]. From this discussion, it is expected that the asymptotic performance of the SOCI will be better in structures I and II than in structure III.

IV. DATA RECOVERY

In this section, the objective is to determine the array weight beamformer $\mathbf{w} = [w_1 \ w_2]$ to achieve the task of data recovery. Several minimization and maximization criteria can be used to optimize the beamformer weights [13]. This includes the use of the reference signal, maximization of signal-to-interference and noise ratio (SINR), and linearly constrained minimum variance of the beamformer output. We compute the optimum beamformer that maximizes the SINR at the receiver output subject to the unit norm constraint $|\mathbf{w}|^2 = 1$.

A. SINR Expression

1) *Structure I*: The receiver SINR is defined as the ratio of the square of the mean to the variance of the correlator output U [14]²

$$\text{SINR}_I = \frac{|E[U]|^2}{\text{Var}[U]} \quad (23)$$

where

$$U = \sum_{n=1}^L \mathbf{w}^H \mathbf{x}(n) c^*(n) \quad (24)$$

where the superscript H denotes the transpose conjugate operator. It is realized that U consists of three different uncorrelated components U_s , U_j , and U_n , which are the output of the correlator due to the desired signal, the interference, and the noise, respectively. That is

$$U = U_s + U_j + U_n \quad (25)$$

where

$$U_s = \mathbf{w}^H \mathbf{h}_1 \sum_{n=1}^L s(n) c^*(n) \quad (26)$$

$$U_j = \mathbf{w}^H \mathbf{h}_2 \sum_{n=1}^L j(n) c^*(n) \quad (27)$$

²Note that this definition is consistent herein only because the variance of the data bit sequence is zero over the chip length.

Therefore

$$U_s = \mathbf{w}^H \sum_{n=1}^L \mathbf{x}(n) c^*(n). \quad (28)$$

$$E[U] = E[U_s] + E[U_j] + E[U_n] \quad (29)$$

$$\text{Var}[U] = \text{Var}[U_s] + \text{Var}[U_j] + \text{Var}[U_n]. \quad (30)$$

The mean value can be easily computed as

$$E[U_s] = E \left[\mathbf{w}^H \mathbf{h}_1 \sum_{n=1}^L s(n) c^*(n) \right] = \pm L \mathbf{w}^H \mathbf{h}_1 \quad (31)$$

$$E[U_j] = E \left[\mathbf{w}^H \mathbf{h}_2 \sum_{n=1}^L j(n) c^*(n) \right] = 0 \quad (32)$$

$$E[U_n] = E \left[\mathbf{w}^H \sum_{n=1}^L \mathbf{n}(n) c^*(n) \right] = 0 \quad (33)$$

where

$$(\pm) = \begin{cases} +1 & \text{if bit 1 is transmitted} \\ -1 & \text{if bit -1 is transmitted.} \end{cases}$$

The zero values in (32) and (33) are the result of the uncorrelation between the zero mean chip sequence and both the jammer and noise sequences. These properties along with the white noise process can be used to obtain the variance expressions

$$\begin{aligned} \text{Var}[U_s] &= 0 \\ \text{Var}[U_j] &= L |\mathbf{w}^H \mathbf{h}_2|^2 \\ \text{Var}[U_n] &= L |\mathbf{w}|^2 \sigma^2. \end{aligned} \quad (34)$$

Accordingly

$$|E[U]|^2 = L^2 |\mathbf{w}^H \mathbf{h}_1|^2 \quad (35)$$

$$\text{Var}[U] = L (|\mathbf{w}^H \mathbf{h}_2|^2 + |\mathbf{w}|^2 \sigma^2) \quad (36)$$

and the correlator SINR is

$$\text{SINR}_I = \frac{L |\mathbf{w}^H \mathbf{h}_1|^2}{|\mathbf{w}^H \mathbf{h}_2|^2 + |\mathbf{w}|^2 \sigma^2}. \quad (37)$$

2) *Structures II and III*: At the output of the beamformer, the SINR corresponding to structures II and III is given by

$$\begin{aligned} \text{SINR}_{II} &= \text{SINR}_{III} \\ &= \frac{|\mathbf{w}^H \mathbf{h}_1|^2 E[\bar{s}(n) \bar{s}(n)^*]}{|\mathbf{w}^H \mathbf{h}_2|^2 E[\bar{j}(n) \bar{j}(n)^*] + \mathbf{w}^H E[\bar{\mathbf{n}}(n) \bar{\mathbf{n}}(n)^*] \mathbf{w}} \end{aligned} \quad (38)$$

where

$$\bar{x}(n) = \sum_{l=1}^L x(n-l) c(l)^*$$

$$\bar{n}(n) = \sum_{l=1}^L \mathbf{n}(n-l) c(l)^*$$

$$\bar{s}(n) = \sum_{l=1}^L s(n-l) c(l)^*$$

and

$$\bar{j}(n) = \sum_{l=1}^L j(n-l)c(l)^*$$

with

$$E[\bar{s}(n)\bar{s}(n)^*] = E\left[\sum_{l,u=1}^L s(n-l)c(l)^* s(n-u)^* c(u)\right] = L^2$$

$$E[\bar{j}(n)\bar{j}(n)^*] = E\left[\sum_{l,u=1}^L j(n-l)c(l)^* j(n-u)^* c(u)\right] = L$$

$$E[\bar{n}(n)\bar{n}(n)^*] = E\left[\sum_{l,u=1}^L n(n-l)c(l)^* n(n-u)^* c(u)\right] = L\sigma^2 \mathbf{I}.$$

Therefore

$$\text{SINR}_{\text{II}} = \text{SINR}_{\text{III}} = \frac{L|\mathbf{w}^H \mathbf{h}_1|^2}{|\mathbf{w}^H \mathbf{h}_2|^2 + |\mathbf{w}|^2 \sigma^2}. \quad (39)$$

3) *Comments:* According to (37) and (39), the two structures lead to the same asymptotic SINR if the same optimal array weights are used. In practice, the optimal weights of structures I and II are computed from the same estimates of the channel coefficients. Therefore, these two structures have the same performance. If K denotes the sample size at the input of the receiver, structures I and II estimate the channel coefficients using K/L sample data. Note also that the input SINR per bit per chip is the same for the three structures. Accordingly, for a same setting, the estimation error on the array weights of structure III is expected to be higher than the corresponding error of structures I and II. Hence, receivers of structures I and II should have better performance but higher numerical complexity than the receiver of structure III, as shown below.

B. Optimum Array Weights

The optimum array weight vector in the sense mentioned above is given by

$$\mathbf{w}_{\text{opt}} = \underset{\mathbf{w}}{\text{Argmax}} \frac{L|\mathbf{w}^H \mathbf{h}_1|^2}{|\mathbf{w}^H \mathbf{h}_2|^2 + |\mathbf{w}|^2 \sigma^2} \text{ subject to } |\mathbf{w}|^2 = 1. \quad (40)$$

The solution to the maximization problem (40) is well known [15] and is given by

$$\mathbf{w}_{\text{opt}} = \frac{\mathbf{Q}^{-1} \mathbf{h}_1}{\sqrt{\mathbf{h}_1^H \mathbf{Q}^{-1} \mathbf{h}_1}} \quad \mathbf{Q} = \mathbf{h}_2 \mathbf{h}_2^H + \sigma^2 \mathbf{I}. \quad (41)$$

A workout of (41) leads to

$$\mathbf{w}_{\text{opt}} = \frac{1}{\sqrt{1 + |\alpha|^2}} [1 \ \alpha]^T \quad (42)$$

$$\alpha = \frac{h_{12}\sigma^2 + h_{21}^* \Delta}{h_{11}\sigma^2 - h_{22}^* \Delta}, \quad \Delta = h_{21}h_{12} - h_{11}h_{22}. \quad (43)$$

In practice, the channel vectors \mathbf{h}_1 , \mathbf{h}_2 and the noise variance σ^2 are replaced by their estimated values.

C. Summary

Based on the previous sections, each proposed spread spectrum receiver consists of the following steps:

- Receiver of Structure I (Fig. 1)
 - estimation of channel coefficients from the array output $x(n)$ using (19)–(22);
 - estimation of the array weight vectors $\hat{\mathbf{w}}$ using (42);
 - recovery of the desired signal by $\hat{s}(n) = \hat{\mathbf{w}}^H \mathbf{x}(n)$;
 - recovery of the data bit sequence b_k by the correlation of $\hat{s}(n)$ with the chip sequence $\{c_l^k\}_{l=1, \dots, L}$.
- Receiver of Structure II (Fig. 2)
 - estimation of channel coefficients from the array output $x(n)$ using (19)–(22);
 - despreading of the sampled received data $x(n)$ by the correlation with the chip sequence $\{c_l^k\}_{l=1, \dots, L}$ to obtain $\bar{x}(n)$;
 - estimation of the array weight vectors $\hat{\mathbf{w}}$ using (42);
 - recovery of the data bit sequence b_k by $\mathbf{w}^H \bar{x}(n)$.
- Receiver of Structure III (Fig. 3)
 - despreading of the sampled received data $x(n)$ by the correlation with the chip sequence $\{c_l^k\}_{l=1, \dots, L}$ to obtain $\bar{x}(n)$;
 - estimation of channel coefficients from $\bar{x}(n)$ using (19)–(22);
 - estimation of the array weight vectors $\hat{\mathbf{w}}$ using (42);
 - recovery of the data bit sequence b_k by $\mathbf{w}^H \bar{x}(n)$.

V. COMPUTATIONAL ANALYSIS

In this section, the computational cost associated with each receiver of structures I–III using SOCI or JADE³ is determined. Table I summarizes the number of computations required for each receiver. The first column indicates the term to be computed. The calculations required to compute each of these terms is quantified in terms of the number of multiplications (\times). A data block size consisting of K data samples is assumed, and N delays for the correlations are considered. The symbol (*) indicated that a specific term is required either for structure I, II, or III using SOCI or JADE.

From Table I, implementing receivers I and II using SOCI require, respectively, $(6 + 2N)K + 22$ and $(4 + (2/L) + 2N)K + 22$ multiplications. For $K = 512$, $L = 64$, and $N = 4$, structure II requires 108 multiplications less than structure I. In comparison, implementing receiver III using SOCI requires $(1 + ((5 + 2N)/L)K + 22$ multiplications. Therefore, the computations required to implement receiver I or II are significantly higher than those required in implementing receiver III. For $K = 512$, $L = 64$, and $N = 4$, the computational cost of receiver I is approximately a factor of 11 greater than the computational cost required for receiver III.

It can be seen from Table I that receivers I and II using JADE require, respectively, $(11 + 18N)K + 21 + 8N$ and

³JADE is a blind identification technique described in [7] and [13] and which uses higher order statistics to estimate the channel coefficients.

TABLE I
COMPUTATIONS REQUIRED FOR STRUCTURES I-III

Term	x	SOC1			JADE		
		S. I	S. II	S. III	S. I	S. II	S. III
\tilde{x}	K		*	*		*	*
T_1	K	*	*				
T_1	K/L			*			
T_2	K	*	*				
T_2	K/L			*			
T_{12}	K	*	*				
T_{12}	K/L			*			
β	$2N K$	*	*				
β	$2N K/L$			*			
h_2	10	*	*	*			
h_1	3	*	*	*			
$h_1 \& h_2$	$(8+18N)K+12+8N$				*	*	
$h_1 \& h_2$	$(8+18N)K/L+12+8N$						*
w	9	*	*	*	*	*	*
s	$2 K$	*			*		
b	K	*			*		
b	$2K/L$		*	*		*	*

$(9+(2/L)+18N)K+21+8N$ multiplications. In comparison, receiver III using JADE requires $(1 + ((9 + 18N)/L)K + 21 + 8N$ multiplications. Again, the computations required to implement receiver I or II are significantly higher than those required in implementing receiver III. The numbers in Table I also show that the computations required when using JADE are higher than those required when using SOC1. For $K = 512$ and $N = 4$, the computational cost of receiver I using JADE is approximately a factor of 6 greater than the computational cost of receiver I using SOC1.

VI. PERFORMANCE EVALUATIONS

In this section, we consider an array of two sensors separated by half a wavelength. In addition to the DS/SS signal, the array receives a jammer through three paths (see Fig. 4). The desired signal is BPSK signal arriving at $\theta_0 = 0^\circ$. The jammer is composed of a chirp signal whose frequencies are $\omega_1 = 0.1\pi$ and $\omega_2 = 0.6\pi$. The direct path of the jammer arrives at $\theta_1 = 2^\circ$, whereas its multipaths arrive at $\theta_2 = 10^\circ$ and $\theta_3 = -10^\circ$, respectively. The noise used is zero-mean white complex Gaussian process. The value of N in (10) is chosen to be equal to 8 and 100 data bits.

Figs. 5 and 6 display the baseband power spectral density over the normalized frequency of the emitted spread spectrum signal and the jammer, respectively. The jammer-to-signal noise ratio (JSR) is 30 dB and $L = 128$ chips/bit. Figs. 7 and 8 present the power spectral density of the array outputs for a signal-to-noise ratio (SNR) of 0 dB. Fig. 9 displays the

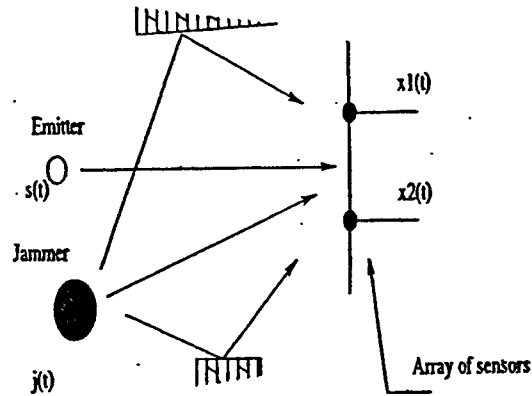


Fig. 4. Scenario of the simulation.

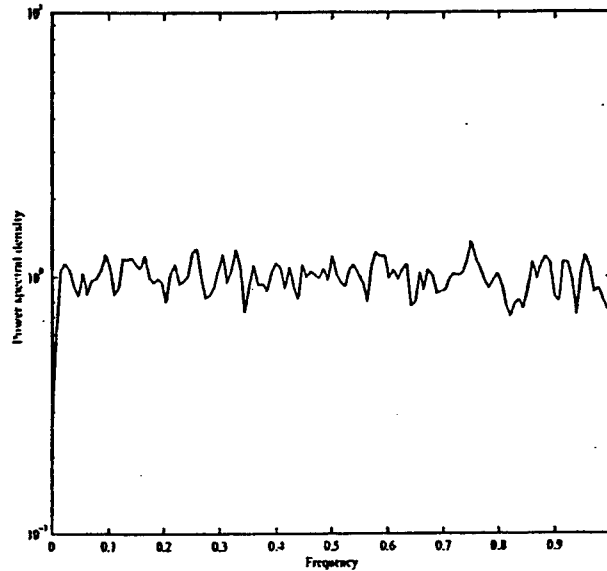


Fig. 5. Spectral density of the emitted SS signal in the baseband.

power spectral density of the recovered signal at the output of the separator and before using SOC1 in structure I. This figure clearly shows that the blind beamformer has well rejected the jammer.

Next, the SINR at the output of the decorrelator is estimated over 100 Monte Carlo runs. Figs. 10–14 show the SINR in decibels when the beamformer is both enabled (either using SOC1 or JADE according to the three structures I–III) and disabled.

In Figs. 10 and 11, the SINR is plotted against SNR for a JSR of 30 and 10 dB, respectively and for both 4 chips/bit⁴ and 64 chips/bit. According to Fig. 10, receivers I and II, which have the same performances, perform better than receiver III, as expected. Fig. 11 shows that receiver I and II using either SOC1 or JADE have comparable performance.

Fig. 12 presents the SINR versus JSR for 0 dB SNR and 64 chips/bit. This figure shows that by using the beamformer, the

⁴The choice of 4 chips/bit in this simulation is just for illustration.

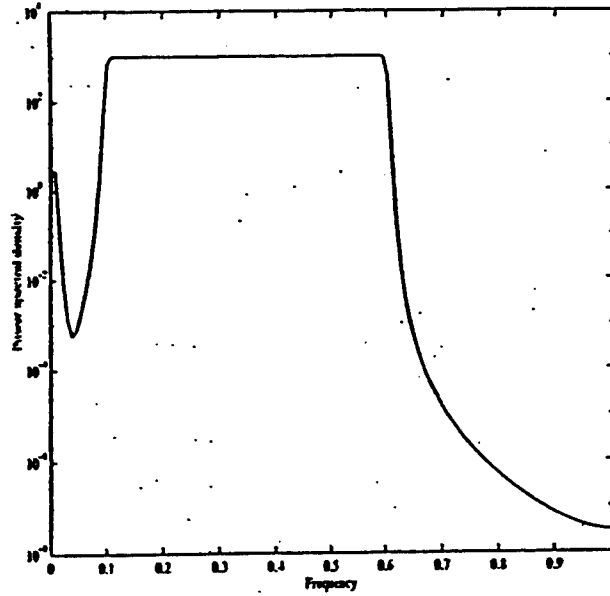


Fig. 6. Spectral density of the jammer in the baseband.

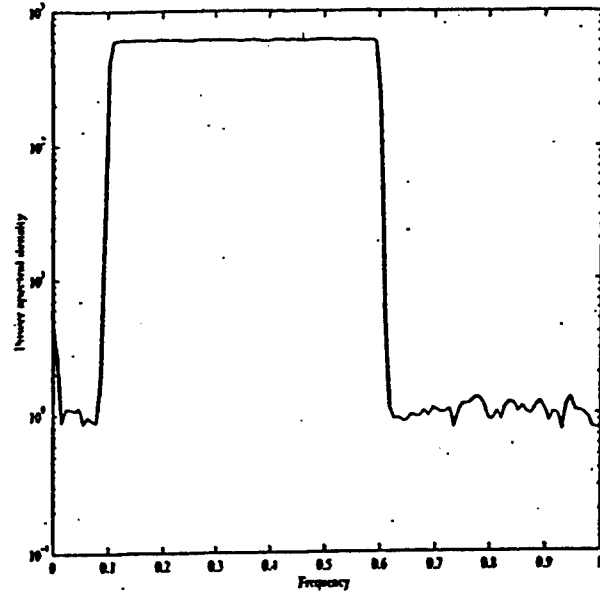


Fig. 8. Spectral density of the array output 2 in the baseband.

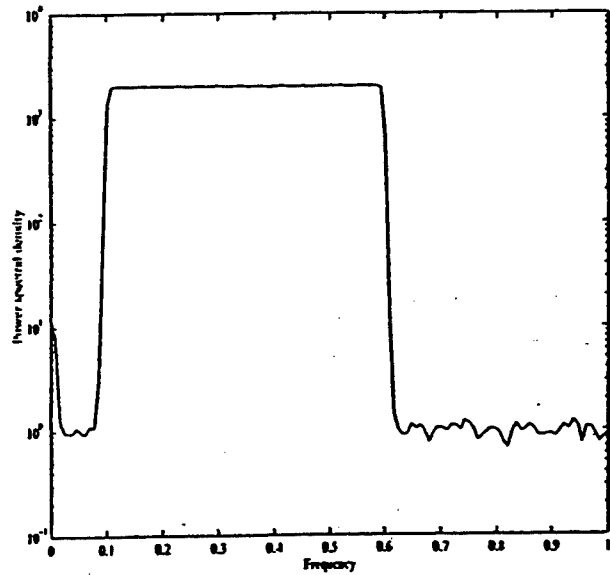


Fig. 7. Spectral density of the array output 1 in the baseband.

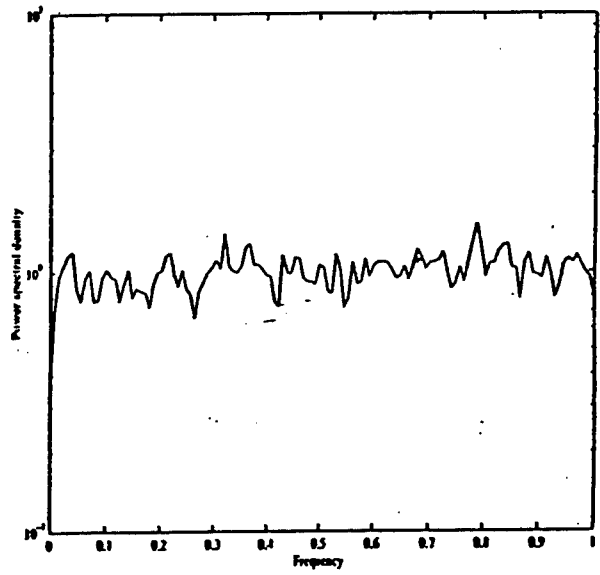


Fig. 9. Spectral density of the recovered signal before despreading using SOCI in structure 1.

demodulator performance becomes insensitive to high levels of the JSR. Figs. 13 and 14 display the SINR versus the number of chips/bit for JSR of 10 and 40 dB, respectively, and for 0 dB SNR. From Fig. 13, it is evident that for 8 chips/bit, the proposed receivers achieve the same performance as the despreader when used alone for 128 chips/bit. These figures support the claim that the proposed method requires small spreading gain and transmission bandwidth.

VII. CONCLUSION

In this paper, we have proposed an efficient two-sensor blind beamformer for single jammer mitigation in spread spectrum communication systems based on second-order statistic blind identification of the channel coefficients. This second order identification has been made possible because of the temporal properties of the spread spectrum signal and the jammer.

Closed-form expressions of the channel coefficients have been derived. Analytical expressions of the optimum beamformer weights have been computed from the maximization

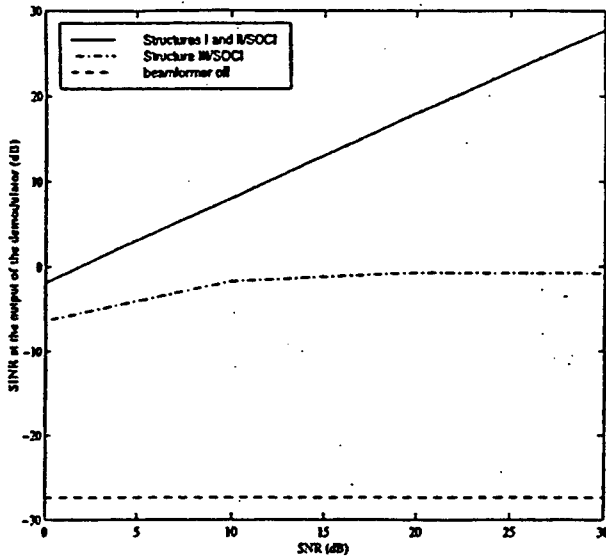


Fig. 10. SINR at the correlator output in decibels versus SNR for JSR = 30 dB and 4 chips/bit.

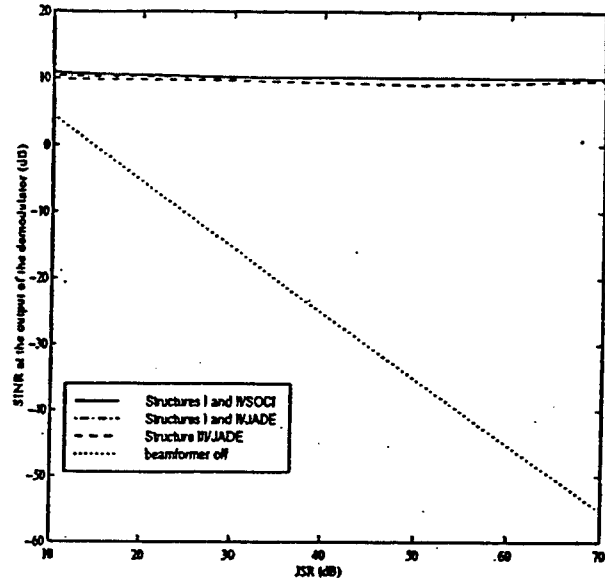


Fig. 12. SINR at the correlator output in decibels versus JSR for SNR = 0 dB and 64 chips/bit.

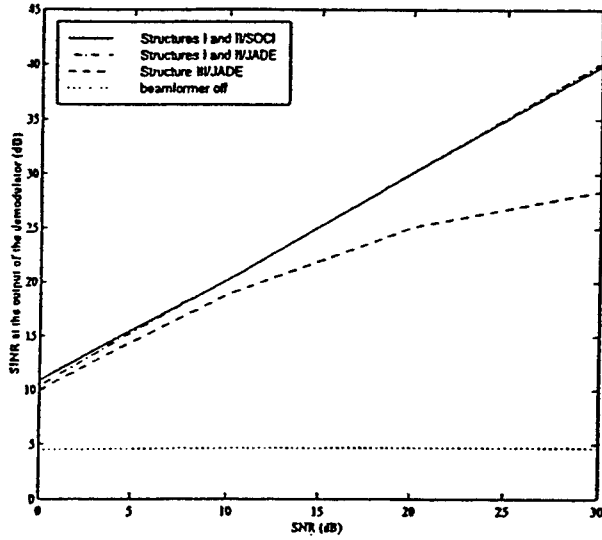


Fig. 11. SINR at the correlator output in decibels versus SNR for JSR = 10 dB and 64 chips/bit.

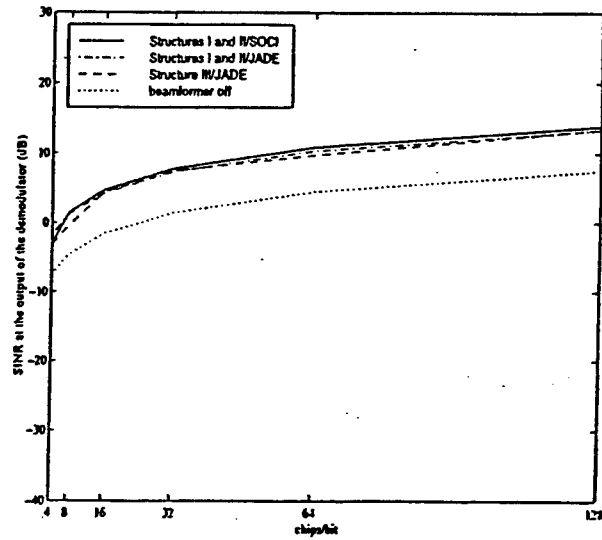


Fig. 13. SINR at the correlator output in decibels versus chips/bit for SNR = 0 dB and JSR = 10 dB.

of the signal-to-interference plus noise ratio at the output of the demodulator. Three structure designs of the mitigation receiver were suggested. While structure III presents a low computational cost, it is less robust than structures I and II. The second-order channel identification (SOCI) was compared with the "JADE" in both terms of computational cost and the achieved SINR. While SOCI has a low computational cost, it represents a comparable performance of JADE when the asymptotic conditions are reached. Because of inherent ambiguity related to the general blind problem [16], [17] solved by JADE, a selection of the desired signal signature and the jammer signature from the estimated signatures should

be performed when using JADE. Some *a priori* knowledge on the desired signal is needed. In contrast, the proposed SOCI does not need this extra processing since it selects implicitly the desired signature during the identification process. We conclude that receivers I and II using SOCI seem to be the best receiver for the mitigation of a single jammer in a two sensor spread spectrum communications system both in terms of performance and computational cost. Simulation results were provided for multipath and coherent signal environment.

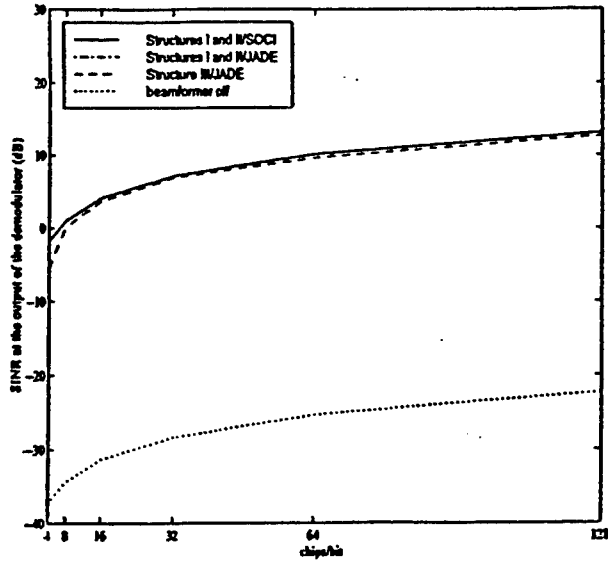


Fig. 14. SINR at the correlator output in decibels versus chips/bit for SNR = 0 dB and JSR = 40 dB.

APPENDIX

With no SS signal arrival, (14)–(18) is reduced to

$$\frac{\tilde{F}_{12}}{\tilde{F}_1} = \frac{\text{off}(\mathbf{R}_{\tilde{\mathbf{x}}_1 \tilde{\mathbf{x}}_2})}{\text{off}(\mathbf{R}_{\tilde{\mathbf{x}}_1 \tilde{\mathbf{x}}_1})} = \frac{\tilde{h}_2^*}{\tilde{h}_1} \quad (44)$$

$$\tilde{\mathbf{T}}_1 = \text{tr}(\mathbf{R}_{\tilde{\mathbf{x}}_1 \tilde{\mathbf{x}}_1}) = \tilde{h}_1^2 \tilde{L} + \tilde{L}\sigma^2 \quad (45)$$

$$\tilde{\mathbf{T}}_{12} = \text{tr}(\mathbf{R}_{\tilde{\mathbf{x}}_1 \tilde{\mathbf{x}}_2}) = \tilde{h}_1^2 \tilde{h}_2^* \tilde{L}\sigma^2 \quad (46)$$

where $\tilde{\mathbf{h}} = [\tilde{h}_1 \ \tilde{h}_2]^T$ and $\tilde{\mathbf{x}} = [\tilde{x}_1 \ \tilde{x}_2]^T$, respectively, represent the channel vector associated with the jammer and the observed data prior to signal transmission. From (44)–(46), we obtain the expression of the background noise variance

$$\sigma^2 = \frac{\tilde{\mathbf{T}}_1}{\tilde{L}} - \frac{\tilde{\mathbf{T}}_{12} \tilde{\mathbf{F}}_{12}}{\tilde{L} \tilde{\mathbf{F}}_1} \quad (47)$$

REFERENCES

- [1] L. B. Milstein, "Interference rejection techniques in spread spectrum communications," *Proc. IEEE*, vol. 66, pp. 657–671, June 1988.
- [2] M. Amin, "Interference mitigation in spread spectrum communications using time-frequency distributions," *IEEE Trans. Signal Processing*, vol. 45, pp. 90–101, Jan. 1997.
- [3] B. D. Van Veen and K. M. Buckley, "Beamforming: A versatile approach to spatial filtering," *IEEE Signal Processing Mag.*, pp. 4–24, Apr. 1988.
- [4] L. Brennan and L. Reed, "Theory of adaptive radar," *IEEE Trans. Aerosp. Electron.*, pp. 237–247, Mar. 1973.
- [5] L. C. Godara, "Application of antenna arrays to mobile communications—II: Beamforming and direction of arrival considerations," *Proc. IEEE*, vol. 87, pp. 1195–1245, Aug. 1997.
- [6] A. F. Naguib, "Adaptive antennas for CDMA wireless networks," Ph.D. dissertation, Stanford Univ., Stanford, CA, 1996.
- [7] M. K. Simon, *Spread Spectrum Communications*. New York: Comput. Sci., 1985.
- [8] B. Ottersten, "Array processing for wireless communications," in *Proc. 8th IEEE Signal Process. Workshop Stat. Signal Array Process.*, Corfu, Greece, June 1996, pp. 466–473.
- [9] J. F. Cardoso, A. Belouchrani, K. Abed Meraim, and E. Moulines, "A blind source separation technique using second order statistics," *IEEE Trans. Signal Processing*, vol. 45, pp. 434–444, Feb. 1997.
- [10] P. Comon, "Independent component analysis," in *Proc. Int. Workshop Higher Order Stat.*, Chamrousse, France, 1991, pp. 111–120.
- [11] J. F. Cardoso and A. Souloumiac, "An efficient technique for blind separation of complex sources," in *Proc. IEEE SP Workshop Higher-Order Stat.*, Lake Tahoe, CA, 1993.
- [12] ———, "Blind beamforming for non Gaussian signals," *IEEE Proceedings*, vol. 140, no. 6, pp. 362–370, 1993.
- [13] R. Monzingo and T. Miller, *Introduction to Adaptive Radar*. New York: Wiley and Sons, 1980.
- [14] J. Ketchum and J. Proakis, "Adaptive algorithms for estimating and suppressing narrow band interference in pss spread spectrum communications," *IEEE Transactions on Communications*, vol. 30, pp. 913–924, May 1982.
- [15] S. Haykin and A. Steinhardt, *Adaptive Radar Detection and Estimation*. New York: Wiley, 1992.
- [16] A. Souloumiac, "Utilization des statistiques d'ordre sup'erieur en traitement d'antenne," Ph.D. dissertation, Telecom Paris, Paris, France, Feb. 1993.
- [17] A. Belouchrani, "Se'paration atmodictate de sources: Algorithmes, performances et application a des signaux experimentaux," Ph.d. dissertation, ENST, Paris, France, July 1995.
- [18] L. B. Milstein and R. Illis, "Signal processing for interference rejection in spread communications," *IEEE Signal Processing Mag.*, vol. 3, pp. 18–31, Apr. 1986.
- [19] G. Saulnier, M. Medley, and P. Das, "Applications of the wavelet transform in spread spectrum communications systems," *SPIE—Wavelet Applications*, Orlando, FL, Apr. 1994.
- [20] M. G. Amin, "Interference excision in spread spectrum communication systems using time-frequency distributions," Tech. Rep., Rome Lab., Rome, NY, Sept. 1994.
- [21] M. Tazebay and A. Akansu, "Adaptive subband transform in time-frequency excisers for DSSS communications systems," *IEEE Trans. Signal Processing*, vol. 43, pp. 2776–2783, Nov. 1995.
- [22] S. Roberts and M. Amin, "Linear vs. bilinear time-frequency methods for interference mitigation in direct sequence spread spectrum communication systems," in *Proc. Asilomar Conf. Signals, Syst., Comput.*, Nov. 1995.

Adel Belouchrani (M'95) received the State Engineering degree in 1991 from the National Polytechnic School of Algiers, Algiers, Algeria, the M.Sc. degree in signal processing from the Institut National Polytechnique de Grenoble (INPG), Grenoble, France, in 1992, and the Ph.D. degree in signal and image processing from Ecole Nationale Supérieure des Telecommunications (ENST), Paris, France, in 1995.

He was a Visiting Scholar at the Electrical Engineering and Computer Sciences Department, University of California, Berkeley, from 1995 to 1996, working on fast adaptive blind equalization and carrier phase tracking. He was with the Department of Electrical and Computer Engineering, Villanova University, Villanova, PA, as a Research Associate from 1996 to 1997. He also served as a Consultant to Comcast Inc., Philadelphia, PA, during the same period. In February 1997, he was a visiting Scientist at the Laboratory for Artificial Brain System, Riken, Japan. From August 1997 to October 1997, he was with Alcatel ETCA, working on very high-speed digital subscriber line (VDSL). He is currently with the Electrical Engineering Department, National Polytechnic School of Algiers, as an Assistant Professor. His research interests are in the areas of digital communications and statistical signal processing including (blind) array processing, performance analysis, blind source separation, blind equalization, systems identification, damped sinusoids estimation, adaptive algorithms, expectation-maximization techniques applied to communications, nonstationary signals, and spread spectrum communications.



Moeness G. Amin (SM'91) received the B.Sc. degree in 1976 from Cairo University, Cairo, Egypt, the M.Sc. degree in 1980 from the University of Petroleum and Minerals, Dhahran, Saudi Arabia, and the Ph.D. degree in 1984 from the University of Colorado, Boulder, all in electrical engineering.

In 1984, he joined the University of Colorado, Denver, as a visiting Assistant Professor. He has been on the Faculty of the Department of Electrical and Computer Engineering, Villanova University, Villanova, PA, since 1985, where he is now a

Professor.

Dr. Amin was an Associate Editor of the IEEE TRANSACTIONS ON SIGNAL PROCESSING and a member of the Technical Committee of the IEEE Signal Processing Society on Statistical Signal and Array Processing. He was a General Chair of the 1994 IEEE International Symposium on Time-Frequency and Time-Scale Analysis and is heading as a General Chair the IEEE Workshop on Statistical Signal and Array Processing to be held in the Poconos Mountains in Pennsylvania in August 2000. He was the recipient of the 1997 IEEE Philadelphia Section Award for "Outstanding Intellectual and Organizational Contributions to the IEEE Philadelphia Section in the Area of Signal Processing." He was also the recipient of the 1997 Villanova University Outstanding Faculty Research Award. Over the past four years, he chaired three All-Day Workshops on Smart Antennas, Recent Trends in Adaptive Filtering, and Advanced Signal Processing Applications in Wireless Communications. His current research interests are in the areas of time-frequency analysis, spread spectrum communications, smart antennas, and blind signal processing.

Dr. Amin is a member of Sigma Xi, Eta Kappa Nu, and Phi Kappa Phi.

Blind Source Separation Based on Time-Frequency Signal Representations

Adel Belouchrani and Moeness G. Amin, *Senior Member, IEEE*

Abstract—Blind source separation consists of recovering a set of signals of which only instantaneous linear mixtures are observed. Thus far, this problem has been solved using statistical information available on the source signals. This paper introduces a new blind source separation approach exploiting the difference in the time-frequency (t - f) signatures of the sources to be separated. The approach is based on the diagonalization of a combined set of “spatial t - f distributions.” In contrast to existing techniques, the proposed approach allows the separation of Gaussian sources with identical spectral shape but with different t - f localization properties. The effects of spreading the noise power while localizing the source energy in the t - f domain amounts to increasing the robustness of the proposed approach with respect to noise and, hence, improved performance. Asymptotic performance analysis and numerical simulations are provided.

I. INTRODUCTION

BLIND SOURCE separation is an emerging field of fundamental research with a broad range of applications. It is motivated by practical problems that involve several source signals and several sensors. Each sensor receives a linear mixture of the source signals. The problem of the blind source separation consists, then, of recovering the original waveforms of the sources without any knowledge of the mixture structure. This mixture is often a convolutive mixture. However, in this paper, our main concern is the blind identification of an instantaneous linear mixture, which corresponds to a linear memoryless channel. This choice is motivated not only by the fact that such a model is mathematically tractable but also by the applicability to various areas, including semiconductor manufacturing process [1], factor analysis [2], narrowband signal processing [3], and image reconstruction [4].

Thus far, the problem of the blind source separation has been solved using statistical information available on the source signals. The first solution to the source separation problem was proposed almost a decade ago [5] and was based on the cancellation of higher order moments assuming non-Gaussian and i.i.d source signals. Since then, other criteria based on minimizations of cost functions, such as the sum of square fourth-order cumulants [6]–[8], contrast functions [7],

[9], or likelihood function [10], have been used by several researchers. Note that in the case of non-i.i.d source signals and even Gaussian sources, solutions based on second-order statistics are possible [11], [12].

Matsuoka *et al.* have shown that the problem of the separation of nonstationary signals can be solved using second-order decorrelation only [14]. They implicitly use the nonstationarity of the signal via a neural net approach. In this paper, we propose to take advantage explicitly of the nonstationarity property of the signals to be separated. This is done by resorting to the powerful tool of time-frequency (t - f) signal representations. The underlying problem can then be posed as a signal synthesis [15] from the t - f plane with the incorporation of the spatial information provided by the multisensor array. With the proposed approach, no masking is required, and the cross terms no longer represent ambiguity in the synthesis of multicomponent signals.

This paper introduces a new blind identification technique based on a joint diagonalization of a combined set of spatial t - f distributions (STFD's) that are a generalization of the t - f distribution to a vector signal. It is shown that under the linear data model the proposed STFD has the similar structure than the data spatial correlation matrix that we commonly use in array signal processing. The benefits of STFD over the spatial correlation matrix in a nonstationary signal environment is the direct exploitation of the information brought by the nonstationarity of the signals. Hence, the new approach exploits the difference between the t - f signatures of the sources. This method presents a number of attractive features. In contrast to blind source separation approaches using second-order and/or high order statistics, the proposed approach allows the separation of Gaussian sources with identical spectral shape but with different t - f localization properties. Moreover, the effects of spreading the noise power while localizing the source energy in the t - f domain amounts to increasing the robustness of the proposed approach with respect to noise.

The paper is organized as follows. In Section II, the problem of blind source separation is stated along with the relevant hypothesis. Spatial t - f distributions are introduced in Section III. Section IV presents the proposed t - f blind identification technique based on the diagonalization of a combined set of spatial t - f distributions (TFD's). In Section V, a closed-form expression of the asymptotic performance of the proposed method is derived. Numerical simulations illustrating the usefulness of the proposed technique are given in Section VI.

Manuscript received September 6, 1996; revised April 10, 1998. This work was supported by Rome Laboratories, Rome, NY, under Contract F30602-96-C-0077. The associate editor coordinating the review of this paper and approving it for publication was Prof. Luis F. Chaparro.

A. Belouchrani is with the Electrical Engineering Department, National Polytechnic School of Algiers, Algiers, Algeria.

M. G. Amin is with the Department of Electrical and Computer Engineering, Villanova University, Villanova, PA 19085 USA (e-mail: moeness@ece.vill.edu).

Publisher Item Identifier S 1053-587X(98)07799-X.

II. PROBLEM FORMULATION

A. Data Model

In most practical situations, we have to process multidimensional observations of the form

$$\mathbf{x}(t) = \mathbf{y}(t) + \mathbf{n}(t) = \mathbf{A}\mathbf{s}(t) + \mathbf{n}(t) \quad (1)$$

where $\mathbf{x}(t)$ is a noisy instantaneous linear mixture of source signals, and $\mathbf{n}(t)$ is the additive noise. This model is commonly used in the field of narrowband array processing. In this context, the vector $\mathbf{s}(t) = [s_1(t), \dots, s_n(t)]^T$ consists of the signals emitted by n narrowband sources, whereas the vector $\mathbf{y}(t) = [y_1(t), \dots, y_m(t)]^T$ contains the array output. Both vectors are sampled at time t . Matrix \mathbf{A} is the transfer function between the sources and the array sensors. In the following, this matrix is referred to as the "array matrix" or the "mixing matrix."

B. Assumptions

The source signal vector $\mathbf{s}(t)$ is assumed to be a nonstationary multivariate process with

$$\begin{aligned} \text{H1): } \mathbf{R}_s &= \lim_{T \rightarrow \infty} \frac{1}{T} \sum_{t=1}^T \mathbf{s}(t+\tau) \mathbf{s}^*(t) \\ &= \text{diag}[r_{11}(\tau), \dots, r_{nn}(\tau)] \end{aligned} \quad (2)$$

where superscript $*$ denotes the conjugate transpose of a vector, $\text{diag}[\cdot]$ is the diagonal matrix formed with the elements of its vector valued argument, and $r_{ii}(\tau) = \lim_{T \rightarrow \infty} \frac{1}{T} \sum_{t=1}^T s_i(t+\tau) s_i^*(t)$ denotes the autocorrelation of $s_i(t)$. Assumption H1) means that the component $s_i(t)$, $1 \leq i \leq n$ are mutually uncorrelated as their cross-correlations are equal to zero.

The additive noise $\mathbf{n}(t)$ is modeled as a stationary, temporally white, zero-mean complex random process independent of the source signals. For simplicity, we also require $\mathbf{n}(t)$ to be spatially white, i.e.,

$$\text{(H2): } E(\mathbf{n}(t+\tau) \mathbf{n}^*(t)) = \sigma^2 \delta(\tau) \mathbf{I} \quad (3)$$

where $\delta(\tau)$ is the Kronecker delta, and \mathbf{I} denotes the identity matrix.

The $m \times n$ complex matrix \mathbf{A} is assumed to have full column rank but is otherwise unknown. In contrast with traditional parametric methods, no specific array geometry or sensor characteristics are assumed, i.e., the array manifold is unknown.

The aim of blind source separation is to identify the mixture matrix and/or to recover the source signals from the array output $\mathbf{x}(t)$ without any *a priori* knowledge of the array manifold.

C. Problem Indeterminacies

This problem of blind source separation has two inherent ambiguities. First, it is not possible to know the original labeling of the sources; hence, any permutation of the estimated sources is also a satisfactory solution. The second ambiguity is that it is inherently impossible to uniquely identify the source

signals. This is because the exchange of a fixed scalar factor between a source signal and the corresponding column of the mixture matrix \mathbf{A} does not affect the observations as is shown by

$$\mathbf{x}(t) = \mathbf{A}\mathbf{s}(t) + \mathbf{n}(t) = \sum_{i=1}^n \frac{\alpha_i}{\alpha_i} \alpha_i s_i(t) + \mathbf{n}(t) \quad (4)$$

where α_i is an arbitrary complex factor, and \mathbf{a}_i denotes the i th column of \mathbf{A} .

We take advantage of the second indeterminacy by treating the source signals as if they have unit power so that the dynamic range of the sources is accounted for by the magnitude of the corresponding columns of \mathbf{A} . This normalization convention turns out to be convenient in the sequel; it does not affect the performance results presented below. Since the sources are assumed to be uncorrelated, we have

$$\mathbf{R}_s = \mathbf{I} \text{ so that } \mathbf{R}_y \stackrel{\text{def}}{=} \lim_{T \rightarrow \infty} \frac{1}{T} \sum_{t=1}^T \mathbf{y}(t) \mathbf{y}^*(t) = \mathbf{A} \mathbf{A}^H \quad (5)$$

where the superscript H denotes the complex conjugate transpose of a matrix. This normalization still leaves undetermined the ordering and the phases of the columns of \mathbf{A} . Hence, the blind source separation must be understood as the identification of the mixing matrix and/or the recovering of the source signals up to a fixed permutation and some complex factors.

III. SPATIAL TIME-FREQUENCY DISTRIBUTIONS

The discrete-time form of the Cohen's class of TFD's, for signal $x(t)$, is given by [16]

$$\begin{aligned} D_{xx}(t, f) &= \sum_{l=-\infty}^{\infty} \sum_{m=-\infty}^{\infty} \phi(m, l) x(t+m+l) \\ &\quad \times x^*(t+m-l) e^{-j4\pi f l} \end{aligned} \quad (6)$$

where t and f represent the time index and the frequency index, respectively. The kernel $\phi(m, l)$ characterizes the distribution and is a function of both the time and lag variables. The cross-TFD of two signals $x_1(t)$ and $x_2(t)$ is defined by

$$\begin{aligned} D_{x_1 x_2}(t, f) &= \sum_{l=-\infty}^{\infty} \sum_{m=-\infty}^{\infty} \phi(m, l) x_1(t+m+l) \\ &\quad \times x_2^*(t+m-l) e^{-j4\pi f l}. \end{aligned} \quad (7)$$

Expressions (6) and (7) are now used to define the following data *spatial t-f distribution* (STFD) matrix,

$$\begin{aligned} D_{xx}(t, f) &= \sum_{l=-\infty}^{\infty} \sum_{m=-\infty}^{\infty} \phi(m, l) x(t+m+l) \\ &\quad \times x^*(t+m-l) e^{-j4\pi f l} \end{aligned} \quad (8)$$

where $[D_{xx}(t, f)]_{ij} = D_{x_i x_j}(t, f)$, for $i, j = 1, \dots, n$.

A more general definition of the STFD matrix can be given as

$$\begin{aligned} D_{xx}(t, f) &= \sum_{l=-\infty}^{\infty} \sum_{m=-\infty}^{\infty} \Phi(m, l) \odot x(t+m+l) \\ &\quad \times x^*(t+m-l) e^{-j4\pi f l} \end{aligned} \quad (9)$$

where \odot designates the Hadamard product, and $[\Phi(m, l)]_{ij} = \phi_{ij}(m, l)$ is the t - f kernel associated with the pair of the sensor data $x_i(t)$ and $x_j(t)$.

Under the linear data model of (1) and assuming noise-free environment, the STFD matrix takes the simple structure in

$$D_{xx}(t, f) = AD_{ss}(t, f)A^H \quad (10)$$

where $D_{ss}(t, f)$ is the signal TFD matrix whose entries are the auto- and cross-TFD's of the sources. We note that $D_{xx}(t, f)$ is of dimension $m \times m$, whereas $D_{ss}(t, f)$ is of $n \times n$ dimension. For narrowband array signal processing applications, matrix A holds the spatial information and maps the auto- and cross-TFD's of the sources into auto- and cross-TFD's of the data.

Expression (10) is similar to that which commonly used in blind source separation [12] and direction-of-arrival (DOA) estimation problems, relating the signal correlation matrix to the data spatial correlation matrix. The two subspaces spanned by the principle eigenvectors of $D_{xx}(t, f)$ and the columns of A are, therefore, identical. Since the off-diagonal elements are crossterms of $D_{ss}(t, f)$, then this matrix is diagonal for each t - f point that corresponds to a true power concentration, i.e., signal auto-term. In the sequel, we consider the t - f points that satisfy this property. In practice, to simplify the selection of autoterms, we apply a smoothing kernel $\phi(m, l)$ that significantly decreases the contribution of the crossterms in the t - f plane. This kernel can be a member of the reduced-interference distribution (RID) introduced in [17], or it can be signal dependent, which matches the underlying signal characteristics [18]–[20].

IV. A TWO-STEP BLIND IDENTIFICATION APPROACH

In this section, we present a new blind identification approach based on two step processing: the first step consists of whitening the data in order to transform the mixing matrix A into a unitary matrix. The second step consists then of retrieving this unitary matrix by joint diagonalizing a set of data-STFD matrices.

A. First Step

The first processing step consists of whitening the signal part $y(t)$ of the observation. This is achieved by applying a whitening matrix W to $y(t)$, i.e., an $n \times m$ matrix satisfying

$$\lim_{T \rightarrow \infty} \frac{1}{T} \sum_{t=1}^T W y(t) y^*(t) W^H = W R_y W^H = I \quad (11)$$

where $R_y = \lim_{T \rightarrow \infty} \frac{1}{T} \sum_{t=1}^T y(t) y^*(t)$ is the autocorrelation matrix of the noiseless array output. Equation (11) shows that if W is a whitening matrix, then WA is a $n \times n$ unitary matrix. It follows that for any whitening matrix W , there exists a $n \times n$ unitary matrix U such that $WA = U$. As a consequence, matrix A can be factored as

$$A = W^{\#} U \quad (12)$$

where the superscript $\#$ denotes the Moore–Penrose pseudoinverse. This whitening procedure reduces the determination of the $m \times n$ mixture matrix A to that of a unitary $n \times n$ matrix U . The whitened data vector $z(t) = Wx(t)$ still obeys a linear model

$$z(t) \stackrel{\text{def}}{=} Wx(t) = W(As(t) + n(t)) = Us(t) + Wn(t). \quad (13)$$

The signal part of the whitened process now is a “unitary mixture” of the source signals. Note that all information contained in the autocorrelation matrix is “exhausted” after the whitening procedure in the sense that changing U in (13) to any other unitary matrix leaves the autocorrelation matrix of $z(t)$ unchanged. Note also that besides whitening the signal part of the observations, multiplication by a whitening matrix W reduces the array output to an n -dimensional vector.

Under the assumption of the linear model (1), the data autocorrelation matrix has the following structure:

$$R \stackrel{\text{def}}{=} \lim_{T \rightarrow \infty} \frac{1}{T} \sum_{t=1}^T x(t) x^*(t) = R_y + \sigma^2 I. \quad (14)$$

Combining (14) and (5), we have

$$AA^H = R - \sigma^2 I \quad (15)$$

Hence, from (11) and (15), the whitening matrix W can be determined from the array output autocorrelation R . As shown by (12), finding a whitening matrix still leaves undetermined some unitary factor in A . This “missing factor” U can be determined from higher order statistics, as investigated in [6], [21], [7], or from second order statistics as proposed in [12]. As explained below, by exploiting the t - f dependence structure (10), the missing rotation may be also retrieved from spatial time frequency distributions at properly chosen t - f points.

B. Second Step

By pre and postmultiplying the STFD matrices $D_{xx}(t, f)$ by W , we obtain the whitened STFD-matrices as

$$D_{zz}(t, f) = W D_{xx}(t, f) W^H \quad (16)$$

which is, in essence, the STFD of the whitened data vector z . From the definition of W and (10), we may express $D_{zz}(t, f)$ as

$$D_{zz}(t, f) = U D_{ss}(t, f) U^H. \quad (17)$$

Since the matrix U is unitary and $D_{ss}(t, f)$ is diagonal, (17) shows that any whitened data STFD-matrix is diagonal in the basis of the columns of the matrix U (the eigenvalues of $D_{zz}(t, f)$ being the diagonal entries of $D_{ss}(t, f)$). As a consequence, the missing unitary matrix U may be obtained as a unitary diagonalizing matrix of a whitened STFD matrix for some t - f point corresponding to a signal autoterm. More formally, we have the following theorem.

Theorem 1 (First Identifiability Condition): Let (t_a, f_a) be a t - f point corresponding to a signal autoterm and V be a unitary matrix such that

$$V^H D_{zz}(t_a, f_a) V = \text{diag}[d_1, \dots, d_n]. \quad (18)$$

For all $1 \leq i \neq j \leq n$ $D_{s_i s_i}(t_a, f_a) \neq D_{s_j s_j}(t_a, f_a)$. (19)

Then

- V is equal to U up to a phase and a permutation of its columns;
- there exists a permutation γ on $\{1, \dots, n\}$ such that

$$[D_{s_{\gamma(1)}}(t_a, f_a), \dots, D_{s_{\gamma(n)}}(t_a, f_a)] = [d_{\gamma(1)}, \dots, d_{\gamma(n)}].$$

This is a direct consequence of the spectral theorem for normal matrices (see [22, Th. 2.5.4]). We recall that an $n \times n$ matrix M is said to be *normal* if $MM^H = M^H M$. According to Theorem 1, for the (t_a, f_a) point, if the diagonal elements of $D_{ss}(t_a, f_a)$ are all distinct, the missing unitary matrix U may be "uniquely" (i.e. up to permutation and phase shifts) retrieved by computing the eigendecomposition of $D_{zz}(t_a, f_a)$. However, when the t - f signatures of the different signals are not highly overlapping or frequently intersecting, which is likely to be the case, the selected (t_a, f_a) point often corresponds to a single signal auto-term, rendering matrix $D_{ss}(t_a, f_a)$ deficient. That is, only one diagonal element of $D_{ss}(t_a, f_a)$ is different from zero. It follows that the determination of the matrix U from the eigendecomposition of a single whitened data STFD-matrix is no longer "unique" in the sense defined above.

The situation is more favorable when considering *simultaneous diagonalization* of a combined set $\{D_{zz}(t_i, f_i) \mid i = 1, \dots, p\}$ of p STFD matrices. This amounts to incorporating several t - f points in the source separation problem.

Theorem 2 (Second Identifiability Condition): Let $(t_1, t_1), (t_2, t_2), \dots, (t_K, t_K)$ be K t - f points corresponding to signal autoterms, and let V be a unitary matrix such that

For all $1 \leq k \leq K$

$$V^H D_{zz}(t_k, f_k) V = \text{diag}[d_1(k), \dots, d_n(k)] \quad (20)$$

For all $1 \leq i \neq j \leq n$ there exists k , $1 \leq k \leq K$

$$D_{s_i s_i}(t_k, f_k) \neq D_{s_j s_j}(t_k, f_k). \quad (21)$$

Then

- V is equal to U up to a phase and a permutation of its columns;
- there exists a permutation γ on $\{1, \dots, n\}$ such that

$$[D_{s_{\gamma(1)}}(t_k, f_k), \dots, D_{s_{\gamma(n)}}(t_k, f_k)] = [d_{\gamma(1)}(k), \dots, d_{\gamma(n)}(k)] \quad 1 \leq k \leq K.$$

This is a consequence of the uniqueness of the joint diagonalization: (see [12, Th. 3]). Again, the existence of a unitary matrix V that simultaneously diagonalizes the set of STFD matrices $\{D_{zz}(t_1, f_1), \dots, D_{zz}(t_K, f_K)\}$ is guaranteed by (17) for any choice of t - f points corresponding to signal autoterms. Condition (21), although it is weaker than condition (19), it is not always satisfied. In particular, in the trivial case where

the sources show identical t - f signatures, the mixing matrix A cannot be identified by resorting to Theorem 2. Conversely, when the source signals have different t - f signatures, it is always possible to find a set of t - f points corresponding to signal autoterms such that condition (21) is met.

C. Joint Diagonalization

The *joint diagonalization* [12], [13] can be explained by first noting that the problem of the diagonalization of a single $n \times n$ normal matrix M is equivalent to the minimization of the criterion [23]

$$C(M, V) \stackrel{\text{def}}{=} - \sum_i |v_i^* M v_i|^2 \quad (22)$$

over the set of unitary matrices $V = [v_1, \dots, v_n]$. Hence, the joint diagonalization of a set $\{M_k \mid k = 1 \dots K\}$ of K arbitrary $n \times n$ matrices is defined as the minimization of the following *JD* criterion:

$$C(V) \stackrel{\text{def}}{=} - \sum_k C(M_k, V) = - \sum_{ki} |v_i^* M_k v_i|^2 \quad (23)$$

under the same unitary constraint.

It is important to note that the above definition of joint diagonalization does *not* require the matrix set under consideration to be exactly and simultaneously diagonalized by a single unitary matrix. This is because we do not require the off-diagonal elements of all the matrices to be cancelled by a unitary transform; a joint diagonalizer is simply a minimizer of the *JD* criterion. If the matrices in $\{M_k \mid k = 1 \dots K\}$ are not exactly joint diagonalizable, the *JD* criterion cannot be zeroed, and the matrices can only be approximately joint diagonalized. Hence, an (approximate) joint diagonalizer defines a kind of an "average eigenstructure." Note that a numerically efficient algorithm for solving (23) exists in [12] and is based on a generalization of the Jacobi technique [23].

D. Summary

Based on the previous sections, we can introduce a time-frequency separation (TFS) algorithm. The TFS is defined by the following implementation.

- 1) Estimate the autocorrelation matrix \hat{R} from T data samples. Denote by $\lambda_1, \dots, \lambda_n$ the n largest eigenvalues and h_1, \dots, h_n the corresponding eigenvectors of \hat{R} .
- 2) Under the white noise assumption, an estimate $\hat{\sigma}^2$ of the noise variance is the average of the $m - n$ smallest eigenvalues of \hat{R} . The whitened signals are $z(t) = [z_1(t), \dots, z_n(t)]^T$ computed by $z_i(t) = (\lambda_i - \hat{\sigma}^2)^{-1/2} h_i^* x(t)$ for $1 \leq i \leq n$. This is equivalent to forming a whitening matrix by $\hat{W} = [(\lambda_1 - \hat{\sigma}^2)^{-1/2} h_1, \dots, (\lambda_n - \hat{\sigma}^2)^{-1/2} h_n]^H$.
- 3) Form K matrices by computing the STFD of $z(t)$ for a fixed set of (t_i, f_i) points, $i = 1, \dots, K$, corresponding to signal autoterms.
- 4) A unitary matrix \hat{U} is then obtained as joint diagonalizer of the set $\{D_{zz}(t_i, f_i) \mid i = 1, \dots, K\}$.
- 5) The source signals are estimated as $\hat{s}(t) = \hat{U}^H \hat{W} x(t)$, and/or the mixing matrix A is estimated as $\hat{A} = \hat{W}^H \hat{U}$.

V. ASYMPTOTIC PERFORMANCE ANALYSIS

In this section, an asymptotic performance analysis of the proposed method is carried out. To ease the derivations, we make the following two assumptions.

H1') Each source signal $s_i(t)$ is a deterministic sequence.

H2') The additive noise $n(t)$ is complex circular Gaussian process.

To eliminate the phase and permutation indeterminacies, we shall assume that they are fixed in such a way that the matrix estimate \hat{A} is closer to the true mixture matrix A than to some other matrix equal to A up to a phase and a permutation of its columns. In addition, the STFD are computed at a set of t - f points $\{(t_i, f_i), i = 1, \dots, K\}$ such that the identifiability condition of Theorem 2 is satisfied.

A. Performance Index

Rather than estimating the variance of the coefficients of the mixing matrix, it is more relevant with respect to the source separation issue to compute an index that quantifies the performance in terms of interference rejection, as follows. Assume that at each time instant t , an estimate of the vector of source signals is computed by applying the pseudoinverse of the estimated mixture matrix to the received signal $x(t)$, i.e.,

$$\hat{s}(t) = \hat{A}^\# x(t) = \hat{A}^\# A s(t) + \hat{A}^\# n(t) \quad (24)$$

where $\hat{A}^\# = \hat{U}^H \hat{W}$. We stress that in general, this procedure is not optimal for recovering the source signals based on an estimate \hat{A} . For large enough sample size T , matrix \hat{A} should be close to the true mixing matrix A so that $\hat{A}^\# A$ is close to the identity matrix. The performance index used in the sequel is the interference-to-signal ratio (ISR), which is defined as

$$\mathcal{I}_{pq} = E|(\hat{A}^\# A)_{pq}|^2. \quad (25)$$

This actually defines an ISR because by our normalization convention (5), we have $\mathcal{I}_{pp} \simeq 1$ for large enough T . Thus, \mathcal{I}_{pq} measures the ratio of the power of the interference of the q th source to the power of the p th source signal estimated as in (25). As a measure of the global quality of the separation, we also define a global rejection level

$$\mathcal{I}_{\text{perf}} \stackrel{\text{def}}{=} \sum_{q \neq p} \mathcal{I}_{pq}. \quad (26)$$

B. Outline of the Performance Analysis

The purpose of this section is to give a closed-form expression of the mean rejection level (25). Giving the details of a rigorous proof goes far beyond the scope of this paper. We present only an outline of the derivation below with additional mathematical details in the Appendix.

The matrix estimate \hat{A} is a "function" of the data autocorrelation matrix R , and the STFD matrices $(D_{xx}(t_1, f_1), D_{xx}(t_2, f_2), \dots, D_{xx}(t_K, f_K))$ of the observed signal $x(t)$. The computation proceeds in two steps: First, we compute the leading term in the Taylor series expansion of $|(\hat{A}^\# A)_{pq}|^2$ (see Lemma 1). Then, by computing the expectation of the aforementioned leading term, we obtain the desired result.

Lemma 1: The Taylor series expansion of $|(\hat{A}^\# A)_{pq}|^2$ is given for $p \neq q$ by

$$\begin{aligned} |(\hat{A}^\# A)_{pq}|^2 &= |\alpha_{pq} C_{pq}|^2 + \sum_{k=1}^K \alpha_{pq} \alpha_{pq}(k) [C_{qp} C_{pq}(k) \\ &\quad + C_{pq} C_{qp}(k)] + \sum_{k=1, l=1}^{K, K} \alpha_{pq}(k) \alpha_{pq}(l) \\ &\quad \times C_{pq}(k) C_{qp}(l) \\ &\quad + O\left(\|\delta R\|^3 + \sum_{k=1}^K \|\delta D_{xx}(t_k, f_k)\|^3\right) \end{aligned}$$

with

$$\begin{aligned} d_r &= [D_{s_r, s_r}(t_1, f_1), \dots, D_{s_r, s_r}(t_K, f_K)]^T \\ \alpha_{pq} &= 1 + \frac{|d_p|^2 - |d_q|^2}{|d_p - d_q|^2} \\ \alpha_{pq}(k) &= \frac{D_{s_r, s_r}^*(t_k, f_k) - D_{s_q, s_q}^*(t_k, f_k)}{|d_p - d_q|^2} \\ C &= -\frac{1}{2} A^\# \delta R A^\# + \frac{\text{Tr}(\Pi \delta R)}{2(m-n)} (A^H A)^{-1} \\ C(k) &= \frac{1}{2} A^\# \delta D_{xx}(t_k, f_k) A^\# \\ \delta R &= \hat{R} - R \\ \delta D_{xx}(t_k, f_k) &= D_{xx}(t_k, f_k) - A \text{diag}[D_{s_1, s_1}(t_k, f_k), \dots, \\ &\quad D_{s_m, s_m}(t_k, f_k)] A^H \\ &= A \{D_{ss}(t_k, f_k) - \text{diag}[D_{s_1, s_1}(t_k, f_k), \dots, \\ &\quad D_{s_m, s_m}(t_k, f_k)]\} A D_{nn}(t_k, f_k) \\ &\quad + D_{ns}(t_k, f_k) A^H + D_{nn}(t_k, f_k) \end{aligned}$$

where $\text{Tr}(\cdot)$ is the trace of the matrix, Π denotes the orthogonal projector on the noise subspace (i.e., the subspace orthogonal to the range of matrix A), and $C_{pq}(\cdot)$ is the pq th element of the matrix $C(\cdot)$.

The proof of the above lemma follows closely the same steps used in [12]. For more details, see Appendix A.

The expectation of $|(\hat{A}^\# A)_{pq}|^2$ can be computed from the expectations of $|C_{pq}|^2$, $C_{qp} C_{pq}(k)$, and $C_{qp}(l) C_{pq}(k)$. Conditions H1') and H2') reduce this computation to simple algebra, yielding

$$\begin{aligned} E(|C_{pq}|^2) &= \frac{1}{4} |r_{T, pq}|^2 + \frac{1}{4T} \left[\sigma^2 (r_{T, pp} J_{qq} + r_{T, qq} J_{pp}) \right. \\ &\quad \left. + \sigma^4 \left(J_{pp} J_{qq} + \frac{|J_{pq}|^2}{m-n} \right) \right] \\ E(C_{qp} C_{pq}(k)) &= -\frac{1}{4} r_{T, qp} D_{s_r, s_r}(t_k, f_k) - \frac{\sigma^2}{4} \left[|r_{T, qp}|^2 J_{r-1} \right. \\ &\quad \left. + \frac{1}{T} (D_{s_r, s_r}(t_k, f_k) J_{qq} \right. \\ &\quad \left. + D_{s_q, s_q}(t_k, f_k) J_{pp}) \right] - \frac{\sigma^4}{4T} J_{qq} J_{pp} \end{aligned}$$

$$E(C_{pq}(k)C_{qp}(l)) = \frac{1}{4}D_{s_p s_q}(t_k, f_k)D_{s_q s_p}(t_l, f_l) + \frac{1}{4}[\sigma^2(D_{s_p s_q}(t_k, f_k)J_{qp} + D_{s_q s_p}(t_l, f_l)J_{pq} + F_{s_p s_q}(k, l)J_{qq} + F_{s_q s_p}(l, k)J_{pp}) + \sigma^4(|J_{pq}|^2 + J_{pp}J_{qq}\phi_{kl})]$$

where we have set

$$\begin{aligned} r_{T_{pq}} &= \frac{1}{T} \sum_{t=1}^T s_p(t)s_q^*(t) \\ J_{pq} &= (A^H A)_{pq}^{-1} \\ F_{s_p s_q}(k, l) &= \sum_{v'=-\infty}^{+\infty} \sum_{v=-\infty}^{+\infty} \left[\sum_{m=-\infty}^{+\infty} \phi(m, v) \right. \\ &\quad \times \phi(m - v - v' + t_k - t_l, v')s_p(t_k + m + v) \\ &\quad \times s_q^*(t_k + m - v - 2v') \Big] e^{-j4\pi f_k v} e^{-j4\pi f_l v'} \\ \phi_{kl} &= \sum_{v=-\infty}^{+\infty} \left[\sum_{m=-\infty}^{+\infty} \phi(m, v)\phi^*(m + (t_k - t_l), v) \right] \\ &\quad \times e^{-j4\pi(f_k - f_l)v} \end{aligned}$$

It can be readily shown that [24]

$$\begin{aligned} \lim_{T \rightarrow \infty} TE\|\delta R\|^3 &= 0 \\ \lim_{T \rightarrow \infty} TE\|\delta D_{xx}(t_k, f_k)\|^3 &= 0. \end{aligned}$$

Using the above results, the ISR is asymptotically given by

$$I_{pq} = I_{pq}^0 + \sigma^2 I_{pq}^1 + \sigma^4 I_{pq}^2 \quad (27)$$

where the coefficients of the expansion are

$$\begin{aligned} I_{pq}^0 &= \frac{1}{4} \left[\alpha_{pq}^2 |r_{T_{pq}}|^2 - \sum_{k=1}^K \alpha_{pq} \alpha_{pq}(k) \right. \\ &\quad \times [r_{T_{pq}} D_{s_p s_q}(t_k, f_k) + r_{T_{qp}} D_{s_q s_p}(t_k, f_k)] \\ &\quad \left. + \sum_{k=1, l=1}^{K, K} \alpha_{pq}(k) \alpha_{pq}(l) D_{s_p s_q}(t_k, f_k) D_{s_q s_p}(t_l, f_l) \right] \\ I_{pq}^1 &= \frac{1}{4} \left[\frac{\alpha_{pq}^2}{T} (r_{T_{pp}} J_{qq} + r_{T_{qq}} J_{pp}) \right. \\ &\quad - \sum_{k=1}^K \alpha_{pq} \alpha_{pq}(k) [r_{T_{pq}} J_{qp} + r_{T_{qp}} J_{pq} \\ &\quad + \frac{2}{T} (D_{s_p s_q}(t_k, f_k) J_{qq} + D_{s_q s_p}(t_k, f_k) J_{pp})] \\ &\quad + \sum_{k=1, l=1}^{K, K} \alpha_{pq}(k) \alpha_{pq}(l) (D_{s_p s_q}(t_k, f_k) J_{qp} \\ &\quad \left. + D_{s_q s_p}(t_l, f_l) J_{pq} + F_{s_p s_q}(k, l) J_{qq} + F_{s_q s_p}(l, k) J_{pp}) \right] \end{aligned}$$

$$\begin{aligned} I_{pq}^2 &= \frac{1}{4} \left[\frac{1}{T} \left[\alpha_{pq}^2 \left(J_{qq} J_{pp} + \frac{|J_{pq}|^2}{m-n} \right) \right. \right. \\ &\quad \left. - 2 \sum_{k=1}^K \alpha_{pq} \alpha_{pq}(k) J_{qq} J_{pp} \right] \\ &\quad \left. + \sum_{k=1, l=1}^{K, K} \alpha_{pq}(k) \alpha_{pq}(l) (|J_{pq}|^2 + \phi_{kl} J_{pp} J_{qq}) \right]. \end{aligned}$$

C. Discussion

For high signal-to-noise ratio, the expansion (27) of the ISR is dominated by the first term I_{pq}^0 . Below, some comments on this term are given.

- If the sources p and q have identical t - f signatures over the chosen t - f points (i.e., $d_p = d_q$), the corresponding ISR $I_{pq} \rightarrow \infty$. This confirms the statement of Theorem 2.
- As the correlation function $r_{T_{pq}}$ of the sources p and q and the crossterms $D_{s_p s_q}(t_k, f_k)$ vanish, the corresponding ISR given by I_{pq} also vanishes, yielding a perfect separation.
- I_{pq}^0 is independent of the mixing matrix. In the array processing context, it means that performance in terms of interference rejection is unaffected by the array geometry and, in particular, by the number of sensors. The performance depends only on the sample size and the t - f signatures of the sources.
- In (27), the sum over k is a sum over time and frequency. Hence, the joint diagonalization can be seen as a kind of averaging. Indeed, the choice of a large number of t - f points increases the performance.

Note that from the above analysis, the choice of the t - f kernel has a direct impact on the performance of the proposed method. Optimal smoothing kernels could, at least theoretically, be obtained by extending the previous derivations. This point is left to further study.

VI. PERFORMANCE EVALUATION

In this section, the performance of the t - f separation (TFS) method, as investigated via computer simulations, is reported. Evaluation of the domain of validity of the asymptotic performance expansion developed in the previous section are also presented.

A. Numerical Experiments

Example 1: This example deals with real source signals.

Two speech signals sampled at 8000 Hz are mixed by the mixing matrix

$$A = \begin{bmatrix} 1.0 & 0.6 & 0.4 \\ 0.5 & 1.0 & 0.8 \end{bmatrix}^T.$$

The plots of the two individual speech signals are shown in Fig. 1 and their TFD's are displayed in Fig. 2. Speech "1" and "2" of a male speaker are the words "Cars" and "Cats," respectively. The TFD's of the observed speech signals at three sensors are shown in Fig. 3. Fig. 4 shows the TFD's of the speech signals estimated by TFS. It is clear that TFS works

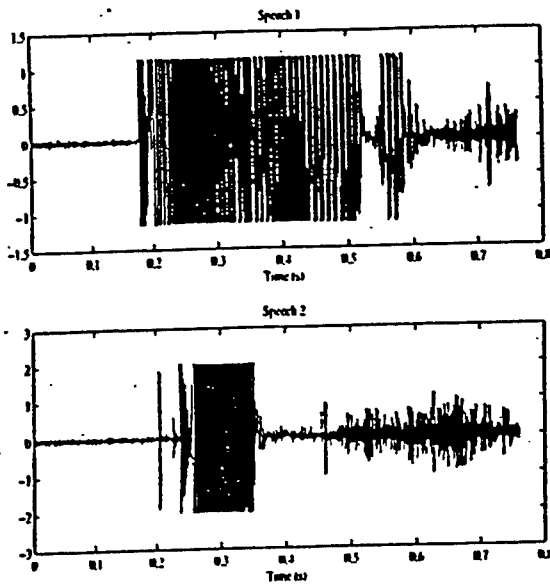


Fig. 1. Plots of individual speeches.

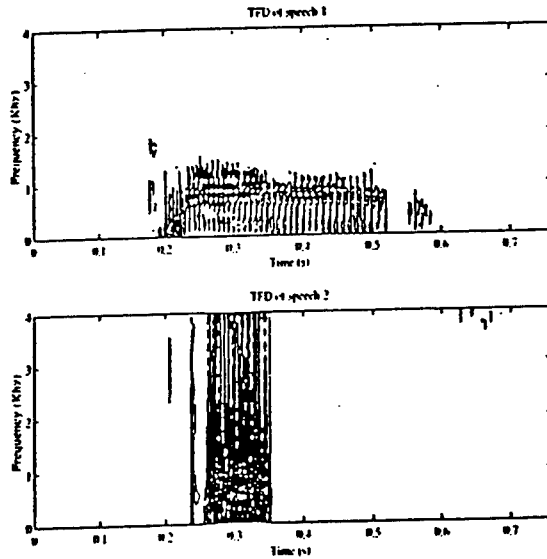


Fig. 2. TFD's of the individual speeches.

well in this case. The purpose of this example is to test the algorithm when speech signals are used. It may not reflect a real speech environment.

To assess the robustness of the TFS algorithm with respect to noise, we corrupt the observed speech signals by an additive white Gaussian noise, and we compare in Fig. 5 the performance of the second-order blind identification (SOBI) algorithm proposed in [12] and the TFS algorithm over the [0–20 dB] range of signal-to-noise ratio (SNR). The mean rejection levels are evaluated here over 100 Monte-Carlo runs

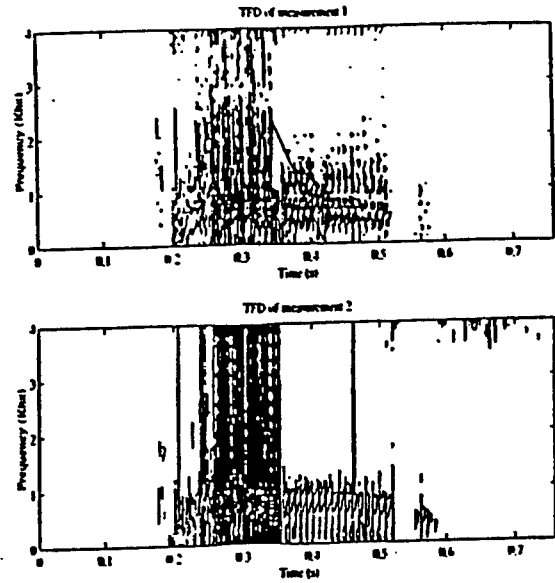


Fig. 3. TFD's of the observed signals.

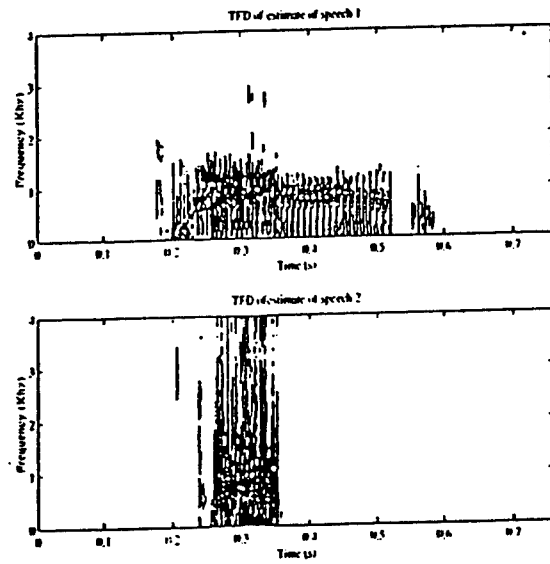


Fig. 4. TFD's of the estimate signals.

with $T = 6084$ samples. It is evident from Fig. 5 that in this case, the TFS algorithm outperforms SOBI algorithm. The increase of this robustness of the TFS algorithm with respect to noise may be explained by the effect of spreading the noise power and of localizing the source energy in the t - f domain.

Example 2: In this example, we consider a uniform linear array of three sensors having half wavelength spacing and receiving signals from two sources in the presence of white Gaussian noise. The sources arrive from different directions: $\phi_1 = 0$ and $\phi_2 = 20^\circ$ (the particular structure of the array manifold is, of course, not exploited here). The source signals are generated by filtering a complex circular white Gaussian

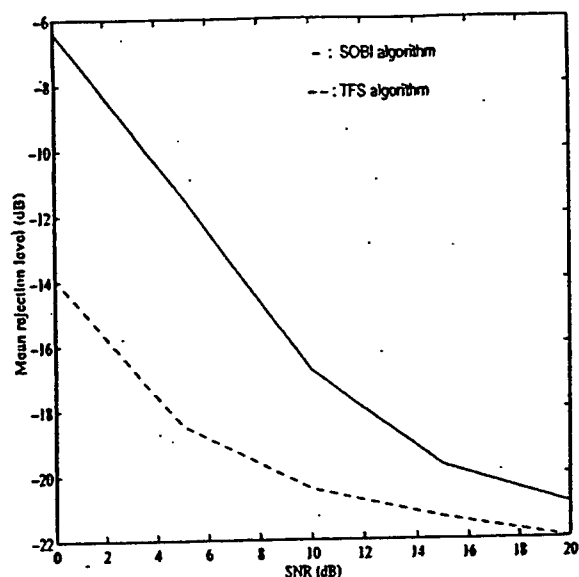


Fig. 5. Performance of SOBI and TFS algorithms versus SNR.

 TABLE I
 PERFORMANCE OF SOBI AND TFS ALGORITHMS VERSUS δf

Spectral shift (δf)	Mean Rejection level in dB	
	SOBI	TFS
0.000	-8.86	-12.22
0.002	-10.07	-12.21
0.010	-10.18	-12.34
0.050	-11.09	-12.53
0.200	-12.92	-12.54

processes by an AR model of order one with coefficient $a_1 = \rho \exp(j2\pi f_1(t))$ and $a_2 = \rho \exp(j2\pi f_2(t))$, where we have

$$f_1(t) = \begin{cases} 0.0625, & \text{for } t = 1 : 400 \\ 0.1250, & \text{for } t = 401 : 450 \\ 0.3750, & \text{for } t = 451 : 850 \end{cases}$$

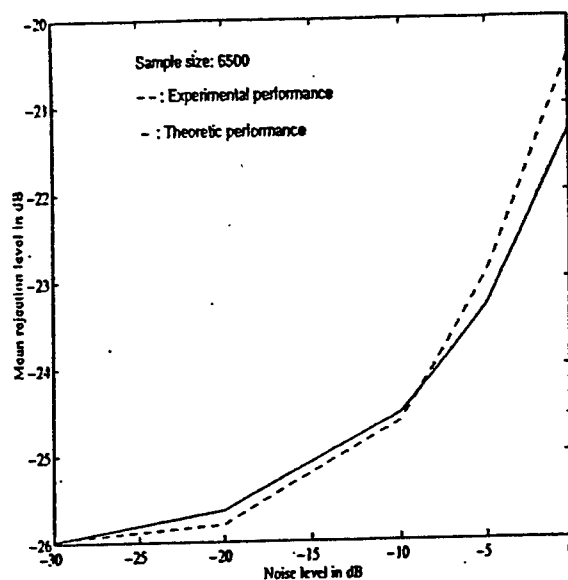
$$f_2(t) = \begin{cases} 0.3750, & \text{for } t = 1 : 400 \\ 0.1250 + \delta f, & \text{for } t = 401 : 450 \\ 0.0625, & \text{for } t = 451 : 850 \end{cases}$$

$$\rho = 0.85.$$

The signal-to-noise ratio (SNR) is set at 5 dB. The kernel used for the computation of the TFD's is the Choi-Williams kernel [16], which provides a good reduction of the crossterms. For the TFS algorithm, eight TFD matrices are considered. The corresponding t - f points are those of the highest power in the t - f domain. The mean rejection level is evaluated over 500 Monte-Carlo runs.

Table I shows the mean rejection level in dB versus the "spectral shift" δf both for the SOBI [12] and TFS algorithms. Note that for $\delta f = 0$, the two Gaussian source signals have identical spectral shape. In this case, while SOBI fails¹ in

¹We admit that a source separation algorithm fails when the mean rejection level is greater than -10 dB.


 Fig. 6. Performance validation versus σ^2 .

separating the two sources, TFS succeeds. Note also that in contrast to SOBI, TFS presents constant performance with respect to δf .

B. Experimental Validation of the Performance Analysis

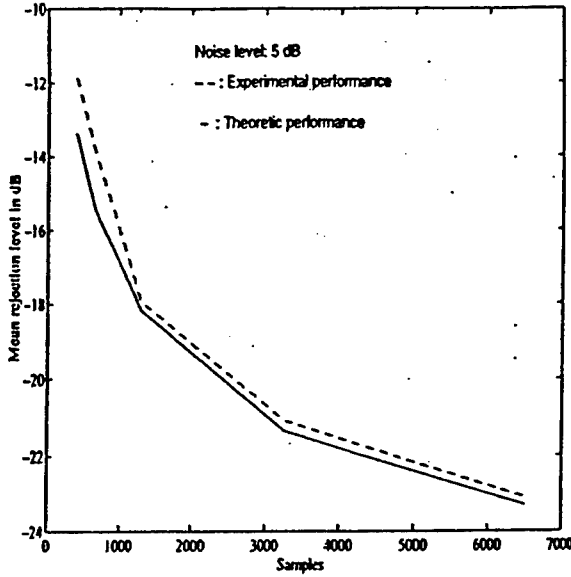
This section deals with the evaluation of the domain of validity of the first-order performance approximation (27).

The same settings than in Example 2 are used, with the exception of the source signals, which are deterministic sinusoids at frequencies $f_1 = 0.4375$ and $f_2 = 0.0625$. The TFD's are computed using windowed Wigner distribution. The chosen window width is $M = 2L + 1$, with $L = 32$. The identification is performed using $\frac{T}{M}$ STFD matrices spaced in time by M samples (T being the sample size). The overall rejection level is evaluated over 500 independent runs.

In Fig. 6, the rejection level $\mathcal{I}_{\text{perf}}$ is plotted in decibels as a function of the noise power σ^2 (also expressed in decibels). In Fig. 7, the rejection level $\mathcal{I}_{\text{perf}}$ is plotted in decibels as against sample size. Both Figs. 6 and 7 show that the approximation is better at high SNR and for large sample size. This means that the asymptotic conditions are reached faster in this range of parameters.

VII. CONCLUSION

In this paper, a new blind separation approach using t - f distributions (STFD's) is introduced. It is devised to primarily separate sources with temporal nonstationary signal characteristics. The new approach is based on the joint diagonalization of a combined set of spatial t - f distribution matrices. The later are made up of the auto- and cross-TFD's of the data snapshots across the multisensor array, and they are expressed in terms of the TFD matrices of the sources. The TFD matrices of the data and sources appear, respectively, in place of the spatial and signal correlation matrices commonly used under stationary

Fig. 7. Performance validation versus samples size (T).

environment. The diagonal structure of the TFD matrix of the sources is essential for the proposed approach and is enforced by incorporating only the T - F points corresponding to the signal autoterms. The off-diagonal elements are crossterms that become negligible by using a reduced-interference distribution kernel. We have focused on the TFD's of Cohen's class, however. We can use any other bilinear t - f distributions signal representations, such as the affine and hyperbolic classes.

The proposed approach shows a number of attractive features. In contrast to blind source separation approaches using second-order and/or high-order statistics, it allows the separation of Gaussian sources with identical spectral shapes but with different t - f localization properties. The effect of spreading the noise power while localizing the source energy in the t - f domain amounts to increasing the robustness of the proposed approach with respect to noise. The paper has included numerical experiments of simple nonstationary signals as well as real source signal data. These experiments have demonstrated the effectiveness of the proposed technique in separating a wide class of signals. The asymptotic performance analysis of the proposed technique has been provided.

APPENDIX A PROOF FOR LEMMA 1

In this section, a sketch of the proof for Lemma 1 is presented. We follow the same steps as in [12]. The square modulus $|\hat{I}_{pq}|^2$ is expressed as

$$|\hat{I}_{pq}|^2 = |(\hat{\mathbf{U}}^H \hat{\mathbf{W}} \mathbf{A})_{pq}|^2. \quad (28)$$

We decompose the matrix $\hat{\mathbf{W}} \mathbf{A}$ under its polar form

$$\hat{\mathbf{V}} \hat{\mathbf{H}} = \hat{\mathbf{W}} \mathbf{A} \quad (29)$$

where $\hat{\mathbf{V}}$ is a unitary matrix, and $\hat{\mathbf{H}}$ is a non-negative semidefinite hermitian matrix; matrix $\hat{\mathbf{H}}$ verifies $\hat{\mathbf{H}}^2 = \mathbf{A}^H \hat{\mathbf{W}}^H \hat{\mathbf{W}} \mathbf{A}$ (see [22, th. 7.3.2, p. 412]). According to the convention

outlined in Section C, matrix $\hat{\mathbf{H}}$ is expected to be close to the identity matrix; let $\delta \mathbf{H} = \hat{\mathbf{H}} - \mathbf{I}$ denote the estimation error of the hermitian part of $\hat{\mathbf{W}} \mathbf{A}$. Using standard perturbation calculus (see, for example, [25]), it can be shown that

$$\delta \mathbf{H} \approx -\frac{1}{2} \mathbf{A}^{\#} \delta \mathbf{R} \mathbf{A}^{\#H} + \frac{1}{2(m-n)} \text{Tr}(\Pi \delta \mathbf{R}) (\mathbf{A}^H \mathbf{A})^{-1} + o(\delta \mathbf{R}). \quad (30)$$

From the polar decomposition (29), the whitened STFD matrices can be similarly approximated at the first order, for all $k \neq 0$, as

$$\begin{aligned} \mathbf{D}_{xx}(t_k, f_k) &= \hat{\mathbf{W}} (\mathbf{A} \text{diag}[D_{s_1 s_1}(t_k, f_k), \dots, D_{s_n s_n}(t_k, f_k)] \mathbf{A}^H \\ &\quad + \mathbf{D}_{xx}(t_k, f_k) - \mathbf{A} \text{diag}[D_{s_1 s_1}(t_k, f_k), \dots, \\ &\quad D_{s_n s_n}(t_k, f_k)] \mathbf{A}^H) \hat{\mathbf{W}}^H \\ &= \hat{\mathbf{V}} (\hat{\mathbf{H}} \text{diag}[D_{s_1 s_1}(t_k, f_k), \dots, D_{s_n s_n}(t_k, f_k)] \hat{\mathbf{H}} \\ &\quad + \hat{\mathbf{V}}^H \hat{\mathbf{W}} \delta \mathbf{D}_{xx}(t_k, f_k) \hat{\mathbf{W}}^H \hat{\mathbf{V}}) \hat{\mathbf{V}}^H. \end{aligned} \quad (31)$$

The joint diagonalization criterion aims at searching the unitary matrix that minimizes the off-diagonal elements of a set of matrices: here, the whitened STFD matrix $\mathbf{D}_{xx}(t_k, f_k)$. It can be shown (see a discussion in [26]) that if the set of matrices entering in the JD are multiplied by a common unitary matrix, then the result of the JD will simply be multiplied by this common matrix. Formally, let $\mathbf{N}_1, \dots, \mathbf{N}_p$ be arbitrary matrices, and let \mathbf{U} be an arbitrary unitary matrix; then, $JD\{\mathbf{U} \mathbf{N}_1 \mathbf{U}^H, \dots, \mathbf{U} \mathbf{N}_p \mathbf{U}^H\} = \mathbf{U} JD\{\mathbf{N}_1, \dots, \mathbf{N}_p\}$. Applying this result in our situation, it comes from (31) that the unitary matrix $\hat{\mathbf{U}}$ resulting from the JD of the set of whitened STFD matrices $\mathbf{D}_{xx}(t_1, f_1), \dots, \mathbf{D}_{xx}(t_K, f_K)$ can be decomposed as

$$\hat{\mathbf{U}} = \hat{\mathbf{V}} \hat{\mathbf{U}}_0$$

where the matrix $\hat{\mathbf{U}}_0$ minimizes the JD criterion for the matrices

$$\begin{aligned} \mathbf{M}_k &\stackrel{\text{def}}{=} \hat{\mathbf{H}} \text{diag}[D_{s_1 s_1}(t_k, f_k), \dots, D_{s_n s_n}(t_k, f_k)] \hat{\mathbf{H}} \\ &\quad + \hat{\mathbf{V}}^H \hat{\mathbf{W}} \delta \mathbf{D}_{xx}(t_k, f_k) \hat{\mathbf{W}}^H \hat{\mathbf{V}} \\ &= \text{diag}[D_{s_1 s_1}(t_k, f_k), \dots, D_{s_n s_n}(t_k, f_k)] \\ &\quad + \text{diag}[D_{s_1 s_1}(t_k, f_k), \dots, D_{s_n s_n}(t_k, f_k)] \delta \mathbf{H} \\ &\quad + \delta \mathbf{H} \text{diag}[D_{s_1 s_1}(t_k, f_k), \dots, D_{s_n s_n}(t_k, f_k)] \\ &\quad + \hat{\mathbf{V}}^H \hat{\mathbf{W}} \delta \mathbf{D}_{xx}(t_k, f_k) \hat{\mathbf{W}}^H \hat{\mathbf{V}} + o(\delta \mathbf{D}_{xx}(t_k, f_k)) \\ &= \text{diag}[D_{s_1 s_1}(t_k, f_k), \dots, D_{s_n s_n}(t_k, f_k)] \\ &\quad + \text{diag}[D_{s_1 s_1}(t_k, f_k), \dots, D_{s_n s_n}(t_k, f_k)] \delta \mathbf{H} \\ &\quad + \delta \mathbf{H} \text{diag}[D_{s_1 s_1}(t_k, f_k), \dots, D_{s_n s_n}(t_k, f_k)] \\ &\quad + \mathbf{A}^{\#} \delta \mathbf{D}_{xx}(t_k, f_k) \mathbf{A}^{\#H} + o(\delta \mathbf{D}_{xx}(t_k, f_k)) \\ &= \text{diag}[D_{s_1 s_1}(t_k, f_k), \dots, D_{s_n s_n}(t_k, f_k)] \\ &\quad + \xi_k + o(\delta \mathbf{D}_{xx}(t_k, f_k)), \quad 1 \leq k \leq K \end{aligned}$$

where

$$\begin{aligned} \xi_k &\stackrel{\text{def}}{=} \text{diag}[D_{s_1 s_1}(t_k, f_k), \dots, D_{s_n s_n}(t_k, f_k)] \delta \mathbf{H} \\ &\quad + \delta \mathbf{H} \text{diag}[D_{s_1 s_1}(t_k, f_k), \dots, D_{s_n s_n}(t_k, f_k)] \\ &\quad + \mathbf{A}^{\#} \delta \mathbf{D}_{xx}(t_k, f_k) \mathbf{A}^{\#H}. \end{aligned}$$

Hence, (28) can be written as

$$|\hat{f}_{pq}|^2 = |(\hat{U}_0^H \hat{H})_{pq}|^2.$$

As shown in [26], the unitary matrix \hat{U}_0 is given at first order by

$$\begin{aligned} \hat{U}_0 &= I + \delta U_0 \\ \delta U_0 &= \frac{1}{2} \sum_{r \neq s} \sum_{k=1}^K (\alpha_{rs}(k) \Pi_r \xi_k \Pi_s + \alpha_{rs}^*(k) \Pi_r \xi_k^H \Pi_s) \\ (\delta U_0^H &= -\delta U_0) \end{aligned} \quad (32)$$

where $\Pi_r = e_r e_r^H$ is the orthogonal projector on the r th vector column e_r of the identity matrix I_n . The performance index becomes

$$\begin{aligned} |\hat{f}_{pq}|^2 &= |(I - \delta U_0)(I + \delta H)|_{pq}^2 \\ &\simeq |\delta H - \delta U_0|_{pq}^2 \quad \text{for } p \neq q. \end{aligned} \quad (33)$$

Including expressions (30) and (32) in (33) leads to the Taylor expansion of Lemma 1.

REFERENCES

- [1] C. M. Berrah, "Parameter yield estimation for a MOSFET integrated circuit," in *Proc. 1990 IEEE ISCAS*, pp. 2260-2263.
- [2] E. E. Cureton and R. B. D'Agostino, *FACTOR ANALYSIS on Applied Approach*. New York: Lawrence Erlbaum, 1983.
- [3] R. Schmidt, "Multiple emitter location and signal parameter estimation," *IEEE Trans. Antennas Propagat.*, vol. AP-34, pp. 276-280, 1986.
- [4] G. Demoment, "Image reconstruction and restoration: Overview of common estimation structures and problems," *IEEE Trans. Acoust., Speech, Signal Processing*, vol. 37, pp. 2024-2036, Oct. 1989.
- [5] C. Julien and J. Héroult, "Détection de grandeurs primitives dans un message composite par une architecture de calcul neuromimétique en apprentissage non supervisé," in *Proc. Gressi*, Nice, France, 1985.
- [6] M. Gaeta and J.-L. Lacoume, "Source separation without a priori knowledge: The maximum likelihood solution," in *Proc. EUSIPCO*, 1990, pp. 621-624.
- [7] P. Comon, "Independent component analysis, a new concept?" *Signal Process.*, vol. 36, pp. 287-314, 1994.
- [8] J.-F. Cardoso and A. Souloumiac, "An efficient technique for blind separation of complex sources," in *Proc. IEEE SP Workshop Higher Order Statist.*, Lake Tahoe, CA, 1993.
- [9] E. Moreau and O. Macchi, "New self-adaptive algorithms for source separation based on contrast functions," in *Proc. IEEE SP Workshop Higher Order Statist.*, Lake Tahoe, CA, 1993.
- [10] A. Belouchrani and J.-F. Cardoso, "Maximum likelihood source separation for discrete sources," in *Proc. EUSIPCO*, 1994, pp. 768-771.
- [11] L. Tong and R. Liu, "Blind estimation of correlated source signals," in *Proc. Asilomar Conf.*, Nov. 1990.
- [12] A. Belouchrani, K. A. Meraim, J.-F. Cardoso, and E. Moulines, "A blind source separation technique using second order statistics," *IEEE Trans. Signal Processing*, vol. 45, pp. 434-444, Feb. 1997.
- [13] M. Wax and J. Sheinvald, "A least-squares approach to joint diagonalization," *IEEE Signal Processing Lett.*, vol. 4, pp. 52-53, Feb. 1997.
- [14] K. Matsuoka, M. Ohya, and M. Kawamoto, "A neural net for blind separation of nonstationary signals," *Neural Networks*, vol. 8, pp. 411-419, 1995.
- [15] F. Hlawatsch and W. Krattenthaler, "Bilinear signal synthesis," *IEEE Trans. Signal Processing*, vol. 40, pp. 352-363, Feb. 1992.
- [16] L. Cohen, *Time-Frequency Analysis*. Englewood Cliffs, NJ: Prentice-Hall, 1995.
- [17] J. Jeong and W. Williams, "Kernel design for reduced interference distributions," *IEEE Trans. Signal Processing*, vol. 40, pp. 402-412, Feb. 1992.
- [18] R. Baraniuk and D. Jones, "A signal dependent time-frequency representation: Optimum kernel design," *IEEE Trans. Signal Processing*, vol. 41, pp. 1589-1603, Apr. 1993.
- [19] B. Ristic and B. Boashash, "Kernel design for time-frequency signal analysis using the Radon transform," *IEEE Trans. Signal Processing*, vol. 41, pp. 1996-2008, May 1993.
- [20] M. Amin, G. Venkatesan, and J. Carroll, "A constrained weighted least square approach for time-frequency kernel design," *IEEE Trans. Signal Processing*, vol. 44, pp. 1111-1123, May 1996.
- [21] J.-F. Cardoso and A. Souloumiac, "Blind beamforming for non Gaussian signals," *Proc. Inst. Elect. Eng.*, vol. 140, no. 6, pp. 362-370, 1993.
- [22] R. Horn and C. Johnson, *Matrix Analysis*. Cambridge, U.K.: Cambridge Univ. Press, 1985.
- [23] G. H. Golub and C. F. Van Loan, *Matrix Computations*. Baltimore, MD: Johns Hopkins Univ. Press, 1989.
- [24] M. Rosenblatt, *Stationary Sequences and Random Fields*. Berlin, Germany: Birkhauser-Verlag, 1985.
- [25] A. Belouchrani, K. Abed-Meraim, J.-F. Cardoso, and E. Moulines, "A second order blind source separation technique: Implementation and performance," Tech. Rep. 94D027, Telecom Paris, Signal Dept., 1994.
- [26] J.-F. Cardoso, "Perturbation of joint diagonalizers," Tech. Rep. 94D023, Telecom Paris, Signal Dept., 1994.



Adel Belouchrani received the State Engineering degree in 1991 from the National Polytechnic School of Algiers, Algiers, Algeria, the M.Sc. degree in signal processing from the Institut National Polytechnique de Grenoble (INPG), Grenoble, France, in 1992, and the Ph.D. degree in signal and image processing from Ecole Nationale Supérieure des Telecommunications (ENST), Paris, France, in 1995.

He was a Visiting Scholar at the Electrical Engineering and Computer Science Department, University of California, Berkeley, from 1995 to 1996, working on fast adaptive blind equalization and carrier phase tracking. He was with the Department of Electrical and Computer Engineering, Villanova University, Villanova, PA, as a Research Associate from 1996 to 1997. He also served as a consultant to Comcast Inc., Philadelphia, PA, during this period. In February 1997, he was a visiting scientist at the Laboratory for Artificial Brain Systems, Riken, Japan. From August 1997 to October 1997, he was with Alcatel ETCA, Belgium, working on the Very High Speed Digital Subscriber Line (VDSL). He is currently with the Electrical Engineering Department, National Polytechnic School of Algiers, as an Assistant Professor. His research interests are in the areas of digital communications and statistical signal processing including (blind) array processing, performance analysis, blind source separation, blind equalization, systems identification, damped sinusoids estimation, adaptive algorithms, expectation-maximization techniques applied to communications, nonstationary signals, and spread spectrum communications.



Moeness G. Amin (SM'91) received the B.Sc. degree in 1976 from Cairo University, Cairo, Egypt, the M.Sc. degree in 1980 from University of Petroleum and Minerals, Dhahran, Saudi Arabia, and the Ph.D. degree in 1984 from the University of Colorado, Boulder, all in electrical engineering.

In 1984, he joined University of Colorado, Denver, as a Visiting Assistant Professor. He has been on the Faculty of the Department of Electrical and Computer Engineering at Villanova University, Villanova, PA, since 1985, where is now a Professor. His current research interests are in the areas of time-frequency analysis, spread spectrum communications, smart antennas, and blind signal processing.

Dr. Amin is currently an Associate Editor of the IEEE TRANSACTIONS ON SIGNAL PROCESSING and a member of the Technical Committee of the IEEE Signal Processing Society on Signal Processing for Communications. He was the General Chair of the 1994 IEEE International Symposium on Time-Frequency and Time-Scale Analysis and is the General Chair of the 2000 IEEE Workshop on Statistical Signal and Array Processing, Poconos, PA. He is the recipient of the 1997 IEEE Philadelphia Section Award for "Outstanding Intellectual and Organizational Contributions to the IEEE Philadelphia Section in the Area of Signal Processing." He is also the recipient of the 1997 Villanova University Outstanding Faculty Research Award. Over the past four years, he chaired three All-Day Workshops on Smart Antennas, Recent Trends in Adaptive Filtering, and Advanced Signal Processing Applications in Wireless Communications. He is a member of Sigma Xi, Eta Kappa Nu, and Phi Kappa Phi.

On the Use of Spatial Time Frequency Distributions For Signal Extraction.

Adel Belouchrani and Moeness G. Amin

Department of Electrical and Computer Engineering,
Villanova University, Villanova PA 19085,
adel,moeness@ece.vill.edu

Abstract

This paper deals with the extraction of signals from their instantaneous linear mixtures using time-frequency distributions. Fundamentally, this problem is a signal synthesis from the time-frequency (t-f) plane. However with the incorporation of the spatial information provided by a multisensor array, the problem can be posed as special case of blind source separation. So far, the blind source separation has been solved using only statistical information available on the source signals. Herein, we propose to solve the aforementioned problem using time-frequency signal representations and the spatial array aperture. The proposed approach relies on the difference in the t-f signatures of the sources to be separated. It is based on the diagonalization of a combined set of spatial time-frequency distribution matrices. A numerical example is provided to illustrate the effectiveness of our method.

1 Introduction

In statistical signal and array processing, the problem of signal extraction has received the name of blind source separation, which becomes an emerging field of fundamental research with a broad range of applications. It is motivated by practical problems that involve several source signals and several sensors. Each sensor receives a linear mixture of the source signals. The problem of the blind source separation consists then of recovering the original waveforms of the sources without any knowledge of the mixture structure. This mixture is often a convolutive mixture. However, in this paper we focus on the blind identification of an instantaneous linear mixture, which corresponds to a linear memoryless channel. This choice is motivated not only by the fact that such model is mathematically tractable, but also by the applicability to various areas, including semiconductor manufacturing process [1], factor analysis [2], narrowband signal processing [3], and image reconstruction [4].

So far, the problem of blind source separations has been solved using statistical information available on the source signals. The first solution to the source separation problem was proposed almost a decade ago [5] and was based on the cancellation of higher order moments assuming non-Gaussian and i.i.d source signals. Other criteria based on minimizations of cost functions, such as the sum of square fourth order cumulants [6], contrast functions [6] or likelihood function [7], have been used by several researchers. In the case of non i.i.d source signals and even Gaussian sources, solutions based on second order statistics are possible [8].

When the frequency content of the source signals is time-varying, one can take advantage of the powerful tool of time-frequency distributions to separate and recover the incoming

signals. The underlying blind source separation problem can be posed as a signal synthesis [9] from the t-f plane with the incorporation of the spatial diversity provided by the multisensor array. In this case, no masking is required and cross-terms no longer represents ambiguity in the synthesis of individual components. Herein, we introduce a new blind identification technique based on a joint diagonalization of a combined set of spatial time-frequency distribution matrices. The new approach exploits the difference between the t-f signatures of the sources. This method presents a number of attractive features. In contrast to blind source separation approaches using second-order and/or high order statistics, the proposed approach allows the separation of Gaussian sources with identical spectra. Moreover, the effects of spreading the noise power while localizing the source energy in the time-frequency domain amounts to increasing the signal to noise ratio (SNR).

2 Data Model

Consider m sensors receiving an instantaneous linear mixture of signals emitted from n sources. The $m \times 1$ vector $\mathbf{x}(t)$ denotes the output of the sensors at time instant t which may be corrupted by an additive noise $\mathbf{n}(t)$. Hence, the linear data model is given by:

$$\mathbf{x}(t) = \mathbf{A}\mathbf{s}(t) + \mathbf{n}(t), \quad (1)$$

where the $m \times n$ matrix \mathbf{A} is called the 'mixing matrix'. The n source signals are collected in the $n \times 1$ vector $\mathbf{s}(t)$. The mixing matrix \mathbf{A} is full column rank but is otherwise unknown. In contrast with traditional parametric methods, no specific structure of the mixture matrix is assumed. The problem of blind source separation has two inherent indeterminacies such that the source signals can only be identified up to a fixed permutation and some complex

factors [8]. In the underlying problem, we are concerned with the separation of signals which may have similar spectra, but still possess different structures and localization properties in the time-frequency domain.

3 Spatial Time-Frequency Distributions

The Cohen's class of time-frequency distributions (TFD) [10] of the signal $x(t)$ is given by

$$D_{xx}(t, f) = \int_{-\infty}^{\infty} \int_{-\infty}^{\infty} \phi(t - u, \tau) x(u + \tau/2) x^*(u - \tau/2) e^{-j2\pi f \tau} du d\tau \quad (2)$$

where t and f represent the time index and the frequency index, respectively. The kernel $\phi(t, \tau)$ is a function of the time and lag variables. The cross-TFD of two signals $x_1(t)$ and $x_2(t)$ is defined by

$$D_{x_1 x_2}(t, f) = \int_{-\infty}^{\infty} \int_{-\infty}^{\infty} \phi(t - u, \tau) x_1(u + \tau/2) x_2^*(u - \tau/2) e^{-j2\pi f \tau} du d\tau \quad (3)$$

Expressions (2) and (3) are now used to define the following data *spatial time-frequency distribution* (STDF) matrix,

$$D_{xx}(t, f) = \int_{-\infty}^{\infty} \int_{-\infty}^{\infty} \phi(t - u, \tau) x(u + \tau/2) x^*(u - \tau/2) e^{-j2\pi f \tau} du d\tau \quad (4)$$

where $[D_{xx}(t, f)]_{ij} = D_{x_i x_j}(t, f)$, for $i, j = 1, \dots, n$.

A more general definition of the spatial time-frequency distribution matrix is given by,

$$D_{xx}(t, f) = \int_{-\infty}^{\infty} \int_{-\infty}^{\infty} \Phi(t - u, \tau) \odot x(u + \tau/2) x^*(u - \tau/2) e^{-j2\pi f \tau} du d\tau \quad (5)$$

where \odot designs the Hadamard product, and $[\Phi(t, \tau)]_{ij} = \phi_{ij}(t, \tau)$ is the kernel associated with the pair of the sensor data $x_i(t)$ and $x_j(t)$.

Under the assumption of the linear data model of Eq.(1) and neglecting the noise, the STFD matrix takes the following simple structure:

$$\mathbf{D}_{xx}(t, f) = \mathbf{A}\mathbf{D}_{ss}(t, f)\mathbf{A}^H \quad (6)$$

where the superscript H denotes the complex conjugate transpose of a matrix and $\mathbf{D}_{ss}(t, f)$ are the signal TFD matrices. We note that $\mathbf{D}_{xx}(t, f)$ is of dimension $m \times m$, whereas $\mathbf{D}_{ss}(t, f)$ is of $n \times n$ dimension. For narrowband array signal processing applications, matrix \mathbf{A} holds the spatial information, and through a similarity transformation, it maps the auto- and cross-TFDs of the sources into auto- and cross-TFDs of the data.

Expression (6) is similar to that which commonly used in blind source separation [8] and direction of arrival (DOA) estimation problems, relating the signal correlation matrix to the data spatial correlation matrix. The two subspaces spanned by the principle eigenvectors of $\mathbf{D}_{xx}(t, f)$ and the columns of \mathbf{A} are, therefore, identical. Since the off-diagonal elements are cross-terms of $\mathbf{D}_{ss}(t, f)$, then this matrix is diagonal for all (t-f) points which correspond only to the signal auto-terms. In the sequel, we consider the (t-f) points, which verify such property. In practice, to simplify the selection of such points of high power localization, we apply the smoothing kernel $\phi(t, \tau)$ that significantly decreases the contribution of the cross-terms in the t-f plane.

4 A Time Frequency Separation Principle

Let \mathbf{W} denotes a $m \times m$ matrix, such that $(\mathbf{W}\mathbf{A})(\mathbf{W}\mathbf{A})^H = \mathbf{U}\mathbf{U}^H = \mathbf{I}$, i.e. $\mathbf{W}\mathbf{A}$ is a $m \times m$ unitary matrix (this matrix is referred to as a whitening matrix, since it whitens the signal part of the observations and can be obtained from the eigendecomposition of the

autocorrelation matrix of the data $x(t)$, see [8] for more details). Pre- and post-multiplying the STFD-matrices $D_{xx}(t, f)$ by W , we then define the *whitened STFD-matrices* as:

$$\underline{D}_{xx}(t, f) = W D_{xx}(t, f) W^H \quad (7)$$

From the definition of W and Eq.(6), we may expressed $\underline{D}_{xx}(t, f)$ as

$$\underline{D}_{xx}(t, f) = U D_{ss}(t, f) U^H \quad (8)$$

Since the matrix U is unitary and $D_{ss}(t, f)$ is diagonal, expression (8) shows that any whitened data STFD-matrix is diagonal in the basis of the columns of the matrix U (the eigenvalues of $\underline{D}_{xx}(t, f)$ being the diagonal entries of $D_{ss}(t, f)$).

If, for a $(t-f)$ point, the diagonal elements of $D_{ss}(t, f)$ are all distinct, the missing unitary matrix U may be 'uniquely' (i.e. up to permutation and phase shifts) retrieved by computing the eigendecomposition of $\underline{D}_{xx}(t, f)$. However, when the $t-f$ signatures of the different signals are not highly overlapping or frequently intersecting, which is likely to be the case, the selected $(t-f)$ point often corresponds to one signal auto-term, rendering matrix $D_{ss}(t, f)$ deficient. That is, only one diagonal element of $D_{ss}(t, f)$ is different from zero. It follows that the determination of the matrix U from the eigendecomposition of a single whitened data STFD-matrix is no longer 'unique' in the sense define above.

The situation is more favorable when considering *joint diagonalization* of a combined set $\{\underline{D}_{xx}(t_i, f_i) | i = 1, \dots, p\}$ of p STFD matrices. This amounts to incorporating several $(t-f)$ points in the source separation problem. It is noteworthy that two source signals with identical $t-f$ signatures can not be separated even with the inclusion of all information in the $t-f$ plane.

The *joint diagonalization* can be explained by first noting that the problem of the diagonalization of a single $n \times n$ normal matrix M is equivalent to the minimization of the criterion $C(M, V) \stackrel{\text{def}}{=} -\sum_i |v_i^* M v_i|^2$ over the set of unitary matrices $V = [v_1, \dots, v_n]$ [11]. Hence, the Joint diagonalization of a set $\{M_k | k = 1..p\}$ of p arbitrary $n \times n$ matrices is defined as the minimization of the criterion:

$$C(V) \stackrel{\text{def}}{=} -\sum_k C(M_k, V) = -\sum_{ki} |v_i^* M_k v_i|^2 \quad (9)$$

under the same unitary constraint. An efficient algorithm for solving (9) already exists in [8] and is the generalization of the Jacobi technique [11].

5 An example

Here we present an illustration that involves real data signals. Two speech signals sampled at 8000 Hz are mixed by the following mixing matrix,

$$A = \begin{bmatrix} 1.0 & 0.5 \\ 0.6 & 1.0 \\ 0.4 & 0.8 \end{bmatrix}.$$

The kernel used for the computation of the TFDs is the Choi-Williams kernel[10], which provide a good cancellation of the cross-terms. Four STFD matrices are considered. The corresponding (t-f) points are those of the highest power in the t-f plane. The TFDs of the two individual speech signals are shown in Fig.1. Speech 1 and 2 of a male speaker are the words "Cars" and "Cats", respectively. The TFDs of the observed speech signals at three sensors are displayed in Fig.2. Figure 3 shows the TFDs of the estimated speech signals by

TFS. It is clear that TFS works well in this case. The purpose of this example is to test the algorithm when speech signals are used.

References

- [1] C. M. Berrah, "Parameter yield estimation for a MOSFET integrated circuit," in *Proc. 1990 IEEE ISCAS*, pp. 2260-2263, 1990.
- [2] E. E. Cureton and R. B. D'Agostino, *FACTOR ANALYSIS An Applied Approach*. Lawrence Erlbaum Associates, 1983.
- [3] R. Schmidt, "Multiple emitter location and signal parameter estimation," *IEEE Trans. on AP*, vol. 34, no. 1, pp. 276-280, 1986.
- [4] G. Demoment, "Image reconstruction and restoration: Overview of common estimation structures and problems," *IEEE Trans. on ASSP*, vol. 37, pp. 2024-22036, Oct. 1989.
- [5] C. Jutten and J. Héroult, "Détection de grandeurs primitives dans un message composite par une architecture de calcul neuromimétique en apprentissage non supervisé," in *Proc. Grets, (Nice)*, 1985.
- [6] P. Comon, "Independent component analysis, a new concept?," *Signal Processing*, vol. 36, pp. 287-314, 1994.
- [7] A. Belouchrani and J.-F. Cardoso, "Maximum likelihood source separation for discrete sources," in *Proc. EUSIPCO*, pp. 768-771, 1994.
- [8] A. Belouchrani and K. Abed Meraim and J.-F. Cardoso and E. Moulines. "A blind source separation technique using second order statistics," *IEEE Trans. on SP*, 1996. To appear.

- [9] F. Hlawatsch and W. Krattenthaler, "Bilinear Signal Synthesis," *IEEE Trans. on SP*, vol. 40, pp. 352-363, Feb. 1992.
- [10] L. Cohen, *Time-frequency analysis*. Prentice Hall, 1995.
- [11] G.H. Golub and C.F. Van Loan, *Matrix computations*. The Johns Hopkins University Press, 1989.

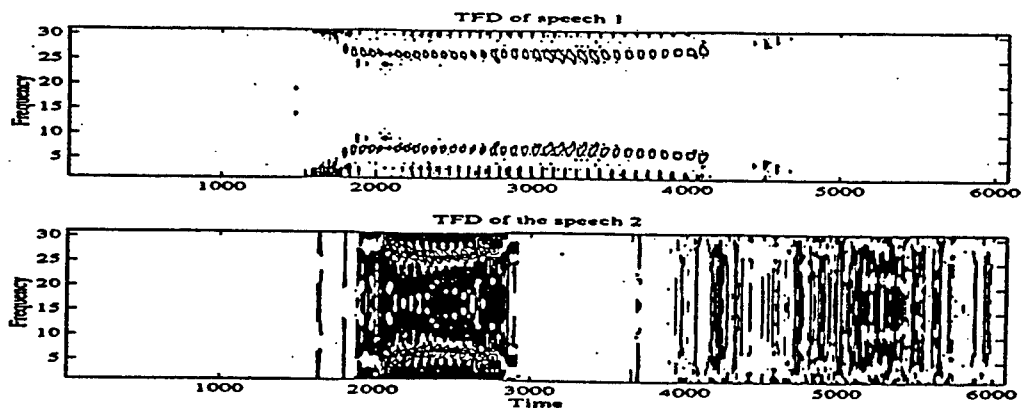


Figure 1. TFDs of the individual speeches.

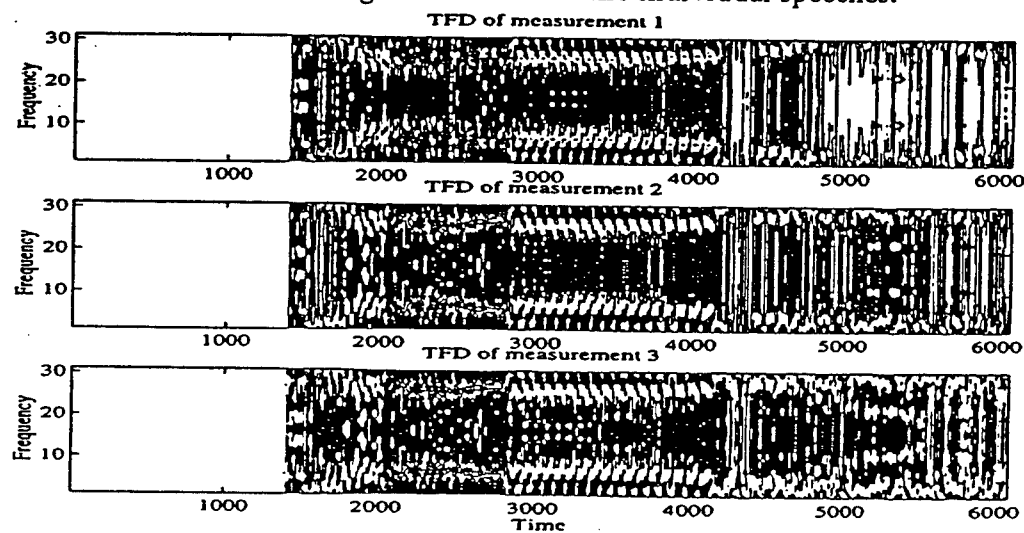


Figure 2. TFDs of the Measurements.

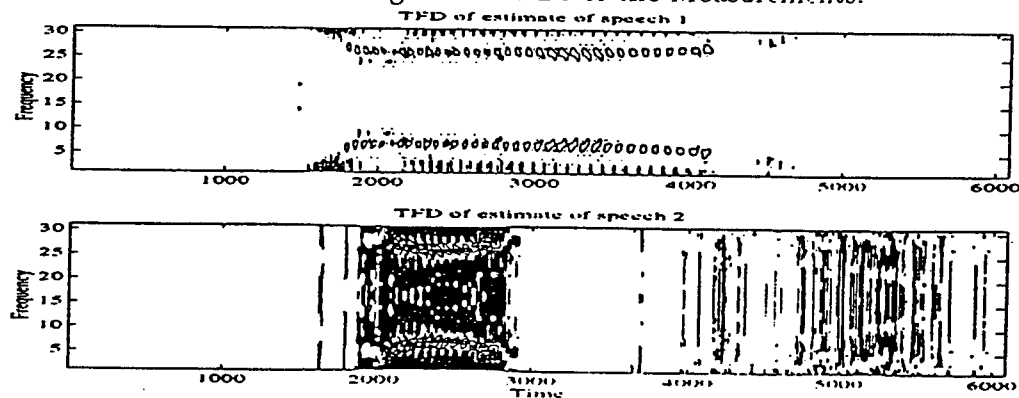


Figure 3. TFDs of the estimate signals.

TWO-SENSOR BLIND BEAMFORMER FOR DIRECT SEQUENCE SPREAD SPECTRUM COMMUNICATIONS

Adel Belouchrani* and Moeness G. Amin**

* Department of Electrical Engineering
Ecole National Polytechnique, Algiers, Algeria

** Department of Electrical and Computer Engineering,
Villanova University, Villanova PA 19085 USA

ABSTRACT

This paper presents an efficient blind beamformer dedicated to the problem of interference mitigation in direct sequence spread spectrum (DSSS) communications systems using a two sensor array. A closed form solution for the blind identification of the communication channel is derived by exploiting the temporal properties of the desired signal and the interference. Three structures of the DSSS receiver are presented. One structure consists of the blind beamformer followed by the spread spectrum demodulator, the two other structures consist of the spread spectrum demodulator followed by the blind beamformer. Simulation results are provided to illustrate the effectiveness of the proposed algorithms.

I INTRODUCTION

Recent development of spread spectrum communications and digital beamforming provides a formidable set of technologies for jam-resistance systems. These technologies are compatible and often used in the same system. The integration of these two technologies can be achieved by cascading their corresponding processing techniques. That is, the multidimension problem can be first translated into a single dimension problem via beamforming, where the sensor array outputs are weighted and added so as to attenuate strong jammer signals received by the multisensor antenna array. Spread spectrum techniques [1] may then be employed to neutralize large numbers of weak jammers that may not be totally eliminated by the spatial filtering implemented by the beamformer. A different order of cascade is to first apply the spread spectrum techniques at the output of each sensor, followed by spatial filtering via the beamformer is employed. This paper investigates the performance of these two approaches. For this purpose, we propose a new beamformer dedicated to the problem of a single jammer mitigation in DSSS communications systems using a two sensor array, and we implement the corresponding DSSS receiver according to the two aforementioned approaches.

II PROBLEM FORMULATION

The DSSS communications system under consideration employs binary phase-shift-keying (BPSK) for both chip and

data modulation. An array of 2 sensors receiving signals from 2 sources (an i.i.d. desired signal and a temporally correlated jammer (H1))¹ is considered. The array output vector $x(t)$ is of dimension 2×1 and is expressed by the following low rank model [2].

$$x(t) = Hy(t) + n(t), \quad y(t) = [s(t) \ j(t)]^T \quad (1)$$

where $y(t)$ is the signal vector whose entries are $s(t)$ and $j(t)$, which represent the desired signal and the jammer signal, respectively. The superscript T denotes the transpose operator. The components of $n(t)$ are zero mean temporally and spatially white noise processes with variance σ^2 (H2). $H = [h_1, h_2]$ is the channel matrix, where h_i is the spatial signature of the i -th signal which defines the array response to the signal direct-path and all its multipaths. The desired signal, the jammer signal, and the noise components are assumed uncorrelated (H3). In the baseband, the desired signal $s(t)$ has the following form

$$s(t) = \sum_{k=-\infty}^{\infty} b_k m_k(t - kT), \quad (2)$$

where

$$m_k(t) = \sum_{l=1}^L c_l^k p(t - (l-1)T_c) \quad (3)$$

In (2)-(3), T^{-1} is the data (bit) rate, and T_c^{-1} is the chip rate. The integer $L = T/T_c$ is the number of chips per bit (SS processing gain). $\{b_k\}$ and $\{c_l^k\}_{l=1, \dots, L}$ represent the k -th bit data sequence and the corresponding chip sequence, and $p(t)$ is the chip pulse. The chip sequence is a pseudo-random signal which is known by both the transmitter and the receiver.

In the blind context, the identification of the channel matrix H can be performed only up to a permutation and a scaling factor of its columns. Hence, it is assumed without any loss of generality, that:

(H4) $s(t)$ and $j(t)$ are treated as if they have unit variance so that their dynamic range is accounted for by the magnitude of the corresponding channel vector.

(H5) The first entries of the channel vectors $h_k, k=1,2$ are real and positive, i.e.,

$$h_{k1} = h_{k1}^*, \quad h_{k1} > 0 \quad k=1,2 \quad (4)$$

where the superscript * denotes the complex conjugate operator. These conventions are shown to be convenient in the sequel.

III RECEIVER DESIGNS

The block diagrams shown in Fig. 1, 2 and 3 illustrate the three structures of the proposed spread spectrum communication receiver. In Fig. 1, structure I describes a receiver which consists of the standard spread spectrum demodulation preceded by a blind beamformer. The task of the beamformer is to fully or partially remove the jammer with minimum distortion to the desired signal. This is achieved by utilizing the spatial diversity provided by the two-sensor array as well as the difference in the temporal characteristics of the two signal arrivals. The demodulation process recovers the original data by despreading the separated desired signal, while spreading the background noise and, in partial nulling, any jammer component which might have escaped to the beamforming output. As depicted in Fig. 2 and 3, structures II and III of the receiver consist of the spread spectrum demodulation applied at each sensor followed by a blind beamformer. The difference between these two structures is in the estimation of the channel coefficients. In structure II, the channel coefficients are estimated from the observed data directly before despreading, whereas in structure III, these coefficients are estimated from the despread data.

IV SECOND ORDER CHANNEL IDENTIFICATION (SO CI)

Consider the following sampled version of the data model,

$$\tilde{x}(n) = H\tilde{y}(n) + \tilde{n}(n), \quad \tilde{y}(n) = [\tilde{s}(n) \tilde{j}(n)]^T \quad (5)$$

where,

- For structures I and II
 $\tilde{x}(n) = x(n)$, $\tilde{n}(n) = n(n)$, $\tilde{s}(n) = s(n)$, and $\tilde{j}(n) = j(n)$
- For structure III
 $\tilde{x}(n) = \sum_{l=1}^L x(n-l)c(l)^*$, $\tilde{n}(n) = \sum_{l=1}^L n(n-l)c(l)^*$,
 $\tilde{s}(n) = \sum_{l=1}^L s(n-l)c(l)^*$, and
 $\tilde{j}(n) = \sum_{l=1}^L j(n-l)c(l)^*$

In the above expressions, $x(n)$, $n(n)$, $s(n)$ and $j(n)$ are the sampled version of $x(t)$, $n(t)$, $s(t)$ and $j(t)$, respectively. $c(l)$ is a zero-mean i.i.d. chip sequence and L is the length of the chip sequence per information bit.

The correlation matrices of $\tilde{x}(n)$ is given by,

$$R_{\tilde{x}\tilde{x}} = h_{11}^2 \bar{L}^2 I + h_{21}^2 \bar{L} R_{jj} + \bar{L} \sigma^2 I \quad (6)$$

$$R_{\tilde{x}\tilde{s}} = |h_{12}|^2 \bar{L}^2 I + |h_{22}|^2 \bar{L} R_{jj} + \bar{L} \sigma^2 I \quad (7)$$

$$R_{\tilde{x}\tilde{j}} = h_{11} h_{12}^* \bar{L}^2 I + h_{21} h_{22}^* \bar{L} R_{jj} \quad (8)$$

where I is the identity matrix and R_{xy} are defined by

$$R_{xy} = E([x(1), \dots, x(N)]^T [y(1), \dots, y(N)]^*) \quad (9)$$

where $E(\cdot)$ is the expectation operator, N is some chosen length of data. The above expressions are derived under the assumptions (H1)-(H5), where

$$\bar{L} = \begin{cases} 1 & \text{if structures I and II} \\ L & \text{if structure III} \end{cases} \quad (10)$$

Let us define the operators $off(\cdot)$ and $tr(\cdot)$ by

$$off(M) = \frac{1}{N(N-1)} \sum_{i \neq j} M_{ij} \quad (11)$$

$$tr(M) = \frac{1}{N} \sum_i M_{ii} \quad (12)$$

where M is any square matrix of dimension $N \times N$ and M_{ij} are the entries of M . By applying these operators to equations (6), (7) and (8), we get the following set of equations,

$$F_1 = off(R_{\tilde{x}\tilde{x}}) = h_{21}^2 \bar{L} off(R_{jj}) \quad (13)$$

$$F_{12} = off(R_{\tilde{x}\tilde{s}}) = h_{21} h_{22}^* \bar{L} off(R_{jj}) \quad (14)$$

$$T_1 = tr(R_{\tilde{x}\tilde{x}}) = h_{11}^2 \bar{L}^2 + h_{21}^2 \bar{L} + \bar{L} \sigma^2 \quad (15)$$

$$T_2 = tr(R_{\tilde{x}\tilde{s}}) = |h_{12}|^2 \bar{L}^2 + |h_{22}|^2 \bar{L} + \sigma^2 \bar{L} \quad (16)$$

$$T_{12} = tr(R_{\tilde{x}\tilde{j}}) = h_{11} h_{12}^* \bar{L}^2 + h_{21} h_{22}^* \bar{L} \quad (17)$$

where $|\cdot|^2$ denotes the square modulus. Note that $off(R_{jj})$ is an unknown which can be eliminated by combining equations (13) and (1).

From equations (13)-(17), we obtain the following expressions of the channel coefficients,

$$h_{21} = \sqrt{\frac{1}{\bar{L}} \frac{T_1 T_2 - |T_{12}|^2 - \bar{L} \sigma^2 (T_1 + T_2) + \bar{L}^2 \sigma_{(18)}^4}{T_2 + T_1 |\beta|^2 - 2 \Re\{\beta T_{12}\} - \bar{L} \sigma^2 (1 + |\beta|^2)}} \quad (18)$$

$$h_{22} = h_{21} \beta^* \quad (19)$$

$$h_{11} = \frac{1}{\bar{L}} \sqrt{T_1 - h_{21}^2 \bar{L} - \bar{L} \sigma^2} \quad (20)$$

$$h_{12} = \frac{1}{\bar{L}} \frac{T_{12} - h_{21}^2 \bar{L} \beta}{\sqrt{T_1 - h_{21}^2 \bar{L} - \bar{L} \sigma^2}} \quad (21)$$

where $\beta = F_{12}/F_1$ and $\Re\{\cdot\}$ denotes the real part operator.

An estimate of the noise variance σ^2 is needed for a robust estimation of the channel coefficients. It can be obtained by eigen-decomposition of the data covariance matrix [3] if a third sensor is available. Otherwise, σ^2 can be estimated using only two sensors before transmission begins, i.e. in the absence of the spread spectrum signal. Note that in practice, the temporal correlation matrices of the data are replaced by their time-averages.

Discussion:

In addition to reducing the jammer power, the despreading in structure III also weakens the temporal coherence of the jammer signal while estimating the channel coefficients. For high number of chips by bit (L), the despreading operation makes the jammer temporally white and, subsequently, the values of F_1 and F_{12} in equations (13) and (14) are reduced

to zero. Hence, equations (15) to (17) become insufficient to solve the identification problem. In this case, one has to use higher order blind identification techniques [4, 5, 6]. From this discussion, it is expected that the asymptotic performance of the SOCI to be better in structures I and II than in structure III.

V DATA RECOVERY

In this Section, we compute the optimum beamformer which maximizes the signal to interference plus noise ratio (SINR) at the output of the receiver, subject to the unit norm constraint $|w|^2 = 1$.

A. SINR Expressions

1. Structure I:

The receiver SINR is defined as the ratio of the square of the mean to the variance of the correlator output U [7]¹,

$$SINR_I = \frac{|E[U]|^2}{Var[U]} \quad (22)$$

where $U = \sum_{n=1}^L w^H x(n) c^*(n)$ and the superscript H denotes the transpose conjugate operator.

The computation of the mean value and the variance of the correlator output yields to

$$|E[U]|^2 = L^2 |w^H h_1|^2 \quad (23)$$

$$Var[U] = L(|w^H h_2|^2 + |w|^2 \sigma^2) \quad (24)$$

Hence, the correlator SINR is given by

$$SINR_I = \frac{L|w^H h_1|^2}{|w^H h_2|^2 + |w|^2 \sigma^2} \quad (25)$$

2. Structures II and III:

At the output of the beamformer, the SINR corresponding to structures II and III is given by,

$$SINR_{II} = SINR_{III} = \frac{L|w^H h_1|^2}{|w^H h_2|^2 + |w|^2 \sigma^2} \quad (26)$$

3. Comments:

According to equations (25) and (26), the two structures lead to the same asymptotic SINR if the same optimal array weights are used in the three structures. In practice, the optimal weights of structures I and II are computed from the same estimates of the channel coefficients. Therefore, these two structures have the same performance.

If K denotes the sample size at the input of the receiver, structures I and II estimate the channel coefficients using K sample data, while, structure II estimated these same coefficients using K/L sample data. Note also that the input SINR per bit or per chip is the same for the three structures. Accordingly, for a same setting, the estimation error on the array weights of structure III is expected to be higher than the corresponding error of structures I and II. Hence, receivers of structures I and II should have better performance, but higher numerical complexity than the receiver of structure III.

B. Optimum array weights

The optimum array weight vector in the sense mentioned above is given by,

$$w_{opt} = \underset{w}{\text{Argmax}} \frac{L|w^H h_1|^2}{|w^H h_2|^2 + |w|^2 \sigma^2} \quad \text{subject to } |w|^2 = 1 \quad (27)$$

The solution to the maximization problem (27) is given by

$$w_{opt} = \frac{1}{\sqrt{1 + |\alpha|^2}} [1 \ \alpha]^T \quad (28)$$

with

$$\alpha = \frac{h_{12}\sigma^2 + h_2^H \Delta}{h_{11}\sigma^2 - h_2^H \Delta}, \quad \Delta = h_{21}h_{12} - h_{11}h_{22} \quad (29)$$

In practice, the channel vectors h_1 , h_2 and the noise variance σ^2 are replaced by their estimated values.

VI PERFORMANCE EVALUATIONS

Consider an array of two sensors separated by half a wavelength. In addition to the DS/SS signal, the array receives a jammer through three paths. The desired signal is a BPSK signal arriving at $\theta_0 = 0^\circ$. The jammer is composed of a chirp signal whose frequencies are $\omega_1 = 0.1\pi$ and $\omega_2 = 0.6\pi$. The direct path of the jammer arrives at $\theta_1 = 2^\circ$ whereas its multipath arrive at $\theta_2 = 10^\circ$ and $\theta_3 = -10^\circ$, respectively. The noise used is zero-mean white complex Gaussian process. The value N in equation (9) is chosen to be equal to 8 and 100 data bits are considered. The SINR at the output of the decorrelator is estimated over 100 Monte-Carlo runs.

Figures 4 to 5 show the SINR in dB when the beamformer is enabled (either using SOCI or JADE according to the three structures I, II and III) and when the beamformer is disabled. In Figures 4, the SINR is plotted against SNR for a JSR of 30 dB and for 4 chips/bit¹. According to Figure 4, receivers I and II, which have the same performance, perform better than receiver III as expected. Figures 5 displays the SINR versus the number of chips/bit for a JSR of 10 dB and for 0 dB SNR. From Figure 5, we see that for 8 chips/bit, the proposed receivers achieve the same performance as the despreader when used alone for 128 chips/bit.

VII CONCLUSION

In this paper, we have proposed an efficient two-sensor array blind beamformer for single jammer mitigation in spread spectrum communications systems based on second order statistic blind identification of the channel coefficients which exploits the temporal properties of the spread spectrum signal and the jammer. Three structure designs of the mitigation receiver were suggested, where structure III is less robust than structures I and II. The second order channel identification (SOCI) was compared to the high order identification technique "JADE". Simulation results were provided for multipath and coherent signal environment.

¹Note that this definition is consistent herein only because the variance of the data bit sequence is zero over the chip length.

¹The choose of 4 chips/bit in this simulation is just for illustration.

REFERENCES

- [1] M. K. Simon, et al, *Spread Spectrum Communications*. Computer Science Press, 1985.
- [2] B. Ottersten, "Array processing for wireless communications," *Proceedings of 8th IEEE Signal Processing Workshop on Statistical Signal and Array Processing, Corfu, Greece*, pp. 466-473, June 1996.
- [3] A. Belouchrani and K. Abed Meraim and J.-F. Cardoso and E. Moulines, "A blind source separation technique using second order statistics," *IEEE Trans. on SP*, vol. 45, pp. 434-444, Feb. 1997.
- [4] P. Comon, "Independent component analysis," in *Proc. Int. Workshop on Higher-Order Stat., Chamrousse, France*, pp. 111-120, 1991.
- [5] A. Belouchrani and K. Abed Meraim, "Constant modulus blind source separation technique: A new approach," in *Proc. ISSPA, Gold Coast, Australia*, August 1996.
- [6] J.-F. Cardoso and A. Souloumiac, "Blind beamforming for non Gaussian signals," *IEE Proceedings-F*, vol. 140, no. 6, pp. 362-370, 1993.
- [7] J. Ketchum and J. Proakis, "Adaptive algorithms for estimating and suppressing narrow band interference in PN spread spectrum systems," *IEEE Trans. on Comm.*, vol. 30, pp. 913-924, May 1982.

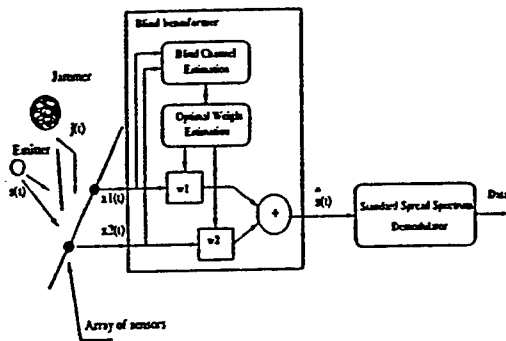


Figure 1. The jammer mitigation system: structure I.

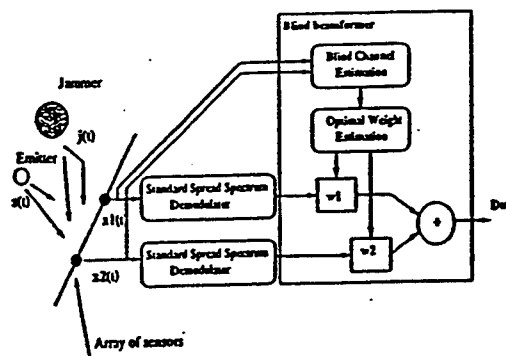


Figure 2. The jammer mitigation system: structure II.

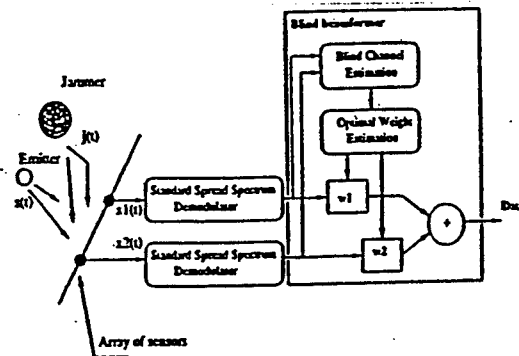


Figure 3. The jammer mitigation system: structure III.

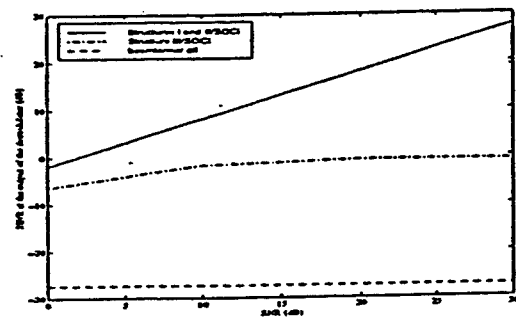


Figure 4. SINR at the correlator output in dB vs SNR for JSR= 30 dB and 4 chips/bit.

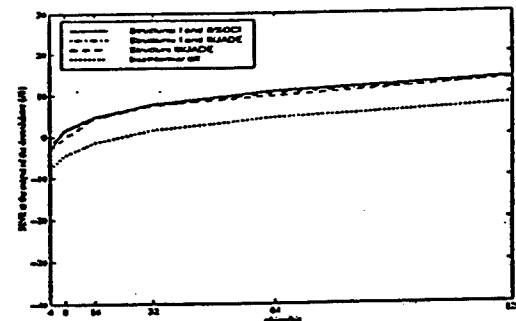


Figure 5. SINR at the correlator output in dB vs chips/bit for SNR= 0 dB and JSR= 10 dB.

Blind source separation using joint signal representations for arbitrary variables.

Adel Belouchrani and Moeness G. Amin

Department of Electrical and Computer Engineering, Villanova University, Villanova PA 19085.
adel,moeness@ece.vill.edu

ABSTRACT

Blind source separation is an emerging field of fundamental research with a broad range of applications. It is motivated by practical problems that involve several source signals and several sensors. Each sensor receives an instantaneous linear mixture of the source signals. The problem of the blind source separation consists then of recovering the original waveforms of the sources without any knowledge of the mixture structure. So far, the problem of the blind source separation has been solved using statistical information available on the source signals. A blind source separation approach for non-stationary signals based on time-frequency representations (TFR) have been recently introduced by the authors (SPIE 1996). Herein, we generalize the TFR based blind source separation approach to arbitrary variables, including time and frequency. 'Spatial joint arbitrary variable distributions' are introduced and used for blind source separation via joint diagonalization techniques.

Key Words: Blind source separation, Time-Frequency representation, Joint signal representation, Spatial joint Arbitrary Variable Distributions, Joint diagonalization.

1 INTRODUCTION

In many signal processing applications, signals are received on small or large antennas aperture. In some of these applications, the multidimensional signal is spatially processed and reduced to one dimension where a desired temporal/spectral processing is applied. The reduction to a one dimensional signal is achieved using linear combiner of the data at the array sensor outputs. Optimum combiner often leads to interference nulling with minimum distortion of the signal. The temporal/spectral processing is applied to the array output to perform filtering, spectral estimation, adaptive linear prediction and notch filters, transient detection and removal, matched filters, time-frequency distribution and synthesis, transform domain analysis, etc.

In some other applications, the multidimensional signal is directly utilized to estimate some signal parameters, such as the number of sources and their directions of arrival. Subspace-based methods exploit this spatial information, which is provided by the multidimensional signal. These methods use a geometrical relation involving the exact moments of the data, commonly the data covariance matrix. The desired signal parameters are then extracted by solving the geometrical relation in some approximate sense, and using sample moments instead of the exact ones. These methods assume stationary signals. Although, when the frequency content of the measured data is time-varying, existing eigenstructure methods can still be applied, they do not, however, fully utilize the data time-frequency information and structures, which if properly used, will significantly improve performance.

The proposed paper develops a new concept which exploits the geometrical relation which no longer involves the exact moments of the data but rather their Spatial Joint Arbitrary Variable Distributions. The spatial joint arbitrary variable distribution (SJAVD) is a generalization of the arbitrary variable distribution to a vector signal. A particular case is the spatial time frequency distribution (STFD) where the two arbitrary variables are time and frequency. In a previous research, the authors have used successfully the concept of STFD to solve the problem of blind source separation for nonstationary signals.¹ The STFDs belong to the general class of Cohen. An alternative solution is to introduce the Spatial Hyperbolic Class of Quadratic Time-Frequency Representations.²

In this paper, we study the application of this new concept of spatial signal representations to the problem of blind source separation.

2 THE BLIND SOURCE SEPARATION PROBLEM

In several applications such as semiconductor manufacturing process,³ factor analysis,⁴ narrow-band signal processing,⁵ and image reconstruction,⁶ one has to process multidimensional observations of the form:

$$\mathbf{x}(t) = \mathbf{y}(t) + \mathbf{n}(t) = \mathbf{A}\mathbf{s}(t) + \mathbf{n}(t), \quad (1)$$

where $\mathbf{x}(t)$ is a noisy instantaneous linear mixture of source signals. This model is commonly used in the field of narrowband array processing. In this context, the vector $\mathbf{s}(t) = [s_1(t), \dots, s_n(t)]^T$ consists of the signals emitted by n narrowband sources; whereas the vector $\mathbf{x}(t) = [x_1(t), \dots, x_m(t)]^T$ contains the array output. Both vectors are sampled at time t . Matrix \mathbf{A} is the transfer function between the sources and the array sensors.

The problem of the blind source separation consists then of recovering the original waveforms $\mathbf{s}(t)$ of the sources without any knowledge of the mixture structure \mathbf{A} . So far, this problem has been solved using statistical information available on the source signals.

The first solution to the source separation problem was proposed almost a decade ago⁷ and was based on the cancellation of higher order moments assuming non-Gaussian and i.i.d source signals. Since then, other criteria based on minimizations of cost functions, such as the sum of square fourth order cumulants,⁸⁻¹⁰ contrast functions^{9,11} or likelihood function,¹² have been used by several researchers. Note that in the case of non i.i.d source signals and even Gaussian sources, solutions based on second order statistics are possible.^{13,14}

In the sequel, we propose to take advantage of the nonstationarity property of the signals to be separated. This is done by resorting to the powerful tool of joint signal representations.

3 SPATIAL ARBITRARY VARIABLES DISTRIBUTIONS

There are several approaches to define joint-variable distributions.¹⁵⁻¹⁹ In this section, we only focus on the characteristic function operator method discussed by Cohen.²⁰

Suppose we have two variables a and b associated with the Hermitian operators A and B , respectively. We seek a joint distribution $D(a, b)$ that indicates the energy content of signals in terms of both a and b simultaneously. The characteristic function for a and b is given by²⁰

$$M(\alpha, \beta) = \langle e^{j\alpha A + j\beta B} \rangle = \iint e^{j\alpha a + j\beta b} D(a, b) da db \quad (2)$$

Hence by Fourier inversion, we have

$$D(a, b) = \langle e^{j\alpha a - j\beta b} \rangle = \int \int M(\alpha, \beta) e^{-j\alpha a - j\beta b} d\alpha d\beta \quad (3)$$

As presented in,²⁰ $M(\alpha, \beta)$ can be computed from the signal by averaging the characteristic function operator $\mathcal{M}(\alpha, \beta)$ by way of

$$M(\alpha, \beta) = \langle \mathcal{M}(\alpha, \beta) \rangle = \int x^*(t) \mathcal{M}(\alpha, \beta) x(t) dt \quad (4)$$

The previous equation leads to,

$$D(a, b) = \int \int \int x^*(t) \mathcal{M}(\alpha, \beta) x(t) dt d\alpha d\beta \quad (5)$$

The characteristic function operator $\mathcal{M}(\alpha, \beta)$ is formed by combining exponentiated versions of the Hermitian operators A and B associated with the variables a and b . There are many possibilities for orderings of $e^{j\alpha A}$ and $e^{j\beta B}$ in $\mathcal{M}(\alpha, \beta)$. To handle the possible orderings, one can choose one particular ordering and introduce a kernel function $\phi(\alpha, \beta)$ to generate the remaining ones. This leads to a general class of joint distributions of the variables a and b . For a specific ordering

$$\mathcal{M}(\alpha, \beta) = \phi(\alpha, \beta) e^{j\alpha A + j\beta B} \quad (6)$$

The discrete form of the aforementioned joint arbitrary variable distribution (JAVD), for signal $x(t)$, is given by

$$D_{xx}(a, b) = \sum_{t, l, m=-\infty}^{\infty} \phi(m, l) x^*(t) \mathcal{M}(m, l) x(t) e^{-jma - jlb} \quad (7)$$

The cross-AVD of two signals $x_1(t)$ and $x_2(t)$ is defined by

$$D_{x_1 x_2}(a, b) = \sum_{t, l, m=-\infty}^{\infty} \phi(m, l) x_2^*(t) \mathcal{M}(m, l) x_1(t) e^{-jma - jlb} \quad (8)$$

Expressions (7) and (8) are now used to define the following data *spatial joint arbitrary-variable distribution* (SJAVD) matrix,

$$D_{xx}(a, b) = \sum_{t, l, m=-\infty}^{\infty} \phi(m, l) x(t) \mathcal{M}(m, l) x^*(t) e^{-jma - jlb} \quad (9)$$

where $[D_{xx}(a, b)]_{ij} = D_{x_i x_j}(a, b)$, for $i, j = 1, \dots, n$.

Under the linear data model of equation (1) and assuming noise-free environment, the SJAVD matrix takes the following simple structure:

$$D_{xx}(a, b) = A D_{ss}(a, b) A^H \quad (10)$$

where $D_{ss}(a, b)$ is the signal JAVD matrix whose entries are the auto- and cross-JAVDs of the sources. We note that $D_{xx}(a, b)$ is of dimension $m \times m$, whereas $D_{ss}(a, b)$ is of $n \times n$ dimension. For narrowband array signal processing applications, matrix A holds the spatial information and maps the auto- and cross-JAVDs of the sources into auto- and cross-JAVDs of the data.

In general terms, since the off-diagonal elements of $D_{ss}(a, b)$ are cross-terms, then this matrix is diagonal for each arbitrary variables (a, b) point which corresponds to a true power concentration, i.e. signal auto-term. In the sequel, we consider the (a, b) points which satisfy this property. In practice, to simplify the selection of auto-terms, a smoothing kernel $\phi(m, l)$ in $\mathcal{M}(m, l)$ can be applied to significantly decrease the contribution of the cross-terms in the a - b plane.

It is important to note that expression (10) is similar to that which has been commonly used in blind source separation and direction of arrival (DOA) estimation problems, relating the signal correlation matrix to the data spatial correlation matrix.

3.1 Cohen Class

The discrete-time form of the Cohen's class of time-frequency distributions (TFD) for signal $x(t)$ is provided by choosing a and b to be time and frequency variables, and \mathcal{A} and \mathcal{B} in (6) to be the time and frequency operators, respectively. This class is given by²⁰

$$D_{xx}(t, f) = \sum_{l, m=-\infty}^{\infty} \phi(m, l) x(t+m+l) x^*(t+m-l) e^{-j4\pi fl} \quad (11)$$

where t and f represent the time index and the frequency index, respectively. The kernel $\phi(m, l)$ characterizes the distribution and is a function of both the time and lag variables. The cross-TFD of two signals $x_1(t)$ and $x_2(t)$ is defined by

$$D_{x_1 x_2}(t, f) = \sum_{l, m=-\infty}^{\infty} \phi(m, l) x_1(t+m+l) x_2^*(t+m-l) e^{-j4\pi fl} \quad (12)$$

Expressions (11) and (12) are used to define the following data *spatial time-frequency distribution* (STFD) matrix,

$$D_{xx}(t, f) = \sum_{l, m=-\infty}^{\infty} \phi(m, l) x(t+m+l) x^*(t+m-l) e^{-j4\pi fl} \quad (13)$$

where $[D_{xx}(t, f)]_{ij} = D_{x_i x_j}(t, f)$, for $i, j = 1, \dots, n$.

As the SJAVD, the STFD verify under the model (1) relation (10), i.e.

$$D_{xx}(t, f) = \mathcal{A} D_{ss}(t, f) \mathcal{A}^H \quad (14)$$

Note that the STFD is a particular case of the SJAVD, where the Hermitian operators \mathcal{A} and \mathcal{B} are the operators $\mathcal{T} = t$ and $\mathcal{W} = \frac{d}{dt}$, respectively.²⁰

3.2 Hyperbolic Class

The discrete form of the Hyperbolic class of time-frequency distributions (HTFD), for signal $x(t)$, is given by²

$$T_{xx}(t, f) = \frac{f_r}{f} \sum_{m, l=-\infty}^{\infty} \phi\left(\frac{f_r}{f} m, \frac{f_r}{f} l\right) X(m) X^*(l) e^{-j2\pi t f \ln(m/l)} \quad (15)$$

where $\phi(m, f)$ is a 2-D kernel function which is independent of the signal, $X(f)$ is the Fourier transform of $x(t)$ and f_r is a fixed reference frequency (or normalization) which is needed to obtain the correct physical dimensions. The cross-HTFD of two signals $x_1(t)$ and $x_2(t)$ is defined by

$$T_{x_1 x_2}(t, f) = \frac{f_r}{f} \sum_{m, l=-\infty}^{\infty} \phi\left(\frac{f_r}{f} m, \frac{f_r}{f} l\right) X_1(m) X_2^*(l) e^{-j2\pi t f \ln(m/l)} \quad (16)$$

Expressions (15) and (16) are now used to define the following data *spatial hyperbolic time-frequency distribution* (SHTFD) *matrix*.

$$T_{xx}(t, f) = \frac{f_r}{f} \sum_{m,l=-\infty}^{\infty} \phi\left(\frac{f_r}{f}m, \frac{f_r}{f}l\right) X(m)X^*(l) e^{-j2\pi t f l n(m/l)} \quad (17)$$

where $[T_{xx}(t, f)]_{ij} = T_{x_i x_j}(t, f)$, for $i, j = 1, \dots, n$.

Under the model (1), the SHTFD also verify relation (10), i.e.

$$T_{xx}(t, f) = A T_{ss}(t, f) A^H \quad (18)$$

4 THE BLIND SOURCE SEPARATION ALGORITHM

Let W denotes a $m \times n$ matrix, such that $(WA)(WA)^H = UU^H = I$, i.e. WA is a $m \times m$ unitary matrix (this matrix is referred to as a whitening matrix, since it whitens the signal part of the observations). Pre- and post-multiplying the JAVD-matrices $D_{xx}(a, b)$ by W , we then define the *whitened JAVD-matrices* as:

$$\underline{D}_{xx}(a, b) = W D_{xx}(a, b) W^H \quad (19)$$

From the definition of W and Eq.(10), we may expressed $\underline{D}_{xx}(a, b)$ as

$$\underline{D}_{xx}(a, b) = U D_{ss}(a, b) U^H \quad (20)$$

Since the matrix U is unitary and $D_{ss}(a, b)$ is diagonal, expression (20) shows that any whitened data SJAVD-matrix is diagonal in the basis of the columns of the matrix U (the eigenvalues of $\underline{D}_{xx}(a, b)$ being the diagonal entries of $D_{ss}(a, b)$).

The unitary matrix U is to be distinguished from the unitary transform¹⁹ that could be used in place of the characteristic function operator method discussed in the previous Section for introducing joint-arbitrary variable distributions. for joint variable signal representation, the unitary transformation operates on the data in the temporal domain whereas matrix U in (20) is developed for spatial processing.

If, for the (a_i, b_i) point, the diagonal elements of $D_{ss}(a_i, b_i)$ are all distinct, the missing unitary matrix U may be 'uniquely' (i.e. up to permutation and phase shifts) retrieved by computing the eigendecomposition of $D_{xx}(a_i, b_i)$. However, when the a-b signatures of the different signals are not highly overlapping or frequently intersecting, which is likely to be the case, the selected (a_i, b_i) point often corresponds to a single signal auto-term, rendering matrix $D_{ss}(a_i, b_i)$ deficient. That is, only one diagonal element of $D_{ss}(a_i, b_i)$ is different from zero. It follows that the determination of the matrix U from the eigendecomposition of a single whitened data SJAVD-matrix is no longer 'unique' in the sense defined above. The situation is more favorable when considering *simultaneous diagonalization* of a combined set $\{\underline{D}_{xx}(a_i, b_i) | i = 1, \dots, p\}$ of p SJAVD matrices. This amounts to incorporating several a-b points in the source separation problem. It is noteworthy that two source signals with identical a-b signatures can not be separated, even with the inclusion of all information in the a-b plane.

Joint diagonalization: The *joint diagonalization*¹⁴ can be explained by first noting that the problem of the diagonalization of a single $n \times n$ normal matrix M is equivalent to the minimization of the criterion²¹

$$C(M, V) \stackrel{\text{def}}{=} - \sum_i |v_i^* M v_i|^2 \quad (21)$$

over the set of unitary matrices $V = [v_1, \dots, v_n]$. Hence, the joint diagonalization of a set $\{M_k | k = 1..K\}$ of K arbitrary $n \times n$ matrices is defined as the minimization of the following JD criterion:

$$C(V) \stackrel{\text{def}}{=} - \sum_k C(M_k, V) = - \sum_{ki} |v_i^* M_k v_i|^2 \quad (22)$$

under the same unitary constraint. An efficient joint approximate diagonalization algorithm exists in¹⁴ and it is a generalization of the Jacobi technique²¹ for the exact diagonalization of a single normal matrix.

4.1 General Conditions on Joint-Variables Representations

The idea of introducing a set of variables different than time and frequency in the underlying blind source separation problem is stemmed from the fact that improved performance may well be achieved by incorporating spatial and temporal matrices in equation (20) which correspond to new variables a and b .

It is clear from (22) that from a perspective of the joint diagonalization techniques, an attractive joint-variable distributions are those which allow the formation of non-singular diagonal matrices $D_{ss}(a, b)$ at the prospective joint-variable points. This property should be viewed in light of the following observations:

1. The off-diagonal elements of $D_{ss}(a, b)$ should be zeros, and as such, distributions that mount the cross-terms on the top of auto-terms should be carefully studied and re-examined for qualification under the proposed application and within the above frame work.
2. Joint-variable distributions that spread cross-terms over the entire joint-variable plane should, using the same argument, lead to improved performance over those distributions which localize the cross-terms in the auto-term regions.
3. Joint variable distributions which reduce, but still localize the cross-terms away from the auto-term regions appear to be most applicable to the diagonal matrix requirements.
4. The joint-variable signatures of the sources, although remain distinct, should intersect as often as possible, producing a large number of candidate points.
5. Joint-variable distributions which reduce the noise variance are of significant importance, as they lead eventually to reliable separation and reconstruction of the source signals.^{22,23}

It is noteworthy that in the time-frequency plane, t-f distribution kernels which handle cross-terms differently in terms of their smoothing and localizations have already been devised. The ZAM,²⁴ Choi-Williams,²⁵ and Born-Jordan kernels²⁰ are good examples of how time-frequency kernels differ in cross-term mitigations. These kernels should be investigated to show their possible distinct offerings in the blind source separation context.

4.2 The Identification Procedure:

Equations (10-22) constitute the blind source separation approach based on SJAVD which is summarized by the following steps

- Determine the whitening matrix \tilde{W} from the eigendecomposition of an estimate of the autocorrelation matrix of the data (see¹⁴ for more details).

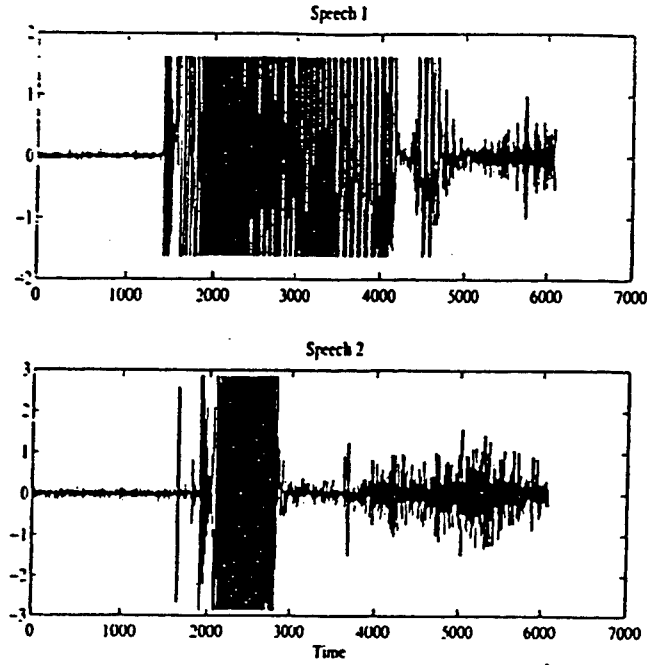


Figure 1: Plots of individual speeches.

- Determine the unitary matrix $\hat{\mathbf{U}}$ by minimizing the joint approximate diagonalization criterion for a specific set of whitened SJAVD matrices $\{\mathbf{D}_{xx}(a_i, b_i) | i = 1, \dots, p\}$,
- Obtain an estimate of the mixture matrix $\hat{\mathbf{A}}$ as $\hat{\mathbf{A}} = \hat{\mathbf{W}}^\# \hat{\mathbf{U}}$, where the superscript $\#$ denotes the pseudo-inverse, and an estimate of the source signals $\hat{\mathbf{s}}(t)$ as $\hat{\mathbf{s}}(t) = \hat{\mathbf{U}}^H \mathbf{W}_x(t)$.

5 ILLUSTRATION

In this section, we consider the Cohen class to illustrate the feasibility of the proposed method.

Example 1 This example deals with real source signals. Two speech signals sampled at 8000 Hz are mixed by the following mixing matrix, $\mathbf{A} = \begin{bmatrix} 1.0 & 0.6 & 0.4 \\ 0.5 & 1.0 & 0.8 \end{bmatrix}^T$.

The plots of the two individual speech signals are shown in Fig.1. Speech “1” and “2” of a male speaker are the words “Cars” and “Cats”, respectively. To assess the robustness of the TFS algorithm with respect to noise, we corrupt the mixed speech signals by an additive white Gaussian noise and we compare in Fig.2 the performance of the second order blind identification (SOBI) algorithm proposed in¹⁴ and the TFS algorithm over [0 - 20 dB] range of signal-to-noise ratio (SNR) in terms of the overall rejection level of the sources in each other.¹⁴ The mean rejection levels are evaluated here over 100 Monte-Carlo runs with $T = 6084$ samples. It is evident from Fig.2 that, in this case, the TFS algorithm outperforms SOBI algorithm. The increase of this robustness of the TFS algorithm with respect to noise may be explain by the effect of spreading the noise power and of localizing the source energy in the time-frequency domain.

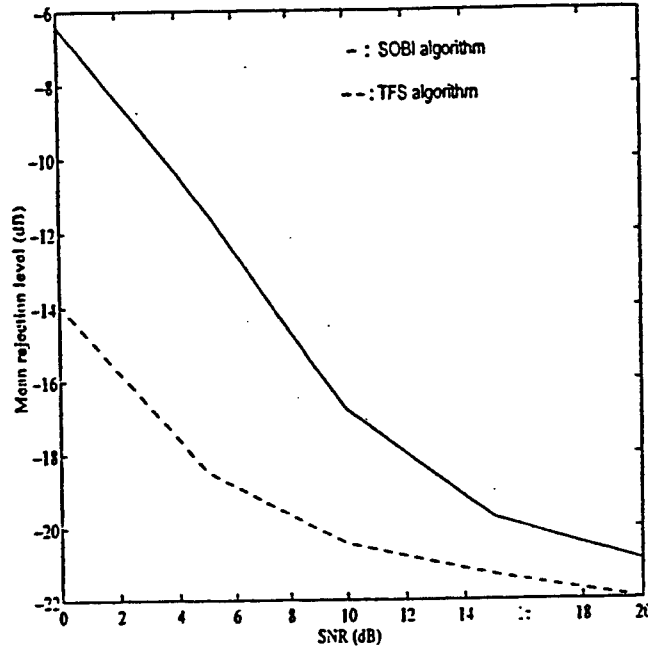


Figure 2: Performance of SOBI and TFS algorithms vs SNR.

Example 2 In this example, we consider a uniform linear array of three sensors having half wavelength spacing and receiving signals from two sources in the presence of white Gaussian noise. The sources arrive from different directions $\phi_1 = 0$ and $\phi_2 = 20$ degrees (the particular structure of the array manifold is of course not exploited here). The source signals are generated by filtering a complex circular white Gaussian processes by an AR model of order one with coefficient $a_1 = \rho \exp(j2\pi f_1(t))$ and $a_2 = \rho \exp(j2\pi f_2(t))$, where we have:

$$f_1(t) = \begin{cases} 0.0625 & \text{for } t = 1 : 400 \\ 0.1250 & \text{for } t = 401 : 450 \\ 0.3750 & \text{for } t = 451 : 850 \end{cases}$$

$$f_2(t) = \begin{cases} 0.3750 & \text{for } t = 1 : 400 \\ 0.1250 + \delta f & \text{for } t = 401 : 450 \\ 0.0625 & \text{for } t = 451 : 850 \end{cases}$$

$$\rho = 0.85$$

The signal to noise ratio (SNR) is set at 5 dB. The kernel used for the computation of the TFDs is the Choi-Williams kernel²⁰, which provides a good reduction of the cross-terms. For the TFS algorithm, eight TFD matrices are considered. The corresponding t-f points are those of the highest power in the t-f domain. The mean rejection level is evaluated over 500 Monte-Carlo runs.

Table 1 shows the mean rejection level in dB versus the 'spectral shift' δf both for SOBI algorithm¹⁴ and TFS algorithm. Note that for $\delta f = 0$, the two Gaussian source signals have identical spectra shape. In this case, while SOBI fails¹ in separating the two sources, TFS succeed. Note also that in contrast to SOBI, TFS presents constant performance with respect to δf .

¹We admit that a source separation algorithm fails when the mean rejection level is greater than -10 dB.

Spectral shift (δf)	Mean Rejection level in dB	
	SOBI	TFS
0.000	-8.86	-12.22
0.002	-10.01	-12.21
0.010	-10.18	-12.34
0.050	-11.09	-12.53
0.200	-12.92	-12.54

Table 1: Performance of SOBI and TFS algorithms vs δf

6 CONCLUSION

In this paper, the problem of blind separation of linear spatial mixture of non-stationary source signal based on arbitrary variable distributions has been investigated. A solution based on the diagonalization of a combined set of spatial arbitrary variable distributions has been proposed. The concept of the spatial joint signal representation is introduced. This concept should prove to be very valuable in multisensor signal analysis and lead to improved performance in the field of array signal processing. Numerical simulations have been provided to illustrate the feasibility of the proposed method.

7 REFERENCES

- [1] A. Belouchrani and M. G. Amin, "Blind Source Separation Based on Time-Frequency Signal Representation," *IEEE Trans. on SP*. Submitted 1996.
- [2] A. Papandreou, F. Hlawatsch and G. F. Boudreaux-Bartels, "The Hyperbolic Class of Quadratic Time-Frequency Representations Part I: Constant-Q Warping, the Hyperbolic Paradigm, Properties, and Members," *IEEE Trans. on SP*, vol. 41, pp. 3425-3444, Dec. 1993.
- [3] C. M. Berrah, "Parameter yield estimation for a MOSFET integrated circuit," in *Proc. 1990 IEEE ISCAS*, pp. 2260-2263, 1990.
- [4] E. E. Cureton and R. B. D'Agostino, *FACTOR ANALYSIS An Applied Approach*. Lawrence Erlbaum Associates, 1983.
- [5] R. Schmidt, "Multiple emitter location and signal parameter estimation," *IEEE Trans. on AP*, vol. 34, no. 1, pp. 276-280, 1986.
- [6] G. Demoment, "Image reconstruction and restoration: Overview of common estimation structures and problems," *IEEE Trans. on ASSP*, vol. 37, pp. 2024-22036, Oct. 1989.
- [7] C. Jutten and J. Héroult, "Détection de grandeurs primitives dans un message composite par une architecture de calcul neuromimétique en apprentissage non supervisé," in *Proc. Grets, (Nice)*, 1985.
- [8] M. Gaeta and J.-L. Lacoume, "Source separation without a priori knowledge: the maximum likelihood solution," in *Proc. EUSIPCO*, pp. 621-624, 1990.
- [9] P. Comon, "Independent component analysis, a new concept?," *Signal Processing*, vol. 36, pp. 287-314, 1994.
- [10] J.-F. Cardoso and A. Souloumiac, "An efficient technique for blind separation of complex sources," in *Proc. IEEE SP Workshop on Higher-Order Stat., Lake Tahoe, USA*, 1993.

- [11] E. Moreau and O. Macchi, "New self-adaptive algorithms for source separation based on contrast functions," in *Proc. IEEE SP Workshop on Higher-Order Stat., Lake Tahoe, USA*, 1993.
- [12] A. Belouchrani and J.-F. Cardoso, "Maximum likelihood source separation for discrete sources," in *Proc. EUSIPCO*, pp. 768-771, 1994.
- [13] L. Tong and R. Liu, "Blind estimation of correlated source signals," in *Proc. Asilomar conference*, Nov. 1990.
- [14] A. Belouchrani and K. Abed Meraim and J.-F. Cardoso and E. Moulines, "A blind source separation technique using second order statistics," *IEEE Trans. on SP*, vol. 45, pp. 434-444, Feb. 1997.
- [15] R.G. Baraniuk and L. Cohen, "On joint distributions of arbitrary variables," *IEEE Signal Processing Letters*, vol. 3, pp. 10-12, Jan. 1995.
- [16] R.G. Baraniuk, "A limitation of the kernel method for joint distributions of arbitrary variables," *IEEE Signal Processing Letters*, vol. 3, Feb. 1996.
- [17] O. Rioul and F. Flandrin, "Time-scale energy distributions: A general class extending wavelet transforms," *IEEE Trans. on SP*, vol. 40, pp. 1746-1757, July 1992.
- [18] J. Bertrand and P. Bertrand, "A class of affine Wigner functions with extended covariance properties," *J. Math. Phys.*, vol. 33, pp. 2515-2527, July 1992.
- [19] R. G. Baraniuk and D. L. Jones, "Unitary equivalence: A new twist on signal processing," *IEEE Trans. on SP*, vol. 43, pp. 2269-2282, Oct. 1995.
- [20] L. Cohen, *Time-frequency analysis*. Prentice Hall, 1995.
- [21] G.H. Golub and C.F. Van Loan, *Matrix computations*. The Johns Hopkins University Press, 1989.
- [22] S. Hearon and M. Amin, "Minimum variance time-frequency distribution kernels," *IEEE Trans. on SP*, vol. 43, pp. 1258-1262, 1995.
- [23] M. Amin, "Minimum variance time-frequency distribution kernels for signals in noise," *IEEE Trans. on SP*, vol. 44, pp. 2352-2356, 1996.
- [24] Y. Zhao, L. Atlas and R. Marks, "The use of cone-shaped kernels for generalized time-frequency representation of nonstationary signals," *IEEE Trans. on ASSP*, vol. 38, pp. 1084-1091, 1990.
- [25] H. Choi and W. Williams, "Improved time-frequency representation of multicomponent signals using exponential kernels," *IEEE Trans. on ASSP*, vol. 37, pp. 862-871, 1989.

INTERFERENCE MITIGATION IN SPREAD SPECTRUM COMMUNICATIONS USING BLIND SOURCE SEPARATION: APPROACH AND ANALYSIS.

Adel Belouchrani and Moeness G. Amin
Department of Electrical and Computer Engineering,
Villanova University, Villanova PA 19085 USA
E-mail:adel,moeness@ece.vill.edu

Abstract

In this paper, a new approach based on blind source separation techniques is proposed to solve the problem of interference mitigation in direct sequence spread spectrum communications systems. This approach strives to separate the interference from the desired signal and as such produce the spread spectrum signal with reduced jammer contamination. The proposed method is robust under multipath and array imperfections, and therefore, is most applicable to coherent arrivals and uncalibrated arrays. The paper presents the performance analysis and evaluation of the spread spectrum receiver incorporating the blind source separator. Closed form expressions of the receiver SNR and the corresponding improvement factors due to the proposed preprocessing scheme are derived. Simulation results are provided to illustrate the effectiveness of the blind source separation-based interference mitigation approach.

I. Introduction

Code division multiple-access (CDMA) using direct-sequence spread spectrum (DS/SS) signaling is among the most promising multiplexing technologies for cellular telecommunications services, such as personal communications, mobile telephony, and indoor wireless networks. The advantages of DS/SS for the aforementioned services include superior operation in multipath environments, increased capacity in bursty or fading channels, flexibility in the allocation of channels, the possibility to operate asynchronously, and the ability to share bandwidth with narrowband communication systems without affecting the performance of either systems. An DS/SS system can be defined simply as one in which the transmitted signal is spread over a bandwidth much wider

than the minimum bandwidth necessary to transmit the information [1], by means of a code independent of the data. The availability of this code at the receiver enables despreading and recovery of data, while spreading and suppression of interference. The processing gain of an DS/SS system, generally defined as the ratio between the transmission and data bandwidths, is a measure of its interference rejection capability [1]. This inherent ability of DS/SS systems to suppress interference is significantly enhanced when a complementary interference rejection techniques [2] is incorporated. These techniques have been first developed for military applications as a means to combat hostile narrowband jamming of the DS/SS signal, but they can also be used to mitigate the effects of unintentional narrowband interference caused by co-existence with conventional communications as well. The use of these techniques allows the CDMA users to communicate reliably with much less power than would otherwise be required in the presence of the narrowband users, and therefore increases the value for the maximum number of CDMA users that can be tolerated, with an acceptable level of degradation for the narrowband users.

In this paper, an approach for interference rejection based on blind source separation techniques is introduced. These techniques operate on the mixture of the desired and undesired signals at the array outputs to separate the DS/SS signal from the interference and its multipath. Blind source separation schemes [3, 4, 5] are known to be robust under multipath, sensor displacement, and array imperfections, and as such, they outperform adaptive array interference nulling algorithms when applied to coherent arrivals and uncalibrated arrays. Upon separation, the desired signal has to be identified for postprocessing, i.e., despreading. Several measures can be used in this regard, including direction-of-arrival, bandwidth, and spectral characteristics. The overall interference rejection DS/SS system is therefore

This work is supported by Rome Lab, NY, contract # F30602-96-C-0077.

composed of a separator, selector, and a correlator followed by a detector. Closed form expressions of the improvement of the receiver SNR for a two-sensor array are derived and Monte-Carlo simulations of the bit error rate (BER) curves illustrating the performance improvement of the proposed scheme for correlated arrivals are presented.

II. Problem formulation

A SS communication system which employs binary phase-shift-keying (BPSK) for both chip and data modulation is considered. We consider also an array of n sensors receiving signals from two sources (a desired signal and a narrowband jammer). The array output denoted by $\mathbf{x}(t)$ is a $n \times 1$ random vector. In the presence of spatially independent additive noise $\mathbf{w}(t)$, the narrowband data model is given by:

$$\mathbf{x}(t) = \mathbf{A}\mathbf{y}(t) + \mathbf{w}(t), \quad \mathbf{y}(t) = [s(t) \ j(t)]^T \quad (1)$$

where $\mathbf{y}(t)$ is the signal vector whose entries $s(t)$ and $j(t)$ are the desired signal and the jammer, respectively. The superscript T denotes the transpose operator. The two waveforms $s(t)$ and $j(t)$ are assumed to be statistically independent. The baseband spread spectrum signal $s(t)$ has the following form

$$s(t) = \sum_{k=-\infty}^{\infty} b_k m_k(t - kT), \quad (2)$$

where

$$m_k(t) = \sum_{l=1}^L c_l^k p(t - (l-1)T_c) \quad (3)$$

In (2)-(3), T^{-1} is the data (bit) rate, and T_c^{-1} is the chip rate. The integer $L = T/T_c$ is the number of chips per bit (SS processing gain). $\{b_k\}$ and $\{c_l^k\}_{l=1,\dots,L}$ represent the k -th bit data sequence and the corresponding chip sequence, and $p(t)$ is the chip pulse. The chip sequence (the PN spreading code) is a pseudo-random signal which is known by both the transmitter and the receiver.

The matrix \mathbf{A} , which in general corresponds to the steering matrix, is assumed to be full column rank, but otherwise is unknown in structure.

III. The proposed system

The block diagram shown in Fig.1 illustrates the proposed spread spectrum communications system. The standard spread spectrum demodulation is augmented by a preprocessor, which consists of a separator followed by

a selector. The separator acts on separating the interference from the signal by utilizing the spatial diversity provided by the multi-sensor array. This separation can be performed only up to a permutation (see below). Hence, a selection device is needed to label the separated waveforms as signal and jammer. The demodulation process recovers the original data by despreading the selected (desired) signal, while spreading the background noise and any interference component which might have not been separated from the signal. In the following, we describe each processing step in details.

A. Separation

The separation of the signal from the interference is achieved by using blind source separation techniques. These techniques strive to recover the source vector $\mathbf{y}(t)$ from the array output $\mathbf{x}(t)$ without the knowledge of matrix \mathbf{A} . The blind source separation techniques are based on the assumption of statistical independence of the source signals.

Various algorithms have been proposed for the blind source separation [3, 6, 7, 8]. In this paper, we only focus on the so called SOBI (Second Order Blind Identification) algorithm [8]. This algorithm is based on the simultaneous diagonalization of a combined set of spatio-temporal correlation matrices of the received signals (for more details see reference [8]).

It is well established that there is two inherent ambiguities in the blind source separation problem. First, there is no direct or indirect way of knowing the original labeling of the sources, hence any permutation of the estimated sources is also a satisfactory solution. The second ambiguity is that it is impossible to uniquely identify the source signals. Hence, the blind source separation is a technique for recovering of the source signals up to a fixed permutation and complex scalar multiplication.

B. Selection

Because of the inherent ambiguity stated above, a selector at the output of the separator is necessary to identify the desired signal for postprocessing. For this purpose, several strategies can be considered. The selection can be based on the signature of the desired signal which may be known by the receiver. As such, the problem of the selection becomes a pure problem of signal classification [9, 10]. Other strategies can be based on some a priori knowledge of the desired signal; for example its directions-of-arrival (DOA). In this case, the component whose steering vector in \mathbf{A} matches the signal DOA is taken as the SS signal. The selection can also be based on the relative power of the separated signals,

which makes use of the fact that the jammer has often a higher power than the spread spectrum signal.

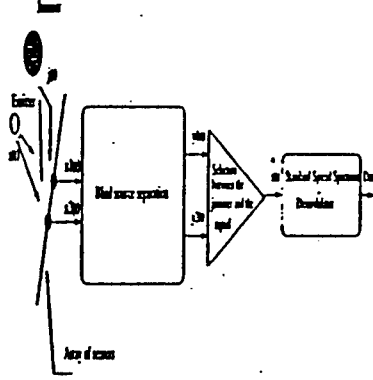


Figure 1: Spread spectrum system using blind source separation.

C. Spread Spectrum Demodulation

This last step consists of despreading the selected signal for recovering the original data bit sequence $\{b_k\}$. This is accomplished by the correlation of the received signal with a synchronized replica of the spreading signal $\{c_i^k\}_{i=1,\dots,L}$ used to spread the information. While the correlator despreads the desired signal, it spreads any interference components which might have escaped to the desired signal in the separation process.

Without interference rejection schemes operating in conjunction with the DS/SS system, the demodulation process improves the signal-to-interference and noise ratio at the receiver by an amount defined as the processing gain (PG). The later is the ratio of the spreading bandwidth to the desired signal information bandwidth (base-band),

$$PG = \frac{\text{Spreading Bandwidth}}{\text{Information Signal Bandwidth}} = \frac{T}{T_c}$$

Since both the spatial diversity and the blind source separation should yield improved performance, we consider in the next section, three receiver SNR improvement factors:

1. The improvement in the receiver SNR, ν_1 , by using a two-element array without SS signal/interference separation over one-element array.
2. The improvement in the receiver SNR, ν_2 , by using a two-element array with SS signal/interference separation over one-element array.
3. The improvement in the receiver SNR, ν_3 , by using a two-element array with SS signal/interference

formed.

IV. Analysis

Throughout the following analysis, the additive noise is assumed to be a zero mean white Gaussian complex circular process with variance σ_w^2 . The desired signal $s(t)$ and the jammer $j(t)$ are treated as if they have unit power. The actual dynamic range of both waveforms are accounted for by the magnitude of the corresponding columns of the steering matrix A . Hence, matrix A has the following structure:

$$A = \begin{bmatrix} \sigma_s & \sigma_j \\ \sigma_s e^{j\theta_s} & \sigma_j e^{j\theta_j} \end{bmatrix} \quad (4)$$

where σ_s^2 and σ_j^2 represent the powers of the signal $s(t)$ and the jammer $j(t)$, respectively, and θ_s and θ_j are their corresponding directions-of-arrival.

Further, in the analysis herein, we assume the transmission of the information bit "1", i.e., $s(n) = c(n)$, and a narrowband jammer of the form:

$$j(n) = e^{j\omega n + \phi}, \quad (5)$$

where ω is the jammer frequency and the phase ϕ is a uniform random variable.

The receiver SNR is defined as the ratio of the square of the mean to the variance of the correlator output U [11],

$$SNR = \frac{|E[U]|^2}{\text{Var}[U]} \quad (6)$$

where

$$U = \sum_{n=1}^L r(n)c(n)^*, \quad (7)$$

In the above equation, $r(n)$ is the sampled version of the correlator input, $c(n)$ is a zero-mean complex circular i.i.d. chip sequence such that $|c(n)|^2=1$ and L is the length of the chip sequence per information bit. Note that the decision of receiving 1 or -1 is based on the sign of the real part of U [12].

A. Pre-processor Disabled

When no DS/SS signal-interference separation is performed, the input to the correlator (the received signal) is the average of the sensor outputs,

$$r(n) = \frac{1}{2}[x_1(n) + x_2(n)] \quad (8)$$

In this case, the computation of the mean value and the variance of the correlator output (7) yields to,

$$E[U] = \frac{1}{2} \sigma_s (1 + e^{j\theta_s}) L \quad (9)$$

$$\text{Var}[U] = \frac{L}{2} [\sigma_j^2 (1 + \cos(\theta_j)) + \sigma_w^2] \quad (10)$$

Hence, the correlator SNR is given by

$$\text{SNR}_{\text{off}} = \frac{(1 + \cos(\theta_s))L}{(1 + \cos(\theta_j))JSR + \frac{1}{\text{SNR}}} \quad (11)$$

where JSR and SNR are the jammer-to-signal and signal-to-noise ratios, respectively.

Since (8) amounts to a beamformer with unit coefficients, then, for a given jammer position, the correlator SNR reaches a maximum value for a broadside desired signal arrival. Adversely, SNR_{off} reaches a minimum value for a given DOA of the desired signal when the jammer DOA is perpendicular to the array.

Since the correlator SNR using only one array sensor and without applying any auxiliary interference excision scheme is

$$\text{SNR}_{\text{one}} = \frac{L\sigma_s^2}{\sigma_j^2 + \sigma_w^2} = \frac{L}{JSR + \frac{1}{\text{SNR}}} \quad (12)$$

Then, the correlator SNR improvement factor achieved via the use of two-sensor array is, in essence, the array gain,

$$\nu_1 = \frac{\text{SNR}_{\text{off}}}{\text{SNR}_{\text{one}}} = \frac{(1 + \cos(\theta_s))(JSR + \frac{1}{\text{SNR}})}{(1 + \cos(\theta_j))JSR + \frac{1}{\text{SNR}}} \quad (13)$$

whose maximum value is $\nu_1 \approx 2$, i.e., 3 dB improvement.

B. Pre-processor Enabled

When the SS signal/interference separation is performed, the correlator input is the selected signal

$$\begin{aligned} r(n) &= \hat{s}(n) \\ &= [\hat{A}^{-1}x(n)]_1 \\ &= [\hat{A}^{-1}A]_{11}s(n) + [\hat{A}^{-1}A]_{12}j(n) \\ &\quad + \{[\hat{A}^{-1}A]_{11}[A^{-1}]_{11} + [\hat{A}^{-1}A]_{12}[A^{-1}]_{21}\} \\ &\quad w_1(n) + \{[\hat{A}^{-1}A]_{11}[A^{-1}]_{12} \\ &\quad + [\hat{A}^{-1}A]_{12}[A^{-1}]_{22}\}w_2(n) \end{aligned} \quad (14)$$

The mixing matrix \hat{A} is estimated by the SOBI algorithm using K correlation matrices. In the following analysis, we make use of the performance study of SOBI algorithm as derived in [8]. Hence, at the first order approximation, we have:

$$[\hat{A}^{-1}A]_{11} \approx 1 \quad (15)$$

$$[\hat{A}^{-1}A]_{12} \approx \sum_{|k| \leq K, k \neq 0} \frac{-\rho_k^*}{2|\rho|^2} [A^{-1}\delta R(k)A^{-1H}]_{12} \quad (16)$$

$$\text{where}$$

$$\rho = [\rho_1, \dots, \rho_K] \quad (18)$$

$$\rho_k = E[j(n)j(n-k)^*], k = 1, \dots, K \quad (19)$$

$$\delta R(k) = \hat{R}(k) - R(k) \quad (20)$$

with

$$\hat{R}(k) = \frac{1}{L} \sum_{n=1}^L x(n)x(n-k)^* \quad (21)$$

$$\begin{aligned} R(k) &= E[x(n)x(n-k)^*] \\ &= AA^H, \text{ for } k \neq 0, \end{aligned} \quad (22)$$

In this case, the derivation of the mean value and the variance of the correlator output (7) yields to the following expressions,

$$E[U] = L - 1 \quad (23)$$

$$\text{Var}[U] = \gamma_0 + \gamma_1\sigma_w^2 + \gamma_2\sigma_w^4 + \gamma_3\sigma_w^6 \quad (24)$$

where

$$\gamma_0 = 1 - \frac{1}{L}$$

$$\begin{aligned} \gamma_1 &= \frac{1}{\sigma_j^2(1 - \cos(\theta_s - \theta_j))} \left[1 + \frac{\sigma_j^2}{\sigma_s^2} (L - 1 + \frac{1}{2K}) \right. \\ &\quad \left. + \frac{1}{L} \left\{ \frac{\sigma_j^2(3 + \cos(\theta_s - \theta_j))}{2\sigma_s^2} + 2 \right. \right. \\ &\quad \left. \left. - \frac{1}{2K} \right\} - \frac{K+1}{L^2} \right] \end{aligned}$$

$$\begin{aligned} \gamma_2 &= \frac{1}{\sigma_j^4(1 - \cos(\theta_s - \theta_j))^2} \left[\frac{1}{2K} + \frac{\sigma_j^2}{\sigma_s^2} \left(1 + \frac{1}{2K} \right) \right. \\ &\quad \left. + \frac{1}{L} \left\{ \frac{1}{2K} + \frac{\sigma_j^2}{\sigma_s^2} \left(1 + \frac{1}{2K} + \frac{(3 + \cos(\theta_s - \theta_j))}{4K} \right) \right\} \right. \\ &\quad \left. - \frac{1}{L^2} \left\{ \frac{K+1}{4K} + \frac{\sigma_j^2}{\sigma_s^2} (K+1) \left(1 + \frac{1}{4K} \right) \right\} \right] \end{aligned}$$

$$\begin{aligned} \gamma_3 &= \frac{1}{\sigma_j^6(1 - \cos(\theta_s - \theta_j))^3} \left[\frac{1}{2K} \frac{\sigma_j^2}{\sigma_s^2} \left(1 - \frac{2}{L} \right. \right. \\ &\quad \left. \left. + \frac{K+1}{2L^2} \right) \right] \end{aligned}$$

From (23) and (24), the correlator output signal-to-noise ratio is

$$\text{SNR}_{\text{on}} = \frac{(L-1)^2}{\gamma_0 + \gamma_1\sigma_w^2 + \gamma_2\sigma_w^4 + \gamma_3\sigma_w^6} \quad (25)$$

It is noteworthy that the above analyses still hold for coherent arrivals. In this case, the vector $[\sigma_j \sigma_j e^{j\theta_j}]^T$ in (4) represents the generalized steering vector (spatial signature) associated to the jammer and all of its multipath.

C. Comments

In the case of a noise free channel, equations (11) and (25) become,

$$SNR_{on} = \frac{(L-1)^2}{\gamma_0} \quad (26)$$

$$SNR_{off} = \frac{(1 + \cos(\theta_s))\sigma_s^2 L}{(1 + \cos(\theta_j))\sigma_j^2} \quad (27)$$

According to (26), SNR_{on} is independent of

- the array geometry.
- the jammer power.
- the number of correlation matrices used in the SOBI algorithm.

This invariance property is not satisfied when the preprocessor is disabled, as shown by relation (27).

Note from (25) that for small jammer power, the detection becomes sensitive to noise through γ_1 , γ_2 and γ_3 . However, as the jammer power σ_j^2 increases, the SNR_{on} increases, leading to conclude that *the higher the jammer power the better the detection*.

For $L \gg 1$ and high SNR, the receiver SNR improvement factor using a two-sensor array and the SOBI algorithm over one-array element is

$$\nu_2 = \frac{SNR_{on}}{SNR_{one}} \approx L(JSR) \quad (28)$$

whereas

the receiver SNR improvement factor with/without the SOBI algorithm in a two-element array is

$$\nu_3 = \frac{SNR_{on}}{SNR_{off}} \approx L \frac{(1 + \cos(\theta_j))}{(1 + \cos(\theta_s))} (JSR) \quad (29)$$

It is clear that $\nu_2 = \nu_3$ for $\theta_s = \theta_j$, as expected.

In figures 2 and 3, we plot expressions (25) and (11) versus the JSR and the number of chips/bit, respectively, for $\theta_s = 0^\circ$, $\theta_j = 9^\circ$ and $K=4$. These figures show the benefit of using the interference separation in the case of high jammer power.

V. Numerical Results

In this Section, we consider a uniform linear array of two sensors separated by half a wavelength. In

addition to the DS/SS signal, the array receives a jammer through three paths. The desired signal is a BPSK signal arriving at $\theta_0 = 0^\circ$. The jammer is composed of three fixed sinusoids whose frequencies are $\omega_1 = \pi/6$, $\omega_2 = \pi/3$ and $\omega_3 = \pi/2$. The direct path of the jammer arrives at $\theta_1 = 2^\circ$ whereas its multipath arrive at $\theta_2 = 10^\circ$ and $\theta_3 = -10^\circ$, respectively. The noise used is zero-mean white complex Gaussian process. Four spatio-temporal correlation matrices at the first four lags $\tau = 1, 2, 3, 4$ are considered in the SOBI algorithm.

Figure 4 presents the Bit Error Rate (BER) in dB versus JSR for 0 dB SNR and 8 chips/bit, 16 chips/bit, 32 chips/bit and 64 chips/bit. Under 32 chips/bit and 64 chips/bit, the proposed method offers no error over 10^6 runs for JSR up to 90 dB. Figures 5 displays the BER versus the number of chips/bit for 0 dB SNR for 60 dB JSR. It is evident that the probability of error is remarkably reduced under the proposed method.

VI. Conclusions

In this paper, we presented a new interference mitigation scheme for spread spectrum communications. Blind source separation techniques are applied to increase the rejection capability of the direct sequence SS communications systems to narrowband interference. The main motivation behind the proposed approach is to further immune the DS/SS system against strong interference and its multipath. The later is most appropriately handled by blind source separation methods, which do not lead to reduced array aperture, as in the case of spatial averaging methods. With the inclusion of blind source separation methods, the overall DS/SS receiver consists of a signal separator, selector, despreader followed by a detector. Although directions-of-arrival estimation is not necessary for the proposed preprocessing interference rejection scheme, it may be used to identify the spread spectrum signal, upon separation. The performance analysis of DS/SS receiver in conjunction with the proposed interference mitigation scheme has been presented. Closed form expressions of the receiver signal-to-noise ratios have been derived. We have considered three improvement factors depicting the gain in performance with/without the spatial diversity and blind source separation. BER curves were provided for multipath and coherent signal environment. These curves clearly show the significant reduction in bit error rates when employing blind source separations.

References

- [1] M. K. Simon, et al. *Spread Spectrum Communications*. Computer Science Press, 1985.

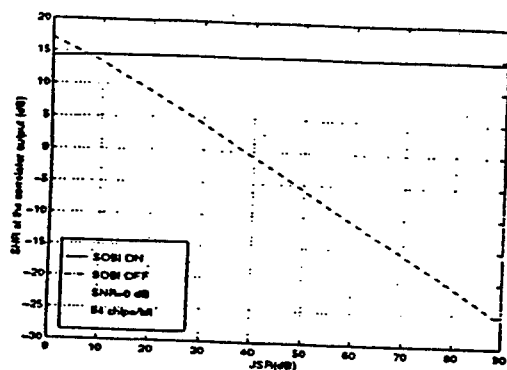


Figure 2: SNR at the correlator output in dB vs JSR.

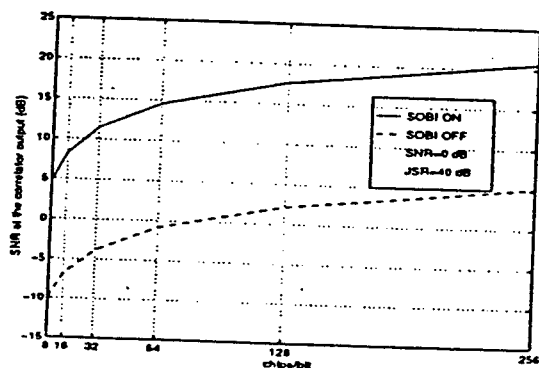


Figure 3: SNR at the correlator output in dB vs chips/bit.

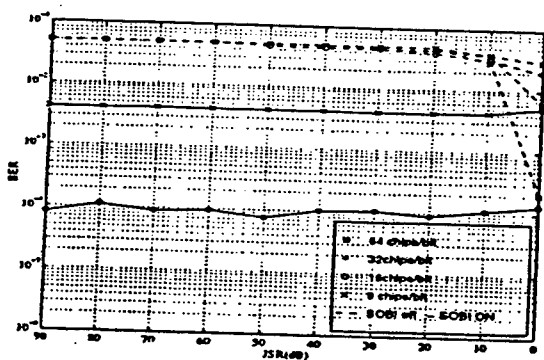


Figure 4: BER in (dB) vs JSR

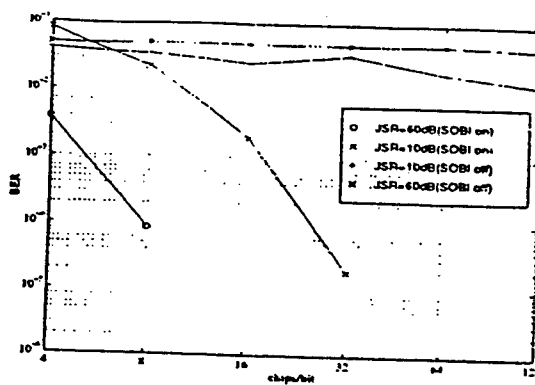


Figure 5: BER in (dB) vs number of chips/bit

- [2] L. B. Milstein, "Interference rejection techniques in spread spectrum communications," *Proc. IEEE*, vol. 66, pp. 657-671, June 1988.
- [3] P. Comon, "Independent component analysis," in *Proc. Int. Workshop on Higher-Order Stat., Chamrousse, France*, pp. 111-120, 1991.
- [4] A. Belouchrani and J.-F. Cardoso, "Maximum likelihood source separation for discrete sources," in *Proc. EU-SIPCO*, pp. 768-771, 1994.
- [5] A. Belouchrani and K. Abed Meraim, "Constant modulus blind source separation technique: A new approach," in *Proc. ISSPA, Gold Coast, Australia*, August 1996.
- [6] M. Gaeta and J.-L. Lacoume, "Source separation without a priori knowledge: the maximum likelihood solution," in *Proc. EUSIPCO*, pp. 621-624, 1990.
- [7] J.-F. Cardoso and A. Souloumiac, "An efficient technique for blind separation of complex sources," in *Proc. IEEE SP Workshop on Higher-Order Stat., Lake Tahoe, USA*, 1993.
- [8] A. Belouchrani and K. Abed Meraim and J.-F. Cardoso and E. Moulines, "A blind source separation technique using second order statistics," *IEEE Trans. on SP*, vol. 45, pp. 434-444, Feb. 1997.
- [9] L. Dominguez, J. Borrallo, J. Garcia, "A general approach to the automatic classification of radiocommunication signals," *Signal Processing*, vol. 22, pp. 239-250, Mar. 1991.
- [10] B. G. Mobasser and S. Rao, "Recognition of Digital Modulation Types Using Constellation Shape Matching," *SPIE, Signal and Image processing, Denver, Colorado*, Aug. 1996.
- [11] J. Ketchum and J. Proakis, "Adaptive algorithms for estimating and suppressing narrow band interference in PN spread spectrum systems," *IEEE Trans. on Comm.*, vol. 30, pp. 913-924, May 1982.
- [12] A. W. Lam and F. M. Ozluturk, "Performance bounds for ds/ssma communications with complex signature sequences," *IEEE Trans. on Comm.*, vol. 40, pp. 512-517, Mar. 1991.

BLIND SOURCE SEPARATION USING TIME-FREQUENCY DISTRIBUTIONS: ALGORITHM AND ASYMPTOTIC PERFORMANCE.

Adel Belouchrani and Moeness G. Amin

Department of Electrical and Computer Engineering,
Villanova University, Villanova PA 19085 USA

ABSTRACT

This paper addresses the problem of the blind source separation which consists of recovering a set of signals of which only instantaneous linear mixtures are observed. A blind source separation approach exploiting the difference in the time-frequency (t-f) signatures of the sources is considered. The approach is based on the diagonalization of a combined set of 'spatial time-frequency distributions'. Asymptotic performance analysis of the proposed method is performed. Numerical simulations are provided to demonstrate the effectiveness of our approach and to validate the theoretical expression of the asymptotic performance.

1. INTRODUCTION

Blind source separation consists of recovering a set of signals of which only instantaneous linear mixtures are observed. The first solution to this problem was based on the cancellation of higher order moments assuming non-Gaussian and i.i.d. source signals [1]. Since then, other criteria based on minimizations of cost functions, such as the sum of square fourth order cumulants [2, 3], contrast functions [2] or likelihood function [4], have been used by several researchers. In the case of non i.i.d. source signals and even Gaussian sources, solutions based on second order statistics are possible [5, 6]. Matsuoka et al. have shown that the problem of the separation of nonstationary signals can be solved using second order decorrelation only [7]. They implicitly use the nonstationarity of the signal via a neural net approach. Herein, we propose to take advantage explicitly of the nonstationarity property of the signals to be separated. This is done by resorting to the powerful tool of time frequency signal representations.

In this paper, we develop an approach based on a joint diagonalization of a combined set of spatial time-frequency distributions. This approach exploits the difference between the t-f signatures of the sources. In contrast to existing methods, the proposed approach allows the separation of Gaussian sources with identical spectra shape but with different time-frequency localization properties. Moreover, the effects of spreading the noise power while localizing the source energy in the time-frequency domain amounts to increase the robustness of the proposed approach with respect to noise.

This work is supported by Rome Lab, NY, contract # F30602-96-C-0077.

2. PROBLEM FORMULATION

Consider m sensors receiving an instantaneous linear mixture of signals emitted from n sources. The $m \times 1$ vector $x(t)$ denotes the output of the sensors at time instant t which may be corrupted by an additive noise $n(t)$. Hence, the linear data model is given by:

$$x(t) = As(t) + n(t), \quad (1)$$

where the $m \times n$ matrix A is called the 'mixing matrix'. The n source signals are collected in a $n \times 1$ vector denoted $s(t)$ which is referred to as the source signal vector. The sources are assumed to have different structures and localization properties in the time frequency domain. The mixing matrix A is full column rank but is otherwise unknown. In contrast with traditional parametric methods, no specific structure of the mixture matrix is assumed.

The problem of blind source separation has two inherent ambiguities. First, it is not possible to know the original labeling of the sources, hence any permutation of the estimated sources is also a satisfactory solution. The second ambiguity is that it is inherently impossible to uniquely identify the source signals. We take advantage of the second indeterminacy by treating the source signals as if they have unit power. This normalization still leaves undetermined the ordering and the phases of the columns of A . Hence, the blind source separation is a technique for the identification of the mixing matrix and/or the recovering of the source signals up to a fixed permutation and some complex factors.

3. SPATIAL TIME-FREQUENCY DISTRIBUTIONS

The discrete-time form of the Cohen's class of time-frequency distributions (TFD), for signal $x(t)$, is given by [8]

$$D_{xx}(t, f) = \sum_{l, m=-\infty}^{\infty} \phi(m, l) x(t+m+l) x^*(t+m-l) e^{-j4\pi fl} \quad (2)$$

where t and f represent the time index and the frequency index, respectively. The kernel $\phi(m, l)$ characterizes the distribution and is a function of both the time and lag variables. The cross-TFD of two signals $x_1(t)$ and $x_2(t)$ is de-

defined by

$$D_{x_1 x_2}(t, f) = \sum_{l, m=-\infty}^{\infty} \phi(m, l) x_1(t+m+l) x_2^*(t+m-l) e^{-j4\pi f l} \quad (3)$$

Expressions (2) and (3) are now used to define the following data *spatial time-frequency distribution* (STFD) matrix,

$$D_{xx}(t, f) = \sum_{l, m=-\infty}^{\infty} \phi(m, l) x(t+m+l) x^*(t+m-l) e^{-j4\pi f l} \quad (4)$$

where $[D_{xx}(t, f)]_{ij} = D_{x_i x_j}(t, f)$, for $i, j = 1, \dots, n$.

Under the linear data model of equation (1) and assuming noise-free environment, the STFD matrix takes the following simple structure:

$$D_{xx}(t, f) = A D_{ss}(t, f) A^H \quad (5)$$

where $D_{ss}(t, f)$ is the signal TFD matrix whose entries are the auto- and cross-TFDs of the sources. We note that $D_{xx}(t, f)$ is of dimension $m \times m$, whereas $D_{ss}(t, f)$ is of $n \times n$ dimension. For narrowband array signal processing applications, matrix A holds the spatial information and maps the auto- and cross-TFDs of the sources into auto- and cross-TFDs of the data.

Since the off-diagonal elements of $D_{ss}(t, f)$ are cross-terms, then this matrix is diagonal for each time-frequency (t-f) point which corresponds to a true power concentration, i.e. signal auto-term. In the sequel, we consider the t-f points which satisfy this property. In practice, to simplify the selection of auto-terms, we apply a smoothing kernel $\phi(m, l)$ that significantly decreases the contribution of the cross-terms in the t-f plane. This kernel can be a member of the reduced interference distribution (RID) introduced in [9] or signal-dependent which matches the underlying signal characteristics [10].

4. PROPOSED ALGORITHM

Let W denotes a $m \times n$ matrix, such that $(WA)(WA)^H = UU^H = I$, i.e. WA is a $m \times m$ unitary matrix (this matrix is referred to as a whitening matrix, since it whitens the signal part of the observations). Pre- and post-multiplying the TFD-matrices $D_{xx}(t, f)$ by W , we then define the *whitened TFD-matrices* as:

$$\underline{D}_{xx}(t, f) = W D_{xx}(t, f) W^H \quad (6)$$

From the definition of W and Eq.(5), we may expressed $\underline{D}_{xx}(t, f)$ as

$$\underline{D}_{xx}(t, f) = U D_{ss}(t, f) U^H \quad (7)$$

Since the matrix U is unitary and $D_{ss}(t, f)$ is diagonal, expression (7) shows that any whitened data STFD-matrix is diagonal in the basis of the columns of the matrix U (the eigenvalues of $\underline{D}_{xx}(t, f)$ being the diagonal entries of $D_{ss}(t, f)$).

If, for the (t_a, f_a) point, the diagonal elements of $D_{ss}(t_a, f_a)$ are all distinct, the missing unitary matrix U may be 'uniquely' (i.e. up to permutation and phase

shifts) retrieved by computing the eigendecomposition of $D_{xx}(t_a, f_a)$. However, when the t-f signatures of the different signals are not highly overlapping or frequently intersecting, which is likely to be the case, the selected (t_a, f_a) point often corresponds to a single signal auto-term, rendering matrix $D_{ss}(t_a, f_a)$ deficient. That is, only one diagonal element of $D_{ss}(t_a, f_a)$ is different from zero. It follows that the determination of the matrix U from the eigendecomposition of a single whitened data STFD-matrix is no longer 'unique' in the sense defined above. The situation is more favorable when considering *simultaneous diagonalization* of a combined set $\{D_{xx}(t_i, f_i) | i = 1, \dots, p\}$ of p STFD matrices. This amounts to incorporating several time-frequency points in the source separation problem. It is noteworthy that two source signals with identical t-f signatures can not be separated even with the inclusion of all information in the t-f plane.

Joint diagonalization: The *joint diagonalization* [6] can be explained by first noting that the problem of the diagonalization of a single $n \times n$ normal matrix M is equivalent to the minimization of the criterion [11]

$$C(M, V) \stackrel{\text{def}}{=} - \sum_i |v_i^* M v_i|^2 \quad (8)$$

over the set of unitary matrices $V = [v_1, \dots, v_n]$. Hence, the joint diagonalization of a set $\{M_k | k = 1..K\}$ of K arbitrary $n \times n$ matrices is defined as the minimization of the following JD criterion:

$$C(V) \stackrel{\text{def}}{=} - \sum_k C(M_k, V) = - \sum_{ki} |v_i^* M_k v_i|^2 \quad (9)$$

under the same unitary constraint. An efficient joint approximate diagonalization algorithm exists in [6] and it is a generalization of the Jacobi technique [11] for the exact diagonalization of a single normal matrix.

Identification Procedure: Equations (5-9) constitute the blind source separation approach based on TFD which is summarized by the following steps

- Determine the whitening matrix \hat{W} from the eigendecomposition of an estimate of the covariance matrix of the data (see [6] for more details).
- Determine the unitary matrix \hat{U} by minimizing the joint approximate diagonalization criterion for a specific set of whitened TFD matrices $\{\underline{D}_{xx}(t_i, f_i) | i = 1, \dots, p\}$,
- Obtain an estimate of the mixture matrix \hat{A} as $\hat{A} = \hat{W}^* \hat{U}$, where the superscript $\#$ denotes the pseudo-inverse, and an estimate of the source signals $\hat{s}(t)$ as $\hat{s}(t) = \hat{U}^H W x(t)$.

5. ASYMPTOTIC PERFORMANCE

The performance is characterized in terms of signal rejection. After identification of the matrix A , the estimated source signals may be obtained as $\hat{s}(t) = \hat{A}^* x(t) = \hat{A}^* A s(t) + \hat{A}^* n(t)$.

The matrix \hat{P} defined by $\hat{P} = \hat{A}^* A$ should be close to some matrix P with only one zero phase term in each row and each column (phase and permutation indeterminacies). For convenience, we assume that \hat{P} is close to a diagonal rather than to some other permutation matrix. The p -th estimated source signal is

$$\hat{s}_p(t) = \sum_{q=1}^n \hat{P}_{pq} s_q(t) + (A^* n(t))_p \quad (10)$$

The power of the q -th source signal residual (interference) in the p -th estimated source signal is: $\mathcal{I}_{pq} = E|\hat{P}_{pq}|^2$ (since the sources have unit power, this quantity is nothing but the interference to signal ratio (ISR) for the q and p -th source). As a global measure of performance, we use the overall rejection level defined as the sum of all the interferences

$$\mathcal{I}_{perf} \stackrel{\text{def}}{=} \sum_{q \neq p} E|\hat{P}_{pq}|^2 = \sum_{q \neq p} \mathcal{I}_{pq} \quad (11)$$

In the case of Gaussian noise and deterministic source signals, we have derived closed form expressions of the rejection index at the limit of large snapshots. Details of the calculation are presented in [12].

$$\mathcal{I}_{pq} = \mathcal{I}_{pq}^0 + \sigma^2 \mathcal{I}_{pq}^1 + \sigma^4 \mathcal{I}_{pq}^2 \quad (12)$$

where the coefficients of the expansion are

$$\begin{aligned} \mathcal{I}_{pq}^0 &= \frac{1}{4} \left[\alpha_{pq}^2 |r_{Tpq}|^2 - \sum_{k=1}^K \alpha_{pq} \alpha_{pqk} \left[r_{Tpq} D_{s_q s_p}(t_k, f_k) + \right. \right. \\ &\quad \left. \left. r_{Tqp} D_{s_p s_q}(t_k, f_k) \right] + \sum_{k,l=1}^K \alpha_{pqk} \alpha_{pql} D_{s_p s_q}(t_k, f_k) D_{s_q s_p}(t_l, f_l) \right] \\ \mathcal{I}_{pq}^1 &= \frac{1}{4} \left[\frac{\alpha_{pq}^2}{T} (r_{Tpp} J_{qq} + r_{Tqq} J_{pp}) - \sum_{k=1}^K \alpha_{pq} \alpha_{pqk} \left[r_{Tpq} J_{qp} \right. \right. \\ &\quad \left. \left. + r_{Tqp} J_{pq} \frac{2}{T} (D_{s_p s_p}(t_k, f_k) J_{qq} + D_{s_q s_q}(t_k, f_k) J_{pp}) \right] + \sum_{k,l=1}^K \alpha_{pqk} \right. \\ &\quad \left. \alpha_{pql} (D_{s_p s_q}(t_k, f_k) J_{qp} + D_{s_q s_p}(t_l, f_l) J_{pq} + F_{s_p s_p}^{k,l} J_{qq} + F_{s_q s_q}^{k,l} J_{pp}) \right] \\ \mathcal{I}_{pq}^2 &= \frac{1}{4} \left[\frac{1}{T} \left[\alpha_{pq}^2 (J_{qq} J_{pp} + \frac{|J_{pq}|^2}{m-n}) - 2 \sum_{k=1}^K \alpha_{pq} \alpha_{pqk} J_{qq} J_{pp} \right] \right. \\ &\quad \left. + \sum_{k,l=1}^K \alpha_{pqk} \alpha_{pql} (|J_{pq}|^2 + \phi_{kl} J_{pp} J_{qq}) \right] \end{aligned}$$

with

$$\begin{aligned} \alpha_{pq} &= 1 + \frac{|d_p|^2 - |d_q|^2}{|d_p - d_q|^2} \\ d_r &= [D_{s_r s_r}(t_1, f_1), \dots, D_{s_r s_r}(t_K, f_K)]^T \\ \alpha_{pqk} &= \frac{D_{s_p s_p}^*(t_k, f_k) - D_{s_q s_q}^*(t_k, f_k)}{|d_p - d_q|^2} \\ r_{Tpq} &= \frac{1}{T} \sum_{t=1}^T s_p(t) s_q^*(t) \end{aligned}$$

$$\begin{aligned} J_{pq} &= (A^H A)_{pq}^{-1} \\ F_{s_p s_p}^{k,l} &= \sum_{v', v, m=-\infty}^{+\infty} \phi(m, v) \phi(m - v - v' + t_k - t_l, v') \\ &\quad s_p(t_k + m + v) s_p^*(t_k + m - v - 2v') e^{-j4\pi f_k v} e^{-j4\pi f_l v'} \\ \phi_{kl} &= \sum_{v, m=-\infty}^{+\infty} \phi(m, v) \phi^*(m + (t_k - t_l), v) e^{-j4\pi (f_k - f_l) v} \end{aligned}$$

For high signal to noise ratio, the expansion (12) is dominated by the first term \mathcal{I}_{pq}^0 . Below, some comments on this term are given:

- If the sources p and q have identical t-f signatures over the chosen t-f points (i.e. $d_p = d_q$), the corresponding ISR $\mathcal{I}_{pq} \rightarrow \infty$.
- As the correlation function r_{Tpq} of the sources p and q and the cross-terms $D_{s_p s_q}(t_k, f_k)$ vanish, the corresponding ISR given by \mathcal{I}_{pq} also vanishes, yielding a perfect separation.
- \mathcal{I}_{pq}^0 is independent of the mixing matrix. In the array processing context, it means that performance in terms of interference rejection are unaffected by the array geometry. The performance depends only on the sample size and the t-f signatures of the sources.

6. PERFORMANCE EVALUATION

Numerical experiments: we consider a uniform linear array of three sensors having half wavelength spacing and receiving signals from two sources in the presence of white Gaussian noise. The sources arrive from different directions $\phi_1 = 0$ and $\phi_2 = 20$ degrees. The source signals are generated by filtering a complex circular white Gaussian processes by an AR model of order one with coefficient $a_1 = 0.85 \exp(j2\pi f_1(t))$ and $a_2 = 0.85 \exp(j2\pi f_2(t))$, where we have:

$$\begin{aligned} f_1(t) &= \begin{cases} 0.0625 & \text{for } t = 1 : 400 \\ 0.1250 & \text{for } t = 401 : 450 \\ 0.3750 & \text{for } t = 451 : 850 \end{cases} \\ f_2(t) &= \begin{cases} 0.3750 & \text{for } t = 1 : 400 \\ 0.1250 + \delta f & \text{for } t = 401 : 450 \\ 0.0625 & \text{for } t = 451 : 850 \end{cases} \end{aligned}$$

The signal to noise ratio (SNR) is set at 5 dB. The kernel used for the computation of the TFDs is the Choi-Williams kernel [8], which provides a good reduction of the cross-terms. Eight TFD matrices are considered. The corresponding t-f points are those of the highest power in the t-f domain. The mean rejection level is evaluated over 500 Monte-Carlo runs.

Table 1 shows the mean rejection level in dB versus the 'spectral shift' δf both for SOBI algorithm [6] and the new algorithm. Note that for $\delta f = 0$, the two Gaussian source signals have identical spectra shape. In this case, while SOBI fails¹ in separating the two sources, the proposed algorithm succeed.

¹ We admit that a source separation algorithm fails when the mean rejection level is greater than -10 dB.

Spectral shift (δf)	Mean Rejection level in dB	
	SOBI	TFS
0.000	-8.86	-12.22
0.002	-10.01	-12.21
0.010	-10.18	-12.34
0.050	-11.09	-12.53
0.200	-12.92	-12.54

Table 1. Performance of SOBI and TFS algorithms vs δf

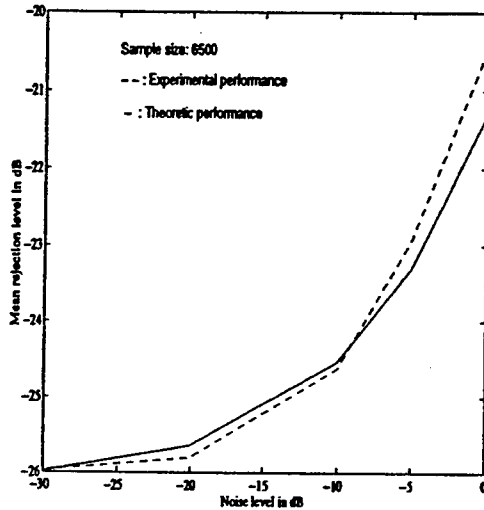


Figure 1. Performance validation vs σ^2 .

Validation of the asymptotic performance: Herein, the evaluation of the domain of validity of the first-order performance approximation (12) is considered. The previous settings are used with the exception of the source signals which are deterministic sinusoids at frequencies $f_1 = 0.4375$ and $f_2 = 0.0625$. The TFDs are computed using windowed Wigner distribution. The chosen window width is $M = 2L + 1$, with $L = 32$. The identification is performed using $\frac{T}{M}$ STFD matrices spaced in time by M samples (T being the sample size). The overall rejection level is evaluated over 500 independent runs.

In Fig.1, the rejection level I_{perf} is plotted in dB as a function of the noise power σ^2 (also expressed in dB). In Fig.2, the rejection level I_{perf} is plotted in dB as against sample size. Both figures 1 and 2 show that the approximation is better at high SNR and for large sample size. This means that the asymptotic conditions are reached faster in this range of parameters.

7. CONCLUSION

In this paper, the problem of blind separation of linear spatial mixture of non-stationary source signal based on time frequency distributions has been investigated. A solution based on the diagonalization of a combined set of spatial time frequency distribution matrices has been proposed. A closed form expression for the performance criterion of the method has been developed. Numerical simulations have been provided to support the theoretical claims.

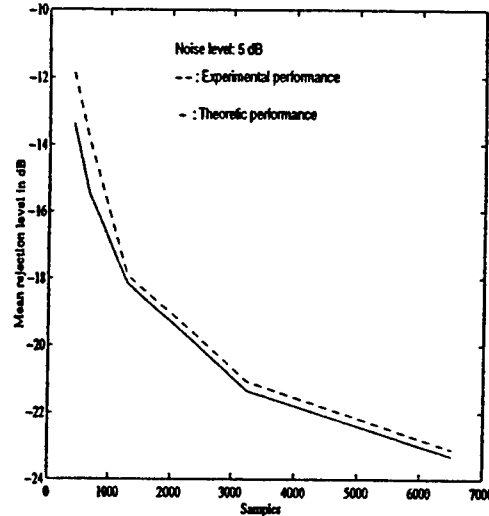


Figure 2. Performance validation vs samples size (T).

REFERENCES

- [1] C. Jutten and J. Héroult, "Détection de grandeurs primitives dans un message composite par une architecture de calcul neuromimétique en apprentissage non supervisé," in *Proc. Grets, (Nice)*, 1985.
- [2] P. Comon, "Independent component analysis, a new concept?," *Signal Processing*, vol. 36, pp. 287-314, 1994.
- [3] J.-F. Cardoso and A. Souloumiac, "An efficient technique for blind separation of complex sources," in *Proc. IEEE SP Workshop on Higher-Order Stat., Lake Tahoe, USA*, 1993.
- [4] A. Belouchrani and J.-F. Cardoso, "Maximum likelihood source separation for discrete sources," in *Proc. EUSIPCO*, pp. 768-771, 1994.
- [5] L. Tong and R. Liu, "Blind estimation of correlated source signals," in *Proc. Asilomar conference*, Nov. 1990.
- [6] A. Belouchrani and K. Abed Meraim and J.-F. Cardoso and E. Moulines, "A blind source separation technique using second order statistics," *IEEE Trans. on SP*, 1996. To appear.
- [7] K. Matsuoka, M. Ohya and M. Kawamoto, "A neural net for blind separation of nonstationary signals," *Neural Networks*, vol. 8, pp. 411-419, 1995.
- [8] L. Cohen, *Time-frequency analysis*. Prentice Hall, 1995.
- [9] J. Jeong and W. Williams, "Kernel design for reduced interference distributions," *IEEE Trans. on SP*, vol. 40, pp. 402-412, Feb. 1992.
- [10] R. Baraniuk and D. Jones, "A signal dependent time-frequency representation: Optimum kernel design," *IEEE Trans. on SP*, vol. 41, pp. 1589-1603, Apr. 1993.
- [11] G.H. Golub and C.F. Van Loan, *Matrix computations*. The Johns Hopkins University Press, 1989.
- [12] A. Belouchrani and M. G. Amin, "Blind Source Separation Based on Time-Frequency Signal Representation," *IEEE Trans. on SP*, 1996. Submitted.

Interference mitigation in spread spectrum communications using blind source separation

Adel Belouchrani, Moeness G. Amin, and Chenshu Wang
Department of Electrical and Computer Engineering,
Villanova University, Villanova, PA 19085
adel,moeness@ece.vill.edu

Abstract

In this paper, we propose to apply blind source separation techniques for jammer mitigation in spread spectrum (SS) communication systems. These techniques strive to separate the jammer from the signal and as such produce a signal with reduced jammer contamination. With the jammer mostly mitigated through the separation process, the SS system requires smaller spreading gain and transmission bandwidth than the case if no separation is performed. The proposed spread spectrum receiver based on source separation improves the SNR at the correlator output and its performance is robust to multipath and coherent jamming environment. Simulation results including the bit error rates are provided to illustrate the effectiveness of the proposed approach.

1 Introduction

Code division multiple-access (CDMA) using direct-sequence spread spectrum (DS/SS) signaling is among the most promising multiplexing technologies for cellular telecommunications services, such as personal communications, mobile telephony, and indoor wireless networks. The advantages of DS/SS for the aforementioned services include superior operation in multipath environments, increased capacity in bursty or fading channels, flexibility in the allocation of channels, the possibility to operate asynchronously, and the ability to share bandwidth with narrowband communication systems without affecting the performance of either systems. An DS/SS system can be defined simply as one in which the transmitted signal is spread over a bandwidth much wider than the minimum bandwidth necessary to transmit the information [1], by means of a code independent of the data. The availability of this code at

the receiver enables despreading and recovery of data, while spreading and suppression of interference. The processing gain of an DS/SS system, generally defined as the ratio between the transmission and data bandwidths, is a measure of its interference rejection capability [1]. This inherent ability of DS/SS systems to suppress interference is significantly enhanced when a complementary interference rejection technique [2] is incorporated. These techniques have been first developed for military applications as a means to combat hostile narrowband jamming of the DS/SS signal, but they can also be used to mitigate the effects of unintentional narrowband interference caused by co-existence with conventional communications as well. The use of these techniques allows the CDMA users to communicate reliably with much less power than would otherwise be required in the presence of the narrowband users, and therefore increases the value for the maximum number of CDMA users that can be tolerated, with an acceptable level of degradation for the narrowband users.

So far, all the proposed interference rejection techniques [2] for spread spectrum communications are interference excision techniques, which relies on applying an excision filter prior to the despreading. Excision filters act on suppressing the interference and thus increase the signal-to-noise ratio at the correlator output of the receiver. These filters can be block or adaptive and may be realized in time [3], frequency [4], or time frequency domain. The later includes the wavelet [5] and Gabor transforms [6] as well as bilinear time frequency distributions [7, 8, 9]. But pre-processing using excision filters may eliminate a significant part of the desired signal, prove impractical and difficult to implement for on line high data rate communications, and yield poor performance in rapidly changing jamming environment. Instead of excising the interference, we propose in this paper to separate the interference from the signal prior to the despreading, by taking advantage of the spatial diversity provided by a multisensor array. This can be accomplished by a blind source separation technique already considered in [10]. It is shown that this technique substantially

This work is supported by Rome Lab., NY, contract # F30602-96-C-0077

reduces the probability of error at the receiver and requires smaller spreading gain and transmission bandwidth than the case if no separation is performed. An important feature in the context of narrowband signals is that the separation technique is robust under multipath and coherent jamming environment.

2 System Model

An SS communication system which employs binary phase-shift-keying (BPSK) for both chip and data modulation is considered. We consider also an array of n sensors receiving signals from two sources (a desired signal and a narrowband jammer). The array output denoted by $\mathbf{x}(t)$ is a $n \times 1$ random vector. In the presence of spatially independent additive noise $\mathbf{n}(t)$, the narrowband data model is given by:

$$\mathbf{x}(t) = \mathbf{A}\mathbf{y}(t) + \mathbf{n}(t), \quad \mathbf{y}(t) = [s(t) \ j(t)]^T \quad (1)$$

where $s(t)$ is the desired signal and $j(t)$ is the jammer. The two waveforms $s(t)$ and $j(t)$ are assumed to be statistically independent. The baseband SS signal $s(t)$ has the following form

$$s(t) = \sum_{k=-\infty}^{\infty} b_k m_k(t - kT), \quad (2)$$

where

$$m_k(t) = \sum_{l=0}^{M-1} c_l^k p(t - lT_c) \quad (3)$$

In (2)-(3), T^{-1} is the data (bit) rate, and T_c^{-1} is the chip rate. The integer $M = T/T_c$ is the number of chips per bit (SS processing gain). $\{b_k\}$ and $\{c_l^k\}_{l=0, \dots, M-1}$ represent the k -th bit data sequence and the corresponding chip sequence. $p(t)$ is the chip pulse.

The matrix \mathbf{A} , which in general corresponds to the steering matrix, is assumed to be full column rank. However no particular structure of this matrix is enforced in the sequel. This relaxation is important to handle interference multipath. In this case, the column vector of \mathbf{A} associated with the jammer becomes the sum of the direct-path and multipath steering vectors multiplied by an exponential phase delay introduced by each path. The resulting vector does not have the phase progression property of a steering vector. Because of the fact that we do not assume any structure of the matrix \mathbf{A} , the performance of the proposed receiver should be unaffected under multipath and coherent environment. It is noteworthy that by considering the direction of arrival of the desired signal equal to $\theta = 0^\circ$, model (1) still holds when $s(t)$ is wideband, since each sensor receives the same signal with no delay or phase change.

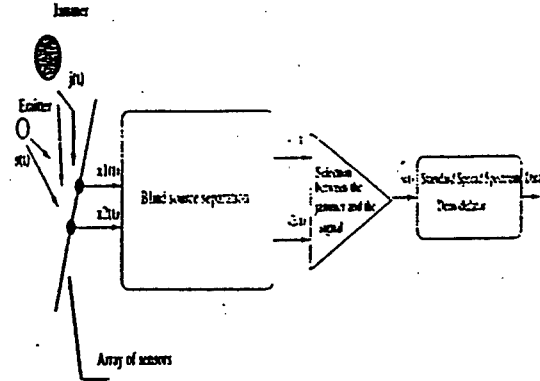


Figure 1. Spread spectrum system using blind source separation.

3 A New Interference Mitigation Design

The block diagram shown in Fig.1 illustrates the proposed interference mitigation spread spectrum communication system. The standard spread spectrum demodulation is preceded by a preprocessor, which consists of a separator followed by a selector. The separator acts on separating the interference from the signal by utilizing the spatial diversity provided by the multi-sensor array. This separation can be performed only up to a permutation (see below). Hence, a selection device is needed to label the separated waveforms as signal and jammer. The demodulation process recovers the original data by despreading the selected (desired) signal, while spreading the background noise and any interference component which might have not been separated from the signal. In the following, we describe each processing step in more details.

3.1 Separation

The separation of the signal from the interference is achieved by using blind source separation techniques. These techniques strive to recover the source vector $\mathbf{y}(t)$ from the array output $\mathbf{x}(t)$ without knowledge of the matrix \mathbf{A} . The benefit of such a 'blind' processing is that the separation is essentially unaffected by errors in the propagation model or in array calibration. Source separation techniques are based on the assumption of statistical independence of the source signals.

Various algorithms have been proposed for the blind source separation [11, 12, 13, 10]. In this paper, we only focus on the so called SOBI (Second Order Blind Identification) algorithm [10]. This algorithm is based on the simultaneous diagonalization of a combined set of spatio-temporal correlation matrices of the received signals (for more details see reference [10]).

It is well established that there is two inherent ambiguities in the blind source separation problem. First, there is no way of knowing the original labeling of the sources, hence any permutation of the estimated sources is also a satisfactory solution. The second ambiguity is that it is impossible to uniquely identify the source signals. This is because the exchange of a fixed scalar factor between a source signal and the corresponding column of the mixture matrix A does not affect the observations, as shown by the relation,

$$x(t) = Ay(t) + n(t) = \sum_{i=1}^2 \frac{\alpha_i}{\alpha_i} \alpha_i y_i(t) + n(t), \quad (4)$$

where α_i is an arbitrary complex factor and α_i denotes the i -th column of A . Hence, the blind source separation must be understood as the recovering of the source signals up to a fixed permutation and some complex factors.

3.2 Selection

Because of the inherent ambiguity stated above, a selector at the output of the separator is necessary to identify the desired signal for postprocessing. For this purpose, several strategies can be considered, the selection can be based on the signature of the desired signal which may be known by the receiver. As such, the problem of the selection becomes a pure problem of signal classification [14, 15]. Other strategies can be based on some a priori knowledge of the desired signal; for example its direction of arrival (DOA). The component whose steering vector in A matches the signal DOA is taken as the SS signal. The selection can also be based on the relative power of the separated signals, which makes use of the fact that the jammer has often a higher power than the spread spectrum signal. In section 4, the selection is based on the a priori knowledge of the direction of arrival of the desired signal.

3.3 Spread Spectrum Demodulation

This last step consists of despreading the selected signal for recovering the original data bit sequence $\{b_k\}$. This is accomplished by the correlation of the received signal with a synchronized replica of the spreading signal $\{c_i^k\}_{i=0, \dots, M-1}$ used to spread the transmitted signal. While the correlator despreads the desired signal, it spreads any interference components which might have escaped to the desired signal in the separation process.

The demodulation process improves the signal-to-interference and noise ratio at the receiver by an amount defined as the processing gain (PG). The later is the ratio of the spreading bandwidth and the desired signal information bandwidth (baseband),

$$PG = \frac{\text{Spreading Bandwidth}}{\text{Information Signal Bandwidth}} = \frac{T}{T_c}$$

4 Simulation

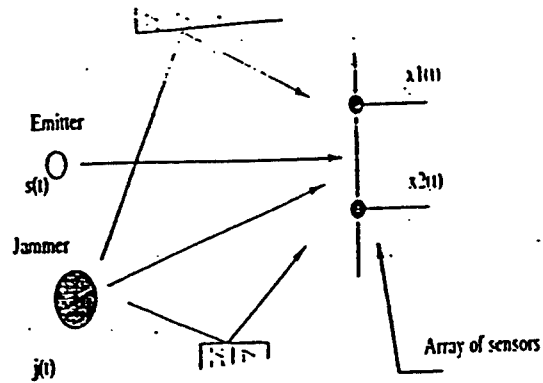


Figure 2. Scenario of the simulation.

Consider a uniform linear array of two sensors separated by half a wavelength and receiving signals from one desired source and one direct-path along two multipath of the same jammer (see Fig.2). The desired signal is a BPSK signal arriving at $\theta_0 = 0^\circ$. The jammer is composed of three fixed sinusoids whose frequencies are $\omega_1 = \pi/6$, $\omega_2 = \pi/3$ and $\omega_3 = \pi/2$. The direct path of the jammer arrives at $\theta_1 = 2^\circ$ and the two multipath of jammer arrive at $\theta_2 = 10^\circ$ and $\theta_3 = -10^\circ$, respectively. The noise used is zero-mean white Gaussian distributed process. Four spatio-temporal correlation matrices at the first four lags $\tau = 1, 2, 3, 4$ are considered in SOBI algorithm. Figure 3 presents the Bit Error Rate (BER) in dB versus the Jammer to Signal Ratio (JSR) for 0 dB SNR both for 8 chips/bit, 16 chips/bit, 32 chips/bit and 64 chips/bit. Under 32 chips/bit and 64 chips/bit, the proposed method offers no error over 10^6 runs for Jammer to Signal Ratio of 90 dB. Figures 4 and 5 display the BER in dB versus respectively the number of chips/bit for 0 dB SNR and the SNR for 60 dB JSR. It is evident that the probability of error is remarkably reduced under the proposed method.

5 Conclusion

In this paper, mitigation of narrowband interference in spread spectrum communication systems is achieved based on a blind source separation technique. Interference excision techniques for spread spectrum communications aim to increase the signal-to-noise ratio at the receiver output by suppressing the interference. But, at meantime, they eliminate a significant part of the desired signal. Instead of excising the interference, the proposed approach separates the interference from the signal prior to the despreading using the spatial diversity provided by the multisensor array. This is accomplished by the blind source separation technique

of [10]. The later referred to as SOBI for second order blind source separation is based on the simultaneous diagonalization of a combined set of spatio-temporal correlation matrices of the received signals. Because of the inherent indeterminacies of the blind source separation problem, a selector at the separator output is needed to label the separated waveforms as signal and jammer. Hence, some strategies of selection are presented in the paper. An important feature of using the blind source separation is that the proposed interference mitigation scheme is robust under multipath and coherent jamming environment. Some simulation results were presented to illustrate the effectiveness of the proposed approach.

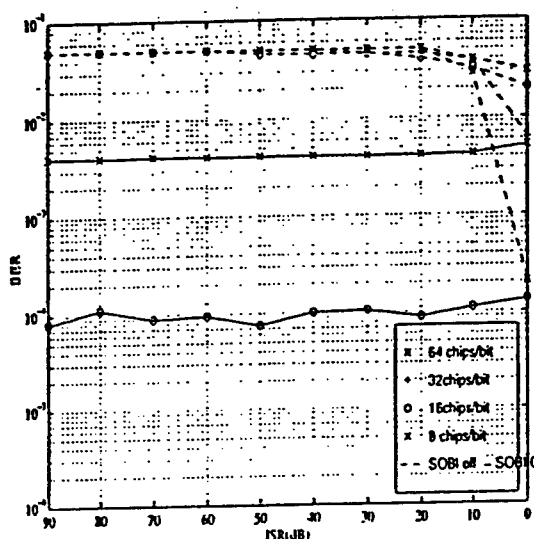


Figure 3. BER in (dB) vs JSR

References

- [1] M. K. Simon, et al. *Spread Spectrum Comm.* Computer Science Press. 1985.
- [2] L. B. Milstein, "Interference rejection techniques in spread spectrum communications," *Proc. IEEE*, vol. 66, pp. 657-671, June 1988.
- [3] J. Ketchum and J. Proakis, "Adaptive algorithms for estimating and suppressing narrow band interference in PN spread spectrum systems," *IEEE Trans. on Comm.*, 1982.
- [4] L. Milstein and R. Iltis, "Signal processing for interference rejection in spread spectrum communications," *IEEE SP Magazine*, vol. 3, pp. 18-31, Apr. 1986.

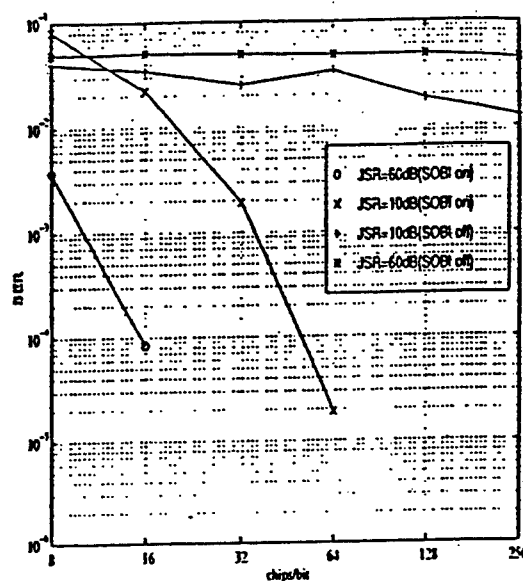


Figure 4. BER in (dB) vs number of chips/bit

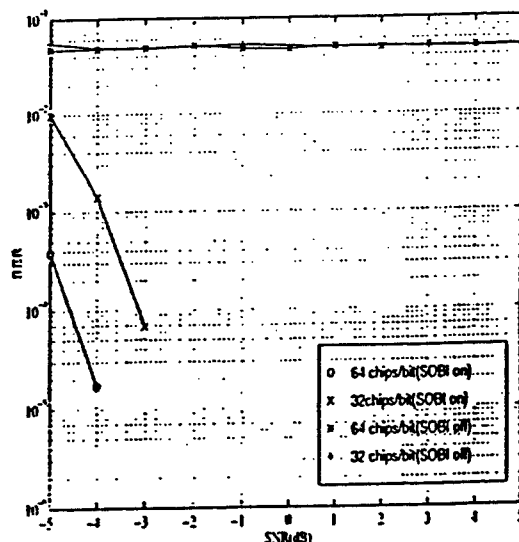


Figure 5. BER in (dB) vs SNR.

- [5] M. Medley, G. Saulnier and P. Das, "Applications of the Wavelet Transform in Spread Spectrum Communications Systems," *SPIE, Wavelet Applic., Orlando, FL*, Apr. 1994.
- [6] S. Roberts and M. Amin, "Linear vs. bilinear time-frequency methods for interference mitigation in direct sequence spread spectrum communication systems," in *Proc. Asilomar conf. on Signals, Systems and Computers*, Nov. 1995.
- [7] M. G. Amin, "Interference excision in spread spectrum communication systems using time-frequency distributions," *Technical Report. Rome Lab*, Sept. 1994.
- [8] M. Amin, "Interference mitigation in spread spectrum communication system using time-frequency distributions," *IEEE Trans. on SP*, Jan. 1997.
- [9] C. Wang and M. Amin, "Performance analysis of interference excisions in spread spectrum communications based on instantaneous frequency estimation," in *ISSPA, Australia*, Aug. 1996.
- [10] A. Belouchrani and K. Abed Meraim and J.-F Cardoso and E. Moulines, "A blind source separation technique using second order statistics," *IEEE Trans. on SP*, 1996. To appear.
- [11] P. Comon, "Independent component analysis," in *Proc. Int. Workshop on Higher-Order Stat., Chamrousse, France*, pp. 111-120, 1991.
- [12] M. Gaeta and J.-L. Lacoume, "Source separation without a priori knowledge: the maximum likelihood solution," in *Proc. EUSIPCO*, pp. 621-624, 1990.
- [13] J.-F. Cardoso and A. Souloumiac, "An efficient technique for blind separation of complex sources," in *Proc. IEEE SP Workshop on Higher-Order Stat., Lake Tahoe, USA*, 1993.
- [14] L. Dominguez, J. Borrallo, J. Garcia, "A general approach to the automatic classification of radiocommunication signals," *Signal Processing*, vol. 22, pp. 239-250, Mar. 1991.
- [15] B. G. Mobasseri and S. Rao, "Recognition of Digital Modulation Types Using Constellation Shape Matching," *SPIE, Signal and Image processing, Denver, Colorado*, Aug. 1996.

A new approach for blind source separation using time frequency distributions.

Adel Belouchrani and Moeness G. Amin

Department of Electrical and Computer Engineering, Villanova University, Villanova PA 19085.
adel,moeness@ece.vill.edu

ABSTRACT

This paper deals with the problem of blind source separation which consists of recovering a set of signals from instantaneous linear mixtures of them. So far, this problem has been solved using statistical information available on the source signals. Here, we propose an approach for blind source separation based on time-frequency (t-f) signal representations. This approach is based on a 'joint diagonalization' of a combined set of time frequency distribution matrices which correspond to different t-f points. It relies on the difference in the t-f signatures of the sources to be separated. In contrast to existing techniques, the proposed approach allows the separation of Gaussian sources with identical spectra shape. Because of changes incurred in the t-f signal structures due to time-delay, the new approach can be employed to separate multipath signals received by multi-sensor array. Moreover, the effects of spreading the noise power while localizing the source energy in the time frequency domain amounts to increasing the signal to noise ratio (SNR) and hence improved performance. Numerical examples are provided to illustrate the effectiveness of our method.

Keywords: Blind source separation, Spatial diversity, Time frequency distributions, Joint diagonalization, Time frequency signatures.

1 Introduction

Blind source separation is an emerging field of fundamental research with a broad range of applications. It is motivated by practical problems that involve several source signals and several sensors. Each sensor receives a linear mixture of the source signals. The problem of the blind source separation consists then of recovering the original waveforms of the sources without any knowledge of the mixture structure. This mixture is often a convolutive mixture. However, in this paper our main concern is the blind identification of an instantaneous linear mixture, which corresponds to a linear memoryless channel. This choice is motivated not only by the fact that such model is mathematically tractable, but also by the applicability to various areas, including semiconductor manufacturing process¹, factor analysis², narrow-band signal processing³, and image reconstruction⁴.

So far, the problem of the blind source separation has been solved using statistical information available on the source signals. The first solution to the source separation problem was proposed almost a decade ago⁵ and was based on the cancellation of higher order moments assuming non-Gaussian and i.i.d source signals. Other criteria based on minimizations of cost functions, such as the sum of square fourth order cumulants⁶⁻⁸, contrast functions^{7,9} or likelihood function¹⁰, have been used by several researchers. Note that in the case of non i.i.d

This work is supported by the Rome Lab., contract # F30602-96-C-0077

source signals and even Gaussian sources, solutions based on second order statistics are possible^{11,12}.

When the frequency content of the source signals is time-varying, one can take advantage of the powerful tool of time frequency signal representations to separate and recover the incoming signals. The underlying problem can be posed as a signal synthesis¹³ from the t-f plane with the incorporation of the spatial diversity provided by the multisensor. With the proposed approach, no masking is required and cross-terms no longer represents ambiguity in the synthesis of individual components. In this paper, we introduce a new blind identification technique based on a joint diagonalization of a combined set of time-frequency distribution matrices. The new approach exploits the difference between the t-f signatures of the sources. It has been established in the literature of the blind source separation that the problem of the separation of Gaussian sources with identical spectra cannot be solved. This may be only true for stationary process. But for sources with different structures and energy localizations in the time-frequency domain, this limitation can be easily overcome. Further, due to the difference of the t-f signatures of the time-delayed signals, the proposed approach can also separate multipath signals.

The paper is organized as follows. In section 2, the problem of blind source separation is stated together with the relevant hypothesis. Section 3 introduces the definition of time frequency distribution matrices. Section 4 presents a time frequency separation technique based on joint diagonalization of a combined set of time frequency distribution matrices. Numerical examples illustrating the effectiveness of this method are presented in section 5.

2 Statement of the problem

2.1 Data Model and assumptions

Consider m sensors receiving an instantaneous linear mixture of signals emitted from n sources. The $m \times 1$ vector $x(t)$ denotes the output of the sensors at time instant t which may be corrupted by an additive noise $n(t)$. Hence, the linear data model is given by:

$$x(t) = As(t) + n(t), \quad (1)$$

where the $m \times n$ matrix A is called the 'mixing matrix'. The n source signals are collected in a $n \times 1$ vector denoted $s(t)$ which is referred to as the source signal vector. The sources are assumed to have different structures and localization properties in the time frequency domain. The mixing matrix A is full column rank but is otherwise unknown. In contrast with traditional parametric methods, no specific structure of the mixture matrix is assumed.

2.2 Indeterminacies

Let us point out that this problem of blind source separation has several inherent ambiguities. First of all, there is no way of knowing the original labeling of the sources, hence any permutation of the estimated sources is also a satisfactory solution.

The second ambiguity is that it is inherently impossible to uniquely identify the source signals. This is because the exchange of a fixed scalar factor between a source signal and the corresponding column of the mixture matrix A does not affect the observations as is shown by the following relation,

$$x(t) = As(t) + n(t) = \sum_{i=1}^n \frac{a_i}{\alpha_i} \alpha_i s_i(t) + n(t). \quad (2)$$

where α_i is an arbitrary complex factor and a_i denotes the i -th column of A . Hence, the blind source separation

must be understood as the identification of the mixing matrix and/or the recovering of the source signals up to a fixed permutation and some complex factors.

3 Time Frequency Distribution Matrices

The Cohen's class of time-frequency distributions (TFD)¹⁴ of the signal $x(t)$ is given by

$$D_{xx}(t, f) = \int_{-\infty}^{\infty} \int_{-\infty}^{\infty} \phi(t - u, \tau) x(u + \tau/2) x^*(u - \tau/2) e^{-j2\pi f \tau} du d\tau \quad (3)$$

where t and f represent the time index and the frequency index, respectively. The kernel $\phi(t, \tau)$ is a function of the time and lag variables. The cross-TFD of two signals $x_1(t)$ and $x_2(t)$ is defined by

$$D_{x_1 x_2}(t, f) = \int_{-\infty}^{\infty} \int_{-\infty}^{\infty} \phi(t - u, \tau) x_1(u + \tau/2) x_2^*(u - \tau/2) e^{-j2\pi f \tau} du d\tau \quad (4)$$

Expressions (3) and (4) are now used to define the following data time frequency distribution matrix,

$$D_{xx}(t, f) = \int_{-\infty}^{\infty} \int_{-\infty}^{\infty} \phi(t - u, \tau) x(u + \tau/2) x^*(u - \tau/2) e^{-j2\pi f \tau} du d\tau \quad (5)$$

where $[D_{xx}(t, f)]_{ij} = D_{x_i x_j}(t, f)$, for $i, j = 1, \dots, n$.

A more general definition of the time frequency distribution matrix is given by,

$$D_{xx}(t, f) = \int_{-\infty}^{\infty} \int_{-\infty}^{\infty} \Phi(t - u, \tau) \odot x(u + \tau/2) x^*(u - \tau/2) e^{-j2\pi f \tau} du d\tau \quad (6)$$

where \odot designs the Hadamard product, and $[\Phi(t, \tau)]_{ij} = \phi_{ij}(t, \tau)$ is the kernel associated with the pair of the sensor data $x_i(t)$ and $x_j(t)$.

Under the assumption of the linear data model of Eq.(1) and neglecting the noise, the TFD matrix takes the following simple structure:

$$D_{xx}(t, f) = A D_{ss}(t, f) A^H \quad (7)$$

where the superscript H denotes the complex conjugate transpose of a matrix and $D_{ss}(t, f)$ are the signal TFD matrices. We note that $D_{xx}(t, f)$ is of dimension $m \times m$, whereas $D_{ss}(t, f)$ is of $n \times n$ dimension. If the kernel $\phi(t, \tau)$ is chosen in such away that the cross-terms in the TFD vanish, the matrix $D_{ss}(t, f)$ will be diagonal. In the sequel, we assume that such property of the kernel $\phi(t, \tau)$ is verified.

4 Time Frequency Separation Principle

Let W denotes a $m \times n$ matrix, such that $(WA)(WA)^H = UU^H = I$, i.e. WA is a $m \times m$ unitary matrix (this matrix is referred to as a whitening matrix, since it whitens the signal part of the observations). Pre- and post-multiplying the TFD-matrices $D_{xx}(t, f)$ by W , we then define the whitened TFD-matrices as:

$$\underline{D}_{xx}(t, f) = W D_{xx}(t, f) W^H \quad (8)$$

From the definition of W and Eq.(7), we may expressed $\underline{D}_{xx}(t, f)$ as

$$\underline{D}_{xx}(t, f) = U D_{ss}(t, f) U^H \quad (9)$$

5 Experimental results

Separation of identical spectra shape signals: In this example, we consider a uniform linear array of three sensors separated by half a wavelength and receiving signals from two sources. The additive noise is a zero mean white Gaussian process. The emitted signals are two sinusoids at the same frequency which turn on and off during different periods. The signal to noise ratio (SNR) is set at 5 dB. The kernel used for the computation of the TFDs is the Choi-Williams kernel¹⁴, which provide a good cancellation of the cross-terms. For the TFS algorithm, four TFD matrices are considered. The corresponding t-f points are those of the highest power in the t-f domain. Figures 1 and 2 display the TFDs of the two emitted signals and the three mixed signals (corresponding to the outputs of the three array sensors), respectively. Figures 3 shows the TFDs of the two estimated signals separated by the proposed approach. Figures 4 shows the TFDs of the two estimated signals separated by the second order blind identification (SOBI) algorithm proposed in¹². According to these figures, the TFS algorithm has clearly succeeded to separate the two emitted signals, while SOBI algorithm fails in this case.

Separation of speech signals: Here we present an illustration that involves real data signals. Two speech signals sampled at 8000 Hz are mixed by the following mixing matrix,

$$A = \begin{bmatrix} 1.0 & 0.5 \\ 0.6 & 1.0 \\ 0.4 & 0.8 \end{bmatrix}.$$

The plots of the two individual speech signals are shown in Fig.5 and their TFDs are displayed in Fig.6. Speech 1 and 2 of a male speaker are the words "Cars" and "Cats", respectively. The observed speech signals at three sensors are shown in Fig.7, while their TFDs are shown in Fig.8. Figures 9 and 10 show the speech signals estimated by TFS and their TFDs, respectively. It is clear that TFS works well in this case. The purpose of this example is to test the algorithm when speech signals are used.

6 Conclusion

In this paper, a new blind source separation approach using time frequency distributions is presented. It is based on the joint diagonalization of a combined set of time frequency distribution matrices. The concept of time-frequency distribution matrix is introduced. This method shows a number of attractive features. In contrast to blind source separation approaches using second-order and/or high order statistics, the proposed approach allows the separation of Gaussian sources with identical spectra. Moreover, the effects of spreading the noise power while localizing of the source energy in the time frequency domain amounts to increasing the signal to noise ratio (SNR). Numerical examples prove that the proposed TFS algorithm is able to separate sources with identical spectra. TFS is also applied to a speech extraction problem and shown to have promising results. Since time-delayed signals present different t-f signatures, it is also possible to separate multipath signals, such feature was not considered in this paper.

7 REFERENCES

- [1] C. M. Berrah, "Parameter yield estimation for a MOSFET integrated circuit," in *Proc. 1990 IEEE ISCAS*, pp. 2260-2263, 1990.
- [2] E. E. Cureton and R. B. D'Agostino, *FACTOR ANALYSIS An Applied Approach*. Lawrence Erlbaum Associates, 1983.

Since the matrix U is unitary and $D_{xx}(t, f)$ is diagonal, expression (9) shows that any whitened data TFD-matrix is diagonal in the basis of the columns of the matrix U (the eigenvalues of $\underline{D}_{xx}(t, f)$ being the diagonal entries of $D_{xx}(t, f)$).

If, for a point (t, f) of the time frequency domain, the diagonal elements of $D_{xx}(t, f)$ are all distinct, the missing unitary matrix U may be 'uniquely' (i.e. up to permutation and phase shifts) retrieved by computing the eigendecomposition of $\underline{D}_{xx}(t, f)$. Indeterminacy occurs in the case of degenerate eigenvalues, i.e. when $D_{i,i}(t, f) = D_{j,j}(t, f)$, $i \neq j$. It does not seem possible to *a priori* determine some value for the point (t, f) such that the diagonal entries of $D_{xx}(t, f)$ are all distinct. Of course, if the source signals have different time frequency signatures, such degeneracy is unlikely to occur. It is expected however, that when some eigenvalues of $\underline{D}_{xx}(t, f)$ comes close to degeneracy, the robustness of determining U from eigendecomposition of a single whitened TFD matrix is seriously impaired. The situation is more favorable when considering joint diagonalization of a combined set $\{D_{xx}(t_i, f_i) | i = 1, \dots, p\}$ of p TFD matrices. This amounts to incorporating several (t, f) points in the source separation problem. It is noteworthy that two source signals with identical t - f signatures can not be separated even with the inclusion of all information in the t - f plane.

4.1 The approximate joint diagonalization

Exact joint diagonalization of arbitrary matrices is generally impossible. Here, we define *approximate* joint diagonalization of a combined set of arbitrary matrices. We start by noting that the diagonalization of a single $n \times n$ normal matrix¹⁵ M may be understood as minimizing under unitary transform the sum of the squared moduli of all the off-diagonal terms. This may be shown to be equivalent to minimizing the criterion

$$C(M, V) \stackrel{\text{def}}{=} - \sum_i |v_i^* M v_i|^2 \quad (10)$$

over the set of unitary matrices $V = [v_1, \dots, v_n]$. Hence, the *joint approximate diagonalization* of a combined set $\{M_k | k = 1..p\}$ of p arbitrary $n \times n$ matrices is defined as the minimization of the criterion:

$$C(V) \stackrel{\text{def}}{=} - \sum_k C(M_k, V) = - \sum_{ki} |v_i^* M_k v_i|^2 \quad (11)$$

under the same unitary constraint. An efficient joint approximate diagonalization algorithm exists in¹² and it is a generalization of the Jacobi technique¹⁶ for the exact diagonalization of a single normal matrix.

4.2 A time frequency separation algorithm (TFS).

Equations (7-11) constitute the blind source separation approach based on TFD which is summarized by the following steps

- Determine the whitening matrix \hat{W} from the eigendecomposition of an estimate of the covariance matrix of the data (see¹² for more details).
- Determine the unitary matrix \hat{U} by minimizing the joint approximate diagonalization criterion for a specific set of whitened TFD matrices $\{\underline{D}_{xx}(t_i, f_i) | i = 1, \dots, p\}$.
- Obtain an estimate of the mixture matrix \hat{A} as $\hat{A} = \hat{W}^* \hat{U}$, where the superscript $*$ denotes the pseudo-inverse, and an estimate of the source signals $\hat{s}(t)$ as $\hat{s}(t) = \hat{U}^* \hat{W} x(t)$.

- [3] R. Schmidt, "Multiple emitter location and signal parameter estimation," *IEEE Trans. on AP*, vol. 34, no. 1, pp. 276-280, 1986.
- [4] G. Demoment, "Image reconstruction and restoration: Overview of common estimation structures and problems," *IEEE Trans. on ASSP*, vol. 37, pp. 2024-22036, Oct. 1989.
- [5] C. Jutten and J. Héroult, "Détection de grandeurs primitives dans un message composite par une architecture de calcul neuromimétique en apprentissage non supervisé," in *Proc. Grets, (Nice)*, 1985.
- [6] M. Gaeta and J.-L. Lacoume, "Source separation without a priori knowledge: the maximum likelihood solution," in *Proc. EUSIPCO*, pp. 621-624, 1990.
- [7] P. Comon, "Independent component analysis, a new concept?," *Signal Processing*, vol. 36, pp. 287-314, 1994.
- [8] J.-F. Cardoso and A. Souloumiac, "An efficient technique for blind separation of complex sources," in *Proc. IEEE SP Workshop on Higher-Order Stat., Lake Tahoe, USA*, 1993.
- [9] E. Moreau and O. Macchi, "New self-adaptive algorithms for source separation based on contrast functions," in *Proc. IEEE SP Workshop on Higher-Order Stat., Lake Tahoe, USA*, 1993.
- [10] A. Belouchrani and J.-F. Cardoso, "Maximum likelihood source separation for discrete sources," in *Proc. EUSIPCO*, pp. 768-771, 1994.
- [11] L. Tong and R. Liu, "Blind estimation of correlated source signals," in *Proc. Asilomar conference*, Nov. 1990.
- [12] A. Belouchrani and K. Abed Meraim and J.-F. Cardoso and E. Moulines, "A blind source separation technique using second order statistics," *IEEE Trans. on SP*, 1996. To appear.
- [13] F. Hlawatsch and W. Krattenthaler, "Bilinear Signal Synthesis," *IEEE Trans. on SP*, vol. 40, pp. 352-363, Feb. 1992.
- [14] L. Cohen, *Time-frequency analysis*. Prentice Hall, 1995.
- [15] R. Horn and C. Johnson, *Matrix analysis*. Cambridge University Press, 1985.
- [16] G.H. Golub and C.F. Van Loan, *Matrix computations*. The Johns Hopkins University Press, 1989.

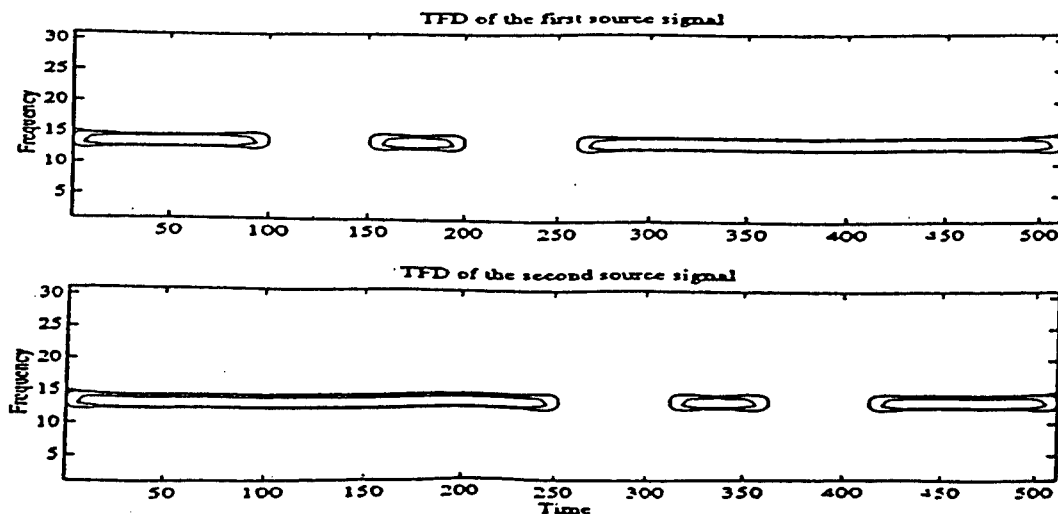


Figure 1. TFDs of emitted signals.

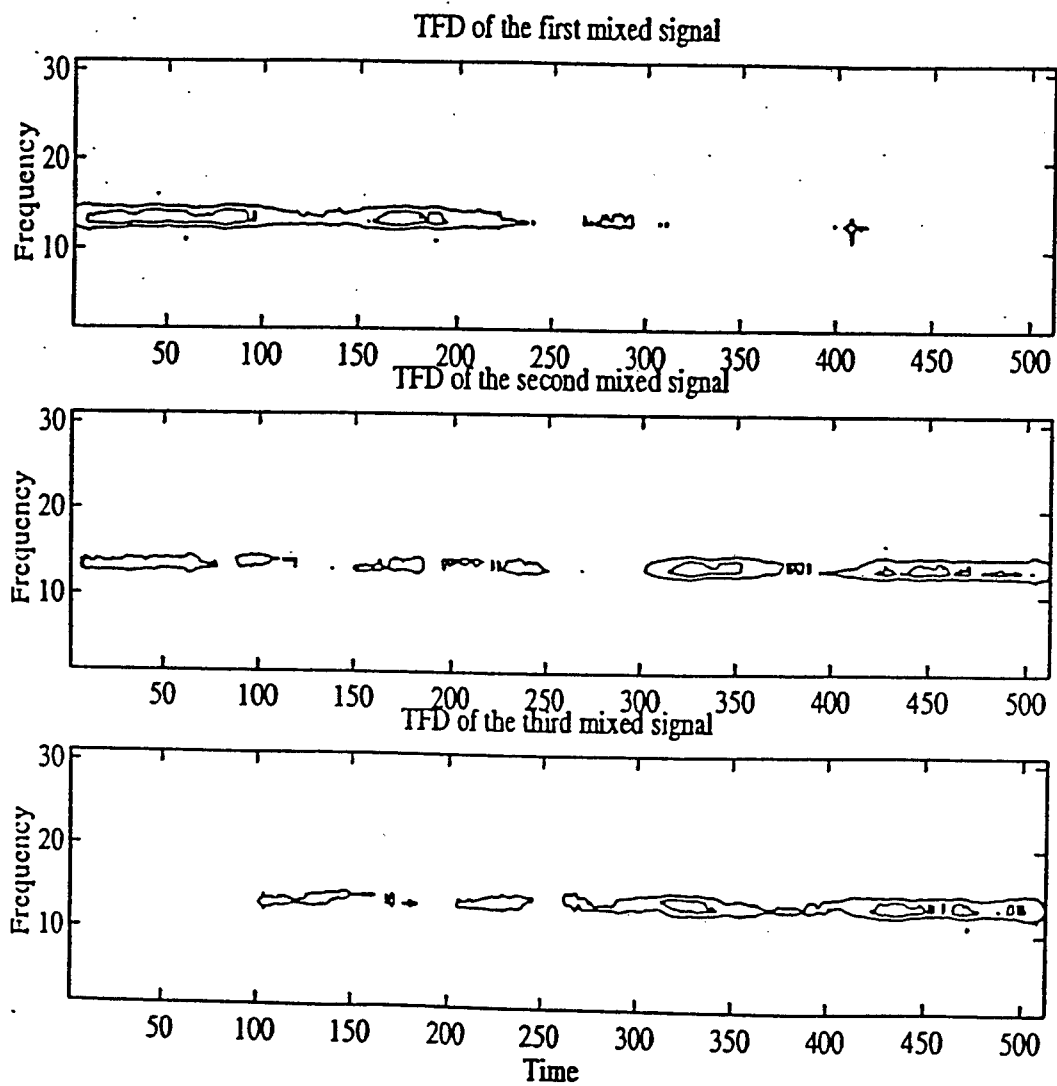


Figure 2. TFDs of received signals.

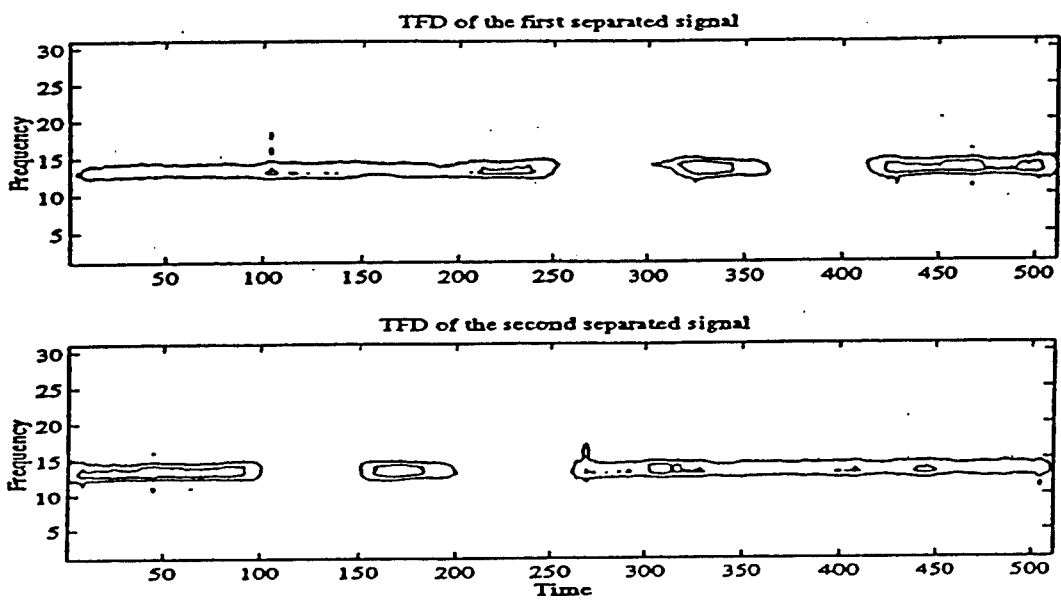


Figure 3. TFDs of the estimated signals by TFS.

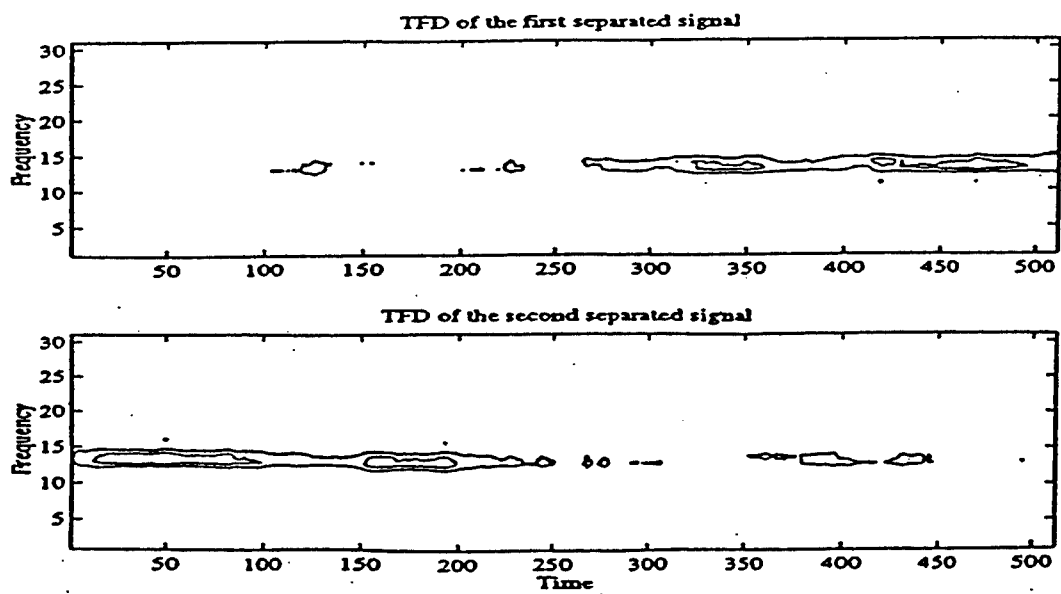


Figure 4. TFDs of the estimated signals by SOBI.

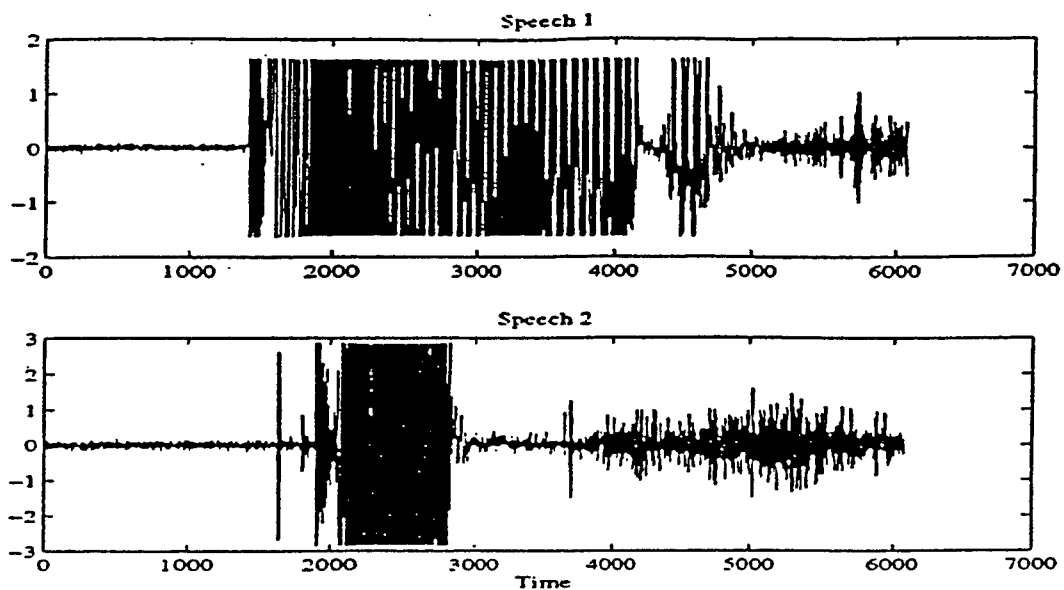


Figure 5. Plots of individual speeches.

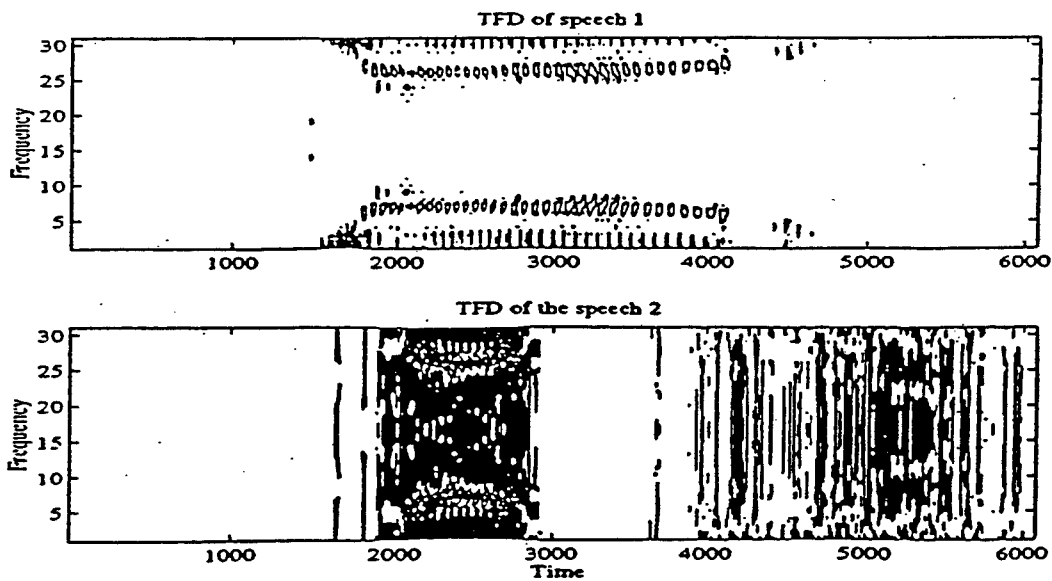


Figure 6. TFDs of the individual speeches.

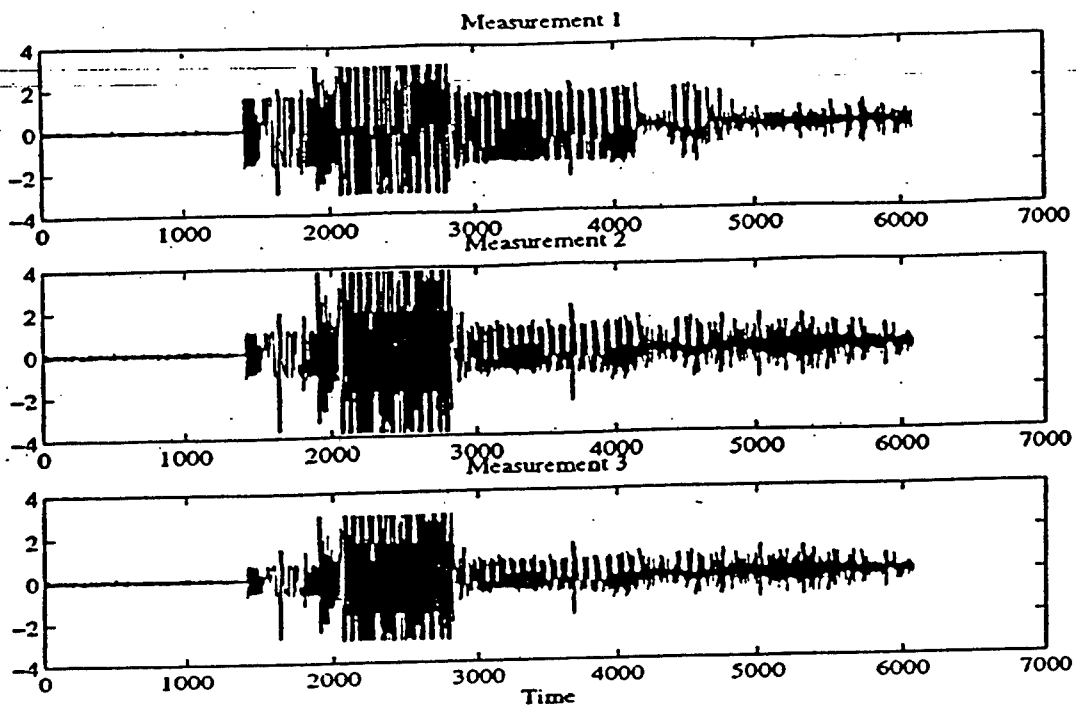


Figure 7. Plots of the Measurements.

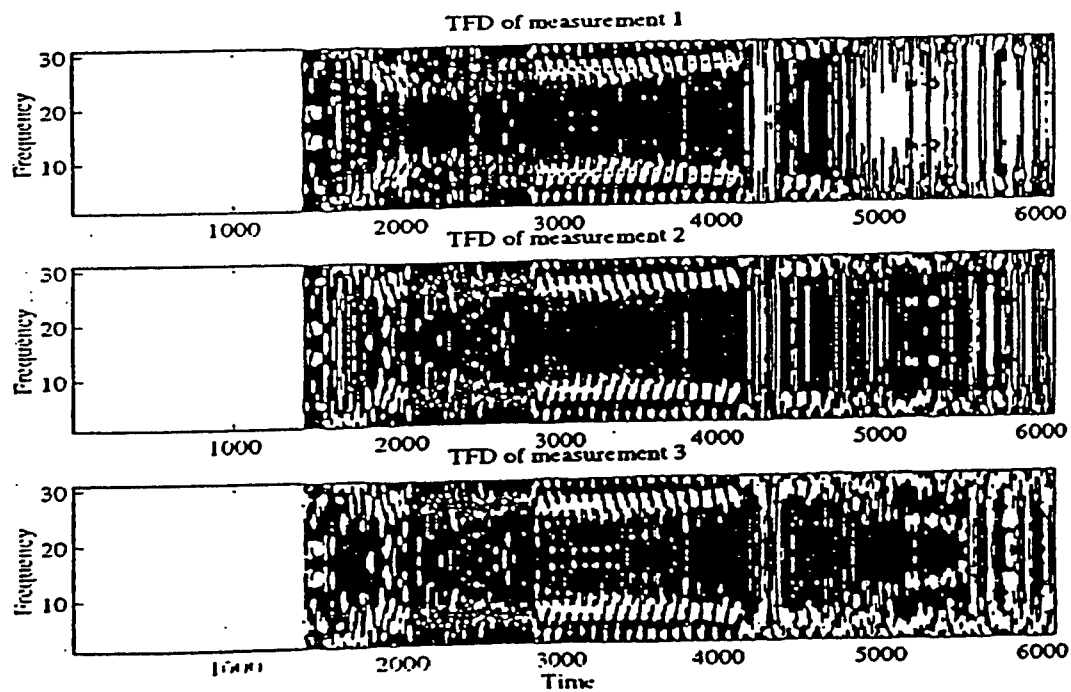


Figure 8 TFDs of the Measurements.

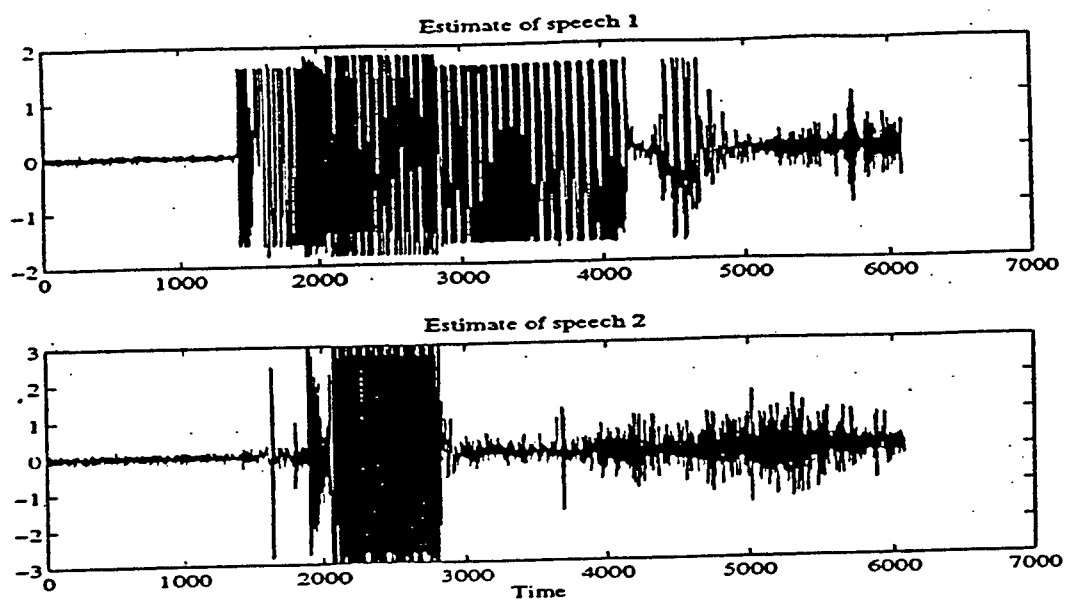


Figure 9. Plots of the estimate signals.

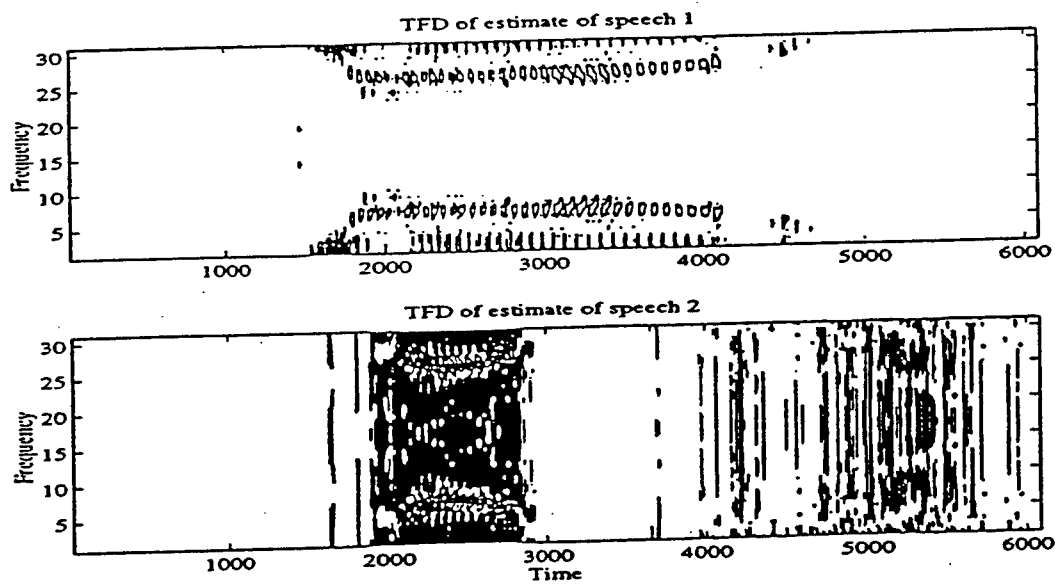


Figure 10. TFDs of the estimate signals.

**Broadband Interference Excision for Software Radio
DSSS Communications Using Time-Frequency
Distribution Synthesis**

Broadband Interference Excision for Software-Radio Spread-Spectrum Communications Using Time-Frequency Distribution Synthesis

Stephen R. Lach, Moeness G. Amin, *Senior Member, IEEE*, and Alan R. Lindsey, *Member, IEEE*

Abstract—A new method is introduced for interference excision in spread-spectrum communications that is conducive to software-radio applications. Spare processing capacity in the receiver permits the use of time-frequency techniques to synthesize a nonstationary interference from the time-frequency domain using least squares methods. The synthesized signal is then subtracted from the incoming data in the time domain, leading to jammer removal and increased signal-to-interference-and-noise ratio at the input of the correlator. The paper focuses on jammers with constant modulus that are uniquely described by their instantaneous frequency characteristics. With this *a priori* knowledge, the jammer signal amplitude is restored by projecting each sample of the synthesized signal to a circle representing its constant modulus. With the phase matching provided by the least squares synthesis method and amplitude matching underlying the projection operation, a significant improvement in receiver performance/bit-error rates is achieved over the case where no projection is performed. Software-radio aspects including computational complexity and processing modes are also discussed.

Index Terms—Interference excision, software radio, spread spectrum, time frequency, Wigner distribution.

I. INTRODUCTION

ONE of the most important applications of direct-sequence (DS) spread-spectrum (SS) communications is that of interference mitigation. A DSSS system is defined as one in which the transmitted signal is spread over a bandwidth much wider than the minimum bandwidth necessary to transmit the information [1] by means of a code independent of the data. The availability of this code at the receiver enables the despreading and recovery of data, while spreading and suppressing the interference. The processing gain of a DSSS system, generally defined as the ratio between the transmission and the data bandwidths, provides the system with a high degree of interference suppression. In principle, any level of interference rejection may be achieved with sufficient processing gain. This, however, may entail increasing the

bandwidth of the transmitted signal beyond the limits of the available frequency spectrum. Therefore, signal processing techniques have been used in conjunction with the DSSS receiver to augment the processing gain, permitting greater interference protection without an increase in bandwidth [2].

Several past contributions deal with the suppression of narrow-band interference [3], [4]. In time-varying environments, adaptive filters are employed to track and remove the nonstationary interference [5]–[7]. Recently, two approaches for broadband interference excision in DSSS communications based on time-frequency analysis have been considered [8]–[12]. One approach is linear and based on multiresolution analysis, whereas the second approach requires bilinear transformation of the data. In linear transform interference excisions, the data are processed using Fourier, Gabor, or wavelet transforms. Excision of the correlated signal components of the received data is then performed by clipping, or gating, the high coefficient values followed by inverse transformation to recover the desired signal.

The recent development of bilinear (quadratic) time-frequency distributions (TFD's) for improved signal power localization in the time-frequency plane has motivated several filtering approaches for nonstationary interference excision in spread-spectrum communications. The most common of these methods uses an open-loop adaptive filter. In this approach, the jammer instantaneous frequency (IF) is estimated, and the received data are then processed by a short-length time-varying finite impulse response (FIR) filter with a notch at the jammer IF. This effectively removes the jammer, and causes the filter output to be essentially interference free. This approach is most applicable to rapidly time-varying environments in which the IF estimate can be obtained via estimation methods such as zero-crossing techniques, the least mean-squares (LMS) algorithm, etc. [13]. An implementation of interference excision systems using TFD's to determine the jammer IF has been thoroughly discussed in [14]–[16]. However, these time-domain notch filtering techniques also create a significant amount of self-noise, which is an induced correlation across the PN sequence. This correlation forms an upper bound on the maximum attainable value of the correlator SNR, and in many cases, the use of these filters makes the performance worse than when the preprocessing is disabled. Also, these techniques become ineffective for

Manuscript received September 25, 1997; revised June 19, 1998. This work was supported by Rome Laboratory under Contract F30602-96-0077.

S. R. Lach was with the Department of Electrical and Computer Engineering, Villanova University, Villanova, PA 19085 USA. He is now with the Air Force Research Laboratory, Eglin AFB, FL 32542 USA.

M. G. Amin is with the Department of Electrical and Computer Engineering, Villanova University, Villanova, PA 19085 USA.

A. R. Lindsey is with the Rome Laboratory, RL/C3BB, Rome, NY 13441 USA.

Publisher Item Identifier S 0733-8716(99)02973-X.

0733-8716/99\$10.00 © 1999 IEEE

the multicomponent interference case. When the jamming signal is composed of more than one term at any time instant, processing the received signal with a filter with multiple notches yields an intolerable degree of self-noise, especially when only a small number of filter coefficients is used. For the above two reasons, alternatives for nonstationary interference excision in spread-spectrum communications are sought.

This paper uses time-frequency (t - f) distributions as a powerful tool for depicting the jammer power over time and frequency. However, contrary to the open-loop adaptive interference excision method, the excision filter is applied in the time-frequency domain, rather than the time domain, to capture the interference signature. Since the interference is characterized by its instantaneous frequency, its signature in the time-frequency domain is distinct from those of both the noise and the spread-spectrum signal, whose spectra are flat, independent of time. Therefore, filtering is achieved by masking the t - f regions of high power concentration, followed by synthesis of the jamming signal. The synthesized jammer signal is then subtracted from the incoming data to remove the interference component in the time domain.

Of particular interest in this paper are jammers with the constant modulus property. In this case, the jamming signal can be estimated more accurately through a two-stage process. First, an estimate of the jammer is generated by masking out the signal and noise components of the data in the t - f domain, and then performing a least squares synthesis procedure. The result of the first stage is improved by taking each sample of the synthesized signal and projecting it on a circle representing the constant modulus of the jammer. The improved estimate of the jammer is independent of the order of the phase-matching and constant modulus projection operations. Subtraction of this estimate from the received signal results in a drastic enhancement in system performance.

Section II summarizes the main steps of the time-frequency synthesis technique introduced in [18]. Section III addresses the issue of phase matching in t - f synthesis applied to interference mitigation in spread-spectrum communications. If the DSSS signal must be recovered from the t - f domain, then phase restoration of the synthesized signal is essential for aligning the PN sequence of the input data with that of the receiver prior to correlation. On the other hand, if the jammer signal is synthesized, effective interference removal is achieved by subtracting a proper copy of the synthesized jammer from the input data. In this case, phase ambiguity remains undesirable since subtraction may lead to doubling the jammer power instead of removing it. Amplitude matching of jammers that are of constant modulus constitutes the key contribution of this paper, and is described in Section IV. Section V addresses the application of this technique to the multicomponent jammer case, where each term of the interference is known to be of constant modulus. In Section VI, the computational requirements of the algorithm are derived and compared with the recently introduced TFD-based interference excision technique outlined in [12]. Section VII presents several computer simulations which show the effect of both projection and phase matching on bit error rate (BER) applied to linear FM signals.

II. TIME-FREQUENCY SIGNAL SYNTHESIS TECHNIQUES

The Wigner-Ville distribution (WVD) $W_x(n, \omega)$ of the discrete-time signal $x(n)$ is defined as [17]

$$W_x(n, \omega) = 2 \sum_{k=-\infty}^{\infty} x(n+k)x^*(n-k)e^{-jk\omega}. \quad (1)$$

There are several desirable properties of the WVD [16], but for the purposes of signal synthesis, it is enough to note that the WVD is always real and periodic in ω (with period π). The synthesis problem is finding the sequence $x(n)$ whose WVD is closest in some sense to a desired real time-frequency distribution $Y(n, \omega)$ that may not represent a valid WVD.

If $Y(n, \omega) = W_x(n, \omega)$ is a valid WVD, a direct calculation of the corresponding time-domain sequence $x(n)$ can be accomplished [17] according to

$$x(n+k)x^*(n-k) = \frac{1}{2\pi} \int_{-\pi/2}^{\pi/2} W_x(n, \omega) e^{j2k\omega} d\omega. \quad (2)$$

If, however, $Y(n, \omega)$ is not a WVD, one must find a sequence $x(n)$ whose WVD best approximates $Y(n, \omega)$. This problem is formulated and solved in a least squares sense [18] by minimizing the error

$$E(x) = \sum_n \frac{1}{\pi} \int_{-\pi/2}^{\pi/2} |Y(n, \omega) - W_x(n, \omega)|^2 d\omega. \quad (3)$$

Using Parseval's theorem, this error can be rewritten as

$$E(x) = \sum_n \sum_m |y(n, m) - 2x(n+m)x^*(n-m)|^2 \quad (4)$$

where

$$y(n, m) = \frac{1}{\pi} \int_{-\pi/2}^{\pi/2} Y(n, \omega) e^{j\omega m} d\omega. \quad (5)$$

By substituting $m = 2r - n$ for even values of the integer $(n+m)$ and $m = 2r - n - 1$ for odd values, (4) becomes

$$E(x) = \sum_n \sum_r |y(n, 2r-n) - 2x(2r)x^*(2n-2r)|^2 + \sum_n \sum_r |y(n, 2r-n-1) - 2x(2r-1)x^*(2n-2r-1)|^2. \quad (6)$$

$E(x)$ now consists of two summations, the first of which depends solely on the even-indexed components of $x(n)$, and the second of which depends on the odd-indexed components. Therefore, minimization of the error in (6) requires minimizing the first summation independently of the second, or equivalently, determining the even- and odd-indexed components of $x(n)$.

Finding the even-indexed samples of $x(n)$ is therefore equivalent to minimizing

$$E_e(x_e) = \sum_n \sum_r |y(n, 2r-n) - 2x_e(r)x_e^*(n-r)|^2 \quad (7)$$

where

$$x_e(n) = x(2n). \quad (8)$$

By setting the partial derivatives of (7) with respect to $x_e(p)$ and $x_e^*(p)$ equal to zero, the following eigenvalue/eigenvector equation is produced:

$$C_e x_e = 4 \|x_e\|^2 x_e \quad (9)$$

where

$$C_e(p+1, m+1) = y(m+p, p-m) + y^*(m+p, m-p) \quad (10)$$

and

$$\|x\|^2 = \sum_n |x(n)|^2. \quad (11)$$

Similarly, finding the odd-indexed samples of $x(n)$ is equivalent to minimizing

$$E_o(x_o) = \sum_n \sum_r |y(n, 2r-n-1) - 2x_o(r)x_o^*(n-r+1)|^2 \quad (12)$$

where

$$x_o(n) = x_o(2n+1). \quad (13)$$

This is accomplished by setting the partial derivatives of (12) with respect to $x_o(p)$ and $x_o^*(p)$ equal to zero, producing the equation

$$C_o x_o = 4 \|x_o\|^2 x_o \quad (14)$$

where

$$C_o(p, m) = y(m+p-1, p-m) + y^*(m+p-1, m-p). \quad (15)$$

C_e and C_o are therefore Hermitian matrices of size P_e and P_o , respectively:

$$P_e = \text{floor} \left[\frac{L+1}{2} \right] \quad (16)$$

and

$$P_o = \text{floor} \left[\frac{L}{2} \right] \quad (17)$$

where L is the length of the signal. It is apparent from (9) and (14) that x_e and x_o are eigenvectors of C_e and C_o . It is shown in [18] that, by choosing the eigenvectors corresponding to the largest eigenvalues of C_e and C_o , the error expression (3) is minimized.

Although this technique produces a sequence that minimizes the error in (3), the solution is not unique. Since a multiplication of the even and odd components of $x(n)$ by the phase constants a_e and a_o does not change the sequence's WVD, signal synthesis can only be achieved up to an arbitrary phase in both the even and odd components of the sequence. However, with a reference signal chosen as the original data sequence, it is possible to find the parameters a_e and a_o by phase matching. That is

$$a_e = \arctan \left[\frac{\text{Imag} \left[\sum_n s(2n)x_e^*(n) \right]}{\text{Real} \left[\sum_n s(2n)x_e^*(n) \right]} \right] \quad (18)$$

$$a_o = \arctan \left[\frac{\text{Imag} \left[\sum_n s(2n+1)x_o^*(n) \right]}{\text{Real} \left[\sum_n s(2n+1)x_o^*(n) \right]} \right] \quad (19)$$

where $s(n)$ is the reference signal.

III. SELECTION OF THE SYNTHESIZED SIGNAL

Two possible approaches apply t - f distribution synthesis techniques to interference mitigation for spread-spectrum communications. The first approach synthesizes the spread-spectrum signal, and correlates it with the PN sequence at the receiver, as shown in Fig. 1(a). The second approach synthesizes the interference signal from the t - f domain, subtracting it from the incoming data to suppress the jammer, as depicted in Fig. 1(b).

The choice of one approach over the other depends on the ability to obtain an accurate synthesized signal. This requires the signal to be synthesized to have a t - f signature that clearly distinguishes it from other signal components. Also, phase matching and restoration of the synthesized signal should be feasible and properly accomplished.

Fig. 2(a)-(c) shows an example of the WVD's computed separately for complex white noise, a complex DSSS signal, and a linear FM interference. Fig. 2(d) shows the WVD of the sum of all three components. One may conclude that synthesizing the spread-spectrum signal from the t - f domain should be avoided because of the following.

- 1) It is difficult to distinguish between the noise and the spread-spectrum signal signatures in the t - f domain. Therefore, t - f synthesis of the DSSS signal does not reduce the effect of noise nor lead to enhanced SNR.
- 2) Masking out the jammer by clipping or gating the high power values in the t - f domain may remove the main lobe, but it leaves behind the sidelobes which may carry significant jammer power.
- 3) The cross terms among the jammer, and the DSSS signal, noise, and jammer self-cross terms are often spread over the entire t - f domain, contaminating the spread-spectrum signal within large regions of time and frequency.
- 4) Phase matching is often performed using the input data as a reference signal. Therefore, even with the assumption that the DSSS signal is perfectly synthesized up to a phase ambiguity, low desired signal power makes it difficult to arrive at the correct phase by simple matching to a data sequence in which the jammer is the dominant component.

Accurate phase matching can therefore be obtained using the input data as a reference signal only through synthesis of the interference, provided that the JSR is relatively high, which is often the case. However, the effectiveness of phase matching is reduced with reduced jammer power.

IV. THE CONSTANT MODULUS PROJECTION OPERATOR

Let P_A define the constant modulus projection operator. When applied to the complex sequence $x(n)$, the resulting

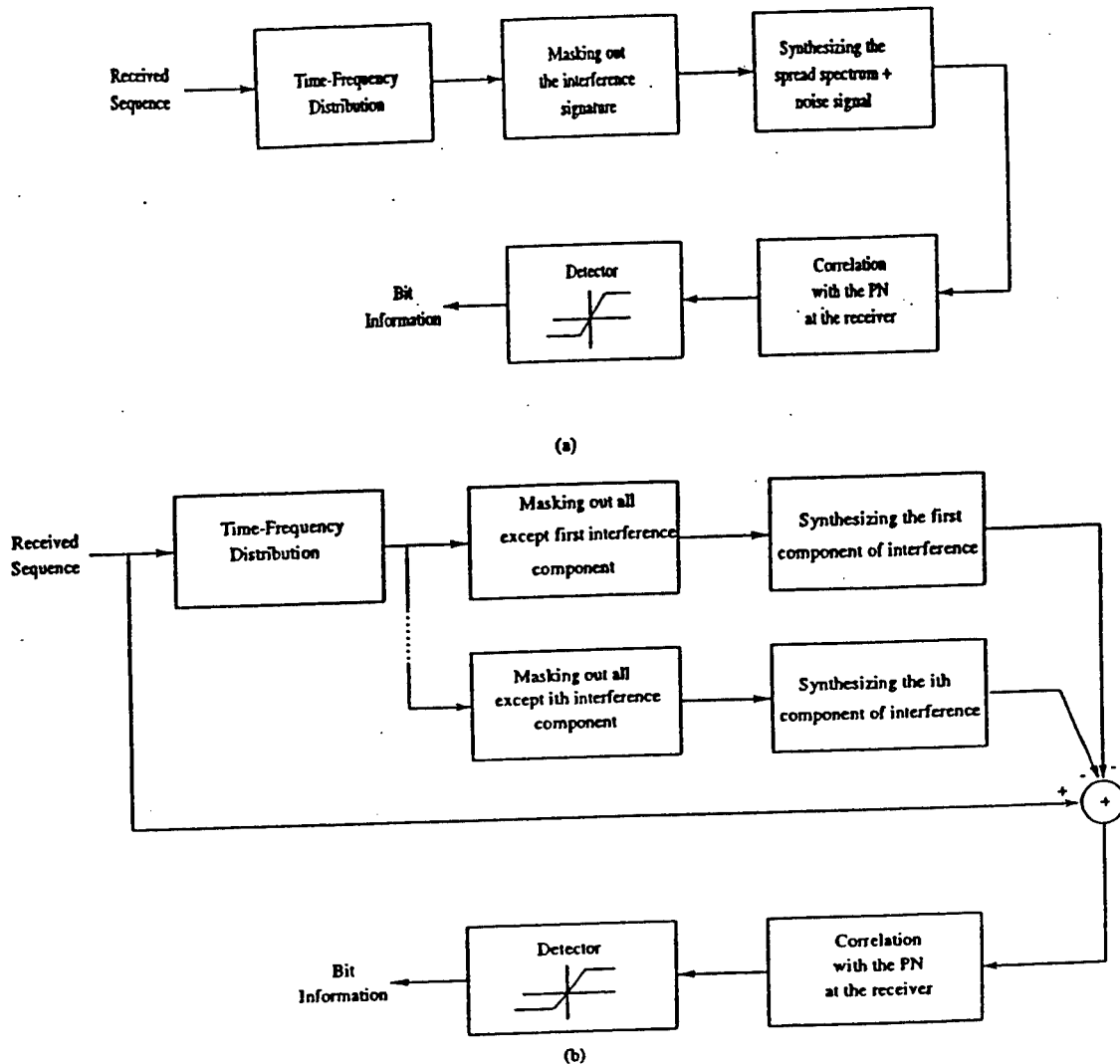


Fig. 1. Two approaches for interference mitigation in DS/SS communication systems: (a) synthesizing the desired signal and (b) synthesizing the interference.

signal $x_A(n)$ retains the phase of each sample of $x(n)$, but changes its amplitude to a constant value A . This is equivalent to projecting each sample of $x(n)$ on the complex plane onto the closest point of a circle of radius A that is centered at the origin, as in Fig. 3. Significant reduction of noise may be achieved through this operation when applied to a signal that is known to be of modulus A whose phase is not significantly distorted or can be recovered by phase matching.

The present t - f synthesis technique uses P_A to subtract an accurate estimate of the interference from the received signal prior to correlation with the PN sequence. Fig. 4(a) depicts the original time-domain chirp jammer signal, and Fig. 4(b) is the synthesized interference estimate obtained from masking out the signal and noise components in the t - f domain where the JSR = 9 dB. The phases of the even and odd samples are not matched either absolutely to the original jammer or relatively to themselves. Projection P_A of the synthesized jammer estimate produces the signal

in Fig. 4(c). Phase matching then produces the final jammer estimate of Fig. 4(d). Each stage of this estimation process is also represented in the complex plane, as seen in Fig. 5. It is clear that phase matching and constant modulus projection significantly improve the jammer estimate.

Several factors may inhibit the effectiveness of P_A . If the constant modulus value A is inaccurate, projection may induce noise into the estimate of the interference. Even with exact knowledge of A , the lack of an accurate phase reference may render projection ineffective.

V. MULTICOMPONENT JAMMERS

When the jammer is composed of more than one component, t - f synthesis may prove effective, provided that each component is distinguishable in the t - f domain. In this situation, each jammer component is individually synthesized from the t - f domain and subtracted from the received signal. The WVD of a jammer composed of two widely spaced linear FM

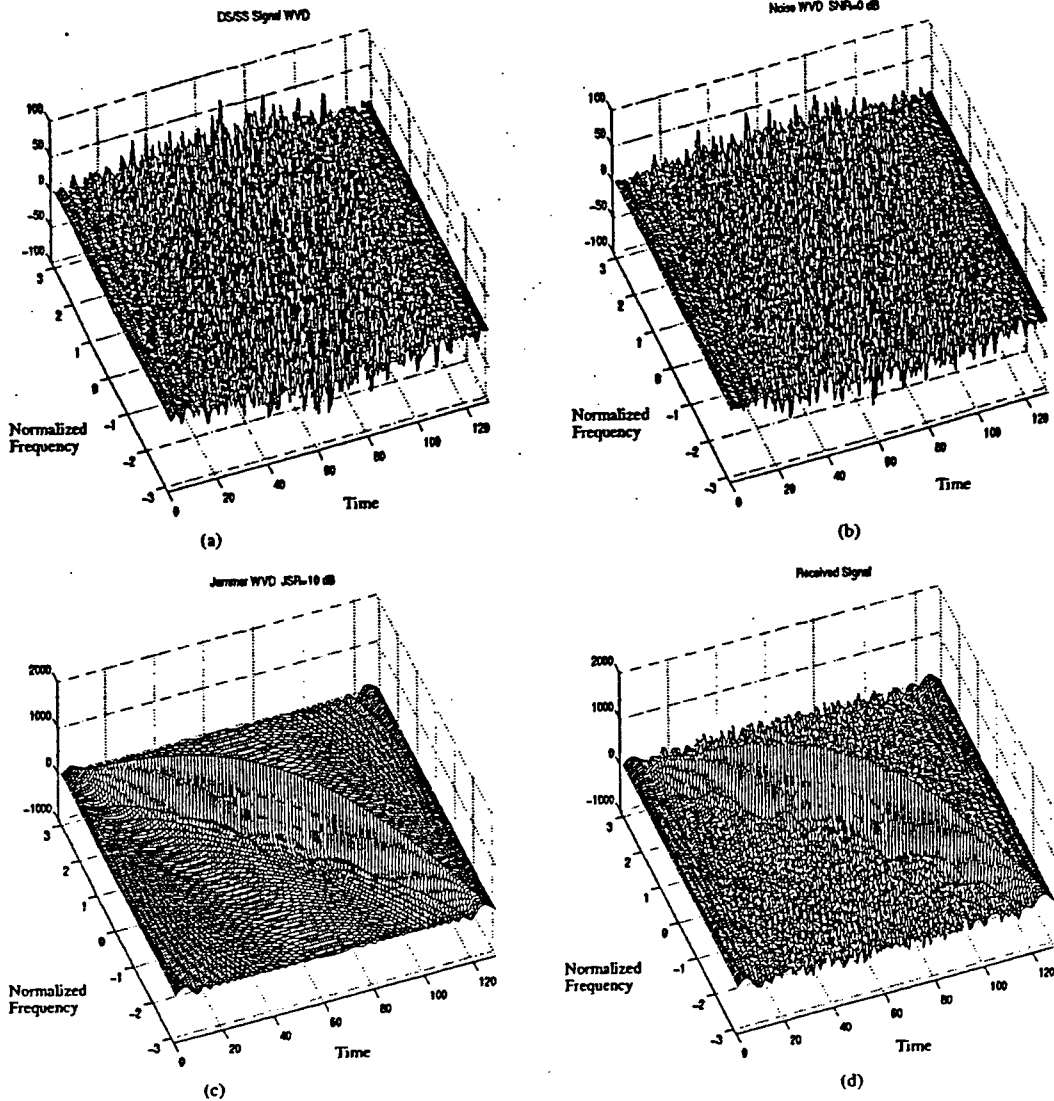


Fig. 2. WVD of the different components of the received signal: (a) WVD of the DS/SS signal, $L = 128$, (b) WVD of the noise, (c) WVD of a chirp interference, and (d) WVD of the sum of the above components.

signals is shown in Fig. 6(a). Masking so as to retain only one of these components produces the distribution in Fig. 6(b). Synthesizing this masked distribution and performing the projection provides a good estimate for this specific jammer. The second jammer component is retained through masking, and is synthesized and projected in the same manner.

With the availability of all jammer components, phase matching is performed. However, the monocomponent jammer signal equations (18) and (19) are no longer adequate. When the reference signal is composed of the sum of several individual components, corresponding components must be phase matched. In this case, a least squares approach must be used. If the even and odd components of the reference signal are denoted by the vectors s_e and s_o , respectively, and x_e and x_o denote matrices where each column is a nonphase-matched signal component, a vector containing the estimated

phase constants of each even and odd component is obtained according to

$$a_e = \arg[x_e^\# s_e] \quad (20)$$

and

$$a_o = \arg[x_o^\# s_o] \quad (21)$$

where $z^\#$ denotes the pseudoinverse of z [20].

Each of the estimated jammer components is to be subtracted from the incoming data to provide an effectively jammer-free received signal.

When masking out all but one of the interference terms, one should ensure that none of the jammer cross terms is included in the synthesis procedure. Inclusion of even a small fraction of these cross terms may induce other interference terms into

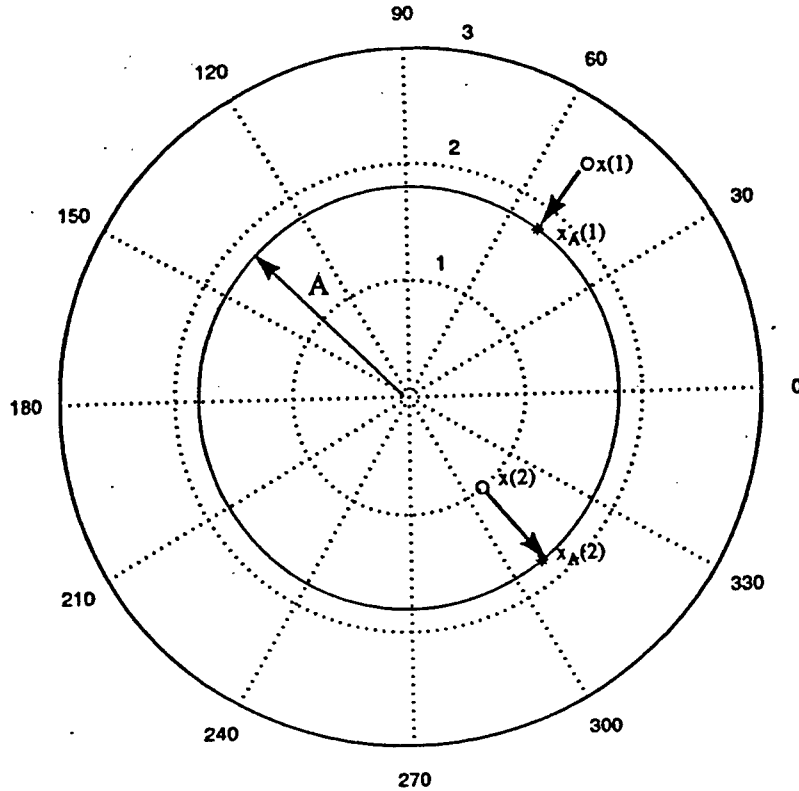


Fig. 3. Constant modulus projection operation (P_A) on the data sequence $x(n)$.

the desired jammer estimate, thus contaminating the overall jammer estimate and reducing system performance.

VI. COMPUTATIONAL REQUIREMENTS

In this section, the computational demands that the proposed algorithm places on the software-radio receiver are considered. As mentioned in Section I, the motivation for using signal-processing techniques is to augment the processing gain of the spread-spectrum system without increasing the bandwidth. This improved performance does have a price, however, since the majority of the preprocessing techniques is computationally intensive.

For the purpose of comparison, the spread-spectrum case with preprocessing disabled should be considered first. The DSSS signal is given by

$$b_k(t) = \sum_{n=1}^M p_k(n)q(t - n\tau_c)$$

where $p_k(n)$ represents the complex output sequence from the PN code generator for the k th information bit $b_k(t)$, and M is the PN sequence length. The chip pulse $q(t)$ is of duration τ_c and unit energy. Assuming that there are M complex chips/bit and only one sample/chip, this decoder thus requires M complex multiplications and $M - 1$ complex additions to process each complex bit. This translates into $4M$ real multiplications and $4M - 2$ real additions, or approximately $4M$ flops.

It was shown in [17] that the pseudo-Wigner-Ville distribution can be realized with $\frac{1}{4}M \log_2 M + 2M$ complex multiplications and $\frac{1}{2}M \log_2 M$ complex additions at each point. Removing the deliberate windowing by considering the signal to be zero outside of the current bit removes M complex multiplications, and we are therefore left with $M^2(\log_2 M + 4)$ real multiplications and $M^2(\frac{3}{2} \log_2 M + 2)$ real additions, or approximately $M^2(\log_2 M + 4)$ flops to achieve an $M \times M$ t - f representation of the received signal.

To synthesize the jammer, the eigenvector corresponding to the largest eigenvalue must be determined for both C_e and C_o , defined by (10) and (15). Using the methods outlined in [19] for a $K \times K$ Hermitian matrix, this operation can be achieved in $K^2 + 2K$ flops, ignoring the calculation of an initializing vector. Therefore, the jammer estimate can effectively be synthesized from the Hermitian matrices C_e and C_o with $P_e^2 + P_o^2 + 2(P_e + P_o)$ flops where P_e and P_o are as defined in Section II. Other methods can be used to find these eigenvectors as well, but many of these algorithm require $O(K^3)$ operations.

In order to achieve the phase matching, a_e and a_o in (18) and (19) must be determined and applied to the sequences $x_e(n)$ and $x_o(n)$ to produce the phase-matched estimate $x(n)$. The determination of a_e requires $2P_e$ real multiplications and $(2P_e - 2)$ real additions since it only involves real terms. Using similar methods for the determination of a_o , the phase-matching operation may be achieved with a total of $2P_e + 2P_o + 4M$ real multiplications and $2(P_e + P_o + M - 2)$

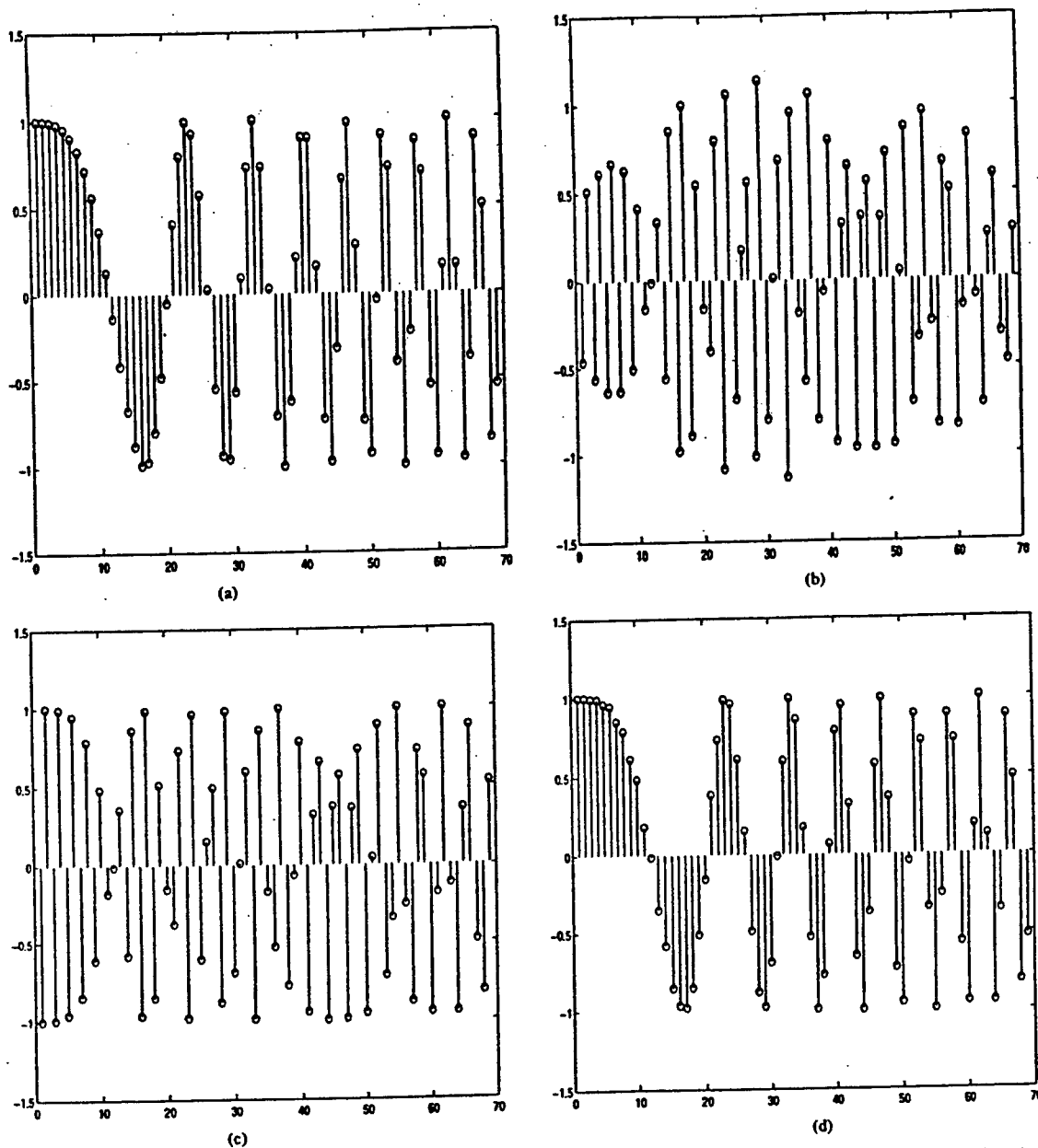


Fig. 4. $\text{Re}\{\text{Jammer estimates}\}$ for a complex chirp: (a) original jammer, (b) masked and synthesized jammer estimate, (c) projection introduced, and (d) projection and phase matching introduced.

real additions, plus four additional flops for the computation of the two inverse tangents.

It is straightforward to show that the projection operation takes at most $3M$ flops, and the subtraction of the jammer estimate from the received signal requires an additional $2M$ real additions. Finally, the $4M$ flops needed for the correlation are also needed for this algorithm. Therefore, the method described in this paper requires approximately $M^2(\log_2 M + \frac{9}{2}) + 17M$ flops to process and decode each bit.

As expected, the computational demands of the proposed algorithm increase significantly with added interference terms.

When the jammer is composed of N distinct signals, the computations needed for Wigner analysis and correlation are unchanged, while the computations required by synthesis, projection, and jammer subtraction are obviously increased by a factor of N . The new phase-matching algorithm is simply a complex least squares operation that requires $(4MN^2 - 4N^3/3)$ flops to determine the least squares solution [20], followed by $2N$ flops to extract the angular information and $4NM$ flops to adjust the phases. This produces a total of approximately $M^2(\log_2 M + 4) + (N/2)M^2 + 4N^2M - (4N^3/3) + 7NM + 4M$ flops to

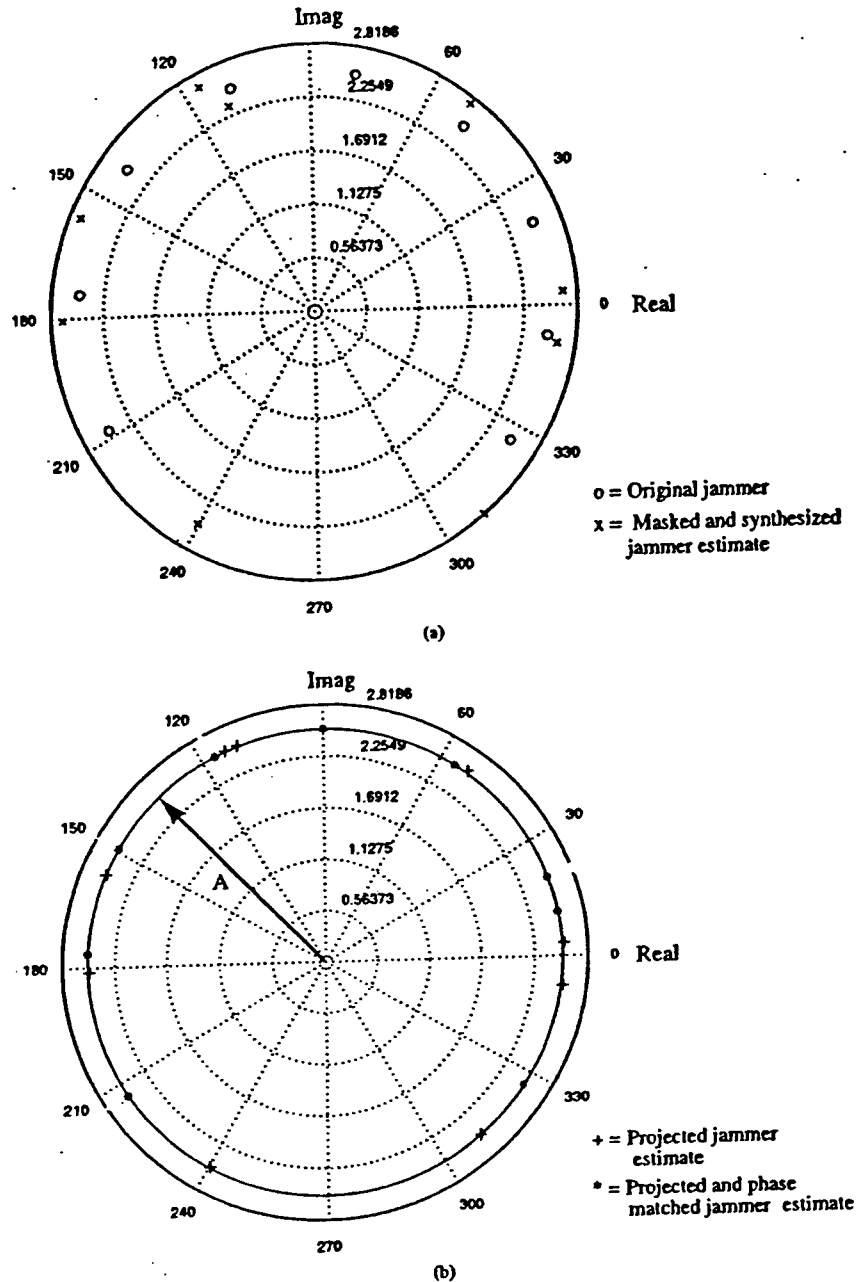


Fig. 5. Jammer estimates for nine data points as seen in the complex plane: (a) original jammer and jammer estimate and (b) projected only and projected then phase matched jammer estimates.

process and decode each bit contaminated by multicomponent interference.

As the interference excision techniques become less sophisticated, the computational costs become less demanding. Methods that rely on the application of a five-tap notch filter in the time domain [11], [12], [15], [16] require at least $24M$ flops to filter and correlate the data for each bit, in addition to the cost of determining the jammer IF. When this IF is found through TFD's, however [12], the computational

requirements are on the order of $M^2(\log_2 M + 4) + 24M$, which is not significantly different than they are for the methods presented in this paper. Placing multiple notches at the multicomponent jammer does not substantially change the complexity of the time-domain excision filter technique. The drawback, however, is a significant increase in the self-noise, rendering this algorithm unsuitable for such an environment. The computational costs for these algorithms are illustrated in Table I.

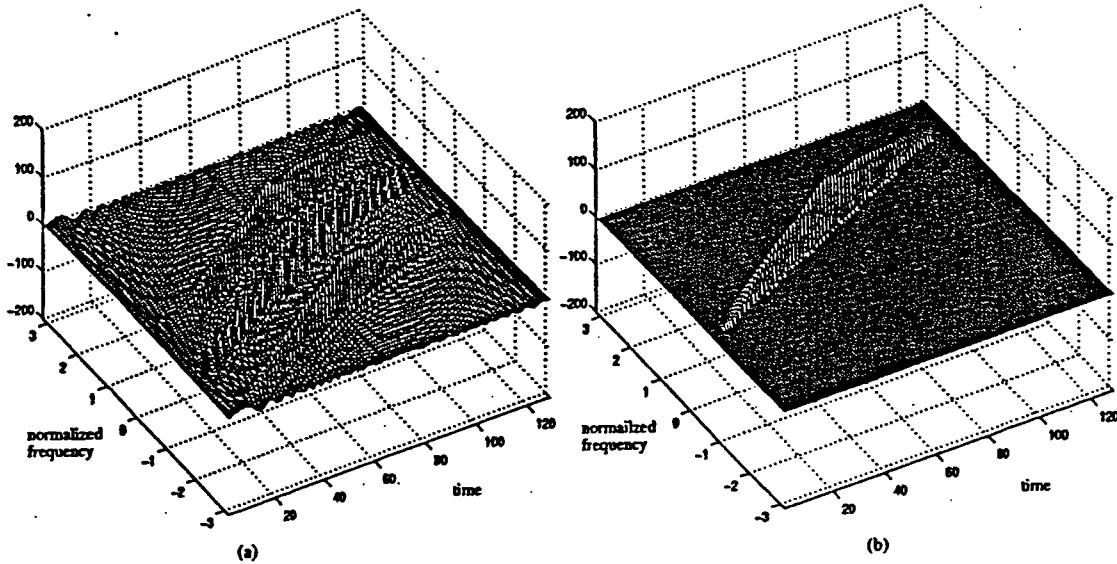


Fig. 6. (a) WVD of interference composed of two terms. Note the Jammer crossterms. (b) Only one jammer component retained.

TABLE I
A COMPARISON OF THE COMPUTATIONAL COMPLEXITY OF TWO
BILINEAR BASED INTERFERENCE EXCISION ALGORITHMS FOR DSSS

Algorithm	Approx. Number of flops required
DS/SS, no preprocessing	$4M$
This paper	
WVD calculation	$M^2(\log_2 M + 4)$
Synthesis	$(M/2)^2 + 2M$
Phase matching	$6M$
Projection	$3M$
Subtraction of jammer estimate	$2M$
Correlation	$4M$
Total	$M^2(\log_2 M + \frac{9}{2}) + 17M$
Multi-component Case	$M^2(\log_2 M + 4) + \frac{N}{2}M^2 + 4N^2M - \frac{4N^3}{3} + 7NM + 4M$
5-tap notch filter with IF estimation via TFD	$M^2(\log_2 M + 4) + 24M$
Multi-component Case	$M^2(\log_2 M + 4) + 24M$

VII. SIMULATION RESULTS

This section presents the results of computer simulations for the methods introduced in this paper. Thirty-two chips/bit are taken at a sampling frequency of one sample/bit for all simulations. In each case, the jammer is a linear FM interference that sweeps the entire frequency band every bit period, with an additive zero-mean white Gaussian noise of SNR = 0 dB.

Fig. 7 includes a benchmark for the other simulations by plotting the BER's against different JSR's for the case when the preprocessing using the t - f interference synthesis excision method is disabled. This allows interference mitigation to be performed using only the DSSS spreading-despreading operations. As the power of the interference rises, the spreading gain loses its ability to compensate for the presence of the jammer in the receiver signal, and consequently, the BER increases.

Fig. 7 also includes the BER curve where a broad mask is applied in the proposed t - f synthesis excision method. This broad mask allows most of the interference sidelobes to be included in the least squares synthesis equations (9) and (14), and therefore it is approximately equivalent to performing "no masking." The monotone decreasing behavior of this curve clearly defines a range of JSR over which the constant modulus projection part of the proposed technique alone is sufficient to yield significant improvement over the benchmark case.

The third BER curve in Fig. 7 shows the improvement in system performance when a very narrow mask is applied around the mainlobe of the interference. For JSR's between 9 and 30, this method of masking produces excellent results since no errors were detected in 1.5 million trials. Unfortunately, as the JSR continues to rise, the removal of the jammer sidelobes induces enough error into the synthesis procedure that this method of masking is not as effective as the broad masking technique. However, increasing the resolution of the TFD by extending the number of chips per bit enlarges the range of JSR where the narrow masking technique outperforms the broad masking method.

It must be emphasized that proper masking in the t - f domain is crucial to producing the best estimate of the interference. The proper masking technique depends upon the magnitude of the jammer sidelobes in the t - f domain relative to the TFD of the desired signal. For a given resolution of the TFD, it has been determined that the bit-error performance of

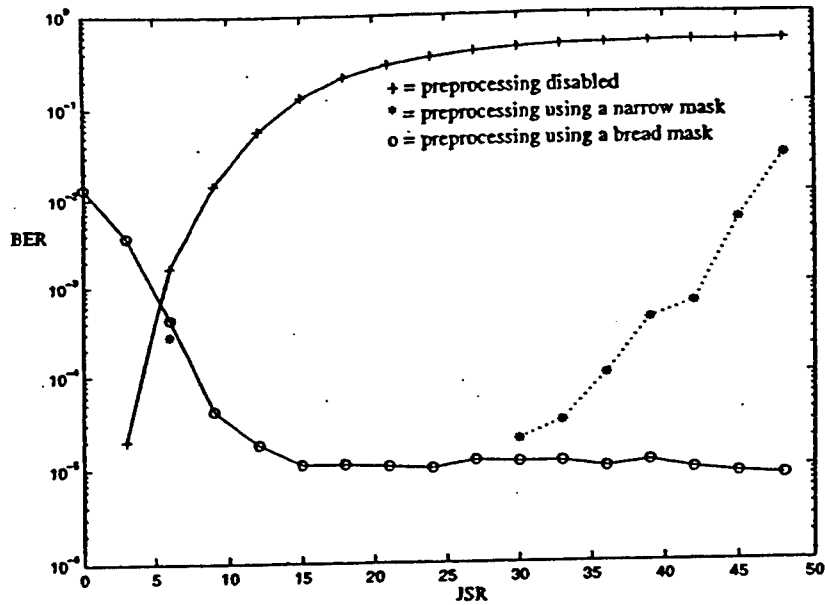


Fig. 7. BER versus JSR for the preprocessing disabled and for the preprocessing enabled cases.

the spread-spectrum system can be maximized by using the appropriate masking techniques for a given range of JSR.

For all simulations, the estimated modulus value used by the projection operator was taken by averaging the modulus of the received signal over each time sample. At low JSR's, enabling preprocessing hinders the DSSS system since the jammer estimate is highly contaminated by the signal and noise. Subtracting this poor jammer estimate actually increases the noise in the signal. It is apparent that interference mitigation using t - f synthesis prior to correlation with the receiver PN sequence starts to produce improved results over the preprocessing disabled case at a JSR of approximately 6 dB, depending on the nature of the interference.

It should be noted that some simulations used 63 chips/bit. However, with this much processing gain, no errors were produced in 200 000 trials at any of the given JSR values when preprocessing was enabled.

VIII. CONCLUSIONS

In this paper, the mitigation of narrow-band nonstationary interference in DSSS communication systems is achieved by subtracting an estimate of the interference from the received signal. This estimate is obtained by masking out the signal and noise components of the received data in the time-frequency domain, and synthesizing the result. When the interference is known *a priori* to be a polynomial phase, which is uniquely described by its instantaneous frequency characteristics, an improved estimate can be generated by projecting the synthesized jammer estimate onto a circle of its constant modulus. The direct synthesis of the spread-spectrum signal, rather than the interference, from the t - f domain is shown to be undesirable due to lack of a clear DSSS t - f signature, the retention of the jammer power in its sidelobes, cross terms of the signal, noise, and jammer spreading over the entire t - f domain, and the loss

of a meaningful phase reference. A method for extending this technique to the multijammer scenario where each term of the interference is of constant modulus is also presented.

Simulations were performed using two masking techniques. It was shown that the lowest bit-error rates are obtained when the jammer estimate is the result of both a phase-matching and a projection operation on a correctly masked t - f distribution. The implementation of this technique in the simulations showed that different masks should be applied to the TFD of the received signal, depending on the relative power of the interference.

In software-radio architectures, the system has the discretion to invoke the proper algorithms, such as the one presented in this paper, should a specific jammer type appear. When no interference signal is present, the receiver should disable preprocessing of the received signal, and rely solely on the spreading gain inherent in DSSS. As the nature of the interference changes and a jammer appears, the receiver can take some corrective action and change modes, depending on the situation. When a single jammer that is of constant modulus is detected, the method described in this paper becomes applicable. On the other hand, when the jammer is amplitude modulated, more appropriate algorithms may be invoked. Although these interference excision techniques are computationally demanding, the processing power of the spare channels on a multiband, multimode system may be dedicated to them when only one channel is in use. By so doing, a signal lost in broadband nonstationary interference may often be recovered.

REFERENCES

- [1] M. K. Simon *et al.*, *Spread Spectrum Communications*. Rockville, MD: Computer Science Press, 1985.
- [2] L. Milstein and R. Litis, "Signal processing for interference rejection in spread spectrum communications," *IEEE Signal Processing Mag.*, vol. 3, pp. 18-31, Apr. 1986.

- [3] L. B. Milstein, "Interference rejection techniques in spread spectrum communications," *Proc. IEEE*, pp. 657-671, June 1988.
- [4] J. Proakis and M. Salehi, *Communication System Engineering*. Englewood Cliffs, NJ: Prentice-Hall, 1994, Sect. 11.
- [5] J. Ketchum and J. Proakis, "Adaptive algorithms for estimating and suppressing narrowband interference in PN spread spectrum systems," *IEEE Trans. Commun.*, pp. 913-924, May 1982.
- [6] L. A. Rusch and H. V. Poor, "Narrowband interference suppression in CDMA spread-spectrum communications," *IEEE Trans. Commun.*, vol. 42, pp. 1969-1979, Apr. 1994.
- [7] H. V. Poor and X. Wang, "Adaptive suppression of narrowband digital interferers from spread-spectrum signals," *Wireless Personal Commun.*, 1997. (Also see *Proc. ICASSP96*, Atlanta, GA, May 1996.)
- [8] M. Medley, G. Saulnier, and P. Das, "Applications of the wavelet transform in spread spectrum communications systems," presented at SPIE, Wavelet Appl., Orlando, FL, Apr. 1994.
- [9] M. Tazebay and A. Akansu, "Adaptive subband transforms in time-frequency excisers for DSSS communication systems," *IEEE Trans. Signal Processing*, pp. 2776-2782, Nov. 1995.
- [10] S. Roberts and M. Amin, "Linear vs. bilinear time-frequency methods for interference mitigation in direct sequence spread spectrum communication systems," in *Proc. Asilomar Conf. Signals, Syst., Comput.*, Pacific Grove, CA, Nov. 1995.
- [11] S. Tyler and M. Amin, "Mitigating interference in direct sequence spread spectrum communication systems," *Rome Lab. Tech. J.*, vol. 1, June 1995.
- [12] M. Amin, "Interference mitigation in spread spectrum communication system using time-frequency distributions," *IEEE Trans. Signal Processing*, vol. 45, pp. 90-102, Jan. 1997.
- [13] B. Boashash, "Estimating and interpreting the instantaneous frequency of a signal, Parts 1 and 2," *Proc. IEEE*, vol. 80, Dec. 1990.
- [14] M. G. Amin, A. Lindsey, and C. Wang, "On the application of time-frequency distributions in the excision of pulse jamming in spread spectrum communication systems," presented at the IEEE Workshop Statistical Signal and Array Processing, Greece, June 1996.
- [15] C. Wang and M. Amin, "Performance analysis of instantaneous frequency based interference excision techniques in spread spectrum communications," *IEEE Trans. Signal Processing*, vol. 46, pp. 1-13, Jan. 1998.
- [16] ———, "Performance analysis of interference excisions in spread spectrum communications based on instantaneous frequency estimation," in presented at the 4th Int. Symp. Signal Processing and Appl., Australia, Aug. 1996.
- [17] T. A. C. M. Claasen and W. F. G. Mecklenbrauker, "The Wigner distribution—A tool for time-frequency signal analysis; Part II: Discrete time signals," *Phillips J. Res.*, vol. 35, pp. 276-300, 1980.
- [18] G. F. Boudreaux-Bartels and T. W. Parks, "Time-varying filtering and signal estimation using Wigner distribution synthesis techniques," *IEEE Trans. Acoust., Speech, Signal Processing*, vol. ASSP-34, pp. 442-451, June 1986.
- [19] D. Tufts and C. Melissinos, "Simple, effective computation of principal eigenvectors and their eigenvalues and application to high-resolution estimation of frequencies," *IEEE Trans. Acoust., Speech, Signal Processing*, vol. ASSP-34, pp. 1046-1053, Oct. 1986.
- [20] G. Golub and C. Van Loan, *Matrix Computations*. Baltimore, MD: Johns Hopkins Univ. Press, 1984.



Stephen R. Lach was born in Colorado Springs, CO, in 1974. He received the B.S.E.E. and M.S. degrees in 1996 and 1998, respectively, from Villanova University.

Since his graduation, he has served as a Lieutenant in the U.S. Air Force, working as an Engineer at the Air Force Research Laboratory at Eglin AFB, FL. He is currently working on antijam technologies for GPS-based systems, and his main interests include time-frequency signal representations, array processing techniques, and GPS technologies.



Moeness G. Amin (S'82-M'83-SM'91) received the Ph.D. degree in electrical engineering in 1984 from the University of Colorado, Boulder.

He has been on the faculty of the Department of Electrical and Computer Engineering at Villanova University since 1985, where he is now a Professor. His current research interests are in the areas of time-frequency analysis, spread-spectrum communications, smart antennas, and blind signal processing.

From 1995 to 1997, Dr. Amin was an Associate Editor of the IEEE TRANSACTIONS ON SIGNAL PROCESSING and a member of the Technical Committee of the IEEE Signal Processing Society on Statistical Signal and Array Processing. He is currently a member of the IEEE Signal Processing Society Technical Committee on Signal Processing for Communications. He was the General Chair of the 1994 IEEE International Symposium on Time-Frequency and Time-Scale Analysis. He is the General Chair of the 2000 IEEE Workshop on Statistical Signal and Array Processing. He is the recipient of the 1997 IEEE Philadelphia Section Award for "Outstanding Intellectual and Organizational Contributions to the IEEE Philadelphia Section in the Area of Signal Processing." He is also the recipient of the 1997 Villanova University Outstanding Faculty Research Award.



Alan R. Lindsey (S'84-M'88) was born in Ohio in 1966. He received the B.S.E.E., M.S.E.E., and Ph.D. degrees in 1989, 1991, and 1995, respectively, from Ohio University, Athens.

Since 1995, he has served the U.S. Air Force as a Civilian Research Scientist for the Information Grid Directorate of the Air Force Research Laboratory in Rome, NY. He is currently responsible for basic research into the problems of interference mitigation in spread-spectrum communication signals and computationally feasible trellis coding in high-dimensional signal spaces. His main interests include digital communication theory, coding and information theory, digital signal processing, adaptive signal processing, digital control systems, wavelet and multiresolution theory, and applications of time-frequency signal representations.

A COMPARISON BETWEEN TWO TIME-FREQUENCY BILINEAR TRANSFORMS FOR INTERFERENCE EXCISIONS IN SPREAD SPECTRUM COMMUNICATIONS

Stephen R. Lach,[†] Alan R. Lindsey,^{††} and Moeness G. Amin[†]

[†] Department of Electrical and Computer Engineering
Villanova University
Villanova, PA 19085
email: slach/moeness@ece.vill.edu

^{††} Air Force Research Laboratory / IFGC
525 Brooks Road
Rome, NY 13441
email: lindsey@rl.af.mil

ABSTRACT

In this paper, a comparison is made between two recently proposed techniques that utilize time-frequency (t-f) bilinear transforms to mitigate interference in direct sequence spread spectrum communications. The first method uses the jammer instantaneous frequency (IF) as obtained from a time-frequency distribution (TFD) to construct an open loop adaptive filter that places a notch at the jammer IF. The second method synthesizes a least squares estimate of the interference from the t-f domain. This jammer estimate is then improved by a constant modulus projection operation, after which it is directly subtracted from the received signal in the time domain. A review of each method is presented, and bit error performance for each technique is displayed and explored for several jamming environments. Computational requirements for both methods are derived.

I. INTRODUCTION

Direct-sequence spread spectrum (DSSS) is a technique of communication whereby the bandwidth of the transmitted waveform is intentionally made much wider than would be necessary to transmit the information over the channel. This spreading is accomplished by superimposing upon the data bits a high-rate spreading sequence, which is typically a pseudorandom noise (PN) sequence. The advantage of using this excess bandwidth is that it makes the system less sensitive to many types of interferences. In fact, any level of interference rejection can be achieved by using sufficient processing gain. This, however, may entail increasing the bandwidth beyond the limits of the available spectrum. Therefore, signal processing techniques have been used in conjunction with the DSSS receiver to augment the processing gain, permitting greater interference protection without an increase in bandwidth. (For more details of the discussions, see the tutorial [7]).

Recently, bilinear time-frequency distributions (TFDs) have been proposed for nonstationary interference excision in DSSS communications. Over the past two years, two approaches based on TFDs have shown great promise in improving the spread spectrum receiver signal-to-noise ratio (SNR) and reducing the BER significantly beyond what is achieved by traditional excision methods [2,6]. Both techniques rely on the localization properties of the TFD for interferers with time-varying characteristics, specifically those which are uniquely characterized by their instantaneous frequencies (IF). The class of jammers considered in this paper are polynomial phase signals with known constant modulus. The two methods are reviewed in the following sections.

II. THE NOTCH FILTER METHOD

In [1,2], the notch filter method of interference excision in DSSS using time-frequency distributions (TFDs) is introduced. This approach characterizes the unwanted interference by estimating its instantaneous frequency (IF) at each time sample through a bilinear t-f transformation. This information is then used to construct an open loop adaptive filter that places a frequency varying notch at the estimated jammer IF, thus rendering the filter output essentially jammer-free. A block diagram illustrating this procedure is shown in Fig. 1. In the original work, filters that place either one or two zeros at the jammer IF were derived and analyzed for both real and complex scenarios [1], but subsequent work in this area has focused primarily on a real interference [9,10]. However, since it is generally recommended that TFDs operate on the analytic signal rather than the real one [2], and

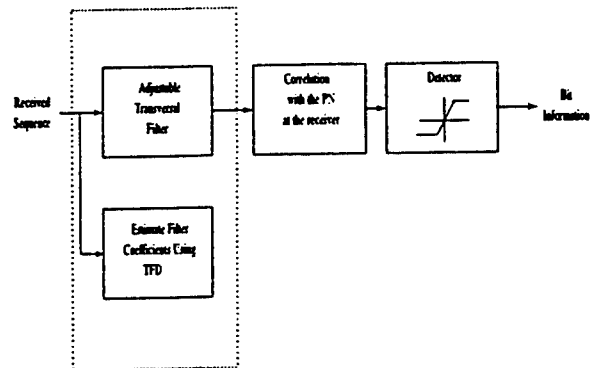


Figure 1. Open loop adaptive (Notch) filter technique

since the WVD synthesis technique operates on a complex interference, only the complex excision filter will be considered in this paper. Therefore, instead of the familiar three and five coefficient real filters, two and three coefficient complex filters will suffice.

For the case of a complex jammer of IF ω_0 , the single-zero notch filter is defined as [1]

$$H(z) = 1 - z^{-1} e^{j\omega_0} \quad (1)$$

The corresponding impulse response is

$$h(n) = \delta(n) - e^{j\omega_0} \delta(n-1) \quad (2)$$

Assuming a constant modulus jammer of fixed frequency ω_0 and phase ϕ ,

$$J(n) = A e^{jn\omega_0 + j\phi} \quad (3)$$

it was shown in [1] that the receiver signal-to-noise ratio is

$$SNR = \frac{L^2}{L-1+(2L-1)\sigma^2} = \frac{L}{1+2\sigma^2} \quad (4)$$

which is only dependent upon the number of chips/bit (L) and the noise power (σ^2). Unlike the real excision filter case, the receiver SNR of the complex filter is frequency independent.

The double-zero complex excision filter is the convolution of (1) with itself; that is

$$H(z) = (1 - z^{-1} e^{j\omega_s})^2 \quad (5)$$

The corresponding impulse response is

$$h(n) = \delta(n) - 2e^{j\omega_s} \delta(n-1) + e^{2j\omega_s} \delta(n-2) \quad (6)$$

Assuming the same jammer as in (3), the SNR is modified to

$$SNR = \frac{L^2}{5L-6+(6L-6)\sigma^2} = \frac{L}{5+6\sigma^2} \quad (7)$$

Although this method of jammer excision promises complete removal of the interference, there are still two drawbacks to its use in practical applications. First, these filters inherently process a portion of the desired signal, inducing an unwanted correlation (commonly referred to as "self-noise") into the spreading PN sequence. Second, this method relies on the fact that the IF of the jammer is constant throughout the filter duration. In situations where the jammer IF is rapidly varying, this assumption no longer holds, and decreased performance is expected. Finally, inaccuracies in the IF estimate may cause the filter zeros (notches) to be placed at an incorrect frequency, thus allowing a percentage of the jammer power to escape the filtering altogether. For these last two reasons, and those stated in reference [2], the double-zero filter, whose bandwidth is wider than that for a single zero, should outperform the single-zero filter in all cases except for that of a pure sinusoidal interference.

It should be noted that in [9], the real filter analysis was expanded to account for inaccuracies in the estimation of the jammer IF, and in [10], a notch depth control parameter was introduced to combat the detrimental effects of self noise at low jammer-to-signal ratios (JSRs). Although, both of these discussions only dealt with the case of a real jammer, the development of these techniques in a complex environment is feasible and straightforward.

III. THE WVD SYNTHESIS/PROJECTION METHOD

In this method, time-varying filtering is achieved by masking the regions of high power concentration in the t-f domain, followed by a synthesis procedure to recover the jamming signal. This constructed jammer is then subtracted from the incoming data to effectively remove the interference component in the time domain, as shown in Fig. 2.

Of particular interest to this technique are jammers having the property of a constant modulus. In this case, the jamming signal can be estimated more accurately through a two stage process. First, an estimate of the jammer is generated by masking out the signal and noise components of the received signal in the t-f domain and then performing a least-squares synthesis procedure. This estimate is then improved by projecting each sample of the synthesized signal on a circle representing the constant modulus of the actual jammer. By retaining the phase and performing this projection at each sample of the synthesized signal, an improved estimate of the jammer is obtained. When this new interference

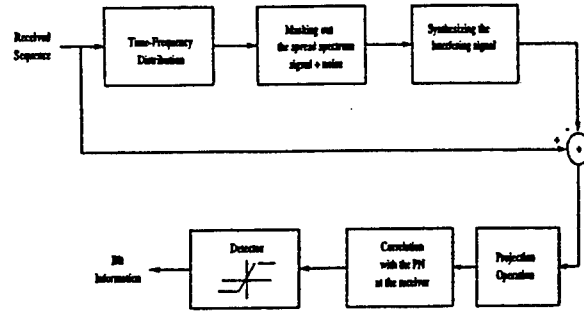


Figure 2. WVD Synthesis/Projection Jammer Excision

estimate is then subtracted from the received signal, a drastic enhancement in the DS/SS system performance is achieved [6].

The synthesis problem is finding the sequence $x(n)$ whose Wigner-ville Distribution (WVD) is closest in some sense to a desired real time-frequency distribution $Y(n, \omega)$ that may or may not represent a valid WVD [3]. Therefore, a minimization of

$$E(x) = \sum_n \frac{1}{\pi} \int_{-\pi/2}^{\pi/2} |Y(n, \omega) - W_x(n, \omega)|^2 d\omega \quad (8)$$

is desired. It was shown in [3] that the even and odd indexed samples of the sequence $x(n)$ could be generated independently by solving the equations

$$C_e x_e = 4 \|x_e\|^2 x_e \quad (9)$$

and

$$C_o x_o = 4 \|x_o\|^2 x_o \quad (10)$$

where x_e and x_o are the eigenvectors corresponding to the largest eigenvalues of C_e and C_o in each equation. C_e and C_o are obtained from $Y(n, \omega)$ according to

$$C_e(p+1, m+1) = y(m+p, p-m) + y^*(m+p, m-p) \quad (11)$$

and

$$C_o(p, m) = y(m+p-1, p-m) + y^*(m+p-1, m-p) \quad (12)$$

where

$$y(n, m) = \frac{1}{\pi} \int_{-\pi/2}^{\pi/2} Y(n, \omega) e^{j\omega n} d\omega \quad (13)$$

Although this technique produces a sequence that minimizes the error in (8), the above solution is not unique. Since a multiplication of the even and odd components of $x(n)$ by the phase constants a_e and a_o does not change the sequence's WVD, signal synthesis can only be achieved up to an arbitrary phase in both the even and odd components of the sequence. However, with the presence of a reference signal often chosen as the original data sequence, it is possible to find the parameters a_e and a_o that bring the synthesized signal as close as possible to the reference signal by phase matching. That is

$$a_e = \arg \left[\sum_n s(2n) x_e^*(n) \right] \quad (14)$$

$$a_o = \arg \left[\sum_n s(2n+1) x_o^*(n) \right] \quad (15)$$

where $s(n)$ is the reference signal.

For the projection portion of this technique, P_A is defined as the constant modulus projection operator which when applied

to the complex sequence $x(n)$, the resulting signal, $x_A(n)$, retains the phase of each sample of $x(n)$, but changes its amplitude to a constant value A [6].

It must be emphasized that there are several factors that may inhibit the effectiveness of projecting the jammer estimate onto a constant modulus circle in order to produce an improved estimation. If the value A of the modulus chosen is inaccurate, the projection operation may actually induce extra noise into the estimate of the interference. Also, even with the exact knowledge of A , if the phase of the estimate is inaccurate, projection may prove ineffective.

IV. BIT ERROR PERFORMANCE

Computer simulations for the methods considered in the preceding sections are now presented. The $L=23$ chips/bit are taken at a sampling frequency of 1 sample/bit for all simulations. In each case, the interference terms are polynomial phase signals with constant amplitude. A zero-mean, white Gaussian noise is added in all cases at an SNR = 0 dB. Although practical applications of these excursions would demand a much larger spreading gain, this reduced number was used in the simulations to lower the bit error rates (BERs) into a reasonable range.

Figure 3 (a) gives a benchmark for the rest of the simulations by plotting the BERs against different JSRs for the non-processed case of a typical monotone interference. Also included in Fig. 3 (a) is the case of a fixed frequency complex sinusoidal jammer filtered either by a two-tap filter or a three-tap filter. As expected, the two-tap filter with the thinner notch outperforms the three-tap filter, as less self-noise is induced on the desired signal in the single-zero case.

Figure 3 (b) uses the same interference, but this time the received signal is processed using the TF synthesis/projection technique. Plots are included for the cases of a narrow mask without projection, and a narrow/broad mask with projection.

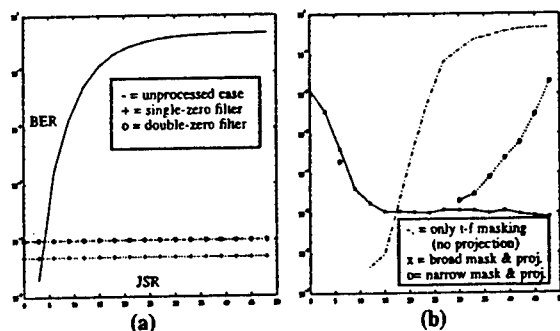


Figure 3. Bit error plots for the case of a complex sinusoidal jammer

Figure 4 introduces a nonstationary interference in the form of a linear FM that sweeps one-half of the frequency range in each bit duration. Since the IF is no longer constant from sample to sample, the performance of the notch filter (Fig. 4 (a)) suffers quite dramatically, although the three-tap filter handles the frequency changes more gracefully than the two-tap filter.

Figure 4 (b) shows that the WVD Synthesis technique handles the chirp interference almost as well as the tone jamming case. For a linear FM jammer, the WVD transforms the interference into a series of impulses, and self crossterms are not introduced. This permits an extremely accurate t-f representation of the received signal, and proper masking is feasible.

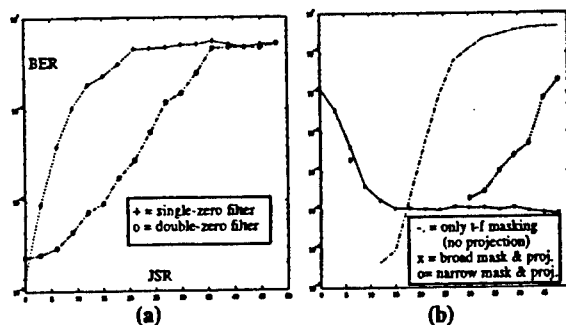


Figure 4. Bit error plots for the case of a complex chirp jammer

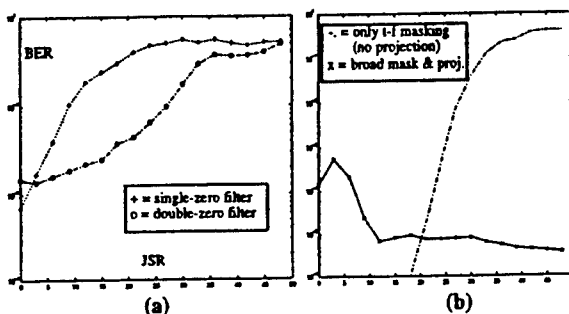


Figure 5. Bit error plots for the case of a third order polynomial phase jammer

In Fig. 5, the interference used is a third order polynomial phase signal with a parabolic t-f signature. In this case, the performance of the notch filters still suffer severely at high JSRs, but the performance of the WVD synthesis method is still surprisingly good. However, due to the nonlinearity of the IF of the jammer, proper masking in this case is difficult, as it becomes hard to distinguish jammer self crossterm regions (which should be retained) from signal and noise regions (which should be masked out). However, through the use of a broad mask, especially at high JSRs, improved system performance may still be obtained.

V. COMPUTATIONAL DEMANDS

In order to provide a more complete comparison between the direct subtraction by synthesis method and the open-loop adaptive filtering method, an analysis of computational requirements is necessary. The authors do not attempt to provide a rigorous analysis adhering to the standards of complexity theory, nor is the subject of efficiency optimization addressed. In the following, computational complexity will be measured by floating point operations, or "flops", which are taken to be single kernel operations - a real multiplication or addition. Implementation on architectures that operate on complex numbers as efficiently as real ones is not considered. In this regard, some perspective on the practical utility of such a notion is provided by Golub and Van Loan's excellent reference [5]. The receivers discussed here decode one bit at a time, so the computational requirements are neatly fenced off on bit boundaries. Thus, for the following calculations, the number of samples per bit, M , which encapsulates the spread spectrum chip rate and sample rate, is the only parameter that affects the computational load of either method.

Now, each frequency slice of a pseudo-WVD for an M -

point signal (one bit) can be accomplished with $.25M\log_2 M + 2M$ complex multiplications and $.5M\log_2 M$ complex additions. Since this application precludes the use of pseudo-Wigner methods, it is assumed that each bit is padded with enough zeros on both sides to avoid deliberate windowing, so this essentially eliminates M complex multiplications. With 6 flops per complex multiplication and 2 flops per complex addition, the total flop count for the WVD is $M^2(2.5\log_2 M + 6)$. This is the dominant process and it, together with the $2M$ flops required for application of the spreading sequence, comprises the two common computations.

The unique processes of the synthesis method are considered next. The synthesis procedure is equivalent to two $M/2$ -length eigenvector (only the principal component) calculations. Using a Lanczos-type algorithm [8] the flops required for each is $.5M^2 + 6M$, for a total of $M^2 + 12M$ flops. Phase matching, as described previously, is directly figured to require $8M$ flops for even and $8M$ flops for odd components, plus an additional $6M$ flops for applying these phases - a total of $22M$ flops. The projection of an M -point complex signal to some constant modulus A is accomplished via a three step process. First the ratio of the real and imaginary components are processed with tangent to determine phase, then each component is scaled via trigonometric identities such that the modulus is A . Trig functions are typically accomplished with lookup tables and so do not contribute to flop count, hence the total for the projection is $3M$ flops. Subtraction of the synthesized jammer from the received signal is obviously a $2M$ flop process, and the last step of correlation with PN sequence is easily shown to take $8M$ flops. The total flop count for this method is then $47M + M^2((2.5)\log_2 M + 7)$.

In the notch filtering approach, using complex-coefficient filters with N taps, the correlation is shown to involve N complex multiplications and $N-1$ complex adds $\Rightarrow 8N-2$ flops, for each point in the M -point output sequence. Thus, the two and three tap filters will require $14M$ and $22M$ flops respectively. The other major processing required for this approach is the calculation of WVD, shown before. Thus the total computations required for this method is either $TFD+14M$ or $TFD+22M$. Now, it becomes clear that the filtering approach has only a slight advantage over direct subtraction, even at very small M . This advantage disappears quickly for any realistic value of M , say 64 or higher. This is illustrated clearly in Fig 6.

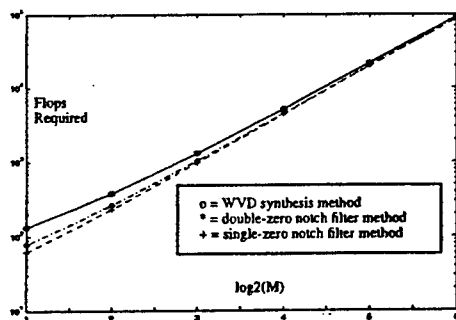


Figure 6. Computational Requirements vs. $\log_2(M)$

VI. CONCLUSIONS

Through bit error comparisons, it has been shown that the WVD synthesis jammer excision technique significantly outperforms the notch filtering method for cases in which the frequency of the interference changes rapidly with time. Although the WVD synthesis method performs best when the jammer can be charac-

terized by a first order polynomial phase signal with constant amplitude, adequate results are obtained even with the presence of self-cross terms or without the use of the projection operator. The reason for the unsatisfactory performance of the notch filter technique in the jammer environments considered in this paper is that the assumption of a constant frequency being maintained throughout the duration of the filter is no longer valid. However, for single tone, slowly varying chirps and frequency hopping interfering scenarios, the notch filter technique may provide adequate results.

REFERENCES

- [1] M. G. Amin, "Time-frequency receiver in spread spectrum communication systems using time-frequency distributions," Rome Lab. Technical Journal, July 1996.
- [2] M. G. Amin, "Interference mitigation in spread spectrum communication system using time-frequency distribution," IEEE Trans. on SP, vol. 45, pp. 90-102, Jan. 1997.
- [3] G. F. Boudreaux-Bartels and T. W. Parks, "Time-varying filtering and signal estimation using Wigner Distribution synthesis techniques," IEEE Trans. Acoust., Speech, Signal Processing, vol. ASSP-34, no. 3, pp. 442-451, June 1986.
- [4] T. Claasen and W. Mecklenbrauker, "The Wigner distribution-A tool for time-frequency signal analysis; Part II: Discrete time signals," Phillips J. Res., vol. 35, pp. 276-300, 1980.
- [5] G. Golub and C.F. Van Loan, *Matrix Computations*, 2nd Edition, Johns Hopkins University Press, Balt., MD, 1989, page 19.
- [6] S. Lach, M. Amin and A. Lindsey, "Broadband nonstationary interference excision for spread spectrum communications using time-frequency synthesis," Proc. ICASSP98, Seattle, WA, May 1998.
- [7] L. Milstein and R. Itlis, "Signal processing for interference rejection in spread spectrum communications," IEEE SP Magazine, vol. 3, pp. 18-31, April 1986.
- [8] D. Tufts and C. Melissinos, "Simple, effective computation of principal eigenvectors and their eigenvalues and application to high-resolution estimation of frequencies," IEEE Trans. ASSP, vol. ASSP-34, no. 5, pp. 1046-1053, October 1986.
- [9] C. Wang and M. Amin, "Performance analysis of instantaneous frequency based interference excision techniques in spread spectrum communications," IEEE Transactions on Signal Processing, vol. 46, no. 1, pp. 70-82, January 1998.
- [10] C. Wang and M. Amin, "Optimum interference excision in spread spectrum communications using time-frequency distribution," Submitted IEEE transactions on Signal Processing.

Algorithm	Number of flops required
DSSS, no preprocessing	$2M$
WVD calculation	$M^2(2.5\log_2(M)+6)$
Synthesis (eigen-analysis)	M^2+12M
Phase matching	$22M$
Projection	$3M$
Subtraction of jammer estimate	$2M$
Correlation	$8M$
Total	$M^2(2.5\log_2(M)+7)+47M$
2-tap complex notch filter with IF estimation via TFD	$TFD+14M$
3-tap complex notch filter with IF estimation via TFD	$TFD+22M$

Table 1: Computational Costs

BROADBAND NONSTATIONARY INTERFERENCE EXCISION FOR SPREAD SPECTRUM COMMUNICATIONS USING TIME-FREQUENCY SYNTHESIS

Stephen R. Lach, Moeness G. Amin
Department of Electrical and Computer Engineering
Villanova University
Villanova, PA 19085

Alan R. Lindsey
Rome Laboratory / C3BB
525 Brooks Road
Rome, NY 13441

ABSTRACT

A new method is introduced for interference excision in spread spectrum communications. Time-frequency synthesis techniques are used to synthesize the nonstationary jammer from the time-frequency domain using least-squares methods. The synthesized jammer is then subtracted from the incoming data in the time domain, leading to increased signal to interference ratio at the input of the correlator. The paper focuses on jammers with constant modulus where the jamming signal is a polynomial phase. With this apriori knowledge, the jammer signal amplitude is restored by projecting each sample of the synthesized signal to a circle representing its constant modulus. With the phase matching provided by the least-squares synthesis method and amplitude matching underlying the projection operation, the paper shows a significant improvement in receiver performance/bit error rates over the case where no projection is performed.

I. INTRODUCTION

One of the primary motivations for direct sequence (DS) spread spectrum (SS) communications is that of interference mitigation. Several past contributions deal with the suppression of narrowband interference [7,8], and approaches for broadband interference excision based on time-frequency analysis have also been considered [1,2,6]. The recent development of bilinear (quadratic) time-frequency distributions (TFDs) for improved signal power localization in the time-frequency plane has motivated several new approaches for nonstationary interference excision in spread spectrum communications [1,3]. An implementation of an interference excision system using time-frequency distributions (TFDs) to determine the jammer IF has been thoroughly discussed [9]. However, this technique also creates a significant amount of self noise that forms an upper bound on the maximum attainable value of the correlator SNR, and in many cases the use of these filters makes the performance worse than when the preprocessing is disabled.

In this paper, the time-frequency (t-f) distribution is used to the fullest extent as a powerful tool for depicting a locally narrowband (FM, hopped, chirp, etc.) jammer over time and frequency. Since the interference is characterized by instantaneous frequency, its signature in the time-frequency domain is distinct from those of the noise and the spread spectrum signal, which have characteristically flat spectra by design. Therefore, time-varying filtering is achieved by masking the regions of high power concentration in the t-f domain, followed by a synthesis technique to recover the jamming signal. This constructed jammer is then subtracted from the incoming data to remove the interference component in the time domain.

Of particular interest in this paper are jammers with the constant modulus property. In this case, the jamming signal can

be estimated more accurately through a two stage process. First, an estimate of the jammer is generated by masking out the signal and noise components of the received signal in the t-f domain and then performing a least-squares synthesis procedure. This estimate is then improved by projecting each sample of the synthesized signal on a circle representing the constant modulus of the actual jammer. By retaining the phase and performing this projection at each sample of the synthesized signal, we obtain an improved estimate of the jammer, which when subtracted from the received signal, a drastic enhancement in the DS/SS system performance is achieved.

II. TIME-FREQUENCY SYNTHESIS

The Wigner-Ville Distribution (WVD) $W_x(n, \omega)$ of the discrete-time signal $x(n)$ is defined by [5] as

$$W_x(n, \omega) = 2 \sum_{k=-\infty}^{\infty} x(n+k)x^*(n-k)e^{-jk\omega} \quad (1)$$

The synthesis problem is finding the sequence $x(n)$ whose WVD is closest in some sense to a desired real time-frequency distribution $Y(n, \omega)$ that may or may not represent a valid Wigner-Ville distribution.

If $Y(n, \omega)$ is indeed a valid Wigner-Ville distribution, a direct calculation of the corresponding time-domain sequence $x(n)$ can be accomplished according to [5]

$$x(n+k)x^*(n-k) = \frac{1}{2\pi} \int_{-\pi/2}^{\pi/2} W_x(n, \omega) e^{j2k\omega} d\omega \quad (2)$$

If, however, $Y(n, \omega)$ is not itself a valid WVD, we then wish to find a sequence $x(n)$ whose WVD best approximates $Y(n, \omega)$. This problem is formulated and solved in a least-squares sense by minimizing [4]

$$E(x) = \sum_n \frac{1}{\pi} \int_{-\pi/2}^{\pi/2} |Y(n, \omega) - W_x(n, \omega)|^2 d\omega \quad (3)$$

It was shown in [4] that the even and odd indexed samples of the sequence $x(n)$ could be generated independently by solving the equations

$$C_e x_e = 4 \|x_e\|^2 x_e \quad (4)$$

and

$$C_o x_o = 4 \|x_o\|^2 x_o \quad (5)$$

where x_e and x_o are the eigenvectors corresponding to the largest eigenvalues of C_e and C_o in each equation. C_e and C_o are obtained from $Y(n, \omega)$ according to

$$C_e(p+1, m+1) = y(m+p, p-m) + y^*(m+p, m-p) \quad (6)$$

and

$$C_o(p, m) = y(m + p - 1, p - m) + y^*(m + p - 1, m - p) \quad (7)$$

where

$$y(n, m) = \frac{1}{\pi} \int_{-\pi/2}^{\pi/2} Y(n, \omega) e^{j\omega n} d\omega \quad (8)$$

The desired sequence $x(n)$ can then be recovered from

$$x_e(n) = x(2n) \quad (9)$$

and

$$x_o(n) = x(2n + 1) \quad (10)$$

Although this technique produces a sequence that minimizes the error in (3), the above solution is not unique. Since a multiplication of the even and odd components of $x(n)$ by the phase constants a_e and a_o does not change the sequence's WVD, signal synthesis can only be achieved up to an arbitrary phase in both the even and odd components of the sequence. However, with the presence of a reference signal often chosen as the original data sequence, it is possible to find the parameters a_e and a_o that bring the synthesized signal as close as possible to the reference signal by phase matching. That is

$$a_e = \frac{\left[\text{Imag} \left[\sum_n s(2n) x_e^*(n) \right] \right]}{\left[\text{Real} \left[\sum_n s(2n) x_e^*(n) \right] \right]} \quad (11)$$

$$a_o = \frac{\left[\text{Imag} \left[\sum_n s(2n-1) x_o^*(n) \right] \right]}{\left[\text{Real} \left[\sum_n s(2n-1) x_o^*(n) \right] \right]} \quad (12)$$

where $s(n)$ is the reference signal.

III. SELECTION OF THE SYNTHESIZED SIGNAL

Two possible approaches can be adapted in the application of t-f distribution synthesis techniques in interference mitigation in spread spectrum communications. The first approach is to synthesize the spread spectrum signal and correlate it with the PN sequence at the receiver, as shown in Fig (1-a). In the second approach, the jammer signal is synthesized from the t-f domain and then subtracted from the incoming data to remove, or at least reduce, the jammer contamination of the desired signal, as depicted in Fig (1-b).

The preference of using one approach over the other depends on the ability to obtain a synthesized signal which is a good copy of its correspondence in the input data. This requires the signal to be synthesized to have a clear t-f signature that distinguishes it from other components of the received data. Also, phase matching and restoration of the synthesized signal should be properly accomplished.

Figure 2 (a,b) shows an example of the Wigner-Ville distributions computed separately of a complex DS/SS signal and a linear FM interference. It is straightforward to conclude that synthesizing the spread spectrum signal from the t-f domain should generally be avoided due to the following reasons:

1) It is very difficult to distinguish between the noise and the spread spectrum signal signatures in the time-frequency domain. Therefore, time-varying filtering does not reduce the effect of noise or enhance the SNR.

2) Masking out the jammer by clipping or gating the high power values in the t-f domain may very well remove the main

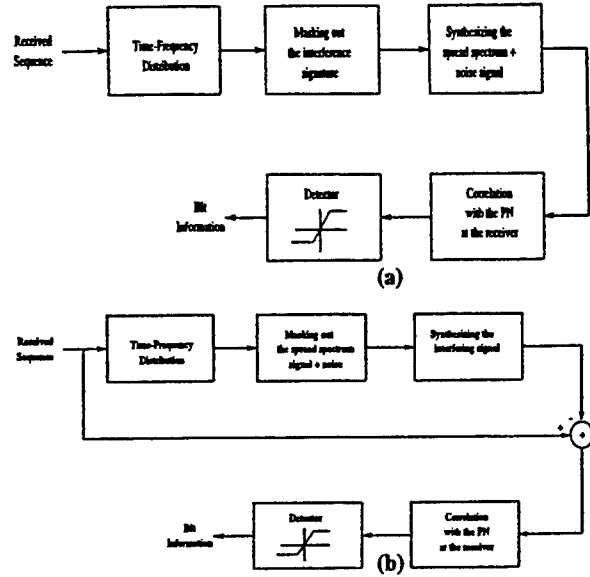


Fig. 1 Two approaches for interference mitigation in DS/SS communication systems (a) synthesizing the desired signal (b) synthesizing the interference

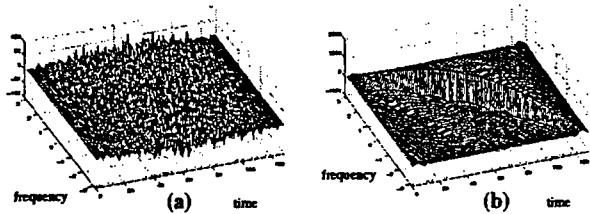


Fig. 2 (a) WVD of the DS/SS signal, L=128 (b) WVD of the chirp interference

lobe, but it leaves behind the sidelobes which carry significant jammer power.

3) The crossterms between the jammer and both the DS/SS signal and noise as well as the jammer self crossterms are often spread over the entire t-f domain, contaminating the spread spectrum signal within large regions of time and frequency.

4) Phase matching is often performed using the input data as a reference signal. Therefore, even with the assumption that the DS/SS signal is perfectly synthesized up to a phase ambiguity, the low desired signal power will make it very difficult to arrive at the correct phase by a simple matching to a data sequence in which the jammer is the dominant component.

Proper phase matching can therefore be obtained using the input data as a reference signal only through the second approach, provided that the JSR is relatively high, which is usually the case. It is expected, however, that the effectiveness of phase matching reduces with reduced jammer power.

IV. CONSTANT MODULUS PROJECTION

Let P_A define the constant modulus projection operator which when applied to the complex sequence $x(n)$, the resulting signal, $x_A(n)$, retains the phase of each sample of $x(n)$, but changes its amplitude to a constant value A . This is equivalent to project-

ing each sample of $x(n)$ on the complex plane onto the closest point of a circle of radius A that is centered at the origin, as depicted in Fig. 3. Significant reduction of noise may be achieved through this operation when it is applied to a signal that is known to be of modulus A , and whose phase is not significantly distorted.

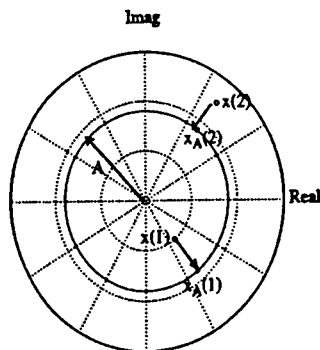


Fig. 3 Constant modulus projection operator (P_A) on the data sequence $x(n)$

In the excision of interference in DS/SS systems, it desirable to subtract an accurate estimate of this interference from the received signal prior to correlation with the PN sequence in order to enhance system performance. As stated in the previous section, a good estimate for this interference may come from synthesizing a masked t-f representation of the received signal. Fig. (4-a) depicts the original time-domain chirp jammer signal, and Fig. (4-b) is the synthesized interference estimate obtained from masking out the signal and noise components in the t-f domain where the JSR = 5 dB. Note that the phase of the even and odd samples are not matched either absolutely to the original jammer or relatively to themselves. After the phase matching operation defined by (16) and (17) is performed on the synthesized jammer estimate, the signal in Fig. (4-c) is produced. Projecting the phase matched synthesized jammer on the constant modulus circle

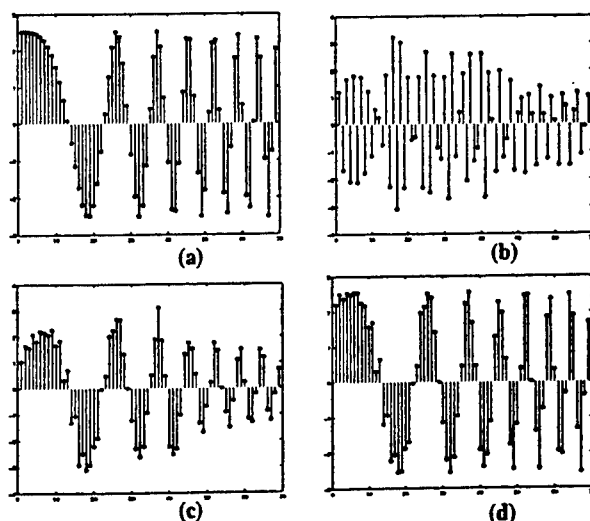


Fig. 4 Jammer estimates for a complex chirp (a) Original Jammer (b) Masked and synthesized jammer estimate (c) Phase matching introduced (d) Projection Introduced

produces the final jammer estimate, as shown in Fig (4-d). It is clear that through the phase matching and constant modulus projection, both the phase and modulus of the jammer estimate are significantly improved.

There are several factors that may inhibit the effectiveness of projecting the jammer estimate onto a constant modulus circle in order to produce an improved estimation. If the value A of the modulus chosen is inaccurate, the projection operation may actually induce extra noise into the estimate of the interference. Also, even with the exact knowledge of A , if the phase of the estimate is inaccurate, projection may prove ineffective.

V. SIMULATION RESULTS

We now present computer simulations for the cases considered in the preceding sections. The $L=23$ chips/bit are taken at a sampling frequency of 1 sample/bit for all simulations. In each case, the interference terms are either linear or sinusoidal FM. The linear FM interference is a chirp that sweeps the entire frequency band every bit period. The sinusoidal FM jammer is an FM signal whose instantaneous frequency (IF) is $\cos(.04 n)$. In this case, the jammer signal is offset to reach its highest IF in the middle of the bit duration. By so doing, we account for most of the self interference terms in the simulations. A zero-mean, white Gaussian noise is added in all cases at an SNR = 0 dB.

Figure 5 gives a benchmark for the rest of the simulations by plotting the bit error rates (BERs) against different JSRs for the case when the preprocessing implementing the t-f interference synthesis is disabled, allowing interference mitigation to be only performed using spreading/despreading operations. Also included in the same figure is the case where the jammer is masked and synthesized with phase-matching, then subtracted from the received signal without the benefit of projection. Note that enabling preprocessing without performing the projection actually increases the overall noise at the receiver, and performance is hindered from the unprocessed case.

Figure 6 shows the improvement in system performance when the masked-synthesized jammer estimate is projected onto a circle of constant modulus before it is subtracted from the received signal. Figure (6-a) illustrates the result of projecting the jammer estimate both before and after the phase matching is performed for the case of chirped interference. A sinusoidal FM jammer is considered in Fig. (6-b). In each case, a comparison with Fig. 5 makes it clear that as the interference increases in power, the estimate of the interference becomes more accurate, and lower bit error rates are produced. For these plots, the estimated modulus value used by the projection operator was taken from the received signal. At low JSRs, enabling preprocessing hinders the DS/SS system since the jammer estimate is highly contaminated by the signal and noise. Subtracting this poor jammer estimate actually serves to increase the noise in the signal. It is apparent that the interference mitigation using t-f synthesis techniques prior to correlation with the receiver PN sequence starts to produce improved results over the preprocessing disabled case around a JSR of 15 dB, depending on the t-f representation of the interference.

Also included in Figure 6 is the ideal case when the exact amplitude of the jammer is known and can be used to define the constant modulus circle used in the projection operation. This produces a further reduction in BER, as the projection always produces an improved estimation of the interference, and additional noise from the inaccuracy of estimating the amplitude of the projected signal is no longer produced.

Simulations were also run to show the effect of synthesiz-

ing the jammer without applying any masking in the t-f domain. Phase matching before and after projection was considered for both the chirp and sinusoidal FM jammers. Note that performing a phase matching prior to projection is equivalent to projecting the received signal in the time-domain and ignoring the t-f domain altogether. This technique also produces better results with increased jammer power, and it outperforms the original DS/SS case for JSRs above 20 dB, depending on the nature of the interference. However, this technique is inferior to the one considered in the previous figure.

VI. CONCLUSIONS

In this paper, mitigation of narrowband nonstationary interference in DS/SS communication systems is achieved by subtracting an estimate of the interference from the received signal. This estimate is obtained by masking out the signal and noise components of the received signal's time-frequency distribution, and synthesizing the result. When the interference is known a priori to be a polynomial phase which is uniquely described by its instantaneous frequency characteristics, an improved estimate can be generated by projecting the synthesized jammer estimate onto a circle of its constant modulus. The direct synthesis of the received signal from the t-f domain is also shown to be undesirable primarily due to the inclusion of the jammer sidelobes and the loss of a meaningful phase reference.

Simulations were performed for two jammer types utilizing several processing techniques. It was shown that the lowest BERs were obtained when the jammer estimate was the result of both a phase matching and a projection operation. The order of these two operations that produce the best system performance, however, depend on the JSR and the time-frequency characteristics of the jammer signal.

REFERENCES

- [1] M. Amin, "Interference mitigation in spread spectrum communication system using time-frequency distribution," *IEEE Trans. on SP*, vol. 45, pp. 90-102, Jan. 1997.
- [2] M. G. Amin, A. Lindsey, and C. Wang, "On the application of time-frequency distributions in the excision of pulse jamming in spread spectrum communication systems," *IEEE Workshop on SSAP*, Greece, June 1996.
- [3] S. Barbarosa, A. Scaglione, and S. Votini, "Adaptive suppression of wideband interferences in spread spectrum communications using the Wigner-Hough Transform," *Proc. of ICASSP*, Munich, Germany, April 1997.
- [4] G. F. Boudreaux-Bartels and T. W. Parks, "Time-varying filtering and signal estimation using Wigner Distribution synthesis techniques," *IEEE Trans. Acoust., Speech, Signal Processing*, vol. ASSP-34, no. 3, pp. 442-451, June 1986.
- [5] T. A. C. M. Claassen and W. F. G. Mecklenbrauker, "The Wigner distribution-A tool for time-frequency signal analysis; Part II: Discrete time signals," *Phillips J. Res.*, vol. 35, pp. 276-300, 1980.
- [6] M. Medley, G. Saulnier, and Das, "Applications of the wavelet transform in spread spectrum communications systems," *SPIE, Wavelet Applic.*, Orlando, FL, April 1994.
- [7] H. V. Poor and X. Wang, "Adaptive suppression of narrowband digital interferers from spread-spectrum signals," *Wireless Personal Communications*, to appear 1997. [Also see *Proc. ICASSP96*, Atlanta, GA, May 1996.]
- [8] J. Proakis and M. Salehi, *Communication System Engineering*, (Section 11), Prentice Hall, Englewood Cliffs, New Jersey, 1994.
- [9] C. Wang and M. Amin, "Performance analysis of instantaneous frequency based interference excision techniques in spread spectrum communications," *IEEE transactions on Signal Processing*, January 1998.

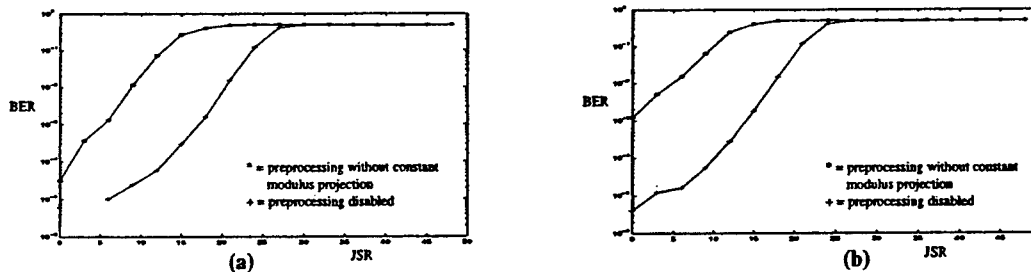


Fig. 5 BERs of the unprocessed and the preprocessed signal without constant modulus projection (a) chirp jammer (b) sinusoidal FM jammer

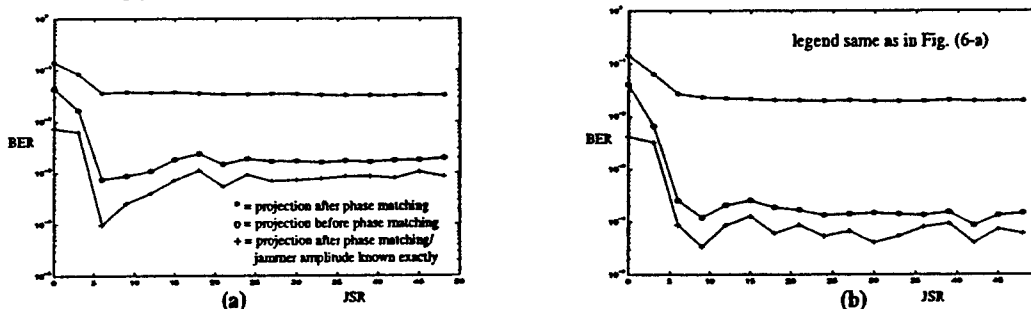


Fig. 6 BERs of the preprocessed signal with phase-matching and constant modulus projection for the cases of estimated and known amplitude of the interference (a) chirp jammer (b) sinusoidal FM

MULTIPLE COMPONENT INTERFERENCE EXCISION IN SPREAD SPECTRUM COMMUNICATIONS USING WIGNER DISTRIBUTION SYNTHESIS TECHNIQUES

Stephen R. Lach and Moeness G. Amin

Department of Electrical and Computer Engineering

Villanova University

Villanova, PA 19085

email: slach/moeness@ece.vill.edu

ABSTRACT

A new method is introduced for interference excision in spread spectrum communications. Time-frequency synthesis techniques are used to synthesize the nonstationary jammer from the time-frequency domain using least-squares methods. Subtraction of the synthesized jammer from the incoming data in the time domain leads to increased signal to interference and noise ratio at the input of the correlator, and hence improved bit error performance. The paper focuses on multi-component jammers, with each component of the jammer being of constant modulus. With this apriori knowledge, an amplitude projection operation which restores jammer amplitude information becomes feasible. Phase matching of the interference is provided by a least squares operation relative to the received signal.

I. INTRODUCTION

One of the fundamental applications of direct sequence (DS) spread spectrum (SS) communications is that of interference mitigation. Frequently, signal processing techniques are used in conjunction with the DS/SS receiver to augment the processing gain, permitting greater interference protection without an increase in bandwidth [6]. The recent development of bilinear time-frequency distributions (TFDs) for improved signal power localization in the time-frequency plane has motivated several new approaches for nonstationary interference excision in DS/SS systems. Utilization of the jammer IF as obtained via TFDs to design an open loop adaptive filter in the time domain has been thoroughly discussed in [1,7]. However, this technique has two major drawbacks. First, it becomes unfeasible to remove more than one jammer component at any time instant. Second, this method creates a significant amount of self noise (induced correlation) that in many cases actually hinders the performance of the spread spectrum system.

An alternate approach to broadband interference excision in DS/SS systems has been presented in [4]. This technique uses the TFD to depict a locally narrowband (FM, hopped, chirp, etc.) jammer over time and frequency. Time-varying filtering is then achieved by masking the regions of high power concentration in the t-f domain, followed by a synthesis technique to recover the jamming signal. This constructed jammer is then subtracted from the incoming data to remove the interference component in the time domain.

This paper clarifies and expands on the methods presented in [4]. Of particular interest in this paper are jammers composed of one or more components, each of which is of constant modulus. In this case, the jamming signal can be estimated more accurately through a two stage process. First, a non phase-matched estimate of each jammer component is generated by masking out the signal and noise components of the received signal in the t-f domain and

then performing a least-squares synthesis procedure. This estimate is then improved by projecting each sample of each synthesized component on a circle representing the constant modulus of the actual jammer term. Performing a least squares phase matching operation then obtains a final estimate of the jammer, which when subtracted from the received signal achieves a drastic enhancement in the DS/SS system performance.

II. TIME-FREQUENCY SYNTHESIS

To explain the Wigner-Ville synthesis algorithm for multi-component signals, the following review of the methods presented in [3] is included.

The Wigner-Ville Distribution (WVD) $W_x(n, \omega)$ of the discrete-time signal $x(n)$ is defined by [5] as

$$W_x(n, \omega) = 2 \sum_{k=-\infty}^{\infty} x(n+k)x^*(n-k)e^{-jk\omega} \quad (1)$$

The synthesis problem is finding the sequence $x(n)$ whose WVD is closest in some sense to a desired real time-frequency distribution $Y(n, \omega)$ that may or may not represent a valid Wigner-Ville distribution.

If $Y(n, \omega)$ is indeed a valid Wigner-Ville distribution, a direct calculation of the corresponding time-domain sequence $x(n)$ can be accomplished according to [5]

$$x(n+k)x^*(n-k) = \frac{1}{2\pi} \int_{-\pi/2}^{\pi/2} W_x(n, \omega) e^{j2k\omega} d\omega \quad (2)$$

If, however, $Y(n, \omega)$ is not itself a valid WVD, we then wish to find a sequence $x(n)$ whose WVD best approximates $Y(n, \omega)$. This problem is formulated and solved in a least-squares sense by minimizing

$$E(x) = \sum_n \frac{1}{\pi} \int_{-\pi/2}^{\pi/2} |Y(n, \omega) - W_x(n, \omega)|^2 d\omega \quad (3)$$

It was shown in [4] that the even and odd indexed samples of the sequence $x(n)$ could be generated independently by solving the equations

$$C_e x_e = 4 \|x_e\|^2 x_e \quad (4)$$

and

$$C_o x_o = 4 \|x_o\|^2 x_o \quad (5)$$

where x_e and x_o are the eigenvectors corresponding to the largest eigenvalues of C_e and C_o in each equation. C_e and C_o are obtained from $Y(n, \omega)$ according to

$$C_e(p+1, m+1) = y(m+p, p-m) + y^*(m+p, m-p) \quad (6)$$

and

$$C_o(p, m) = y(m+p-1, p-m) + y^*(m+p-1, m-p) \quad (7)$$

where

$$y(n, m) = \frac{1}{\pi} \int_{-\pi/2}^{\pi/2} Y(n, \omega) e^{j\omega n} d\omega \quad (8)$$

The desired sequence $x(n)$ can then be recovered from

$$x_e(n) = x(2n) \quad (9)$$

and

$$x_o(n) = x(2n+1) \quad (10)$$

Although this technique produces a sequence that minimizes the error in (3), the above solution is not unique. Since a multiplication of the even and odd components of $x(n)$ by the phase constants a_e and a_o does not change the sequence's WVD, signal synthesis can only be achieved up to an arbitrary phase in both the even and odd components of the sequence. However, with the presence of a reference signal which is often chosen as the original data sequence, it is possible to find the parameters a_e and a_o that bring the synthesized signal as close as possible to the reference signal by phase matching. That has conventionally been achieved according to

$$a_e = \arg \left[\sum_n s(2n) x_e^*(n) \right] \quad (11)$$

and

$$a_o = \arg \left[\sum_n s(2n+1) x_o^*(n) \right] \quad (12)$$

where $s(n)$ is the reference signal.

However, when the reference signal is composed of the sum of several individual components, and a phase matching of several signals to corresponding components is desired, a least squares solution must be utilized. If the even and odd components of the reference signal in this case are denoted by the vectors s_e and s_o respectively, and x_e and x_o denote matrices with each column being a non phase-matched signal component, a vector containing the desired phase constants of each even and odd component may be obtained according to

$$a_e = \arg \{ x_e^\# s_e \} \quad (13)$$

and

$$a_o = \arg \{ x_o^\# s_o \} \quad (14)$$

where $z^\#$ denotes the pseudo-inverse of z .

III. SELECTION OF THE SYNTHESIZED SIGNAL

It was shown in [4] that two possible approaches can be adapted in the application of t-f distribution synthesis techniques in interference mitigation in spread spectrum communications. The first approach is to synthesize the spread spectrum signal and correlate it with the PN sequence at the receiver, as shown in Fig 1 (a). In the second approach, each jammer component is synthesized from the t-f domain and then subtracted from the incoming data to remove, or at least reduce, the jammer contamination of the desired signal, as depicted in Fig 1 (b).

The preference of using one approach over the other depends on the ability to obtain a synthesized signal which is a good copy of its correspondence in the input data. This requires the signal to be synthesized to have a clear t-f signature that distinguishes it from other components of the received data. Also, phase matching and restoration of the synthesized signal should

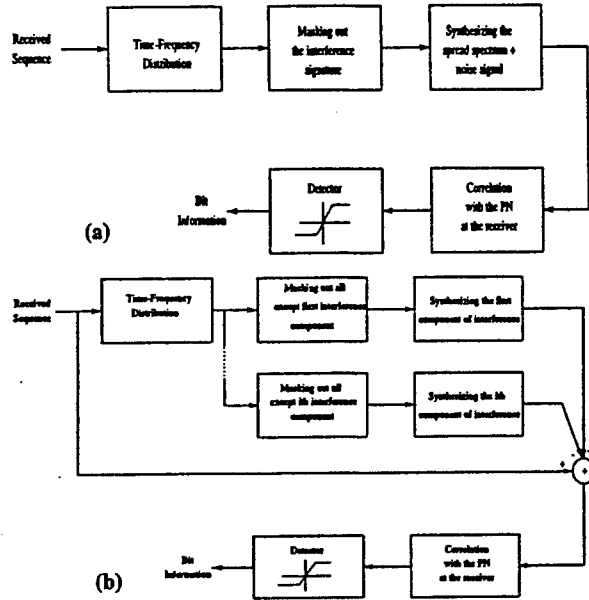


Fig. 1 Two approaches for interference mitigation in DS/SS communication systems (a) synthesizing the desired signal (b) synthesizing the interference

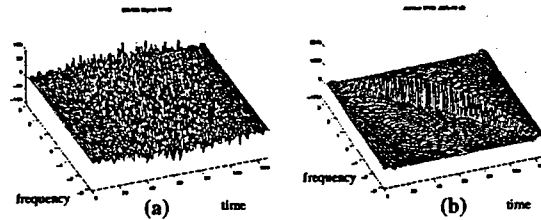


Fig. 2 (a) WVD of the DS/SS signal, $L=128$ (b) WVD of the chirp interference

be properly accomplished.

Figure 2 shows an example of the Wigner-Ville distributions computed separately of a complex DS/SS signal and a linear FM interference. It is straightforward to conclude that synthesizing the spread spectrum signal from the t-f domain should generally be avoided due to the following reasons:

1) It is very difficult to distinguish between the noise and the spread spectrum signal signatures in the time-frequency domain. Therefore, time-varying filtering does not reduce the effect of noise or enhance the SNR.

2) Masking out the jammer by clipping or gating the high power values in the t-f domain may very well remove the main lobe, but it leaves behind the sidelobes which carry significant jammer power.

3) The crossterms between the jammer and both the DS/SS signal and noise as well as the jammer self crossterms are often spread over the entire t-f domain, contaminating the spread spectrum signal within large regions of time and frequency.

4) Phase matching is often performed using the input data as a reference signal. Therefore, even with the assumption that the DS/SS signal is perfectly synthesized up to a phase ambiguity, the low desired signal power will make it very difficult to arrive at the correct phase by a simple matching to a data sequence in

which the jammer is the dominant component.

Proper phase matching can therefore be obtained using the input data as a reference signal only through the second approach, provided that the JSR is relatively high, which is usually the case. It is expected, however, that the effectiveness of phase matching reduces with reduced jammer power.

IV. CONSTANT MODULUS PROJECTION

Let P_A define the constant modulus projection operator which when applied to the complex sequence $x(n)$, the resulting signal, $x_A(n)$, retains the phase of each sample of $x(n)$, but changes its amplitude to a constant value A . This is equivalent to projecting each sample of $x(n)$ on the complex plane onto the closest point of a circle of radius A that is centered at the origin, as depicted in Fig 3. Significant reduction of noise may be achieved through this operation when it is applied to a signal component that is known to be of modulus A , and whose phase can be recovered.

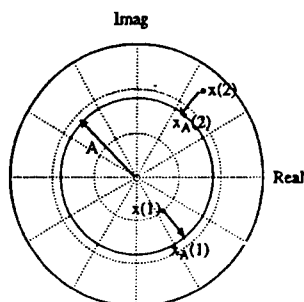


Fig. 3 Constant modulus projection operator (P_A) on the data sequence $x(n)$

In the excision of interference in DS/SS systems, it desirable to subtract an accurate estimate of this interference from the received signal prior to correlation with the PN sequence in order to enhance system performance. As stated in the previous section, a good estimate for this interference may come from synthesizing a masked t-f representation of the received signal. Figure 4 (a) depicts the original time-domain chirp jammer signal, and Fig 4 (b) is the synthesized interference estimate obtained from masking out the signal and noise components in the t-f domain where the JSR = 5 dB. Note that the phase of the even and odd samples are not matched either absolutely to the original jammer or relatively to themselves. After the projection operation is performed on the synthesized jammer estimate, the signal in Fig 4 (c) is produced. Phase matching the projected synthesized jammer produces the final jammer estimate, as shown in Fig 4 (d). It is clear that through the phase matching and constant modulus projection, both the phase and modulus of the jammer estimate are significantly improved.

There are several factors that may inhibit the effectiveness of projecting the jammer estimate onto a constant modulus circle in order to produce an improved estimation. If the value A of the modulus chosen is inaccurate, the projection operation may actually induce extra noise into the estimate of the interference. Also, even with the exact knowledge of A , if the phase of the estimate is inaccurate, projection may prove ineffective.

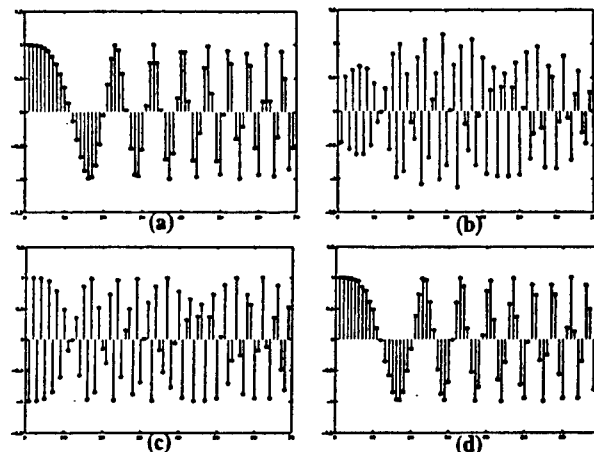


Fig. 4 Re(Jammer estimates) for a complex chirp (a) Original Jammer (b) Masked and synthesized jammer estimate (c) Projection Introduced (d) Phase Matching Introduced

V. MULTI-COMPONENT JAMMERS

When the jammer is composed of more than one component, the technique presented in this paper may still prove effective, provided that each interference term is distinguishable in the t-f domain. In this situation, each jammer component is individually synthesized from the t-f domain and subtracted from the received signal.

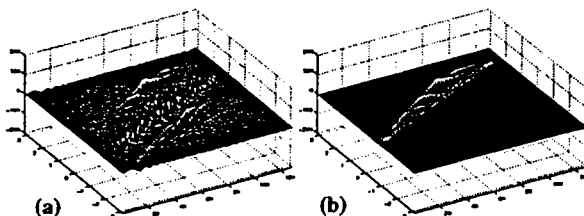


Fig. 5 (a) WVD of interference composed of two terms. Note the jammer crossterms. (b) Only one jammer component retained

The Wigner-Ville distribution of a jammer composed of two widely spaced linear FM signals is shown in Fig 5 (a). Masking so as to retain only one of these components produces the distribution in Fig 5 (b). Synthesizing this masked distribution and performing the projection provides a good estimate for this term. Next, the second jammer component is retained through masking, and is synthesized and projected in the same manner. Phase matching is now performed according to (13) and (14), and estimates for each of the jammer components are obtained. Each of these jammer is now subtracted from the incoming data to provide an effectively jammer-free received signal.

When masking out all but one of the interference terms, care should be taken so as to ensure that none of the jammer crossterms are included in the synthesis procedure. Inclusion of even a small fraction of these crossterms may induce other interference terms into the desired jammer estimate, thus contaminating the overall jammer estimate and hindering system performance.

VI. SIMULATION RESULTS

We now present the results of computer simulations for the methods introduced in this paper. The $L=23$ chips/bit are taken at a sampling frequency of 1 sample/bit for all simulations. In each case, the jammer is a linear FM interference that sweeps the entire frequency band every bit period, and zero-mean, white Gaussian noise is added at an SNR = 0 dB.

Figure 6 gives a benchmark for the rest of the simulations by plotting the bit error rates (BERs) against different JSRs for the case when the preprocessing implementing the t-f interference synthesis is disabled, allowing interference mitigation to be only performed using spreading/despreading operations. Also included in the same figure is the case where the jammer is masked and synthesized with phase-matching, then subtracted from the received signal without the benefit of projection. Note that enabling preprocessing without performing the projection actually increases the overall noise at the receiver at high JSRs, and performance is slightly hindered from the unprocessed case.

Table 1 shows the improvement in system performance when the masked-synthesized jammer estimate is projected onto a circle of constant modulus before it is subtracted from the received signal. This table illustrates the result of projecting the jammer estimate both before and after the phase matching is performed for the case of a single chirped interference. For each column, 800,000 trials were used. It is clear that as the interference increases in power, the estimate of the interference becomes more accurate, and lower bit error rates are produced. For these simulations, the estimated modulus value used by the projection operator was taken by averaging the modulus of the received signal over each time sample. At low JSRs, enabling preprocessing hinders the DS/SS system since the jammer estimate is highly contaminated by the signal and noise. Subtracting this poor jammer estimate actually serves to increase the noise in the signal. It is apparent that the interference mitigation using t-f synthesis techniques prior to correlation with the receiver PN sequence starts to produce improved results over the preprocessing disabled case around a JSR of 9 dB, depending on the nature of the interference.

Also included in Table 1 is the ideal case when the exact amplitude of the jammer is known and can be used to define the constant modulus circle used in the projection operation. This produces a further reduction in BER, as the projection always produces an improved estimation of the interference, and additional noise from the inaccuracy of estimating the amplitude of the projected signal is no longer produced.

It should be noted that simulations were also run using 63 chips/bit. However, with this much processing gain, no errors were produced in 100,000 trials at any of the given JSR values

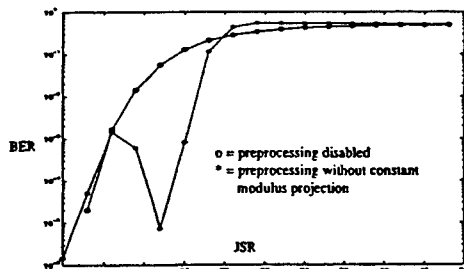


Fig. 6 BER vs. JSR for the preprocessing disabled and for the preprocessing enabled without projection cases

when preprocessing was enabled. Simulation results for the multi-component case are given in [2]

VII. CONCLUSIONS

In this paper, mitigation of multi-component nonstationary interference in DS/SS communication systems is achieved by subtracting an estimate of the interference from the received signal. This estimate is obtained by masking out the SS signal and noise components of the received signal's time-frequency distribution, and synthesizing the result. When the interference is known a priori to be the sum of polynomial phase signals which are uniquely described by their instantaneous frequencies, an improved estimate can be generated by projecting the synthesized jammer component estimates onto circles of their constant modulus values.

Simulations were performed for a linear FM jammer utilizing several processing techniques. It was shown that the lowest BERs were obtained when the jammer estimate was the result of both a projection and a phase matching operation.

REFERENCES

- [1] M. Amin, "Interference mitigation in spread spectrum communication system using time-frequency distribution," IEEE Trans. on SP, vol. 45, pp. 90-102, Jan. 1997.
- [2] M. Amin, et al., "Time-frequency receivers for nonstationary interference excision in spread spectrum communications systems," Technical Report, Rome Lab, April 1998.
- [3] G. F. Boudreaux-Bartels and T. W. Parks, "Time-varying filtering and signal estimation using Wigner Distribution synthesis techniques," IEEE Trans. Acoust., Speech, Signal Processing, vol. ASSP-34, no. 3, pp. 442-451, June 1986.
- [4] S. Lach, M. Amin and A. Lindsey, "Broadband nonstationary interference excision for spread spectrum communications using time-frequency synthesis," Proc. ICASSP98, Seattle, WA, May 1998.
- [5] T. A. C. M. Claassen and W. F. G. Mecklenbrauker, "The Wigner distribution-A tool for time-frequency signal analysis; Part II: Discrete time signals," Phillips J. Res., vol. 35, pp.276-300, 1980.
- [6] L. Milstein and R. Illis, "Signal processing for interference rejection in spread spectrum communications," IEEE SP Magazine, vol. 3, pp. 18-31, April 1986.
- [7] C. Wang and M. Amin, "Performance analysis of instantaneous frequency based interference excision techniques in spread spectrum communications," IEEE Trans. on Signal Processing, January 1998.

JSR	Project Before Phase Match	Project After Phase Match	Project Before onto Exact Mod
0	1	143	1
3	48	1730	40
6	3746	14622	1560
9	314	585	182
12	0	0	0
15	0	0	0
18	8	8	4
21	4	4	1
24	3	3	0
27	1	1	0
30	6	6	4
33	4	4	2
36	9	9	3
39	7	7	3
42	6	6	2
45	5	5	0
48	7	7	2

Table 1 Number of bit errors out of 800,000 trials

Linear Interference Excision in DSSS Communications Using Short Time Fourier Transforms

Short-Time Fourier Transform Receiver for Nonstationary Interference Excision in Direct Sequence Spread Spectrum Communications*

Xuemei Ouyang and Moeness G. Amin

Department of Electrical and Computer Engineering
Villanova University
Villanova, PA 19085
Email: ouyang, moeness@ece.vill.edu

EDICS 2.8.1

ABSTRACT

A new adaptive excision approach for nonstationary interference excision in direct sequence spread spectrum(DS/SS) communications is introduced. The proposed excision approach is based on the attractive localization properties of the impulse responses of the multiple pole filters. These impulse responses have Gaussian-like shapes and decrease in bandwidth with higher pole multiplicities. When used as data windows, they yield a large class of computationally efficient short-time Fourier transforms(STFTs). Localization measures can be applied for determining the optimum window which maximally concentrates the interference in the time-frequency domain. Interference mitigation is then achieved by applying a binary excision mask to the corresponding STFT for each data bit. We show that the proposed interference excision method permits both data-dependent windowing and time-varying filtering, and leads to improved BER performance of the DS/SS system.

*This work is supported by US Air Force, Rome Lab, contract No. F30602-96-C-0077

I. INTRODUCTION

Interference excision in spread spectrum communication is an important problem in both military and civilian applications. There are several techniques which have been proposed for this task. These techniques include adaptive notch filtering, decision feedback[1] and transform domain methods[2]. For jammer signals with broadband frequency characteristics, but yet possess narrowband instantaneous bandwidths, time-frequency methods have been shown to be very effective in improving the receiver performance and reducing the bit error rates. One class of these methods implements linear excisions in which the data is processed using the wavelet transform or M-band/subband filter banks [3,4]. Another class applies bilinear transformations using time-frequency distributions for instantaneous frequency estimation, followed by time-domain excision filtering [5,6].

The short-time Fourier transform (STFT) is a linear time-frequency signal representation which inherently suffers from the trade-off between temporal and spectral resolution [7]. The STFT employing a short data window provides a good temporal resolution, whereas that using a window of long time extent has fine spectral resolution. One solution of this incompatibility problem is to generate a large class of STFTs which employ different windows with distinct characteristics. Some members of this class should be appropriate to describe slowly time-varying signals, while others must be set to provide better localization in rapidly time-varying environments. For a given nonstationary signal, the STFT within this class that yields the best temporal/spectral trade-off, or the highest possible concentration in time-frequency domain, should be chosen for t-f signal representations. Several concentration measures including those introduced in [7, 8] can be used for this purpose.

The application of STFT for interference excision in DS/SS communications using sparse grid

and overdetermined time-frequency tilings is discussed in [9] and [10], respectively. In this paper, we extend the application of the STFT to nonstationary interference mitigation in DS/SS communications. The generation of a class of different short-time Fourier transforms by using a multiple pole infinite impulse response filter, realized in cascading form is considered. Members of this class have sufficient diversity in their temporal/spectral trade-off and are easily updated in time. Further, the STFT using an impulse response of one filter can be recursively generated from those members corresponding to smaller filter orders or pole multiplicities. The choice of the optimum window (impulse response) can be made using localization test criteria such as those discussed in [7,8]. Interference excision is then performed by either clipping or gating the high power values of the optimum window STFT. The process is repeated for each bit or block of data and the choice of the window could therefore vary with time.

We present the analysis of the receiver signal-to-noise ratio, SNR_o , using binary excisions on STFTs. It is shown that different data windows applied to the same jammer waveform will result in a different value of SNR_o . The proper data windows, selected by concentration measures, maximize the jammer localization and thus limit the interference spread in the t-f domain. By confining the jammer to small number of t-f bins, binary excisions can effectively remove the jammer energy, causing a minimum distortion to the spread spectrum signal and, in turn, improving receiver SNR. We stress the fact that not only the jammer power affects the receiver SNR, but also its t-f signature. The best and the worst jammer power distributions in the t-f domain in view of STFT-based interference excision are delineated.

Section II presents the STFT analysis and synthesis method. Multiple pole windows and their temporal/spectral localization properties are discussed in Section III. Section IV summarizes two concentration measures for the optimum data window selection. The overall scheme for the pro-

posed adaptive STFT method for jammer excisions is given in Section V. Receiver SNR analysis for the DS/SS communication system implementing the STFT as jammer excision method is given in Section VI. Performance dependency on the jammer's t-f signature is analyzed in Section VII. Computer simulations showing the BER for both adaptive and fixed window STFT-based interference excisions in DS/SS communication are presented in Section VIII.

II. SHORT-TIME FOURIER TRANSFORM

Short-time Fourier transform can be presented using two perspectives, namely the filter bank and Fourier transform[11]. From the Fourier transform perspective, the STFT $X(n,k)$ of the signal $x(n)$ is given by

$$X(n, k) = \sum_m w(n-m)x(m)e^{-j2\pi mk/N} \quad (1)$$

where k is the frequency sample number, N is the number of total frequency samples, and w is the moving data window. The synthesis method corresponding to the Fourier transform perspective is the Overlap-Add(OLA)[12] method which can be expressed as

$$y(n) = \sum_m \sum_{k=0}^{L-1} X_m(e^{j\omega_k})e^{j\omega_k n} = \sum_m y_m(n) = \sum_m Lx(n)w(m-n) = Lx(n)\sum_m w(m-n) \quad (2)$$

where $y_m(n)$ is the inverse discrete Fourier transform at the time sample m . It can be readily shown that if $w(n)$ is sampled at sufficiently dense rate, then[12]

$$\sum_m w(m-n) = W(e^{j0}), \quad y(n) = Lx(n)W(e^{j0}) \quad (3)$$

It is clear from (3) that without altering the values of the STFT, the synthesized signal is the same as the original signal,

$$x(n) = \frac{y(n)}{LW(e^{j0})} = \frac{1}{LW(e^{j0})} \sum_m \sum_{k=0}^{L-1} X_m(e^{j\omega_k}) e^{j\omega_k n} \quad (4)$$

In many applications, however, it is desired to synthesize a signal from a time-frequency function formed by modifying the STFT. For example, the purpose of the STFT method in DS/SS jammer excision problem is to concentrate the jammer in a small area in t-f domain and remove its t-f signature via a binary mask. The synthesis is then performed on the masked STFT to recover the jammer-free original signal. If the STFT $X(n,k)$ is modified, then the synthesized signal becomes a time-varying convolution between data sequence $x(n)$ and a function $p(n,m)$, which is referred to as a time-varying filter.

III. ORDER RECURSIVE SHORT TIME FOURIER TRANSFORM (ORFT)

The order recursive short-time Fourier transform was introduced in [13] as an approach to generate a large class of STFTs whose members are generated from one another through simple recursions. The recursions are made possible by setting the analysis window $h_k(n)$ equal to the impulse response of a multiple pole linear time-invariant filter. The transfer function of $h_k(n)$ can be expressed in the Z-domain as

$$H_k(z) = \frac{(1-\gamma)^k}{(1-\gamma z^{-1})^k} \quad (5)$$

where γ is the filter pole and the superscript k denotes the pole multiplicity. The corresponding impulse response is given by

$$h_k(n) = (1-\gamma)^k \frac{n(n+k-1)!}{n!(k-1)!} \gamma^n \quad (6)$$

It can be readily shown that the above sequence possesses the recursive property[13]

$$h_k(n) = \gamma h_k(n-1) + (1-\gamma)h_{(k-1)}(n) \quad (7)$$

Using the impulse response (7) as the analysis window in STFT yields a similar recursion

$$F_{k+1}(n, \omega) = \gamma F_{k+1}(n-1, \omega) + (1-\gamma)F_k(n, \omega) \quad (8)$$

where $F_k(n, \omega)$ denotes the STFT which corresponds to the filter order k , calculated at time n and frequency ω . Equation (8) defines the order recursive Fourier transform (ORFT), in which the FT is recursive in both time n and filter order k . The block diagram of ORFT consisting of systems connected in cascade is depicted in Fig.1. The STFTs $F_k(n, \omega)$, $k=1,2,\dots,K$ offer different trade-off between temporal and spectral resolutions. The trade-off is decided by the two variables in the problem, the filter pole and its multiplicity. Fig.2(a) shows the windows corresponding to $k=1,2,\dots,9$ with $\gamma = 0.7$, whereas Fig.2(b) shows the data window for a single pole filter with γ changing over the range $[0.5, 0.9]$. Fig.3 shows the time and frequency characteristics of the window corresponding to different filter orders for $\gamma = 0.9$. It is evident that higher filter order and pole values lead to longer extent data windows, and subsequently, finer spectral resolution. The fast computational property of the members of the above recursive class of STFTs as well as the significant variation of temporal/spectral resolutions as a function of the analysis window parameters makes multiple pole window STFTs as an attractive tool for nonstationary interference excision, as shown below.

IV. CONCENTRATION MEASURE

The main objective of adaptive STFT is to decide, without human intervention or extensive prior knowledge of the underlying signal characteristics, on the analysis window which offers the best time-frequency resolution[14]. Procedures based on mathematical optimal criteria appears

most promising. Renyi information of the third order has been shown to provide a valuable and effective information measure in the context of time-frequency distributions[8],

$$v_1 = -\frac{1}{2} \sum_n \sum_\omega \log \|STFT(n, \omega)\|^3 \quad (9)$$

It is recognized that the maximum value of v_1 in (9) is the one corresponding to the highest t-f concentration of the underlying t-f signal. Using the recursive class of STFTs presented in the previous section, we first proceed to calculate v_1 for all members $F_k(n, \omega)$. The maximum concentration measure is then determined, and the respective STFT is chosen as the most appropriate t-f signal representation.

Another effective local concentration measure was introduced in [7] as:

$$v_2 = \frac{\sum_n \sum_\omega |STFT(n, \omega)|^4}{\left(\sum_n \sum_\omega |STFT(n, \omega)|^2 \right)^2} \quad (10)$$

The basis for choosing the optimum window rests on the intuition that high value of v_2 reflects good time-frequency localization and high resolution. The ratio of the L_4 norm to the L_2 norm of the STFT favors “peaky” distributions that place much of the signal energy into small region of the time-frequency plane, thus achieving a concentrated representation.

Figure.4(a,b,c,d) depicts the STFTs of a chirp jammer signal using three rectangular data windows. The jammer-to-DS/SS signal ratio(JSR) is 20dB, where SNR is set to 0dB. The PN sequence length is set to $L=128$. The values of the two concentration measures as functions of the window length are shown in Fig.4(e). In both cases, the maximum value is reached when the window length is 30 data samples. Indeed, by comparing Fig.4(b,c,d), it is clear that the STFT with window length of 30 samples is more concentrated than the other two based on the window

lengths of 10 and 110 samples. Next, we consider the two cases of sinusoidal and impulse jammers. For both cases, STFTs using rectangular, Hamming, and Hanning windows are computed. For each type of window, the two aforementioned concentration measures are evaluated for different window length. The results for the sinusoidal jammer are shown in Fig.5(a,c), whereas those for impulse jammer are depicted in Fig.5(b,d). For the sinusoid jammer, both measures under all three windows point to the maximum window length as the one leading to the highest t-f concentration. The opposite is true for the impulse jammer. It is clear that both concentration measures (9) and (10) give results consistent with Fourier analysis of windowed signals.

V. ADAPTIVE STFT IN DS/SS SYSTEMS

Fig.6 shows the flow chart describing the steps in implementing the proposed recursive STFT-based interference excision method in PN spread spectrum communications. These steps can be lumped into five consecutive stages: selecting of the analysis window parameters; computing STFTs; selecting the optimum STFT using concentration measures; masking the selected STFT; synthesizing the jammer-free signal; forming the decision variable and detecting the transmitted bit. In this section we expand an important issue relating to window selection and decision variable.

Generating a class of infinite numbers of STFTs is neither feasible or necessary. In the following, we provide a mechanism to set the window parameters γ , K to take a finite number of values consistent with the PN length as well as the required temporal and spectral resolutions. According to [13], the effective window length is defined as

$$L_k = 1 / \left(\sum_{n=0}^{\infty} h_k(n)^2 \right) \quad L_1 = \frac{1+\gamma}{1-\gamma} \quad (11)$$

which increases with increased values of k and γ . Since the minimum value of $L_k(\gamma) = L_{min}$ is obtained at $k=1$, for a given γ , then the highest temporal resolution is achieved when using a single pole filter. By setting $L_1 = L_{min}$, the value of γ can be determined from (11). The maximum effective window length $L_k(\gamma) = L_{max}$ is reached at the maximum multiplicity $k=K$. A reasonable value of L_{max} is the PN sequence length L . In the absence of the closed form expressions for $h_k(\gamma)$, $k>1$, given L and γ , the maximum order K can be numerically determined by computing (11). The relation between γ and K for $L=1024$ is shown in Fig.7. It is evident from this figure that as γ increases, fewer analysis windows can be generated in between L_1 and L_k , which, in turn, narrows down the possible and available choices of the STFTs.

For the detection of the information symbol, the decision variable g can be formed from the correlation

$$g = \sum_{n=0}^{N-1} \hat{x}(n)p^*(n) \quad (12)$$

where, $p(n)$ represents the receiver PN sequence, N is the number of chips per information bit (we assume one sample/chip), and $\hat{x}(n)$ is the synthesized signal. From Section II, if there is no modification made in the t-f domain, then the synthesized signal is equal to the original signal $x(n) = \hat{x}(n)$. By substituting equation (4) in (12), we obtain

$$g = \frac{1}{LW(e^{j\omega_0})} \sum_{k=0}^{L-1} P^*(e^{j\omega_k}) \sum_m X_m(e^{j\omega_k}) \quad (13)$$

where $P(e^{j\omega_k})$ is the discrete Fourier transform of the PN sequence. Since all the functions in (13) are in the transform domain, then the detection can be performed without the need to apply

inverse transformations. If the excision function $A_m(k)$ is applied to the STFT, then the synthesized signal is modified to

$$y(n) = \sum_m \sum_{k=0}^{L-1} A_m(k) X_m(e^{j\omega_k}) e^{j\omega_k n} \quad (14)$$

In this case,

$$g = \frac{1}{LW(e^{j0})} \sum_{k=0}^{L-1} P^*(e^{j\omega_k}) \sum_m A_m(k) X_m(e^{j\omega_k}) \quad (15)$$

The scheme to perform the correlation in the time domain and the transform domain, respectively given by (12) and (15), is depicted in Fig.8(a),(b). The STFT domain detection scheme allows computational saving in two ways. First, the time domain correlation requires m inverse DFT to be performed, whereas only one DFT operation is required for the PN sequence in (15). Second, if the PN sequence is repetitive, its DFT remains fixed for every bit, which in turn reduces on-line computations in the correlation scheme of Fig.8(b).

VI. RECEIVER SNR

If bit “1” is transmitted, then the baseband received signal can be expressed as*

$$r(i) = p(i) + j(i) + n(i) \quad (16)$$

where $\{p(i)\}$ represents the PN sequence, which is known to both the transmitter and the receiver, $\{j(i)\}$ is the jammer sequence, which is of zero-mean and covariance $\{R_j(i)\}$, and $\{n(i)\}$ is an additive white Gaussian noise sequence with zero mean and variance σ_n^2 . It is assumed that the above three sequences are uncorrelated. The decision variable at the output of the correlator is

*In this section, we use r in place of x to represent the received signal.

given by

$$g = \sum_{i=0}^{L-1} r(i)p(i) \quad (17)$$

If jammer excision is performed prior to despreading, then the received signal is modified to $r'(i)$, and the corresponding decision variable becomes

$$g' = \sum_{i=0}^{L-1} r'(i)p(i) \quad (18)$$

The receiver SNR is often used as a performance measure. It is defined in [15] as

$$SNR_o = \frac{E^2[g']}{var[g']} \quad (19)$$

The primary objective of all interference excision techniques in spread spectrum communication is to maximize SNR_o for a large class of interfering signals. The STFT-based interference excision system is most effective in mitigating jammers which can be highly localized in the t-f domain.

The signal synthesis from the STFT can be simply performed using the overlap-add(OLA) method described in Section II. If the binary excision function $A_m(k)$ is applied to the STFT at time m and frequency k , then the synthesized signal is modified to

$$\begin{aligned} r'(n) &= \frac{1}{LW(e^{j0})} \sum_m \sum_{k=0}^{L-1} A_m(k) R_m(e^{j\omega_k}) e^{j\omega_k n} \\ &= \frac{1}{LW(e^{j0})} \sum_m \sum_{k=0}^{L-1} \sum_{l=0}^{L-1} A_m(k) r(l) w_m(l) e^{j\omega_k(n-l)} \end{aligned} \quad (20)$$

where R and W are the DFTs of the received signal and the data window, $w_m(l)$, respectively.

From (19) and (20), the decision variable can be expressed by the sum of three different terms corresponding to the three components of the input data,

$$\begin{aligned}
g' &= \frac{1}{LW(e^{j0})} \sum_{n=0}^{L-1} \sum_m \sum_{k=0}^{L-1} \sum_{l=0}^{L-1} A_m(k) w_m(l) e^{j\omega_k(n-l)} p(l) p(n) \\
&+ \frac{1}{LW(e^{j0})} \sum_{n=0}^{L-1} \sum_m \sum_{k=0}^{L-1} \sum_{l=0}^{L-1} A_m(k) w_m(l) e^{j\omega_k(n-l)} j(l) p(n) \\
&+ \frac{1}{LW(e^{j0})} \sum_{n=0}^{L-1} \sum_m \sum_{k=0}^{L-1} \sum_{l=0}^{L-1} A_m(k) w_m(l) e^{j\omega_k(n-l)} n(l) p(n) \\
&= g'_1 + g'_2 + g'_3
\end{aligned} \tag{21}$$

Since the three components of r are independent, then

$$E(g') = E(g'_1) + E(g'_2) + E(g'_3) \quad \text{var}(g') = \text{var}(g'_1) + \text{var}(g'_2) + \text{var}(g'_3) \tag{22}$$

The mean values in (22) are derived in Appendix A and are given by

$$E(g'_1) = \frac{1}{LW(e^{j0})} \sum_{n=0}^{L-1} \sum_m \sum_{k=0}^{L-1} A_m(k) w_m(n) \quad E(g'_2) = E(g'_3) = 0 \tag{23}$$

whereas the variances in (22), as shown in Appendix A, are given by

$$\text{var}(g'_1) = 0 \tag{24}$$

$$\text{var}(g'_2) = \frac{1/L}{W^2(e^{j0})} \sum_m \sum_{k=0}^{L-1} \sum_{l=0}^{L-1} \sum_{m_1} \sum_{l_1=0}^{L-1} A_m(k) A_{m_1}(k) w_m(l) w_{m_1}(l_1) R_j(l, l_1) e^{-j\omega_k(l-l_1)} \tag{25}$$

$$\text{var}(g'_3) = \frac{\sigma_n^2/L}{W^2(e^{j0})} \sum_m \sum_{k=0}^{L-1} \sum_{l=0}^{L-1} \sum_{m_1} A_m(k) A_{m_1}(k) w_m(l) w_{m_1}(l) \tag{26}$$

Using equations (22-26), the receiver SNR_o is given by

$$SNR_o = \frac{E^2[g'_1]}{\text{var}(g'_2) + \text{var}(g'_3)} \tag{27}$$

If there is no jammer excision, then $A_m(k)=1$ and the above expression simplifies to the well

known formula[16]

$$SNR_{wo} = \frac{(L^2 W(e^{j0}))^2 / L}{L^2 R_j(0) W^2(e^{j0}) + L^2 \sigma_n^2 W^2(e^{j0})} = \frac{L}{R_j(0) + \sigma_n^2} \quad (28)$$

In order to gain insights into the SNR_o in (27), we examine, in the following, the two specific cases of impulse and sinusoidal jammers.

A. Impulse Jammer

If the jammer is an impulse, i.e., $j(i) = \delta(i - i_0)$, the SNR_o takes the form

$$SNR_o = \frac{(1/L) \left(\sum_{n=0}^{L-1} \sum_{m=0}^{L-1} \sum_{k=0}^{L-1} A_m(k) w_m(n) \right)^2}{\sum_{m=0}^{L-1} \sum_{m_1=0}^{L-1} \sum_{k=0}^{L-1} A_m(k) A_{m_1}(k) w_m(i_0) w_{m_1}(i_0) + \sigma_n^2 \sum_{m=0}^{L-1} \sum_{k=0}^{L-1} \sum_{l=0}^{L-1} \sum_{m_1=0}^{L-1} A_m(k) A_{m_1}(k) w_m(l) w_{m_1}(l)} \quad (29)$$

All signals in the t-f region (m,k) , $m \in Q$, where Q is a set of integer values chosen from $[1,L]$, is removed by setting the binary coefficients $A_m(k)=0$, $m \in Q$, whereas all signals in the complement t-f region (m,k) , $m \in \bar{Q}$ is left intact by setting the binary coefficients $A_m(k)=1$, $m \in \bar{Q}$. These two conditions simplify equation (29) to the form below

$$SNR_o = \frac{\left(\sum_{m \in \bar{Q}} W_m(0) \right)^2}{\left(\sum_{m \in \bar{Q}} w_m(i_0) \right)^2 + \sigma_n^2 \left\{ \left(\sum_{m \in \bar{Q}} W_m(0) \right)^2 + \sum_{m \in \bar{Q}} \sum_{m_1 \in \bar{Q}, m \neq m_1} \sum_{l=0}^{L-1} w_m(l) w_{m_1}(l) \right\}} \quad (30)$$

Two important observations about SNR_o in (30) are in order: 1) the first summation term in the denominator is zero if $i_0 \in Q$, and the span of the data window is equal to or smaller than that of

the t-f strip $m \in Q$. 2) the term with overlapping windows in the denominator takes a minimum value if $w_m(i) = \delta(m - i)$, i.e., the window is a unit sample sequence. In this case, SNR_o reaches its maximum value

$$SNR_o = \frac{(L-1)}{\sigma_n^2} \quad (31)$$

In (31), the jammer is entirely removed with the cost of only decreasing the processing gain by one. For high spread spectrum processing gain, $L \gg 1$, jammer removal causes insignificant change in SNR_o .

B. Sinusoidal Jammer

If the jammer is a sinusoidal function, $j(i) = Be^{j\frac{2\pi}{L}k_0 i}$, then the corresponding DFT is $B\delta(k - k_0)$. In this case, it can be readily shown that the DS/SS receiver SNR implementing STFT is given by

$$SNR_o = \frac{(1/L) \left(\sum_{n=0}^{L-1} \sum_m \sum_{k=0}^{L-1} A_m(k) w_m(n) \right)^2}{D_1 + D_2} \quad (32)$$

where

$$D_1 = B^2 \sum_m \sum_{k=0}^{L-1} \sum_{m_1} A_m(k) A_{m_1}(k) W_m(k - k_0) W_{m_1}(k - k_0)$$

and

$$D_2 = \sigma_n^2 \sum_m \sum_{k=0}^{L-1} \sum_{l=0}^{L-1} \sum_{m_1} A_m(k) A_{m_1}(k) w_m(l) w_{m_1}(l)$$

If we only set the peak value of the STFT at the frequency $k=k_0$ to zero, i.e., $A_m(k_0)=0$ and

$A_m(k)=1, k \neq k_0$, then equation (32) simplifies to

$$SNR_o = \frac{(1/L)(L-1)^2 L^2 W^2(e^{j0})}{B^2 \sum_m \sum_{k=0, k \neq k_0}^{L-1} \sum_{m_1} W_m(k-k_0) W_{m_1}(k-k_0) + \sigma_n^2 (L-1) L W^2(e^{j0})} \quad (33)$$

It should be noted that by doing so, the jammer is not totally removed, as evident by the appearance of B^2 in the denominator of equation (33). The entire removal of the jammer can, however, be achieved by setting $W_m(k-k_0) = 0, k \neq k_0$, which amounts to using a rectangular data window with the appropriate length. In this case, SNR_o is maximized and given by

$$SNR_o = \frac{(L-1)}{\sigma_n^2} \quad (34)$$

On the other hand, if the jammer frequency does not coincide with any of the STFT frequency bins, then its power leaks over the entire t-f plane. Mitigating the interference in this case may be achieved by carefully selecting the region of highest jammer concentration and setting the corresponding coefficients $A_m(k)$ to zero. If C denotes the jammer power remained after setting q t-f bins to zero, then the receiver SNR_o becomes

$$SNR_o = \frac{(L-q)}{C + \sigma_n^2} \quad (35)$$

The trade-off between jammer removal and desired signal distortion is evident in equation (35). As the number of t-f binary coefficients assuming zero-value increases, i.e., q increases, the numerator is reduced, but also less jammer power is retained, i.e., C decreases.

VII PERFORMANCE DEPENDENCY ON JAMMER SIGNITURE

The main purpose of this section is to highlight the fact that the receiver performance not only

depends on the number of t-f bins contaminated by the jammer signature, but also on where these bins lie in the time-frequency domain. Suppose the jammer occupies L t-f bins, which are to be removed by proper masking. The following analysis shows that the positions of these L bins significantly influence the SNR performance.

Under the assumption that the jammer is entirely removed by setting the corresponding M t-f binary coefficients to zeros, equation (27) simplifies to

$$SNR_o = \frac{\left(\sum_{n=0}^{L-1} \sum_{k=0}^{L-1} \left(\sum_m A_m(k) w_m(n) \right) \right)^2}{L \sigma_n^2 \sum_{k=0}^{L-1} \sum_{l=0}^{L-1} \left(\sum_m A_m(k) w_m(l) \right) \left(\sum_{m_1} A_{m_1}(k) w_{m_1}(l) \right)} \quad (36)$$

The numerator of SNR_o can be expressed in matrix form as

$$Numerator = W^2(0) \left[\begin{matrix} 1 & 1 & \dots & 1 \end{matrix} \right] \left[\begin{matrix} A_1(0) & A_2(0) & \dots & A_M(0) \\ A_1(1) & A_2(1) & \dots & A_M(1) \\ \vdots & \vdots & \ddots & \vdots \\ A_1(L-1) & A_2(L-1) & \dots & A_M(L-1) \end{matrix} \right] \left[\begin{matrix} 1 \\ 1 \\ \vdots \\ 1 \end{matrix} \right]^2 = W^2(0) (c' A c)^2 \quad (37)$$

where c is a vector whose elements are all ones. The denominator in (36) can be expressed as

$$Denominator = L \delta_n^2 trace[B R_w]$$

where B is the product of the binary excision coefficient matrix

$$B = \left[\begin{matrix} A_1(0) & A_1(1) & \dots & A_1(L-1) \\ A_2(0) & A_2(1) & \dots & A_2(L-1) \\ \vdots & \vdots & \ddots & \vdots \\ A_M(0) & A_M(1) & \dots & A_M(L-1) \end{matrix} \right] \left[\begin{matrix} A_1(0) & A_2(0) & \dots & A_M(0) \\ A_1(1) & A_2(1) & \dots & A_M(1) \\ \vdots & \vdots & \ddots & \vdots \\ A_1(L-1) & A_2(L-1) & \dots & A_M(L-1) \end{matrix} \right] = A^T A \quad (38)$$

Similarly, R_w is the window correlation matrix,

$$R_w = \begin{bmatrix} \sum_{l=0}^{L-1} w^2(l) & \sum_{l=0}^{L-2} w(l)w(l+1) & \dots & w(0)w(L-1) \\ \sum_{l=0}^{L-2} w(l)w(l+1) & \ddots & \ddots & \vdots \\ \vdots & \ddots & \ddots & \sum_{l=0}^{L-2} w(l)w(l+1) \\ w(0)w(L-1) & \dots & \sum_{l=0}^{L-2} w(l)w(l+1) & \sum_{l=0}^{L-1} w^2(l) \end{bmatrix} \quad (39)$$

Suppose the jammer is concentrated in M t-f bins. By setting the corresponding excision values to zero, then

$$\text{Numerator} = \left(W(0) \times \sum_{k=0}^{L-1} \sum_{m=1}^M A_m(k) \right)^2 = ((L-1)MW(0))^2 \quad (40)$$

$$\begin{aligned} \text{Denominator} = & \sum_{i=1}^L B(i, i) \sum_{l=0}^{L-1} w^2(l) + 2 \sum_{i=1}^{L-1} B(i, i+1) \sum_{l=0}^{L-2} w(l)w(l+1) + \dots \\ & + 2B(1, L)w(0)w(L-1) \end{aligned} \quad (41)$$

From (40) and (41), since the optimum window is assumed to have already been selected, the only parameters that can affect SNR are the elements of B matrix $B(i, j)$, where

$$B(i, j) = \begin{bmatrix} A_i(0) & A_i(1) & \dots & A_i(L-1) \end{bmatrix} \begin{bmatrix} A_j(0) \\ A_j(1) \\ \vdots \\ A_j(L-1) \end{bmatrix} \quad (42)$$

With nonnegative analysis window, the maximum values of the denominator is achieved by maximizing each summation coefficient in (41). The maximum values of

$\sum_{i=1}^{L-j+1} B(i, i+j), j = 0, 1, \dots, L-1$ are obtained when all the elements along one column of \mathbf{A}

are zeros, i.e.

$$\mathbf{A} = \begin{bmatrix} A_1(0) & A_1(1) & \dots & 0 & \dots & A_1(L-1) \\ A_2(0) & A_2(1) & \dots & 0 & \dots & A_2(L-1) \\ \vdots & \vdots & \ddots & \vdots & \ddots & \vdots \\ A_M(0) & A_M(1) & \dots & 0 & \dots & A_M(L-1) \end{bmatrix}$$

which corresponds to a single tone jammer. In this case, equation (41) becomes

$$\begin{aligned} \text{Denominator} = & M(L-1) \sum_{l=0}^{L-1} w^2(l) + 2(M-1)(L-1) \sum_{l=0}^{L-2} w(l)w(l+1) + \dots \\ & + 2(L-1)w(0)w(L-1) \end{aligned} \quad (43)$$

An important conclusion that can be drawn from above analysis is that, for all jammers which occupy M t-f bins, a single tone interference results in the smallest SNR, i.e., the worst receiver performance.

The above analysis cannot be applied to examine the interference signature leading to the best receiver performance. It should be noted that the solution space of \mathbf{A} is discrete. Therefore, the best or worst performance cannot be achieved via constrained minimum mean square error optimization methods. In the underlying problem, exhaustive search of all possible combinations of “1” and “0” can be used to obtain the performance bounds. We have consistently found that, independent of the PN sequence length, the highest SNR_0 is achieved when the interference has the orthogonal signature of that of the minimum SNR_0 , i.e., the jammer puts all of its power into one time slice, which describes an impulse form of jamming.

One interpretation of the above result lies in the fact that for STFT, due to the moving win-

dow, yields a redundancy in the information along the time axis, yet there is no redundancy along the frequency axis. If the data in one time slice is removed, the adjacent time slice will still include most of the data samples, depending on the overlapping pattern of the moving window. As long as the overlap is not sparse, the information lost is insignificant. The signal may, however, encounter some energy attenuation. This kind of binary excision will not substantially decrease the receiver performance although some degradation to the SNR_0 may occur. On the other hand, if the data in one frequency bin is removed, the information at that frequency is lost and cannot be recovered in the synthesis procedure. In this case, the SNR suffers the largest degradation.

VIII. SIMULATIONS

The first simulation example deals with the generation of the best STFT over a finite number of analysis windows defined by the recursive class discussed in Section III. A synthetic signal which contains impulse, sinusoid and chirp components is generated. The result of using the optimum window selections is shown in Fig.9(a). The optimum window changes over different parts of the jammer signal according to the changes in the Renyi concentration measure. For comparison, three STFTs with fixed window lengths are shown in Fig.9(b,c,d), in which the impulse, the sinusoid, and the chirp signals separately exhibit good time-frequency resolution.

In the second simulation example, we implement the proposed jammer excision scheme and compute the respective BER. The signal is BPSK and the jammer over every information symbol randomly selects one out of three forms, an impulse, a sinusoid and a chirp signal. The BER curve is shown in Fig.10. For comparison, the BER curves with fixed window of $k=1$ and $k=5$ are also given in Fig.10. It is evident from this figure that the proposed adaptive method offers improved

interference excision performance.

CONCLUSIONS

In this paper, a new adaptive time-frequency technique for interference excision in direct sequence spread spectrum communication was introduced. The proposed technique implements recursive analysis windows to allow efficient generation of a large class of STFTs with different spectral/temporal resolution properties. Concentration measures were applied to select the analysis window with the best jammer time-frequency power concentration. Central to our contribution is the demonstration that the strength as well as the localization of the jammer power in the t-f domain affects the STFT receiver performance. This demonstration underscores the fact that knowledge of the type of the interference excision system deployed at the receiver can be used by the jammer to reduce the system effectiveness in interference suppression. The paper presented simulation examples to illustrate the advantage of the proposed adaptive STFT excision approach over its fixed-window STFT counterpart.

APPENDIX A

In order to obtain the mean value and the variance of the decision variable, we recall

$$E(p(l)p(n)) = \delta(n-l), E(j(l)p(n)) = E(j(l))E(p(n)) = 0$$

$$E(n(l)p(n)) = E(n(l))E(p(n)) = 0$$

$$\begin{aligned} E(g'_1) &= \frac{1}{LW(e^{j0})} \sum_{n=0}^{L-1} \sum_{m=0}^{L-1} \sum_{k=0}^{L-1} \sum_{l=0}^{L-1} A_m(k) w_m(l) e^{j\omega_k(n-l)} E(p(l)p(n)) \\ &= \frac{1}{LW(e^{j0})} \sum_{n=0}^{L-1} \sum_{m=0}^{L-1} \sum_{k=0}^{L-1} A_m(k) w_m(n) \end{aligned} \quad (\text{A.1})$$

$$E(g'_2) = \frac{1}{LW(e^{j0})} \sum_{n=0}^{L-1} \sum_{m=0}^{L-1} \sum_{k=0}^{L-1} \sum_{l=0}^{L-1} A_m(k) w_m(l) e^{j\omega_k(n-l)} E(j(l)p(n)) = 0 \quad (\text{A.2})$$

$$E(g'_3) = \frac{1}{LW(e^{j0})} \sum_{n=0}^{L-1} \sum_{m=0}^{L-1} \sum_{k=0}^{L-1} \sum_{l=0}^{L-1} A_m(k) w_m(l) e^{j\omega_k(n-l)} E(n(l)p(n)) = 0 \quad (\text{A.3})$$

The variance,

$$E(g_1'^2) = \left(\frac{1}{LW(e^{j0})} \right)^2 \sum_{n=0}^{L-1} \sum_{m=0}^{L-1} \sum_{k=0}^{L-1} \sum_{l=0}^{L-1} \sum_{n_1=0}^{L-1} \sum_{m_1=0}^{L-1} \sum_{k_1=0}^{L-1} \sum_{l_1=0}^{L-1} A_m(k) A_{m_1}(k_1) w_m(l) w_{m_1}(l_1) e^{j\omega_k(n-l)} e^{-j\omega_{k_1}(n_1-l_1)} E(p(l)p(n)p(l_1)p(n_1)) \quad (\text{A.4})$$

Since $E(p(l)p(n)p(l_1)p(n_1)) = \delta(l-n)\delta(l_1-n_1)$, then

$$E(g_1'^2) = \left(\frac{1}{LW(e^{j0})} \right)^2 \sum_{n=0}^{L-1} \sum_{m=0}^{L-1} \sum_{k=0}^{L-1} \sum_{n_1=0}^{L-1} \sum_{m_1=0}^{L-1} \sum_{k_1=0}^{L-1} A_m(k) A_{m_1}(k_1) w_m(n) w_{m_1}(n_1) = \left(\frac{1}{LW(e^{j0})} \right)^2 \left(\sum_{n=0}^{L-1} \sum_{m=0}^{L-1} \sum_{k=0}^{L-1} A_m(k) w_m(n) \right)^2 \quad (\text{A.5})$$

$$\begin{aligned} E(g_2'^2) &= \left(\frac{1}{LW(e^{j0})} \right)^2 \sum_{n=0}^{L-1} \sum_{m=0}^{L-1} \sum_{k=0}^{L-1} \sum_{l=0}^{L-1} \sum_{n_1=0}^{L-1} \sum_{m_1=0}^{L-1} \sum_{k_1=0}^{L-1} \sum_{l_1=0}^{L-1} A_m(k) A_{m_1}(k_1) w_m(l) w_{m_1}(l_1) \\ &\quad (l_1) e^{j\omega_k(n-l)} e^{-j\omega_{k_1}(n_1-l_1)} E(j(l)j(l_1)) E(p(n)p(n_1)) \\ &= \left(\frac{1}{LW(e^{j0})} \right)^2 \sum_{n=0}^{L-1} \sum_{m=0}^{L-1} \sum_{k=0}^{L-1} \sum_{l=0}^{L-1} \sum_{m_1=0}^{L-1} \sum_{k_1=0}^{L-1} \sum_{l_1=0}^{L-1} A_m(k) A_{m_1}(k_1) w_m(l) w_{m_1}(l_1) \\ &\quad R_j(l, l_1) e^{j\omega_k(n-l)} e^{-j\omega_{k_1}(n-l_1)} \\ &= L \left(\frac{1}{LW(e^{j0})} \right)^2 \sum_{m=0}^{L-1} \sum_{k=0}^{L-1} \sum_{l=0}^{L-1} \sum_{m_1=0}^{L-1} \sum_{k_1=0}^{L-1} A_m(k) A_{m_1}(k_1) w_m(l) w_{m_1}(l_1) R_j(l, l_1) e^{-j\omega_k(l-l_1)} \quad (\text{A.6}) \end{aligned}$$

$$\begin{aligned}
E(g_3'^2) &= \left(\frac{1}{LW(e^{j0})} \right)^2 \sum_{n=0}^{L-1} \sum_{m=0}^{L-1} \sum_{k=0}^{L-1} \sum_{l=0}^{L-1} \sum_{n_1=0}^{L-1} \sum_{m_1=0}^{L-1} \sum_{k_1=0}^{L-1} \sum_{l_1=0}^{L-1} A_m(k) A_{m_1}(k_1) w_m(l) w_{m_1}(l_1) \\
&\quad e^{j\omega_k(n-l)} e^{-j\omega_{k_1}(n_1-l_1)} E(n(l)n(l_1)) E(p(n)p(n_1)) \\
&= \left(\frac{\sigma_n}{LW(e^{j0})} \right)^2 \sum_{m=0}^{L-1} \sum_{k=0}^{L-1} \sum_{l=0}^{L-1} \sum_{m_1=0}^{L-1} \sum_{k_1=0}^{L-1} A_m(k) A_{m_1}(k_1) w_m(l) w_{m_1}(l) e^{-j(\omega_k - \omega_{k_1})l} \sum_{n=0}^{L-1} e^{j(\omega_k - \omega_{k_1})n} \\
&= L \left(\frac{\sigma_n}{LW(e^{j0})} \right)^2 \sum_{m=0}^{L-1} \sum_{k=0}^{L-1} \sum_{l=0}^{L-1} \sum_{m_1=0}^{L-1} A_m(k) A_{m_1}(k) w_m(l) w_{m_1}(l) \quad (A.7)
\end{aligned}$$

$$\begin{aligned}
\text{var}(g_1') &= E(g_1'^2) - E^2(g_1') = \left(\frac{1}{LW(e^{j0})} \right)^2 \left(\sum_{n=0}^{L-1} \sum_{m=0}^{L-1} \sum_{k=0}^{L-1} A_m(k) w_m(n) \right)^2 \\
&\quad \left(\frac{1}{LW(e^{j0})} \sum_{n=0}^{L-1} \sum_{m=0}^{L-1} \sum_{k=0}^{L-1} A_m(k) w_m(n) \right)^2 = 0 \quad (A.8)
\end{aligned}$$

$$\begin{aligned}
\text{var}(g_2') &= E(g_2'^2) - E^2(g_2') \\
&= L \left(\frac{1}{LW(e^{j0})} \right)^2 \sum_{m=0}^{L-1} \sum_{k=0}^{L-1} \sum_{l=0}^{L-1} \sum_{m_1=0}^{L-1} \sum_{k_1=0}^{L-1} A_m(k) A_{m_1}(k) w_m(l) w_{m_1}(l) R_j(l, l_1) e^{-j\omega_k(l-l_1)} \quad (A.9)
\end{aligned}$$

$$\text{var}(g_3') = E(g_3'^2) - E^2(g_3') = L \left(\frac{\sigma_n}{LW(e^{j0})} \right)^2 \sum_{m=0}^{L-1} \sum_{k=0}^{L-1} \sum_{l=0}^{L-1} \sum_{m_1=0}^{L-1} A_m(k) A_{m_1}(k) w_m(l) w_{m_1}(l) \quad (A.10)$$

References

- [1] J. Laster and J. Reed, "Interference rejection in digital wireless communication," *IEEE signal processing magazine*, pp. 37-62, May 1997.
- [2] L. Milstein and P. Das, "An analysis of a real-time transform domain filtering digital communication system--part I: narrow-band interference rejection," *IEEE Trans. on Comm.*, pp. 816-824, vol. 28, no. 6, June 1980.

- [3] M. Medley, G. Saulnier, and Das, "Applications of the wavelet transform in spread spectrum communications systems," *SPIE, Wavelet Applic.*, Orlando, FL, April 1994.
- [4] M. Tazebay and A. Akansu, "Adaptive subband transforms in time-frequency excisers for DSSS communication systems," *IEEE Trans. on SP*, pp. 2776-2782, November 1995.
- [5] M. Amin, "Interference mitigation in spread spectrum communications using time-frequency distributions," *IEEE Trans. on SP*, vol. 45, no. 1, January 1996.
- [6] C. Wang and M. Amin, "Performance analysis of instantaneous frequency-based interference excision techniques in spread spectrum communications," *IEEE Trans. on SP*, vol. 46, no. 1, January 1998.
- [7] D. Jones and T. Parks, "A high resolution data-adaptive time-frequency representation," *IEEE Trans. on ASSP*, vol. 38, pp. 2127-2135, December 1990.
- [8] W. Williams, M. Brown, and A. Hero, "Uncertainty, information and time-frequency distributions," *SPIE*, vol. 1566, pp. 144-156, 1991.
- [9] S. Roberts and M. Amin, "Linear vs. bilinear time-frequency methods for interference mitigation in direct sequence spread spectrum communication systems," *Asilomar Conf. on Signals, Systems and Computers*, Pac. Grove, Ca, November 1995.
- [10] B. Krongold, M. Kramer, K. Ramchandran and D. Jones, "Spread spectrum interference suppression using adaptive time-frequency tilings," *Proceedings of ICASSP*, Munich, Germany, April 1997.
- [11] J. Lim and A. Oppenheim, *Advanced Topics in Signal Processing*, Chapter 6, Prentice Hall, Englewood Cliffs, New Jersey, 1988.
- [12] J. Allen and L. Rabiner, "A unified approach to short-time Fourier analysis and synthesis," *Proc. IEEE*, vol. 65, no. 11, November 1977.
- [13] M. Amin and K. Feng, "Short-time Fourier transform using cascade filter structures," *IEEE Transactions on Circuits and Systems*, vol. 42, pp. 631-641, October 1995.
- [14] D. Jones and R. Baraniuk, "A simple scheme for adapting time-frequency representations," *IEEE Trans. on SP*, vol. 42, December 1994.
- [15] F. M. Hsu and A. A. Giordano, "Digital whitening techniques for improving spread spectrum communications performance in the presence of narrow-band jamming and interference," *IEEE trans. Comm.*, vol. COM-26, pp. 209-216, February 1978.
- [16] J. Ketchum and J. Proakis, "Adaptive algorithms for estimating and suppressing narrowband interference in PN spread spectrum systems," *IEEE Trans. on Comm.*, May 1982.

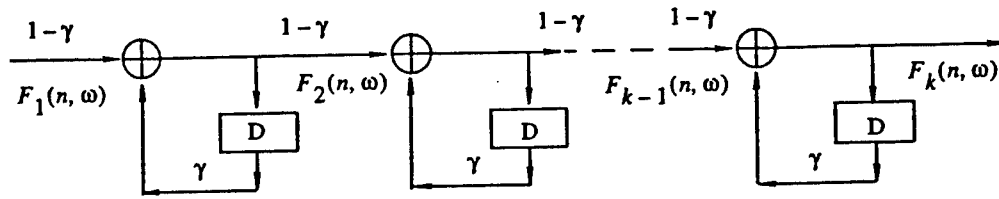
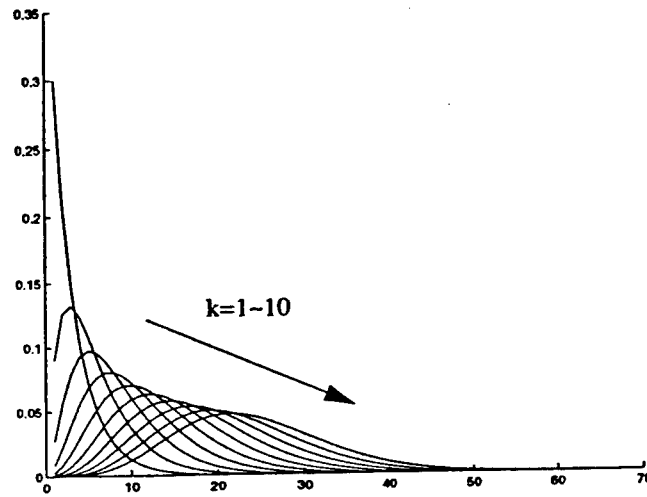
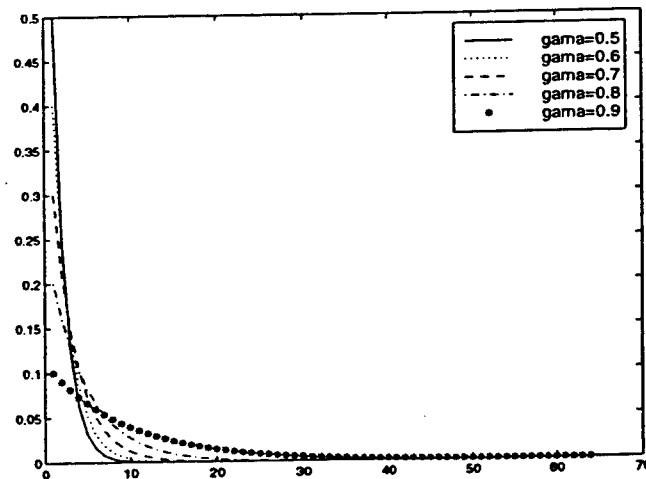


Fig.1 Order recursive Fourier transform

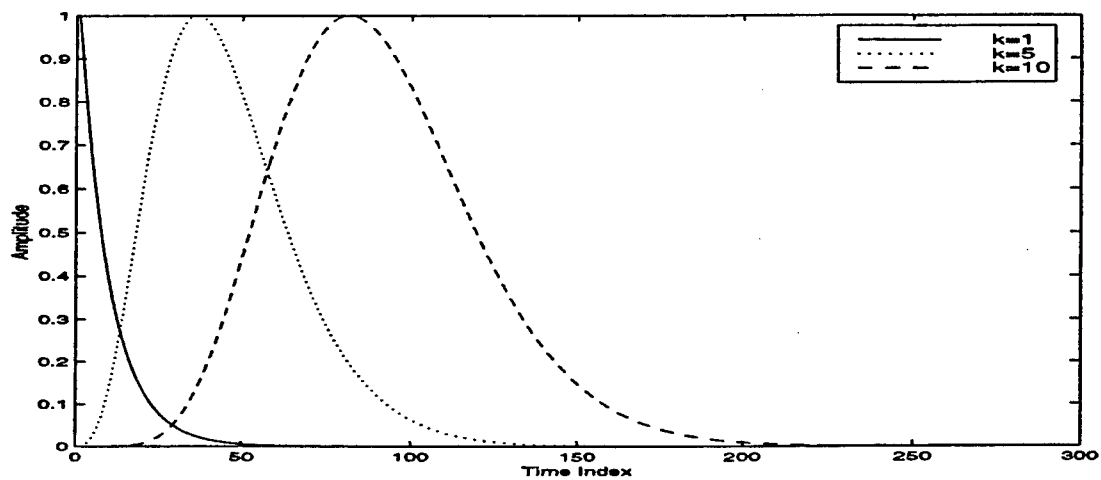


(a)

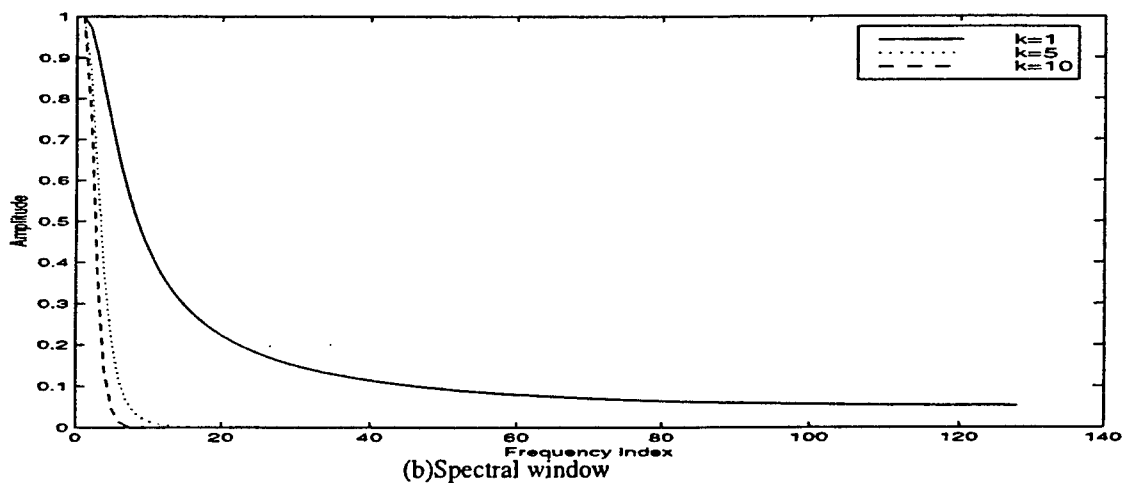


(b)

Fig.2 pole position and order effect on the impulse response. (a) order effect when $\gamma = 0.7$; (b) pole position effect when order fixed ($k=1$)



(a) Impulse response



(b) Spectral window

Fig.3 Time and spectral windows(normalized) for multiple-pole filters $\gamma = 0.9$

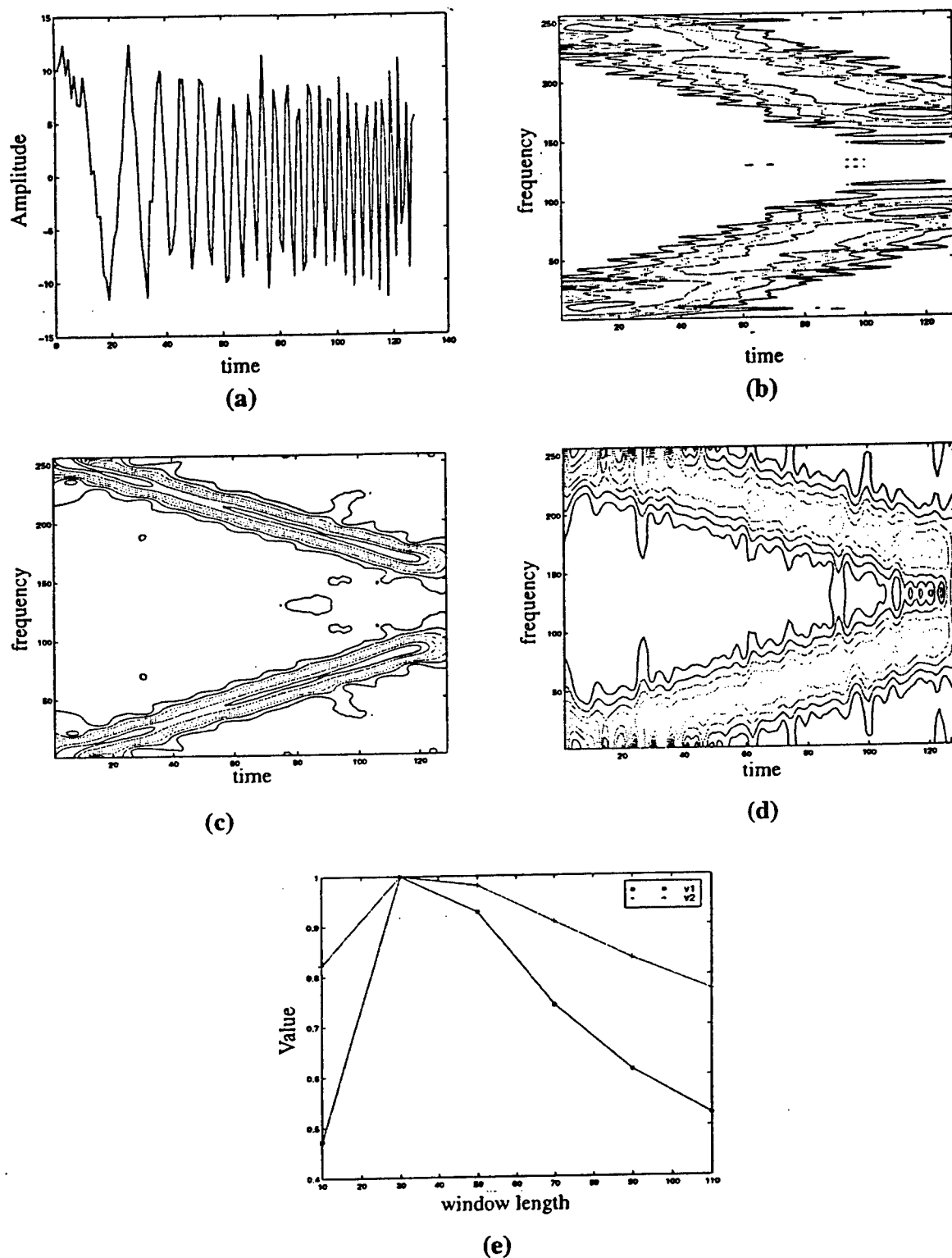
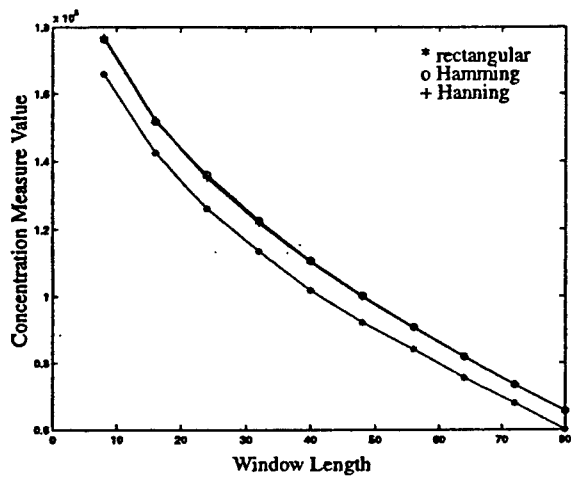
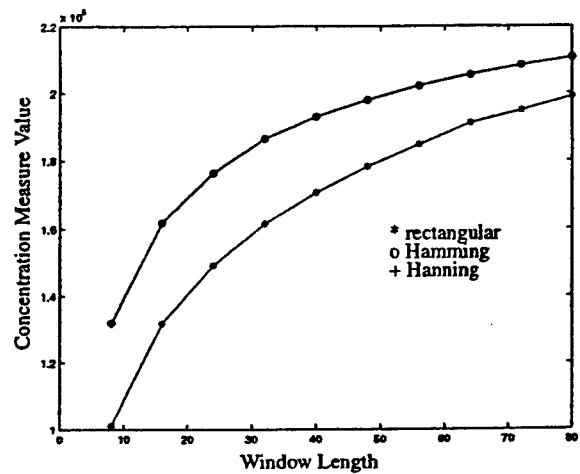


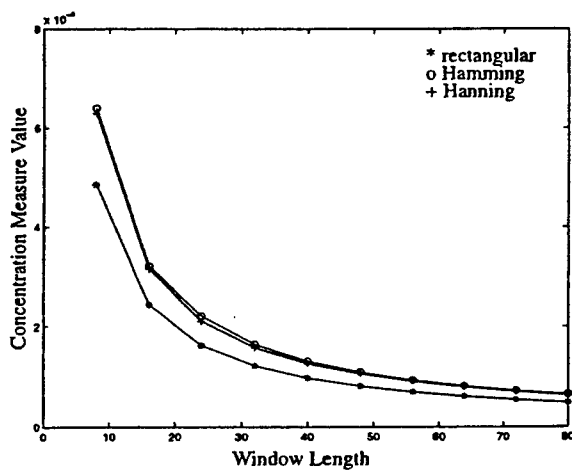
Fig.4 Concentration measures for a chirp signal at different window(rectangular) length.
(a) received signal, (b)window length=10, (c)window length=30, (d)window length=110,
(e)concentration measures



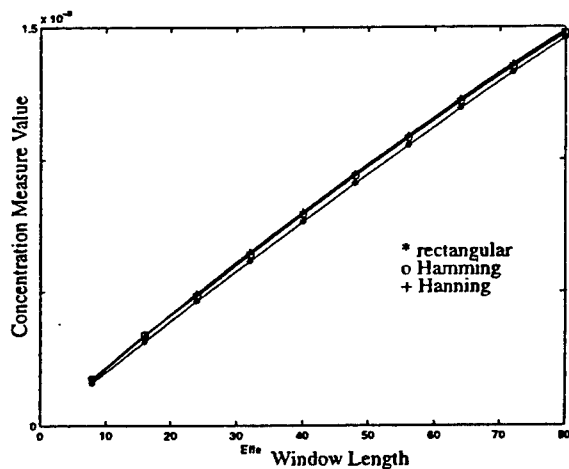
(a) Concentration measure(16) for impulse jammer with three different kind of window with different effective window length



(b) Concentration measure(16) for sinusoid jammer with three different kind of window with different effective window length



(c) Concentration measure(17) for impulse jammer with three different kind of window with different effective window length



(d) Concentration measure(17) for impulse jammer with three different kind of window with different effective window length

Fig.5 Concentration measures for different window with different length on sinusoidal and impulsive signal

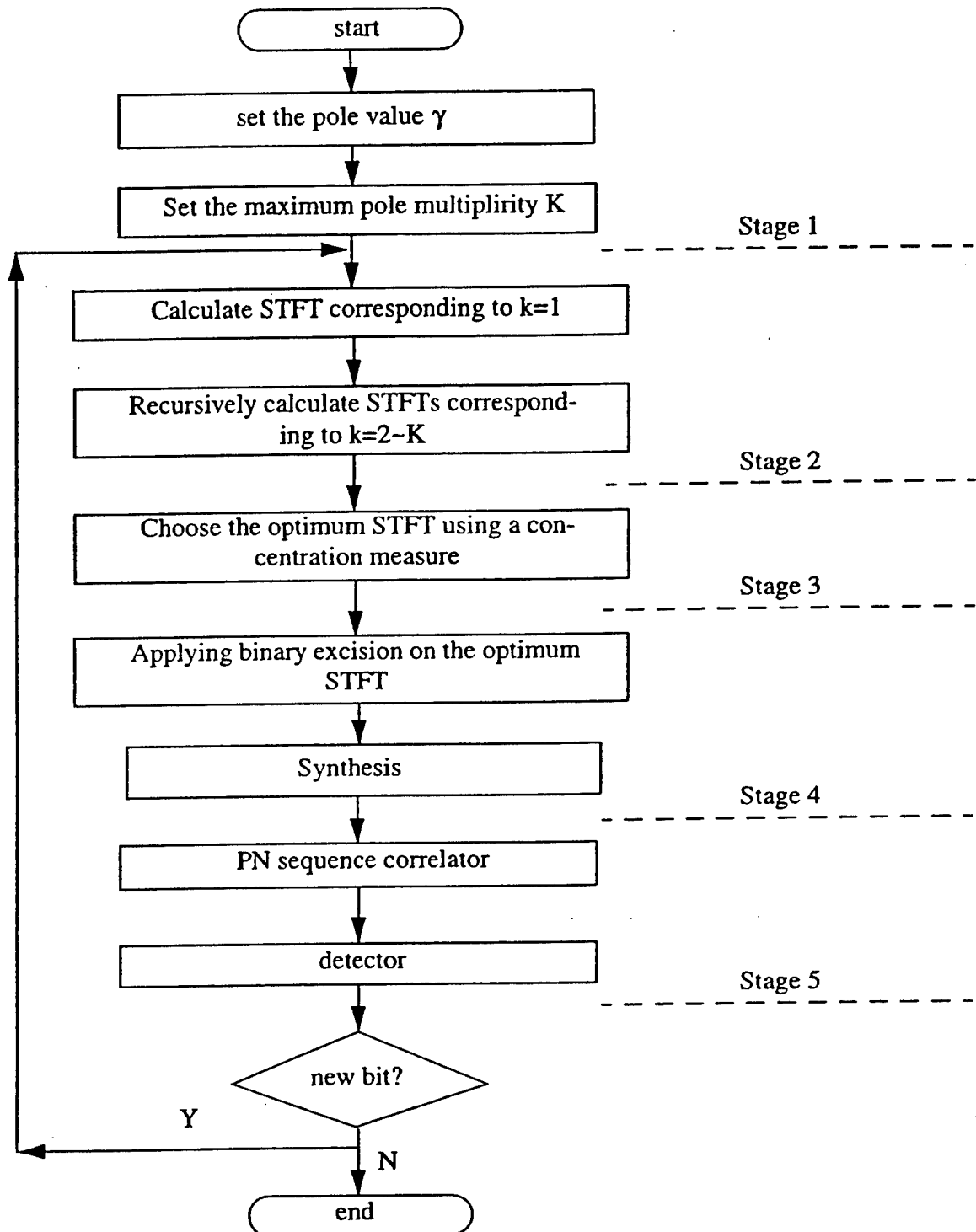


Fig.6 Flow chart for proposed adaptive interference excision method

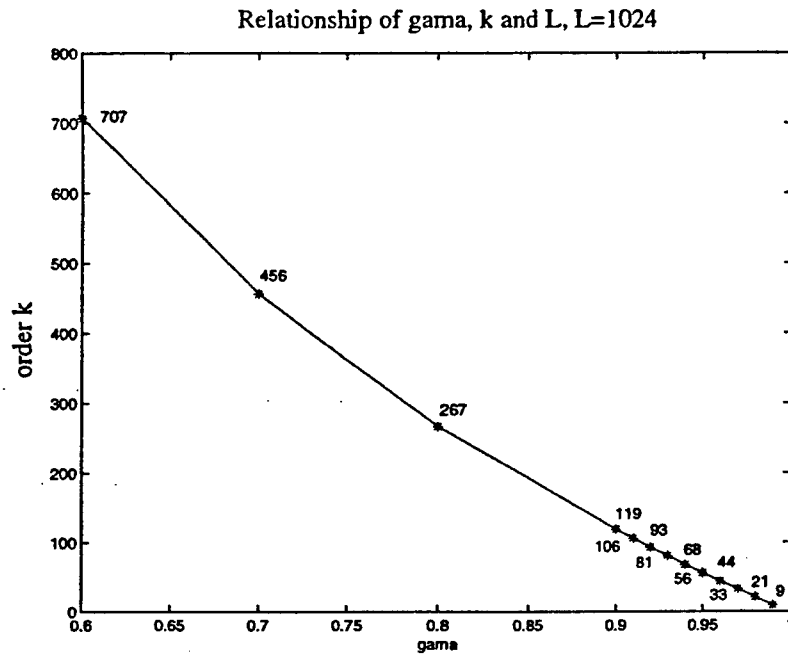


Fig.7 Relationship between γ , K , and L

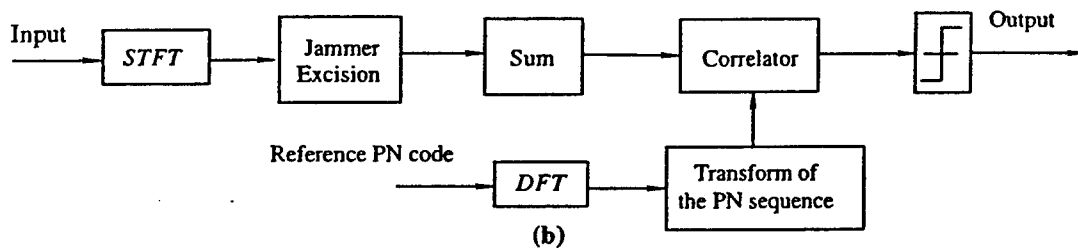
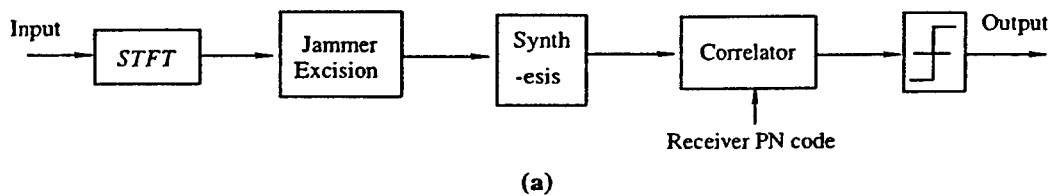
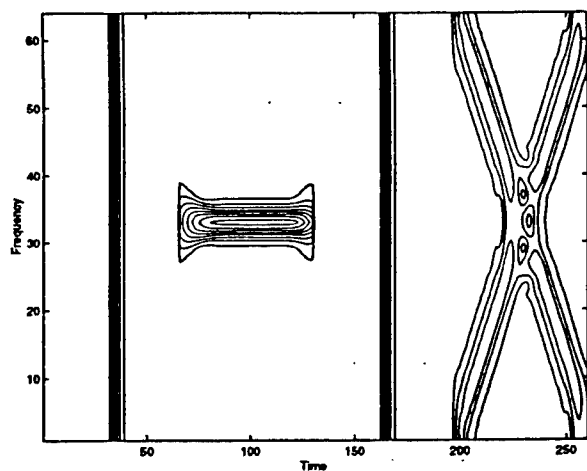
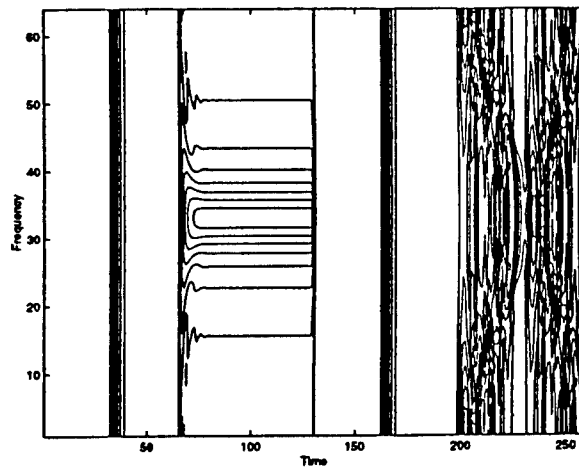


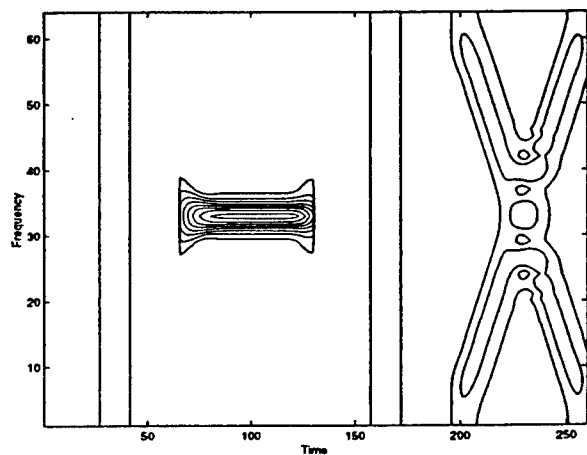
Fig.8 (a) Time domain decision (b) Transform domain decision



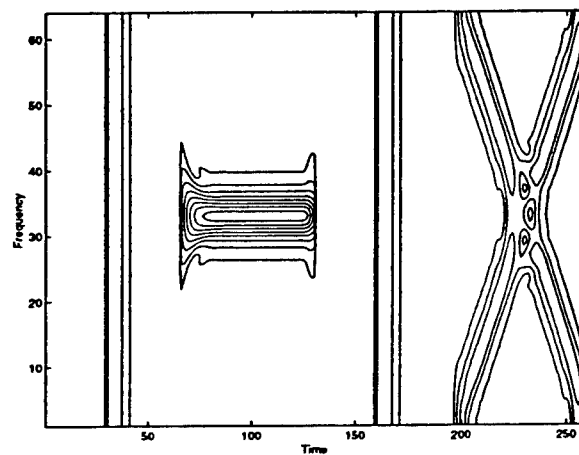
(a) TFD of adaptive STFT



(b) TFD with fixed window length with small k



(c) TFD with fixed window length with large k



(d) TFD with fixed window length with medium k

Fig.9 TFD of adaptive STFTs and STFT with fixed windows

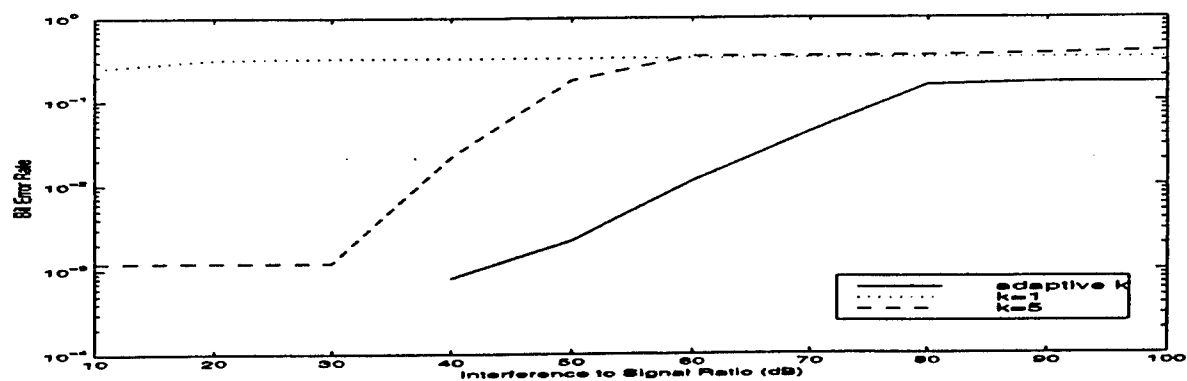


Fig.10 BER performance of the proposed spread spectrum

Suppression of Nonstationary Interference in Direct Sequence Spread Spectrum Communications using the Short Time Fourier Transform

Moeness G. Amin and Xuemei Ouyang

Department of Electrical and Computer Engineering

Villanova University, Villanova, PA 19085.

Email: moeness@ece.vill.edu

ABSTRACT

In this Chapter, the short-time Fourier transform (STFT) is employed for the rejection of nonstationary interference in direct sequence spread spectrum (DSSS) communication systems. The proposed interference excision approach is based on the attractive localization properties of the impulse responses of the multiple pole filters. These impulse responses have Gaussian-like shapes and decrease in bandwidth with higher pole multiplicities. When used as data windows, they yield a large class of computationally efficient STFTs. Localization measures can be applied for determining the optimum window that maximally concentrates the interference in the time-frequency domain. Interference mitigation is then achieved by applying a binary excision mask to the corresponding STFT for each data bit. The optimum correlator for the reconstructed jammer free signal is developed, and closed form expressions for the receiver SNR are derived. Simulations show that there is a significant improvement in performance of the optimum receiver compared to its suboptimal counterpart, which is simply obtained by performing the correlation between the output of the excision filter and the original PN sequence.

1. INTRODUCTION

Interference excision in direct sequence spread spectrum communication (DSSS) is an important problem in both military and civilian applications. There are several techniques that have been proposed for this task. These techniques include adaptive notch filtering, decision feedback [1] and transform domain methods [2]. For jammer signals with broadband frequency characteristics, but yet possess narrowband instantaneous bandwidths, time-frequency methods have recently been shown to be very effective in improving the receiver performance and reducing the bit error rates. One class of these methods implements linear excisions in which the data is processed using the wavelet transform or M-band/subband filter banks [3,4]. Another class applies bilinear transformations using time-frequency distributions for instantaneous frequency estimation, followed by time-domain excision filtering [5,6].

The short-time Fourier transform (STFT) is a linear time-frequency signal representation that inherently suffers from the trade-off between temporal and spectral resolution [7]. The STFT employing a short data window provides a good temporal resolution, whereas that using a window of long time extent has fine spectral resolution. One solution of this incompatibility problem is to generate a large class of STFTs, which employ different windows with distinct characteristics. Some members of this class should be appropriate to describe slowly time-varying signals, while others must be set to provide better localization in rapidly time-varying environments. For a given nonstationary signal, the STFT within this class that yields the best temporal/spectral trade-off, or the highest possible concentration in time-frequency domain, should be chosen for t-f signal representations. Several concentration measures including those introduced in [8,9] can be used for this purpose.

The application of STFT for interference excision in DS/SS communications using sparse grid and overdetermined time-frequency tilings is discussed in [10,11] and [12], respectively. In this chapter, we provide a new approach and a general framework for the application of the STFT to nonstationary interference mitigation in DSSS communications. In this approach, a large class of different short-time Fourier transforms is generated using a multiple-pole infinite impulse response filter realized in cascading form is considered.

Members of this class have sufficient diversity in their temporal/spectral trade-off and are easily updated in time. Further, the STFT using an impulse response of one filter can be recursively generated from those members corresponding to smaller filter orders or pole multiplicities. The choice of the optimum analysis window (impulse response) can be made using localization test criteria such as those discussed in [8,9]. Interference excision is then performed by either clipping or gating the high power values of the optimum window STFT. The process is repeated for each bit or block of data and the choice of the window could therefore vary with time. We present the analysis of the receiver signal-to-noise ratio SNR, using binary excisions on STFTs. It is shown that different data windows applied to the same jammer waveform will result in a different value of SNR. The proper data window that is selected by the concentration measures maximizes the jammer localization and thus limits the interference spread in the t-f domain. By confining the jammer to small number of t-f bins, binary excisions can effectively remove the jammer energy, causing a minimum distortion to the spread spectrum signal and, in turn, improving the receiver performance.

In traditional spread spectrum receivers, the signal is correlated with the PN sequence, which is known to both the transmitter and the receiver. When filtering techniques are applied for jammer excision, leading to enhanced receiver performance, the modified PN sequence and the original PN sequence will no longer be identical, and their correlation leads to suboptimal solutions. An optimum correlator, therefore, should be developed to combat the induced distortion of the PN sequence caused by the preprocessing excision filtering stage. The optimum correlator associated with STFT based interference excision system is derived and shown to depend on the analysis window, the interference time-frequency signature, and the white noise power.

Section 2 gives a brief presentation of the STFT analysis and synthesis method. Multiple pole windows and their temporal/spectral localization properties are discussed in Section 3. Section 4 summarizes two concentration measures for the optimum data window selection. The overall scheme for the proposed adaptive STFT method for jammer excisions is given in Section 5. The closed form expression for the optimum receiver SNR is given in Section 6. The performance of the traditional receiver implementing the STFT excision system is

also considered in Section 6. Simulation results are presented in Section 7.

2. SHORT-TIME FOURIER TRANSFORM

Short-time Fourier transform can be presented using two perspectives, namely the filter bank and Fourier transform[7,13]. Form the Fourier transform perspective, the STFT $X_m(e^{j\omega_k})$ of the signal $x(n)$ is given by

$$X_m(e^{j\omega_k}) = \sum_m w(n-m)x(m)e^{-j2\pi mk/N} \quad (1)$$

where k is the frequency sample number, N is the total of frequency samples, and $w(n)$ is the moving data window. The synthesis method corresponding to the Fourier transform perspective is the Overlap-Add(OLA) method [13], which can be expressed as

$$y(n) = \sum_m \sum_{k=0}^{L-1} X_m(e^{j\omega_k})e^{j\omega_k n} = \sum_m y_m(n) = Lx(n) \sum_m w(m-n) \quad (2)$$

where $y_m(n)$ is the inverse discrete Fourier transform at the time sample m . It can be readily shown that if $w(n)$ is sampled at sufficiently dense rate, then[13]

$$\sum_m w(m-n) = W(e^{j0}), \quad y(n) = Lx(n)W(e^{j0}) \quad (3)$$

It is clear from (3) that without altering the values of the STFT, the synthesized signal is the same as the original signal,

$$x(n) = \frac{y(n)}{LW(e^{j0})} = \frac{1}{LW(e^{j0})} \sum_m \sum_{k=0}^{L-1} X_m(e^{j\omega_k})e^{j\omega_k n} \quad (4)$$

In many applications, however, it is desired to synthesize a signal from a time-frequency function formed by modifying the STFT. For example, the purpose of the STFT method in DSSS jammer excision problem is to concentrate the jammer in a small area in t-f domain and remove its t-f signature via a binary mask. The synthesis is then performed on the masked STFT to recover the jammer-free original signal. If the STFT $X(n,k)$ is modified, then the synthesized signal becomes a time-varying convolution between the input data sequence $x(n)$ and an impulse response of a linear time-varying filter.

3. ORDER RECURSIVE SHORT TIME FOURIER TRANSFORM (ORFT)

The order recursive short-time Fourier transform was introduced in [14] as an approach to generate a large class of STFTs whose members are generated from one another through simple recursions. The recursions are made possible by setting the analysis window $h_k(n)$ equal to the impulse response of a multiple pole linear time-invariant filter. The transfer function of $h_k(n)$ can be expressed in the Z-domain as

$$H_k(z) = \frac{(1 - \gamma)^k}{(1 - \gamma z^{-1})^k} \quad (5)$$

where γ is the filter pole and the superscript k denotes the pole multiplicity. The filter corresponding impulse response is given by

$$h_k(n) = (1 - \gamma)^k \frac{(n + k - 1)!}{n!(k - 1)!} \gamma^n \quad (6)$$

It can be readily shown that the above sequence possesses the recursive property[14]

$$h_k(n) = \gamma h_k(n - 1) + (1 - \gamma)h_{k-1}(n) \quad (7)$$

Using the impulse response (7) as the analysis window in STFT leads to a similar recursion,

$$F_{k+1}(n, \omega) = \gamma F_{k+1}(n - 1, \omega) + (1 - \gamma)F_k(n, \omega) \quad (8)$$

where $F_k(n, \omega)$ denotes the STFT which corresponds to the filter order k , calculated at time n and frequency ω . Equation (8) defines the order recursive Fourier transform(ORFT), in which the FT is recursive in both time n and filter order k . The block diagram of ORFT consisting of systems connected in cascade is depicted in Fig.1. The STFTs $F_k(n, \omega)$, $k=1,2,\dots,K$ offer different trade-off between temporal and spectral resolutions. The trade-off is decided by the two variables in the problem, the filter pole and its multiplicity. Fig.2(a) shows the windows corresponding to $k=1,2,\dots,9$ with $\gamma = 0.7$, whereas Fig.2(b) shows the data window for a single pole filter with γ changing over the range $[0.5, 0.9]$. Figure 3 shows the time and frequency characteristics of the window corresponding to different filter orders for $\gamma = 0.9$. It is evident that higher filter order and pole values lead to longer extent data windows, and subsequently, finer spectral resolution. The fast

computational property of the members of the above recursive class of STFTs as well as the significant variation of temporal/spectral resolutions as a function of the analysis window parameters cast multiple pole window STFTs as an attractive tool for nonstationary interference excision, as shown below.

4. CONCENTRATION MEASURES

The main objective of adaptive STFT is to decide, without human intervention or extensive prior knowledge of the underlying signal characteristics, on the analysis window which offers the best time-frequency resolution. Procedures based on mathematical optimal criteria appears most promising. Renyi information of the third order has been shown to provide a valuable and effective information measure in the context of time-frequency distributions[8],

$$v_1 = -\frac{1}{2} \sum_n \sum_\omega \log \|STFT(n, \omega)\|^3 \quad (9)$$

It is recognized that the maximum value of v_1 in (9) is the one corresponding to the highest t-f concentration of the underlying t-f signal. Using the recursive class of STFTs presented in the previous section, we first proceed to calculate v_1 for all members $F_k(n, \omega)$. The maximum concentration measure is then determined, and the respective STFT is chosen as the most appropriate t-f signal representation. Another effective local concentration measure was introduced in [9] as:

$$v_2 = \frac{\sum_n \sum_\omega |STFT(n, \omega)|^4}{(\sum_n \sum_\omega |STFT(n, \omega)|^2)^2} \quad (10)$$

The basis for choosing the optimum window rests on the intuition that high value of v_2 reflects good time-frequency localization and high resolution. The ratio of the L_4 norm to the L_2 norm of the STFT favors "peaky" distributions that places much of the signal energy into small region of the time-frequency plane, thus achieving a concentrated representation.

Figure.4(a,b,c,d) depicts the STFTs of a chirp jammer signal using three rectangular data windows. The jammer-to-DSSS signal ratio(JSR) is 20dB, where SNR is set to 0dB. The PN sequence length is set to $L=128$. The values of the two concentration measures as

functions of the window length are shown in Fig.4(e). In both cases, the maximum value is reached when the window length is 30 data samples. Indeed, by comparing Fig.4(b,c,d), it is clear that the STFT with window length of 30 samples is more concentrated than the other two based on the window lengths of 10 and 110 samples. Next, we consider the two cases of sinusoidal and impulse jammers. For both cases, STFTs using rectangular, Hamming, and Hanning windows are computed. For each type of window, the two aforementioned concentration measures are evaluated for different window lengths. The results for the sinusoidal jammer are shown in Fig.5(a,c), whereas those for the impulse jammer are depicted in Fig.5(b,d). For the sinusoid jammer, both measures under all three windows point to the maximum window length as the one leading to the highest t-f concentration. The opposite is true for the impulse jammer. It is clear that both concentration measures (9) and (10) give results consistent with Fourier analysis of windowed signals.

5. ADAPTIVE STFT IN DSSS SYSTEMS

Fig.6 shows the flow chart describing the steps in implementing the proposed recursive STFT-based interference excision method in PN spread spectrum communications. These steps can be lumped into five consecutive stages: selecting of the analysis window parameters; computing STFTs; selecting the optimum STFT using concentration measures; masking the selected STFT; synthesizing the jammer-free signal; forming the decision variable and detecting the transmitted bit. In this section, we discuss an important issue relating to window selection and decision variable.

Generating a class of infinite numbers of STFTs is neither feasible or necessary. In the following, we provide a mechanism to set the window parameters γ , K to take a finite number of values consistent with the PN length as well as the required temporal and spectral resolutions. According to [14], the effective window length is defined as

$$L_k = 1 / \left(\sum_{n=0}^{\infty} h_k(n)^2 \right) \quad L_1 = \frac{1+\gamma}{1-\gamma} \quad (11)$$

which increases with increased values of k and γ . Since the minimum value of $L_k(\gamma) = L_{min}$ is obtained at $k=1$, for a given γ , then the highest temporal resolution is achieved when using a single pole filter. By setting $L_1 = L_{min}$, the value of γ can be determined from (11). The maximum effective window length $L_k(\gamma) = L_{max}$ is reached at the maximum

multiplicity $k=K$. A reasonable value of L_{max} is the PN sequence length L . In the absence of the closed form expressions for $h_k(\gamma)$, $k > 1$, given L and , the maximum order K can be numerically determined by computing (11). The relation between γ and K for $L=1024$ is shown in Fig.7. It is evident from this figure that as γ increases, fewer analysis windows can be generated in between L_1 and L_K , which, in turn, narrows down the possible and available choices of the STFTs.

Suboptimum detection of the information symbol, the decision variable can be formed from the correlation

$$g = \sum_{n=0}^{N-1} \hat{x}(n)p^*(n) \quad (12)$$

where, $p(n)$ represents the receiver PN sequence, N is the number of chips per information bit (we assume one sample/chip), and $\hat{x}(n)$ is the synthesized signal. From Section 2, if there is no modification made in the t-f domain, then the synthesized signal is equal to the original signal $x(n) = \hat{x}(n)$. By substituting equation (4) in (12), we obtain

$$g = \frac{1}{LW(e^{j0})} \sum_{k=0}^{L-1} P^*(e^{j\omega_k}) \sum_m X_m(e^{j\omega_k}) \quad (13)$$

where $P(e^{j\omega_k})$ is the discrete Fourier transform of the PN sequence. Since all the functions in (13) are in the transform domain, then the detection can be performed without the need to apply inverse transformations. If the binary excision function $A_m(k)$ is applied to the STFT, then the synthesized signal is modified to

$$y(n) = \sum_m \sum_{k=0}^{L-1} A_m(k) X_m(e^{j\omega_k}) e^{j\omega_k n} \quad (14)$$

In this case,

$$g = \frac{1}{LW(e^{j0})} \sum_{k=0}^{L-1} P^*(e^{j\omega_k}) \sum_m A_m(k) X_m(e^{j\omega_k}) \quad (15)$$

The STFT domain suboptimum detection scheme allows computational saving in two ways. First, the time domain correlation requires m inverse DFT to be performed, whereas only one DFT operation is required for the PN sequence in (15). Second, if the PN sequence is

repetitive, its DFT remains fixed for every bit, which in turn reduces on-line computations in the correlation scheme of Fig.8(b).

6. TRADITIONAL AND OPTIMUM CORRELATOR

Assuming "1" is transmitted, the baseband received signal can be expressed as

$$r(i) = s(i) + j(i) + n(i) \quad (16)$$

where $s(i)$ represents the PN sequence, $j(i)$ is the jammer sequence, which is of zero-mean and covariance $R_j(i)$, and $n(i)$ is an additive white Gaussian noise sequence with zero mean and variance σ_n^2 . It is assumed that the above three sequences are uncorrelated.

In order to use the STFT presentations in Sections 2 and 5, we replace $x(n)$ by $r(n)$ and the STFT $X_m(e^{j\omega_k})$ by $R_m(e^{j\omega_k})$. We also denote the desired signal as $s(n)$ rather than $p(n)$. With the application of the binary excision function $A_m(k)$ to the STFT at time m and frequency k , it can be readily shown that the synthesized signal is modified to

$$r'(n) = \frac{1}{LW(e^{j0})} \sum_{l=0}^{L-1} r(l) \sum_{m=1}^M \sum_{k=0}^{L-1} A_m(k) w_m(l) e^{j\omega_k(n-l)} \quad (17)$$

where R and W are the DFTs of the received data and the data window, $w_m(l)$, respectively.

The performance of the traditional suboptimum and optimum correlators can be analysed by expressing the reconstructed signal in the matrix form. The two inner summations of equation (17) can be written as

$$\sum_{m=1}^M \sum_{k=0}^{L-1} A_m(k) w_m(l) e^{j\omega_k(n-l)} = \bar{A}^t(n, l) \bar{W}(l) \quad (18)$$

where superscript 't' denotes matrix or vector transpose, and

$$\bar{A}(n, l) = [A_1(1)e^{j\omega_1(n-l)} \dots A_1(L)e^{j\omega_L(n-l)}, \dots, A_M(1)e^{j\omega_1(n-l)} \dots A_M(L)e^{j\omega_L(n-l)}]^t$$

$$\bar{W}(l) = [W_1(l) \dots W_1(l), \dots, W_M(l) \dots W_M(l)]^t \quad (19)$$

Accordingly,

$$r'(n) = \sum_{l=0}^{L-1} r(l) \sum_{m=1}^M \sum_{k=0}^{L-1} A_m(k) w_m(l) e^{j\omega_k(n-l)} = \sum_{l=0}^{L-1} r(l) \bar{A}^t(n, l) \bar{W}(l) = \bar{A} \bar{W}^t \mathbf{R} \quad (20)$$

where

$$\bar{A} \bar{W} = [\bar{A}^t(n, 1) \bar{W}(1) \dots \bar{A}^t(n, L) \bar{W}(L)]^t, \quad \mathbf{R} = [r(1) \dots r(L)]^t \quad (21)$$

Then, the vector \mathbf{Y} of the output samples in (2) can be expressed as

$$\mathbf{Y} = \begin{bmatrix} y(1) \\ \vdots \\ y(L) \end{bmatrix} = \begin{bmatrix} \bar{A}^t(1, 1) \bar{W}(1) & \dots & \bar{A}^t(1, L) \bar{W}(L) \\ \vdots & \vdots & \vdots \\ \bar{A}^t(L, 1) \bar{W}(1) & \dots & \bar{A}^t(L, L) \bar{W}(L) \end{bmatrix} \begin{bmatrix} r(1) \\ \vdots \\ r(L) \end{bmatrix} = \mathbf{B} \mathbf{R} \quad (22)$$

Since binary jammer excision fully removes the jammer power, the only components in (22) are the signal and the white noise,

$$\mathbf{Y} = \mathbf{B} \mathbf{R} = \mathbf{B} \mathbf{S} + \mathbf{B} \mathbf{N} = \mathbf{Y}_S + \mathbf{Y}_N \quad (23)$$

where

$$\mathbf{S} = [s(1) \ s(2) \dots s(L)]^t, \quad \mathbf{N} = [n(1) \ n(2) \dots n(L)]^t$$

$$\mathbf{Y}_S = \mathbf{B} \mathbf{S} = \begin{bmatrix} \bar{A}^t(1, 1) \bar{W}(1) & \dots & \bar{A}^t(1, L) \bar{W}(L) \\ \vdots & \vdots & \vdots \\ \bar{A}^t(L, 1) \bar{W}(1) & \dots & \bar{A}^t(L, L) \bar{W}(L) \end{bmatrix} \begin{bmatrix} s(1) \\ \vdots \\ s(L) \end{bmatrix}$$

$$\mathbf{Y}_N = \mathbf{B} \mathbf{N} = \begin{bmatrix} \bar{A}^t(1, 1) \bar{W}(1) & \dots & \bar{A}^t(1, L) \bar{W}(L) \\ \vdots & \vdots & \vdots \\ \bar{A}^t(L, 1) \bar{W}(1) & \dots & \bar{A}^t(L, L) \bar{W}(L) \end{bmatrix} \begin{bmatrix} n(1) \\ \vdots \\ n(L) \end{bmatrix} \quad (24)$$

Unlike the traditional receiver, where the decision variable is obtained via (12), in the case of optimum receiver, the receiver PN is modified before the correlation with $r'(n)$. Denote the modified PN sequence at the receiver as $h(n)$. Then, the decision variable is given by

$$g' = \sum_{i=0}^{L-1} r'(i)h(i) = \frac{1}{LW(e^{j0})} \mathbf{H}^H \mathbf{Y} = \frac{1}{LW(e^{j0})} \mathbf{H}^H \mathbf{Y}_S + \frac{1}{LW(e^{j0})} \mathbf{H}^H \mathbf{Y}_N \quad (25)$$

where $\mathbf{H} = [h(1) \dots h(L)]^H$, and superscript 'H' denote the Hermitian operator. The receiver signal-to-noise ratio, SNR_{out} , is

$$SNR_{out} = \frac{|\mathbf{H}^H \mathbf{Y}_S|^2}{E[\mathbf{H}^H \mathbf{Y}_S \mathbf{Y}_S^H \mathbf{H}] - |\mathbf{H}^H \mathbf{Y}_S|^2 + E|\mathbf{H}^H \mathbf{Y}_N|^2} = \frac{E^2[g']}{Var[g']} \quad (26)$$

Since

$$E(\mathbf{Y}_N \mathbf{Y}_N^H) = E[\mathbf{B} \mathbf{N} \mathbf{N}^H \mathbf{B}^H] = \mathbf{B} E[\mathbf{N} \mathbf{N}^H] \mathbf{B}^H = \sigma_n^2 \mathbf{B} \mathbf{B}^H$$

then

$$SNR_{out} = \frac{\mathbf{H}^H \mathbf{Y}_S \mathbf{Y}_S^H \mathbf{H}}{E[\mathbf{H}^H \mathbf{Y}_S \mathbf{Y}_S^H \mathbf{H}] - |\mathbf{H}^H \mathbf{Y}_S|^2 + \sigma_n^2 \mathbf{H}^H \mathbf{B} \mathbf{B}^H \mathbf{H}} \quad (27)$$

The sequence \mathbf{H} must be correlated with the original PN sequence \mathbf{S} . Therefore, $E[\mathbf{H}^H \mathbf{Y}_S \mathbf{Y}_S^H \mathbf{H}]$ is a fourth order function of \mathbf{S} . If we define the relationship between \mathbf{H} and \mathbf{S} by the modification matrix \mathbf{C} , then $\mathbf{H} = \mathbf{C} \mathbf{S}$ and

$$E[\mathbf{H}^H \mathbf{Y}_S \mathbf{Y}_S^H \mathbf{H}] = E[\mathbf{S}^H \mathbf{C}^H \mathbf{B} \mathbf{S} \mathbf{S}^H \mathbf{B}^H \mathbf{C} \mathbf{S}] \quad (28)$$

Let $\mathbf{D} = \mathbf{C}^H \mathbf{B}$, then

$$E[\mathbf{H}^H \mathbf{Y}_S \mathbf{Y}_S^H \mathbf{H}] = E[\mathbf{S}^H \mathbf{D} \mathbf{S} \mathbf{S}^H \mathbf{D}^H \mathbf{S}] = E|\mathbf{S}^H \mathbf{D} \mathbf{S}|^2 \quad (29)$$

Since

$$\mathbf{S}^H \mathbf{D} \mathbf{S} = \sum_j \sum_i S(i) D(i, j) S(j) \mathbf{S}_i,$$

then

$$\begin{aligned} E|\mathbf{S}^H \mathbf{D} \mathbf{S}|^2 &= E \left[\sum_i \sum_j \sum_k \sum_l S(i) D(i, j) S(j) S(k) D^*(l, k) S(l) \right] \\ &= \sum_i \sum_j \sum_k \sum_l D(i, j) D^*(l, k) E(S(i) S(j) S(k) S(l)) \end{aligned}$$

$$= \sum_i \sum_k D(i,i)D(k,k) + \sum_i \sum_j |D(i,j)|^2 + \sum_i \sum_j D(i,j)D^*(j,i) - 2 \sum_i |D(i,i)|^2 \quad (30)$$

and

$$E[H^H Y_S Y_S^H H] - H^H Y_S Y_S^H H = \left(\sum_i \sum_j |D(i,j)|^2 + \sum_i \sum_j D(i,j)D^*(j,i) - 2 \sum_i |D(i,i)|^2 \right) \quad (31)$$

Define

$$C^H = \begin{bmatrix} c_1 \\ c_2 \\ \vdots \\ c_L \end{bmatrix}, B = \begin{bmatrix} b_1 & b_2 & \cdots & b_L \end{bmatrix}$$

where c_i is a row vector and b_i is a column vector, and

$$C1^H = \begin{bmatrix} c_1 & c_2 & \cdots & c_L \end{bmatrix}_{1 \times L^2} \quad B1 = \begin{bmatrix} b_1 & 0 & \cdots & 0 \\ 0 & b_2 & \cdots & 0 \\ \vdots & \vdots & \ddots & 0 \\ 0 & 0 & \cdots & b_L \end{bmatrix}_{L^2 \times L} \quad B2 = \begin{bmatrix} B & 0 & \cdots & 0 \\ 0 & B & \cdots & 0 \\ \vdots & \vdots & \ddots & 0 \\ 0 & 0 & \cdots & B \end{bmatrix}_{L^2 \times L^2}$$

$$B3 = \begin{bmatrix} b_1 & 0 & \cdots & 0 & b_2 & 0 & \cdots & 0 & b_3 & \cdots & \cdots & b_L & 0 & \cdots & 0 \\ 0 & b_1 & 0 & \cdots & 0 & b_2 & 0 & \cdots & 0 & b_3 & \cdots & \cdots & b_L & \cdots & 0 \\ \vdots & & & & & & & & & & & & & \\ 0 & \cdots & 0 & b_1 & 0 & \cdots & 0 & b_2 & 0 & \cdots & 0 & b_3 & \cdots & \cdots & 0 & b_L \end{bmatrix}_{L^2 \times L} \quad B4 = \begin{bmatrix} b_1 \\ b_2 \\ \vdots \\ b_L \end{bmatrix}$$

Using the above matrices,

$$\sum_i |D(i,i)|^2 = C1^H B1 B1^H C1, \quad \sum_i \sum_j |D(i,j)|^2 = C1^H B2 B2^H C1,$$

$$\sum_i \sum_j D(i,j)D^*(j,i) = C1^H B2 B3^H C1.$$

Accordingly,

$$(E[H^H Y_S])^2 = C1^H (B4 B4^H) C1 = C1^H Q C1 \quad (32)$$

$$E(|H^H Y_S|^2) - (E[H^H Y_S])^2 = C1^H (B2 B2^H + B2 B3^H - 2 B1 B1^H) C1 \quad (33)$$

$$\mathbf{H}^H E(\mathbf{Y}_N \mathbf{Y}_N^H) \mathbf{H} = \sigma_n^2 \mathbf{C}_1^H (\mathbf{B}_2 \mathbf{B}_2^H) \mathbf{C}_1 \quad (34)$$

The receiver SNR in (26) can be written as

$$\begin{aligned} SNR_{out} &= \frac{(E |\mathbf{H}^H \mathbf{Y}_s|^2)}{E(|\mathbf{H}^H \mathbf{Y}_s|^2) - (E |\mathbf{H}^H \mathbf{Y}_s|^2)^2 + E |\mathbf{H}^H \mathbf{Y}_s|^2} \\ &= \frac{\mathbf{C}_1^H \mathbf{Q} \mathbf{C}_1}{\mathbf{C}_1^H ((1 + \sigma_n^2) \mathbf{B}_2 \mathbf{B}_2^H + \mathbf{B}_2 \mathbf{B}_3^H - 2 \mathbf{B}_1 \mathbf{B}_1^H) \mathbf{C}_1} = \frac{\mathbf{C}_1^H \mathbf{Q} \mathbf{C}_1}{\mathbf{C}_1^H \mathbf{P} \mathbf{C}_1} \end{aligned} \quad (35)$$

where

$$\mathbf{Q} = \mathbf{B}_4 \mathbf{B}_4^H, \mathbf{P} = (1 + \sigma_n^2) \mathbf{B}_2 \mathbf{B}_2^H + \mathbf{B}_2 \mathbf{B}_3^H - 2 \mathbf{B}_1 \mathbf{B}_1^H \quad (36)$$

A. Traditional receiver

For the traditional correlator, \mathbf{H} is set equal to the PN sequence, i.e., $\mathbf{C} = \mathbf{I}$. Performing the correlation between the synthesized signal and \mathbf{H} leads to suboptimal performance, since this process doesn't take into account the distortion effect of the excision filter on the original PN sequence. The distortion entailed on the PN sequence depends on the binary excision mask. In Fig.9, we show the PN sequence distortion under the impulse, sinusoidal and chirp jammer excision. It is evident from the figure that the sinusoidal jammer excision results in the worst PN distortion, whereas the impulse jammer causes the least distortion. The impulse jammer concentrates on a relatively small area in the t -f domain. In this case, after excision and signal reconstruction, the only change in the PN sequence is just the energy, and as much, the information in the PN sequence is preserved. Yet for sinusoidal jammer, after excision, since we lose several frequency bins in the PN sequence which one is recoverable, the reconstructed PN will encounter severe distortion.

B. Optimum receiver

In equation (35), since all elements in analysis window and excision mask are non-negative, matrix \mathbf{P} is symmetric, nonnegative, and positive definite. Equation (25) may be viewed as the Rayleigh Quotient problem. Define $\tilde{\mathbf{C}}_1^H = \mathbf{P}^{1/2} \mathbf{C}_1$, where $\mathbf{P}^{1/2} =$

$\sum_i \lambda_i^{1/2} v_i v_i'$. The variables λ_i and v_i are the i th eigenvalue and its respective eigenvector of P . Equation (35) can then be expressed as

$$SNR_{out} = \frac{\tilde{C}1^H[(P^{-1/2})^H Q P^{-1/2}]\tilde{C}1}{\tilde{C}1^H \tilde{C}1} \quad (37)$$

It is well known that $(SNR_{out})_{max}$ corresponds to the largest eigenvalue of $(P^{-1/2})^H Q P^{-1/2}$. If the corresponding eigenvector is denoted by $\tilde{C}1_{max}$, then the optimum correlator is given by $C1_{opt} = P^{-1/2} \tilde{C}1_{max}$. Once the modification matrix C is obtained, the correlation between $r'(n)$ and $h(n)$ can be performed.

7. SIMULATIONS

Computer simulations are given below to show the improvement in the receiver SNR using the solution in (36). In general, with the cancellation of the jammer in the t-f domain, white noise and signal components at the excised t-f bins are removed as well. This in turn will result in the distortion of the reconstructed PN sequence. In Fig.8, the impairment of the PN sequence under jammer signal cancellation is shown. The length of PN sequence is taken as 128, and a rectangular window of 4 samples is employed. Ten time slices are cancelled for the impulse jammer (index 59 to 69), ten frequency slices for the sinusoidal jammer (index 59 to 69) and ten diagonal slices for the chirp jammer (main diagonal and the adjacent upper and lower diagonals). Fig.8 (a), (b), (c) depicts the degree of the distortion due to the impulse, sinusoid, and chirp jammer signals. The results show that the worst distortion occurs under the sinusoidal jammer case, whereas the best one is achieved in the case of impulse jammer. For the sinusoidal jammer, the entire 128 PN sequence is impaired. Yet for the impulse signal cancellation, only few chips of the original PN sequence are distorted in amplitude, while the rest are left intact. The number of distorted chips depends on the analysis window length as well as the number of excised t-f bins. The results clearly show that, in all three cases, the original PN sequence doesn't match the reconstruction PN sequence.

Figure 9 shows the receiver SNR for both the suboptimal and optimum receivers. The length of the PN sequence used is 16. A rectangular analysis window with length equal to 8 was employed. It is evident from the figure that the higher the number of the excised t-f bins the worse the performance of the traditional receiver. On the other hand, the optimum

receiver maintains the same performance level for both impulse and chirp jammers. It should be noted, however, that the optimum receiver performance will deteriorate when the number of t-f slices excised exceeds the window length, in which case the removed desired signal becomes unrecoverable. For a sinusoidal jammer, although the receiver SNR for the optimum receiver SNR monotonically decreases with increased number of the t-f bins cancelled, yet the performance is still better than that of the suboptimum one. The prime reason for the difference in performance between the sinusoidal jammer and the other two types of jammer signals is that in the STFT analysis, there is redundancy along the time index which does not exist along the frequency axis. When several consecutive time slices are cancelled, the information in the cancelled t-f bins can be restored with the information held in the rest t-f bins. Yet if one frequency bin is cancelled, the STFT will lose the information in that bin, and the reconstructed PN will be considerably different from the original one.

Also shown in Fig. 9 the receiver performance when the receiver PN sequence is distorted in the same exact way as the received PN sequence. That is, the sequence encounters the same binary excision applied to the incoming data. The performance is at best equal to that of suboptimum receivers, which is achieved for the sinusoidal jammer case.

8. CONCLUSIONS

In this Chapter, a new adaptive time-frequency technique for interference excision in direct sequence spread spectrum communication was introduced. The proposed technique implements recursive analysis windows to allow efficient generation of a large class of STFTs with different spectral/temporal resolution properties. Concentration measures were applied to select the analysis window that provides the best jammer time-frequency power concentration. The jammer signal is excised in t-f domain using a binary mask. Central to our contribution is the demonstration that the strength as well as the localization of the jammer power in the t-f domain affects the STFT receiver performance. This demonstration underscores the fact that knowledge of the type of the interference excision system deployed at the receiver can be exploited by the jammer to reduce the system effectiveness to interference suppression.

We have also derived the optimum receiver for interference excision based on STFT

analysis. Traditional detectors correlate the receiver PN sequence with the reconstructed PN sequence from STFT. The proposed optimum scheme, however, takes into account the distortion of the PN sequence caused by the jammer cancellation and is shown to yield enhanced receiver performance. Simulation results show significant improvement in the receiver SNR when the optimum receiver is implemented in place of its suboptimum counterpart.

Acknowledgements

The authors would like to thank Dr. Alan Lindsey at the Air Force Research Lab, Rome, NY for his valuable insights on the interference excision problem, and also thank Mr. Ce Zhang at Villanova University for typing and preparing this chapter according to the publisher format.

References

- [1] J. Laster and J. Reed, "Interference rejection in digital wireless communication," IEEE Signal Processing Magazine, pp. 37-62. May 1997.
- [2] L. Milstein and P. Das, "An Analysis of a real-time transform domain filtering digital communication system-Part I: Narrowband interference rejection," IEEE Trans. on Communications, pp. 816-824, vol. 28, no. 6, June 1980.
- [3] M. Medley, G. Saulnier, and Das, "Applications of the wavelet transform in spread spectrum communications systems," SPIE, Wavelet Applications., Orlando, FL, April 1994.
- [4] M. Tazebay and A. Akansu, "Adaptive subband transforms in time-frequency excisers for DSSS communication systems," IEEE Trans. on Signal Processing, pp. 2776-2782, Nov. 1995.
- [5] M. Amin, "Interference mitigation in spread spectrum communications using time-frequency distributions," IEEE Trans. on Signal Processing, vol. 45, no. 1, pp. 90-102, January 1997.
- [6] C. Wang and M. Amin, "Performance analysis of instantaneous frequency-based interference excision techniques in spread spectrum communications," IEEE Trans. on Signal Processing, vol. 46, no. 1, pp. 70-82, January 1998.

- [7] J. Lim and A. Oppenheim, *Advanced Topics in Signal Processing*, Chapter 6, Prentice Hall, Englewood Cliffs, New Jersey, 1988.
- [8] W. Williams, M. Brown, and A. Hero, "Uncertainty, information and time-frequency distributions," *SPIE*, vol. 1566, pp. 144-156, 1991.
- [9] D. Jones and T. Parks, "A high resolution data-adaptive time-frequency representation," *IEEE Trans. on ASSP*, vol. 38, pp. 2127-2135, December 1990.
- [10] S. Roberts and M. Amin, "Linear vs. bilinear time-frequency methods for interference mitigation in direct sequence spread spectrum communication systems," *Asilomar Conf. on Signals, Systems and Computers*, Pacific Grove, Ca, Nov. 1995.
- [11] D. Wei, D. Harding, and A. Bovik, "Interference rejection in DSSS communications using the discrete Gabor transform," *Proceedings of the IEEE Workshop on DSP*, Bryle Canyon, VT, Aug. 1998.
- [12] B. Krongold, M. Kramer, K. Ramchandran, and D. Jones, "Spread spectrum interference suppression using adaptive time-frequency tilings," *Proceedings of ICASSP-97*, Munich, Germany, April 1997.
- [13] J. Allen and L. Rabiner, "A Unified Approach to Short-Time Fourier Analysis and Synthesis," *Proc. IEEE*, vol. 65, no. 11, Nov. 1977.
- [14] M. Amin and K. Feng, "Short-time Fourier transform using cascade filter structures," *IEEE Transactions on Circuits and Systems*, vol. 42, pp. 631-641, October 1995.

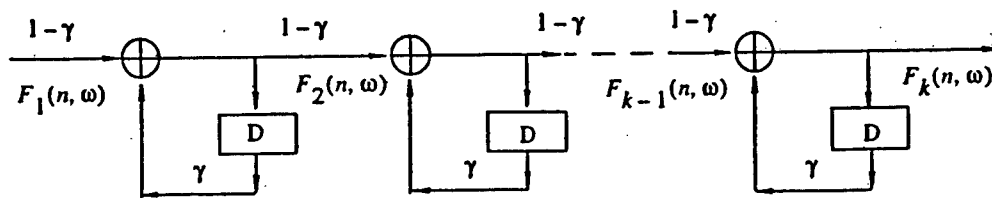
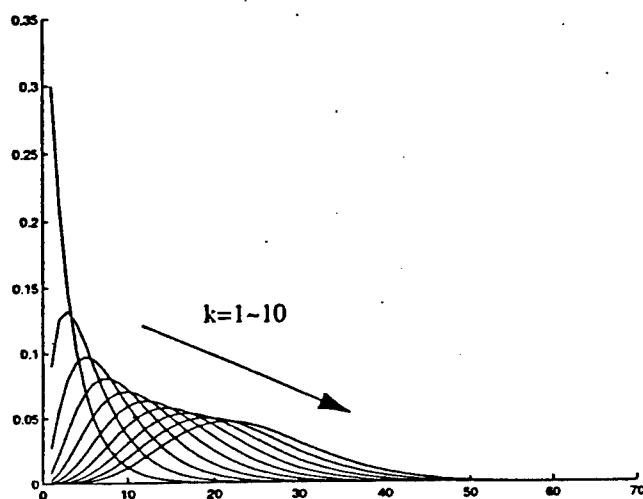
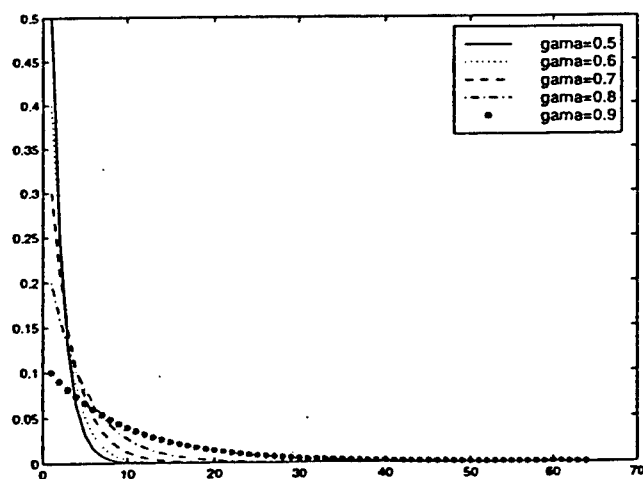


Fig.1 Order recursive Fourier transform



(a)



(b)

Fig.2 pole position and order effect on the impulse response. (a) order effect when $\gamma = 0.7$; (b) pole position effect when order fixed ($k=1$)

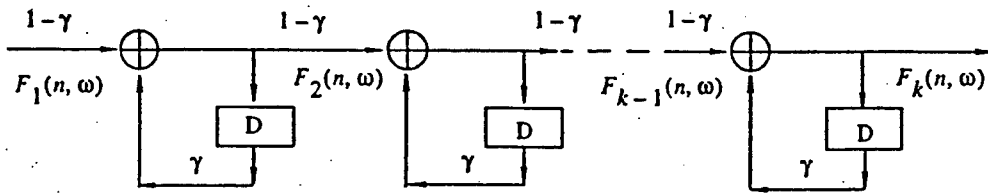
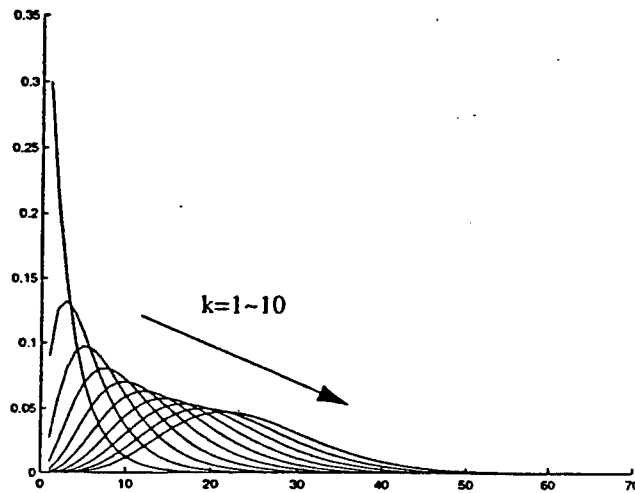
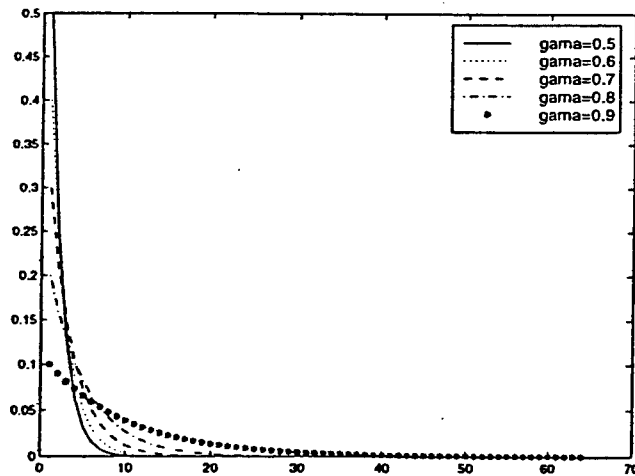


Fig.1 Order recursive Fourier transform

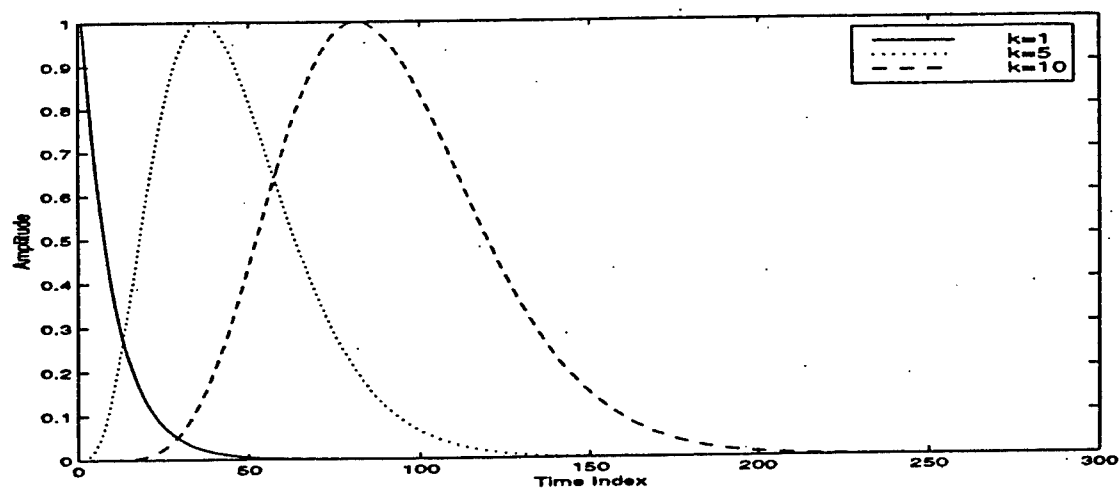


(a)

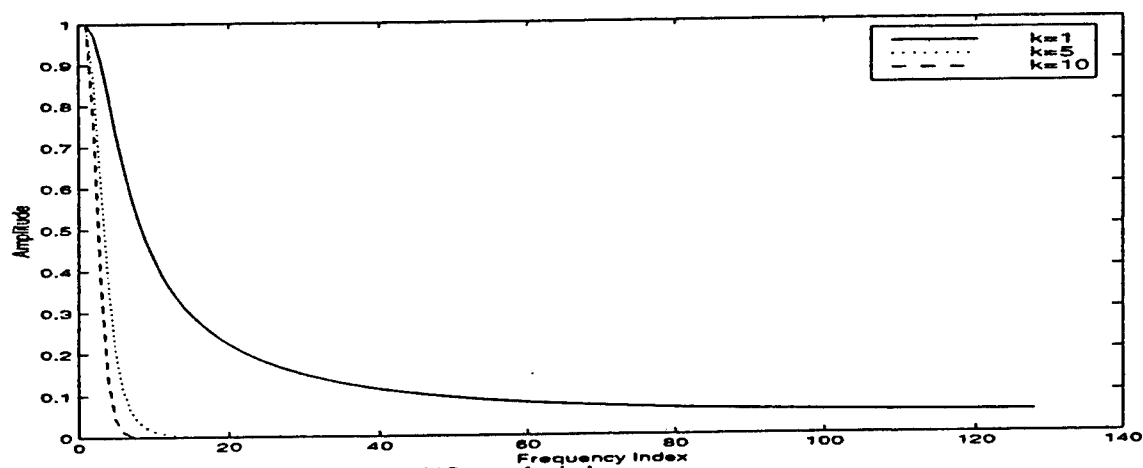


(b)

Fig.2 pole position and order effect on the impulse response. (a) order effect when $\gamma = 0.7$; (b) pole position effect when order fixed ($k=1$)



(a) Impulse response



(b) Spectral window

Fig.3 Time and spectral windows(normalized) for multiple-pole filters $\gamma = 0.9$

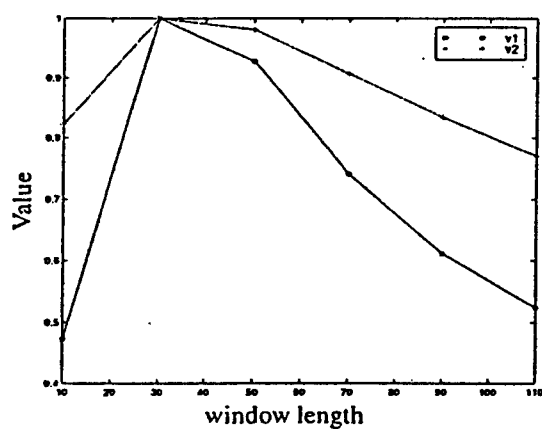
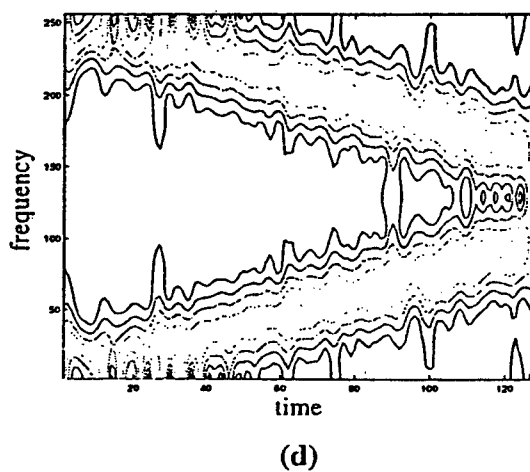
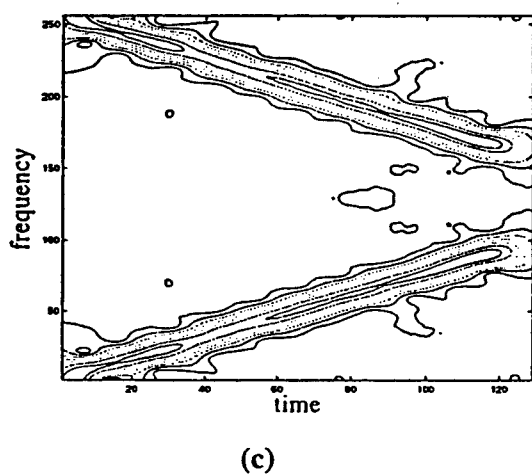
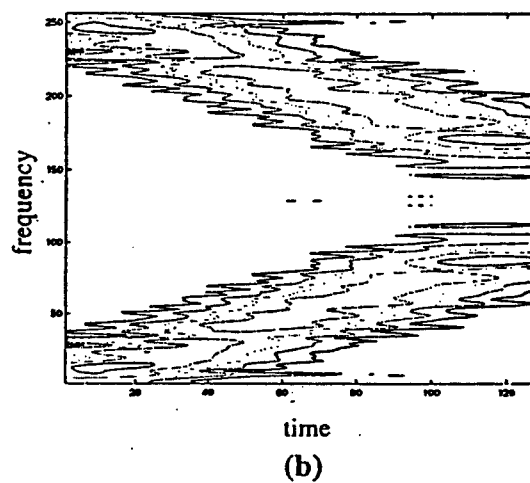
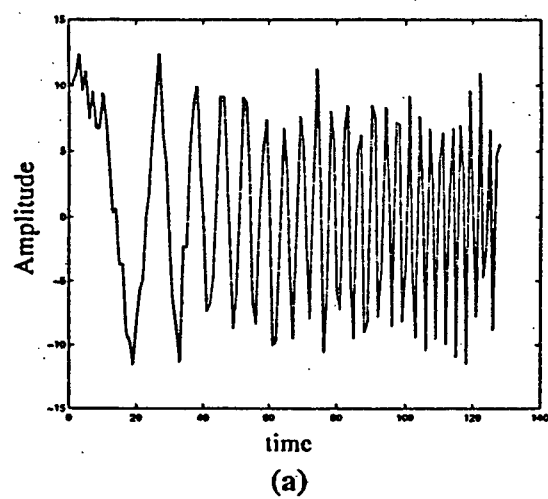
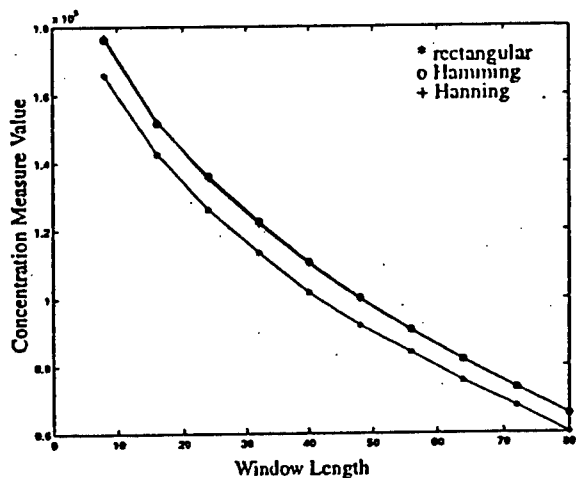
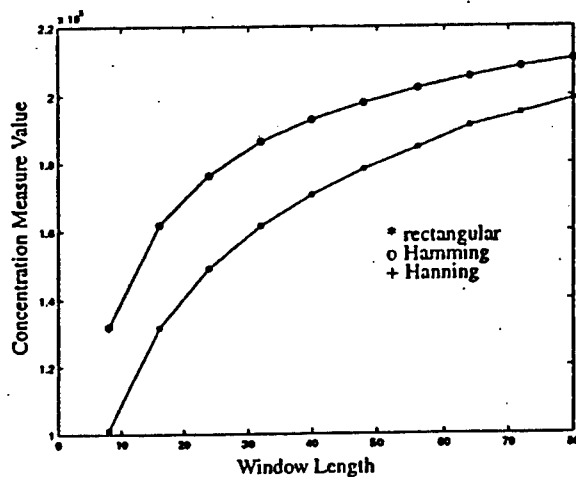


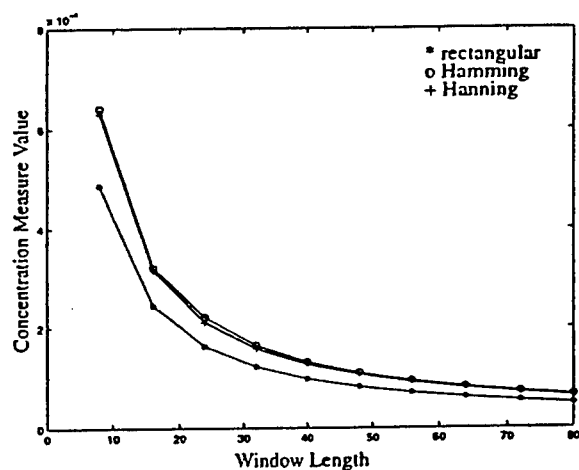
Fig.4 Concentration measures for a chirp signal at different window(rectangular) length. (a) received signal, (b)window length=10, (c)window length=30, (d)window length=110, (e)concentration measures



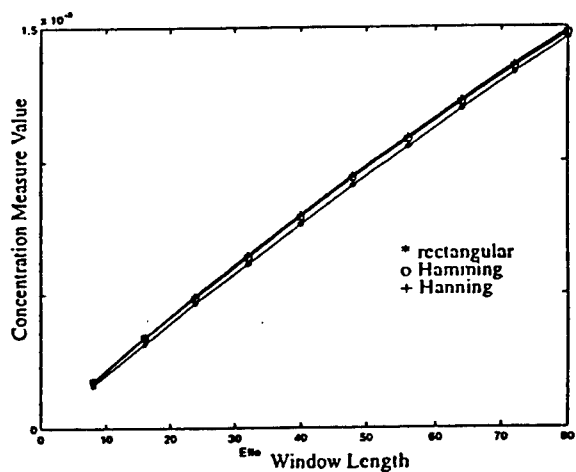
(a) Concentration measure(16) for impulse jammer with three different kind of window with different effective window length



(b) Concentration measure(16) for sinusoid jammer with three different kind of window with different effective window length



(c) Concentration measure(17) for impulse jammer with three different kind of window with different effective window length



(d) Concentration measure(17) for impulse jammer with three different kind of window with different effective window length

Fig.5 Concentration measures for different window with different length on sinusoidal and impulsive signal

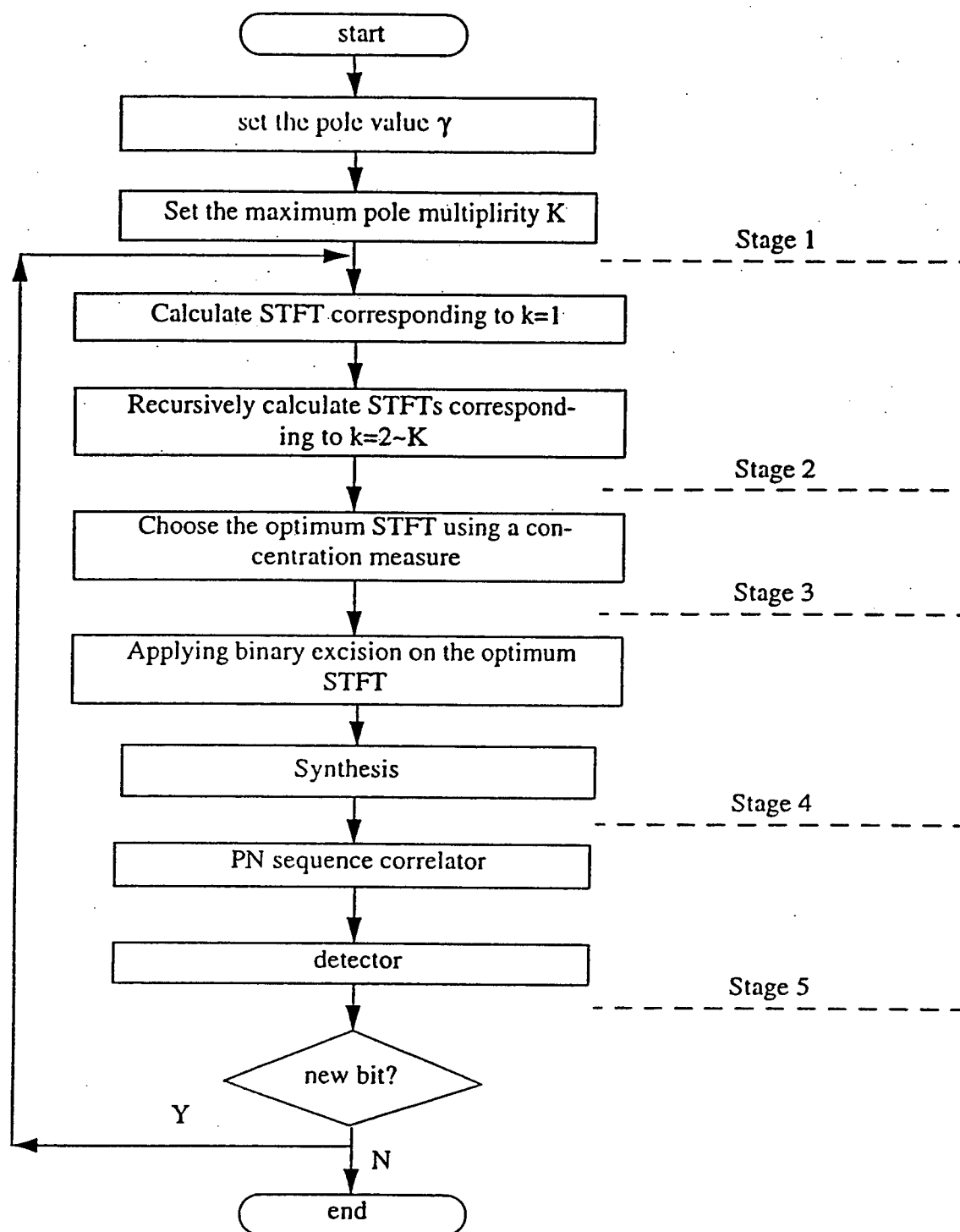


Fig.6 Flow chart for proposed adaptive interference excision method

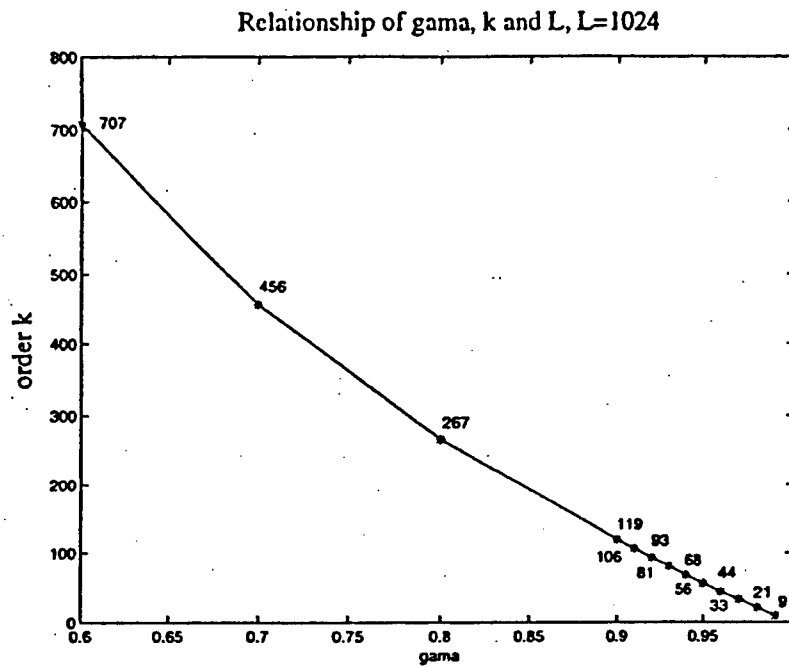
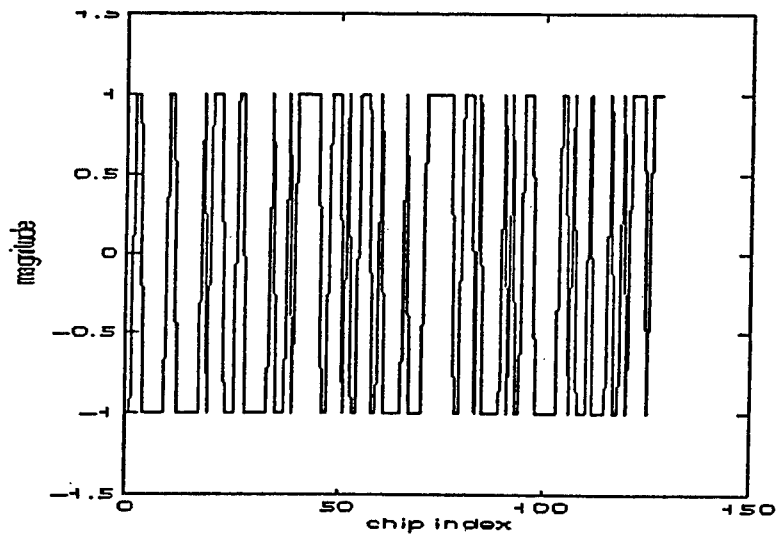
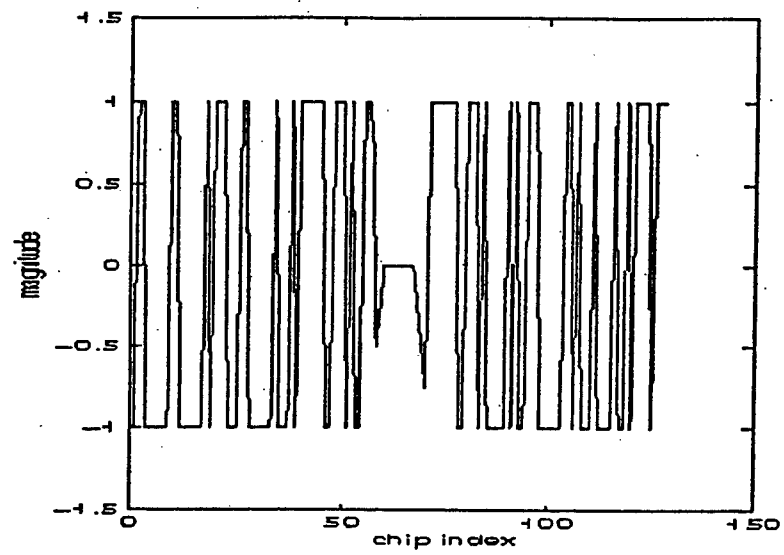
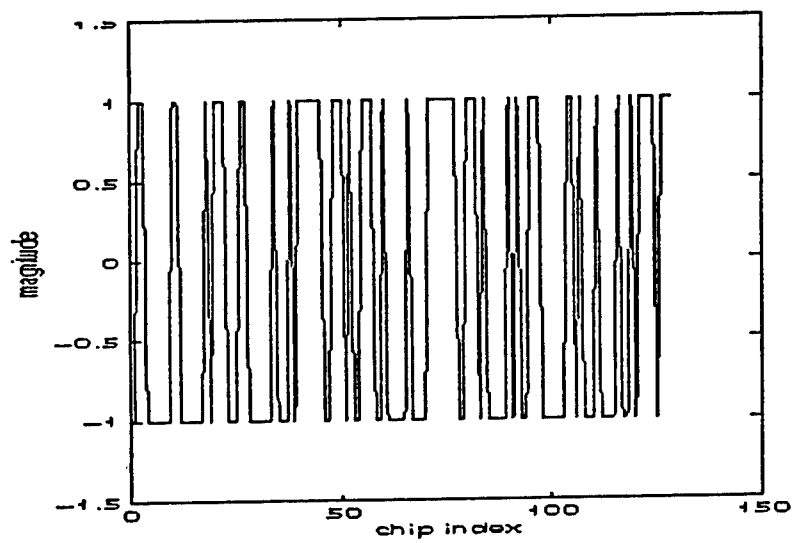
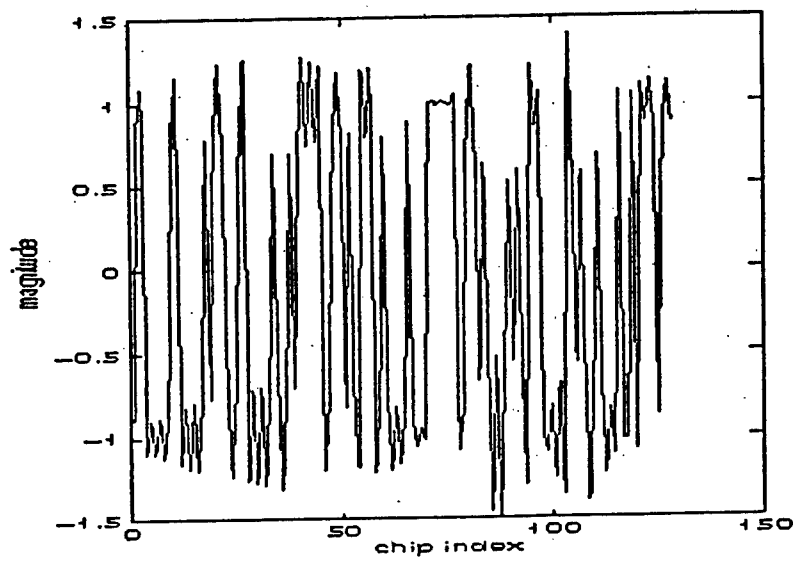


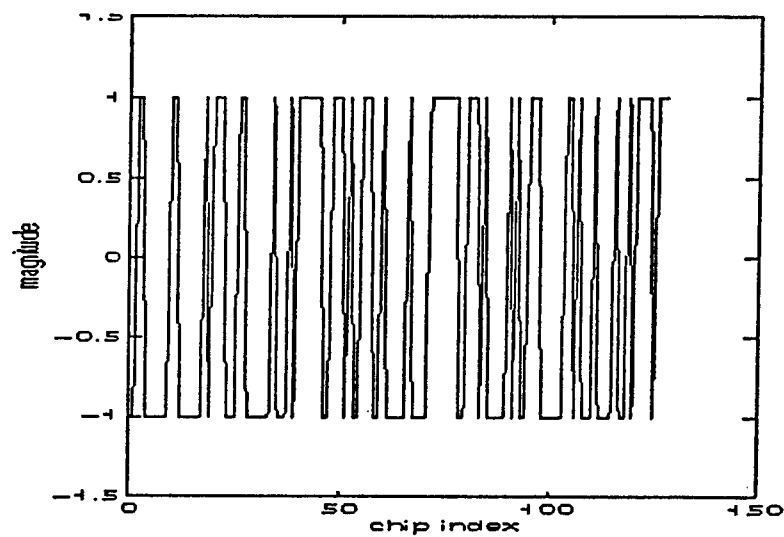
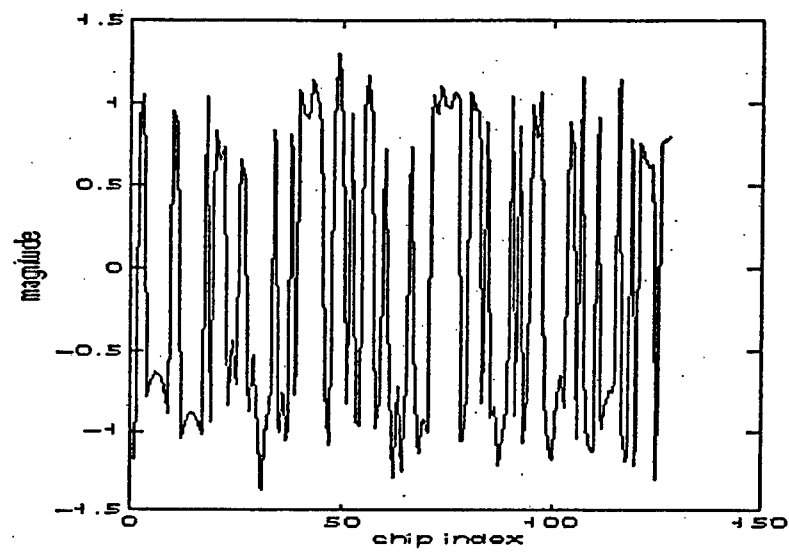
Fig.7 Relationship between γ , K, and L



(a) PN sequence reconstruction for the impulse jammer binary excision



(b) PN sequence reconstruction for the sinusoid jammer binary excision



(c) PN sequence reconstruction for the chirp jammer binary excision

Fig.8 PN sequence distortion under the binary excision on the STFT

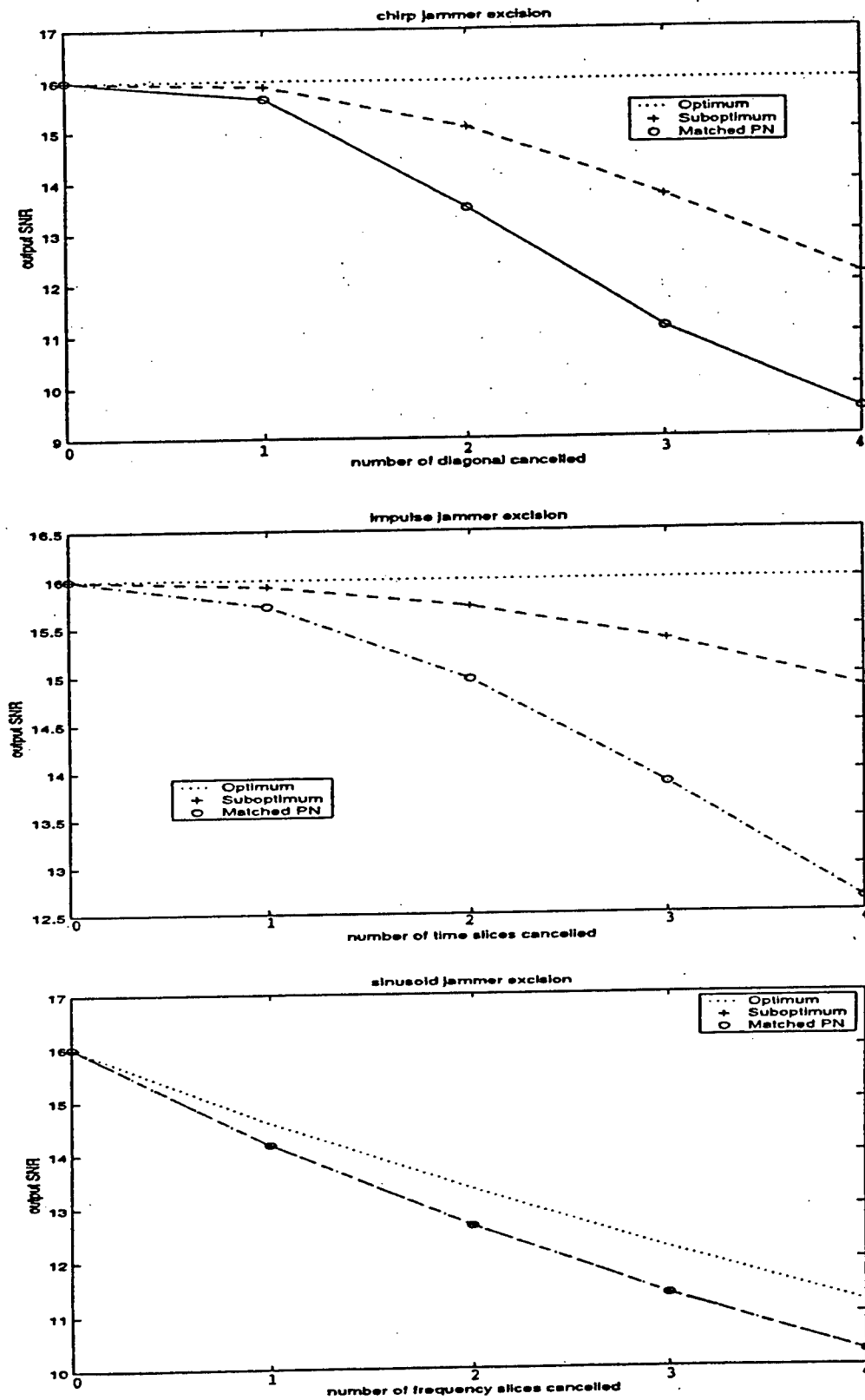


Fig.9 Receiver SNR for chirp, sinusoid and impulse jammers

Performance Analysis of The DS/SS Communications Receiver Implementing A Short Time Fourier Transform Interference Excision System

Xuemei Ouyang and Moeness G. Amin

Department of Electrical and Computer Engineering
Villanova University
Villanova, PA 19085
Email: ouyang, moeness@ece.vill.edu

ABSTRACT

In this paper, the short-time Fourier transform(STFT) is employed for nonstationary jammer excision in direct sequence spread spectrum(DS/SS) communication systems. The received signal is first analyzed by STFT. The localized interferers in the t-f domain are then removed by binary excisions. Finally, the synthesized signal is correlated with the PN sequence and passed to the detector. The selection of both the data window and the distribution of the binary excision values in the t-f domain are key to effective removal of the jammer with a minimum distortion of the DS/SS communication signal. Proper data windows localize the interference in as few t-f bins as possible, whereas good binary excision assigns zero values to only those t-f bins contaminated by the jammer t-f signature. The closed form expression of the receiver SNR is derived as a function of the binary excision values in the t-f domain. The specific cases of impulsive and sinusoidal jammers are analyzed.

1. INTRODUCTION

Interferer excision in spread spectrum communication is an important problem in both military and civilian applications. There are several techniques which have been proposed for this task. These technique include adaptive notch filtering, decision feedback[1] and transform domain methods[2]. For jammer signals which have broadband frequency characteristics, but yet possess narrowband instantaneous bandwidths, time-frequency method have been shown to be very effective in improving the receiver performance and reducing the bit error rate[3,4,5,6]. The application of STFT for interference excision in DS/SS communications using sparse grid and overdetermined time-frequency tilings is discussed in [7] and [8], respectively. In this paper, we extend the application of the STFT to nonstationary interference mitigation in DS/SS communications. We present the analysis of the receiver signal-to-noise ratio, SNR, using binary excisions on STFTs. It is shown that different data windows applied to the same jammer waveform will result in a different value of SNR.

Proper data windows maximize the jammer localization and

thus limit the interference spread in the t-f domain. By confining the jammer to a small number of t-f bins, binary excisions can effectively remove the jammer energy, causing a minimum distortion to the spread spectrum signal. We stress the fact that not only the jammer power affects the receiver SNR, but also its t-f signature. The best and the worst jammer power distributions in the t-f domain in view of STFT-based interference excision are delineated.

The receiver SNR using binary t-f excision applied to STFT is analyzed in Section 2. The window effect on SNR with two special cases, namely, impulsive and sinusoidal jammers are considered in Section 3. The binary excision is represented in Section 4 by a masking matrix. The effect of the structure of this matrix on the receiver SNR is also discussed.

2. RECEIVER SNR

The DS/SS system is shown Fig.1. Assuming "1" is transmitted, the baseband received signal can be expressed as

$$r(i) = p(i) + j(i) + n(i) \quad (1)$$

where $\{p(i)\}$ represents the PN sequence, which is known to both the transmitter and the receiver, $\{j(i)\}$ is the jammer sequence, which is of zero-mean and covariance $\{R_j(i)\}$, and $\{n(i)\}$ is an additive white Gaussian noise sequence with zero mean and variance σ_n^2 . It is assumed that the above three sequences are uncorrelated. The decision variable at the correlator output is given by

$$g = \sum_{i=0}^{L-1} r(i)p(i) \quad (2)$$

where L is the length of PN sequence. If jammer excision is performed prior to despreading, then the received signal is modified to $r'(i)$, and the corresponding decision variable becomes

$$g' = \sum_{i=0}^{L-1} r'(i)p(i) \quad (3)$$

The receiver SNR is commonly defined as[9]

$$SNR_o = \frac{E^2[g']}{var[g']} \quad (4)$$

This work is supported by Rome Lab, contract No. F30602-96-C-0077.

The primary objective of all interference excision techniques is to maximize SNR_o for a large class of interfering signals. The STFT-based interference excision system is most effective in mitigating jammers which are highly localizable in the t-f domain.

The signal synthesis from the STFT can be simply performed using the overlap addition (OLA) method described in [10]. If the binary excision function $A_m(k)$ is applied to the STFT at time m and frequency k , then the synthesized signal is modified to

$$\begin{aligned} r'(n) &= \frac{1}{LW(e^{j0})} \sum_{m=0}^{L-1} \sum_{k=0}^{L-1} A_m(k) R_m(e^{j\omega_k}) e^{j\omega_k n} \\ &= \frac{1}{LW(e^{j0})} \sum_{m=0}^{L-1} \sum_{k=0}^{L-1} \sum_{l=0}^{L-1} A_m(k) r(l) w_m(l) e^{j\omega_k(n-l)} \end{aligned} \quad (5)$$

where R and W are the DFTs of the received signal and the data window, $w_m(l)$, respectively. From (3) and (5),

$$\begin{aligned} g' &= \frac{1}{LW(e^{j0})} \sum_{n=0}^{L-1} \sum_{m=0}^{L-1} \sum_{k=0}^{L-1} \sum_{l=0}^{L-1} A_m(k) w_m(l) e^{j\omega_k(n-l)} (p(l)p(n)) \\ &+ \frac{1}{LW(e^{j0})} \sum_{n=0}^{L-1} \sum_{m=0}^{L-1} \sum_{k=0}^{L-1} \sum_{l=0}^{L-1} A_m(k) w_m(l) e^{j\omega_k(n-l)} j(l)p(n) \\ &+ \frac{1}{LW(e^{j0})} \sum_{n=0}^{L-1} \sum_{m=0}^{L-1} \sum_{k=0}^{L-1} \sum_{l=0}^{L-1} A_m(k) w_m(l) e^{j\omega_k(n-l)} n(l)p(n) \\ &= g'_1 + g'_2 + g'_3 \end{aligned} \quad (6)$$

Since the three components in the received signal are independent,

$$E(g') = E(g'_1) + E(g'_2) + E(g'_3)$$

$$\text{var}(g') = \text{var}(g'_1) + \text{var}(g'_2) + \text{var}(g'_3)$$

Using the properties of $p(i)$, $j(i)$ and $n(i)$, we have

$$E(g'_2) = E(g'_3) = 0$$

$$E(g'_1) = \frac{1}{LW(e^{j0})} \sum_{n=0}^{L-1} \sum_{m=0}^{L-1} \sum_{k=0}^{L-1} A_m(k) w_m(n) \quad (7)$$

The expressions of the variances of the above three components are given in [11]. From these expressions and above mean value equations, the general expression of the receiver SNR_o is given by equation (8). If the preprocessing is disabled, i.e., there is no jammer excision, then $A_m(k)=1$ and the SNR_o simplifies to [12]

$$SNR_{wo} = \frac{L}{R_j(0) + \sigma_n^2} \quad (9)$$

3. WINDOW EFFECT ON SNR

In the following, we examine the effect of the data window on SNR_o expression (8) with the two specific cases of impulsive and sinusoidal jammers.

If the jammer is an impulse, i.e., $j(i) = \rho \delta(i - i_0)$, the SNR_o takes the form (10). All signals in the t-f region (m, k) , $m \in Q$, where Q is a set of integer values chosen from $[1, L]$, are removed by setting the binary coefficients $A_m(k)=0$, $m \in Q$, whereas all signals in the complement t-f region (m, k) , $m \in \bar{Q}$ is left intact by setting the binary coefficients $A_m(k)=1$, $m \in \bar{Q}$. These two conditions simplify equation (10) to the form (11). Two observations are in order: 1) The first summation term in the denominator is zero if $i_0 \in Q$ and the data window span is equal to or smaller than that of the t-f strip $m \in Q$. 2) The term with overlapping windows in the denominator takes a minimum value if $w_m(i) = \delta(m - i)$, i.e., the window is a unit sample sequence.

In this case SNR_o is maximum and equal to

$$SNR_o = \frac{(L-1)}{\sigma_n^2} \quad (12)$$

$$SNR_o = \frac{(1/L) \left(\sum_{n=0}^{L-1} \sum_{m=0}^{L-1} \sum_{k=0}^{L-1} A_m(k) w_m(n) \right)^2}{\sum_{m=0}^{L-1} \sum_{k=0}^{L-1} \sum_{l=0}^{L-1} \sum_{m_1=0}^{L-1} \sum_{k_1=0}^{L-1} A_m(k) A_{m_1}(k) w_m(l) w_{m_1}(l) R_j(l, l_1) e^{-j\omega_k(l-l_1)} + \sigma_n^2 \sum_{m=0}^{L-1} \sum_{k=0}^{L-1} \sum_{l=0}^{L-1} \sum_{m_1=0}^{L-1} A_m(k) A_{m_1}(k) w_m(l) w_{m_1}(l)} \quad (8)$$

$$SNR_o = \frac{(1/L) \left(\sum_{n=0}^{L-1} \sum_{m=0}^{L-1} \sum_{k=0}^{L-1} A_m(k) w_m(n) \right)^2}{\rho^2 \sum_{m=0}^{L-1} \sum_{k=0}^{L-1} \sum_{l=0}^{L-1} A_m(k) A_{m_1}(k) w_m(i_0) w_{m_1}(i_0) + \sigma_n^2 \sum_{m=0}^{L-1} \sum_{k=0}^{L-1} \sum_{l=0}^{L-1} \sum_{m_1=0}^{L-1} A_m(k) A_{m_1}(k) w_m(l) w_{m_1}(l)} \quad (10)$$

$$SNR_o = \frac{\left(\sum_{m, m \in \bar{Q}} w_m(0) \right)^2}{\rho^2 \left(\sum_{m, m \in \bar{Q}} w_m(i_0) \right)^2 + \sigma_n^2 \left\{ \left(\sum_{m, m \in \bar{Q}} w_m(0) \right)^2 + \sum_{m, m \in \bar{Q}} \sum_{m_1, m_1 \in \bar{Q}, m \neq m_1} \sum_{l=0}^{L-1} w_m(l) w_{m_1}(l) \right\}} \quad (11)$$

If the jammer is a sinusoid, $j(i) = \rho \exp(j(2\pi/L)k_0 i)$, then the corresponding DFT is $\rho \delta(k - k_0)$. It can be readily shown that for a sinusoidal jammer, the signal-to-noise ratio of the DS/SS receiver implementing STFT is (13).

If we only set the peak value of the STFT at the frequency $k=k_0$ to zero, i.e., $A_m(k_0)=0$ and $A_m(k)=1, k \neq k_0$, then (13) simplifies to (14). It should be noted that by doing so, the jammer is not entirely removed, as evident by the appearance of ρ^2 in the denominator of equation (14). The jammer is removed in its entirety, however, if we set $W_m(k - k_0) = 0, k \neq k_0$, which amounts to using a rectangular data window with the appropriate length. In this case, SNR_o can be expressed as

$$SNR_o = \frac{(L-1)}{\sigma_n^2} \quad (15)$$

If the jammer frequency does not coincide with any of the STFT frequency bins, then its power leaks over the entire t-f plane. Mitigating the interference may then be achieved by carefully selecting the region of highest jammer concentration and setting the corresponding coefficients $A_m(k)$ to zero. If we denote C as the jammer power remained after setting q t-f bins to zero, then the receiver SNR_o becomes

$$SNR_o = \frac{(L-q)}{C + \sigma_n^2} \quad (16)$$

The trade-off between jammer removal and desired signal distortion is evident in equation (16). As the number of t-f binary coefficients assuming zero-value increases, i.e., q increase, the numerator in (16) decreases, but also less jammer power is retained, i.e., C decreases.

Concentration measures such as those introduced in [13,14] can help in selecting the optimum windows.

4. MASKING EFFECT ON SNR

Not only the jammer power will affect the receiver SNR, but also its position in t-f domain. Jammer position determines the binary excision(mask) function matrix. Suppose the jammer occupies L t-f bins, which are to be removed by proper masking. the following analysis shows that the positions of these L bins influence the SNR performance.

Under the assumption that the jammer is entirely removed by setting the corresponding L t-f binary coefficients to zeros, equation (8) simplifies to (17). Let $X = \sum_m \left(A_m(k) w_m(n) \right)$, which

can be expressed in the matrix form (18). If $x_{k,l}$ denote the elements of X , then the SNR expression (17) becomes

$$SNR_o = \frac{\left(\sum_{k=0}^{L-1} \sum_{l=0}^{L-1} x_{k,l} \right)^2}{L \sigma_n^2 \sum_{k=0}^{L-1} \sum_{l=0}^{L-1} x_{k,l}^2} \quad (19)$$

Since all the elements in the masking matrix A and the window samples are nonnegative, all the elements in X are nonnegative, then

$$\left(\sum_{k=0}^{L-1} \sum_{l=0}^{L-1} x_{k,l} \right)^2 \geq \sum_{k=0}^{L-1} \sum_{l=0}^{L-1} x_{k,l}^2 \quad (20)$$

The equality holds when there is only one nonzero element in the summation. The closest the values of $x_{k,l}$, the larger the SNR_o .

$$SNR_o = \frac{(1/L) \left(\sum_{n=0}^{L-1} \sum_{m=0}^{L-1} A_m(k) w_m(n) \right)^2}{\rho^2 \sum_{m=0}^{L-1} \sum_{k=0}^{L-1} A_m(k) A_{m_1}(k) W_{m_1}(k - k_0) W_m(k - k_0) + \sigma_n^2 \sum_{m=0}^{L-1} \sum_{k=0}^{L-1} \sum_{l=0}^{L-1} A_m(k) A_{m_1}(k) w_m(l) w_{m_1}(l)} \quad (13)$$

$$SNR_o = \frac{(1/L)(L-1)^2 L^2 W^2(e^{j0})}{\rho^2 \sum_{m=0}^{L-1} \sum_{k=0, k \neq k_0}^{L-1} W_m(k - k_0) W_{m_1}(k - k_0) + \sigma_n^2 (L-1) L W^2(e^{j0})} \quad (14)$$

$$SNR_o = \frac{\left(\sum_{n=0}^{L-1} \sum_{m=0}^{L-1} A_m(k) w_m(n) \right)^2}{L \sigma_n^2 \sum_{m=0}^{L-1} \sum_{k=0}^{L-1} \sum_{l=0}^{L-1} A_m(k) A_{m_1}(k) w_m(l) w_{m_1}(l)} = \frac{\left(\sum_{n=0}^{L-1} \sum_{k=0}^{L-1} \left(\sum_m A_m(k) w_m(n) \right) \right)^2}{L \sigma_n^2 \sum_{k=0}^{L-1} \sum_{l=0}^{L-1} \left(\sum_m A_m(k) w_m(l) \right) \left(\sum_m A_{m_1}(k) w_{m_1}(l) \right)} \quad (17)$$

$$X = \begin{bmatrix} A_1(0) & A_2(0) & \dots & A_M(0) \\ A_1(1) & A_2(1) & \dots & A_M(1) \\ \vdots & \vdots & \ddots & \vdots \\ A_1(L-1) & A_2(L-1) & \dots & A_M(L-1) \end{bmatrix}_{L \times M} \begin{bmatrix} w_1(0) & w_1(1) & \dots & w_1(L-1) \\ w_2(0) & w_2(1) & \dots & w_2(L-1) \\ \vdots & \vdots & \ddots & \vdots \\ w_M(0) & w_M(1) & \dots & w_M(L-1) \end{bmatrix}_{M \times L} = AW \quad (18)$$

It is clear from (18) that the removal of L elements from one row in A matrix yields the largest difference among the elements in X , i.e., the smallest SNR_o . In this case, $x_{k,l}$ range from 0 to $W(e^{j0})$. If the L elements are removed from one column of A , i.e., cancelling the coefficients in one time slice, $x_{k,l}$ will have the smallest range, which is $[W(e^{j0}) - \max(w(n)), W(e^{j0})]$. This leads to the largest SNR_o . One interpretation of the above result lies in the fact that for STFT, due to the moving window, there is a redundancy in the information along the time axis, yet there is no redundancy along the frequency axis. If the data in one time slice is removed, the adjacent time slice will still include most of the data samples, depending on the overlapping pattern of the moving window. As long as the overlap is not sparse, the information lost is insignificant. The signal may, however, encounter some energy attenuation. This kind of binary excision will not substantially decrease the receiver performance although some degradation to the SNR_o may occur. On the other hand, if the data in one frequency bin is removed, the information at that frequency is lost and can not be recovered in the synthesis procedure. In this case, the SNR suffers the largest degradation.

5. CONCLUSION

The receiver performance of DS/SS communication system implementing the STFT and binary excision for jammer mitigation is analyzed. The closed form expression of the receiver SNR has been obtained. Based on this expression, the window and masking effects on the SNR have been delineated. It is shown that different windows depict the jammer in t-f domain with different resolutions. The best resolution combined with the proper binary mask yield the highest receiver SNR. The position of the jammer in the t-f domain, i.e. the structure of the masking matrix significantly affects the receiver performance. It is shown that the highest SNR is obtained by masking a time slice, while the lowest SNR is a result of masking a frequency bin when only L coefficients can be removed.

REFERENCES

[1] J. Laster and J. Reed, "Interference Rejection in Digital Wireless Communication," *IEEE signal processing magazine*, pp37-

62, May, 1997.

[2] L. Milstein and P. Das, "An Analysis of a Real-Time Transform Domain Filtering Digital Communication System--Part I: Narrow-band Interference Rejection," *IEEE Trans. on Comm.*, pp816-824, vol.28, No.6, June, 1980.

[3] M. Amin, "Interference mitigation in spread spectrum communications using time-frequency distributions", *IEEE Trans. on SP*, vol.45, No.1, Jan. 1996.

[4] C. Wang and M. Amin, "Performance analysis of instantaneous frequency-based interference excision techniques in spread spectrum communications," *IEEE Trans. on SP*, vol.46, No.1, Jan. 1998.

[5] M. Medley, G. Saulnier, and Das, "Applications of the wavelet transform in spread spectrum communications systems," *SPIE, Wavelet Applic.*, Orlando, FL, April 1994.

[6] M. Tazebay and A. Akansu, "Adaptive subband transforms in time-frequency excisers for DSSS communication systems," *IEEE Trans. on SP*, pp. 2776-2782, Nov. 1995.

[7] S. Roberts and M. Amin, "Linear vs. bilinear time-frequency methods for interference mitigation in direct sequence spread spectrum communication systems," *Asilomar Conf. on Signals, Systems and Computers*, Pac. Grove, Ca, Nov. 1995.

[8] B. Krongold, M. Kramer, K. Ramchandran and D. Jones, "Spread spectrum interference suppression using adaptive time-frequency tilings," *Proceedings of ICASSP97*, Munich, Germany, April 1997.

[9] F. Hsu and A. Giordano, "Digital whitening techniques for improving spread spectrum communications performance in the presence of narrow-band jamming and interference," *IEEE Trans. on Comm.*, vol. 26, pp.209-216, Feb 1978.

[10] J. Allen and L. Rabiner, "A Unified Approach to Short-Time Fourier Analysis and Synthesis," *Proc. IEEE*, vol. 65, No. 11, Nov. 1977.

[11] X. Ouyang and M. G. Amin, "Time-Frequency Concentration Measures for Nonstationary Interference Excisions in DS/SS Communications," *IEEE Sarnoff Symposium on Advances in Wired and Wireless Communications*, New Jersey, March, 1998.

[12] J. Ketchum and J. Proakis, "Adaptive algorithms for estimating and suppressing narrowband interference in PN spread spectrum systems," *IEEE Trans. on Comm.*, May 1982.

[13] D. Jones and R. Baraniuk, "A Simple Scheme for Adapting Time-Frequency Representations," *IEEE Trans. on SP*, vol. 42, Dec. 1994.

[14] W. Williams, M. Brown, and A. Hero, "Uncertainty, information and time-frequency distributions," *SPIE*, vol.1566, pp.144-156, 1991.

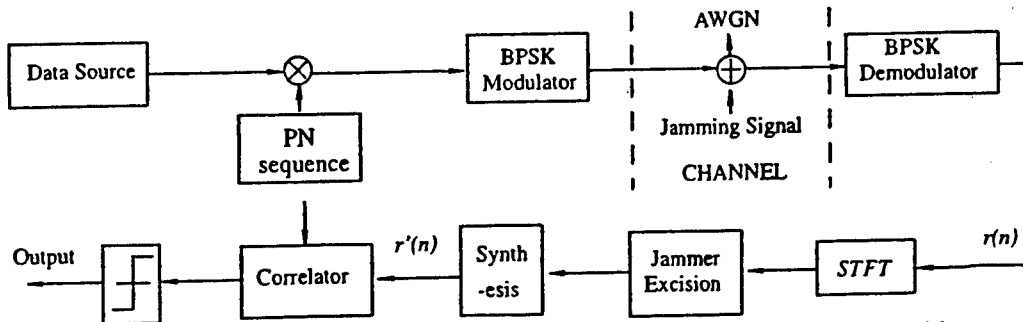


Fig.1 Block diagram of a direct sequence spread spectrum system with STFT jammer excision

Time-Frequency Concentration Measures for Nonstationary Interference Excisions in DS/SS Communications

Xuemei Ouyang and Moeness G. Amin

Department of Electrical and Computer Engineering
Villanova University
Villanova, PA 19085
Email: ouyang, moeness@ece.vill.edu

ABSTRACT

In this paper, we show the effectiveness of applying concentration measures in the time-frequency (t-f) plane to remove nonstationary interference in direct sequence spread spectrum communications. These measures are used to select the optimum window in short-time-Fourier transform (STFT). This window yields improved localization of the jammer and, subsequently, allows its excision with minimum distortion of the desired signal. The expression of the receiver SNR is derived as a function of the binary excision values in the t-f domain. The two specific cases of impulsive and sinusoidal jammers are analyzed.

I. INTRODUCTION

The application of STFT for interference excision in DS/SS communications using sparse grid and overdetermined time-frequency tilings is discussed in [1] and [2], respectively.

In this paper, we extend the application of the STFT to nonstationary interference mitigation in DS/SS communications. We present the analysis of the receiver signal-to-noise ratio, SNR_o , using binary excisions on STFTs. It is shown that different data windows applied to the same jammer waveform will result in a different value of SNR_o . The proper windows maximize the jammer localization and thus limit the interference spread in the t-f domain. By confining the jammer to small number of t-f bins, binary excisions can effectively remove the jammer energy, causing a minimum distortion to the spread spectrum signal. A concentration measure is applied to select the window of maximum interference localization.

The receiver SNR using binary t-f excision applied to STFT is analyzed in Section II. Two Special cases are considered, namely, impulsive and sinusoidal jammers. The concentration measure for optimum window selection and computer simulations are discussed in Section III.

II. RECEIVER SNR

The DS/SS system is shown Fig.1. Assume "1" is transmitted, the baseband received signal can be expressed as

$$r(i) = p(i) + j(i) + n(i) \quad (1)$$

where $\{p(i)\}$ represents the PN sequence, which is known to both the transmitter and the receiver. $\{j(i)\}$ is the jammer sequence,

which is of zero-mean and covariance $\{R_j(i)\}$, and $\{n(i)\}$ is an additive white Gaussian noise sequence with zero mean and variance σ_n^2 . It is assumed that the above three sequences are uncorrelated. The decision variable at the output of the correlator is given by

$$g = \sum_{i=0}^{L-1} r(i)p(i) \quad (2)$$

where L is the length of PN sequence. If jammer excision is performed prior to despreading, then the received signal is modified to $r'(i)$, and the corresponding decision variable becomes

$$g' = \sum_{i=0}^{L-1} r'(i)p(i) \quad (3)$$

The receiver SNR is defined as [3]

$$SNR_o = \frac{E^2[g']}{var[g']} \quad (4)$$

The primary objective of all interference excision techniques in spread spectrum communication is to maximize SNR_o for a large class of interfering signals. The STFT-based interference excision system is most effective in mitigating jammers which can be highly localized in the t-f domain.

The signal synthesis from the STFT can be simply performed using the overlap addition (OLA) method described in [4]. If the binary excision function $A_m(k)$ is applied to the STFT at time m and frequency k , then the synthesized signal is modified to

$$\begin{aligned} r'(n) &= \frac{1}{LW(e^{j0})} \sum_{m=0}^{L-1} \sum_{k=0}^{L-1} A_m(k) R_m(e^{j\omega_k}) e^{j\omega_k n} \\ &= \frac{1}{LW(e^{j0})} \sum_{m=0}^{L-1} \sum_{k=0}^{L-1} \sum_{l=0}^{L-1} A_m(k) r(l) w_m(l) e^{j\omega_k(n-l)} \end{aligned} \quad (5)$$

where R and W are the DFTs of the received signal and, the data window, $w_m(l)$, respectively. From (3) and (5)

$$\begin{aligned} g' &= \frac{1}{LW(e^{j0})} \sum_{n=0}^{L-1} \sum_{m=0}^{L-1} \sum_{k=0}^{L-1} \sum_{l=0}^{L-1} A_m(k) w_m(l) e^{j\omega_k(n-l)} p(l) p(n) \\ &\quad + \frac{1}{LW(e^{j0})} \sum_{n=0}^{L-1} \sum_{m=0}^{L-1} \sum_{k=0}^{L-1} \sum_{l=0}^{L-1} A_m(k) w_m(l) e^{j\omega_k(n-l)} j(l) p(n) \\ &\quad + \frac{1}{LW(e^{j0})} \sum_{n=0}^{L-1} \sum_{m=0}^{L-1} \sum_{k=0}^{L-1} \sum_{l=0}^{L-1} A_m(k) w_m(l) e^{j\omega_k(n-l)} n(l) p(n) \\ &= g'_1 + g'_2 + g'_3 \end{aligned} \quad (6)$$

*This work is supported by Rome Lab, contract No. F30602-96-C-0077

Since the three components in the received signal are independent, then

$$E(g') = E(g'_1) + E(g'_2) + E(g'_3) \quad (7)$$

$$\text{var}(g') = \text{var}(g'_1) + \text{var}(g'_2) + \text{var}(g'_3) \quad (8)$$

It can be readily shown that $E(g'_2) = E(g'_3) = 0$, and

$$E(g'_1) = \frac{1}{LW(e^{j0})} \sum_{n=0}^{L-1} \sum_{m=0}^{L-1} A_m(k) w_m(n).$$

The variances of the above three components are given by (9), (10), (11). The corresponding SNRo is given in (12). If there is no jammer excision, $A_m(k)=1$ and the SNRo simplifies to the well known formula [5]

$$SNR_{wo} = \frac{(L^2 W(e^{j0}))^2 / L}{L^2 R_j(0) W^2(e^{j0}) + L^2 \sigma_n^2 W^2(e^{j0})} = \frac{L}{R_j(0) + \sigma_n^2} \quad (13)$$

In the following, we examine two specific cases of the general SNRo expression (12) under impulsive and sinusoidal jammers.

A. Impulsive Jammer

If the jammer is an impulse, i.e., $j(i) = \delta(i - i_0)$, the SNRo takes the form (14). All signals in the t-f region (m, k) , $m \in Q$, where Q is a set of integer values chosen from $[1, L]$, is removed by setting the binary coefficients $A_m(k)=0$, $m \in Q$, whereas all signals in the complement t-f region (m, k) , $m \in \bar{Q}$ is left intact by setting the binary coefficients $A_m(k)=1$, $m \in \bar{Q}$. These two conditions simplify equation (14) to the form (15). Two observations are in order: 1) The first summation term in the denominator is zero if $i_0 \in Q$ and the data window span is equal to or smaller than

that of the t-f strip $m \in Q$. 2) The term with overlapping windows in the denominator takes a minimum value if $w_m(i) = \delta(m - i)$, i.e., the window is a unit sample sequence. In this case SNRo is maximum and equal to

$$SNR_o = \frac{(m-1)^2}{\sigma_n^2(m-1)^2} = \frac{1}{\sigma_n^2} \quad (16)$$

B. Sinusoidal Jammer

If the jammer is sinusoid, $j(i) = B e^{j \frac{2\pi}{L} k_0 i}$, then the corresponding DFT is $B \delta(k - k_0)$. It can be readily show that for a sinusoidal jammer, the signal-to-noise ratio of the DS/SS receiver implementing STFT is given by (17). If we only set the peak value of the STFT at the frequency $k=k_0$ to zero, i.e., $A_m(k_0)=0$ and $A_m(k)=1$, $k \neq k_0$, then equation (17) simplifies to (18). It should be noted that by doing so, the jammer is not entire removed, as evident by the appearance of B^2 in the denominator of equation (18). The jammer is entirely removed if we set $w_m(k - k_0) = 0$, $k \neq k_0$, which amounts to using a rectangular data window with the appropriate length. In this case, SNRo can be expressed as

$$SNR_o = \frac{(L-1)}{\sigma_n^2} \quad (19)$$

On the other hand, if the jammer frequency does not coincide with any of the STFT frequency bins, then its power leaks over the entire t-f plane. Mitigating the interference may then be achieved by carefully selecting the region of highest jammer concentration and setting the corresponding coefficients $A_m(k)$ to zero. If we donate C as the jammer power remained after setting q t-f bins to

$$\text{var}(g'_1) = \left(\frac{1}{LW(e^{j0})} \right)^2 \left(\sum_{n=0}^{L-1} \sum_{m=0}^{L-1} A_m(k) w_m(n) \right)^2 - \left(\frac{1}{LW(e^{j0})} \sum_{n=0}^{L-1} \sum_{m=0}^{L-1} A_m(k) w_m(n) \right)^2 = 0 \quad (9)$$

$$\text{var}(g'_2) = \left(\frac{\sqrt{L}}{LW(e^{j0})} \right)^2 \sum_{m=0}^{L-1} \sum_{k=0}^{L-1} \sum_{l=0}^{L-1} \sum_{m_1=0}^{L-1} A_m(k) A_{m_1}(k) w_m(l) w_{m_1}(l_1) R_j(l-l_1) e^{-j\omega_k(l-l_1)} \quad (10)$$

$$\text{var}(g'_3) = \left(\frac{\sqrt{L} \sigma_n}{LW(e^{j0})} \right)^2 \sum_{m=0}^{L-1} \sum_{k=0}^{L-1} \sum_{l=0}^{L-1} A_m(k) A_{m_1}(k) w_m(l) w_{m_1}(l) \quad (11)$$

$$SNR_o = \frac{(1/L) \left(\sum_{n=0}^{L-1} \sum_{m=0}^{L-1} A_m(k) w_m(n) \right)^2}{\sum_{m=0}^{L-1} \sum_{k=0}^{L-1} \sum_{l=0}^{L-1} \sum_{m_1=0}^{L-1} A_m(k) A_{m_1}(k) w_m(l) w_{m_1}(l_1) R_j(l-l_1) e^{-j\omega_k(l-l_1)} + \sigma_n^2 \sum_{m=0}^{L-1} \sum_{k=0}^{L-1} \sum_{l=0}^{L-1} A_m(k) A_{m_1}(k) w_m(l) w_{m_1}(l)} \quad (12)$$

$$SNR_o = \frac{(1/L) \left(\sum_{n=0}^{L-1} \sum_{m=0}^{L-1} A_m(k) w_m(n) \right)^2}{\sum_{m=0}^{L-1} \sum_{k=0}^{L-1} A_m(k) A_{m_1}(k) w_m(i_0) w_{m_1}(i_0) + \sigma_n^2 \sum_{m=0}^{L-1} \sum_{k=0}^{L-1} \sum_{l=0}^{L-1} A_m(k) A_{m_1}(k) w_m(l) w_{m_1}(l)} \quad (14)$$

$$SNR_o = \frac{\left(\sum_{m \in \bar{Q}} w_m(0) \right)^2}{\left(\sum_{m \in Q} w_m(i_0) \right)^2 + \sigma_n^2 \left\{ \left(\sum_{m \in Q} w_m(0) \right)^2 + \sum_{m \in Q} \sum_{m_1 \in Q} \sum_{l=0}^{L-1} w_m(l) w_{m_1}(l) \right\}} \quad (15)$$

zero, then the receiver SNR becomes

$$SNR_o = \frac{(L-q)}{C + \sigma_n^2} \quad (20)$$

The trade-off between jammer removal and desired signal distortion is evident in equation (20). As the number of t-f binary coefficients assuming zero-value increases, i.e., q increase, the numerator in (20) decreases, but also less jammer power is retained, i.e., C decreases.

III. CONCENTRATION MEASURE

The main objective of adaptive STFT is to decide, without human intervention and extensive prior knowledge of the underlying signal characteristics, on the analysis window which offers the best time-frequency resolution[6]. Procedures based on mathematical optimal criteria appears most promising. Renyi information of the third order has been shown to provide a valuable and effective information measure in the context of time-frequency distributions[7].

$$v_1 = -\frac{1}{2} \sum_n \sum_\omega \log |STFT(n, \omega)|^3 \quad (21)$$

It is recognized that the value of v corresponding to the highest resolution t-f signal representation should be larger than others. As such, we proceed to calculate v for different windows and window length of STFTs and examine its value. The window maximum concentration measure is determined and the respective STFT is chosen as the most appropriate t-f representation.

Another local concentration measure is introduced in [8] as:

$$v_2 = \frac{\sum_n \sum_\omega |STFT(n, \omega)|^4}{\left(\sum_n \sum_\omega |STFT(n, \omega)|^2 \right)^2} \quad (22)$$

The basis for choosing the optimum window rests on the intuition that high value of v reflects good time-frequency localization and high resolution. The ratio of the L_4 norm to the L_2 norm of the STFT favors "peaky" distributions that place much of the signal energy into small region of the time-frequency plane, thus achieving a concentrated representation.

In Fig.(2,3), a spread spectrum signal is generated with L is 128. In order to find the effect of the different window length on the concentration measures, we change the lengths for three types of the windows, namely rectangular, Hamming and Hanning window. The sinusoidal jammer is considered in Fig.2 and the impulsive jammer is considered in Fig.3. And the criterion (21) is employed. The same simulations are performed using the criterion (22) and the results are shown in Fig.4 and Fig.5. For sinusoid jammer, it is clear that the longer the window length, the better the concentration of the jammer signal in t-f domain and is repre-

sented by larger value of concentration measure. The opposite is true for impulsive jammer.

IV. CONCLUSION

In this paper, we provided closed form expressions for the receiver SNR while implementing STFT-based interference excision in DS/SS communications. Both the data window of STFT and the binary excision values applied in the t-f domain are important to effectively remove the jammer without distorting the desired spread spectrum signal. Proper data windows localize the interference in as few t-f bins as possible whereas good binary excision assign zero values to only those t-f bins contaminated by the jammer t-f signature. In order to select the proper data windows, concentration measures can be applied to STFTs of different data windows to select the one which is of high localization.

Reference

- [1] S. Roberts and M. Amin, "Linear vs. bilinear time-frequency methods for interference mitigation in direct sequence spread spectrum communication systems", *Asilomar Conf. on Signals, Systems and Computers*, Pac. Grove, Ca, Nov. 1995.
- [2] Brian S. Krongold, Michael L. Kramer, Kannan Ramchandran and Douglas L. Jones, "Spread spectrum interference suppression using adaptive time-frequency tilings", *Proceedings of ICASSP97*, Munich, Germany, April 1997.
- [3] F.M. Hsu and A. A. Giordano, "Digital whitening techniques for improving spread spectrum communications performance in the presence of narrow-band jamming and interference," *IEEE trans. Commun.*, vol. COM-26, pp.209-216, Feb 1978.
- [4] J. B. Allen and L. R. Rabiner, "A Unified Approach to Short-Time Fourier Analysis and Synthesis", *Proc. IEEE*, vol. 65, No. 11, Nov. 1977.
- [5] J. Ketchum and J. Proakis, "Adaptive algorithms for estimating and suppressing narrowband interference in PN spread spectrum systems", *IEEE Trans. on Comm.*, May 1982.
- [6] D. Jones and R. Baraniuk, "A Simple Scheme for Adapting Time-Frequency Representations", *IEEE Tran. on SP*, vol. 42, Dec. 1994.
- [7] D. Jones and T. Parks, "A high resolution data-adaptive time-frequency representation", *IEEE Trans. on ASSP*, vol. 38, pp.2127-2135, December 1990.
- [8] W. Williams, M. Brown, and A. Hero, "Uncertainty, information and time-frequency distributions," *SPIE*, vol.1566, pp.144-156, 1991.
- [9] D. Jones and T. Parks, "A high resolution data-adaptive time-frequency representation", *IEEE Trans. on ASSP*, vol. 38, pp.2127-2135, December 1990.

$$SNR_o = \frac{(1/L) \left(\sum_{n=0}^{L-1} \sum_{m=0}^{L-1} A_m(k) w_m(n) \right)^2}{B^2 \sum_{m=0}^{L-1} \sum_{m_1=0}^{L-1} A_m(k) A_{m_1}(k) w_m(k-k_0) w_{m_1}(k-k_0) + \sigma_n^2 \sum_{m=0}^{L-1} \sum_{m_1=0}^{L-1} A_m(k) A_{m_1}(k) w_m(l) w_{m_1}(l)} \quad (17)$$

$$SNR_o = \frac{(1/L)(L-1)^2 L^2 w^2(e^{j0})}{B^2 \sum_{m=0}^{L-1} \sum_{m_1=0}^{L-1} w_m(k-k_0) w_{m_1}(k-k_0) + \sigma_n^2 (L-1) L w^2(e^{j0})} \quad (18)$$

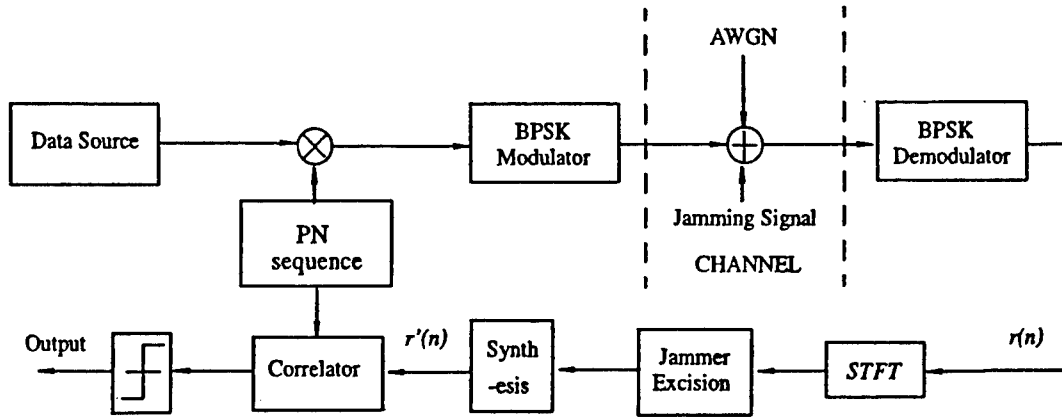


Fig.1 Block diagram of a direct sequence spread spectrum system with STFT jammer excision

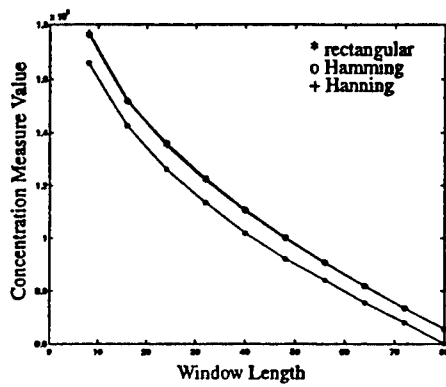


Fig2. Concentration measure(21) for impulse jammer with three different kind of window with different effective window length

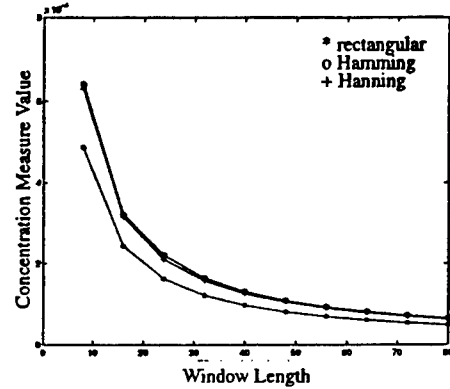


Fig4. Concentration measure(22) for impulse jammer with three different kind of window with different effective window length

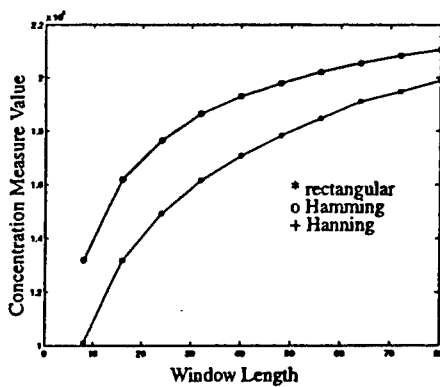


Fig3. Concentration measure(21) for sinusoid jammer with three different kind of window with different effective window length

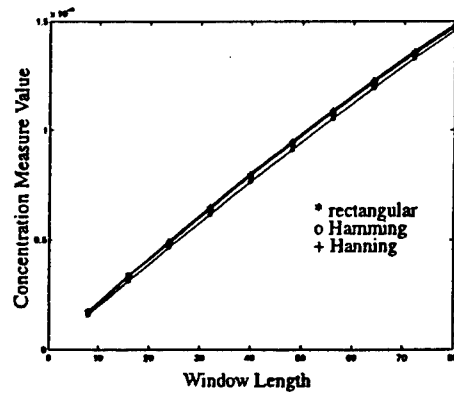


Fig5. Concentration measure(22) for sinusoid jammer with three different kind of window with different effective window length

Recursive Fourier Transform for Interference Suppression in PN Spread Spectrum Communications

Moeness G. Amin[†], Xuemei Ouyang[†], and Alan Lindsey^{**}

[†] Department of Electrical and Computer
Engineering
Villanova University
Villanova, PA 19085
Email: moeness, ouyang@ece.vill.edu

^{**} Rome Laboratory
RL/C3BB
525 Brooks Road
Rome, NY 13441-4505
Email: lindsey@rl.af.mil

Abstract

In this paper, we use recursive short-time Fourier transforms (STFT) for interference excision in PN spread spectrum communication systems. The proposed excision method is based on the attractive localization properties of the impulse responses of the multiple pole filters. These impulse responses have Gaussian-like shapes and decrease in bandwidth with higher pole multiplicities. When used as data window before Fourier transformation, they result in a large class of computationally efficient STFTs. Localization measures can be applied to determine the proper window (impulse response), which maximally concentrates the jammer in the time-frequency domain. Interference mitigation is then achieved by applying a binary excision to the STFT employing the optimum window for each data bit. We show that this method permits both data-dependent windowing and filtering, and leads to improved BER performance of the DS/SS system.

I. Introduction

The short-time Fourier transforms (STFT) is a linear time-frequency signal representations which inherently suffers from the trade-off between temporal and spectral resolution [1]. The STFT employing a short data window provides good temporal resolution whereas that using a window of long time extent has fine spectral resolution. The solution of this incompatibility problem is to generate a large class of STFTs which employ different windows with distinct characteristics. Some members of this class

should be more appropriate to describe slowly time-varying signals, while others are set to provide better localization in rapidly time-varying environments. For a given nonstationary signal, the member which yields the best temporal/spectral trade-off, or the highest possible concentration should be chosen for t-f representation. Several concentration measures including those introduced in [1, 2] can be used for this purpose.

The application of STFT for interference excision in DS/SS communications using sparse grid and overdetermined time-frequency tilings was discussed in [3] and [4], respectively. Other techniques for the suppression of nonstationary interference include (1) adaptive linear predictions to track and remove the time-varying frequency characteristics of the coherent interference [5], (2) linear excisions in which the data is processed using the wavelet transform or M-band/subband filter banks [6,7], (3) bilinear transformations using time-frequency distributions for instantaneous frequency estimation, followed by time-domain excision filtering [8,9].

In this paper, we extend the application of the short time Fourier transform to nonstationary interference mitigation in DS/SS communications. We apply a simple, but effective concentration measure to a computationally efficient class of STFTs in order to select the data-dependent STFT which provides the most improved localization of the interference in the time-frequency domain. Specifically, we consider the generation of a class of different short-time Fourier transforms by using a multiple pole infinite impulse response filter, realized in cascading form. Members of this class have sufficient diversity in their temporal/spectral trade-off and are easily updated in time. Further, the STFT using an impulse response of one filter can be recursively generated from those members corresponding to smaller filter orders or pole multiplicities. The choice of the optimum window (impulse response) can be

This work is supported by Rome Lab, contract No. F30602-96-C-0077

made using localization test criteria such as the one discussed in [2]. Interference excision is then performed by either clipping or gating the high power values of the optimum window STFT. The process is repeated for each bit or block of data and the choice of the window could then vary with time.

Section II presents the multiple pole windows and discusses the difference in their temporal/spectral localization properties. The time- and transform- domain generations of the decision variable for detection are given in Section III. The scheme for the proposed adaptive STFT method for jammer excisions is given in Section IV. Computer simulations showing the BER for both adaptive and fixed window STFT-based interference excision in DS/SS communication are presented in Section V.

II. Order Recursive Short Time Fourier Transform(ORFT)

For the short-time Fourier transform, the analysis window $h(n)$ can be set equal to an impulse response of a linear time-invariant filter. If the filter is only made up of a multiple-pole of multiplicity k , then the transfer function of $h(n)$ is given by

$$H_k(z) = \frac{(1-\gamma)^k}{(1-\gamma z^{-1})^k} \quad (1)$$

The corresponding impulse response is given by

$$h_k(n) = (1-\gamma) \frac{k(n+k-1)!}{n!(k-1)!} \gamma^n \quad (2)$$

It can be readily shown that the above sequence possesses the recursive property[10]

$$h_k(n) = \gamma h_k(n-1) + (1-\gamma)h_{k-1}(n) \quad (3)$$

Using the impulse response (2) as the analysis window in STFT yields a similar recursive expression to (4),

$$F_{k+1}(n, \omega) = \gamma F_{k+1}(n-1, \omega) + (1-\gamma)F_k(n, \omega) \quad (4)$$

where $F_k(n, \omega)$ denotes the STFT which corresponds to the filter order k , calculated at time n and frequency ω . Equation (4) defines the order recursive Fourier transform(ORFT), in which the FT is recursive in both time n and filter order k . The block diagram of ORFT consisting of systems connected in cascade is depicted in Fig.1. The STFTs $F_k(n, \omega)$, $k=1,2,\dots,K$ offer different trade-off between temporal and spectral resolutions. The trade-off is decided by the two variables in the problem, the filter pole and its multiplicity. Fig.2 shows the windows corresponding to $k=1,5,10$, $\gamma = 0.9$. It is evident that higher values of the filter order lead to longer extent windows, and subsequently, finer spectral resolution.

III. Decision Variable in the Transform Domain

The signal-to-jammer ratio (SJR) can be improved by eliminating the time and frequency samples of the STFT corresponding to the interference, and then synthesizing the result. The synthesized signal $\hat{x}(n)$ is used to obtain the decision variable g for improved detection, through the correlation

$$g = \sum_{n=0}^{N-1} \hat{x}(n)p^*(n) \quad (5)$$

In the above equation, $p(n)$ represents the receiver PN sequence and N is the number of chips per information bit(we assume one sample/chip). The short-time Fourier transform(STFT) is defined as

$$X(f, t) = \int_{-\infty}^{\infty} w(t-\tau)x(\tau)e^{-j2\pi f\tau}d\tau \quad (6)$$

where $w(t)$ is the analysis window and $x(t)$ is the received(original) signal. Let T denote the time-period over which $w(t)$ is significant, and F represent the effective window bandwidth. According to [11], there is no significant information lost if the short-time Fourier transform $X(f, t)$ is sampled at the two Nyquist periods $1/F$ and $1/T$, leading to

$$X_{nm} = X(m/T, n/F) = \sum_{k=0}^{T-1} w(nD-k)x(k)e^{-j2\pi km/T} \quad (7)$$

where n and m are integer numbers and $D = 1/F$. The above expression is obtained using the minimum sampling rate in both the time and frequency domains. For the over-sampled STFT,

$$X_m(e^{j\omega_1}) = \sum_{n=0}^{L-1} w(m-n)x(n)e^{-j\omega_1 n} \quad (8)$$

where $L \geq N$. In this case, the signal synthesis from the STFT can be simply performed using the overlap addition(OLA) method described in [12],

$$y(n) = \sum_m \sum_{k=0}^{L-1} X_m(e^{j\omega_1})e^{j\omega_1 n} = \sum_m y_m(n) \quad (9)$$

where $y_m(n)$ is the inverse discrete Fourier transform at the time sample m ,

$$y_m(n) = Lx(n)w(m-n) \quad (10)$$

From (9) and (10),

$$y(n) = \sum_m y_m(n) = Lx(n) \sum_m w(m-n) \quad (11)$$

It can be readily shown that if $w(n)$ is sampled at sufficiently dense rate, then[12]

$$\sum_m w(m-n) = W(e^{j0}), \quad y(n) = Lx(n)W(e^{j0}) \quad (12)$$

It is clear from (12) that without modifying the STFT, the synthesized signal is the same as the original signal,

$$x(n) = \frac{y(n)}{LW(e^{j0})} = \frac{1}{LW(e^{j0})} \sum_{m=0}^{L-1} \sum_{k=0}^{L-1} X_m(e^{j\omega_k}) e^{j\omega_k n} \quad (13)$$

The decision variable at the output of the correlator (5) can be expressed using transform domain variables. By substituting (13) in (5), we obtain

$$g = \frac{1}{LW(e^{j0})} \sum_{k=0}^{L-1} P^*(e^{j\omega_k}) \sum_m X_m(e^{j\omega_k}) \quad (14)$$

where $P(e^{j\omega_k})$ is the discrete Fourier transform of the PN sequence. Since all the functions in (14) are in the transform domain, then the detection can be performed without the need to apply inverse transformations.

If the excision function $\alpha_m(k)$ is applied to the STFT, then the synthesized signal is modified to

$$y(n) = \sum_{m=0}^{L-1} \sum_{k=0}^{L-1} \alpha_m(k) X_m(e^{j\omega_k}) e^{j\omega_k n} \quad (15)$$

In this case,

$$g = \frac{1}{LW(e^{j0})} \sum_{k=0}^{L-1} P^*(e^{j\omega_k}) \sum_m \alpha_m(k) X_m(e^{j\omega_k}) \quad (16)$$

The scheme to perform the correlation in the time domain and the transform domain, respectively given by (5) and (16), is depicted in Fig.3(a),(b). The STFT domain detection scheme allows computational saving in two ways. First, the time domain correlation requires m inverse DFT to be performed, whereas only one DFT operation is required for the PN sequence in (16). Second, if the PN sequence is repetitive, its DFT remains fixed for every bit, which in turn reduces on-line computations in the correlation scheme of Fig.3(b).

IV. Adaptive STFT method for jammer excision in DS/SS

The main objective of adaptive STFT is to decide, without human intervention and extensive prior knowledge of the underlying signal characteristics, on the analysis window which offers the best time-frequency resolution[13]. Procedures based on mathematical optimal criteria appears most promising. Renyi information of the third order has been shown to provide a valuable and effective information measure in the context of time-frequency distributions[2],

$$C_k = -\frac{1}{2} \sum_n \sum_\omega \log [F_k(n, \omega)]^3 \quad (17)$$

It is recognized that the value of C_k corresponding to the highest resolution t-f signal representation should be larger than others. As such, we proceed to calculate C_k for all

members of the proposed class of STFTs and examine its value as a function of k . The filter order of maximum concentration measure is determined and the respective STFT is chosen as the most appropriate t-f representation.

Fig.4 shows the block diagram of the proposed recursive STFT-based interference excision method in PN spread spectrum communications. The method is summarized in the following steps: <1>The maximum value of the filter order k is set a priori. We have found that $K = 10$ is appropriate for a PN sequence length of 64. <2>The STFTs corresponding to $k = 1$ is computed over the entire bit. <3>The STFTs corresponding to $k = 2, 3, \dots, K$ are computed at the beginning of the bit and then recursively updated in time and order using equation (4). <4>The STFT of maximum concentration measure is chosen. <5>A binary excision is applied to the STFT in step <4> to remove the time-frequency samples with power exceeding a preset threshold. <6>The result in step <5> and the transform of the PN sequence are correlated using equation (16) and detection is applied.

V. Simulations

In order to test the effectiveness of the proposed method, we choose a synthetic signal which contains impulse, sinusoid, and chirp components. The result of the new adaptive method is shown in Fig.5(a). For comparison, the STFTs with fixed window lengths are shown in Fig.5(b,c,d). It is evident that different fixed windows are appropriate for different components of the signal.

In Fig.6, the BER is generated for 0dB SNR spread spectrum signal with $N=64$. Over each bit, the jammer randomly takes an impulse, a sinusoid, or a chirp waveform. For comparison, we have also included the BER for the fixed windows corresponding to $k=1, 5$. It is clear from the BER curves that the proposed adaptive method leads to improved system performance.

VI. Conclusion

In this paper, the impulse response of the multiple pole filter is employed as an analysis window in the calculations of the STFT. By fixing the pole location, the STFT becomes parameterized by only the pole multiplicity. This parameter controls the temporal/spectral resolution and can be set to yield the optimum concentration for a given nonstationary environment. One major attraction of the impulse responses of the above filters is that the corresponding STFTs are inter-related and also recursive in time. This allows a simple generation of a large class of STFTs with different localization properties. We have provided the detailed scheme to perform interference excision in PN spread spectrum communications based on recur-

sive STFTs. It is argued that it is much simpler for the receiver correlator to act on the STFTs of both the excised signal and the PN sequence than to deal with their time-domain representations. Computer simulations of the bit error rate were presented for both fixed and data-adaptive recursive STFTs. It was demonstrated that by applying the Renyi concentration measure to select the most appropriate STFT a significant improvement in the receiver performance can be achieved.

References

- [1] D. Jones and T. Parks, "A high resolution data-adaptive time-frequency representation", *IEEE Trans. on ASSP*, vol. 38, pp.2127-2135, December 1990.
- [2] W. Williams, M. Brown, and A. Hero, "Uncertainty, information and time-frequency distributions," *SPIE*, vol.1566, pp.144-156, 1991.
- [3] S. Roberts and M. Amin, "Linear vs. bilinear time-frequency methods for interference mitigation in direct sequence spread spectrum communication systems", *Asilomar Conf. on Signals, Systems and Computers*, Pac. Grove, Ca, Nov. 1995.
- [4] Brian S. Krongold, Michael L. Kramer, Kannan Ramchandran and Douglas L. Jones, "Spread spectrum interference suppression using adaptive time-frequency tilings", *Proceedings of ICASSP97*, Munich, Germany, April 1997.
- [5] J. Ketchum and J. Proakis, "Adaptive algorithms for estimating and suppressing narrowband interference in PN spread spectrum systems", *IEEE Trans. on Comm.*, May 1982.
- [6] M. Medley, G. Saulnier, and Das, "Applications of the wavelet transform in spread spectrum communications systems", *SPIE, Wavelet Applic.*, Orlando, FL, April 1994.
- [7] M. Tazebay and A. Akansu, "Adaptive subband transforms in time-frequency excisers for DSSS communication systems", *IEEE Trans. on SP*, pp. 2776-2782, Nov. 1995.
- [8] M. Amin, "Interference mitigation in spread spectrum communications using time-frequency distributions", *IEEE Trans. on SP*, Jan. 1996.
- [9] C. Wang and M. Amin, "Performance analysis of instantaneous frequency-based interference excision techniques in spread spectrum communications," *IEEE Trans. on SP*, Jan. 1998.
- [10] M. Amin and K. Feng, "Short-Time Fourier Transform Using Cascade Filter Structures", *IEEE Trans. on Circuits and Systems*, vol.42, pp.631-641, October 1995.
- [11] J. B. Allen, "Short-term spectral analysis and synthesis and modification by discrete Fourier transform", *IEEE Trans. on ASSP*, vol. ASSP-25, no. 3, pp. 235-238, June, 1977.
- [12] J. B. Allen and L. R. Rabiner, "A Unified Approach to Short-Time Fourier Analysis and Synthesis", *Proc. IEEE*, vol. 65, No. 11, Nov. 1977.
- [13] D. Jones and R. Baraniuk, "A Simple Scheme for Adapting Time-Frequency Representations", *IEEE Trans. on SP*, vol. 42, Dec. 1994.

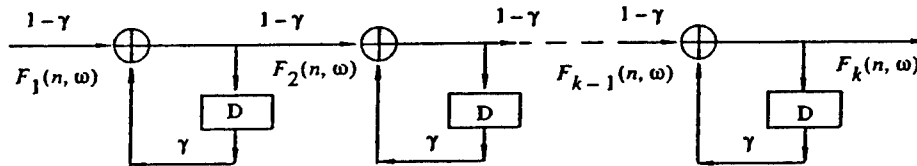
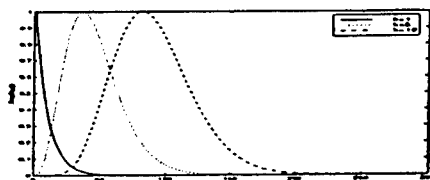
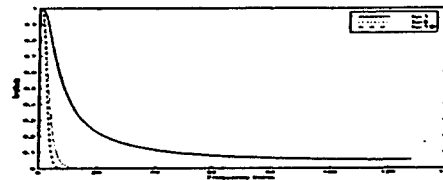


Fig.1 Order recursive Fourier transform

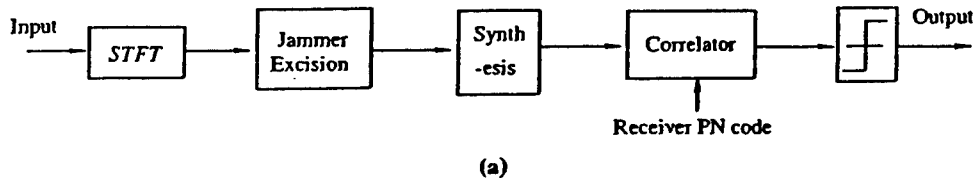


(a) Impulse response



(b) Spectral window

Fig.2. Time and spectral windows for multiple-pole filters $\gamma = 0.9$



(a)

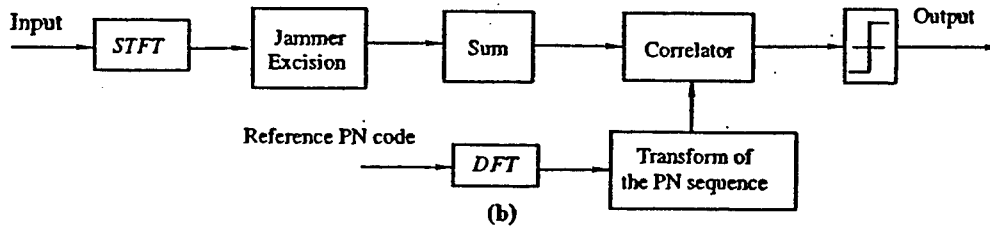


Fig.3 (a) Time domain decision (b) Transform domain decision

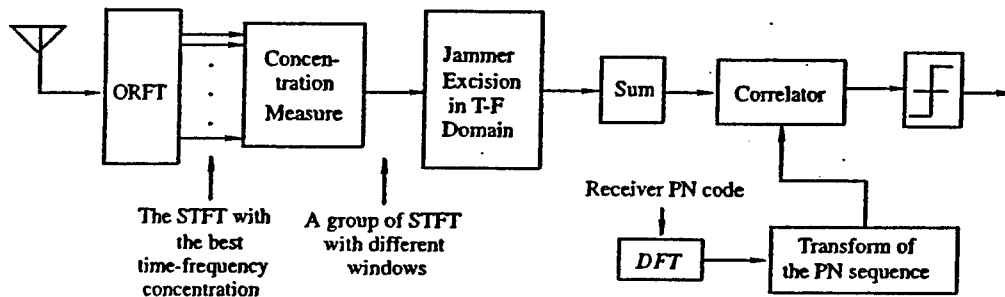


Fig.4 Jammer Excision Scheme with ORFT

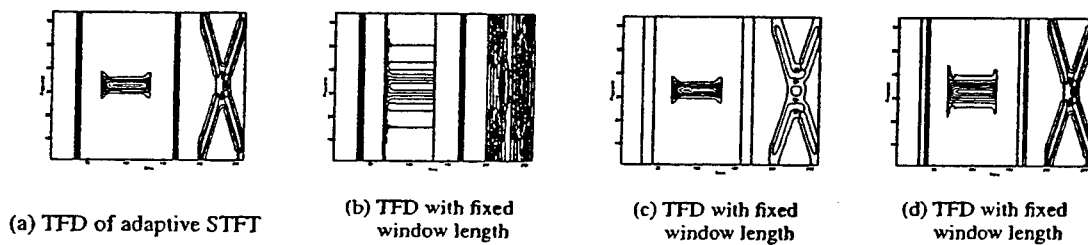


Fig.5 TFD of adaptive STFT and STFT with fixed window

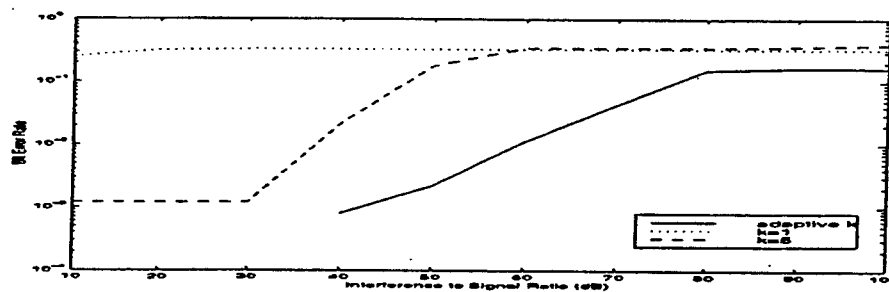


Fig.6 BER performance of the spread spectrum system

Interference Excision in DSSS Communications Using Projection Techniques

Suppression of FM Interference in DSSS Communication Systems Using Projection Techniques¹

Moeness G. Amin, Raja S. Ramineni
Dept. of Elect. and Comp. Eng.
Villanova University, Villanova, PA 19085.

Alan R. Lindsey
USAF Research Laboratory / IFGC
Rome, NY 13441.

Abstract

This paper presents an orthogonal subspace based technique for nonstationary interference excision in direct sequence spread spectrum (DSSS) communications. The interference is an FM signal, which is uniquely characterized by its instantaneous frequency (IF). In the proposed technique, the received data over one symbol period is partitioned into blocks. The data in each block is projected on the subspace orthogonal to the respective interference subspace, which is provided using the IF estimate. The results of the projection are then combined and correlated with the PN sequence at the receiver. The paper shows the receiver performance as a function of the number of blocks and the noise variance. It compares the proposed projection approach with the recently introduced notch filtering techniques for nonstationary interference excisions in DSSS.

1. Introduction

In this paper, the problem of nonstationary interference rejection in DSSS systems is approached using projection-filtering techniques. Orthogonal projection methods currently in the literature are more applicable to stationary signals [1],[2]. However, for this work frequency modulated (FM) interfering signals with constant amplitude over a bit period are considered. These nonstationary signals are uniquely characterized by their instantaneous frequencies (IF), and referred to as constant modulus signals, and include the important class of polynomial phase signals. The FM signals are localizable in the time-frequency domain and confined to a small t-f region, whereas both the additive noise and the DSSS signal components of the received data cover the entire time-frequency (TF) plane. Their IF can be estimated using numerous methods, including time-frequency distributions [3],[4],[5].

Once the IF is estimated, the interference signal vector can be constructed and the basis vector of its respective one-dimensional subspace can easily be defined. Since the PN sequence is uniformly extended in all dimensions, removing the PN component along the interference subspace causes full jammer excision with minimum distortion of the desired signal. Interference removal is simply achieved by projecting the input data vector over one bit period on the subspace orthogonal to the interference subspace. A general framework of the above projection approach is developed by partitioning the input data vector over one symbol period into successive blocks, where the projection on the orthogonal subspace of the jammer signal is applied over each block separately. The results of the projections over all blocks are combined to reconstruct the jammer-free data symbol.

Several approaches have been introduced for nonstationary interference rejections in DSSS. One important excision approach, which will be used for comparison, is also based on IF estimation [6]. In this approach, the IF information provided from the time-frequency plane is used to construct a time-varying excision notch filter which effectively removes the interference. The notch filtering excision techniques, although relatively simple, cause significant distortions to the desired signal leading to undesired receiver performance, specifically under low jammer-to-noise ratio (JNR). In section 4, simulations are presented that show the performance of the proposed excision technique evaluated against the five coefficient notch filter approach introduced in [7].

The general expression of the receiver SNR is derived and shown to depend on the noise variance, the PN sequence length, and the number of blocks per symbol. The tradeoff between receiver performance and complexity is demonstrated by presenting the computational requirements as a function of the block length.

¹ This work is supported by the Air Force Research Laboratory, / IFGC, Rome, NY, contract no. F30602-96-C-0077

2. Notation

The subject system utilizes a direct sequence spread spectrum signal with BPSK modulation

$$s(t) = \sum_i I_i \underbrace{\sum_{n=1}^L p_i(n) q(t - iT_b - n\tau_c)}_{b_i(t - iT_b)}, \quad I_i \in \{-1, 1\} \forall i \quad (1)$$

where I_i is the information sequence (represented by sign in this binary case) and the expression in horizontal brackets amounts to the i^{th} bit as a length L pseudonoise sequence pulse shaped by q . T_b is the bit interval and τ_c is the chip duration in seconds. Block processing over individual bits is the focus of this work so it suffices to drop the i subscripts and model the received signal as a discrete sequence in which a particular bit after demodulation and sampling at the chip rate is considered, without loss of generality, as

$$x(n) = p(n) + w(n) + j(n), \quad 1 \leq n \leq L \quad (2)$$

where receiver hardware and propagation have induced noise $w(n)$ and interference $j(n)$ respectively. The noise statistics assume autoindependence, zero mean, and no cross correlation to the jammer. In vector form, (2) becomes

$$\mathbf{x} = \mathbf{p} + \mathbf{w} + \mathbf{j} \quad (3)$$

where $\mathbf{x} = [x(1), x(2), \dots, x(L)]^T$, $\mathbf{p} = [p(1), p(2), \dots, p(L)]^T$, $\mathbf{w} = [w(1), w(2), \dots, w(L)]^T$, and $\mathbf{j} = [j(1), j(2), \dots, j(L)]^T$.

3. Interference Suppression Using Orthogonal Projection

The orthogonal projection method is based on the fact that a monocomponent jammer with a clearly detectable instantaneous frequency law forms a single-dimensional subspace in the L -dimensional space of the received data vector. Forming the $(L-1)$ -dimensional subspace orthogonal to the interfering signal allows a projection of the received signal into this interference-free space as per Figure 1. Even if the input data of L samples over one bit period is partitioned into K blocks \mathbf{x}_k of N samples each, i.e. $L = NK$, the jammer remains an FM signal with one-dimensional subspace of each block's vector space. The interference can then be removed from the individual blocks by projecting the received data in the respective block on the corresponding orthogonal subspace. *The instantaneous frequency (IF) information provided by any appropriate algorithm determines the jammer signal, and hence the orthogonal jammer-free subspace.*

To formalize this concept, let \mathbf{u}_k be the basis vector for the interference subspace of the k^{th} block (which has been estimated from the IF information,) and define the $N \times N$ projection matrix

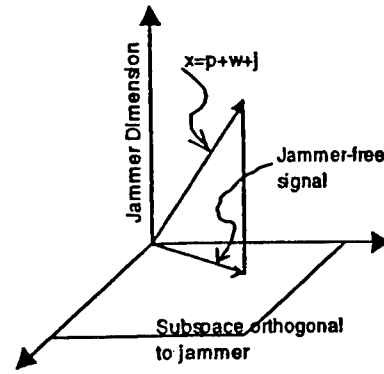


Figure 1. Interference Excision Using Orthogonal Projection.

$$\mathbf{V}_k = \mathbf{I} - \mathbf{u}_k \mathbf{u}_k^T \quad (4)$$

The result of the projection in the k^{th} data block is

$$\bar{\mathbf{x}}_k = \mathbf{V}_k \mathbf{x}_k \quad (5)$$

Using the three different components that make up the input vector (3), the output of the projection filter can be written as

$$\bar{\mathbf{x}}_k = \mathbf{V}_k [\mathbf{p}_k + \mathbf{w}_k + \mathbf{j}_k] \quad (6)$$

It is assumed that the IF estimator provides exact parameterization of the jammer so that projection in this fashion annihilates the interference perfectly, i.e. $\mathbf{V}_k \mathbf{j}_k = \mathbf{0}$. Thus,

$$\begin{aligned} \bar{\mathbf{x}}_k &= \mathbf{V}_k \mathbf{p}_k + \mathbf{V}_k \mathbf{w}_k \\ &= \bar{\mathbf{p}}_k + \bar{\mathbf{w}}_k \end{aligned} \quad (7)$$

Correlating the filter output $\bar{\mathbf{x}}_k$ with the corresponding k^{th} block of the receiver PN sequence and summing the results over the K blocks yields the decision variable y , as in

$$y = \sum_{k=0}^{K-1} \bar{\mathbf{x}}_k^T \mathbf{p}_k \quad (8)$$

In terms of the constituent signals, the decision variable becomes

$$\begin{aligned} y &= \mathbf{p}_k^T \mathbf{V}_k^T \mathbf{p}_k + \mathbf{w}_k^T \mathbf{V}_k^T \mathbf{w}_k \\ &= y_1 + y_2 \end{aligned} \quad (9)$$

where

$$y_1 = \sum_{k=0}^{K-1} \sum_{i=1}^N \sum_{j=1}^N p(kN+i) v_{ji}(k) p(kN+j) \quad (10)$$

is the contribution of the PN sequence to the received signal decision variable, and

$$y_2 = \sum_{l=0}^{K-1} \sum_{m=1}^N \sum_{n=1}^N w(lN+m) v_{nm}(l) p(lN+n) \quad (11)$$

the contribution of the noise. In the absence of the projection filter, y_1 is constant and equal to L . However, application of \mathbf{V}_k induces randomness on y_1 , and y_2 is clearly a random variable. Therefore the statistical

expectations of each must be studied, along with cross-statistics, so that received signal, noise and interference energies (or ratios to be precise) may be developed. We are ultimately looking for two important statistics, $E\{y\}$ and $E\{y^2\}$. Using the properties and the structure of the projection matrix, it can be shown that

$$E\{y_1\} = \sum_{k=0}^{K-1} \text{Tr}(\mathbf{V}_k) = K(N-1) \quad (12)$$

$$= L - K$$

and since $E\{y_2\} = 0$, the noise term does not contribute to the mean of the decision variable. Neither is there a cross correlation, i.e. $E\{y_1 y_2\} = 0$, of the noise and the pseudo noise sequences. Therefore

$$E\{y\} = L - K \quad (13)$$

from Eq (12). It can also be shown that

$$E\{y_1^2\} = \sum_{k=0}^{K-1} \left\{ \sum_{l=0}^{K-1} \text{Tr}(\mathbf{V}_k) \cdot \text{Tr}(\mathbf{V}_l) + 2\|\mathbf{V}_k\|_F^2 - 2\sum_{i=1}^N |v_{ii}(k)|^2 \right\} \quad (14)$$

where $\text{Tr}(\cdot)$ is the matrix trace and $\|\mathbf{V}_k\|_F^2$ denotes the Frobenius norm of the matrix \mathbf{V}_k . It is easy to show that $\|\mathbf{V}_k\|_F^2$ is equal to $(N-1)$. The third term in the equation is equal to $2\frac{(N-1)^2}{N}$ and for $N \gg 1$, it approximates to $(N-2)$. Accordingly, using the above information with (12) yields

$$E\{y_1^2\} = K^2(N-1)^2 + 2K(N-1) - 2K\frac{(N-1)^2}{N} \quad (15)$$

so that

$$\begin{aligned} \text{var}\{y_1\} &= E\{y_1^2\} - E^2\{y_1\} \\ &= 2K(N-1) - 2K\frac{(N-1)^2}{N} \end{aligned} \quad (16)$$

Now, due to the whiteness properties of the white noise and PN sequences, and the fact that they are uncorrelated, the reader may verify that

$$E\{y_2^2\} = \sigma^2 \sum_{k=0}^{K-1} \|\mathbf{V}_k\|_F^2 = \sigma^2 K(N-1) \quad (17)$$

Since $E\{y_2\} = 0$, $\text{var}\{y_2\} = E\{y_2^2\}$, so that

$$\begin{aligned} \text{var}\{y\} &= \text{var}\{y_1\} + \text{var}\{y_2\} \\ &= (L-K) \left[\sigma^2 + \frac{2}{N} \right] \end{aligned} \quad (18)$$

Thus the signal to interference noise ratio (SINR) at the receiver, defined statistically as the received signal power, $E^2\{y\}$, normalized by the variance, is given by

$$\begin{aligned} \text{SINR} &= \frac{E^2\{y\}}{\text{var}\{y\}} = \frac{L-K}{\sigma^2 + \frac{2}{N}} \\ &= \frac{L-K}{\sigma^2} \quad \text{for } N \gg 1 \end{aligned} \quad (19)$$

This shows the intuitively pleasing result that, in the approximate sense, the receiver SINR decreases linearly with the number of blocks per bit, and reaches its maximum value when the excision is performed once over the entire bit period. It should be noticed that, by performing block wise excision, ones loses in two ways – by a decrease in mean and an increase in the variance of the decision variable. However, the computational advantages to block processing will provide an interesting tradeoff in a fielded system.

4. Simulations

Figure 2 shows a family of SINR curves vs. N , for different values of σ^2 . As eq. (19) shows, increasing N (which decreases K) reduces the second term in the denominator, thereby increasing the SINR. This result is consistent with the fact that smaller block size means more blocks, each of which loses a dimension in the projection excision process thereby causing more of the PN sequence to be lost. It is also evident from Figure 2 that the rate of increase in SINR vs. block length is more pronounced for higher noise levels because the denominator of eq. (19) is more dependent on the term $\frac{2}{N}$ than on the noise power when σ^2 is small ($\ll 1$).

If the jammer is not present and preprocessing (projection/excision/filtering) is disabled the SINR expression reduces to the standard result, $\frac{L}{\sigma^2}$, the matched filter bound. It represents the upper bound on performance when implementing interference excision techniques, including the proposed method. The lower bound on performance depends on the jammer power and the time-frequency signature. This bound is often reached when the excision projection filter is disabled, in which case $\mathbf{V}_k = \mathbf{I}$. For a sinusoidal jammer of power ρ^2 , the lower bound on the receiver SINR is $\frac{L}{\sigma^2 + \rho^2}$ as in [8].

The upper and lower bounds for tone jammers are depicted in Figure 3.

Figure 4 shows the receiver SINR vs. JSR for the case of a tone jammer when various excision techniques and parameters are employed, including the optimal adaptive notch filtering technique recently proposed in [7]. The projection method and the non-adaptive notch filtering method both are presumed to exactly annihilate interference, decoupling the performance of these

strategies from the jammer power. Hence the horizontal lines in Figure 4. It is clear from the figure that the projection filtering technique, when $N=L=128$, outperforms the optimum five-coefficient notch filtering and yields a 4.12 dB improvement over the case of full jammer excision with a notch filter.

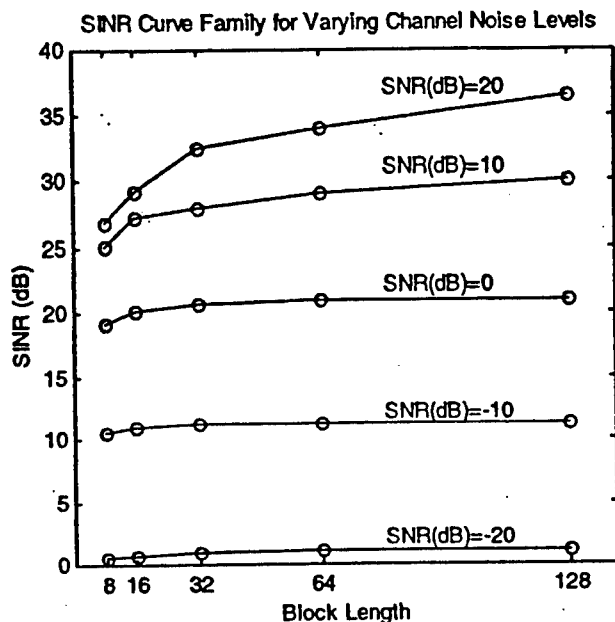


Figure 2. Plot of SINR vs. Block length for varying noise levels.

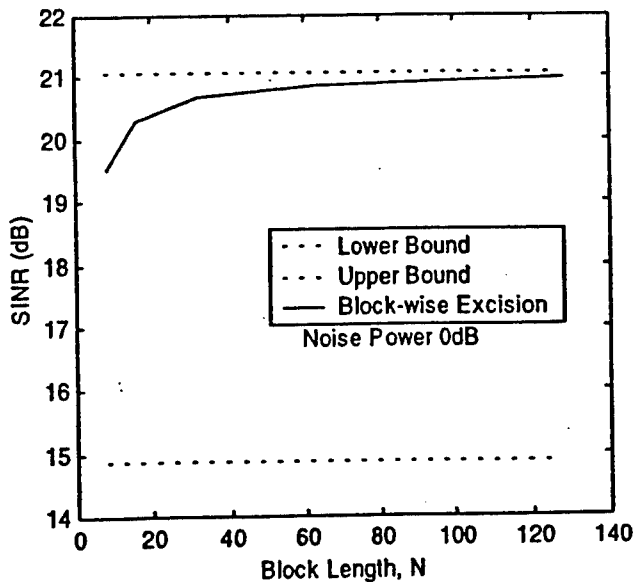


Figure 3. Bounds on SINR: Tone jamming with $L=128$.

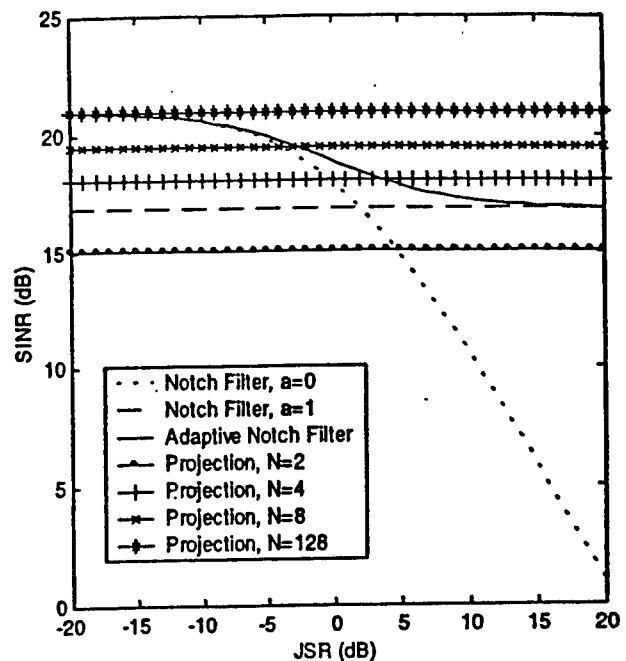


Figure 4. Excision Methods SINR Comparison. $L=128$, $SNR=0dB$.

5. References

- [1] A. Haimovich and A. Vadhri, "Rejection of Narrowband Interferences in PN Spread Spectrum Systems Using an Eigenanalysis Approach," *Proceedings of the 7th SP Workshop on Statistical and Array processing, Quebec City, Canada, June, 26-29 1994*.
- [2] C - M. S. See, B. K. Poli, T. S. Quek and A. C. Kot., "Suppression of Strong Narrowband Interference Using an Eigen-structure-based Algorithm," *Proceedings of MILCOM*, pp. 1205-1208, 1995.
- [3] L. Cohen, "Time-frequency Distributions - A Review," *Proc. of the IEEE*, vol. 77, no. 7, pp. 941-981, July 1989.
- [4] B. Boashash, *Time-Frequency Signal Analysis, Vols. 1&2*, Prentice-Hall, Englewood Cliffs, New Jersey, 1990.
- [5] F. Hlawatsch and G. Boudreaux-Bartels, "Linear and Quadratic Time-frequency Signal Representations," *IEEE Signal Processing Magazine*, vol. 9, no. 2, pp. 21-68, April 1992.
- [6] M. G. Amin, "Interference Mitigation in Spread-spectrum Communication Systems Using Time-frequency Distributions," *IEEE Trans. on Signal Processing*, vol. 45, no. 1, pp. 90-102, January 1997.
- [7] C. Wang, M.G. Amin and A.R. Lindsey, "Optimum Interference Excision in Spread Spectrum Communications using Open Loop Adaptive Filters," *IEEE Trans. on Signal Processing*, vol. 47, no. 7, pp. 1966-1976, July 1999.
- [8] J. Ketchum and J. Proakis, "Adaptive Algorithms for Estimating and Suppressing Narrowband Interference in PN Spread Spectrum Systems," *IEEE Transactions on Communications*, vol. COM-30, pp. 913-924, May, 1982.

Interference Excision in DSSS Communication Systems Using Projection Techniques

Moeness G. Amin[†], Raja S. Ramineni

Dept. of Elect. and Comp. Engg.

Villanova University, Villanova, PA 19085.

Alan R. Lindsey

US AF Research Laboratory, IFGC

Rome, NY 13441.

[†]Corresponding Author:

Phone: (610) 519 7305

Fax: (610) 519 4436

email: moeness@ece.vill.edu

EDICS: 3-INTF

Abstract

This paper presents a subspace-based technique for nonstationary interference excision in direct sequence spread spectrum (DSSS) communications. The interference is a frequency modulated (FM) signal which is uniquely characterized by its instantaneous frequency (IF). In the proposed technique, the received data over one symbol period is partitioned into blocks. The data in each block is projected on the subspace orthogonal to the respective interference subspace, which is provided using an IF estimate. The projected results are then combined and correlated with the PN sequence at the receiver. This paper examines the receiver performance as a function of the number of blocks and the noise variance. It applies the block-based processing to handle the cases in which errors arise in the IF estimate over segments of the bit period, due to changes in interference, noise and cross-term characteristics. This paper shows that the proposed projection approach outperforms the recently introduced notch filtering techniques for nonstationary interference excisions in DSSS. The paper also discusses the performance and computational complexity issues related to the data block size.

Permission to publish this abstract separately has been granted.

This work is supported by the US Air Force Research Laboratory, Rome, NY, contract no. F30602-96-C-0077.

I. Introduction

The primary motivation for using PN direct sequence spread spectrum (DSSS) communication systems is its inherent capability of interference mitigation. Any level of interference can be effectively overcome with sufficiently long PN sequence. However, increasing the number of chips per symbol period, which translates into higher processing gain, may lead to an increase in the spectrum bandwidth of the transmitted signal beyond available limits or intractable complexity for given requirements. This necessitates the use of efficient signal processing techniques in conjunction with a DSSS receiver to achieve acceptable interference rejection levels without intruding on adjacent communication channels [1], [2], [3] or decreasing quality of service.

Several approaches have been introduced for nonstationary interference rejection in DSSS [4], [5], [6], [7], [8], [9]. One of the important excision approach, which will be used for comparison, is also based on IF estimation [9]. In this approach, the IF information provided from the time-frequency plane is used to construct a time-varying excision notch filter which effectively removes the interference. The notch filtering excision techniques, although relatively simple, cause significant distortions to the desired signal leading to undesired receiver performance, specifically under low jammer to noise ratio (JNR).

In order to balance the effect of the excision filter on the DSSS signal, a modification of the receiver PN sequence was proposed in [10],[5],[11]. Amin [10] suggested to process the receiver PN sequence with the same excision filter prior to correlation. He also proposed in [5] to use a zero-phase five-coefficient filter so as to implement the equivalence of a matched filter applied to the output from a three-coefficient excision filter. Barbarossa and Scaglione [11] derived the optimum spreading sequence that maximizes the ratio between the output

and the input SNR's. They also proposed to use the Wigner-Hough transform to effectively estimate the jammer IF under high noise power levels.

In this paper, a new and effective tool is introduced, not yet considered in the recently developed methods for the mitigation of nonstationary interference in DSSS systems. Interference excision is performed using projection filtering techniques. Orthogonal projection methods currently in literature are more applicable to stationary signals [12],[13]. However, for this work frequency modulated (FM) interfering signals with constant amplitude over a bit period are considered. These nonstationary signals are uniquely characterized by their instantaneous frequencies (IF), and referred to as constant modulus signals, and include the important class of polynomial phase signals. The FM signals are localizable in the time-frequency domain and confined to a small t-f region, whereas both the additive noise and the DSSS signal components of the received data cover the entire time-frequency (TF) plane. Their IF can be estimated using various methods, including time-frequency distributions [14],[15],[16].

Once the IF is estimated, the interference signal vector can be constructed, up to ambiguity in phase and possibly in amplitude. The normalized basis vector the interference respective one-dimensional subspace can, therefore, be easily defined. Since the PN sequence is uniformly extended in all dimensions, removing the PN component along the interference subspaces causes full jammer excision with minimum distortion of the desired signal. Interference removal is simply achieved by projecting the input data vector over one bit period on the subspace orthogonal to the interference subspace. A general framework of the above projection approach is developed by partitioning the input data vector over one symbol period into successive blocks, where the projection on the orthogonal subspace of the jammer signal is applied over each block separately. The results of the projection over all

blocks are combined to reconstruct the jammer-free data symbol. Block-processing provides the flexibility to discard the portions of the data bit, over which there are significant errors in the IF estimates, although at the cost of increasing receiver noise variance. This trade off is explored and recommendations are put forth.

In section II, the DSSS signal is presented along with the vector representations of the different components that make up the received data stream. In section III, the interference excision using orthogonal projection is introduced and the receiver SINR expression is developed as a function of the block length and the noise power. Section IV deals with the case where errors in the IF estimates are induced due to the presence of cross terms, high noise power, and changes in jammer signal characteristics. It is shown that block processing becomes very effective when the IF errors only contaminate segments of the filtered DSSS signal, over the entire bit period. The simulation examples included in section IV illustrate the advantages of block processing in the case of significant IF errors. Appendix A highlights the computational requirements for the proposed approach. Appendix B gives the modified SINR expression when using blocks of unequal lengths.

II. Received Data Structure

A BPSK-modulated DSSS signal may be expressed as

$$s(t) = \sum_i I_i b_i(t - iT_b) \quad I_i \in \{-1, 1\} \forall i \quad (1)$$

where I_i represents the binary information sequence and T_b is the bit interval. The i^{th} binary information bit, $b_i(t)$ is further decomposed as a superposition of L pseudo noise samples, $p_i(n)$, pulse shaped by a unit-energy function, $q(t)$, of duration of τ_c .

$$b_i(t) = \sum_{n=1}^L p_i(n) q(t - n\tau_c) \quad (2)$$

The shape of $q(t)$ is determined by design requirements. The PN sequence is known to both the transmitter and the receiver, and it is assumed for this work that timing and synchronization are exact. A metric commonly referred to as processing gain, roughly equivalent to $10\log L$, represents the improvement in SNR due to spreading/despreading of the desired signal at the transmitter/receiver. The communication channel adds both noise and interference to the DSSS signal, as shown in Fig.1. Since block processing over individual bits is the focus of this work, it suffices to drop the dependence on i and concentrate on any particular bit, assumed "+1" without loss of generality. The signal for one bit at the receiver, after demodulation, which strips off $q(t)$, sampled at chip rate, becomes

$$x(n) = p(n) + w(n) + j(n) \quad 1 \leq n \leq L \quad (3)$$

where $p(n)$ is the chip sequence, $w(n)$ is the white noise, and $j(n)$ is the interfering signal. It is assumed that the chip sequence and the white noise sequence are both temporally uncorrelated and of zero mean, and their cross correlation is zero. That is

$$\begin{aligned} E\{w(n)w(n+l)\} &= \sigma^2\delta(l), \quad E\{p(n)p(n+l)\} = \delta(l) \\ E\{p(n)w(n+l)\} &= 0 \quad \forall l \end{aligned}$$

The above equation can be put in the vector form

$$\mathbf{x} = \mathbf{p} + \mathbf{w} + \mathbf{j} \quad (4)$$

where

$$\begin{aligned} \mathbf{x} &= \begin{bmatrix} x(1) & x(2) & x(3) & \cdots & x(L) \end{bmatrix}^T, \quad \mathbf{p} = \begin{bmatrix} p(1) & p(2) & p(3) & \cdots & p(L) \end{bmatrix}^T \\ \mathbf{w} &= \begin{bmatrix} w(1) & w(2) & w(3) & \cdots & w(L) \end{bmatrix}^T, \quad \mathbf{j} = \begin{bmatrix} j(1) & j(2) & j(3) & \cdots & j(L) \end{bmatrix}^T \end{aligned}$$

All vectors are of dimension $L \times 1$, and 'T' denotes vector or matrix transposition.

III. Interference excision using Orthogonal Projection

The signal space is generated by all linear combinations of all possible samples of the received signal vector \mathbf{x} . As such, it contains L dimensions, due to the randomness of the $p(n)$ and the white noise sequence. The jammer, assumed for this work to be a member of the general class of frequency modulated (FM) signals, is determined and constructed via estimates of the instantaneous frequency. It occupies a single dimension in the L -dimensional signal space.

The orthogonal projection method makes use of the fact that an FM jammer has a one dimensional subspace in the the L -dimensional space of the received data vector. In the proposed interference excision approach, the data vector is partitioned into K blocks, each of length N , i.e. $L = NK$. In each block, the jammer remains an FM signal with one-dimensional subspace in an N -dimensional subspace. The interference can be removed from each block by projecting the received data in the respective block on the corresponding orthogonal subspace of the interfering signal as shown in Fig. 2. This subspace is estimated using the IF information. The projection matrix for the k^{th} block is

$$\mathbf{V}_k = \mathbf{I} - \mathbf{u}_k \mathbf{u}_k^T \quad (5)$$

The vector \mathbf{u}_k is the basis vector that span the subspace of the interfering signal. The result of the projection in the k^{th} data block is

$$\bar{\mathbf{x}}_k = \mathbf{V}_k \mathbf{x}_k \quad (6)$$

where \mathbf{x}_k is the input data vector. Using the three different components that make up the input vector in (1), the output of the projection filter \mathbf{V}_k can be written as

$$\bar{\mathbf{x}}_k = \mathbf{V}_k [\mathbf{p}_k + \mathbf{w}_k + \mathbf{j}_k] \quad (7)$$

Since we assume total interference excision through the projection operation, then

$$\mathbf{V}_k \mathbf{j}_k = \mathbf{0}, \quad \bar{\mathbf{x}}_k = \mathbf{V}_k \mathbf{p}_k + \mathbf{V}_k \mathbf{w}_k = \bar{\mathbf{p}}_k + \bar{\mathbf{w}}_k \quad (8)$$

The decision variable y is obtained by correlating the filter output $\bar{\mathbf{x}}_k$ with the corresponding k^{th} block of the receiver PN sequence and summing the results over the K blocks. That is,

$$y = \sum_{k=0}^{K-1} \bar{\mathbf{x}}_k^T \mathbf{p}_k \quad (9)$$

The above variable can be written in terms of the constituent signals as

$$\begin{aligned} y &= \mathbf{p}_k^T \mathbf{V}_k^T \mathbf{p}_k + \mathbf{w}_k^T \mathbf{V}_k^T \mathbf{p}_k = y_1 + y_2 \\ y_1 &= \sum_{k=0}^{K-1} \sum_{i=1}^N \sum_{j=1}^N p(kN+i) v_{ji}(k) p(kN+j) \\ y_2 &= \sum_{l=0}^{K-1} \sum_{m=1}^N \sum_{n=1}^N w(lN+m) v_{nm}(l) p(lN+n) \end{aligned} \quad (10)$$

where y_1 and y_2 are the contributions of the PN and noise sequences to the decision variable, respectively. The mean value of the decision variable is given by

$$E\{y\} = E\{y_1\} + E\{y_2\} \quad (11)$$

Without the pre-processing filter, y_1 is constant and equal to L . However, by applying the projection operator \mathbf{V}_k , y_1 becomes a random variable with the mean value

$$\begin{aligned} E\{y_1\} &= E\{\mathbf{p}_k^T \mathbf{V}_k^T \mathbf{p}_k\} = E\left\{ \sum_{k=0}^{K-1} \sum_{i=1}^N \sum_{j=1}^N p(kN+i) v_{ji}(k) p(kN+j) \right\} \\ &= \sum_{k=0}^{K-1} \sum_{i=1}^N \sum_{j=1}^N v_{ji}(k) E\{p(kN+i) p(kN+j)\} \\ &= \sum_{k=0}^{K-1} \sum_{i=j=1}^N v_{ii}(k) = \sum_{k=0}^{K-1} \text{Tr}(\mathbf{V}_k) \\ &= K \text{Tr}\left(\frac{(N-1)}{N} \mathbf{I}_N\right) = K(N-1) = L - K \end{aligned} \quad (12)$$

where $E[\cdot]$ is the expectation operator, $\text{Tr}[\cdot]$ is the matrix trace, and \mathbf{I}_N is a identity matrix

of order N . If the block length increases to L , then the projection is performed only once over the entire bit period. In this case, $K = 1$ and $E\{y_1\}$ takes the maximum possible value $L - 1$, which is approximately equal to the correlation obtained when the excision filter is disabled. From equation (12), one observation is in order. Because of the uniform energy distribution of the PN sequence over all basis vectors, the energy in the PN sequence over any block will always be reduced by one upon the removal of a one-dimensional jammer signal via the proposed method. Therefore, the total loss in the PN energy when successively applying the interference excision projection filters over K blocks, one at a time, is K , independent of the block length. From this perspective, interference suppression with minimum distortion of the PN sequence is achieved if excision is performed once over the entire bit period.

The contribution of the noise term to the mean is zero, $E\{y_2\} = 0$, as the PN and the noise sequences are uncorrelated. Since the cross-correlations, $E\{y_1 y_2\}$ is zero due to the zero mean property of the noise, the mean square value of the decision variable is made up of only two terms,

$$E\{y^2\} = E\{y_1^2\} + E\{y_2^2\} \quad (13)$$

The first term in the mean square value of y_1 ,

$$\begin{aligned} E\{y_1^2\} &= E\{\mathbf{p}_k^T \mathbf{V}_k^T \mathbf{P}_k \mathbf{p}_k^T \mathbf{V}_k^T \mathbf{P}_k\} \\ E\{y_1^2\} &= E\left\{\left(\sum_{k=0}^{K-1} \sum_{i=1}^N \sum_{j=1}^N p(kN+i) v_{ji}(k) p(kN+j)\right) \right. \\ &\quad \left. \left(\sum_{l=0}^{K-1} \sum_{m=1}^N \sum_{n=1}^N p(lN+m) v_{nm}(l) p(lN+n)\right)\right\} \\ &= \sum_{k=0}^{K-1} \sum_{i=1}^N \sum_{j=1}^N \sum_{l=0}^{K-1} \sum_{m=1}^N \sum_{n=1}^N v_{ji}(k) v_{nm}(l) \\ &\quad E\{p(kN+i) p(kN+j) p(lN+m) p(lN+n)\} \end{aligned} \quad (14)$$

The above expectation is zero except for the following three cases: (i) $i = j$ and $m = n \forall l, k$ (ii) $m = i, j = n$ and $k = l$ (iii) $m = j, i = n$ and $k = l$. It should be noted that the terms that have the indices $i = j = m = n$ are included in each of the summation terms under conditions (i), (ii) and (iii). Therefore, we must subtract twice the value of these terms from the summations. Equation (14) may be simplified to

$$\begin{aligned}
 E\{y_1^2\} &= \sum_{k=0}^{K-1} \sum_{l=0}^{K-1} \sum_{i=j=1}^N \sum_{m=n=1}^N v_{ii}(k) v_{mm}(l) \\
 &+ 2 \sum_{k=0}^{K-1} \sum_{i=m=1}^N \sum_{j=n=1}^N v_{ji}(k) v_{ji}(k) - 2 \sum_{k=0}^{K-1} \sum_{i=n=j=m=1}^N v_{ii}(k) v_{ii}(k) \\
 &= \sum_{k=0}^{K-1} \sum_{l=0}^{K-1} [Tr(V_k)] [Tr(V_l)] + 2 \sum_{k=0}^{K-1} \|V_k\|_F^2 - 2 \sum_{k=0}^{K-1} \sum_{i=1}^N |v_{ii}(k)|^2
 \end{aligned} \quad (15)$$

In the above equation, $\|\cdot\|_F^2$ means the square of the Frobenius norm of the matrix. It is easy to show that $\|V_k\|_F^2$ is equal to $(N-1)$. The inner summation in the third term is equal to $(N-1)^2/N$ and approximates to $(N-2)$ for $N \gg 1$. Accordingly,

$$E\{y_1^2\} = K^2 (N-1)^2 + 2 K (N-1) - 2K \frac{(N-1)^2}{N} \quad (16)$$

From eqns. (12) and (16), the variance of y_1 is

$$\sigma_{y_1}^2 = var[y_1] = \frac{2 K (N-1)}{N} = 2 K \left(1 - \frac{1}{N}\right) = 2 \frac{(L-K)}{N}$$

which can approximated by $2K$ for $N \gg 1$. If the data record is not partitioned into blocks, and jammer excision is only performed once over the entire bit period, then $N = L$, $K = 1$, and the above equation simplifies to

$$var[y_1] = 2 \left(\frac{L-1}{L}\right) = 2\left(1 - \frac{1}{L}\right) \approx 2 \quad L \gg 1$$

The mean square value of y_2 is

$$E\{y_2^2\} = E\{w_k^T V_k^T P_k w_k^T V_k^T P_k\}$$

$$\begin{aligned}
&= E\left\{ \sum_{k=0}^{K-1} \sum_{i=1}^N \sum_{j=1}^N w(kN+i) v_{ji}(k) p(kN+j) \right. \\
&\quad \left. \sum_{l=0}^{K-1} \sum_{m=1}^N \sum_{n=1}^N w(lN+m) v_{nm}(l) p(lN+n) \right\} \\
&= \sum_{k=0}^{K-1} \sum_{i=1}^N \sum_{j=1}^N \sum_{l=0}^{K-1} \sum_{m=1}^N \sum_{n=1}^N v_{ji}(k) v_{nm}(l) \\
&\quad E\{w(kN+i) p(kN+j) w(lN+m) p(lN+n)\}
\end{aligned} \tag{17}$$

Due to the uncorrelation between the noise and the PN sequences and the whiteness property of both sequences, the above expectation is zero unless $l = k$, $j = n$ and $i = m$,

$$\begin{aligned}
E\{y_2^2\} &= \sigma^2 \sum_{k=0}^{K-1} \sum_{i=m=1}^N \sum_{j=n=1}^N v_{ji}(k) v_{ji}(k) \\
&= \sigma^2 \sum_{k=0}^{K-1} \|V_k\|_F^2 = \sigma^2 K (N-1) = \sigma^2 (L-K)
\end{aligned} \tag{18}$$

Since $E\{y_2\} = 0$, then $\sigma_{y_2}^2 = E\{y_2^2\}$. From eqns.(15-18),

$$\begin{aligned}
\text{var}\{y\} &= \sigma_{y_1}^2 + \sigma_{y_2}^2 \\
&= 2K(1 - \frac{1}{N}) + \sigma^2 K (N-1) = (L-K) \left[\sigma^2 + \frac{2}{N} \right]
\end{aligned} \tag{19}$$

The receiver SINR is given by

$$\begin{aligned}
\text{SINR} &= \frac{E^2\{y\}}{\text{var}\{y\}} = \frac{L-K}{\sigma^2 + 2/N} \\
&= \frac{L-K}{\sigma^2} \quad \text{for } N \gg 1
\end{aligned} \tag{20}$$

The above equation shows that, in approximate sense, the receiver SINR increases linearly with the number of blocks per bit, and reaches its maximum value when the excision is performed once over the entire bit period. It should be noticed that, by performing block wise excision, we lose on both fronts, by a decrease in mean and an increase in the variance of the decision variable. However, as shown in Appendix A, increasing the number of blocks

reduces the computational requirements necessary to carry out the proposed excision method.

Figure 3 shows the SINR vs. N , for $L = 128$ and different values of σ^2 . An increase in the value of N causes a decrease in the value of K , and subsequently reduces both the numerator and the second term in the denominator, thereby increasing the SINR. This result is consistent with the fact that with a smaller block size, more of the PN sequence is lost in the projection process. It is also evident from Fig. 3 that the rate of increase of SINR vs. block length is more pronounced for higher values of input SNR's. This is so because, for $\sigma^2 \ll 1$, the denominator of eq.(20) is more dependent on the term $2/N$ than on the noise power.

If the jammer is not present, then with the projection preprocessing operation disabled, the SINR expression reduces to the standard result $\frac{L}{\sigma^2}$. This quantity is known as the matched filter bound [13], and it represents the upper bound on the receiver performance implementing interference excision techniques, including the proposed method. The lower bound on performance depends on the jammer power and its time-frequency signature. This bound is often reached when the excision projection filter is disabled, in which case the matrix \mathbf{V}_k becomes an identity matrix. For a sinusoidal jammer of power ρ^2 , the lower bound on the receiver SINR is $L/(\sigma^2 + \rho^2)$ [17]. The upper and lower bounds for sinusoidal jammer are depicted in Fig. 4

Figure 5. shows the receiver SINR vs JSR for the case of a sinusoidal jammer, using i) the proposed projection approach, ii) the full jammer excision notch filter approach [5], iii) the optimum five-coefficient excision notch filter approach, recently proposed in [9]. The first and the second approaches provide full interference excision and, therefore, their performances are independent of the jammer power, and shown in Fig. 5 as straight horizontal lines. We used block lengths of $N = 2, 4, 8, 128$. It is evident from Fig. 5 that the projection

filtering technique for $N = L = 128$, outperforms the optimum five-coefficients notch filtering and yields a 4.12 dB improvement over the case of full jammer excision using the notch filter.

Comparing the receiver SINR's of equation (20) and that of reference [9], it can be readily shown that the performance of the full excision five-coefficient notch filter [9], in the proposed projection approach, can be reached by using only a block size of three ($N=3$), which is evident in Fig. 5.

In Appendix B, we consider the general case in which the block length may vary from one block to another. We re-derive eqns. (12-20) and show the "best" and the "worst" partitioning of the bit period from the receiver performance perspective.

IV. Effect of IF errors on the projection operation

Errors in estimating the IF can be divided into two types, namely, "resolution errors" and "estimation errors". Resolution errors arise due to the limited number of frequency bins used in the DFT. These errors have a uniform distribution over $[-1/2M, 1/2M]$ for a DFT of M bins. On the other hand, estimation errors occur in situations, where it becomes difficult to ascertain the IF, due to noise, cross-terms or smart jamming techniques. In most cases, the frequency resolution errors are small when compared to the errors due to the estimation of IF. In the following analysis, we consider both sources of IF errors.

Let the complex FM jammer vector be presented as

$$\mathbf{u}^T = \frac{1}{\sqrt{L}} \begin{bmatrix} e^{j\phi(1)} & e^{j\phi(2)} & \dots & e^{j\phi(L)} \end{bmatrix} \quad (21)$$

where normalization by \sqrt{L} ensures unit energy. The estimated jammer signal is given by the normalized vector

$$\hat{\mathbf{u}}^T = \frac{1}{\sqrt{L}} \begin{bmatrix} e^{j\phi(1)} & e^{j\phi(2)} & \dots & | & e^{j(\phi(k)+\Delta\phi(k))} & \dots & e^{j(\phi(m)+\Delta\phi(m))} & | & \dots & e^{j\phi(L)} \end{bmatrix} \quad (22)$$

The above vector is assumed to be in error in the consecutive chips $k \dots m$. The IF estimation errors in the IF at different chips are assumed to be i.i.d random variables with a zero mean Gaussian distribution and variance σ_{Δ}^2 . The projection matrix onto the subspace orthogonal to the estimated jammer vector is

$$\mathbf{V} = [v_{il}] = \mathbf{I} - \frac{1}{L} \hat{\mathbf{u}} \hat{\mathbf{u}}^H = \begin{bmatrix} \mathbf{V}_1 & \mathbf{V}_2 & \mathbf{V}_3 \\ \mathbf{V}_4 & \mathbf{V}_5 & \mathbf{V}_6 \\ \mathbf{V}_7 & \mathbf{V}_8 & \mathbf{V}_9 \end{bmatrix}_{L \times L} \quad \mathbf{V} = \mathbf{V}^H \quad (23)$$

Due to the assumed error structure, the projection matrix may be expressed using block matrices, \mathbf{V}_i , $i = 1, \dots, 9$. The elements of matrix \mathbf{V} are

$$\begin{aligned} v_{il} &= \frac{-e^{j[\phi(i)-\phi(l)]}}{L} \quad i \neq l, \quad 1 \leq i, l \leq (k-1) \\ &= \frac{L-1}{L} \quad i = l, \quad 1 \leq i, l \leq (k-1) \quad \left. \vphantom{\frac{-e^{j[\phi(i)-\phi(l)]}}{L}}} \right\} \mathbf{V}_1 \\ v_{il} &= \frac{-e^{j[\phi(i)+\Delta\phi(i)-\phi(l)-\Delta\phi(l)]}}{L} \quad i \neq l, \quad k \leq i, l \leq m \\ &= \frac{L-1}{L} \quad i = l, \quad k \leq i, l \leq m \quad \left. \vphantom{\frac{-e^{j[\phi(i)+\Delta\phi(i)-\phi(l)-\Delta\phi(l)]}}{L}}} \right\} \mathbf{V}_5 \\ v_{il} &= \frac{-e^{j[\phi(i)-\phi(l)]}}{L} \quad i \neq l, \quad (m+1) \leq i, l \leq L \\ &= \frac{L-1}{L} \quad i = l, \quad (m+1) \leq i, l \leq L \quad \left. \vphantom{\frac{-e^{j[\phi(i)-\phi(l)]}}{L}}} \right\} \mathbf{V}_9 \\ v_{il} &= \frac{-e^{j[\phi(i)-\phi(l)-\Delta\phi(l)]}}{L} \quad i \neq l, \quad 1 \leq i \leq (k-1), \quad k \leq l \leq m \quad \left. \vphantom{\frac{-e^{j[\phi(i)-\phi(l)-\Delta\phi(l)]}}{L}}} \right\} \mathbf{V}_2, \mathbf{V}_4^H \\ v_{il} &= \frac{-e^{j[\phi(i)-\phi(l)]}}{L} \quad i \neq l, \quad 1 \leq i \leq (k-1), \quad (m+1) \leq l \leq L \quad \left. \vphantom{\frac{-e^{j[\phi(i)-\phi(l)]}}{L}}} \right\} \mathbf{V}_3, \mathbf{V}_7^H \\ v_{il} &= \frac{-e^{j[\phi(i)+\Delta\phi(i)-\phi(l)]}}{L} \quad i \neq l, \quad k \leq i \leq m, \quad (m+1) \leq l \leq L \quad \left. \vphantom{\frac{-e^{j[\phi(i)+\Delta\phi(i)-\phi(l)]}}{L}}} \right\} \mathbf{V}_6, \mathbf{V}_8^H \end{aligned} \quad (24)$$

In the block projection matrix \mathbf{V} , the errors in the IF vector spread into the blocks \mathbf{V}_2 , \mathbf{V}_4 , \mathbf{V}_5 , \mathbf{V}_6 and \mathbf{V}_8 . It should be noted that although all the elements of the matrix block \mathbf{V}_5 are obtained from IF values that are all in error, the diagonal elements of the matrix are still error free. This is by virtue of the the complex conjugation product operation.

Since there are errors in the IF estimates, the orthogonal projection technique proposed in section III does not entirely remove the interference signal. The contribution of the jammer

signal to the decision variable y can no longer be ignored. When the IF estimates are not equal to the exact values, then the decision variable is given by

$$y = \mathbf{p}^H \mathbf{V}^H \mathbf{p} + \mathbf{w}^H \mathbf{V}^H \mathbf{w} + \mathbf{j}^H \mathbf{V}^H \mathbf{j} = y_1 + y_2 + y_3 \quad (25)$$

where y_1, y_2 and y_3 represent the contribution of the PN sequence, the white noise sequence and the interference signal, respectively. The mean value of the decision variable is

$$\begin{aligned} E\{y\} &= E\{y_1\} = E\{\mathbf{p}^H \mathbf{V}^H \mathbf{p}\} \\ &= E \left\{ \begin{bmatrix} \mathbf{p}_1^H & \mathbf{p}_2^H & \mathbf{p}_3^H \end{bmatrix} \begin{bmatrix} \mathbf{V}_1^H & \mathbf{V}_4^H & \mathbf{V}_7^H \\ \mathbf{V}_2^H & \mathbf{V}_5^H & \mathbf{V}_8^H \\ \mathbf{V}_3^H & \mathbf{V}_6^H & \mathbf{V}_9^H \end{bmatrix} \begin{bmatrix} \mathbf{p}_1 \\ \mathbf{p}_2 \\ \mathbf{p}_3 \end{bmatrix} \right\} \end{aligned} \quad (26)$$

where $\mathbf{p}_1, \mathbf{p}_2$ and \mathbf{p}_3 are the blocks of the PN vector of sizes $k-1$, $m-k+1$ and $L-m$, respectively, and \mathbf{p}_2 is the erroneous block.

$$\begin{aligned} E\{y_1\} &= E\{\mathbf{p}_1^H \mathbf{V}_1^H \mathbf{p}_1\} + E\{\mathbf{p}_3^H \mathbf{V}_9^H \mathbf{p}_3\} + E\{\mathbf{p}_2^H \mathbf{V}_5^H \mathbf{p}_2\} \\ &= \text{Tr}[\mathbf{V}_1] + \text{Tr}[\mathbf{V}_9] + \text{Tr}[\mathbf{V}_5] = L-1 \end{aligned} \quad (27)$$

It is evident from the above equation that the mean of the decision variable is not affected by the errors in the IF vector nor does it depend on the order and/or number of chips in error. The reason is that the error in the IF does not effect the diagonal elements of the projection matrix. The mean square value of the decision variable is given by the equation

$$E\{|y|^2\} = E\{(y_1 + y_2 + y_3)(y_1^* + y_2^* + y_3^*)\} \quad (28)$$

The cross-correlation $E\{y_i y_j^*\} = 0$, $i \neq j$, and

$$\begin{aligned} E\{|y_1|^2\} &= E\{y_1 y_1^*\} = E\{\mathbf{p}^H \mathbf{V}^H \mathbf{p} \mathbf{p}^H \mathbf{V} \mathbf{p}\} \\ &= E\left\{ \left(\sum_{i=1}^L \sum_{j=1}^L p_i^* v_{ji} p_j \right) \left(\sum_{m=1}^L \sum_{n=1}^L p_m^* v_{mn} p_n \right) \right\} \end{aligned} \quad (29)$$

$$\begin{aligned}
&= \sum_{i=1}^L \sum_{j=1}^L \sum_{m=1}^L \sum_{n=1}^L E\{p_i^* v_{ji}^* p_j p_m^* v_{mn} p_n\} \\
&= \sum_{i=1}^L \sum_{j=1}^L \sum_{m=1}^L \sum_{n=1}^L E\{v_{ji}^* v_{mn}\} E\{p_i^* p_j p_m^* p_n\}
\end{aligned}$$

Since the IF errors are random variables, independent of the PN sequence, the elements of the projection matrix below are also random variables. Using the properties of the PN sequence, eqn. (29) can be simplified to

$$\begin{aligned}
E\{|y_1|^2\} &= \sum_{i=j=1}^L \sum_{m=n=1}^L E\{v_{ii}^* v_{mm}\} + \sum_{i=n=1}^L \sum_{m=j=1}^L E\{v_{ji}^* v_{ji}\} - \sum_{i=j=m=n=1}^L E\{v_{ii}^* v_{ii}\} \\
&= \text{Tr}[\mathbf{V}] \text{Tr}[\mathbf{V}] + \sum_{i=n=1}^L \|\mathbf{V}\|_F^2 - \sum_{i=j=m=n=1}^L E\{v_{ii}^* v_{ii}\} \\
&= (L-1)^2 + (L-1) - \frac{(L-1)^2}{L} \\
\sigma_{y_1}^2 &= (L-1) - \frac{(L-1)^2}{L} = \frac{L-1}{L}
\end{aligned} \tag{30}$$

Again, the above equation shows that the contribution of the PN sequence to the variance of the decision variable is dependent only on the diagonal elements of the projection matrix, and hence is not affected by the errors in the IF. It can also be shown that the contribution of the white noise sequence to the variance of the decision variable is independent of the error variance and equal to that derived in section III,

$$E\{|y_2|^2\} = \sigma_{y_2}^2 = E\{y_2 y_2^*\} = \sigma^2 \|\mathbf{V}\|_F^2 = \sigma^2 (L-1) \tag{31}$$

The contribution of the interference signal to the variance of the decision variable is not zero, and is given by

$$\begin{aligned}
E\{|y_3|^2\} &= E\{y_3 y_3^*\} = E\{\mathbf{j}^H \mathbf{V}^H \mathbf{p} \mathbf{p}^H \mathbf{V} \mathbf{j}\} = \rho^2 E\{\mathbf{u}^H [\mathbf{I} - \hat{\mathbf{u}} \hat{\mathbf{u}}^H] \mathbf{p} \mathbf{p}^H [\mathbf{I} - \hat{\mathbf{u}} \hat{\mathbf{u}}^H] \mathbf{u}\} \\
E\{|y_3|^2\} &= \rho^2 E\{\mathbf{u}^H \mathbf{p} \mathbf{p}^H \mathbf{u} + \mathbf{u}^H \hat{\mathbf{u}} \hat{\mathbf{u}}^H \mathbf{p} \mathbf{p}^H \hat{\mathbf{u}} \hat{\mathbf{u}}^H \mathbf{u}\}
\end{aligned}$$

$$- \mathbf{u}^H \hat{\mathbf{u}} \hat{\mathbf{u}}^H \mathbf{p} \mathbf{p}^H \mathbf{u} - \mathbf{u}^H \mathbf{p} \mathbf{p}^H \hat{\mathbf{u}} \hat{\mathbf{u}}^H \mathbf{u} \quad (32)$$

where ρ is the jammer power. It can be shown that $\mathbf{u}^H \hat{\mathbf{u}} = \frac{1}{L} [(L-m+k-1) + \sum_{i=k}^m e^{j\Delta\phi(i)}]$.

The value of the second term in eq. (32)

$$\begin{aligned} E\{\mathbf{u}^H \hat{\mathbf{u}} \hat{\mathbf{u}}^H \mathbf{p} \mathbf{p}^H \hat{\mathbf{u}} \hat{\mathbf{u}}^H \mathbf{u}\} &= \frac{1}{L^3} \sum_{i=1}^L \sum_{n=1}^L E\{[(L-m+k-1) + \sum_{l=k}^m e^{j\Delta\phi(l)}] \\ &\quad \hat{u}_i^* p_{in} \hat{u}_n [(L-m+k-1) + \sum_{o=k}^m e^{-j\Delta\phi(o)}]\} \\ &= \frac{1}{L^3} \sum_{i=n=1}^L E\{[(L-m+k-1) + \sum_{l=k}^m e^{j\Delta\phi(l)}] \\ &\quad \hat{u}_i^* p_{ii} \hat{u}_i [(L-m+k-1) + \sum_{o=k}^m e^{-j\Delta\phi(o)}]\} \\ &= \frac{1}{L^2} E\{[(L-m+k-1) + \sum_{l=k}^m e^{j\Delta\phi(l)}] [(L-m+k-1) + \sum_{o=k}^m e^{-j\Delta\phi(o)}]\} \\ &= \frac{1}{L^2} [(L-m+k-1)^2 + (L-m+k-1) E\{\sum_{l=k}^m e^{j\Delta\phi(l)} + \sum_{o=k}^m e^{-j\Delta\phi(o)}\} \\ &\quad + E\{\sum_{l=k}^m e^{j\Delta\phi(l)} \sum_{o=k}^m e^{-j\Delta\phi(o)}\}] \\ &= \frac{1}{L^2} [(L-m+k-1)^2 + 2(L-m+k-1)(m-k+1)e^{-\sigma_\Delta^2/2} \\ &\quad + (m-k)(m-k+1)e^{-\sigma_\Delta^2} + (m-k+1)]. \end{aligned} \quad (33)$$

The value of the third in eq. (32) is

$$\begin{aligned} E\{\mathbf{u}^H \hat{\mathbf{u}} \hat{\mathbf{u}}^H \mathbf{p} \mathbf{p}^H \mathbf{u}\} &= \frac{1}{L^2} \sum_{i=1}^L \sum_{n=1}^L E\{[(L-m+k-1) + \sum_{o=k}^m e^{j\Delta\phi(o)}] \hat{u}_n p_{in} u_i^*\} \\ &= \frac{1}{L^2} \sum_{i=n=1}^L E\{[(L-m+k-1) + \sum_{o=k}^m e^{j\Delta\phi(o)}] \hat{u}_i p_{ii} u_i^*\} \\ &= \frac{1}{L^2} \sum_{i=n=1}^{k-1} E\{[(L-m+k-1) + \sum_{o=k}^m e^{j\Delta\phi(o)}] \hat{u}_i p_{ii} u_i^*\} \\ &\quad + \sum_{i=n=k}^m E\{[(L-m+k-1) + \sum_{o=k}^m e^{j\Delta\phi(o)}] \hat{u}_i p_{ii} u_i^*\} \\ &\quad + \sum_{i=n=m+1}^L E\{[(L-m+k-1) + \sum_{o=k}^m e^{j\Delta\phi(o)}] \hat{u}_i p_{ii} u_i^*\} \end{aligned}$$

$$\begin{aligned}
&= \frac{1}{L^2} [(L-m+k-1)E\{[(L-m+k-1) + \sum_{o=k}^m e^{j\Delta\phi(o)}]\}] \\
&+ E\{\sum_{i=k}^m e^{-j\Delta\phi(i)} [(L-m+k-1) + \sum_{o=k}^m e^{j\Delta\phi(o)}]\}] \\
&= \frac{1}{L^2} [(L-m+k-1)^2 + 2(L-m+k-1)(m-k+1)e^{-\sigma_\Delta^2/2} \\
&+ (m-k)(m-k+1)e^{-\sigma_\Delta^2} + (m-k+1)] \quad (34)
\end{aligned}$$

In the absence of IF error, i.e., $\sigma_\Delta^2 = 0$, eqn. (34) reduces to 1. The value of the fourth term can be similarly obtained. It should be noted that the second, third and the fourth terms have the same mean square value. This is due to the fact that the product of $\mathbf{p}\mathbf{p}^H$ gives rise to an Identity matrix in each of the terms, and $\hat{\mathbf{u}}^H \hat{\mathbf{u}} = 1$. The variance due to the jammer signal is given by the expression

$$\begin{aligned}
\sigma_{y_3}^2 &= E\{|y_3|^2\} = \frac{\rho^2}{L^2} [L^2 - [(L-m+k-1)^2 + 2(L-m+k-1)(m-k+1)e^{-\sigma_\Delta^2/2} \\
&+ (m-k)(m-k+1)e^{-\sigma_\Delta^2} + (m-k+1)]] \quad (35)
\end{aligned}$$

which is a function of the jammer power, the error variance σ_Δ^2 , and the number of samples in error, $(m-k+1)$. In this case the receiver SINR is

$$SINR = \frac{E^2\{y\}}{\sigma_{y_1}^2 + \sigma_{y_2}^2 + \sigma_{y_3}^2} \quad (36)$$

If the IF estimates are equal to the exact values, σ_Δ^2 tends to zero, and $\sigma_{y_3}^2 = 0$, indicating full interference excision. In the case the error is spread over the entire bit, $m = L$, $k = 1$ and eqn. (35) reduces to

$$\sigma_{y_3}^2 = \frac{\rho^2}{L^2} [L^2 - [L(L-1)e^{-\sigma_\Delta^2/2} + L]] \quad (37)$$

It is straightforward to show that when considering the frequency resolution errors, equations

(35) and (37) become, respectively,

$$\sigma_{y_3}^2 = \frac{\rho^2}{L^2} \left[L^2 - [(L-m+k-1)^2 + \frac{2(L-m+k-1)(m-k+1)\sin\epsilon}{\epsilon} + \frac{(m-k)(m-k+1)\sin^2\epsilon}{\epsilon^2} + (m-k+1)] \right] \quad (38)$$

$$\sigma_{y_3}^2 = \frac{\rho^2}{L^2} \left[L^2 - \left[\frac{L(L-1)\sin^2\epsilon}{\epsilon^2} + L \right] \right] \quad (39)$$

where ϵ is equal to $1/2M$.

For block processing, using K blocks, each of N samples, equations (27,30,31) for both resolution and estimation errors, become

$$E\{y_1\} = K(N-1), \sigma_{y_1}^2 = K(N-1) - K \frac{(N-1)^2}{N}, \sigma_{y_2}^2 = \sigma^2 K(N-1) \quad (40)$$

The variance $\sigma_{y_3}^2$, however, will depend on whether we deal with resolution or estimation errors. Providing that IF errors span only one block, $\sigma_{y_3}^2$ can be obtained simply by replacing L by N in (35-39). The main advantage of block-wise processing is that the block effected by the IF estimation error does not contaminate the desired signal in other blocks upon projection. We note that if the decision is to remove the erroneous blocks, then the parameters in equation (40) become

$$E\{y_1\} = (K-q)(N-1), \sigma_{y_1}^2 = (K-q)(N-1) - (K-q) \frac{(N-1)^2}{N}$$

$$\sigma_{y_2}^2 = \sigma^2(K-q)(N-1)$$

where q is the number of blocks in error. In this case, the receiver performance is given by

$$SINR = \frac{L - K - Nq + q}{\sigma^2 + 1/N} \quad (41)$$

Figure. 6 depicts the performance of the proposed projection excision filter for $K = 1$, for two different values of IF error variance. It is clear from the figure that the receiver SINR decreases with increased σ_{Δ}^2 , and this behaviour is more pronounced at higher JSR.

Figure. 7 shows the receiver SINR with and without block processing. The errors in the IF were assumed to be entirely due to IF spreading. For low JSR's, the amount of power leaking through the projection filter (using a single block) is very small and hence the performance of the projection filter for $K = 1$ is better than block-wise projections. But, as the jammer power increases, the residual jammer power degrades the performance for a single block excision to the extent that it becomes inferior to block-wise excision. In this example $L=128$, $K=8$ and $N=16$.

V. Conclusions

This paper has presented a subspace-based approach for nonstationary interference excision in DSSS. In this approach, the interference is removed by projecting the data vector on the interference orthogonal subspace formed from the IF estimate. The projection may be performed once over the entire bit period or successively over blocks of the data in the bit period. A closed form expression was derived for the receiver SINR implementing the block-wise excision technique. The performance of the block-wise processing was compared to that of a single block projection receiver and was shown to be computationally efficient, with very small loss in performance.

Two types of IF errors were considered, namely the errors due to the finite length DFT and those due to poor IF estimates over some or all data blocks. A closed form expression was derived to show the effect of each type of errors on the excision process. The receiver performance in the presence of IF errors was evaluated by calculating the jammer power escaping through the projection filter. The performance of the block-wise excision receiver was shown to be less sensitive to errors in IF.

Appendix A

Computational Complexity

Computational cost C_N for processing a block of length N is given in table 1.

$$C_N = 2 N^3 + 4 N^2 + 2 N \quad (\text{A-1})$$

The total computational cost C for processing one symbol will involve K additions, and is given by

$$\begin{aligned} C &= K (2 N^3 + 4 N^2 + 2 N) + K \\ &= K N (2 N^2 + 4 N + 2) + K \\ &= L (2 N^2 + 4 N + 2) + K \end{aligned} \quad (\text{A-2})$$

which should be compared with $L(2L^2 + 4L + 2)$ for the case when only one projection is performed over the entire data bit. If $L = 256, K = 32, N = 8$, then block processing requires 0.122% of the computations required if only $K = 1$ is used.

Table. 1

Algorithm for Real PN sequence& Computational Complexity	
Step	Flops
$I - \mathbf{j} * \mathbf{j}^T$	$2N^2$
$\mathbf{V} = \mathbf{u} \mathbf{u}^H$	$2N^3$
$\bar{\mathbf{x}}_k = \mathbf{V}(n) \mathbf{x}_k$	$2N^2$
$y_k = \bar{\mathbf{x}}_k^H \mathbf{p}_k$	$2N$
Computational cost for processing block C_N	$2N^3 + 4N^2 + 2N$

Appendix B

Block wise interference excision with unequal Block Sizes

As in the case of equal block sizes, the received data vector is divided into blocks. However, the size of the k^{th} block is now N_k , which is dependent on the block number, k . The constraint on the block sizes is

$$\sum_{k=0}^{K-1} N_k = L, \quad N_k \neq 0 \quad (B-1)$$

The projection matrix for the k^{th} block is

$$V_k = I - u_k u_k^T \quad (B-2)$$

The output of the projection operation is

$$\bar{X}_k = V_k X = V_k [p_k + w_k + j_k] \quad (B-3)$$

The decision variable is

$$\begin{aligned} y &= \sum_{k=0}^{K-1} \bar{X}_k^T p_k = \sum_{k=0}^{K-1} [p_k^T + w_k^T + j_k^T] V_k^T p_k \\ &= y_1 + y_2 \end{aligned} \quad (B-4)$$

y_1 and y_2 represent the contribution of the PN sequence and the white noise sequence respectively, to the decision variable, while the interference signal is assumed to have been cancelled.

The means of y_1 is

$$\begin{aligned} E\{y_1\} &= E\{p_k^T V_k^T p_k\} = E\left\{\sum_{k=0}^{K-1} \sum_{i=1}^{N_k} \sum_{j=1}^{N_k} p\left(\sum_{a=1}^k N_a + i\right) v_{ji}(k) p\left(\sum_{a=1}^k N_a + j\right)\right\} \\ &= \sum_{k=0}^{K-1} \sum_{i=1}^{N_k} \sum_{j=1}^{N_k} v_{ji}(k) E\left\{p\left(\sum_{a=1}^k N_a + i\right) p\left(\sum_{a=1}^k N_a + j\right)\right\} = \sum_{k=1}^K \text{Tr}[V_k] \\ &= \sum_{k=1}^K (N_k - 1) \end{aligned} \quad (B-5)$$

The mean of the variable y_2 is

$$\begin{aligned} E\{y_2\} &= E\{w_k^T V_k^T p_k\} \\ &= E\left\{\sum_{l=0}^{K-1} \sum_{m=1}^{N_l} \sum_{n=1}^{N_l} w\left(\sum_{a=1}^l N_a + m\right) v_{nm}(k) p\left(\sum_{a=1}^l N_a + n\right)\right\} = 0 \end{aligned} \quad (B-6)$$

as the noise and the PN sequence are uncorrelated with each other. The variance of the decision variable is

$$E\{y^2\} = E\{y_1^2\} + E\{y_2^2\} \quad (B-7)$$

$$\begin{aligned} E\{y_1^2\} &= E\{p_k^T V_k^T p_k p_k^T V_k p_k\} \\ &= E\left\{\sum_{k=0}^{K-1} \sum_{i=1}^{N_k} \sum_{j=1}^{N_k} p\left(\sum_{a=1}^k N_a + i\right) v_{ji}(k) p\left(\sum_{a=1}^k N_a + j\right) \right. \\ &\quad \left. \sum_{l=0}^{K-1} \sum_{m=1}^{N_l} \sum_{n=1}^{N_l} p\left(\sum_{a=1}^l N_a + m\right) v_{ji}(l) p\left(\sum_{a=1}^l N_a + n\right)\right\} \end{aligned} \quad (B-8)$$

The above expectation operation yields non-zero value only if (i) $i = j$ and $m = n$ (ii) $k = l, j = n$ and $i = m$ (iii) $k = l, j = m$ and $i = n$

$$\begin{aligned} E\{y_1^2\} &= \sum_{k=0}^{K-1} \sum_{l=0}^{K-1} \sum_{i=j=1}^{N_k} \sum_{m=n=1}^{N_l} v_{ji}(k) v_{mn}(l) + 2 \sum_{k=0}^{K-1} \sum_{i=m=1}^{N_k} \sum_{j=n=1}^{N_k} v_{ji}(k) v_{ji}(k) \\ &\quad - 2 \sum_{k=0}^{K-1} \sum_{i=m=j=n=1}^{N_k} v_{ii}(k) v_{ii}(k) \\ &= \sum_{k=0}^{K-1} \text{Tr}[V_k] \sum_{l=0}^{K-1} \text{Tr}[V_l] + 2 \sum_{k=0}^{K-1} \|V_k\|_F^2 - 2 \sum_{k=0}^{K-1} \sum_{i=1}^{N_k} |V_{ii}(k)|^2 \\ &= \left[\sum_{k=0}^{K-1} (N_k - 1) \right]^2 + 2 \sum_{k=0}^{K-1} (N_k - 1) - 2 \sum_{k=0}^{K-1} \frac{(N_k - 1)^2}{N_k} \end{aligned} \quad (B-9)$$

The contribution of the white noise to the variance of the decision variable is

$$\begin{aligned} E\{y_2^2\} &= E\{w_k^T V_k^T p_k p_k^T V_k w_k\} \\ &= E\left\{\sum_{k=0}^{K-1} \sum_{i=1}^{N_k} \sum_{j=1}^{N_k} w\left(\sum_{a=1}^k N_a + i\right) v_{ji}(k) p\left(\sum_{a=1}^k N_a + j\right) \right. \end{aligned}$$

$$E\{y_2^2\} = \sum_{l=0}^{K-1} \sum_{m=1}^{N_l} \sum_{n=1}^{N_l} w\left(\sum_{a=1}^l N_a + m\right) v_{ji}(l) p\left(\sum_{a=1}^l N_a + n\right) \sigma^2 \sum_{k=0}^{K-1} (N_k - 1) = \sigma^2 (L - K) \quad (\text{B-10})$$

It should be noted that the contribution of the white noise sequence to the variance of the decision variable has not changed, even if the block sizes are not equal. This is not the case with the variance of the variable y_1 , which is dependent on the block sizes. The SINR of receiver is

$$\begin{aligned} \text{SINR} &= \frac{\left[\sum_{k=0}^{K-1} (N_k - 1)\right]^2}{(2 + \sigma^2) \sum_{k=0}^{K-1} (N_k - 1) - 2 \sum_{k=0}^{K-1} \frac{(N_k - 1)^2}{N_k}} \\ &= \frac{[L - K]^2}{(2 + \sigma^2)(L - K) - 2 \left[L - 2K + \sum_{k=0}^{K-1} \frac{1}{N_k}\right]} \end{aligned} \quad (\text{B-11})$$

It can readily be shown [18] that the term $\sum_{k=0}^{K-1} 1/N_k$ reaches its minimum value when $N_k = N$, i.e., all blocks of equal length. In this case, SINR is minimum, implying the worst case receiver performance. On the other hand, the above term takes a maximum value when one block is of length $L - K + 1$ and all other $K - 1$ blocks are of equal length, which is a unit sample.

References

- [1] H. V. Poor and L. A. Rusch, "Narrowband interference suppression in spread spectrum CDMA," *IEEE Personal Comm. Magazine*, vol. 1, pp. 14-27, August 1994.
- [2] J. D. Laster and J. H. Reed, "Interference rejection in digital wireless communications," *IEEE Signal Processing Magazine*, pp. 37-62, May 1997.
- [3] M.J. Medley, P.K. Das and G.J. Saulnier, "A chapter in subband and wavelet transforms: design and applications," *Wavelets and Filterbanks in spread-spectrum communication systems*, A.N.Akansu and M.J.T. Smith, Eds., Norwell, MA:Kluwer, 1996.
- [4] M.V. Tazebay and A.N. Akansu, "Adaptive subband transforms in time-frequency excisers for DSSS communication systems," *IEEE Trans. on Signal Processing*, vol. 43, pp. 2776-2783, November 1995.
- [5] M. G. Amin, "Interference mitigation in spread-spectrum communication systems using time-frequency distributions," *IEEE Trans. Signal Processing*, vol. 45, no. 1, pp. 90-102, January 1997.
- [6] A. Bultan, "A novel time-frequency exciser in spread spectrum communications for chirp like interference," *Proc. of ICASSP*, Seattle, WA, May 1998.
- [7] O. Akay and G.F. Boudreaux-Bartels, "Broadband interference excision in spread spectrum communications systems via fractional fourier transforms," *32nd Asilomar conference on Signals Systems and Computers*, Pacific Grove, CA, November, 1998.
- [8] M.G. Amin and A. Akansu, "Time-frequency for interference excision in spread-spectrum communications," *Highlights of Signal Processing for Communications, Celebrating a half Century of Signal Processing*, editor: G. Giannakis, *IEEE SP Magazine*, vol. 16, no. 2, March 1999.
- [9] C. Wang, M. G. Amin and A. Lindsey, "Optimum interference excision in spread spectrum communications using open loop adaptive filters," *IEEE Trans. on Signal Processing*, vol. 47, no. 7, pp. 1966-1976, July 1999.
- [10] M. Amin, "Time-frequency receiver in spread spectrum communication systems using time-frequency distributions," *Tech. report.*, Rome Lab, July, 1996.
- [11] S. Barbarossa and A. Scaglione, "Adaptive time varying cancelation of wideband interferences in spread spectrum communications based on time-frequency distributions," *IEEE Trans. on Signal Processing*, vol. 47, no. 4, pp. 957-965, 1999.

- [12] A. Haimovich and A. Vadhri, "Rejection of narrowband interferences in pn spread spectrum systems using an eigenanalysis approach," *Proc. of the 7th SP Workshop on Statistical and Array processing*, Quebec City, Canada, June 26-29, 1994.
- [13] B. K. Poh, T. S. Quek, C. M. S. See and A. C. Kot, "Suppression of strong narrowband interference using an eigen-structure-based algorithm," *Proc. of MILCOM*, pp. 1205-1208, July, 1995.
- [14] L. Cohen, "Time-frequency distributions - a review," *Proc. of the IEEE*, vol.77 no.7, pp. 941-981, July 1989.
- [15] B. Boashash, *Time-frequency signal analysis*, vol. 1 and 2, Prentice-Hall, Englewood Cliffs, New Jersey, 1990.
- [16] F. Hlawatsch and G. Boudreaux-Bartels, "Linear and quadratic time-frequency signal representations," *IEEE Signal Processing Magazine*, vol. 9, no. 2, pp. 21-68, April 1992.
- [17] J. Ketchum and J. Proakis, " Adaptive algorithms for estimating and suppressing narrowband interference in PN spread spectrum systems," *IEEE Trans. on Communications*, vol. COM-30, pp. 913-924, May, 1982.
- [18] R. S. Ramineni, "Nonstationary interference rejection in DSSS communications using filtering and projection methods," *Master's Thesis, ECE Dept., Villanova University*, December, 1999.

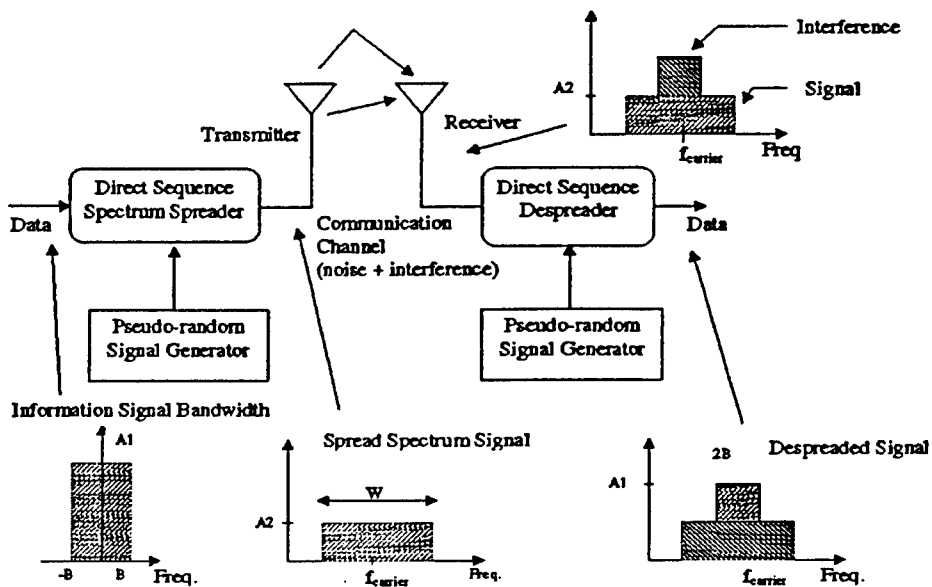


Fig. 1. DSSS Block diagram

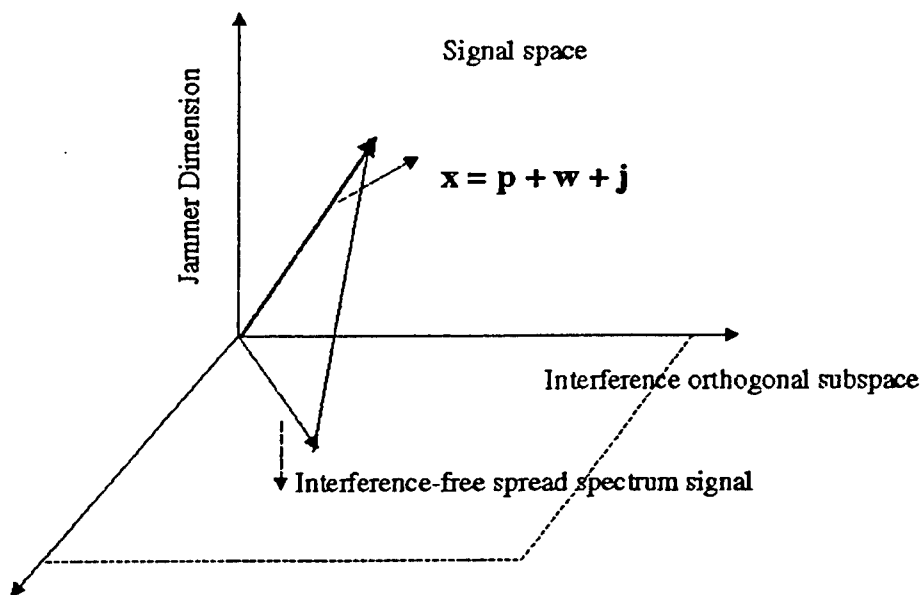


Fig. 2. Interference excision using Orthogonal Projection

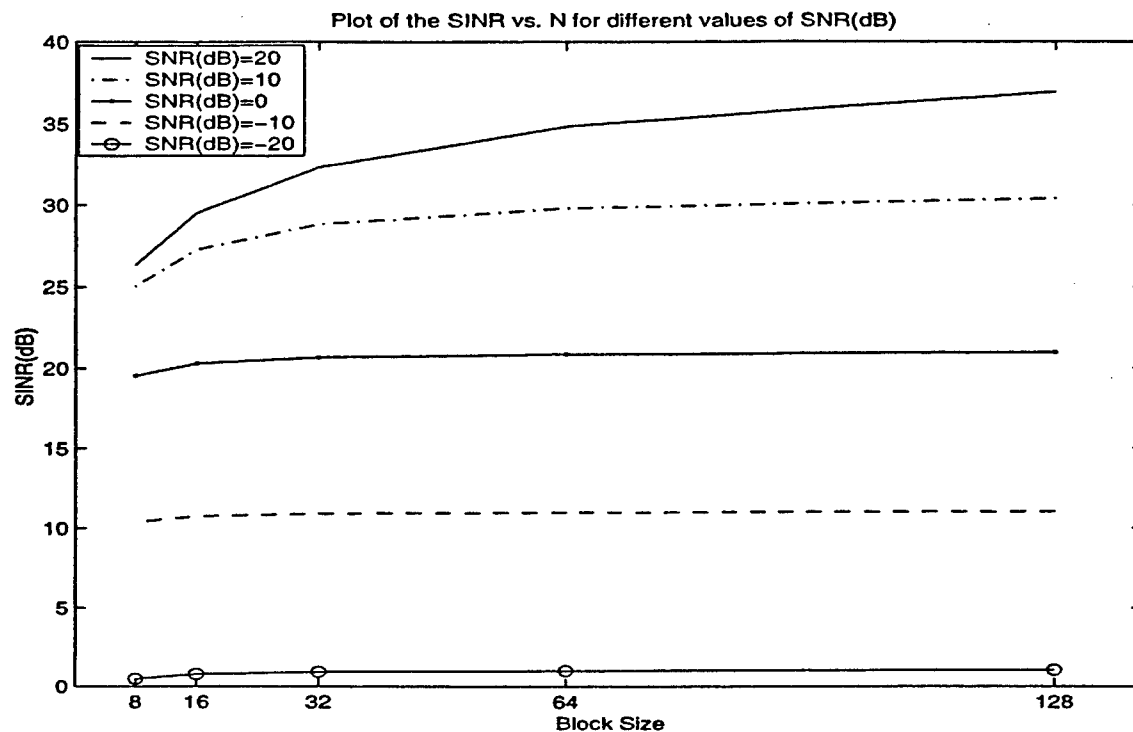


Fig. 3. The plot of the SINR (dB) vs. Block length for different values of input SNR(dB).

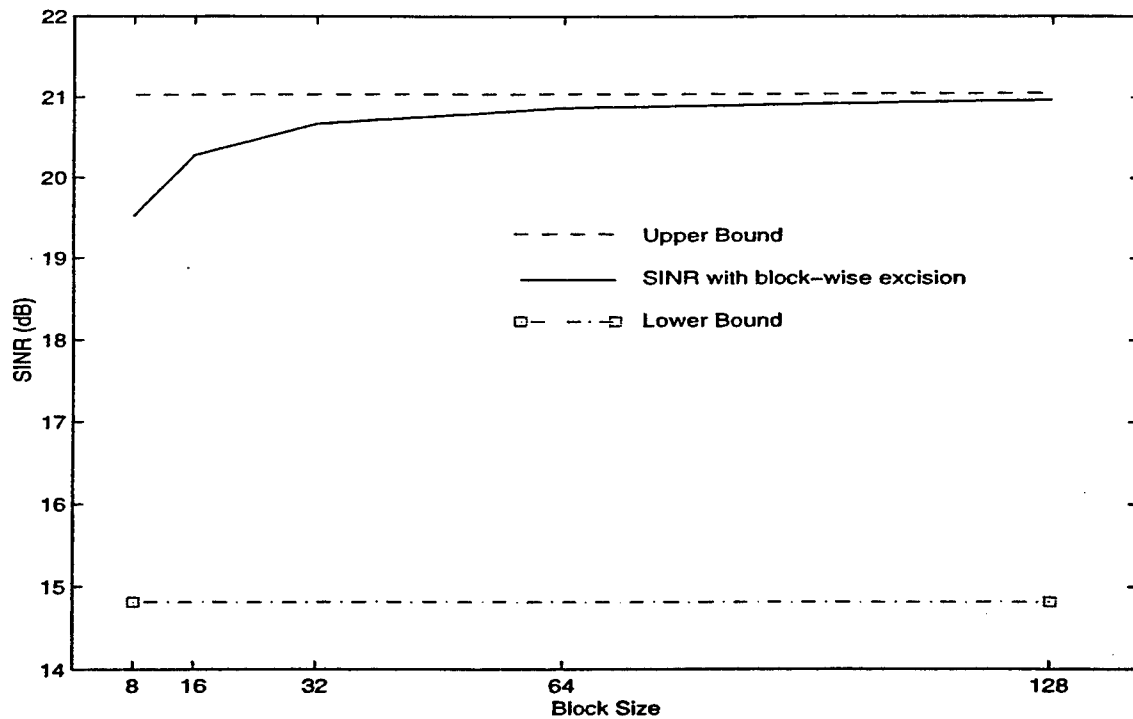


Fig. 4. The Bounds on SINR, for a sinusoidal jammer and $L=128$. The input SNR = 0 dB.

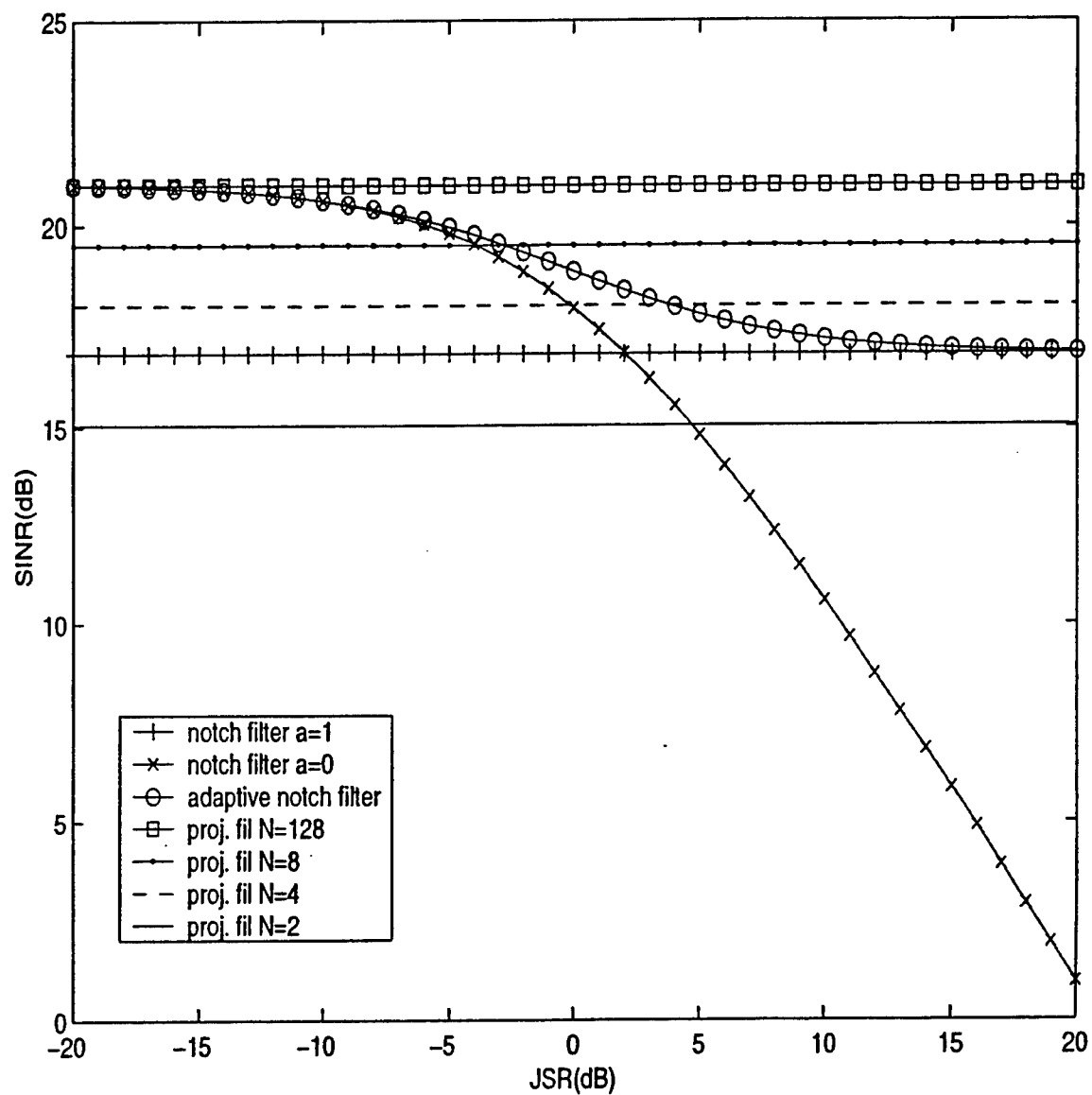


Fig. 5. Comparison of the receiver SINR for different excision methods. The number of chips/bit $L = 128$. The input SNR = 0dB.

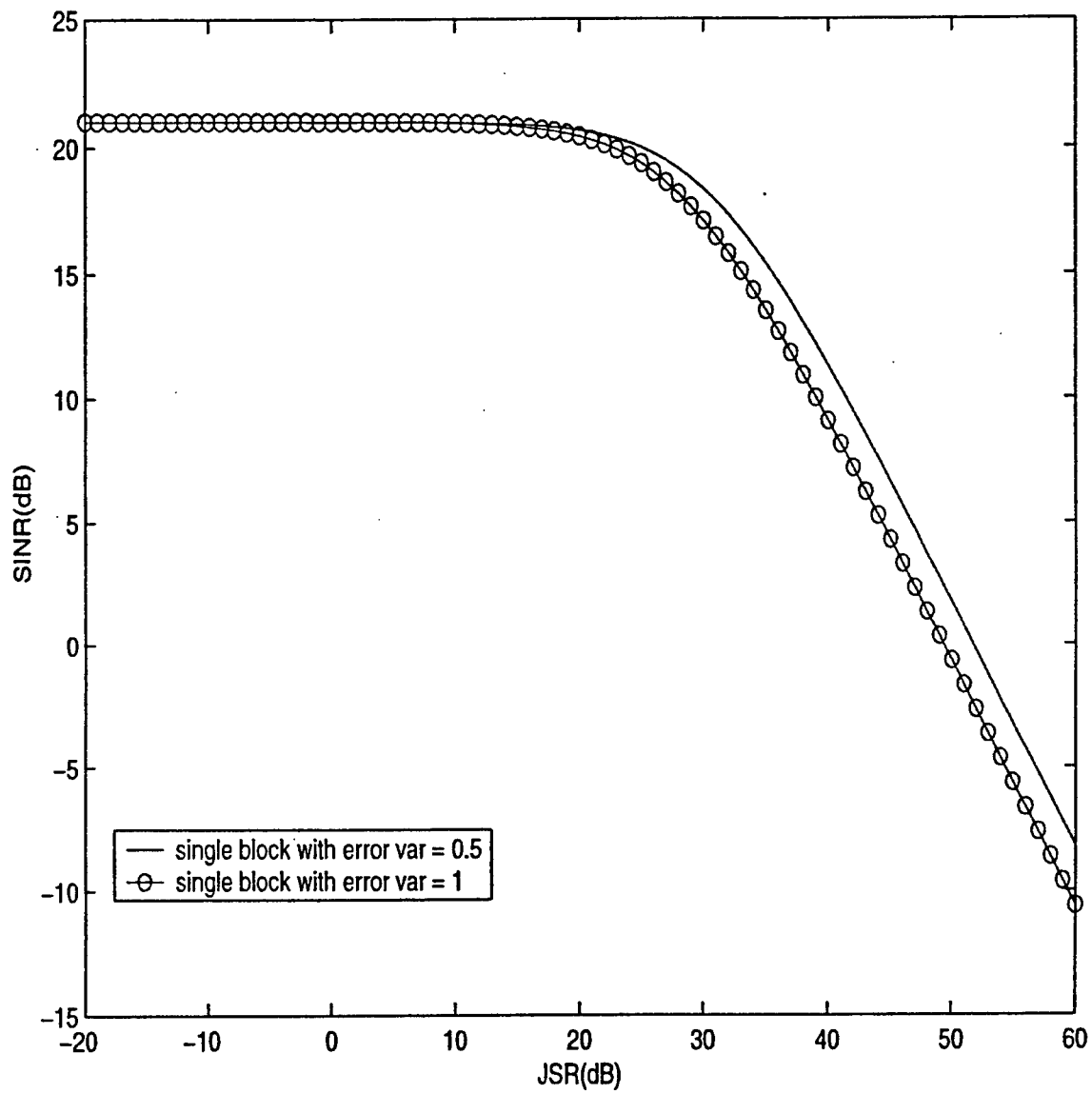


Fig. 6. Projection technique Receiver SINR with different spreading error in IF. Number of chips/bit $L = 128$, $K=1$. The input SNR = 0dB.

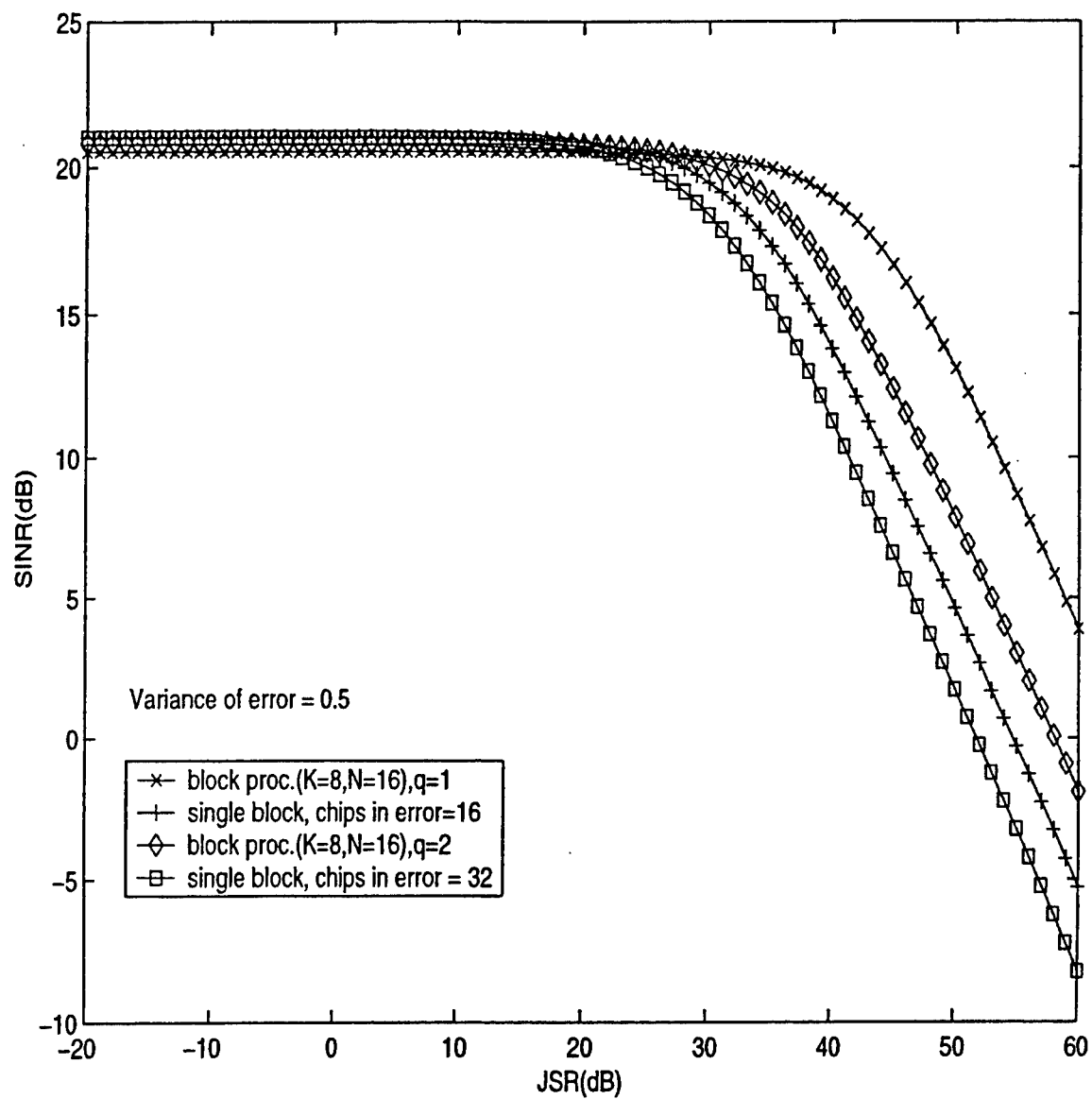


Fig. 7. Receiver SINR with Spreading error in IF. Number of chips/bit (L) = 128. The input SNR = 0 dB.

Analysis of Nonstationary Interference Excision in Spread Spectrum Communications Using Orthogonal Projections

Raja S. Ramineni and Moeness G. Amin

Department of Electrical and Computer Engineering

Villanova University, Villanova, PA 19085

email: moeness@ece.vill.edu

Abstract—This paper presents an orthogonal subspace based technique for nonstationary interference excision in direct sequence spread spectrum communications. The interference is a polynomial phase signal, which is uniquely characterized by its instantaneous frequency. In the proposed technique, the received data over one symbol period is partitioned into blocks. The data in each block is projected on the subspace orthogonal to the respective interference subspace. The projected results are then combined and correlated with the PN sequence at the receiver. The paper presents the analysis that shows the tradeoff between performance and computational complexity as the data block size increases.

I. Introduction

The primary motivation for using PN direct sequence spread spectrum (DSSS) communication systems is its inherent capability of interference mitigation. Any level of interference can be effectively overcome with sufficiently long PN sequences. However, increasing the number of chips per symbol period, which translates into higher processing gain, may lead to an increase in the spectrum bandwidth of the transmitted signal beyond available limits. This necessitates the use of signal processing techniques in conjunction with a DSSS receiver to achieve acceptable interference rejection levels without intruding on adjacent communication signal platforms.

In this paper, we examine interference rejection in DSSS communications using signal processing projection filtering techniques. Orthogonal projection methods have been considered for the underlying problems in references[1],[2],[3],[4]. However, in this paper, we address different issues and focus on the class of polynomial phase interference signals. Members of this class are uniquely characterized by their instantaneous frequency (IF), which can be easily estimated using numerous techniques [5],[6], including time-frequency distri-

butions[7],[8],[9],[10],[11]. Once the IF is estimated, then the interference temporal waveform can be obtained up to an ambiguity in phase and amplitude. With this information, the interference is represented by an L -dimensional vector, where L is the number of chips/symbol. The interference respective subspace is one dimensional and can be easily constructed from the knowledge of its IF. For a multicomponent jammer with q different polynomial phase signals, atmost the jammer subspace is q -dimensional and can be obtained by estimating the component IF's. Since the PN sequence is uniformly extended in all dimensions, removing the PN component along the interference subspace causes full jammer excision with minimum distortion of the desired signal. This interference removal is simply achieved by projecting the data vector over each symbol period on the subspace orthogonal to that of the interference.

The interference orthogonal subspace is computed by applying the singular value decomposition (SVD) to the interference vector. The eigenvectors corresponding to the zero eigen values constitute the basis of the subspace containing the jammer-free signal. In this respect, the key difference between the proposed excision method and others based on eigen analysis, is that in the proposed method, the SVD is performed on the estimated jammer waveform rather than on the data matrix or the correlation matrix.

As the PN sequence length increases, the amount of its energy along the one-dimensional interference subspace becomes smaller relative to its total energy. It is expected, therefore, that the rejection performance of proposed technique improves with more signal spreading, i.e., with higher processing gain. On the other hand, the computations required to perform SVD becomes considerably high and difficult to implement using real time signal processing, specifically for long PN sequences. Accordingly, in the context of interference rejection using

This work is supported by the Air Force Research Laboratory, Rome, NY, Contract #F30602-96-C-0077

subspace projection techniques, there is a clear tradeoff between receiver performance and computational requirements.

In this paper, we allow the user to tradeoff the above two competing requirements by partitioning the input data over each symbol into successive blocks. The projection filtering is applied over each block separately. The results of the projections over all blocks are combined to reconstruct the jammer-free spreaded data symbol. The despreading is obtained by the correlation with the receiver PN sequence. The general expression of the receiver signal to interference and noise ratio (SINR) is derived and shown to depend on the noise variance, the PN sequence length as well as the number of blocks per symbol. The tradeoff between the receiver performance and complexity is demonstrated by presenting the computational requirements as a function of the block length.

II. Interference excision

The received data vector is the sum of the PN sequence \mathbf{P} , the white noise sequence \mathbf{W} , and the interfering signal \mathbf{J} . The received data vector can be represented as

$$\mathbf{X} = \mathbf{P} + \mathbf{W} + \mathbf{J} \quad (1)$$

Let L denote the PN sequence length over one symbol period. The PN sequence is partitioned into K blocks, each of length N . The projected data vector over the k^{th} block on the respective interference orthogonal subspace is given by

$$\bar{\mathbf{X}}_k = \mathbf{V}_k \mathbf{X}_k \quad (2)$$

The orthogonal projection matrix \mathbf{V}_k is of size $N \times N$ and is obtained as

$$\mathbf{V}_k = \mathbf{U}_k \mathbf{U}_k^T \quad (3)$$

The columns of the N -by- $(N-1)$ matrix \mathbf{U} are the orthonormal basis vectors that span the subspace orthogonal to the interfering signal. The output of the projection filter is thus given by

$$\bar{\mathbf{X}}_k = \mathbf{V}_k [\mathbf{P}_k + \mathbf{W}_k + \mathbf{J}_k] \quad (4)$$

The output of the projection filter over the k^{th} block is correlated with the corresponding k^{th} block of the receiver PN sequence. The correlation yields the decision variable y

$$y = \sum_{k=0}^{K-1} \bar{\mathbf{X}}_k^T \mathbf{P}_k \quad (5)$$

The decision variable can be written in terms of the constituent signals as

$$\begin{aligned} y &= \sum_{k=0}^{K-1} \sum_{i=1}^N \sum_{j=1}^N p(kN+i) v_{ji}(k) p(kN+j) \\ &+ \sum_{l=0}^{K-1} \sum_{m=1}^N \sum_{n=1}^N w(lN+m) v_{nm}(l) p(lN+n) \\ y &= y_1 + y_2 \end{aligned} \quad (6)$$

In the above equation, we assume total interference excision. Therefore, the interference contribution to the decision variable is zero. The values y_1 and y_2 are the contributions of the PN sequence and white noise, respectively, to the decision variable y .

III. Receiver SINR Analysis

The analysis provided below is for a monocomponent interference signal, but it can be easily extended to the multicomponent case. The mean value of the decision variable is obtained by taking the expectation of y in eq. 6.

$$E\{y\} = E\{y_1\} + E\{y_2\} \quad (7)$$

$$\begin{aligned} E\{y_1\} &= E\left\{ \sum_{k=0}^{K-1} \sum_{i=1}^N \sum_{j=1}^N p(kN+i) v_{ji}(k) p(kN+j) \right\} \\ &= \sum_{k=0}^{K-1} \sum_{i=1}^N \sum_{j=1}^N v_{ji}(k) E\{p(kN+i) p(kN+j)\} \\ &= \sum_{k=0}^{K-1} \sum_{i=j=1}^N v_{ii}(k) = \sum_{k=0}^{K-1} \text{Trace}(\mathbf{V}_k) \\ E\{y_1\} &= K(N-1) \end{aligned} \quad (8)$$

The contribution of the noise term to the mean is zero, as the PN and the noise sequences are uncorrelated with each other.

$$E\{y_2\} = 0 \quad (9)$$

The variance of the decision variable is

$$\begin{aligned} E\{y^2\} &= E\{y_1^2\} + E\{y_2^2\} + \\ &E\{y_1 y_2\} + E\{y_2 y_1\} \\ E\{y_1^2\} &= E\left\{ \left(\sum_{k=0}^{K-1} \sum_{i=1}^N \sum_{j=1}^N p(kN+i) v_{ji}(k) p(kN+j) \right)^2 \right\} \\ &= \sum_{k=0}^{K-1} \sum_{i=1}^N \sum_{j=1}^N v_{ji}(k) p(kN+i) p(kN+j) \cdot \\ &\quad \left(\sum_{l=0}^{K-1} \sum_{m=1}^N \sum_{n=1}^N p(lN+m) v_{nm}(l) p(lN+n) \right) \end{aligned}$$

$$\begin{aligned}
& v_{nm}(l) p(lN+n))\} \\
& = \sum_{k=0}^{K-1} \sum_{i=1}^N \sum_{j=1}^N \sum_{l=0}^{K-1} \sum_{m=1}^N \sum_{n=1}^N v_{ji}(k) v_{nm}(l) \cdot \\
& \quad E\{p(kN+i) p(kN+j) p(lN+m) \cdot \\
& \quad p(lN+n)\}
\end{aligned} \tag{10}$$

The above expectation takes nonzero values only if

- (i) $i = j$ and $m = n$ ($l \neq k$ and $l = k$)
- (ii) $l = k$, $i = m$ and $j = n$
- (iii) $l = k$, $i = n$ and $j = m$

It should be noted that the terms that have the indices $i = j = m = n$ are included in each of the summation terms in conditions (i), (ii) and (iii). The expected value of the mean square value of y is

$$\begin{aligned}
E\{y_1^2\} & = \sum_{k=0}^{K-1} \sum_{l=0}^{K-1} \sum_{i=j=1}^N \sum_{m=n=1}^N v_{ii}(k) v_{mm}(l) \\
& + 2 \sum_{k=0}^{K-1} \sum_{i=m=1}^N \sum_{j=n=1}^N v_{ji}(k) v_{ji}(k) \\
& - 2 \sum_{k=0}^{K-1} \sum_{i=n=j=m=1}^N v_{ii}(k) v_{ii}(k) \\
& = \sum_{k=0}^{K-1} \sum_{l=0}^{K-1} [\text{Trace}(\mathbf{V}_k)] [\text{Trace}(\mathbf{V}_l)] \\
& + 2 \sum_{k=0}^{K-1} \|\mathbf{V}_k\|_F^2 - 2 \sum_{k=0}^{K-1} \sum_{i=1}^N |v_{ii}(k)|^2 \tag{11}
\end{aligned}$$

$\text{Trace}(\mathbf{V}_k)$ indicates the trace of the matrix \mathbf{V}_k and is equal to $K(N-1)$. $\|\mathbf{V}_k\|_F^2$ represents the Frobenius norm of \mathbf{V}_k and is equal to $K(N-1)$. The fourth term in the equation is equal to $K(N-2)$ for $N \gg 1$. Accordingly

$$E\{y_1^2\} = K^2(N-1)^2 + 2K$$

the expectation of the mean square value of y_2 is

$$\begin{aligned}
E\{y_2^2\} & = E\left\{ \sum_{k=0}^{K-1} \sum_{i=1}^N \sum_{j=1}^N w(kN+i) \right. \\
& \quad v_{ji}(k) p(kN+j) \sum_{l=0}^{K-1} \sum_{m=1}^N \sum_{n=1}^N w(lN+m) \\
& \quad \left. v_{nm}(l) p(lN+n) \right\} \\
& = \sum_{k=0}^{K-1} \sum_{i=1}^N \sum_{j=1}^N \sum_{l=0}^{K-1} \sum_{m=1}^N \sum_{n=1}^N v_{ji}(k) v_{nm}(l) \\
& \quad E\{w(kN+i) p(kN+j)
\end{aligned}$$

$$w(lN+m) p(lN+n)\} \tag{12}$$

Due to the uncorrelation between the noise and the PN sequences, the above expected value is zero, unless $k = l$, $j = n$ and $i = m$,

$$\begin{aligned}
E\{y_2^2\} & = \sigma^2 \sum_{k=0}^{K-1} \sum_{i=m=1}^N \sum_{j=n=1}^N v_{ji}(k) v_{ji}(k) \\
& = \sigma^2 \sum_{k=0}^{K-1} \|\mathbf{V}_k\|_F^2 = \sigma^2 K(N-1) \tag{13}
\end{aligned}$$

From Eqs. (8)-(13) the variance of y can be written as

$$\text{Var}\{y\} = 2K + \sigma^2 K(N-1) \tag{14}$$

The SINR of the receiver is given by

$$\begin{aligned}
\text{SINR} & = \frac{E^2\{y\}}{\text{var}\{y\}} \\
& = \frac{K^2(N-1)^2}{2K + \sigma^2 K(N-1)} \\
& = \frac{K(N-1)}{2/(N-1) + \sigma^2} \tag{15}
\end{aligned}$$

It can be seen that the value of the SINR increases with increased values of N . Smaller block sizes result in lower SINR, as more of the PN sequence is lost during the projection process.

In the special case of no projection, the matrix \mathbf{V}_k becomes an identity matrix, and the SINR expression reduces to the standard result $\frac{L}{\sigma^2}$

IV. Computational Complexity

The total computational cost for processing the input data over a symbol period using the proposed technique can be obtained as [12]

$$\begin{aligned}
& K(10N^3 + 7N^2 + 2N) + K \\
& = L(10N^2 + 7N + 2) + K
\end{aligned}$$

which is related to the square of the block size. Figure 1. shows the computation cost as a function of the block size.

V. Simulations

In this section we present computer simulations to show the effectiveness of the proposed orthogonal subspace based projection filtering approach for interference excision as well as highlight the tradeoff between the performance and the computation complexity. Figure 2 shows the receiver SINR for different block sizes. The approximated values of SINR given by (15) are very close to the exact SINR values.

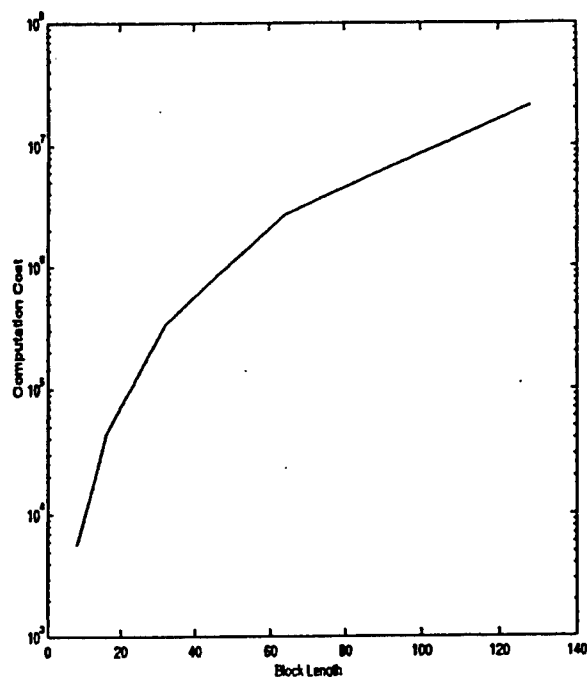


Fig. 1. The Computational cost as a function of block size

Figures. 1 and 2 illustrate that the reduction in computational cost, with the use of smaller block sizes, comes at the expense of receiver the performance. This can be seen from the fact that small block sizes result in lower SINR. Therefore, the user can select the block size based on acceptable performance levels and processing times specific to his/her own application.

VI. Conclusions

This paper has presented a simple orthogonal subspace based technique for nonstationary interference excision in DSSS communications. Closed form expressions of the receiver SINR were derived. It was shown that the receiver performance deteriorates when excision is separately performed on successive data blocks rather than over the entire symbol period. The motivation behind segmenting the symbol interval to smaller length data blocks is to avoid a very high computational cost, which arises due to subspace estimation using SVD of large matrices. The effectiveness of the proposed technique in chirp-like interference was demonstrated by a simulation example.

References

- [1] A. Haimovich and A. Vadhri. Rejection of narrow-band interference in PN spread spectrum systems using an eigenanalysis

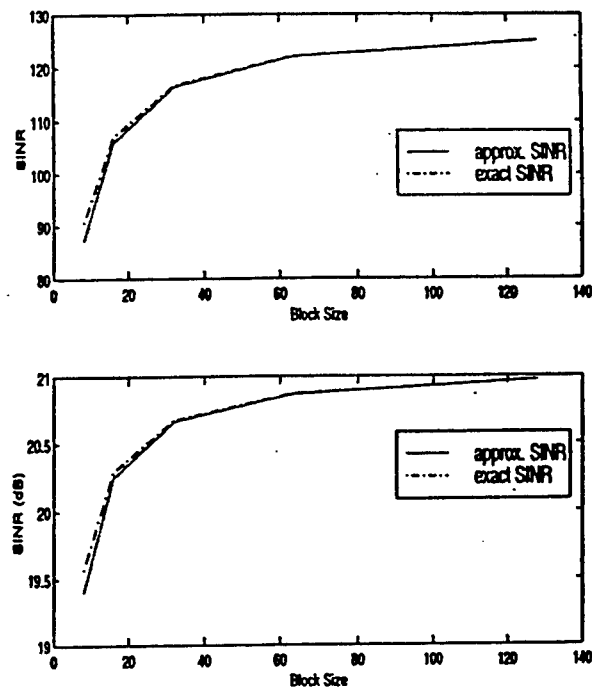


Fig. 2. The SINR of the receiver as function of number of blocks

- approach. *Proceedings of the 7th SP workshop on Statistical and Array processing, Quebec City, Canada, June, 26-29 1994.*
- [2] H. Fathallah and L. A. Rusch. A subspace approach to adaptive narrow-band interference suppression in DSSS. *IEEE Transactions on Communications*, 45:1575-1585, June 1994.
- [3] M. G. Amin and G. R. Mandapati. Nonstationary interference excision in spread-spectrum communication using projection filtering methods. *Proceedings of the Asilomar Conference on Signals, systems, and Computers*, November 1998.
- [4] J. D. Laster and J.H. Reed. Interference rejection in digital wireless communications. *IEEE Signal Processing Magazine*, 14:37-62, May 1997.
- [5] B. Boashash. Estimating and interpreting the instantaneous frequency of a signal. *Proceedings of the IEEE*.
- [6] S. Kay. A fast and accurate single frequency estimator. *IEEE Transactions on Acoustics, Speech, and Signal Processing*, December 1979.
- [7] L. Cohen. Time-frequency distributions- a review. *Proceedings of the IEEE*, pp. 941-981, 1989.
- [8] B. Boashash. *Time-frequency signal analysis*. Prentice-Hall, 1990.
- [9] F. Hlawatsch and G. Boudreaux-Bartels. Linear and quadratic time-frequency signal representations. *IEEE Signal Processing Magazine*, pp. 21-68, 1992.
- [10] L. Cohen. *Time-frequency analysis*. Prentice-Hall, New Jersey, 1995.
- [11] S. Qian and D. Chen. *Joint time-frequency analysis - methods and applications*. Prentice-Hall, New Jersey, 1996.
- [12] G. H. Golub and C. F. Van Loan. *Matrix Computations*. The Johns Hopkins University Press, 1989.
- [13] C. M. S. See B. K. Poh, T. S. Quek and A. C. Kot. Suppression of strong narrowband interference using an eigenstructure based algorithm. *MILCOM*, pp. 1205-1208, 1995.

PERFORMANCE ANALYSIS OF SUBSPACE PROJECTION TECHNIQUES FOR INTERFERENCE EXCISION IN DSSS COMMUNICATIONS

Raja S. Ramineni, Moeness G. Amin *

Dept. of Electrical and Computer Engineering,
Villanova University, Villanova, PA, 19085.
moeness,ramineni@ece.vill.edu

Alan R. Lindsey

USAF Research Laboratory/IFGC
Rome, NY 13441.
lindsey@rl.af.mil

ABSTRACT

This paper presents the performance analysis of the interference excision techniques in direct sequence spread spectrum (DSSS) communications using orthogonal subspace projections. It is shown that this technique is sensitive to the errors in the instantaneous frequency (IF) estimate of the interference over segments of the bit period. This paper discusses the effect of two different types of errors on the receiver SINR and compares the performance of the block-wise processing to the single block projection approach.

1. INTRODUCTION

FM interference excision in DSSS using block-wise orthogonal projection has been recently introduced [1]. This method uses the property that the FM signals are uniquely characterized by their instantaneous frequencies (IF) and that they are localizable to a small area in the time-frequency domain, while the received data and the white noise are spread over the entire t-f plane. The interference signal can be provided from the IF estimate to an ambiguity in phase and amplitude, by using the t-f distributions. Once the interference signal has been estimated, its excision can be achieved by projecting the received data onto the interference orthogonal subspace. The interference can be excised by performing the orthogonal projection once per bit period or over successive blocks within the bit period. It has been shown in [1] that the projection approach outperforms the notch filter approach introduced in [6], as it yields higher receiver performance.

The performance of the orthogonal projection method depends on the accuracy in estimating the IF of the jammer signal. Errors in estimating IF occur as a result of limited number of discrete frequency bins or due to the presence of large scale noise and absence of localization in the t-f distribution. These errors lead to

leakage of some of the jammer signal to the projection filter output. This paper considers the effect of the IF errors on the receiver performance, with the receiver SINR as a measure. Expressions are derived to calculate the amount of jammer leaking and the corresponding receiver SINR. The performance of the receiver implementing the block-wise excision technique is compared with that of the single block projection receiver.

2. RECEIVED DATA STRUCTURE

The signal for one bit at the receiver, after demodulation, sampled at chip rate, becomes

$$x(n) = p(n) + w(n) + j(n) \quad 1 \leq n \leq L \quad (1)$$

where $p(n)$ is the chip sequence, $w(n)$ is the white noise, and $j(n)$ is the interfering signal. It is assumed that the chip sequence and the white noise sequence are both temporally uncorrelated and of zero mean, and their cross correlation is zero. The above equation can be put in the vector form

$$\mathbf{x} = \mathbf{p} + \mathbf{w} + \mathbf{j} \quad (2)$$

All vectors are of dimension $L \times 1$, and 'T' denotes vector or matrix transposition.

3. EFFECT OF IF ERRORS ON THE PROJECTION OPERATION

Let the complex FM jammer vector be presented as

$$\mathbf{u}^T = \frac{1}{\sqrt{L}} [e^{j\phi(1)} \quad e^{j\phi(2)} \quad \dots \quad e^{j\phi(L)}]$$

where normalization by \sqrt{L} ensures unit energy. Errors in estimating the IF can be divided into two types, namely, "resolution errors" and "spreading errors". Resolution errors arise due to the limited number of frequency bins used in the DFT (This is the case for IF estimation techniques based on Fourier transform). For a DFT of M bins, these errors have a uniform distribution over $[-1/2M, 1/2M]$. On the other hand, the spreading

* This work is supported by the US Air Force Research Laboratory, Rome, NY, contract no. F30602-96-C-0077

errors occur in situations, where it becomes difficult to ascertain the interference IF, due to noise, cross-terms or smart jamming techniques. These errors have Gaussian distributions. In most cases, the frequency resolution errors are small when compared to the errors due to the spreading of IF. In the following analysis, we consider both sources of IF errors.

The estimated jammer signal is given by the normalized vector

$$\hat{\mathbf{u}}^T = \frac{1}{\sqrt{L}} \begin{bmatrix} e^{j\phi(1)} & e^{j\phi(2)} & \dots & e^{j(\phi(k)+\Delta\phi(k))} \\ \dots & e^{j(\phi(m)+\Delta\phi(m))} & \dots & e^{j\phi(L)} \end{bmatrix} \quad (3)$$

The above vector is assumed to be in error in the consecutive chips $k \dots m$. The IF spreading errors in the IF at different chips are assumed to be i.i.d random variables with a zero mean. The projection matrix onto the subspace orthogonal to the estimated jammer vector is

$$\mathbf{V} = [\mathbf{v}_{ii}] = \mathbf{I} - \frac{1}{L} \hat{\mathbf{u}} \hat{\mathbf{u}}^H = \begin{bmatrix} \mathbf{V}_1 & \mathbf{V}_2 & \mathbf{V}_3 \\ \mathbf{V}_4 & \mathbf{V}_5 & \mathbf{V}_6 \\ \mathbf{V}_7 & \mathbf{V}_8 & \mathbf{V}_9 \end{bmatrix}, \quad \mathbf{V} = \mathbf{V}^H \quad (4)$$

In the block projection matrix \mathbf{V} , the errors in the IF vector spread into the blocks $\mathbf{V}_2, \mathbf{V}_4, \mathbf{V}_5, \mathbf{V}_6$ and \mathbf{V}_8 . It should be noted that although all the elements of the matrix block \mathbf{V}_5 are obtained from IF values that are all in error, the diagonal elements of the matrix are still error free. This is by virtue of the the complex conjugation product operation.

Since the orthogonal projection technique does not entirely remove the interference signal, the contribution of the jammer signal to the decision variable y can no longer be ignored. The decision variable is given by

$$\begin{aligned} y &= \mathbf{p}^H \mathbf{V}^H \mathbf{p} + \mathbf{w}^H \mathbf{V}^H \mathbf{w} + \mathbf{j}^H \mathbf{V}^H \mathbf{j} \\ &= y_1 + y_2 + y_3 \end{aligned} \quad (5)$$

where y_1, y_2 and y_3 represent the contributions of the PN sequence, the white noise sequence, and the interference signal, respectively. The mean value of the decision variable is

$$\begin{aligned} E\{y\} &= E\{y_1\} = E\left\{ \begin{bmatrix} \mathbf{p}_1^H & \mathbf{p}_2^H & \mathbf{p}_3^H \end{bmatrix} \begin{bmatrix} \mathbf{V}_1^H & \mathbf{V}_2^H & \mathbf{V}_3^H \\ \mathbf{V}_4^H & \mathbf{V}_5^H & \mathbf{V}_6^H \\ \mathbf{V}_7^H & \mathbf{V}_8^H & \mathbf{V}_9^H \end{bmatrix} \begin{bmatrix} \mathbf{p}_1 \\ \mathbf{p}_2 \\ \mathbf{p}_3 \end{bmatrix} \right\} \quad (6) \end{aligned}$$

where $\mathbf{p}_1, \mathbf{p}_2$ and \mathbf{p}_3 are the blocks of the PN vector of sizes $k-1, m-k+1$ and $L-m$, respectively, and \mathbf{p}_2 is the erroneous block.

$$\begin{aligned} E\{y_1\} &= E\{\mathbf{p}_1^H \mathbf{V}_1^H \mathbf{p}_1 + \mathbf{p}_3^H \mathbf{V}_9^H \mathbf{p}_3 + \mathbf{p}_2^H \mathbf{V}_5^H \mathbf{p}_2\} \\ &= \text{Tr}[\mathbf{V}_1] + \text{Tr}[\mathbf{V}_9] + \text{Tr}[\mathbf{V}_5] = L-1 \quad (7) \end{aligned}$$

It is evident from the above equation that the mean of the decision variable is not affected by the errors in the IF vector nor does it depend on the order and/or number of chips in error. The reason is that the error in the IF does not effect the diagonal elements of the projection matrix. The mean square value of the decision variable is given by the equation

$$E\{|y|^2\} = E\{(y_1 + y_2 + y_3)(y_1^* + y_2^* + y_3^*)\} \quad (8)$$

The cross-correlation $E\{y_i y_j^*\} = 0, i \neq j$, and

$$\begin{aligned} E\{|y_1|^2\} &= E\{y_1 y_1^*\} = E\{\mathbf{p}^H \mathbf{V}^H \mathbf{p} \mathbf{p}^H \mathbf{V} \mathbf{p}\} \quad (9) \\ &= E\left\{ \left(\sum_{i=1}^L \sum_{j=1}^L \mathbf{p}_i^* \mathbf{v}_{ji}^* \mathbf{p}_j \right) \left(\sum_{l=1}^L \sum_{n=1}^L \mathbf{p}_l^* \mathbf{v}_{ln} \mathbf{p}_n \right) \right\} \\ &= \sum_{i=1}^L \sum_{j=1}^L \sum_{l=1}^L \sum_{n=1}^L E\{\mathbf{p}_i^* \mathbf{v}_{ji}^* \mathbf{p}_j \mathbf{p}_l^* \mathbf{v}_{ln} \mathbf{p}_n\} \\ &= \sum_{i=1}^L \sum_{j=1}^L \sum_{l=1}^L \sum_{n=1}^L E\{\mathbf{v}_{ji}^* \mathbf{v}_{ln}\} E\{\mathbf{p}_i^* \mathbf{p}_j \mathbf{p}_l^* \mathbf{p}_n\} \end{aligned}$$

Because the IF errors are random variables, the elements of the projection matrix are also random and are independent of the PN sequence. Using the properties of the PN sequence, eqn. (9) can be simplified to

$$\begin{aligned} E\{|y_1|^2\} &= \sigma_{y_1}^2 = \sum_{i,j=1}^L \sum_{l,n=1}^L E\{\mathbf{v}_{ii}^* \mathbf{v}_{ll}\} + \\ &\quad \sum_{i,n=1}^L \sum_{l,j=1}^L E\{\mathbf{v}_{ji}^* \mathbf{v}_{ji}\} - \sum_{i,j,l,n=1}^L E\{\mathbf{v}_{ii}^* \mathbf{v}_{ii}\} \\ &= [\text{Tr}[\mathbf{V}]]^2 + \sum_{i,n=1}^L \|\mathbf{V}\|_F^2 - \sum_{i,j,l,n=1}^L E\{\mathbf{v}_{ii}^* \mathbf{v}_{ii}\} \\ \sigma_{y_1}^2 &= (L-1) - \frac{(L-1)^2}{L} = \frac{L-1}{L} \quad (10) \end{aligned}$$

Again, the above equation shows that the contribution of the PN sequence to the variance of the decision variable is dependent only on the diagonal elements of the projection matrix, and hence is not affected by the errors in the IF. It can also be shown that the contribution of the white noise sequence to the variance of the decision variable is independent of the error variance,

$$E\{|y_2|^2\} = \sigma_{y_2}^2 = \sigma^2 \|\mathbf{V}\|_F^2 = \sigma^2 (L-1) \quad (11)$$

The contribution of the interference signal to the variance of the decision variable is not zero, and is given by

$$E\{|y_3|^2\} = E\{\mathbf{j}^H \mathbf{V}^H \mathbf{p} \mathbf{p}^H \mathbf{V} \mathbf{j}\}$$

$$\begin{aligned}
&= \rho^2 E\{u^H [I - \hat{u}\hat{u}^H] pp^H [I - \hat{u}\hat{u}^H] u\} \\
&= \rho^2 E\{u^H pp^H u + u^H \hat{u}\hat{u}^H pp^H \hat{u}\hat{u}^H u \\
&\quad - u^H \hat{u}\hat{u}^H pp^H u - u^H pp^H \hat{u}\hat{u}^H u\} \quad (12)
\end{aligned}$$

where ρ is the jammer power. It can be shown that $u^H \hat{u} = \frac{1}{L}[(L-m+k-1) + \sum_{i=k}^m e^{j\Delta\phi(i)}]$. The value of the second term in eq. (12)

$$\begin{aligned}
&E\{u^H \hat{u}\hat{u}^H pp^H \hat{u}\hat{u}^H u\} \\
&= \frac{1}{L^3} \sum_{i=1}^L \sum_{n=1}^L E\{[(L-m+k-1) + \sum_{l=k}^m e^{j\Delta\phi(l)}] \\
&\quad \hat{u}_i^* p_{in} \hat{u}_n [(L-m+k-1) + \sum_{o=k}^m e^{-j\Delta\phi(o)}]\} \\
&= \frac{1}{L^2} E\{[(L-m+k-1) + \sum_{l=k}^m e^{j\Delta\phi(l)}] \\
&\quad [(L-m+k-1) + \sum_{o=k}^m e^{-j\Delta\phi(o)}]\} \\
&= \frac{1}{L^2} [(L-m+k-1)^2 + 2(L-m+k-1) \\
&\quad (m-k+1)e^{-\sigma_\Delta^2/2} + (m-k) \\
&\quad (m-k+1)e^{-\sigma_\Delta^2} + (m-k+1)] \quad (13)
\end{aligned}$$

The value of the third term in eq. (12) is

$$\begin{aligned}
&E\{u^H \hat{u}\hat{u}^H pp^H u\} \\
&= \frac{1}{L^2} \sum_{i=1}^L \sum_{n=1}^L E\{[(L-m+k-1) \\
&\quad + \sum_{o=k}^m e^{j\Delta\phi(o)}] \hat{u}_n p_{in} u_i^*\} \\
&= \frac{1}{L^2} \left[\sum_{i,n=1}^{k-1} E\{[(L-m+k-1) + \sum_{o=k}^m e^{j\Delta\phi(o)}] \hat{u}_i p_{ii} u_i^*\} \right. \\
&\quad + \sum_{i,n=k}^m E\{[(L-m+k-1) + \sum_{o=k}^m e^{j\Delta\phi(o)}] \hat{u}_i p_{ii} u_i^*\} \\
&\quad + \sum_{i,n=m+1}^L E\{[(L-m+k-1) + \sum_{o=k}^m e^{j\Delta\phi(o)}] \hat{u}_i p_{ii} u_i^*\} \left. \right] \\
&= \frac{1}{L^2} [(L-m+k-1)^2 + 2(L-m+k-1) \\
&\quad (m-k+1)e^{-\sigma_\Delta^2/2} + (m-k)(m-k+1)e^{-\sigma_\Delta^2} \\
&\quad + (m-k+1)] \quad (14)
\end{aligned}$$

In the absence of IF error, the error variance, $\sigma_\Delta^2 = 0$, eqn. (14) reduces to 1. The value of the fourth term can be similarly obtained. It should be noted that the second, third and the fourth terms have the same mean square value. This is due to the fact that the product

of pp^H gives rise to an Identity matrix in each of the terms, and $\hat{u}^H \hat{u} = 1$. The variance due to the jammer signal is given by the expression

$$\begin{aligned}
\sigma_{y_s}^2 &= \frac{\rho^2}{L^2} [L^2 - [(L-m+k-1)^2 \\
&\quad + 2(L-m+k-1)(m-k+1)e^{-\sigma_\Delta^2/2} \\
&\quad + (m-k)(m-k+1)e^{-\sigma_\Delta^2} + (m-k+1)]] \quad (15)
\end{aligned}$$

which is a function of the jammer power, the error variance σ_Δ , and the number of samples in error, $(m-k+1)$. In this case, the receiver SINR is

$$SINR = \frac{E^2\{y\}}{\sigma_{y_1}^2 + \sigma_{y_2}^2 + \sigma_{y_s}^2} \quad (16)$$

When the IF estimates equals to the exact values, σ_Δ tends to zero, $\sigma_{y_s}^2 = 0$, indicating full interference excision. In the case when the error is spread over the entire bit, $m = L$ and $k = 1$ and eqn. (15) reduces to

$$\sigma_{y_s}^2 = \frac{\rho^2}{L^2} [L^2 - [L(L-1)e^{-\sigma_\Delta^2/2} + L]] \quad (17)$$

It is straightforward to show that when considering the frequency resolution errors, equations (15) and (17) become, respectively,

$$\begin{aligned}
\sigma_{y_s}^2 &= \frac{\rho^2}{L^2} [L^2 - [(L-m+k-1)^2 \\
&\quad + \frac{2(L-m+k-1)(m-k+1)\sin\epsilon}{\epsilon} \\
&\quad + \frac{(m-k)(m-k+1)\sin^2\epsilon}{\epsilon^2} + (m-k+1)]] \quad (18)
\end{aligned}$$

$$\sigma_{y_s}^2 = \frac{\rho^2}{L^2} [L^2 - [\frac{L(L-1)\sin^2\epsilon}{\epsilon^2} + L]] \quad (19)$$

where ϵ is equal to $1/2M$. For block processing, using K blocks, each of N samples, equations (7,10,11) for both resolution and spreading errors, become

$$\begin{aligned}
E\{y_1\} &= K(N-1), \sigma_{y_1}^2 = K(N-1) - K\frac{(N-1)^2}{N}, \\
\sigma_{y_2}^2 &= \sigma^2 K(N-1) \quad (20)
\end{aligned}$$

The variance $\sigma_{y_s}^2$, however will depend on whether we deal with resolution or spreading errors. Providing that IF errors span only one block, $\sigma_{y_s}^2$ can be obtained by replacing L by N in (15-19). The main advantage of block-wise processing is that the block effected by the IF estimation error does not contaminate the desired signal in other blocks upon projection.

4. SIMULATIONS

Figure. 1 depicts the performance of the proposed projection excision filter for $K = 1$, for two different values

of IF error variance. It is clear from the figure that the receiver SINR decreases with increased σ_{Δ}^2 , and this behaviour is more pronounced at higher JSR.

Figure. 2 shows the receiver SINR with and without block processing. The errors in the IF were assumed to be entirely due to IF spreading. For low JSR's, the amount of power leaking through the projection filter (using a single block) is very small and hence the performance of the projection filter for $K = 1$ is better than block-wise projections. But, as the jammer power increases, the residual jammer power degrades the performance for a single block excision to the extent that it becomes inferior to block-wise excision. In this example $L=128$, $K=8$ and $N=16$.

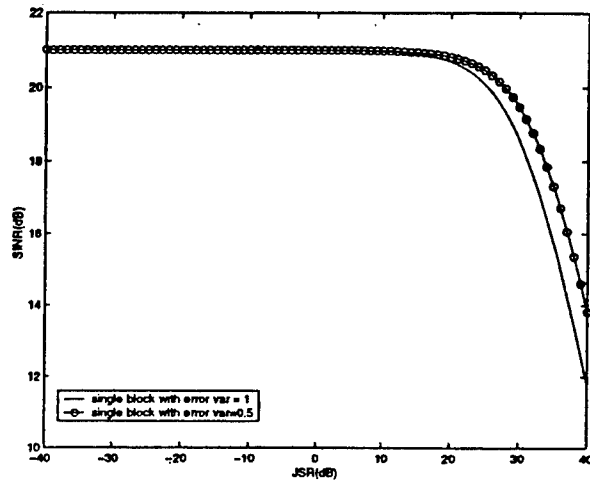


Figure 1: Receiver SINR with different spreading errors. $L = 128$, $K=1$. The input SNR = 0dB.

5. CONCLUSIONS

This paper has presented the performance analysis of the block-wise FM interference excision technique in DSSS. A closed form expression was derived for the case of the interference signal leaking through the projection filter, due to the errors in the IF estimates. The performance of the block-wise projection receiver was compared to that of a single block receiver and was shown to be less sensitive to IF estimate errors.

6. REFERENCES

- [1] M. G. Amin, R. S. Ramineni and A. R. Lindsey, "Suppression of FM interferences in DSSS communications using projection techniques", *Proc. of the 33rd ASILOMAR conference*, Monterey, CA, October 1999.
- [2] B. K. Poh, T. S. Quek, C. M. S. See and A. C. Kot, "Suppression of strong narrowband interference using an eigen-structure-based algorithm", July, 1995.

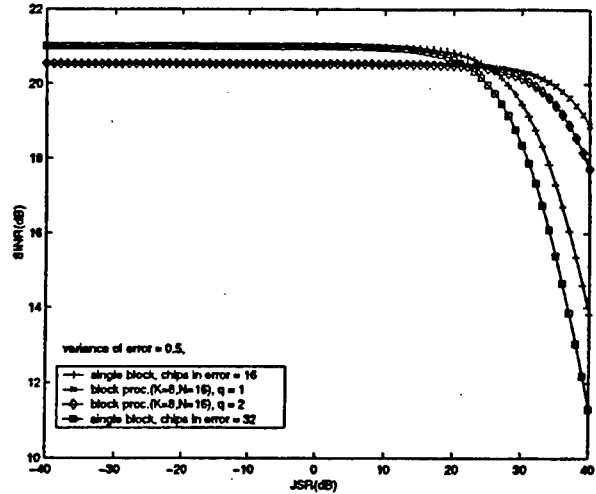


Figure 2: Receiver SINR with Spreading error in IF. $L = 128$. The input SNR = 0 dB.

- [3] A. Haimovich and A. Vadhri, "Rejection of narrow-band interferences in pn spread spectrum systems using an eigenanalysis approach," 1994.
- [4] M.G. Amin, "Time-frequency for interference excision in spread-spectrum communications," *IEEE Signal Processing Magazine*, pp. 33-34, March 1999.
- [5] B. Boashash, "Time-frequency signal analysis," vol. 1 and 2, Prentice-Hall, Englewood Cliffs, New Jersey, 1990.
- [6] M. G. Amin, "Interference mitigation in spread-spectrum communication systems using time-frequency distributions," *IEEE Trans. Signal Processing*, vol. 45, no. 1, pp. 90-102.
- [7] C. Wang, M. G. Amin and A. Lindsey, "Optimum interference excision in spread spectrum communications using open loop adaptive filters," *IEEE Transactions on Signal Processing*, vol. 47, no. 7, pp. 1966-1976, July 1999.
- [8] A. Bultan, "A novel time-frequency exciser in spread spectrum communications for chirp like interference", *Proc. of IEEE International conference on Acoustics, Speech and Signal Processing*, Seattle, WA, May 1998.
- [9] J. Ketchum and J. Proakis, "Adaptive algorithms for estimating and suppressing narrow band interference in PN spread spectrum systems," *IEEE Transactions on Communications*, vol. COM-30, pp. 913-924, May, 1982.

High Resolution Time-Frequency Distributions

- [4] P. Craven and G. Wahba, "Smoothing noisy data with spline functions," *Numerische Mathematik*, vol. 31, pp. 377-403, 1979.
- [5] M. Stone, "Cross-validated choice and assessment of statistical predictions," *J. R. Stat. Soc.*, vol. B36, pp. 111-147, 1974.
- [6] L. R. Rabiner and B. Gold, *Theory and Application of Digital Signal Processing*. Englewood Cliffs, NJ: Prentice-Hall, 1975.
- [7] T. W. Parks and J. H. McClellan, "A program for the design of linear phase finite impulse response digital filters," *IEEE Trans. Audio Electroacoust.*, vol. AU-20, pp. 195-199, 1972.
- [8] W. F. Trench, "Inversion of Toeplitz band matrices," *Math. Comput.*, vol. 28, pp. 1089-1095, 1974.

High Spectral Resolution Time-Frequency Distribution Kernels

Moeness G. Amin and William J. Williams

Abstract—A new class of time-frequency distribution (TFD) kernels is introduced. Members in this class satisfy the desirable TFD properties and simultaneously provide local autocorrelation functions (LAF) that are amenable to high-frequency resolution modeling techniques. It is shown that members of the proposed class are product kernels, fast implementation multiplication-free kernels, recursive kernels, and optimum kernels with respect to autoterm localization.

I. INTRODUCTION

Time-frequency distributions (TFD's) along with their temporal and spectral resolutions are uniquely defined by the employed t - f kernels. Potential kernels seek to map, at every time sample, the time-varying signals in the data into approximately fixed frequency sinusoids in the local autocorrelation function (LAF). Applying the FT to the LAF, therefore, provides a peaky spectrum where the location of the peaks are indicative to the signals' instantaneous power concentrations. The sinusoidal components in the LAF, however, generally appear with some type of amplitude modulations (AM), which are highly dependent on the kernel composition. Such modulation presents a limitation on spectral resolution in the t - f plane, as it is likely to spread both the auto and crossterms to localizations over a wide range of frequencies.

Because of the kernel modulation effects on the various terms, closely spaced frequencies may not be resolved. Further, since TFD's are Fourier-based, then in addition to the amplitude modulation imposed by the kernels, the spectral resolution is limited by and highly dependent on the extent of LAF, i.e., the lag window employed. However, increasing the length of the LAF will not always yield improved resolution. We maintain that events occurring over short periods of time do not require large kernels, which

Manuscript received March 20, 1997; revised April 13, 1998. This work was supported in part by Rome Laboratory under Contract F30602-96-C-0077 and by ONR under Grants N00014-90-J-1654 and N00014-97-1-0072. The associate editor coordinating the review of this paper and approving it for publication was Dr. Frans M. Coetzee.

M. G. Amin is with the Department of Electrical and Computer Engineering, Villanova University, Villanova, PA 19085 USA (e-mail: moeness@ece.vill.edu).

W. J. Williams is with the Department of Electrical Engineering and Computer Science, The University of Michigan, Ann Arbor, MI 48019 USA (e-mail: wjw@gabor.eecs.umich.edu).

Publisher Item Identifier S 1053-587X(98)07078-0.

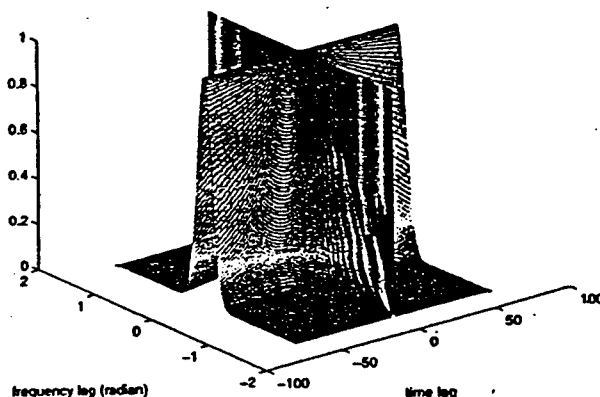


Fig. 1. Binomial kernel.

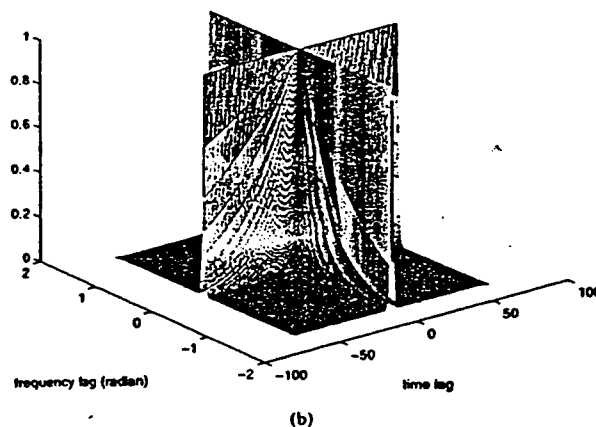
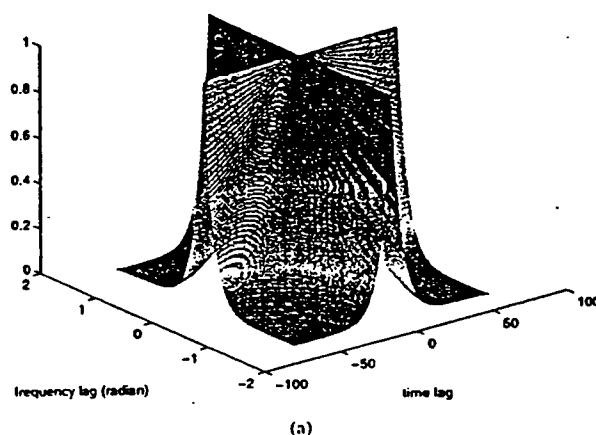


Fig. 2. High-resolution exponential kernel. (a) $\alpha = 1$. (b) $\alpha = 10$.

may only lead to increased crossterm contributions from distant events and obscure the local autoterms. Limited availability of data samples may also provide another reason for using small-extent kernels. In these cases, improving spectral resolution of a TFD can be achieved by parameterizing its local autocorrelation

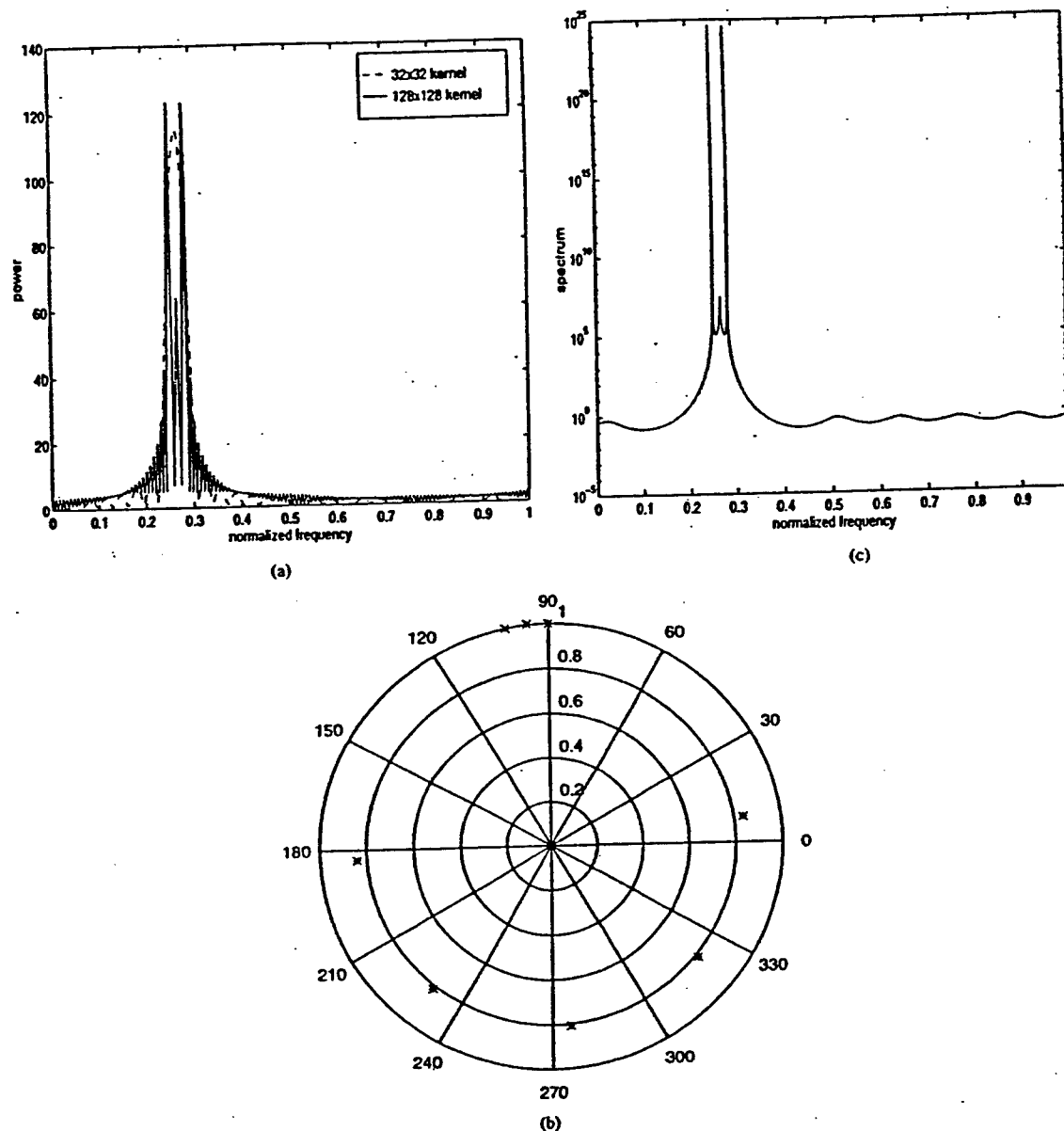


Fig. 3. Binomial kernel. (a) TFA. (b) High-resolution spectrum. (c) Zero diagram.

function via autoregressive (AR) modeling techniques [1]–[4]. Such parameterization seeks to fit a least-squares random model to the second-order statistics of the LAF at different time instants. The AR modeling techniques, however, view the LAF as a stationary process along the lag dimension. Since t - f distribution kernels translate deterministic signals into others of deterministic nature, it will be more appropriate to fit a deterministic, rather than a stochastic, model to the LAF. Further, all modeling techniques applied in the TFD context thus far have only dealt with Pseudo Wigner-Ville distribution (PWVD) or the smoothed PWVD (SPWVD) kernels. We maintain that in addition to PWVD and SPWVD of separable time and lag windows, there exists a large class of t - f kernels for which the LAF are amenable to high spectral resolution techniques. Members of this class not only yield LAF's that can be accurately

parameterized but also satisfy the desirable t - f properties, including reduced interference. The high spectral resolution t - f kernels can be separable or inseparable kernels, product kernels, and computationally efficient kernels, as well as optimum kernels in terms of autoterm localizations.

In this correspondence, we use Prony's method and its least-squares reduced-order approximation based on the singular value decomposition (SVD) [5], [6] in the t - f context. This method is shown to be applicable to high spectral resolution TFD problems, specifically when the underlying LAF is made up of a sum of exponentially damped/undamped sinusoids or chirp-like signals. We derive a class of TFD kernels in which the autoterms and the crossterms of the sinusoidal components in the data are, respectively, mapped into undamped and damped sinusoids. By using the backward

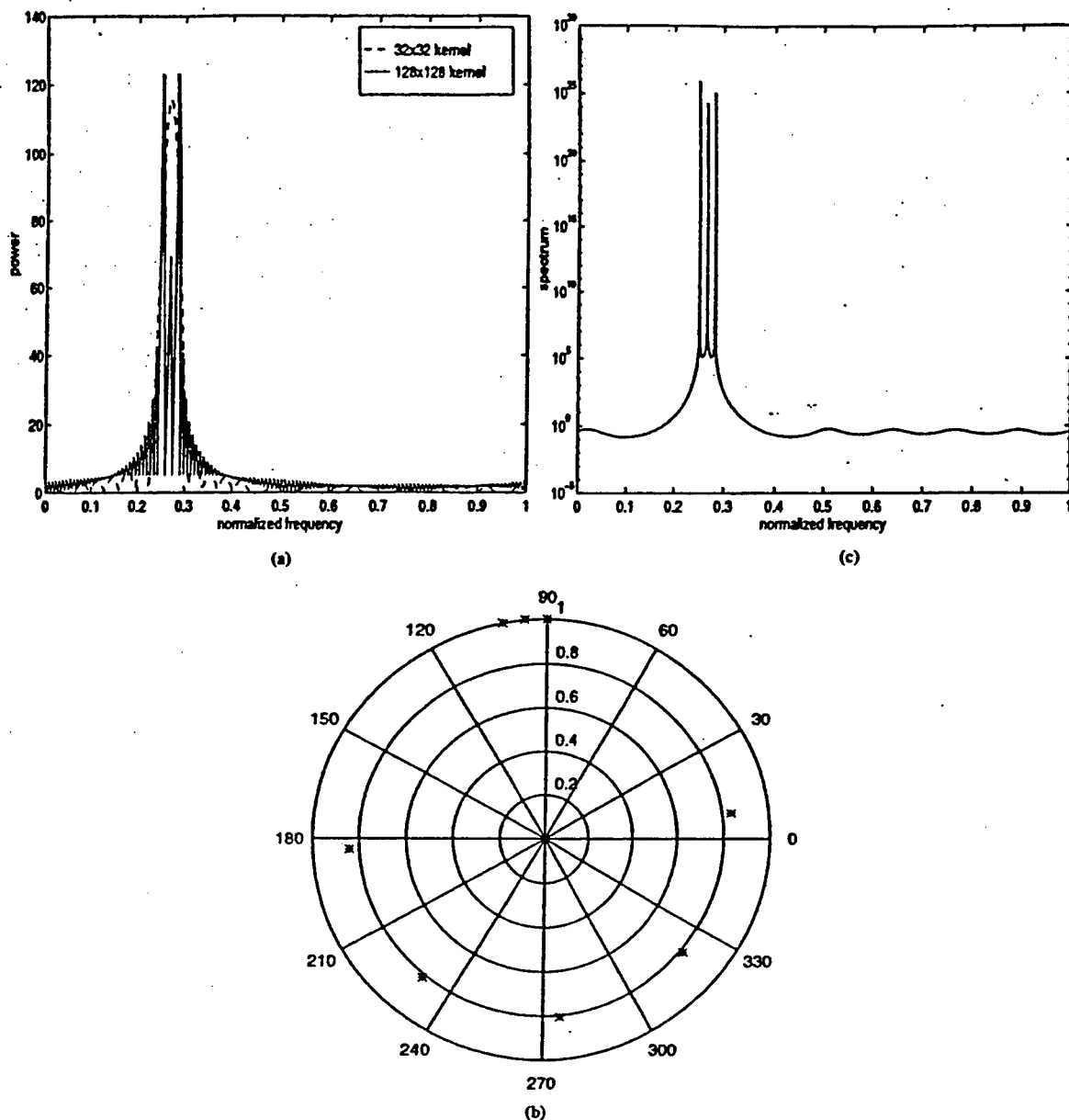


Fig. 4. PWD kernel. (a) TFD. (b) High-resolution spectrum. (c) Zero diagram.

linear prediction frequency estimation approach [5], these two sets of components produce a linear predictor error filter whose zeros lie on and outside the unit circle, respectively. With the extraneous zeros of the polynomial lying inside the unit circle, fitting a deterministic model to the LAF of the proposed class of t - f kernels not only yields accurate estimates of the frequencies of the sinusoids but also provides a mechanism to distinguish between the true and false distribution terms.

In Section II, we introduce the high spectral resolution TFD kernels and state the requirements that permit the application of Prony's method to the corresponding local autocorrelation functions. This application is constrained by the fact that the initial phase of all sinusoidal components in the LAF is either 0 or 180°. Computer simulations are presented in Section III.

II. HIGH SPECTRAL RESOLUTION t - f KERNELS

The ambiguity function of the data $x(n)$ is given by

$$D(\theta, l) = \sum_{n=-\infty}^{\infty} x(n+l)x^*(n-l)e^{-j2\theta l} \quad (1)$$

if the data $x(n)$ consist of p undamped sinusoids in the form

$$x(n) = \sum_{k=1}^p A_k e^{j\omega_k n} \quad (2)$$

where A_k is the complex amplitude of the k th sinusoid. Then

$$D(\theta, l) = \sum_{k=1}^p T_{ii}(l) + \sum_{\substack{i, m=1 \\ i \neq m}}^p T_{im}(l) \quad (3)$$

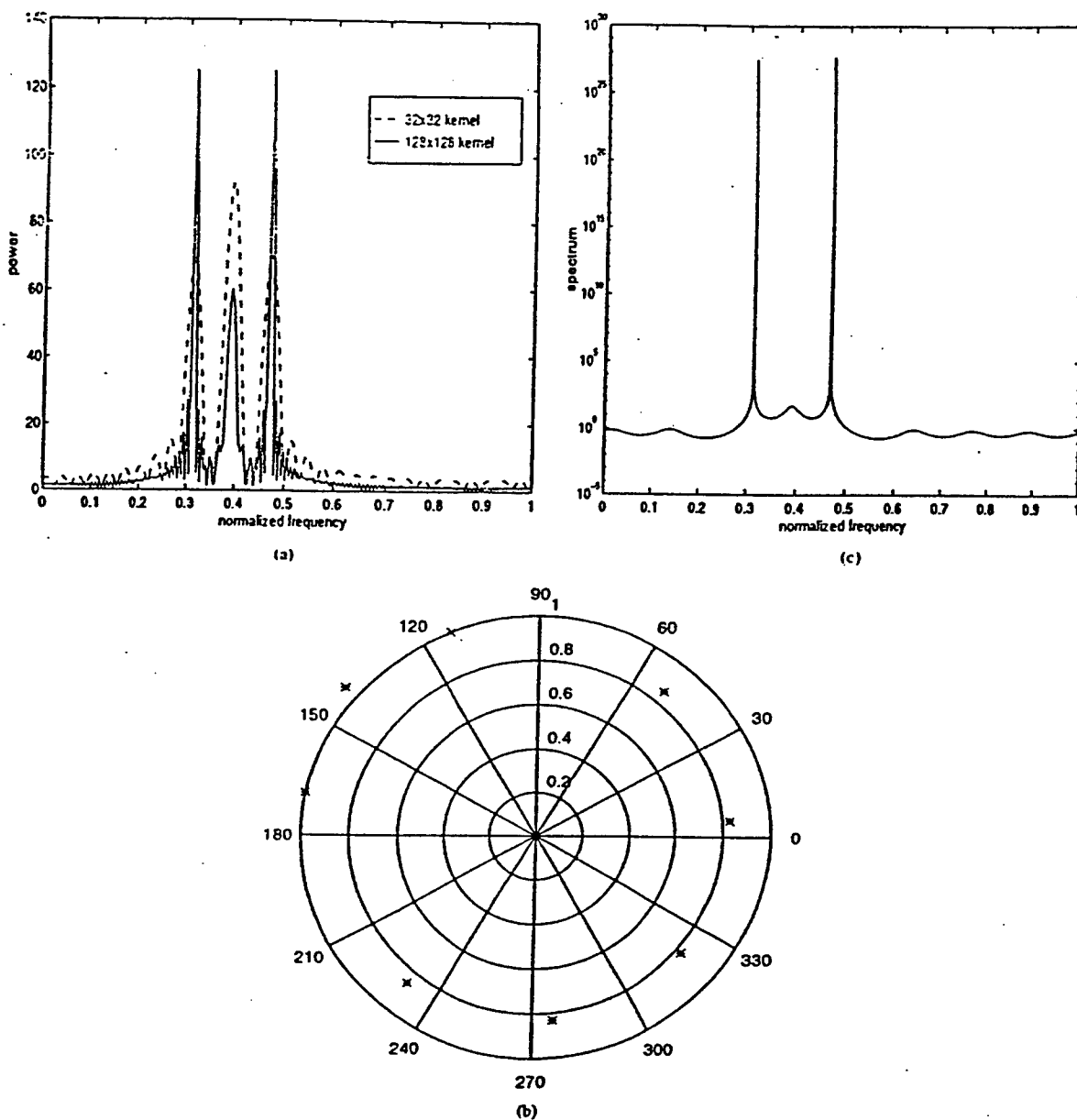


Fig. 5. Binomial kernel. (a) TFD. (b) High-resolution spectrum. (c) Zero diagram.

$$T_{ii}(l) = 2\pi |A_{ii}|^2 e^{j2\omega_i l} \sum_{q=-\infty}^{\infty} \delta(\theta - q\pi)$$

$$T_{im}(l) = 2\pi A_i A_m^* e^{j(\omega_i - \omega_m)l} \sum_{q=-\infty}^{\infty} \delta\left(\theta - \frac{\omega_i - \omega_m}{2} - q\pi\right). \quad (4)$$

The terms in the first summation correspond to the signals' autoterms and lie on the $\theta = 0$ axis. In the second summation, the cross-term $T_{im}(l)$ associated with each pair of sinusoids (ω_i, ω_m) is presented by a train of impulses that lie on a line parallel to the $\theta = 0$ axis and with a distance defined by the frequency separation ($\omega_i - \omega_m$). The application of the t - f kernel, respectively, modulate the autoterms and the cross-terms by $\phi(0, 1)$ and $\phi[(\omega_i - \omega_m)/2, l]$. The new local autocorrelation function is computed by taking the

inverse FT of $D(\theta, l)$. If the kernel satisfies the frequency marginal property, then $\phi(0, l) = 1$, and the LAF is given by

$$r(l) = \sum_{i=1}^P |A_{ii}|^2 e^{j2\omega_i l} + 2 \sum_{\substack{i, m=1 \\ i \neq m}}^P \text{Re}\left(A_i A_m^* e^{j(\omega_i - \omega_m)l/2}\right) \phi\left(\frac{\omega_i - \omega_m}{2}, l\right) e^{j(\omega_i - \omega_m)l}, \quad l \geq 0. \quad (5)$$

The first term is similar to the original data sequence x , except all sinusoids now appear with zero phase. Since the LAF is Hermitian, the frequency information can be extracted from either of its sides. For the cross-terms to be damped exponentially, we require

$$\phi\left(\frac{\omega_i - \omega_m}{2}, l\right) = \beta_{im}^l \quad \forall i, m, \quad i \neq m$$

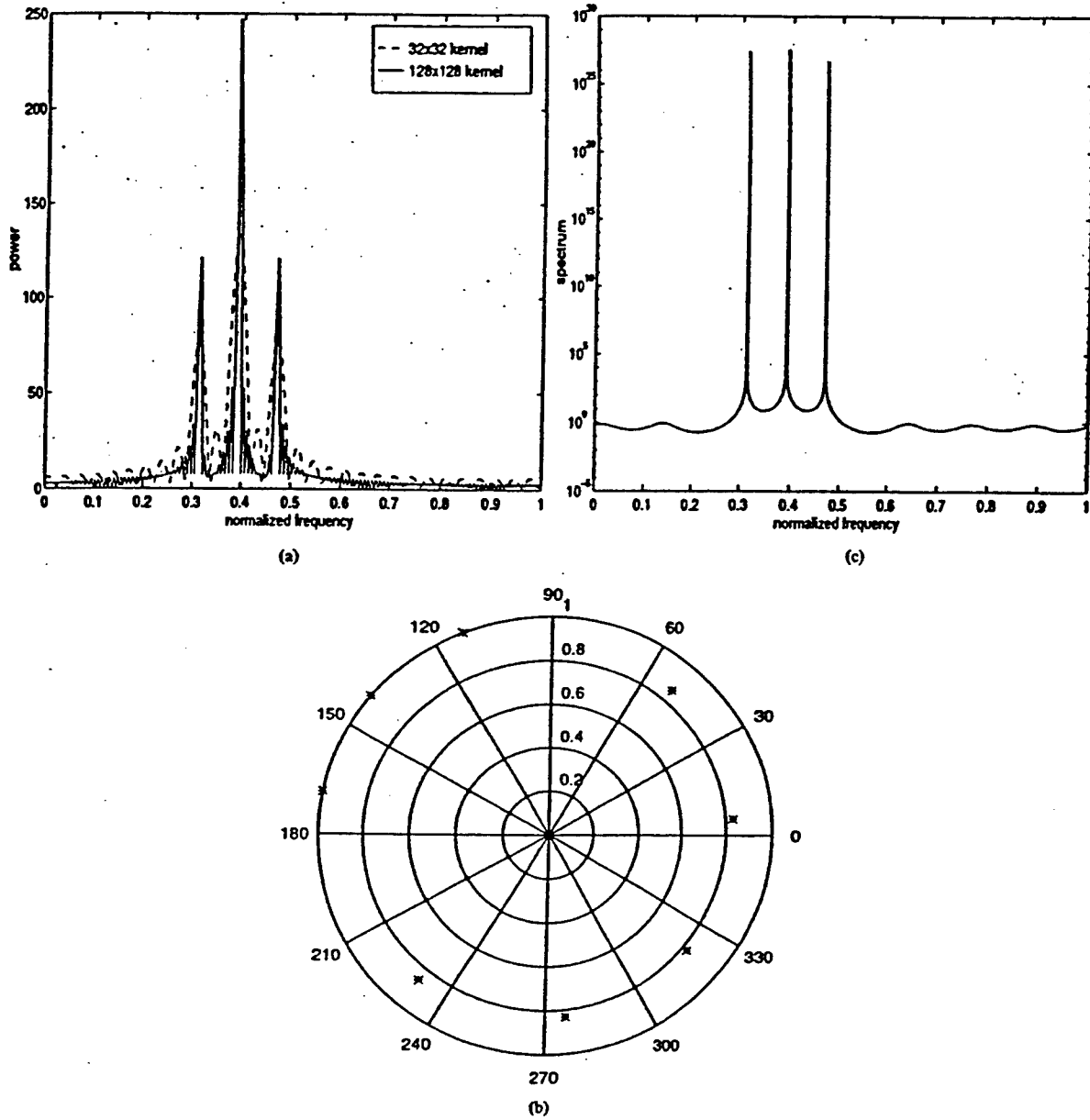


Fig. 6. PWD kernel. (a) TFD. (b) High-resolution spectrum. (c) Zero diagram.

i.e.,

$$\phi(\theta, l) = \beta^l(\theta), \quad \beta(\theta) < 1 \text{ for constant } \theta. \quad (6)$$

The two kernels shown in Figs. 1 and 2

$$\phi_1(\theta, l) = e^{-l\theta/l}, \quad \phi_2(\theta, l) = \cos^{ll}(\theta) \quad (7)$$

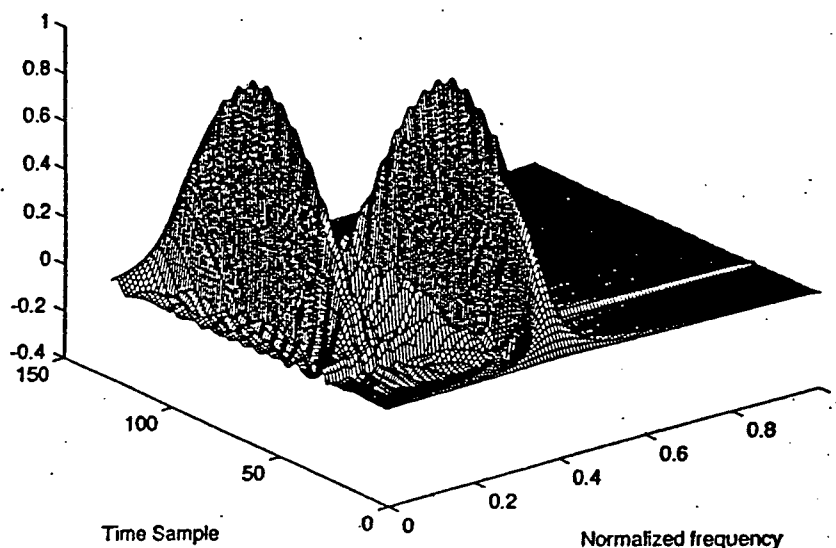
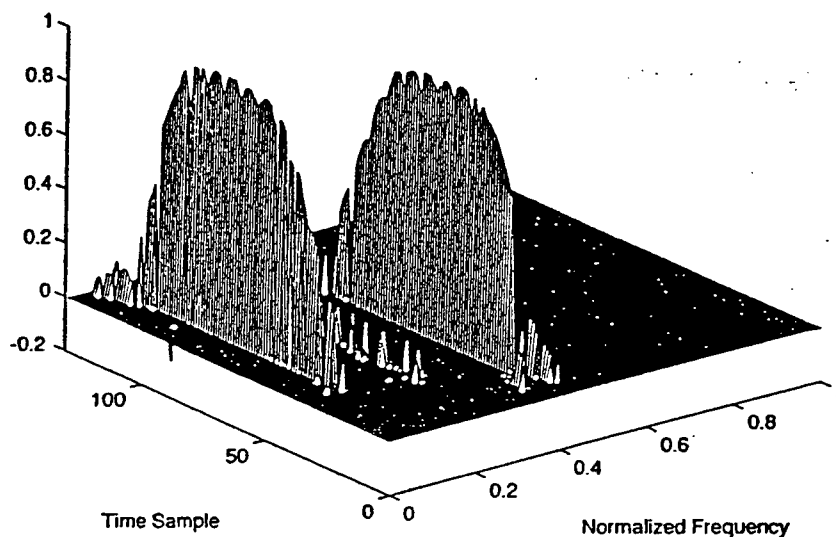
satisfy the above condition. The kernel ϕ_1 is a product kernel but does not satisfy the support property, whereas the second kernel ϕ_2 is not a product kernel but satisfies the time-support property. It is noteworthy that ϕ_2 is a computationally efficient kernel for which the LAF can be generated without any multiplication and is known as the binomial kernel [7]. The kernel ϕ_1 , on the other hand, has recently been shown to be optimum in terms of autoterm localization [8].

It is easily shown that (6) is satisfied by all t - f kernels in the forms

$$\phi(\theta, l) = \beta^{ll(\theta)l} \quad f(0) = 0, \quad f(\theta) = \pm f(-\theta). \quad (8)$$

The t - f kernels satisfying (6) along with all desired t - f properties form a class of high spectral resolution kernels. When $\beta < 1$, the proposed high-resolution t - f kernels have lowpass filter characteristics in the ambiguity domain and, in turn, act on smoothing out the crossterms in the WVD. The Pseudo WVD kernel is obtained by setting $\beta = 1$. In this case, all sinusoidal components become undamped, and a more suitable high-resolution technique can be used [6]. It is important to note that several SPWVD kernels are also members of the proposed high spectral resolution class. All separable t - f kernels in the form

$$\phi(\theta, l) = \alpha^{ll} f(\theta) \quad (9)$$

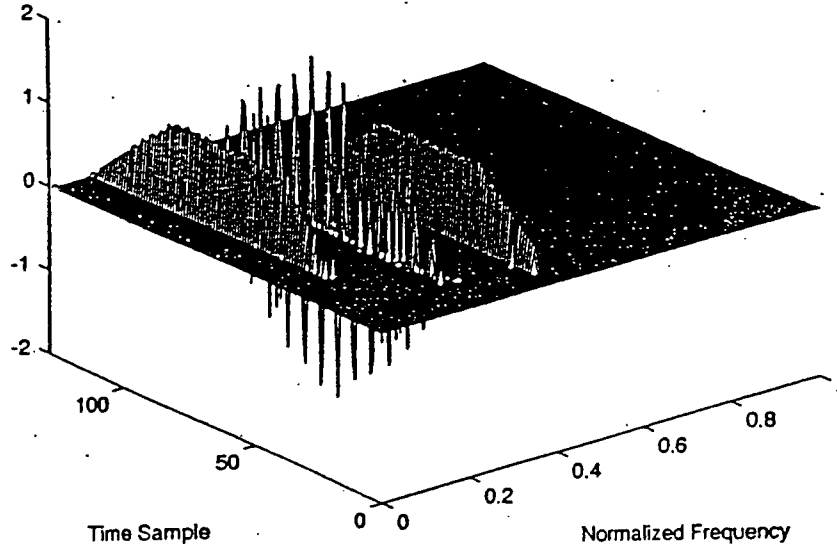
Fig. 7. Binomial TFD results for $z(n)$.Fig. 8. High-resolution binomial TFD for $z(n)$.

damp the crossterms exponentially and, as such, are amenable to the data modeling (1). In [9] and [10], the kernel form (9) is recognized as a recursive t - f kernel for which the TFD can be recursively updated every data sample with a number of computations independent of the time extent of the kernel.

Using the proposed class of kernels, we can proceed with Prony's high-resolution frequency estimation techniques. In the t - f context, the LAF sequence $r(l)$, $l = 1, 2, 3, \dots, N$ replaces the input data sequence, whereas the rank q of the backward data matrix now represents the sum of the autoterms and crossterms, i.e., $q = [p + p(p-1)/2]$. According to [5], the zeros in the backward predictor error filter polynomial corresponding to the undamped autoterm sinusoidal components lie on the unit circle, whereas those corresponding to the damped crossterm sinusoids are positioned outside the unit circle. These zeros are denoted by z_i , $i = 1, 2, \dots, q$. The remaining

polynomial zeros are approximately uniformly distributed inside the unit circle. In general, the frequency estimates will appear with twice the true value, which is due to excluding the terms corresponding to odd lags from (1). This multiplicative factor can be eliminated by using nonaliasing techniques [11].

The power of the sinusoids in the data can be obtained using least squares Prony's method [6]. Let Z define the Vandermonde matrix of dimension $N \times q$, where the ij th element is given by $z_{ij} = z_j^{i-1}$. The q -dimensional vector b includes the different powers in (5). Vector c is of length N and includes the autocorrelation sequence $r(l)$. The unknown vector b is obtained by least square solution of $Zb = c$ [6]. In order to incorporate the fact that in the underlying problem, the initial phase of all sinusoidal components in the LAF at $r(0)$ is either zero or 180° , the least-squares solution should be constrained

Fig. 9. High-resolution TFD for $z(n)$ using the raw LAF values (PWD equivalent).

and modified as

$$\|Zb - c\|_2, \quad \text{subject to } b = b^*. \quad (10)$$

By using the method of Lagrange multipliers, we define

$$\begin{aligned} e(\lambda, b) &= \|Zb - c\|_2^2 + \lambda'(b - b^*) \\ &= (b^H Z^H Z b - b^H Z^H c - c^H Z b + c^H c) \\ &\quad + \lambda'(b - b^*). \end{aligned} \quad (11)$$

Differentiating with respect to b and b^* , we obtain

$$(Z^H Z)^* b^* + \lambda = (Z^H c)^*, \quad (Z^H Z)b - \lambda = Z^H c. \quad (12)$$

By adding (11) and (12) and satisfying the hard constraint $b = b^*$, we obtain the real least-squares optimum sinusoidal amplitude vector

$$b = (\text{Re}(Z^H Z)^{-1} \text{Re}(Zc)). \quad (13)$$

III. SIMULATIONS

The data samples $x(n)$, which consist of two sinusoids

$$x(n) = \exp(j(\pi/4)n) + \exp(j(9\pi/32)n), \quad n = 1, 2, \dots, N \quad (14)$$

are analyzed by the high spectral resolution binomial kernel of dimension 32×32 and 128×128 . N is the data record length and is set equal to 256. Conforming to the simulation results given in [12], Fig. 3(a) shows the corresponding binomial TFD computed at one time instant in the middle of the data record. The small extent kernel provides poor resolution, whereas the large extent kernel resolves the two sinusoids and the crossterm. Due to missing even autocorrelation lags, these sinusoids appear at twice their frequencies. Because of the presence of three sinusoids (two of them are undamped and one is damped), the singular values of the data matrix will have three nonzero values. Applying the reduced-rank Prony's method using an eighth-order prediction filter and the smaller kernel, i.e., a 16-lag LAF, we obtain the polynomial roots of Fig. 3(b). It is clear that the two autoterm components are presented by two zeros on the unit circle. Because of the exponential modulation caused by the binomial kernel, the crossterm zero shows a divergence from the unit circle. All extraneous zeros are approximately uniformly distributed inside the unit circle. The damping effect on the crossterm becomes

more evident in the corresponding high-frequency resolution spectrum presented in Section II and shown in Fig. 3(c). This spectrum is computed via 1024-point FFT with $L = 16$. Fig. 3(c) shows only two dominant spectral lines that correspond to the autoterm components. The TFD, the zero diagram, and the high-resolution spectrum corresponding to PWVD using the same data matrix as in the binomial TFD are depicted in Fig. 4(a)–(c). Due to the equal weighing of the autoterms and crossterms by the PWVD kernel, the crossterm sinusoid, in this case, is undamped and subsequently persists in the spectrum.

To further illustrate the point, we choose two widely spaced sinusoids in additive noise. The SNR is 20 dB. The two normalized frequencies are $(5/16)$ and $(15/32)$. The TFD, the zeros of the backward error predictor filter polynomial of order 8 ($L = 8$), and the corresponding high-frequency spectrum, are depicted in Figs. 5 and 6, for the binomial and PWVD TFD's, respectively. Since the damping factor of the crossterm using the binomial kernel is proportional to the frequency separation, the crossterm zero appears further away from the unit circle than the case in Fig. 3(b).

The following simulations illustrate the effectiveness of the high-resolution TFD's. A test signal was constructed that consisted of two complex exponentials as

$$\begin{aligned} x(n) &= \exp(j2\pi 12.5n/128), \quad y(n) = \exp(j2\pi 51.2n/128) \\ n &= 0, 1, 2, \dots, 127. \end{aligned} \quad (15)$$

Then

$$z(n) = y(n) + x(n - 30). \quad (16)$$

These two signals have normalized frequencies of 0.1 and 0.4 Hz respectively. First, the binomial TFD was computed using the alias free formulation [11] for comparison. The LAF, which extended to ± 128 points, was computed, and the binomial kernel was applied to it. Applying an FFT across the lags produced the result shown in Fig. 7. The two components are well resolved, and the crossterm interference is low. Fig. 8 shows the high-resolution TFD result using the binomial kernel. Only even lag terms were used in the LAF. We can see that the results are similar to the binomial TFD, but the resolution is higher. In addition, the crossterms are small and generally fall between the autoterms and are not spread, as is the case for the binomial TFD.

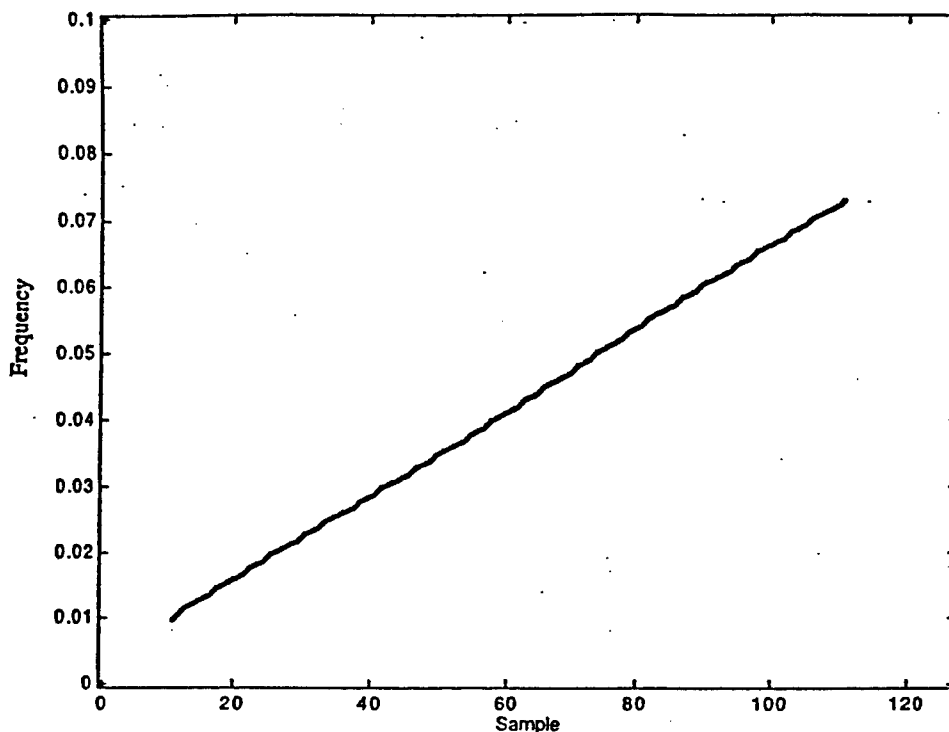


Fig. 10. High-resolution result for a complex exponential signal over 128 time samples (sampling rate assumed to be 1/s). The starting frequency was 0.05 Hz, and the chirp rate was 0.06 Hz/sample.

Fig. 9 shows the results obtained using the raw LAF values, which is equivalent to the PWD. The autoterms are well resolved, but the crossterms are as large as in the conventional PWD and fall between the crossterms. A 20-point analysis window was used to find the Hankel structure for the odd positive lags obtained from the same LAF used to form the binomial TFD. The number of terms included from the SVD computation were limited by excluding all terms with magnitudes less than 15% of the largest singular value.

The effectiveness of the approach with a nonstationary chirp is shown in Fig. 10. Here, a complex exponential with a starting frequency of 0.05 Hz and a positive chirp rate of 0.6×10^{-4} Hz/sample is analyzed using the alias-free binomial LAF. Here, 0.1 Hz spans 100 frequency samples. We can see that the method provides a very nice estimate of the t - f course of the signal. The granularity is due to the choice of 100 frequency samples/0.1 Hz. The granularity could be decreased by choosing a larger number of frequency samples over the presentation range.

IV. CONCLUSIONS

A new class of time-frequency distribution kernels is introduced. The members of this class satisfy the desirable time-frequency properties for power localization in nonstationary environment, yet they produce local autocorrelation functions that are amenable to exponential deterministic modeling during periods of stationarity. The proposed high spectral resolution kernels are required to meet two basic conditions: 1) the frequency marginal and 2) an exponential behavior in the ambiguity domain for constant values of θ . In dealing with sinusoidal data, the first property guarantees that the autoterm sinusoids in the LAF are undamped. The second property enforces an exponential damping on all crossterms. As a result, the sinusoidal components in the data translate into damped/undamped sinusoids in

the local autocorrelation function. High-resolution techniques such as reduced rank approximation of the backward linear prediction data matrix can then be applied for frequency estimation. All simulations are presented using noise-free signals. The effect of the noise on the performance of the proposed class of kernels is briefly discussed in [13].

REFERENCES

- [1] B. Boashash, B. Lovell, and H. Whitehouse, "High resolution time-frequency signal analysis by parametric modeling of the Wigner-Ville distribution," in *Proc. ISSPA*, Brisbane, Australia, Aug. 1987.
- [2] P. Ramamoorthy, V. Iyer, and Y. Ploysongsang, "Autoregressive modeling of the Wigner spectrum," in *Proc. IEEE Int. Conf. Acoust., Speech, Signal Process.*, Dallas, TX, Apr. 1987.
- [3] E. F. Velez and R. G. Absher, "Smoothed Wigner-Ville parametric modeling for the analysis of nonstationary signals," in *Proc. IEEE Int. Symp. Circuits Syst.*, May 1989, pp. 507-510.
- [4] —, "Wigner half kernel modeling," *Signal Process.*, vol. 26, no. 2, pp. 162-175, Feb. 1992.
- [5] R. Kumaresan, "On the zeros of the linear prediction error filter for deterministic signals," *IEEE Trans. Signal Processing*, vol. ASSP-31, pp. 217-220, Feb. 1983.
- [6] S. L. Marple, Jr., *Digital Spectral Analysis with Applications*. Englewood Cliffs, NJ: Prentice-Hall, 1987, ch. 11.
- [7] W. J. Williams and J. Jeong, "Reduced interference time-frequency distributions," in *Time-Frequency Signal Processing: Methods and Applications*, B. Boashash, Ed. Melbourne, Australia: Longman Cheshire, 1992.
- [8] L. J. Stankovic, "Auto-term representation by the reduced interference distributions: A procedure for kernel design," *IEEE Trans. Signal Processing*, vol. 44, pp. 1557-1563, June 1996.
- [9] M. Amin, "Spectral smoothing and recursion based on the nonstationarity of the autocorrelation function," *IEEE Trans. Signal Processing*, vol. 39, pp. 183-185, Jan. 1991.
- [10] —, "The running time-frequency distributions," *Circuits, Syst., Signal Process.*, vol. 14, pp. 401-414, 1995.

- [11] J. Jeong and W. J. Williams, "Alias-free generalized discrete-time time-frequency distributions," *IEEE Trans. Signal Processing*, vol. 40, pp. 2757-2765, Nov. 1992.
- [12] M. Amin and W. J. Williams, "High spectral resolution time-frequency distribution kernels," in *Proc. SPIE Conf. Adv. Algorithms Architectures Signal Process.*, 1992, vol. 1770, pp. 302-314.
- [13] —, "Deterministic exponential modeling techniques for high spectral resolution time-frequency distributions," in *IEEE Int. Conf. Acoust., Speech, Signal Process.*, Minneapolis, MN, Apr. 1993, vol. 3, pp. 249-252.

Method for Defining a Class of Fractional Operations

Peter Kraniuskas, Gianfranco Cariolaro, and Tomaso Erseghe

Abstract—The fractional Fourier transform permits a variety of associated fractional operations. This correspondence proposes a systematic method, based on the structure of the FRT, which not only provides unambiguous extensions of ordinary operations but permits writing the applicable expressions simply by inspection. The approach also exposes the possible paths for implementing such operations.

Index Terms—Fourier transform, fractional convolution theorem, fractional Fourier transform, fractional operations.

I. INTRODUCTION

The fractional Fourier transform (FRT) is effectively an extension of the ordinary Fourier transform (FT) with suitably extended properties. Since its inception, various attempts have been made to define certain *fractional operations* as counterparts to corresponding ordinary operations encountered in Fourier methods. However, the structure of the FRT lends itself to various, nonequivalent extensions of any given operation, which can lead to confusion.

This correspondence proposes a systematic method for *defining fractional operations* that exploits the relevant properties of the ordinary FT embedded in the FRT definition. This strategy not only permits writing the applicable expressions for both the *reference domain* (fraction $\alpha = 0$) and the *fractional domain* α merely by inspection but also provides possible implementation paths with the relevant expressions. No elaborate derivations are required as the burden of proof is carried by the ordinary FT at the center, whose properties are well known.

The fractional convolution theorem is first derived as an extension of the familiar convolution theorem of the ordinary FT and serves as a basis for unambiguously defining a whole class of fractional operations.

Manuscript received August 11, 1997; revised April 7, 1998. The associate editor coordinating the review of this paper and approving it for publication was Prof. Moeness Amin.

P. Kraniuskas is an Independent Consultant, Southampton, U.K.
G. Cariolaro is with the Dipartimento di Elettronica ed Informatica, Università di Padova, Padova, Italy.
T. Erseghe is with Snell and Wilcox Ltd., Hampshire, U.K.
Publisher Item Identifier S 1053-587X(98)07079-2.

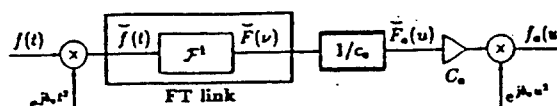


Fig. 1. FRT structure.

II. FRT DEFINITION

Based on the ordinary FT definition

$$F(\omega) = \frac{1}{\sqrt{2\pi}} \int_{-\infty}^{\infty} f(t) e^{-j\omega t} dt \quad (1)$$

taken to be of order $\alpha = 1$, the FRT of order α is typically defined as

$$f_n(u) = C_n e^{j b_n u^2} \frac{1}{\sqrt{2\pi}} \int_{-\infty}^{\infty} [f(t) e^{j b_n t^2}] e^{-j c_n u t} dt \quad (2)$$

where b_n , c_n , and C_n are coefficients associated with each fraction α

$$b_n = \frac{1}{2 \tan \alpha}, \quad c_n = \frac{1}{\sin \alpha}, \quad C_n = \sqrt{|c_n|} e^{-j[\pm \pi/4 - \alpha n/2]}$$

in which $\alpha = \alpha\pi/2$ expresses α as a fraction of $\pi/2$, and the \pm choice represents $\text{sgn}(\sin \alpha)$.

The sequence of internal operations in (2) is shown in Fig. 1 and consists of first chirping the input signal $f(t)$ by adding quadratic phase of rate b_n , followed by an ordinary FT in the "frequency" variable $\nu = c_n u$, and then scaling the frequency ν to the fractional domain variable $u = \nu/c_n$, thus giving $\tilde{F}_n(u) = \tilde{F}(\nu/c_n)$, which is then amplitude scaled by C_n and chirped with rate b_n in u to finally yield $f_n(u)$. The integral character of the FRT thus resides in the ordinary FT link at its center, and this provides the *basis for the method*.

Several properties of the FRT are presented in the literature as extensions of corresponding properties of the FT, including the FRT of operations involving two functions, notably *ordinary multiplication and convolution* [1]. Under the ordinary FT (1), the latter operations are very simply related by the convolution theorem, which states that a convolution in one domain transforms to a multiplication in the alternative domain. For time domain convolution, we have

$$\begin{aligned} f(t) * h(t) &= g(t) \\ \downarrow \mathcal{F}^1 & \quad \downarrow \mathcal{F}^1 \quad \downarrow \mathcal{F}^1 \\ F(\omega) \sqrt{2\pi} \times H(\omega) &= G(\omega) \end{aligned} \quad (3)$$

and for time domain multiplication (or modulation) scaled for symmetry, we have

$$\begin{aligned} f(t) \sqrt{2\pi} \times h(t) &= g(t) \\ \downarrow \mathcal{F}^1 & \quad \downarrow \mathcal{F}^1 \quad \downarrow \mathcal{F}^1 \\ F(\omega) * H(\omega) &= G(\omega). \end{aligned} \quad (4)$$

Thus, (scaled) multiplication is the *dual FT counterpart* of convolution and vice versa.

Under the FRT, the expressions for dual counterparts of ordinary operations are more elaborate versions of corresponding FT duals [1].

III. FRT STRUCTURE OF A FRACTIONAL OPERATION

Our strategy for defining a fractional operation between two functions, represented generically by $\tilde{\circ}$, is encapsulated in Fig. 2.

Broadband Interference Mitigation in Multi-sensor Arrays Using Wavelets and Subbands

Performance of uniform and nonuniform subband constrained adaptive beamforming
under broadband correlated arrivals

Ismail I. Jouny
Dept. of Electrical Engineering
Lafayette College
Easton, PA

Moeness G. Amin
Department of Electrical and
Computer Engineering
Villanova University
Villanova, PA

ABSTRACT

Several array processing architectures have been devised for mitigation of multipath interference. Those algorithms have focused on rejection of terrain scattered interference, sidelobe and mainlobe clutter, and hot clutter. Two adaptive array architectures for rejection of broadband coherent interference are developed in this paper. Both techniques involve uniform subbanding using the Discrete Fourier transform (DFT) or non-uniform subbanding using the wavelet transform (WT). In the first approach, adaptation and weight computation is performed independently in each subband, and in the second technique the Frost constrained LMS algorithm is applied to all subbands in the transform domain. Due to the correlated nature of the jamming signal, spatial averaging is utilized in both cases. The mitigation performance of both algorithms is compared for various scenarios of coherent broadband interference. This paper also focuses on evaluating and rejecting multipath interference due to propellers or rotor of the radar receiver aircraft or helicopter (see Figure 5). This type of interference is characterized by an induced doppler spread proportional to the angular velocity of the propeller or the rotor. Furthermore the reflected signal represents the near-field component of the propeller scattering signatures. Spatial averaging followed by a transform-domain adaptive beamformer based on the Frost algorithm is used to reject this type of propeller generated multipath interference.

Keywords: Adaptive arrays, coherent signals, radars, multipath

I. INTRODUCTION & MOTIVATION

Several results that have recently appeared in the literature show that the rate of convergence as well as the capability of jammer suppression of Frost adaptive array beamformer can be improved by adaptation in the frequency domain or the scale (wavelet) domain. Although all optimum transform domain weight solutions are equivalent, convergence can vary from one transform to another, depending on the attained decorrelation between different bins.

In sensor array processing, however, there exists the problem of correlated and coherent signal arrivals which is not present in temporal processing. This type of interference commonly known as hot clutter or terrain scattered interference (TSI) has received considerable attention in the last few years particularly with the availability of a large clutter database known as the Mountaintop data. Conventional broadband Frost array beamformers perform poorly in the presence of correlated arrivals even when the constrained adaptive algorithm is implemented in the transform domain. An attractive alternative is to decorrelate the received signal via spatial averaging prior to transform-domain adaptation. Adaptation can then be either performed independently in each subband or according to the conventional Frost array beamforming architecture.

II. BROADBAND MITIGATION ARCHITECTURES

A. Full-band Adaptation

The first approach to rejection of coherent broadband interference utilizes the architecture shown in Figure 1, using an array of M sensors each followed by K tap-delay elements. After demodulation, spatial averaging using the algorithm presented in [2] is first implemented. The received signal is then transformed into the frequency domain via DFT or into the scale domain via wavelet transform. The Constrained LMS algorithm (CLMS) is then applied in the corresponding transform domain. Let

$$x(t) = [x_1(t), x_2(t), \dots, x_M(t)] \quad (1)$$

denote a snapshot of the received signal at M sensors. Spatial averaging generates smoothed estimates of the covariance matrix using

$$R = \frac{1}{P} \sum_{k=1}^P R_z(k) \quad (2)$$

where R_z is the estimated covariance matrix for a sub-array of L antennas with a received signal $z(k) = [x_k(t), \dots, x_{k+L}(t)]$. An array of M sensors is therefore operated as an array of L sensors where $L < M$. The Frost algorithm is then applied to transformed signal as shown in Figure 1 for an array of L sensors and K tap delay elements per sensor. The weights are computed using the iteration

$$W(t+1) = P[W(t) - \mu y(t)X(t)] + F \quad (3)$$

where W is a weight vector of L sub-vectors each is of length K and p and F are associated with a predetermined constraint (see [4] for details of the algorithm). Figure 3 shows a sample result of the performance of the full-band adaptation algorithm described in Figure 1 where the beam pattern of an array of 6 sensors is shown. The received signal includes samples due to two fully correlated jammers at 40 db jammer-to-noise ratio arriving at

angles of -15 and 30 degrees respectively. The desired signal is complex exponential with a 0 db signal-to-noise ratio. The complex version of the Daubechies-6 wavelet [15]

$$\begin{aligned}\Re(c) &= [-0.066291, 0.110485, 0.662912, 0.662912, 0.110485, -0.066291] \\ \Im(c) &= [-0.085581, -0.085558, 0.171163, 0.171163, -0.085558, -0.085581]\end{aligned}\quad (4)$$

(where \Re and \Im denote the real and imaginary components of the wavelet filter coefficients) is then used to compute the transform of the received signal vector. The wavelet transform is computed as matrix \times vector product $y = Tx$ where

$$T = \begin{bmatrix} c_0 & c_1 & c_2 & c_3 & c_4 & c_5 & 0 & 0 & 0 & 0 \\ c_5 & -c_4 & c_3 & -c_2 & c_1 & -c_0 & 0 & 0 & 0 & 0 \\ 0 & 0 & c_0 & c_1 & c_2 & c_3 & c_4 & c_5 & 0 & 0 \\ 0 & 0 & c_5 & -c_4 & c_3 & -c_2 & c_1 & -c_0 & 0 & 0 \\ 0 & 0 & 0 & 0 & c_0 & c_1 & c_2 & c_3 & c_4 & c_5 \\ 0 & 0 & 0 & 0 & c_5 & -c_4 & c_3 & -c_2 & c_1 & -c_0 \\ c_4 & c_5 & 0 & 0 & 0 & 0 & c_0 & c_1 & c_2 & c_3 \\ c_1 & -c_0 & 0 & 0 & 0 & 0 & c_5 & -c_4 & c_3 & -c_2 \end{bmatrix} \quad (5)$$

operating on a signal of length 10. Permutation is performed after each wavelet transformation where the low-pass components $\{l\}$ of the transform are kept in the top half and the high pass components $\{h\}$ are rearranged in the bottom half.

$$\begin{bmatrix} y_1 \\ y_2 \\ y_3 \\ y_4 \\ y_5 \\ y_6 \\ y_7 \\ y_8 \\ y_9 \\ y_{10} \end{bmatrix} \rightarrow \begin{bmatrix} l_1 \\ h_1 \\ l_2 \\ h_2 \\ l_3 \\ h_3 \\ l_4 \\ h_4 \\ l_5 \\ h_5 \end{bmatrix} \rightarrow \begin{bmatrix} l_1 \\ l_2 \\ l_3 \\ l_4 \\ l_5 \\ h_1 \\ h_2 \\ h_3 \\ h_4 \\ h_5 \end{bmatrix} \quad (6)$$

A wavelet transformation matrix with only half the dimension of the previous one is applied next to the low pass components of y followed by permutation and so on.

Figure 3 indicates that the best rejection performance of correlated arrivals is achieved via uniform subbanding using the Discrete Fourier transform. The poor performance of wavelet transform-domain full-band adaptation is an indication of insufficient signal decorrelation when block adaptive processing is applied to a non-uniformly subbanded signal.

B. Sub-band Adaptation

A transform-domain adaptive beamforming scheme based on FROST's constrained LMS concept is devised for mitigation of correlated broadband arrivals. The incoming broadband signals are first decorrelated via spatial averaging as described in [7]. Non-overlapping data

segments (32 samples) arriving at each sensor are then transformed either into the frequency domain (using the FFT) or the time-scale domain (using the wavelet transform) to produce 32 separate channels (narrow-band). The constrained FROST LMS adaptive algorithm is then applied to the signals present in each channel. The task of mitigating broadband correlated arrivals is thus transformed into a group of transform-domain narrowband adaptation schemes.

Figure 2 shows a schematic diagram of the proposed alternative approach to rejection of correlated broadband interference. The incoming signal is received by an array of M sensors each followed by K tap-delay elements. Spatial averaging as described above is also implemented in this case where signal components received by M sensors are used to generate a smoothed covariance matrix for an array of L sensors. The received signal is then subbanded into uniform contiguous subbands using the DFT or into non-uniform subbands using the wavelet transform. The corresponding weight in each subband is then computed adaptively by applying the conventional narrow-band Frost algorithm to non-overlapping data segments each of length K . This technique is less computationally demanding than the full-band adaptation scheme described earlier and convergence is generally achieved with fewer snapshots.

Figure 4 shows the beam pattern obtained using the same correlated jamming scenario of Figure 3. Adaptation in this case is performed independently in each frequency or scale bin. Figure 4 shows that adaptation in each bin of the wavelet transform domain results in better rejection of correlated interference.

III. MITIGATION OF PROPELLER GENERATED MULTIPATH

Radar returns due to scattering from a rapidly rotating structure such as a helicopter rotor or an engine propeller have been examined in some detail from an electromagnetics standpoint. The effect of such nonstationary scattering components on the detection and recognition performance of an airborne radar could be severe. Correlated multipath returns generated by a rotating scatterer may also pose a serious threat to an airborne phased array radar systems. The impact of this type of interference could be similar to that of hot clutter or terrain scattered interference depending on the size of the rotating propeller and its azimuth position with respect to the mainlobe of the airborne receiving antenna. In particular, propeller generated multipath jamming becomes a significant interference problem when the array-based radar receiver operates in a broadband mode.

A model for scattering from a thin rotating scatterer is used to study the significance of propeller generated multipath interference. An adaptive antenna array system based on the Frost beamformer operating in the transform domain is then devised for mitigation of broadband propeller generated interference.

A. Radar Returns From Rotating Aircraft Blades

Returned signals received by airborne radars are subjected to amplitude and phase modulation due to the rotating blades of the radar aircraft. The blades length, pitch, shape,

number, and frequency of rotation are all factors that determine the modulation extent of aircraft propellers. Several studies have examined the radar returned signal of rotors and propellers [5, 6], where FM modulation was depicted as the dominant effect of rotating blades over amplitude modulation. Furthermore, propeller blades are characterized by a finite number of scattering centers, namely tips of the blades and rotor hub. Radar returns from a propeller of P blades, each of length $L_2 - L_1$ with L_1 and L_2 being the distances of the blade near and far edges from the center of rotation respectively, are modeled in [5] as

$$I(t) = \sum_{p=0}^{P-1} A(L_2 - L_1) e^{j(\omega_c t - \frac{4\pi}{\lambda} (R + vt + \frac{L_1 + L_2}{2} \cos \theta \sin(\omega_r t + \frac{2\pi n}{P})))} \text{sinc} \left(\frac{4\pi}{\lambda} \frac{L_2 - L_1}{2} \cos(\theta) \sin \left(\omega_r t + \frac{2\pi n}{N} \right) \right) \quad (7)$$

where λ , ω_c , ω_r , θ , v , R and A are the wavelength and frequency of transmitted signal, the rotational frequency of blades, angle between propeller plane and the radar line of sight to its center, the radial velocity and the range of the propeller center, and a scale factor respectively. A sample of the signal using typical aircraft parameters is shown in Figure 6.

The doppler frequency shift generated by propeller FM modulation is in the range of few KHz for a typical aircraft propeller (see Figure 7). In broadband array processing this type of coherent multipath interference with doppler shift results in a time-dependent array covariance matrix and limits the performance of an adaptive processor.

B. Performance Analysis

A transform-domain broadband Frost beamformer is devised to suppress blade generated interference. Although this type of multipath interference is broadband coherent, spatial averaging prior to adaptation does not help as depicted by experimental results obtained during the course of this study. The reason is that multipath interference includes delayed replicas of the desired signal and spatial averaging a propeller modulated version of the desired signal does not decorrelate the interference.

The study assumes that the airborne radar array may be steered away from the center of the rotor or propeller and does not include components of multipath jamming entering the main beam of the array. Preliminary results indicate that a conventional Frost beamformer with tap-delay elements to compensate for the broadband nature of the interference is capable of mitigating propeller generated multipath. The number of array elements is also a significant factor where an array of eight to twelve auxiliaries is needed to mitigate multipath due to a single jammer. In summary, a broadband Frost beamformer with a relatively large number of degrees of freedom is capable of mitigating propeller generated multipath interference assuming that the scattering center of the rotor or propeller does not fall within the mainbeam of the receiving array.

IV. CONCLUSIONS

Two adaptive antenna architectures are proposed for mitigation of broadband coherent interference. Both techniques rely on spatial averaging prior to adaptation, and both incorporate transform domain adaptation using either the discrete Fourier transform or the wavelet transform. The first technique applies the constrained frost LMS algorithm on a block of data, the latter approach applies the Frost adaptation method at each frequency or scale bin of the received signal. While they differ in processing time, both techniques provide sufficient mitigation of broadband interference. Transform domain adaptation helps not only in expediting the convergence of each array, but also in decorrelating the received signal. Finally propeller generated multipath interference was modeled and mitigated using transform domain Frost-based adaptive architecture. Propeller generated multipath interference poses a serious threat to adaptive antenna systems which cannot be sufficiently mitigated using spatial averaging followed by transform domain adaptation. Further investigation in this regard will focus on implementing a form of spatial filtering prior to adaptation.

REFERENCES

- [1] O. Frost III, "An Algorithm for Linearly Constrained Adaptive Array Processing," *Proceedings of IEEE*, Vol. 60, No. 8, pp. 926-935, August, 1972.
- [2] T. Shan and T. Kailath, "Adaptive Beamforming for Coherent Signals and Interference", *IEEE Transactions on Acoustics, Speech, and Signal Processing*, Vol. ASSP-33, No. 3, pp. 527-536, June 1985.
- [3] S. Chern, C Sung, and K. Yang, "The transformed domain hybrid adaptive beamformer for multiple jammers suppression", *Journal of Acoustical Society of America*, Vol. 95, No. 2, pp. 866-876, February 1994.
- [4] O. Frost III, "An Algorithm for Linearly Constrained Adaptive Array Processing," *Proceedings of IEEE*, Vol. 60, No. 8, pp. 926-935, August, 1972.
- [5] J. Martin and B. Mulgrew, "Analysis of the theoretical radar return signal from aircraft propeller blades", *Proceedings of the 1990 IEEE International Radar Conference*, pp. 569-572, 1990.
- [6] H. E. Green, "Electromagnetic Backscattering from a Helicopter Rotor in the Decametric Wave Band Regime", *IEEE Transactions on Antennas and Propagation*, Vol. 42, No. 4, pp. 501-509, April 1994.
- [7] S. Chern, C Sung, and K. Yang, "The transformed domain hybrid adaptive beamformer for multiple jammers suppression", *Journal of Acoustical Society of America*, Vol. 95, No. 2, pp. 866-876, February 1994.
- [8] L. C. Godara, "Beamforming in the presence of broadband correlated arrivals", *Journal of Acoustical Society of America*, Vol. 92, No. 5, pp. 2702-2708, 1992.

- [9] S. Hosur and A. Tzefik, "Wavelet transform domain LMS algorithm," *International Conference on Acoustics, Speech, and Signal Processing*, ICASSP '93, pp. III(508-510), 1993.
- [10] J. Martin and B. Mulgrew, "Analysis of the theoretical radar return signal from aircraft propeller blades", *IEEE International Radar Conference*, pp. 569-572, 1990.
- [11] F. Lorenzelli, A. Wang, D. Korompis, R. Hudson, and K. Yao, "Optimization and performance of broadband microphone arrays", *SPIE Proceedings*, Vol. 2563, pp. 158-169, 1995.
- [12] J. S. Goldstein, E. J. Holder, and M. A. Ingram, "The application of two-dimensional wavelets and filter-banks for convergence enhancement in adaptive arrays for space communications," *Asilomar Conference on Signals Systems and Computers*, 1993.
- [13] S. Attallah and M. Najim, "On The Convergence Enhancement of The Wavelet Transform Based LMS," *Proceedings of International Conference on Acoustics, Speech, and Signal Processing*, ICASSP '95, pp. 973-976, Detroit, MI, May 1995.
- [14] A. J. Fenn, "Near-Field Testing of Adaptive Radar Systems," *The Lincoln Laboratory Journal*, pp. 23-40, Vol. 3, No. 1, 1990.
- [15] W. Lawton, "Applications of Complex Valued Wavelet Transforms to Subband Decomposition," *IEEE Transactions on Signal Processing*, Vol. 41, No. 12, pp. 3566-3568, December 1993.